Indian Institute of Technology Guwahati
*Department of Physics*

---

# *Nonperturbative Aspects of Reheating and Its Signatures on Cosmological Relics*

A thesis submitted by:

**Ayan Chakraborty**

to

**Indian Institute of Technology Guwahati**
in partial fulfillment of the requirements
for the award of the degree of
Doctor of Philosophy in Physics

May 2026

# Statement

.

The work contained in the thesis entitled "**Nonperturbative Aspects of Reheating and Its Signatures on Cosmological Relics**" has been carried out at the Department of Physics, Indian Institute of Technology Guwahati, India, by me, under the supervision of Prof. Debaprasad Maity. The content of this thesis is original and has not been submitted elsewhere for any other degree or diploma. Works presented in the thesis are all my own unless referenced to the contrary in the text.

Ayan Chakraborty
Roll Number: 206121007
PhD student
Department of Physics
Indian Institute of Technology Guwahati
Guwahati, Assam, India-781039
Date: 22/05/2026

# Disclaimer

.

The bibliography included in this thesis is, by no means, complete; rather, it contains the ones I went through thoroughly. I apologize for inadvertently missing out on some of the research papers, review articles, and other scientific documents relevant to this thesis, which also should have been cited. For the sake of illustration, some of the figures in this thesis are excerpted from other sources, which are properly cited.

# Certificate

.

It is certified that the work contained in the thesis entitled "**Nonperturbative Aspects of Reheating and Its Signatures on Cosmological Relics**" by Ayan Chakraborty (Roll number-206121007), a PhD student of the Department of Physics, IIT Guwahati, was carried out under my supervision. The content of this thesis is original and has not been submitted elsewhere for any other degree or diploma.

Debaprasad Maity 22/05/2026
.....
(Signature of the supervisor)

Prof. Debaprasad Maity
Professor,
Indian Institute of Technology Guwahati,
Guwahati-781039, Assam, India
Date: 22/05/2026

# Acknowledgements

.

I would like to express my sincere gratitude to my PhD advisor, Prof. Debaprasad Maity, for his continuous guidance, insightful discussions, and unwavering support throughout the course of this research programme. His encouragement, critical perspective, and intuitive thoughts have been invaluable in shaping both the direction and depth of this work. A short and substantial lesson I have received from him, "In PhD, you have to learn how to learn", has left a deep impression on my mind, and it has continued to inspire me throughout this journey.

I am grateful to the members of my doctoral advisory committee, Dr. Bibhas Ranjan Majhi, Prof. Santabrata Das, Dr. Sovan Chakraborty, for their encouragement and insightful comments, which immensely helped me to improve my presentation skills and also my understanding of my work. I am especially thankful to Dr. Bibhas Ranjan Majhi for his insightful questions regarding my work, which have made me think about my work from a different point of view. My thanks also to all the faculty members and non-teaching staff of the Department of Physics, Indian Institute of Technology Guwahati, for their constructive feedback and academic support at various stages of my doctoral journey. I also acknowledge the stimulating research environment provided by the department, which greatly contributed to the development of this thesis.

I sincerely thank my collaborators, Subhasis Maiti, Dr. Rajesh Mondal, Dr. Md Riajul Haque, Simon Clery, and Prof. Yann Mambrini for prolific discussions, technical assistance, and a collegial atmosphere that made this research experience both productive and enjoyable.

I would like to express my gratitude to my senior and current PhD group mates- Dr. Mousumi Maitra, Dr. Rajesh Karmakar, Dr. Banarshree Baishya, Dr. Sourav Pal, Gargi Sen, Dr. Sovan Sau, Dr. Rajesh Mondal, Subhasis Maiti, Jitumani Kalita and Sitesh Kumar Panda-for all the enriching discussions we have had among ourselves. I express my special gratitude to my group mates, Subhasis Maiti and Dr. Rajesh Mondal, not only for all the stimulating physics discussions but also for having an amicable association in this long journey. I am fortunate enough to have a companion like Subhasis, who would always treat me as his brother. He has always been my strongest support and solace in all of my sorrows in this academic environment. I thank him from the bottom of my heart.

My heartiest thanks to all other beloved friends, juniors and seniors, including Niloy, Abhik, Sourav, Indrajit, Nayan, Sanjib, Amit, Dipendu Bhandari, Dipankar, Shubhankar, Pratim, Sanket da, Surajit da, Sovan da, Shantanu da, Disha, Sounak, Debalina, Sonakshi. I will be cherishing the beautiful memories in this long association with all of them.

I express my deepest gratitude to my parents and my elder sister for their constant encouragement, patience, and understanding throughout this journey. Their ceaseless support and unconditional love have been a source of enormous strength and motivation during tough times. While battling with numerous hurdles, although sometimes I would

doubt my ability to tide over them, their kind words would always carry this message to me: be bold, be resolute; there is a silver lining in every cloud. I am eternally grateful to them.

Finally, I attribute everything to the feet of the Almighty for making these beautiful connections with beautiful people.

# Abstract

.

Over the past decades, the advancement in precision observational cosmology has widened the window to a great extent to look into the early universe. The early reheating phase is an integral part of the inflationary cosmology, which bridges the enormous gap in energy and time scales between the end of inflation and the beginning of the hot Big Bang nucleosynthesis (BBN). This phase not only generates initial conditions for the hot, thermal universe, but also produces various cosmological relics, namely, gravitational waves (GWs), Dark Matter (DM), Dark Radiation etc. The absence of direct observational evidence has left this important phase of the early universe poorly constrained, both at present and in the foreseeable future. However, the distinct imprints of this phase on cosmic relics offer us a promising avenue for its indirect probe through various cosmological observables. In this thesis, we have taken a little step towards this pursuit of deciphering the non-perturbative imprints of the reheating phase on various cosmological relics.

We come across several non-equilibrium and highly non-linear phenomena at the early reheating phase, known as *preheating*, that occur at an incredibly high energy. For the proper investigation of this early reheating era, governed by various complex non-linear processes, an involved non-perturbative framework is indispensable. Another notable area where the non-perturbative dynamics inherently appear is the domain of Cosmological Gravitational Particle Production(CGPP). Of late, this gravitational particle production in the early era has gained significant attention. However, due to its pure gravitational nature, it becomes an unavoidable natural mechanism for producing dark matter, dark radiation, gravitational waves, and all sorts of fundamental particles. Throughout the present thesis, we have meticulously focused on these various non-perturbative aspects of reheating and their distinct signatures on cosmic relics.

We first concentrate on the non-equilibrium *preheating* phase. We studied in detail the phenomena of quantum particle production via resonance, and explored the underlying connection with squeezing, chaos in a cosmological setting. We have particularly focused on bosonic particle production. In the post-inflationary reheating phase, the inflaton oscillates coherently around its minimum and acts as a periodic driving force, which excites chaotic fluctuation owing to the inherent *parametric resonance instability*. To quantify this chaotic nature, we work in the framework of quantum squeezing, and compute one of the important diagnostics of quantum chaos, namely OTOC or *out-of-time-order correlator* of the phase space variables. The dynamics of the squeezing parameters depend on the type of interacting field theory we consider. We take trilinear and quartic, two well-studied interactions between the bosonic fluctuations and the inflaton background. Interestingly, our analysis reveals an intrinsic interconnection among the growth of OTOC, the squeezing parameter, and the parametric resonance instability. Due to background expansion, the periodic driving source gradually loses its strength, resulting in the eventual relaxation of the fluctuation system from the chaotic instability to a thermalized state. Thermalization is believed to be deeply connected to the chaotic behavior of a system, which is conjectured

by proposing an inequality relating the Lyapunov exponent (a measure of chaos) and the system temperature under consideration (well-known Maldacena-Shenker-Stanford or MSS bound). We calculate the approximate lower limit of temperature by using this bound. We further conjecture a relation between the system temperature and quantum squeezing averaged over phase space, consistent with MSS bound and the well-known Rayleigh-Jeans formula for the temperature. Finally, we come up with the findings that the thermalized temperature of the squeezed system at the end of chaotic instability nicely follows the bosonic distribution function in this early reheating era. This indeed establishes a plausible connection between the non-equilibrium squeezed quantum system with the non-equilibrium preheating phase in the early universe.

We next turn our attention towards the non-perturbative aspect of gravitational particle production during inflation and post-inflationary reheating. In this work, we have extensively studied the long-wavelength(IR) and short-wavelength(UV) number density spectrum of *minimally coupled* scalar field, considering general reheating equation of state (EoS). This study also explains the small-scale (UV) oscillation in the momentum space of the number density spectrum through the appearance of an *interference term* in the analytically obtained spectrum. Further, we do a comparative study of the small-scale UV spectra obtained through perturbative or *Boltzmann* and non-perturbative or *Bogoliubov* treatment, indicating the equivalence and non-equivalence of their predictions for a general reheating background. We finally study the possibility of gravitational reheating in a completely non-perturbative framework.

In the last two works, we have extended the minimally coupled scalar field dynamics to a non-minimal one coupled with the Ricci scalar. The inclusion of non-minimal coupling results in the appearance of post-inflationary *tachyonic instability* for higher reheating EoS and coupling strength, signalling a striking departure from the dynamics of a minimally coupled system, particularly for the large-scale (IR) modes. We have further studied the generation of secondary gravitational waves(SGWs) induced by those non-minimally coupled IR scalar fluctuations. Owing to the distinctive non-perturbative large-scale instability effect of the source field, the induced GWs in the low and intermediate-frequency ranges are found to be strong enough to be detected by *Planck* and future gravitational wave detectors like LISA, BBO, DECIGO and ET. Finally, utilizing the Cosmic Microwave Background(CMB) constraints on tensor-to-scalar ratio, isocurvature, and the total number of relativistic degrees of freedom, we have deduced tight constraints on the non-minimal coupling strength between gravity and the spectator scalar fluctuation, depending upon the reheating equation of state.

We further propose a novel reheating scenario facilitated by the aforementioned non-minimal coupling-induced large-scale (infrared) fluctuations generated during inflation. We call this *infrared gravitational reheating* . We also do a comparative study with the prediction of reheating parameters made by perturbative and non-perturbative analyses in the presence of non-minimal curvature coupling. Finally, embedding this infrared reheating scenario into the well-known $\alpha-$attractor inflationary model, we examine possible constraints on the model parameters in light of the latest Atacama Cosmology Telescope (ACT), Dark Energy Spectroscopic Instrument (DESI) results. The strong, detectable GW signal in the present

reheating background indeed opens up a possibility of probing such a reheating scenario through future GW observatories.

These last two studies are devoted to the exploration of non-perturbative effects in the gravitational portal for a nonminimally coupled system during early inflation and reheating, and decode their signature on the gravitational wave spectrum today.

x

# List of Publications

.

## Thesis Works :

1. **Ayan Chakraborty** Debaprasad Maity *"Squeezing, Chaos and Thermalization in Periodically Driven Quantum Systems: The Case of Bosonic Preheating"*. JHEP 02 (2024) 110. arXiv: 2309.10116 [hep-th]

2. **Ayan Chakraborty**, Subhasis Maiti, Debaprasad Maity, *"Probing non-minimal coupling through super-horizon instability and secondary gravitational waves"*. Phys. Rev. D 111, 083505 (2025) arXiv: 2408.07767 [astro-ph.CO]

3. **Ayan Chakraborty**, Simon Clery, Md Riajul Haque, Debaprasad Maity, Yann Mambrini, *"Generalizing the Bogoliubov vs Boltzmann approaches in gravitational production"*. Phys. Rev. D 112 043511 (2025) arXiv: 2503.21877 [gr-qc]

4. **Ayan Chakraborty**, Debaprasad Maity, Rajesh Mondal *"Nonminimal infrared gravitational reheating in light of ACT observation"*. Phys. Rev. D 112, 123547 (2025) arXiv: 2506.02141 [astro-ph.CO]

## Other Works :

1. **Ayan Chakraborty**, Md Riajul Haque, Debaprasad Maity, Rajesh Mondal *"Inflaton phenomenology via reheating in light of primordial gravitational waves and the latest BICEP/Keck data"*. Phys. Rev. D 108, 023515 (2023). arXiv: 2304.13637 [astro-ph.CO]

2. **Ayan Chakraborty**, Rajesh Mondal, Sourav Mondal *"Constraining Reheating Temperature, Inflaton-SM Coupling and Dark Matter Mass in Light of ACT DR6 Observations"*. arXiv: 2505.13387 [hep-ph], JCAP (Accepted for publication)

3. **Ayan Chakraborty**, Debaprasad Maity, Rajesh Mondal *"Dark matters are Inert, or FIMPy, or WIMPy or UFOy: An inflationary gravitational particle production"*. arXiv: 2603.04155 [hep-ph]

# Conference Participations

.

1. **Indian Association for General Relativity and Gravitation(IAGRG), December 19-21, 2022, at IISER KOLKATA**
2. **"Less Travelled Path to the Dark Universe" held during 13 – 24 March 2023 at ICTS-TIFR, Bengaluru, India**
3. An oral presentation at the **10th International Conference on Gravitation and Cosmology: New Horizons and Singularities in Gravity 06-09 December 2023, at IIT Guwahati**
4. An oral presentation at the **Paris-Saclay AstroParticle Symposium 2024, Institut Pascal, Université Paris-Saclay, France, from November 12th to November 29th, 2024.**
5. An oral presentation at the **Hearing beyond the standard model with cosmic sources of Gravitational Waves: Theories and challenges in this era, 30 December 2024 to 10 January 2025, ICTS-TIFR, Bengaluru, India**
6. An oral presentation at the **Cosmic Connections: Bridging the Early and Late Universe, July 28 to August 1, 2025, IMSc Chennai, India**

# Notations and Conventions

.

Throughout this thesis, we use natural units $\hbar$=$c$=$k_B$=1. In this unit, Reduced Planck mass is given by $M_{\rm pl} = \frac{1}{\sqrt{8\pi G}} = 2.435 \times 10^{18}$ GeV.

Greek indices $\mu$,$\nu$ and so on go over the four space-time co-ordinates $x^\mu = [x^0, x^1, x^2, x^3]^T$ with $x^0$ for the time coordinate.

Minkowski metric is given by $\eta_{\mu\nu} = diag[-1, 1, 1, 1]$.

Latin labels $i, j, k$ and so on go over the three spatial co-ordinates.

The Ricci tensor, defined in terms of the Christoffel symbols, is

$$R_{\mu\nu} = \partial_\lambda \Gamma^\lambda_{\mu\nu} - \partial_\nu \Gamma^\lambda_{\mu\lambda} + \Gamma^\lambda_{\lambda\rho}\Gamma^\rho_{\mu\nu} - \Gamma^\rho_{\mu\lambda}\Gamma^\lambda_{\nu\rho}, \tag{1}$$

and the Ricci scalar is $R = g^{\mu\nu}R_{\mu\nu}$ .

# Contents

CHAPTER 1

# Introduction and Motivation

*" The Cosmos is all that is or was or ever will be. Our feeblest contemplations of the Cosmos stir us – there is a tingling in the spine, a catch in the voice, a faint sensation, as if a distant memory, of falling from a height. We know we are approaching the greatest of mysteries. "*

— *Carl Sagan, Cosmos*

Human inquisitiveness has been the impetus behind the civilization's journey from the darkest phase of ignorance to the brightest phase of knowledge in the modern era. From the deep, dark den, the ancient human beings would gaze at the night sky with utter wonder, and the radiance of millions of effulgent stars would enthral them with their majestic beauty. It is curiosity that first posed the question: what is our origin, and how did we come into existence in this vast expanse? To attempt to answer this question, since time immemorial, numerous scientific ideas and theories have been proposed by many great minds across places and eras. Notable among them are Nicolaus Copernicus (1473–1543), Tycho Brahe (1546–1601), Johannes Kepler (1571–1630), Galileo Galilei (1564–1642), and Isaac Newton (1643–1727) in the era of the Renaissance Revolution. Important to mention that long before the era of Renaissance Revolution, Indian astronomers such as Āryabhaṭa (476–550 CE) had already introduced profound ideas —most notably the rotation of the Earth and precise mathematical descriptions of planetary motion—that stand as important conceptual precursors in the global history of cosmology. With the progress of time and the advancement of observation by the revolutionary invention of the improved version of the telescope for astronomical observations by Galileo Galilei in 1609 paved the way to observe distant planets and countless stars in the Milky Way with significant clarity. It is Galileo Galilei, the father of observational astronomy, who first provided the observational evidence that turned heliocentrism, proposed by Copernicus in 1543, into scientific reality. However, in 1687, Issac Newton, one of the greatest scientific minds of all time, first formulated the universal law of gravitation governing the dynamics of the tiniest terrestrial object to

a gigantic celestial body in the infinite universe, and hence established the cosmological studies on a strong foundation of a unified, coherent physical framework. Although Newton envisioned an infinite, static, eternal universe filled with evenly distributed stars through mutual gravitational pulls, his own laws of gravitation clearly contradict the concept of the immutability of the universe. In such a universe governed by the attractive gravitational force, all matter would inevitably be pulled toward a central point of matter distribution, leading to an unstable state of the matter distribution that would eventually collapse. Despite several cosmological challenges, like the *Olbers' paradox* or *dark night paradox*, Newtonian cosmology reigned for more than two centuries with its full glory until Einstein's theory of relativity refuted its infallibility, indicating the strong limitations of this theory and giving much deeper insight into the large-scale structure of the universe. In the trajectory from the pre-Newtonian to the Newtonian era, the universe came to be conceived as a perfectly deterministic and mechanical system, governed by universal laws of motion and gravitation, with space and time considered absolute and independent of the observer. Newton's classical picture, together with Maxwell's electrodynamics(1865), created an impression of a complete description of nature, built upon continuity, determinism, and the predictability of all phenomena on all scales.

By the stroke of the 20th century, the advent of two conceptual revolutions—Einstein's theories of Special (1905) and General Relativity (1915), together with quantum theory—first exposed the fundamental cracks in the edifice of Newtonian philosophy, and made this age-old theory stand before a serious question of its strong limitations in explaining both microscopic dynamics and the dynamics of the cosmos. The theory of Special Relativity abolished absolute space and time, unifying them into spacetime and establishing the constancy of the speed of light. This theory also introduced the mass-energy equivalence. A decade later, General Relativity (1915) replaced Newton's gravitational force with the geometric curvature of spacetime, opening up a new horizon to understand the underlying design of this vast cosmos and the interactions between matter and the dynamical fabric of spacetime. At the same time, the failures of classical physics at microscopic scales led to the birth of quantum theory. The transition from classical to quantum ideas was spearheaded by several distinguished figures. Planck, in 1900, introduced energy quantization to resolve the nature of the blackbody spectrum. Later on, building on the concept of quantized light (photons), Einstein explained the photoelectric effect in 1905. Bohr's atomic model (1913) stabilized the hydrogen atom using quantized orbits. This was followed by the complete formulation of modern quantum mechanics by Heisenberg, Schrödinger, and Dirac (1925–1926), introducing the probabilistic nature of physical laws and fundamentally challenging Newtonian determinism, and establishing a clear demarcation between the classical and quantum worlds. In this world, the description of a localized particle is given in terms of its associated wave function and different classical observables, like position, linear and angular momentum, total energy, are replaced by noncommutative operators. Initially, relativity and quantum theory addressed different domains, yet the unification of the quantum description of matter with the relativistic structure of spacetime became a central challenge. The first remarkable step was the Klein–Gordon equation,

derived in the 1920s as a relativistic generalization of Schrödinger's wave equation. This equation correctly incorporated Lorentz invariance and described spin-0 particles, but it also faced interpretational difficulties, such as negative probability densities, which limited its physical application. Nonetheless, it established the idea that relativistic particles must be described by underlying quantum fields, rather than just wave functions. The next significant advancement of this effort came with Dirac's relativistic wave equation (1928), which not only merged quantum principles with special relativity by successfully resolving the previous issue of probability interpretation but also predicted the existence of antimatter. This marked the dawn of relativistic quantum theory. Building on these insights, Heisenberg, Pauli, Fermi, and later Schwinger, Feynman, and Dyson developed the framework of Quantum Field Theory (QFT), where fields are the fundamental entities of nature. Particles are nothing but the excitations of the underlying fields, and interactions are mediated by the exchange of quanta. These major breakthroughs of the 20th century changed our perception of the microscopic to large cosmological scale dynamics forever. The Relativity and Quantum Field Theory, a synthesis of Relativity with Quantum Mechanics, are two cornerstones upon which the modern cosmology is firmly established. The discussion so far has depicted a historical roadmap of how ideas evolve to attain their present form.

Shortly after the development of these paradigms, people were inclined towards the study of early universe evolution within the newly established theoretical and mathematical frameworks. At the dawn of this revolution, cosmology remained primarily a subject of theoretical curiosity for physicists, largely due to the absence of precise observations capable of validating the models. The period was dominated by debates and doubts between the Big Bang framework and the Steady-State model proposed by Bondi, Gold, and Hoyle in 1948. During the 1950s and 1960s, the lack of precise astronomical surveys caused the key parameters, such as the Hubble constant, the average density of matter, and the age of the Universe, to be highly uncertain, leading to persistent conceptual tensions such as the age problem. A decisive shift occurred in 1965 with the accidental discovery of the Cosmic Microwave Background(CMB) by Penzias and Wilson [1, 2], a persistent, uniform radio signal coming from all directions in the sky, which turned out to be the afterglow of the Big Bang; hence, it strongly supported the Big Bang picture. A few decades later, in the 1990s, another dramatic shift occurred through the COBE(Cosmic Background Explorer) satellite's detection of anisotropies in the CMB in 1992 [3, 4] provided the first quantitative evidence in favor of inflationary cosmology. This discovery marked the transition of cosmology from a primarily theoretical playground to a precision observational science.

After COBE, the subsequent missions(WMAP, Planck) refined the measurements of the CMB anisotropies with unprecedented precision, and hence, significantly enhanced our understanding of the cosmic history of the universe. These precise measurements of the temperature anisotropies in the CMB [5–8] have not only revealed the homogeneity and isotropy of the universe on large scales, but also tiny fluctuations of the matter and energy density on small scales. These primordial density perturbations are the seed of the large-scale structure formation of the universe that we see today. Further, CMB observation data fit well with the negligible spatial curvature and the near scale invariance of the primordial

curvature perturbation power spectrum. The standard cosmological ΛCDM model fails to naturally explain the observed near isotropy of the CMB (the Horizon problem), since widely separated regions of the sky should never have been in causal contact. Similarly, it struggles to account for the flatness of spatial geometry (the Flatness problem), which requires extreme fine-tuning of initial conditions. The model also lacks a mechanism to explain the origin of the nearly scale-invariant primordial density perturbations. Inflationary cosmology, introduced in the early 1980s, provides a natural resolution to these aforementioned issues. According to inflationary cosmology, the very early universe underwent a brief epoch of accelerated phase of expansion known as cosmic inflation [9–23]. This brief accelerated expansion epoch not only resolves the horizon and flatness issues but also explains the origin of primordial density perturbations through the fluctuations of the inflaton field, predicting a nearly scale-invariant spectrum that matches CMB observations with remarkable precision. Inflation is believed to happen at an enormous energy scale as high as $\sim 10^{16}$ GeV, with the substantially small duration $\gtrsim 10^{-36}$ seconds. The fast dilution of all the pre-existed matter components because of extremely rapid expansion within a very short period, the universe was left in a supercool state of vanishing number and entropy density at the end of inflation. Moreover, according to the predictions of Big Bang nucleosynthesis (BBN), the first light elements started forming at cosmic time $\sim 1$ s at the equilibrium temperature $\sim 1$ MeV in the hot, thermal, dense universe. Therefore, connecting these two contrasting phases, inflation and BBN, has become a major challenge in the recent study of early universe cosmology. The intermediate phase, connecting the early inflation and BBN, filling up the huge gap in energy and time scales, is least understood to date and very poorly constrained by current observations. Although collider experiments can probe intermediate phenomena like electroweak symmetry breaking, $E_{EW} \sim 100$ GeV, and QCD phase transitions, $E_{QCD} \sim 100$ MeV, the vast energy range between the end of inflation and the beginning of hot BBN shall remain unreachable in the near future. Most of the information about the complex dynamics following inflation gets washed out by the subsequent non-linear evolutionary phases of the universe. Therefore, this intermediate phase is far beyond the scope of direct probe by current cosmological experiments.

## Importance of reheating phase

To bridge the gap in energy and time scales between the end of inflation and the beginning of the BBN phase, the theoretically proposed intermediate phase is the post-inflationary reheating. At the beginning of the post-inflationary reheating phase, the total energy budget of the universe is dominated by the classical, homogeneous inflaton field. To transit from a cold, dark, inflaton-dominated state to a hot, thermal, radiation-dominated phase, one natural expectation is the eventual decay of the high-energetic classical inflaton field into Standard Model radiation degrees of freedom (DOFs), which subsequently thermalize and give rise to a post-reheating radiation-dominated universe. Therefore, it is imperative to study how the energy transfer occurred between the inflaton and all kinds of Standard Model(SM) elementary particles populating the present universe. Getting a clearer picture



TH-4015_206121007

of reheating dynamics requires an understanding of various complex non-equilibrium field dynamics, as well as interactions among different degrees of freedom in the early universe. This reheating phase not only generates initial conditions for the hot, thermal universe but also produces other cosmological relics, for instance, gravitational waves(GWs), dark matter, dark radiation, baryonic matter, etc. Although the reheating phase is highly unconstrained due to the lack of direct observational evidence, it leaves distinct signatures on these cosmological relics and also subtle imprints on CMB anisotropies, by which this important phase of the early universe can be indirectly constrained. This very important transition phase influences the early universe dynamics mainly in two significant ways:

- **Modified expansion history:** The post-inflationary dynamics of the universe during the reheating era is mainly governed by the nature of the inflaton potential by modifying the effective equation of state. While constraining any inflation model, the reheating phase plays a crucial role because of its connection to the CMB observables.

- **Modified thermal history:** During reheating, the background inflaton transfers its energy to all kinds of standard model and beyond standard model particles, which eventually produce the hot, thermal bath for Big Bang nucleosynthesis. Unlike the standard radiation-dominated era, this gradual energy transfer from the inflaton to thermal bath particles through various mechanisms noticeably alters the thermal evolution of the universe during this phase, which has a significant impact on the production of dark matter, gravitational waves, matter-antimatter asymmetry(Baryogenesis), etc., during reheating.

Thus, this intermediate reheating phase, connecting the early inflation and BBN, has a great phenomenological impact on the late universe. Therefore, it is crucial to gain a proper theoretical understanding of the rich dynamics of this phase. The theoretical study of reheating is broadly classified into two aspects: perturbative and non-perturbative aspects of reheating.

## Importance of perturbative framework of reheating

To study the transfer of energy from inflaton to radiation during reheating, the widely known and useful framework is the perturbative or Boltzmann approach. Using the quantum field theoretic technique of the scattering matrix elements, we compute the interaction rate of a particular interaction process. In the area of High-Energy Physics, Astroparticle Physics, and Cosmology, this framework is rigorously employed while dealing with the evolution of the number and energy density of a system in the presence of interactions. In this description, the decay and scattering of inflaton quanta into lighter particles are tracked through Boltzmann equations, which encode the time evolution of the number and energy densities of different species. This approach allows one to capture the interplay between particle production, dilution due to cosmic expansion, and backreaction effects. Furthermore, it provides a quantitative framework to compute the reheating temperature, the thermalization history, and possible relic abundances of dark matter or other beyond–Standard Model



TH-4015_206121007

species. For these reasons, the perturbative Boltzmann approach remains a robust and versatile tool in the study of early universe cosmology.

## Limitations of perturbative framework and importance of non-perturbative framework of reheating

- **Existence of non-linear preheating phase:** *Preheating* is known to be a highly energetic non-perturbative phenomenon when inflaton and radiation are assumed to be strongly coupled. In this early reheating phase, naturally, the previous perturbation series in the weak coupling regime fails to study the production of radiation quanta from the decay of the inflaton. Just after the end of inflation, the inflaton field amplitude is expected to be very high, that is, of the order of the Planck mass. Consequently, the energy stored in this field is also incredibly high. In this stage, instead of behaving like an individual inflaton particle(quanta), the entire field behaves like a *coherently oscillating inflaton field*. Therefore, any other fields directly/indirectly coupled with this coherently oscillating inflaton will experience a periodic driving force, and if the coupling strength is sufficiently strong, the field amplitude will be resonantly enhanced. The violent draining of energy from the background inflaton to the fluctuations through the *parametric resonance instability* is a prominent feature of this early reheating phase. Due to rapid energy transfer, the energy density of the produced fluctuations becomes comparable to the background energy very soon, thereby causing significant backreaction and backscattering effects during this phase. The dynamics of this phase lead to many interesting phenomena, for example, the production of solitons that can delay the thermalization of the decay products in the thermal bath, required as an initial condition for BBN [24], field configurations evolving self-similarly in a turbulent manner [25, 26], non-thermal phase transitions and the production of cosmic defects [27–29]. The proper investigation of this non-linear phase requires an involved non-perturbative framework studying the coupled field dynamics of the inflaton and a daughter field system.

- **Importance of large-scale Infrared (IR) fluctuations:** The perturbative approach always deals with the interactions happening in the causal scales. At a given instant, all sorts of interactions are taking place inside the Hubble horizon, and we study only the evolution of the interacting system for the causal scales in the perturbative treatment. However, the expansion history of the universe suggests that the early inflationary phase produced the large-scale or super-horizon fluctuations of all fields due to the shrinking inverse Hubble scale during inflation. Different wavelengths of those fluctuations left the horizon at different instants during inflation, and re-enter the horizon at some later phase as the Hubble horizon started growing over time after inflation. In perturbative reheating analyses, such super-horizon modes are ignored due to their very acausal nature. Production of super-horizon perturbations, therefore, is a unique feature of inflation which is indeed observed in Cosmic Microwave Background(CMB) temperature anisotropy. Those are identified

with the massless inflaton fluctuation. However, at the inflation scale of order $10^{16}$ GeV, all the Standard Model (SM) fields are massless and can be generated amply at super-horizon scales during inflation. Such inflationary super-horizon production, therefore, becomes sub-horizon in the post-inflationary period and can contribute to subsequent dynamics of the universe. To track the evolution of these large-scale fluctuations, we should start studying their dynamics when they were deep inside the horizon during inflation. This study of the dynamics of large-scale or Infrared(IR) fluctuations is a pure non-perturbative study, as the perturbative treatment completely fails to capture this acausal picture. A major part of this thesis work focuses on the rich dynamics of the non-perturbative large-scale fluctuations of the light fields during early inflation and reheating, and their indelible signatures on various cosmological relics.

However, to get an exhaustive picture of the reheating dynamics, both the perturbative and non-perturbative studies are indispensable. Another very important aspect addressed in this thesis is the comparative analysis of the two approaches(perturbative and non-perturbative), and exploring the equivalence and non-equivalence of their predictions in the arena of early universe physics.

## Key focus of the thesis

This thesis mainly focuses on the non-perturbative aspects of particle production during inflation and the post-inflationary reheating phase. Parametric resonance, *tachyonic instability* are some distinctive features of the non-perturbative phenomena in the early era. For instance, in the early reheating era(*preheating*), plenty of elementary particles were produced within a very short period through the mechanism of *parametric resonance instability* as described earlier. Another notable aspect where non-perturbative effects become instrumental is the Cosmological Gravitational Particle Production(CGPP). This CGPP is the quantum mechanical particle production in a time-dependent dynamical background. These particles can play an important role in cosmic history, being possible candidates for dark matter, gravitational wave radiation, dark radiation, etc. Our study also sheds light on various non-perturbative signatures of gravitational particle production, both in minimalistic (no coupling to gravity) and non-minimalistic (non-zero coupling to gravity) scenarios.

We have made unprecedented progress in observational cosmology after the detection of gravitational waves. In this thesis, one of the prime objectives is to decipher various non-perturbative signatures of different early universe phenomena through their imprint on gravitational waves. These ideas construct the main foundation of this thesis work.

The thesis is organized into seven chapters. It begins with an introduction and motivation of the thesis work, which is then followed by the overview of the Standard and Non-standard cosmology, its successes and limitations, a short description of the importance of squeezed-state formalism and the description of a diagnostic of quantum chaos(*out-of-time-order*

*correlator*(OTOC)), and a chapterwise description of each work carried out in the thesis. Finally, in chapter seven, we conclude the thesis with a potential future outlook.

CHAPTER 2

# Standard and Non-standard cosmology

*..everything can be created from nothing, And "everything might include a lot more than what we can see. In the context of inflationary cosmology, it is fair to say that the universe is the ultimate free lunch."*

*Alan Guth in 'THE INFLATIONARY COSMOLOGY'*

In this chapter, we present an overview of the Standard Big Bang cosmology. After describing the successes and important drawbacks of this model, we then introduce the inflationary Non-standard cosmology.

## 2.1 Standard FLRW Cosmology

Our current understanding of the universe's evolution is strongly based upon the Friedmann-Lemaître-Robertsom-Walker (FLRW) cosmological model. The basic principles of this model construct the Standard cosmology. Our universe is observed to be homogeneous and isotropic on the large scales, which supports the assumption of the Cosmological Principle. The uniformity of the CMB radiation indicates a remarkably high degree of homogeneity and isotropy of the universe on large scales at the epoch of last scattering of the CMB radiation. To study the homogeneous, isotropic, and expanding universe satisfying the Cosmological Principle, the widely known metric is the FLRW metric, which is expressed in the following form.

$$ds^2 = -dt^2 + a^2(t)\left[\frac{dr^2}{1-\mathcal{K}r^2} + r^2d\theta^2 + r^2\sin^2\theta d\phi^2\right] \tag{2.1}$$

where ($t$, $r$, $\theta$, $\phi$) are the cosmic time coordinate and three spatial coordinates in spherical polar coordinate system respectively, the dimensionless quantity $a(t)$ is the scale factor,

giving the measure of the spatial expansion of the universe, $\mathscr{K}$, the spatial curvature, can be chosen to be $+1$, $-1$, and 0, represents the closed, open and flat universe, respectively. In the metric (2.1), the time-dependent scale factor only implicitly carries the information of the expanding universe. To study the dynamics of the expanding universe, we solve the evolution of the scale factor using the Einstein equations,

$$G_{\mu\nu} = \left(R_{\mu\nu} - \frac{1}{2} R\, g_{\mu\nu}\right) = 8\pi\, G\, T_{\mu\nu} - \Lambda\, g_{\mu\nu},\ \nabla_\mu T^{\mu\nu} = 0\,, \tag{2.2}$$

where $G_{\mu\nu}$ is the Einstein tensor, $G$ is the Newton's gravitation constant, $g_{\mu\nu}$ represent the spacetime metric components, $R_{\mu\nu}$ is the Ricci tensor, $R = g^{\mu\nu} R_{\mu\nu}$ is the Ricci curvature scalar, and $T_{\mu\nu}$ is the stress-energy tensor of all fields(matter, radiation etc.). We have also included the Cosmological Constant, $\Lambda$, in the Einstein equations. The Ricci tensor $R_{\mu\nu}$ can be written in terms of Christoffel symbols as follows:

$$R_{\mu\nu} = \partial_\alpha \Gamma^\alpha_{\mu\nu} - \partial_\nu \Gamma^\alpha_{\mu\alpha} + \Gamma^\alpha_{\alpha\beta}\Gamma^\beta_{\mu\nu} - \Gamma^\beta_{\mu\alpha}\Gamma^\alpha_{\nu\beta}\,, \tag{2.3}$$

where $\Gamma^\alpha_{\mu\nu}$ are the Christoffel symbols.
The symmetry of the FLRW metric(all the vanishing off-diagonal elements) demands the stress-energy tensor to be also diagonal, and by isotropy, the spatial components must be equal. Such a stress-energy tensor can be realized by an ideal fluid characterized by a time-dependent energy density, $\rho(t)$, and pressure $P(t)$ as

$$T^\mu_\nu = (\rho + P)\, U^\mu_\nu + P\delta^\mu_\nu = \mathrm{diag}\,(-\rho,\, P,\, P,\, P)\,, \tag{2.4}$$

where $U^\mu$ is the relative four-velocity between the fluid and the observer. For a comoving observer, this will be $U^\mu = (1, 0, 0, 0)$. In the cosmological context, any kind of matter component is generally associated with an equation of state parameter, "$w$". There exists a linear relationship between the energy density and pressure of a barotropic cosmological fluid

$$P = w\rho\,, \tag{2.5}$$

where $w$ is the equation of state(EoS) parameter of the fluid. For example, $w = 0$ corresponds to a non-relativistic dust-like component having vanishing pressure. From (2.4), we find the trace of this tensor, $T^\mu_\mu = (3P - \rho)$. For relativistic radiation-like components, the requirement of the tracelessness of the stress tensor, $T^\mu_\mu = 0$, gives the radiation EoS to be $w_{\rm r} = 1/3$. This suggests that a universe dominated by the radiation-like components has the property of conformal invariance. For all physical gravitating objects, the strong energy condition(SEC), $(\rho + 3P) > 0$ or, $(1 + 3w) > 0$, must be satisfied. In our subsequent discussion, all the fluids we shall work with satisfy this strong energy condition. On the contrary, the cosmological constant "$\Lambda$" with $w_\Lambda = -1$ violates the strong energy condition.

**Friedmann equations**

In the isotropic, homogeneous FLRW background, the Einstein equations (2.2) give the following set of equations

$$\left(H^2 + \frac{\mathscr{K}}{a^2}\right) = \frac{\rho}{3M_{\rm pl}^2} + \frac{\Lambda}{3}$$
$$\left(\dot{H} + H^2\right) = -\frac{(\rho + 3P)}{6M_{\rm pl}^2} + \frac{\Lambda}{3}\,. \tag{2.6}$$

where $M_{\rm pl} = 1/\sqrt{8\pi G} = 2.435 \times 10^{18}$ GeV, is the reduced *Planck* mass. This set of equations is the well-known Friedmann equations, which are used to study the dynamics of the expanding universe. The dot represents the derivative with respect to cosmic time. The above equation (2.6) shows that the evolution of the Hubble scale, $H = (\dot{a}(t)/a(t))$ is directly related to the energy density of the dominating fluid component. Therefore, in the presence of several energy components, the time evolution of the dominating component decides the background dynamics.

From the conservation of the stress-energy tensor, we get the evolution equation of the energy density of different matter components. The conservation equation, $\nabla_\mu T^{\mu\nu} = 0$ leads to the following continuity equation

$$\dot{\rho} + 3H(\rho + P) = 0 \Rightarrow \dot{\rho} + 3H(1+w)\rho = 0\,. \tag{2.7}$$

The solution of the continuity equation gives the time evolution of the energy density as

$$\rho\, a^{3(1+w)} = \text{constant}\,. \tag{2.8}$$

This relation suggests that the universe, dominated by different fluid components, evolves differently depending upon the corresponding EoS parameters. For instance,

$$\begin{aligned} \rho_{\rm m}\, a^3 &= \text{constant} \quad \text{(Matter)} \\ \rho_{\rm r}\, a^4 &= \text{constant} \quad \text{(Radiation)} \\ \rho_\Lambda &= \text{constant} \quad \text{(Vacuum energy)}\,, \end{aligned} \tag{2.9}$$

where $\rho_{\rm m}, \rho_{\rm r}, \rho_\Lambda$ represent the matter, radiation and vacuum energy densities, respectively. The Cosmological Constant is also identified with the vacuum energy.

Let's now define the dimensionless density parameters at the present time, $t = t_0$.

$$\Omega_{{\rm I},\,0} \equiv \frac{\rho_{\rm I,0}}{\rho_{\rm crit,0}}\,, \tag{2.10}$$

where "I" indicates different fluid components, and $\rho_{\rm I,0}$ is the present-day energy density of any fluid component "I". The present-day critical density is defined as [7]

$$\rho_{\rm crit,0} = \frac{3H_0^2}{8\pi G} = 3M_{\rm pl}^2 H_0^2 = 1.87h^2 \times 10^{-29}{\rm g.cm}^{-3} = 8.1h^2 \times 10^{-47}{\rm GeV}^4\,, \tag{2.11}$$

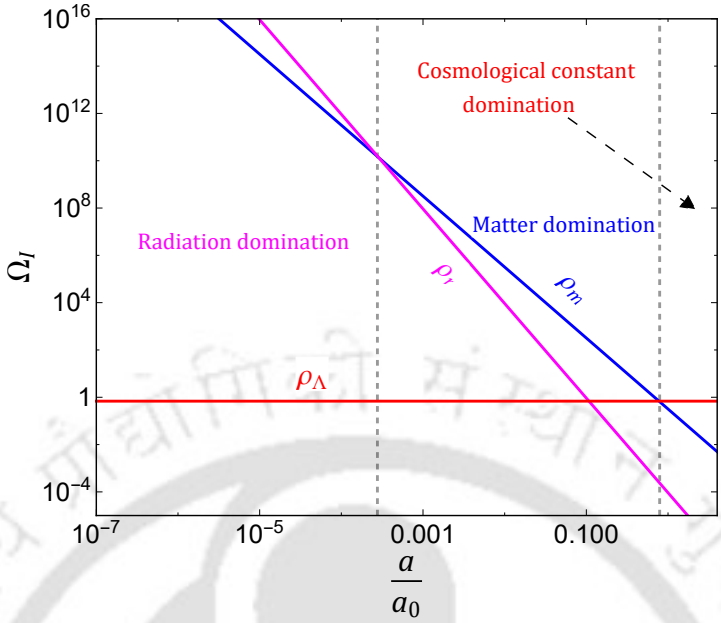


Figure 2.1: *Figure represents the evolution of the energy densities of matter(blue), radiation(magenta) and dark energy(red) in the universe with the normalized scale factor* $(a/a_0)$.

where "$h$" is the dimensionless scaling factor, with a value typically around 0.7.

In terms of the critical density parameter, the Friedmann equation (2.6) can now be recast as

$$H^2(a) = H_0^2 \left[\Omega_{\mathrm{r},0}\left(\frac{a_0}{a}\right)^4 + \Omega_{\mathrm{m},0}\left(\frac{a_0}{a}\right)^3 + \Omega_{\mathscr{K},0}\left(\frac{a_0}{a}\right)^2 + \Omega_{\Lambda,0}\right], \tag{2.12}$$

where the curvature density parameter is defined as $\Omega_{\mathscr{K},0} \equiv -(\mathscr{K}/(a_0 H_0)^2)$ with present-day scale factor and Hubble scale $a_0$, $H_0$ respectively. Following the conventional normalization, the present-day scale factor is set to be unity, $a_0 \equiv 1$. The equation (2.12) now boils down to

$$\frac{H^2}{H_0^2} = \Omega_{\mathrm{r},0}a^{-4} + \Omega_{\mathrm{m},0}a^{-3} + \Omega_{\mathscr{K},0}a^{-2} + \Omega_{\Lambda,0}\,. \tag{2.13}$$

**ΛCDM:**

According to the current observations, the present universe is filled with radiation(r), matter(m), and dark energy($\Lambda$) or vacuum energy with the following critical density parameters [7]:

$$\Omega_{\mathscr{K},0} \simeq -0.007 \pm 0.0019,\ \Omega_{\mathrm{r},0} \simeq 9.2 \times 10^{-5},\ \Omega_{\mathrm{m},0} \simeq 0.32,\ \Omega_{\Lambda,0} \simeq 0.685\,. \tag{2.14}$$

The matter content consists of 5% ordinary matter (baryons) and 27% cold dark matter(CDM). It is seen that even today, the curvature contribution is less than 1% to the total cosmic energy budget. From Eq.(2.9), the matter and radiation energy scale as $a^{-3}$ and $a^{-4}$

respectively, whereas the curvature contribution increases as $a^{-2}$ in the past. Therefore, from a very early epoch, the curvature contribution can always be neglected in comparison with the radiation and matter contents. This fact also confirms the spatial flatness of the universe on large scales. The very early universe was radiation-dominated(RD phase), the adolescent phase was dominated by matter(MD phase), and the adult or present universe is dominated by the Cosmological Constant or Dark Energy(ΛD phase)(see Fig.(2.1)). To study the evolution of the early radiation or matter-dominated universe, the Friedmann equation (2.6) can be further simplified by dropping the curvature($\mathscr{K}$) and Dark energy(Λ) contributions as

$$H^2 = \frac{\rho}{3M_{\rm pl}^2}, \quad \left(\dot{H} + H^2\right) = -\frac{(\rho + 3P)}{6M_{\rm pl}^2}\,. \tag{2.15}$$

Solving the Friedmann equation (2.15) together with the evolution of energy density (2.8), we study the time evolution of the scale factor as well as the Hubble scale in different epochs can be expressed as

$$a(t) \propto \begin{cases} t^{\frac{2}{3(1+w_{\rm I})}} & w_{\rm I} \neq -1 \begin{cases} t^{2/3} & \text{Matter} \quad (w_{\rm m} = 0) \\ t^{1/2} & \text{Radiation } (w_{\rm r} = 1/3) \end{cases} \\ e^{Ht} & w_\Lambda = -1 \qquad \text{Cosmological Constant}\,. \end{cases} \tag{2.16}$$

The associated Hubble scale evolves as

$$H(t) \propto \begin{cases} \frac{1}{t} & w_{\rm I} \neq -1 \\ \text{constant} & w_{\rm I} = -1\,. \end{cases} \tag{2.17}$$

Another important quantity, which also depends upon the Hubble scale, is the Ricci scalar $R$. Subject to the FLRW metric, using Eq.(2.3), we calculate the expression of the Ricci scalar [21, 30]

$$R = g^{\mu\nu} R_{\mu\nu} = 6\left(\frac{\ddot{a}}{a} + \frac{\dot{a}^2}{a^2}\right) = 6\left(\dot{H} + 2H^2\right)\,. \tag{2.18}$$

Following the evolution of the Hubble scale in (2.17), we get the evolution of the Ricci scalar.

$$R(t) \propto \begin{cases} \frac{6}{t^2} & w_{\rm I} \neq -1 \\ \text{constant} & w_{\rm I} = -1\,. \end{cases} \tag{2.19}$$

The Standard FLRW cosmology, built on the assumptions of large-scale homogeneity and isotropy, gives a plausible description of the overall dynamics of the Universe from the early

hot Big Bang epoch to the present Dark Energy-dominated epoch. Within the framework of General Relativity, the FLRW metric leads to the Friedmann equations, which govern the evolution of the cosmic scale factor. This standard cosmological model provides a natural explanation for the Hubble expansion, the thermal history of the Universe, and the synthesis of light elements during Big Bang nucleosynthesis(BBN). It also accurately accounts for the CMB radiation as a remnant of the hot early Universe. The nice concordance of the theoretical predictions with a wide range of observations—from the CMB to Baryon Acoustic Oscillations(BAO) and the accelerated expansion—proclaims a remarkable success of the Standard FLRW cosmology. Despite these notable successes, the FLRW cosmology encounters several conceptual and observational limitations when extrapolated to the earliest stages of the Universe. It neither explains the observed near-isotropy of the CMB background across causally disconnected regions (the Horizon problem), nor accounts for the extreme fine-tuning required for the present-day spatial flatness (the Flatness problem). Moreover, it suffers from the lack of a natural mechanism to suppress unwanted relics predicted by high-energy theories, such as magnetic monopoles (the Monopole problem). Perhaps, most importantly, FLRW cosmology does not provide an origin for the nearly scale-invariant spectrum of primordial density perturbations that seeded the large-scale structures we observe today. These shortcomings motivated us to invoke the non-standard cosmological models, in particular the Inflationary Cosmology, which extends the FLRW framework to resolve these fundamental puzzles. In the Non-standard Cosmology, we introduce an accelerated phase of expansion, preceding the hot Big Bang phase, which offers us a promising way to resolve the aforesaid issues of Standard Cosmology.

## 2.2 Shortcomings of Standard Cosmology and Introduction to Inflationary Non-standard Cosmology

This section begins with a brief description of the aforementioned problems faced by the Standard Cosmology.

### 2.2.1 The Horizon Problem

The Horizon problem appears to be a serious challenge faced by the Standard Cosmology in explaining the amazing uniformity of the CMB radiation over widely separated spatial regions. The CMB radiation, the afterglow of the Big Bang singularity, originating from the last scattering surface at $t \sim 3.8 \times 10^5$ years after the hot Big Bang phase, is observed to be highly isotropic up to one part in $10^5$ today. This incredible uniformity of the observed radiation signals the causal connections of those widely separated regions at the time of the CMB formation, that is, the time of last scattering. However, Standard Cosmology predicts that the universe consisted of nearly $10^4$ causally disconnected patches at that epoch. Further, from the epoch of Big Bang singularity to the CMB decoupling phase, this

time span is too small to have an overlapping past light cones for those widely separated regions. This fact suggests that they could have communicated neither at the time of CMB formation nor at any earlier epoch. Therefore, the natural question arises: why do we observe such a uniform CMB temperature($T_0 = 2.725 \pm 0.01$ K) over a wide range across the sky (see Fig.2.2)? This conflict between the prediction of Standard Cosmology and observation is well-known as the Horizon problem [9, 11].

To give a quantitative description of this problem, we first introduce the concept of *particle horizon*($R_{\rm ph}$). It is the maximum distance traveled by the photon from the beginning of the universe to a later time at which the $R_{\rm ph}$ is being defined.

$$R_{\rm ph} = a \int_{a_{\rm int}}^{a(t)} (aH)^{-1} d(\ln a) \tag{2.20}$$

where $a_{\rm int}$, $a(t)$ are considered to be the scale factors at the beginning of the universe, and later epoch, respectively. The quantity $(aH)^{-1}$ is the *comoving Hubble radius*. For the universe, dominated by a fluid having EoS $w$, this comoving Hubble radius evolves as $(aH)^{-1} \sim a^{\frac{1+3w}{2}}$ (see the equations (2.16) and (2.17)). The particle horizon, therefore, scales as

$$R_{\rm ph} \sim H^{-1} \,. \tag{2.21}$$

The ratio of any physical length scale, $\lambda_{\rm phy} = a\lambda$, to the particle horizon becomes

$$\frac{\lambda_{\rm phy}}{R_{\rm ph}} = a\lambda H = \dot{a}\lambda \,. \tag{2.22}$$

where $\lambda$ is the comoving length scale. As the FLRW cosmology always predicts the decelerated expansion, $\ddot{a} < 0$, of the universe at any phase, the above ratio (2.22) decreases in the entire cosmic history due to the ever-growing comoving Hubble radius $(aH)^{-1}$. This confirms that many causal regions were outside the particle horizon at the time of last scattering. To have an estimate of the causally disconnected patches at that time, we connect the present-day particle horizon $R_{\rm ph,0}$ with that at the time of last scattering $R_{\rm ph,ls}$.

$$R_{\rm ph,0} = R_{\rm ph,\,ls} \frac{H_{\rm ls}}{H_0} \tag{2.23}$$

where $H_{\rm ls}$, $H_0$ are the Hubble scales at the time of last scattering and present day, respectively. As CMB decoupling happens inside the MD phase, the Hubble scale evolves as $H \propto a^{-3/2} \sim T^{3/2}$, with the temperature of the universe $T$. The expression (2.23) can be written in terms of temperature as follows:

$$\frac{R_{\rm ph,0}}{R_{\rm ph,\,ls}} = \frac{H_{\rm ls}}{H_0} = \left(\frac{T_{\rm ls}}{T_0}\right)^{3/2} \sim 10^4 \tag{2.24}$$

where $T_{\rm ls} = 0.23$ eV is the universe temperature at the time of last scattering, and $T_0 = 2.35 \times 10^{-13}$ GeV is the present-day CMB temperature. Therefore, as already stated,

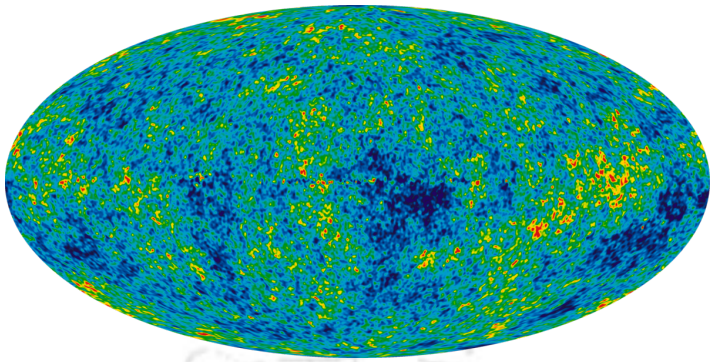

Figure 2.2: *The full sky CMB temperature map. Image courtesy [NASA Universe Web Team]*

these large number of spatial regions were causally disconnected at the time of decoupling or last scattering, whereas the uniformity in the CMB radiation is observed over these widely separated regions, essentially indicating a causal contact between them in the past. In order to reconcile this contradiction between observation and theoretical prediction, we invoke the Non-standard cosmology, introducing the early inflationary era, which precedes the hot Big Bang phase.

### 2.2.2 The Flatness problem

This is another very puzzling phenomenon faced by the Standard Cosmology, which demands a tremendously fine-tuned energy density parameter of the spatial curvature to satisfy the current observational near flatness of the universe on large scales.

We define the dimensionless density parameter of curvature at any time during evolution as

$$\Omega_{\mathscr{K}} = -\frac{\mathscr{K}}{a^2 H^2}\,. \tag{2.25}$$

During the early hot Big bang phase, $H \propto a^{-2}$, and the subsequent matter phase, $H \propto a^{-3/2}$. This leads to the evolution of the density parameter as $|\Omega_{\mathscr{K}}| \propto a^2$ during the Big Bang era(radiation-dominated phase), and $|\Omega_{\mathscr{K}}| \propto a$ during the matter era. However, the current observation tightly constrains the spatial curvature to an extremely small value, $|\Omega_{\mathscr{K},0}| < 0.001$ [7]. As in the entire expansion history, this quantity always grows over time; to satisfy the present-day observationally favored near flatness, the curvature parameter must have been extremely fine-tuned to an incredibly small value in the early epoch.

The degree of fine-tuning required at an early epoch($a_{\rm int}$) to satisfy the present observation is estimated as follows [24, 31]:

$$\left|\frac{\Omega_{\mathscr{K}}}{|\Omega_{\mathscr{K}},0|}\right| = \left(\frac{a_0}{a_{\rm int}}\right)^2 \left(\frac{H_0}{H_{\rm int}}\right)^2 = \left(\frac{a_0}{a_{\rm eq}}\right)^2 \left(\frac{a_{\rm eq}}{a_{\rm int}}\right)^2 \left(\frac{H_0}{H_{\rm eq}}\right)^2 \left(\frac{H_{\rm eq}}{H_{\rm int}}\right)^2$$
$$= \left(\frac{a_{\rm int}}{a_0}\right)\left(\frac{a_{\rm int}}{a_{\rm eq}}\right) \simeq \frac{T_{\rm eq}T_0}{T_{\rm int}^2}\,. \tag{2.26}$$

where $a_{\rm eq}$, $H_{\rm eq}$ are the scale factor and Hubble scale near the radiation-matter equality. As we have assumed that the universe evolved from the early RD to the MD era, and therefrom to the present ΛD era, hence implying $a_{\rm int} < a < a_{\rm eq}$ in RD era, $a_{\rm eq} < a < a_0$ in the MD era until today. $T_{\rm int}$ is the universe temperature at an early epoch, $T_{\rm eq} \sim 1$ eV is the temperature around the radiation-matter equality.

If we take the initial epoch to be the epoch of nucleosynthesis, when light elements were formed at $T_{\rm int} \equiv T_{\rm BBN} \sim 1$ MeV, from (2.26), we get the degree of fine-tuning

$$\left|\frac{\Omega_{\mathscr{K}}}{|\Omega_{\mathscr{K}},0|}\right| \simeq 10^{-16}\,. \tag{2.27}$$

If we now take a daring step and go back to the Planck era, with the temperature $T_{\rm int} \equiv T_{\rm pl} \sim 10^{19}$ GeV, the required degree of fine-tuning comes out to be even more horrible!

$$\left|\frac{\Omega_{\mathscr{K}}}{|\Omega_{\mathscr{K}},0|}\right| \simeq 10^{-60} \tag{2.28}$$

Such extreme sensitivity to the initial conditions implies that, without an extraordinarily flat early universe, it would have either recollapsed too quickly or expanded too rapidly for structures to form. This requirement of the unexplained fine-tuning gives rise to the Flatness problem.

### 2.2.3 The Monopole problem

A widely known difficulty in Standard Cosmology, particularly in the context of grand unified theories (GUTs), is the so–called Monopole problem. GUTs, at the temperature around $T_{\rm GUT} \sim 10^{16}$ GeV, generically predict the formation of heavy, stable magnetic monopoles(hypothetical particles with non-vanishing magnetic charge) as topological defects during the symmetry–breaking phase transitions in the early universe. Since these monopoles are non-relativistic and extremely massive, their number density dilutes as $a^{-3}$ with the expansion of the universe. Simple estimates show that their expected abundance is exceedingly larger than the observed critical density of the universe, leading to a severe overclosure problem. The absence of any experimental evidence for monopoles in the present universe is in sharp contradiction with such predictions, thus generating the Monopole problem. A successful resolution to this issue is provided by cosmic inflation, which causes the dilution of any pre–existing monopole population exponentially, rendering their present abundance negligible and consistent with present observations.

### 2.2.4 Possible resolution to the problems and introduction to Inflation

The central issue of all three problems is the growing comoving Hubble radius $(aH)^{-1}$ in the entire cosmic history, as proposed by the Standard FLRW Cosmology. This ever-growing nature of the Hubble radius also implies the decelerating phase of expansion throughout the journey of the universe. It is Alan Guth(1980) who first introduced the concept of an early accelerated exponential phase of expansion, called *cosmic inflation*[9], which first gave a plausible resolution to all the long-standing problems. This accelerating phase of expansion is associated with the shrinking Hubble sphere, implying $\frac{d}{dt}(aH)^{-1} < 0$, as $\ddot{a} > 0$. This early accelerated expansion, being tied to the shrinking Hubble radius, can solve all the puzzles of the Standard Cosmology. All the causally disconnected regions in the space at the time of CMB formation were in causal contact in the remote past during the early inflation. Two causally connected points are stretched out of the Hubble horizon due to rapid accelerated expansion during inflation. In the post-inflationary era, those regions again reenter the horizon due to the growing Hubble sphere; hence, they come into causal contact. This dynamic horizon exit, entry of a comoving scale is shown in Fig.(2.3). We now estimate the approximate duration of inflation to solve the Horizon problem.

- **Solution of Horizon problem:**

  In the modified expansion history from the early inflation to the present day, we can consider that the observable universe today perfectly fits the comoving Hubble radius at the beginning of inflation, implying

  $$(a_0 H_0)^{-1} < (a_I H_I)^{-1}\,, \tag{2.29}$$

  where $a_I$, $H_I$ are the scale factor and Hubble scale at the beginning of inflation. From the expansion history of the universe, the early inflation is followed by the radiation and matter-dominated phase to reach the present ΛD phase. We then compute

  $$\frac{a_0 H_0}{a_{\rm end} H_{\rm end}} = \left(\frac{a_{\rm end}}{a_{\rm eq}}\right)^{1/2} \left(\frac{a_{\rm end}}{a_0}\right)^{1/2} \simeq \frac{\sqrt{T_{\rm eq} T_0}}{T_{\rm end}} \simeq 10^{-26}\,. \tag{2.30}$$

  Here, we take the temperature of the universe at the end of inflation $T_{\rm end} \sim 10^{15}$ GeV. Using the above ratio in Eq.(2.29), we get

  $$(a_I H_I)^{-1} > 10^{26} (a_{\rm end} H_{\rm end})^{-1}\,. \tag{2.31}$$

  The above relation tells us that for inflation to solve the Horizon problem, the Hubble radius $(aH)^{-1}$ should shrink by a factor of the order $10^{26}$. Assuming a constant Hubble scale during inflation $H_I \approx H_{\rm end}$, we write

  $$\left(\frac{a_{\rm end}}{a_I}\right) > 10^{26} \Rightarrow N_k = \ln\left(\frac{a_{\rm end}}{a_I}\right) > 60\,. \tag{2.32}$$

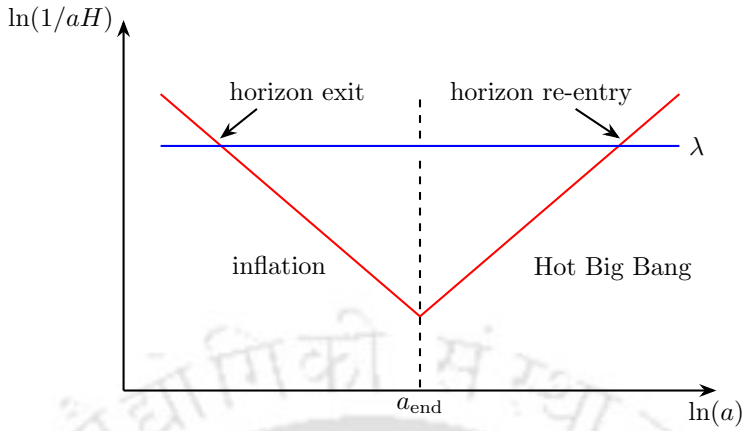


FIGURE 2.3: *The evolution of the comoving Hubble horizon* $(aH)^{-1}$ *during inflation and the post-inflationary epoch. A comoving length scale* $\lambda$ *exits the horizon at some point during inflation, and again reenters the horizon in the hot Big Bang phase, following the early inflation. The shrinking Hubble radius during inflation solves the Horizon problem.*

Therefore, to solve the Horizon problem, the early inflation should last for at least $N_k = 60$ inflationary e-folding number [21, 31].

There is a very subtle issue regarding the resolution of the Horizon problem. Inflation settles this problem by justifying the causal contact between two largely separated acausal points at CMB decoupling during the inflationary era. However, to explain the present-day observed uniformity of the CMB radiation over a large distance, the CMB photons must have communicated with each other in the past, much before the last scattering occurred. Interestingly, as the CMB photos were produced in the post-inflationary era, no photons existed inside the inflationary Hubble sphere to interact with themselves to generate an amazingly uniform radiation background that we observe today. One can readily ask the question, *how does the causal connection between two mere spatial points without any radiation component explain the observed uniformity of the CMB spectrum?* The answer to this question lies in the state of the quantum fields, rather than the photon interaction. Inflation ensures that these fields were smoothed out across the entire region that later became our observable Universe. After inflation, the inflaton's energy gets transferred into the hot thermal bath of particles, including photons. As the pre-inflationary patch had already been homogenized, this newly created plasma inherited that uniformity. Much later, when photons decoupled at the era of last scattering, they naturally carried the imprint of that homogenized early state, which gives rise to today's observed uniformity.

- **Solution of Flatness problem**

  To solve the Flatness problem, we need an extremely fine-tuned small value of spatial curvature as an initial condition at the end of inflation. If there is some initial spatial

curvature at the beginning of inflation, at the end of the exponentially accelerated phase of expansion with $H \approx$ constant, it turns out to be from the eq.(2.25)

$$\left|\frac{\Omega_{\mathscr{K},\text{end}}}{\Omega_{\mathscr{K},I}}\right| \sim e^{-2N_k} \,. \tag{2.33}$$

If we consider the curvature parameter to be of order unity at the beginning of inflation $|\Omega_{\mathscr{K},I}| \sim \mathcal{O}(1)$, then $\Omega_{\mathscr{K},\text{end}} \sim 10^{-52}$ at the end of inflation. Therefore, the very dynamics of inflation suffice for the need for extreme fine-tuning of curvature in the Standard Cosmology.

- **Solution of Monopole problem**

  The Standard FLRW Cosmology predicts that the stable magentic monopoles were abundantly produced during symmetry-breaking phase transitions in the very early Universe at the GUT scale, with a relic density far exceeding observational limits. This creates a severe conflict between theoretical expectations and experimental non-detection today. The dynamics of cosmic inflation also resolves this issue. If the GUT phase transition occurred before or during the inflationary era, any monopoles produced must have been diluted away exponentially fast with the expansion. If $n_M$ is the number density of the monopoles around the beginning of inflation, it then decreases to

  $$n_{M,\text{end}} \propto a^{-3} \sim e^{-3N_k} \approx 10^{-78} \,, \tag{2.34}$$

  almost a vanishingly small value at the end of inflation for $N_k \gtrsim 60$. Thus, the rapid inflationary expansion makes the monopoles unobservable today, while still allowing their possible formation in the early Universe.

Thus, addressing these long-standing cosmological puzzles proclaims a grand success of the Non-standard cosmological model.

## 2.3 Dynamics of Inflation

### 2.3.1 Condition for inflation

- **Accelerated expansion and shrinking Hubble sphere**

  The primary condition for inflation is the shrinking Hubble radius owing to an accelerated expansion. These are two, although not independent, fundamental conditions for inflation, which result in the successful resolution of the cosmological puzzles as already discussed. It can be easily shown that the accelerated expansion and the contraction of the Hubble volume are intimately tied to each other

  $$\frac{d}{dt}(aH)^{-1} = \frac{d}{dt}(\dot{a})^{-1} = -\frac{\ddot{a}}{\dot{a}^2} \,. \tag{2.35}$$

The above relation shows that for the comoving Hubble radius to shrink, the universe must accelerate $\ddot{a} > 0$.

- **Slowly-varying Hubble scale**

  This is also another consequence of the shrinking Hubble sphere.

$$\frac{d}{dt}(aH)^{-1} = -\frac{1}{a}(1-\epsilon_{\rm H})\,, \quad \epsilon_{\rm H} = -\frac{\dot{H}}{H^2}\,. \tag{2.36}$$

  This gives $\epsilon_{\rm H} < 1$, implying a slow time variation of the Hubble scale during inflation. Therefore, the accelerated expansion as well as the slow variation of $H$ are the byproducts of the shrinking Hubble radius and vice versa during inflation.

- **Non-constancy of Hubble scale**

  For perfect de Sitter inflation $\epsilon_{\rm H} = 0$, the spacetime becomes

$$ds^2 = -dt^2 + e^{2Ht}dx^2\,. \tag{2.37}$$

  Although in a perfect de Sitter-type inflation, the Hubble scale $H$ during inflation is considered to be constant, in a real scenario, inflation has to end, implying a departure from the perfect de Sitter space. However, for small and non-zero $\epsilon_{\rm H} \neq 0$, the line element (2.37) is still a good approximation for the inflationary background. Hence, we often call inflation *quasi de Sitter inflation*. Furthermore, the non-vanishing $\epsilon_{\rm H}$ plays a crucial role in connecting the tiny CMB fluctuations to the primordial perturbation during inflation, which we shall study in the subsequent section.

- **Negative pressure**

  Now, we shall study the nature of the fluid causing this accelerated expansion. From the Friedmann equation (2.15), we write

$$\dot{H} + H^2 = -\frac{H^2}{2}\left(1+\frac{3P}{\rho}\right) \Rightarrow \epsilon_{\rm H} = -\frac{\dot{H}}{H^2} = \frac{3}{2}\left(1+\frac{P}{\rho}\right)\,. \tag{2.38}$$

  From the above relation (2.38), to satisfy $\epsilon_{\rm H} < 1$, we require $w \equiv \frac{P}{\rho} < -\frac{1}{3}$. Therefore, inflation requires an exotic fluid that violates the strong energy condition(SEC) and generates a negative pressure acting as repulsive gravity.

- **Constant energy density**

  Combining the Eq.(2.38) with the continuity equation (2.7) we obtain the relation

$$\left|\frac{d\ln\rho}{d\ln a}\right| = 2\epsilon_{\rm H} < 1\,. \tag{2.39}$$

  For small $\epsilon_{\rm H} < 1$, the energy density of the fluid is nearly constant during inflation. Although the energy density of all usual fluids dilutes due to the background expansion, we encounter something unusual here for the exotic fluid, which we shall explore soon while studying the dynamics of inflation, driven by the classical inflaton field($\phi$).

These conditions for inflation suggest that for inflation to occur, the parameter $\epsilon_{\rm H}$ must be small, $\epsilon_{\rm H} < 1$. Additionally, to solve the Horizon, Flatness-like problems, the inflationary phase must last for a sufficient number of Hubble times, or e-folds($N$). It requires another parameter, defining the variation of $\epsilon_{\rm H}$, which is parametrized by

$$\eta_{\rm H} \equiv \frac{d(\ln\epsilon_{\rm H})}{dN} = \frac{d\ln(\epsilon_{\rm H})}{d\ln(a)} = \frac{\dot{\epsilon_{\rm H}}}{H\epsilon_{\rm H}}\,. \tag{2.40}$$

For inflation to persist for a sufficient time, $|\eta_{\rm H}| < 1$ must be satisfied.

So far, we have presented a brief discussion on the necessary conditions required for inflation to occur. Now, we shall proceed to study the dynamics of this phase, driven by a classical, homogeneous field, called inflaton($\phi(t)$), which carries the whole energy budget of the universe during the inflationary era in a single field inflationary model. The very dynamics of the inflaton field will naturally produce all the necessary conditions for inflation, as already discussed.

### 2.3.2 Dynamics of the inflaton field

In a single-field inflationary model, the dominant classical scalar inflaton field $\phi$ sourced the early accelerated expansion of the universe, with the action of the form

$$S = \int \sqrt{-g}\, d^4x\, \mathcal{L} = \int \sqrt{-g}\, d^4x \left[ -\frac{M_{\rm pl}^2}{2} R \underbrace{-\frac{1}{2}\partial_\mu\phi\partial^\mu\phi - V(\phi)}_{\mathcal{L}_\phi} \right] + S_{\rm matter}\,. \tag{2.41}$$

where $\sqrt{-g} = a^3(t)$ for the FLRW metric in cosmic time($t$) coordinate, $V(\phi)$ is the potential energy of the inflaton. We shall introduce the observationally favored specific form of the inflaton potential as we proceed along. In this action, we have considered the inflaton field minimally coupled to gravity. $S_{\rm matter}$ is the matter action, representing the action of all other matter components, including the Standard Model Lagrangian as well as the beyond Standard Model fields to which the inflaton is coupled. By varying the above action for the inflaton field [*], we get

$$\partial_\mu\left(\frac{\delta(\sqrt{-g}\mathcal{L}_\phi)}{\delta(\partial_\mu\phi)}\right) - \left(\frac{\delta(\sqrt{-g}\mathcal{L}_\phi)}{\delta\phi}\right) = 0 \Rightarrow \left(\ddot{\phi} + 3H\dot{\phi} - \frac{\nabla^2\phi}{a^2} + \frac{\partial V(\phi)}{\partial\phi}\right) = 0\,. \tag{2.42}$$

In this dynamical equation, $3H\dot{\phi}$ is the Hubble friction term experienced by the inflaton field due to background expansion while rolling down the inflaton potential. The homogeneity and isotropy of the FLRW metric demand that the inflaton field, governing the background dynamics, will be homogeneous; hence, it will only depend on time, $\phi(t)$. By homogeneity, the dynamical Eq.(2.42) becomes

$$\left(\ddot{\phi} + 3H\dot{\phi} + \frac{\partial V(\phi)}{\partial\phi}\right) = 0\,. \tag{2.43}$$

[*]Here we have ignored all other interactions of the inflaton field, which are contained in $S_{\rm matter}$.

This is the Klein-Gordon equation for the dynamics of the inflaton field.

The stress-energy tensor of the scalar inflaton is written as

$$T^{\phi}_{\mu\nu} = \frac{-2}{\sqrt{-g}}\frac{\delta(\sqrt{-g}\mathcal{L}_{\phi})}{\delta g^{\mu\nu}} = \partial_{\mu}\phi\partial_{\nu}\phi - g_{\mu\nu}\left(\frac{1}{2}\partial_{\alpha}\phi\partial^{\alpha}\phi + V(\phi)\right) . \tag{2.44}$$

The non-zero $T^{\phi}_{00}$ and $T^{\phi}_{ii}$ components correspond to the energy $\rho_{\phi}$ and pressure density $P_{\phi}$ of the inflaton field.

$$\begin{aligned} \rho_{\phi} &= -T^{\phi\,0}_{0} = \left(\frac{1}{2}\dot{\phi}^2 + V(\phi)\right) , \\ P_{\phi} &= T^{\phi\,i}_{i} = \left(\frac{1}{2}\dot{\phi}^2 - V(\phi)\right) . \end{aligned} \tag{2.45}$$

Substituting the expression of $\rho_{\phi}$ from (2.45) to the Friedmann equation (2.15), we get

$$H^2 = \frac{1}{3M^2_{\rm pl}}\left(\frac{1}{2}\dot{\phi}^2 + V(\phi)\right) . \tag{2.46}$$

The time-derivative of Eq.(2.46) leads to

$$2H\dot{H} = \frac{1}{3M^2_{\rm pl}}\left(\frac{1}{2}\dot{\phi}\ddot{\phi} + V'(\phi)\dot{\phi}\right) \Rightarrow \dot{H} = -\frac{\dot{\phi}^2}{2M^2_{\rm pl}} , \tag{2.47}$$

where $V'(\phi) \equiv \left(\frac{\partial V(\phi)}{\partial\phi}\right)$. To reach the final step of the above Eq.(2.47), we use the field dynamical equation (2.43). One of the conditions for inflation, $\epsilon_{\rm H} = -\frac{\dot{H}}{H^2} < 1$ gives $\dot{\phi}^2/M^2_{\rm pl} < 1$, implying that the inflaton field slowly rolls over the flat surface of the inflationary potential, as depicted in Figure (2.4). Therefore, the potential energy $V(\phi)$ dominates over the kinetic energy $\frac{1}{2}\dot{\phi}^2$ of the inflaton field during the inflationary era. This fact results in an interesting outcome, $P_{\phi} \approx -\rho_{\phi} \Rightarrow w_{\phi} = -1$ from Eq.(2.45), where $w_{\phi}$ is the inflaton EoS. The negative pressure of the inflaton field complies with the existence of the shrinking Hubble sphere as well as the accelerated expansion during inflation. This fact also confirms the exotic nature of the inflaton field during inflation, and inflation is driven by the vacuum energy of the inflaton field.

- **Slow-roll conditions:**

  Plugging the expression (2.47) into the Eq.(2.38) we find

  $$\epsilon_{\rm H} = \frac{\dot{\phi}^2}{2M^2_{\rm pl}H^2} . \tag{2.48}$$

  This expression tells us that inflation occurs only if the kinetic energy makes an ignorable contribution to the total energy, $\rho_{\phi} = 3M^2_{\rm pl}H^2$. This situation is well

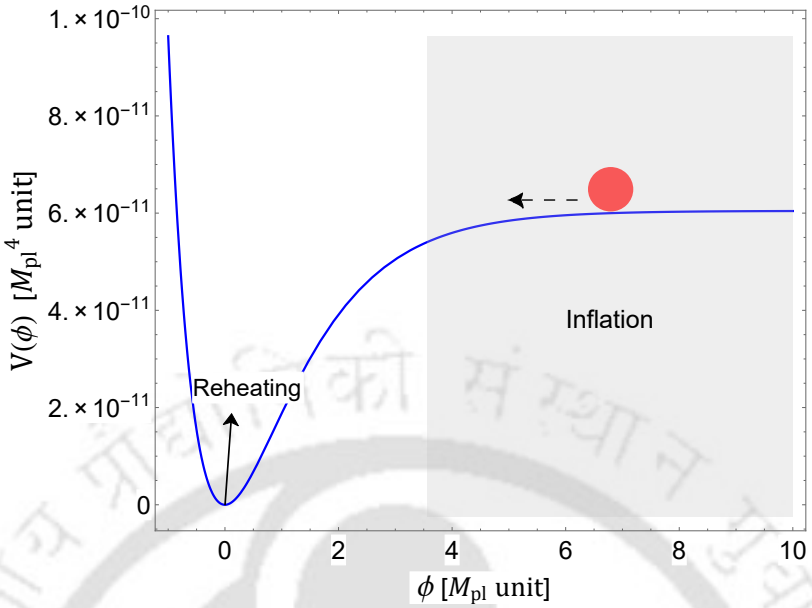


Figure 2.4: *Figure represents the slow-roll inflationary and the post-inflationary oscillatory phase of the inflaton field. The shaded region shows the inflationary era. In the shaded region, the red ball stands for the inflaton field which rolls over the flat surface of the potential during inflation, and the leftward dashed arrow indicates the direction of its rolling over the potential. At the end of inflation, it comes down to the bottom of the potential, and reheating begins(solid arrow).*

known as *slow-roll inflation*. For inflation to persist for a sufficient number of e-folds, the acceleration of the scalar field has to be small. Here, it is useful to define the dimensionless acceleration per Hubble time as follows:

$$\delta_{\rm H} \equiv -\frac{\ddot{\phi}}{H\dot{\phi}} < 1\,. \tag{2.49}$$

Using the time derivative of $\epsilon_{\rm H}$(Eq.(2.48)) and the parameter $\delta_{\rm H}$, we define the other slow-roll parameter $\eta_{\rm H}$ as follows:

$$\eta_{\rm H} = \frac{\dot{\epsilon_{\rm H}}}{H\epsilon_{\rm H}} = 2\frac{\ddot{\phi}}{H\dot{\phi}} - 2\frac{\dot{H}}{H^2} = 2(\epsilon_{\rm H} - \delta_{\rm H})\,. \tag{2.50}$$

Hence, $\{\epsilon_{\rm H},\, |\delta_{\rm H}|\} << 1$ implies $\{\epsilon_{\rm H},\, |\eta_{\rm H}|\} << 1$.

The smallness of $\epsilon_{\rm H}$ implies $\frac{1}{2}\dot{\phi}^2 << V(\phi)$, which further simplifies the Friedmann equation(2.15) during inflation as

$$H^2 \approx \frac{V(\phi)}{3M_{\rm pl}^2}\,. \tag{2.51}$$

The smallness of $|\delta_{\rm H}| << 1$ also simplifies the dynamical equation of the inflaton (2.43) during inflation

$$3H\dot{\phi} \approx -\left(\frac{\partial V}{\partial \phi}\right) . \tag{2.52}$$

Now, utilizing these two expressions (2.51) and (2.52), we write the slow-roll parameter $\epsilon$ as a function of inflation potential $V(\phi)$ as

$$\epsilon_{\rm V} \approx \frac{M_{\rm pl}^2}{2}\left(\frac{V'}{V}\right)^2 . \tag{2.53}$$

The time-derivative of (2.52) $\left(3\dot{H}\dot{\phi} + 3H\ddot{\phi}\right) = -V''\dot{\phi}$ leads to the relation

$$\delta_{\rm H} + \epsilon_{\rm H} \approx M_{\rm pl}^2 \frac{V''}{V} . \tag{2.54}$$

Hence, for a given inflationary potential $V(\phi)$, the possibility of slow-roll inflation is decided by the following slow-roll parameters,

$$\epsilon_{\rm V} = \epsilon_{\rm H} \approx \frac{M_{\rm pl}^2}{2}\left(\frac{V'}{V}\right)^2 , \quad \eta_{\rm V} = \left(2\epsilon_{\rm H} - \frac{\eta_{\rm H}}{2}\right) \approx M_{\rm pl}^2 \frac{V''}{V} . \tag{2.55}$$

Likewise, for successful slow-roll inflation, $\{\epsilon_{\rm V},\, |\eta_{\rm V}|\} << 1$.

The duration of the accelerated expansion is measured by the e-folding number $N_k$

$$N_k = \int_{a_I}^{a_{\rm end}} d\ln a = \int_{t_I}^{t_{\rm end}} H\, dt\,, \tag{2.56}$$

where $t_I(a_I)$, $t_{\rm end}(a_{\rm end})$ are cosmic times defined at the onset and the end of inflation. The end of inflation is given by the condition $\epsilon_{\rm H}(t_{\rm end}) \equiv \epsilon_{\rm end} = 1$. In the slow-roll inflationary phase, we can approximately write

$$H\, dt = \frac{H}{\dot{\phi}} d\phi = \frac{1}{2\sqrt{\epsilon_{\rm H}}}\frac{d\phi}{M_{\rm pl}} = \frac{1}{2\sqrt{\epsilon_{\rm V}}}\frac{d\phi}{M_{\rm pl}} . \tag{2.57}$$

In the field space, the inflationary e-folding number $N_k$ is expressed as

$$N_k = \int_{\phi_I}^{\phi_{\rm end}} \frac{1}{2\sqrt{\epsilon_{\rm V}}}\frac{d\phi}{M_{\rm pl}} \gtrsim 60\,, \tag{2.58}$$

where $\phi_I$ and $\phi_{\rm end}$ are the amplitudes of the inflaton at the onset and the end of inflation. For the successful resolution of the cosmological puzzles(Horizon problem, Flatness problem, etc.), $N_k$ has been shown to be around or greater than 60.

## 2.4 End of slow-roll inflation and beginning of the post-inflationary reheating

Inflation is really a wonderful phenomenon. But every good thing must end at some time. In the New or slow-roll inflationary model proposed by Albrecht–Steinhardt, Linde in 1982 [11, 12], the inflaton field smoothly transits from the accelerated inflationary era to the decelerated post-inflationary phase, when the kinetic energy of the inflaton becomes comparable with the potential energy stored in it. In the slow-roll model, the flat region of the potential(see Fig.(2.4)) sets the inflationary era. At the end of this flat surface, inflaton slowly rolls down to the bottom of the potential, thereby causing the universe to smoothly and continuously exit from the inflationary phase by making $(\epsilon_V, \eta_V) = 1$ at the end of inflation. In the right panel of Fig.(2.5), the evolution of $\epsilon_V$ shows the continuous transition of the universe from early inflation to the post-inflationary reheating phase. The post-inflationary oscillation of $\epsilon_H$ around unity is essentially caused by the oscillatory nature of the inflaton field after inflation. The left panel of Fig.(2.5) shows the time evolution of the inflaton field during inflation and the post-inflationary reheating phase. The oscillation feature during reheating will be investigated in the subsequent discussion of the present section.

However, in contrast, in the Old inflation model by Alan Guth in 1981[9], inflation happened because the inflaton field was trapped in a metastable false vacuum state of high energy density. The inflaton transits from the false to the true vacuum by *quantum tunneling effect*, forming the bubbles of true vacuum inside the false vacuum. Crucially, this tunneling is an inherently local process, leading to inhomogeneous nucleation of bubbles of true vacuum within an exponentially expanding false vacuum background. For the inflationary expansion to end globally in the entire space, these bubbles must grow and collide to convert all space into a true vacuum. But the accelerated exponential expansion of space during inflation, happening in the false vacuum, drags the bubbles far away; hence, they never percolate efficiently. This failure to achieve a successful phase transition from inflation to the post-inflationary phase is called the *graceful exit problem*. The inhomogeneous nature of the tunneling probability underlies the graceful exit problem of the Old inflation. However, the slow-roll inflation model successfully resolves this issue of the exit problem and saves the universe from the state of eternal inflation by introducing a flat portion in the inflationary potential for the inflaton to roll slowly over it during inflation without resorting to any trapping mechanism in the high-energy false vacuum state, and at the end of the flat portion, inflation ends with the violation of the slow-roll conditions. The Chaotic inflation models [32, 33] are a class of models which naturally avoid the graceful exit problem. In these models, at the end of the slow rolling phase, the inflaton starts oscillating around the minima of the potentials, which sets the scene for the post-inflationary reheating(see Fig.(2.4)), where the inflaton's energy is transferred to all kinds of particles(Standard Model and beyond Standard Model(BSM)) through many different non-trivial processes. The underlying mechanism of the energy transfer during reheating is broadly classified into two parts: Perturbative and Non-perturbative reheating. Before discussing these two aspects

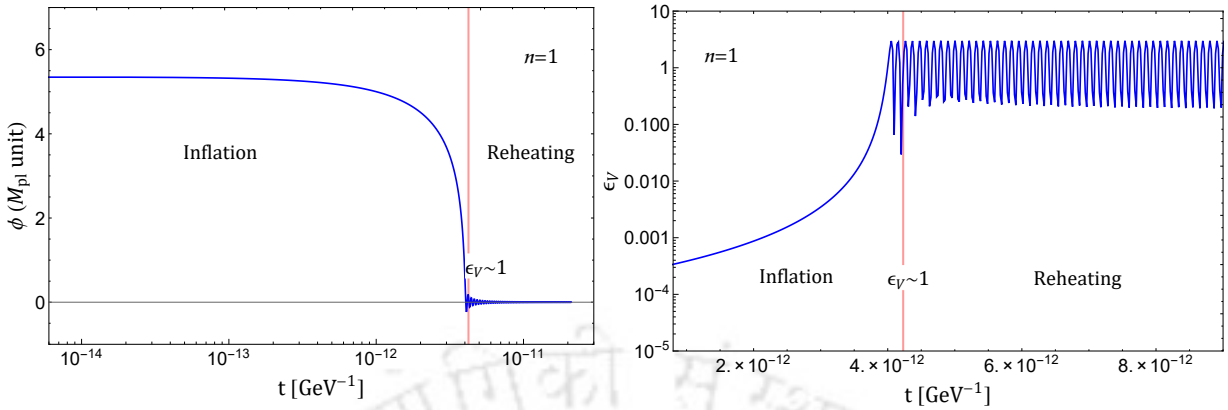


FIGURE 2.5: ***Left Panel:*** *Figure represents the time evolution of the inflaton field during inflation and the post-inflationary reheating era. It is clearly seen that during slow-roll inflation, the field amplitude is nearly constant, making* $\epsilon_V << 1$. *After inflation, the oscillation of the inflaton at the potential minima is nicely imprinted on the field evolution(see also Fig.(2.6) to get the field oscillation during reheating.).* ***Right Panel:*** *It represents the time evolution of the slow-roll parameter during inflation and reheating. The dynamics of* $\epsilon_V$ *shows the continuous transition of the universe from early inflation to the reheating phase. In this figure, we have taken* $\alpha$*-attractor E-type potential model with* $\alpha = 1$, $n = 1$.

of reheating, we now study the evolution of all the background quantities(dynamics of inflaton, scale factor, Hubble scale, etc.) during the post-inflationary reheating phase. In the Chaotic inflation models, the potentials assume a power-law form, $V(\phi) \sim |\phi|^{2n}$ with $n$ being the exponent of the potential, and the inflaton field oscillates around the minima of this potential during reheating. During the reheating era, the oscillatory inflaton field can be written as

$$\phi(t) = \phi_0(t)\mathcal{P}(t)\,, \tag{2.59}$$

where $\phi_0(t)$ is the time-dependent amplitude of the inflaton field, which decays over a large time-scale due to expansion, $\mathcal{P}(t)$ is the time-dependent oscillation profile, encoding the (an)harmonicity of the short time-scale oscillations in the potential. As the oscillation time-scale is much shorter than the inflaton amplitude($\phi_0$) redshift time-scales, the time-averaging over one complete oscillation of the dynamical equation of motion(EoM) (2.43) by multiplying with $\phi$ leads to

$$\langle\dot{\phi}^2\rangle \simeq \langle\phi V'(\phi)\rangle \Rightarrow \frac{1}{2}\langle\dot{\phi}^2\rangle \simeq n\langle V(\phi)\rangle\,. \tag{2.60}$$

This is the well-known Virial theorem, establishing the relation between the average kinetic and potential energy density.

From the Eq.(2.45), the time-averaged energy and pressure density are given by

$$\langle \rho_\phi \rangle = \left( \frac{1}{2}\langle \dot{\phi}^2 \rangle + \langle V(\phi) \rangle \right) \simeq (n+1)\langle V(\phi) \rangle \,,$$
$$\langle P_\phi \rangle = \left( \frac{1}{2}\langle \dot{\phi}^2 \rangle - \langle V(\phi) \rangle \right) \simeq (n-1)\langle V(\phi) \rangle \,. \tag{2.61}$$

The ratio of the time-averaged pressure and energy density leads to the EoS parameter, $w_\phi = \langle P_\phi \rangle / \langle \rho_\phi \rangle = (n-1)\,/\,(n+1)$ for a power-law type potential. Interestingly, for this kind of potential, variation of the exponent $n$ defines different kinds of fluid components. For instance, $n = 1$ gives matter-like behavior of the inflaton background with vanishing pressure, $w_\phi = 0$, $n = 2$ gives a radiation-like background with $w_\phi = 1/3$, for all higher $n$ values, the background behaves like a stiff fluid.

In order to study the redshift behavior of the inflaton amplitude $\phi_0$ for general reheating EoS, we exploit the continuity equation (2.7) with the time-averaged energy density.

$$\begin{aligned} &\langle \dot{\rho}_\phi \rangle + 3H(1+w_\phi)\langle \rho_\phi \rangle \simeq 0 \\ &\Rightarrow \frac{d}{dt}\left(V(\phi_0)\right) + 3H\frac{2n}{n+1}V(\phi_0) \simeq 0 \\ &\Rightarrow \dot{\phi_0} = -\frac{3H}{n+1}\phi_0 \quad \Rightarrow \quad \phi_0(a) = \phi_{\rm end}\left(\frac{a}{a_{\rm end}}\right)^{-\frac{3}{n+1}} , \end{aligned} \tag{2.62}$$

where $\phi_{\rm end}$ and $a_{\rm end}$ are the inflaton amplitude and scale factor at the end of inflation. Here, we have used $\langle \mathcal{P}^{2n} \rangle = 1/(n+1)$(this can be justified by numerical time-averaging of the oscillatory part of the background oscillation), this results in $\langle \rho_\phi \rangle = V(\phi_0)$. Likewise Eq.(2.8), solving the continuity equation (2.7), we find the evolution of the inflaton energy density

$$\rho_\phi(a) = \rho_{\rm end}\left(\frac{a}{a_{\rm end}}\right)^{-3(1+w_\phi)} = \rho_{\rm end}\left(\frac{a}{a_{\rm end}}\right)^{-\frac{6n}{n+1}} . \tag{2.63}$$

At the end of inflation $a = a_{\rm end}$, the condition $\epsilon_{\rm H} = 1$ gives $V(\phi_{\rm end}) \equiv V_{\rm end} = 2M_{\rm pl}^2 H_{\rm end}^2$, and the total energy density $\rho(a_{\rm end}) \equiv \rho_{\rm end} = 3M_{\rm pl}^2 H_{\rm end}^2$, implying $\rho_{\rm end} = \frac{3}{2}V_{\rm end}$. From the Friedmann equation (2.15), we get the post-inflationary evolution of the amplitude of the Hubble scale for general EoS as follows:

$$\bar{H}(a) = H_{\rm end}\left(\frac{a}{a_{\rm end}}\right)^{-\frac{3}{2}(1+w_\phi)} = H_{\rm end}\left(\frac{a}{a_{\rm end}}\right)^{-\frac{3n}{n+1}} . \tag{2.64}$$

Integrating the above Eq.(2.64), we get the behavior of the scale factor in the post-inflationary era as a function of cosmic time $t$

$$a(t) = a_{\rm end}\left(\frac{t}{t_{\rm end}}\right)^{\frac{2}{3(1+w_\phi)}} = a_{\rm end}\left(\frac{t}{t_{\rm end}}\right)^{\frac{n+1}{3n}} . \tag{2.65}$$

where the cosmic time at the end of inflation "$t_{\rm end}$" is calculated to be, $t_{\rm end} = \frac{2}{3(1+w_\phi)H_{\rm end}}$. So far, we have studied the amplitude redshift of the different background quantities for general reheating EoS. We now introduce the nature of the oscillation profile of the inflaton field $\mathcal{P}(t)$ and study how the inflaton oscillation will source the oscillation feature in all the background quantities. In the study of the non-perturbative aspect of reheating dynamics later, we shall see that these minute oscillations of the background quantities will have a great impact on the particle production for small-scale fluctuations. The oscillatory behavior of the inflaton field is strongly influenced by the nature of the potential near its minimum. At this stage, from Eq.(2.59), the inflaton $\phi$ with the quasi-periodic oscillatory function $\mathcal{P}(t)$ can be expressed as

$$\phi(t) = \phi_0(t)\mathcal{P}(t) = \phi_0(t)\sum_{\nu\neq 0}\mathcal{P}_\nu e^{i\nu\omega t} = \phi_0(t)\sum_{\nu\neq 0}\mathcal{P}_\nu\cos(\nu\omega t)\,. \tag{2.66}$$

where the quasi-periodic oscillatory function $\mathcal{P}(t)$ has the fundamental frequency $\omega$ [34], and $\mathcal{P}_\nu$ are the different Fourier coefficients. This function $\mathcal{P}$ being real gives $\mathcal{P}^*_\nu = \mathcal{P}_{-\nu}$ and $\mathcal{P}^*_{-\nu} = \mathcal{P}_\nu$. To find the oscillation frequency $\omega$, using Eq.(2.45), we write the following dynamical equation for the quasi-periodic function,

$$\dot{\mathcal{P}} \simeq \pm\frac{\sqrt{2(\rho_\phi - V(\phi))}}{\phi_0} \simeq \pm\frac{m_\phi}{\sqrt{n(2n-1)}}\sqrt{1-\mathcal{P}^{2n}}\,, \tag{2.67}$$

where $m_\phi$ is the effective mass of the inflaton field during the post-inflationary oscillation phase. Here, we take the amplitude $\phi_0(t)$ to be almost constant over one oscillation time period. This assumption is valid as long as the oscillation time-scale is much shorter than the background expansion time-scale. The effective inflaton mass $m_\phi = \sqrt{\partial^2 V(\phi)/\partial\phi^2}$ is defined with respect to the envelope of the inflaton field $\phi_0(t)$ as given below.

$$m_\phi = \frac{\sqrt{2n(2n-1)V(\phi_0)}}{\phi_0} \tag{2.68}$$

This oscillation profile can be thought of as a pendulum, oscillating around its equilibrium position at the origin. If it starts its motion from the origin, then, at $t = T/4$, $\mathcal{P}(t) = 1$, where $T = (2\pi/\omega)$ is the time-period of oscillation. Using this fact as an initial condition, straightforward integration of (2.67) gives the frequency of oscillation $\omega$.

$$\int_0^1 \frac{d\,\mathcal{P}}{\sqrt{1-\mathcal{P}^{2n}}} = \frac{m_\phi}{\sqrt{n(2n-1)}}\int_0^{T/4} dt \Rightarrow \frac{2\pi}{T} = \omega = m_\phi \underbrace{\sqrt{\frac{\pi n}{(2n-1)}}\frac{\Gamma\left(\frac{1}{2}+\frac{1}{2n}\right)}{\Gamma\left(\frac{1}{2n}\right)}}_{\gamma} \tag{2.69}$$

From now on, we write the time-dependent frequency of background oscillation as $\omega(t) = \gamma\, m_\phi(t)$ for general reheating EoS. Once the time-variation of inflaton amplitude is computed for general $n$, using (2.62) together with its oscillatory part $\mathcal{P}(t)$, we can express the leading

order behavior of the Hubble scale in Eq. (2.15) in terms of the decaying amplitude and quasi-periodic oscillatory function [35, 36] as follows:

$$H(a) \simeq \bar{H}\left(1+\underbrace{\frac{\mathcal{P}\sqrt{6(1-\mathcal{P}^{2n})}}{2(n+1)}\left(\frac{\phi_{\rm end}}{M_{\rm pl}}\right)\left(\frac{a}{a_{\rm end}}\right)^{-\frac{3}{n+1}}}_{H_{\rm fast}}\right), \tag{2.70}$$

where the first term $\bar{H}(a)$ is the slowly varying decaying term as shown in Eq.(2.64), and the second term inside the bracket can be identified with the fast varying oscillatory part in Hubble scale $H_{\rm fast}$. The detailed derivation of this expression is found in Appendix 7.2. As an example, using equations (2.66) and (2.70), we now write the approximate solutions for $n = 1,\ 2,\ 3$. We define a dimensionless time variable $z_n \equiv \frac{m_\phi^{\rm end}(n)\,t}{2\pi}$ to produce the numerical results for the time evolution of the inflaton field and Hubble scale in the post-inflationary phase in Fig.(2.6) for three reheating EoS, where "$m_\phi^{\rm end}(n)$" is the mass of inflaton at the inflation end, $m_\phi^{\rm end} = m_\phi|_{\phi_0=\phi_{\rm end}}$. At the inflation end, the dimensionless time variable is defined as $z_n^{\rm end} = \frac{m_\phi^{\rm end}(n)\,t_{\rm end}}{2\pi}$. †

- For $n = 1$: The model corresponds to an average EoS $w_\phi \simeq 0$; hence, the background inflaton field behaves like a non-relativistic matter. An approximate analytic solution can be recovered from Eq. (2.66) and (2.70).

$$\phi(z_1) \approx \phi_{\rm end}\left(\frac{z_1^{\rm end}}{z_1}\right)\cos(2\pi z_1), \quad H(z_1) \approx H_{\rm end}\left(\frac{z_1^{\rm end}}{z_1}\right)\left(1+\frac{\sin(4\pi z_1)}{4\pi z_1}\right). \tag{2.71}$$

  For $n = 1$, non-negligible contribution comes from only the first Fourier component $\mathcal{P}_1$, which is $|\mathcal{P}_1| = 1/2$.
  With the knowledge of the oscillatory function $\mathcal{P}(t)$ for any general $w_\phi$, we obtain the values of the Fourier components $\mathcal{P}_\nu$ by solving the following integral numerically.

$$\mathcal{P}_\nu = \frac{1}{T}\int_{t_{\rm end}}^{T}\mathcal{P}(t)\,e^{-i\nu\omega t}\,dt \tag{2.72}$$

- For $n = 2$: Approximate analytic solutions for $n = 2$ are obtained as

$$\begin{aligned}\phi(z_2) &\approx \phi_{\rm end}\left(\frac{z_2^{\rm end}}{z_2}\right)^{\frac{1}{2}}\mathcal{P}(z_2)\\ H(z_2) &\approx H_{\rm end}\left(\frac{z_2^{\rm end}}{z_2}\right)\left(1+\frac{\mathcal{P}(z_2)\sqrt{6(1-\mathcal{P}^4(z_2))}}{6}\left(\frac{\phi_{\rm end}}{M_{\rm pl}}\right)\left(\frac{z_2^{\rm end}}{z_2}\right)^{\frac{1}{2}}\right).\end{aligned} \tag{2.73}$$

†For convenience, we shall also use an alternative symbol "$m_\phi^{{\rm end}\,(n)}$" to denote the quantity $m_\phi^{\rm end}(n)$ for varying $n$.

We numerically obtain $|\mathcal{P}_1| = 0.47$ and $|\mathcal{P}_3| = 0.02$. In terms of these Fourier components, $\mathcal{P}(z_2)$ takes the form $\mathcal{P}(z_2) \approx \left(\mathcal{P}_1 \cos\left(\frac{2\pi\omega}{m_\phi^{\text{end (2)}}} z_2\right) + \mathcal{P}_3 \cos\left(\frac{6\pi\omega}{m_\phi^{\text{end (2)}}} z_2\right)\right)$. We indeed recover the leading order solution for the scale factor $a(t) \propto t^{1/2}$, which corresponds to average EoS $w_\phi \simeq 1/3$, implying radiation-like behavior of the inflaton background.

- For $n = 3$:

  For this case, we have a sextic-type potential $V \sim \phi^6$, and approximate analytic solutions are derived as

$$\phi(z_3) \approx \phi_{\text{end}} \left(\frac{z_3^{\text{end}}}{z_3}\right)^{\frac{1}{3}} \mathcal{P}(z_3)$$
$$H(z_3) \approx H_{\text{end}} \left(\frac{z_3^{\text{end}}}{z_3}\right) \left(1 + \frac{\mathcal{P}(z_3)\sqrt{6(1-\mathcal{P}^6(z_3))}}{8} \left(\frac{\phi_{\text{end}}}{M_{\text{pl}}}\right) \left(\frac{z_3^{\text{end}}}{z_3}\right)^{\frac{1}{3}}\right). \tag{2.74}$$

  We numerically obtain $|\mathcal{P}_1| = 0.46$ and $|\mathcal{P}_3| = 0.03$. In terms of these Fourier components, $\mathcal{P}(z_3)$ takes the form $\mathcal{P}(z_3) \approx \left(\mathcal{P}_1 \cos\left(\frac{2\pi\omega}{m_\phi^{\text{end (3)}}} z_3\right) + \mathcal{P}_3 \cos\left(\frac{6\pi\omega}{m_\phi^{\text{end (3)}}} z_3\right)\right)$. We again recover the leading order scale factor $a(t) \propto t^{4/9}$, implying a stiff background with $w_\phi \simeq 1/2$.

## 2.5 Introduction to inflationary potential: $\alpha$-attractor E-type potential model

So far, we have not specified any inflationary potential model, which explains the early inflationary and post-inflationary phase of the universe's evolution. Although the works carried out in this thesis are not model dependent, to estimate different background quantities, model specification is important. More recently, a broad and unifying class of models, known as $\alpha$-attractor models, has attracted significant attention for their strong theoretical motivation and remarkable agreement with cosmological observations. Inspired by Supergravity and Conformal field theory, these models feature potentials that flatten exponentially at large field values, ensuring a stable slow-roll regime. In this thesis, we consider a class of observationally favored single-field $\alpha$-attractor E-model. The universality and consistency with the latest CMB constraints make the $\alpha$-attractor E-model one of the most compelling frameworks for realistic inflationary cosmology. We write the form of the $\alpha$-attractor E-type potential model[37–42]

$$V(\phi) = \Lambda^4 \left(1 - e^{-\sqrt{\frac{2}{3\alpha}} \cdot \frac{\phi}{M_{\text{pl}}}}\right)^{2n}. \tag{2.75}$$

The amplitude of the potential "$\Lambda$", defining the energy scale of inflation, is constrained by the CMB measurement, and is related to the scalar spectral index $n_s$, the amplitude of the

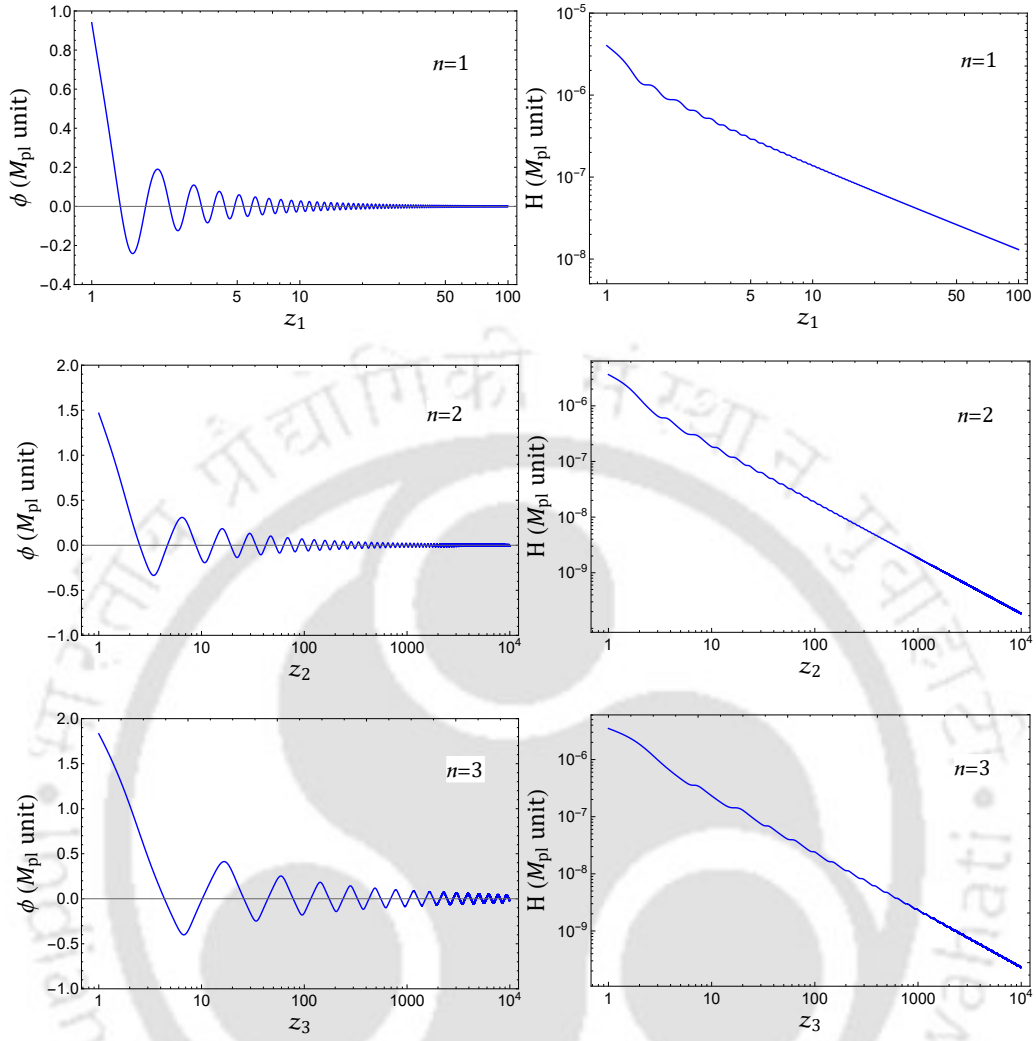


Figure 2.6: *All three plots in the left column represent the decaying oscillatory behavior of the inflaton field during the reheating era for three EoS $w_\phi = 0,\ 1/3,\ 1/2$. The plots in the right column represent the behavior of the Hubble scale during reheating. Oscillations in the inflaton field induce the oscillatory feature in the Hubble scale. In this figure, we have set $\alpha = 1$ for the $\alpha$-attractor E-type model.*

inflaton fluctuation measured as CMB normalization $A_s = 2.12 \times 10^{-9}$, and the tensor to scalar ratio $r$. During inflation, the constancy of $\Lambda$ gives the behavior of a Cosmological Constant dominated accelerated universe. The parameters $(n,\ \alpha)$ in $V(\phi)$ determine the shape of the potential. Expanding the potential (2.75) around its minima, we get the approximated power-law chaotic potential for general "$n$", as

$$V(\phi) \sim \Lambda^4 \Big(\frac{2}{3\alpha}\Big)^n \Big(\frac{\phi}{M_{\rm pl}}\Big)^{2n}. \tag{2.76}$$

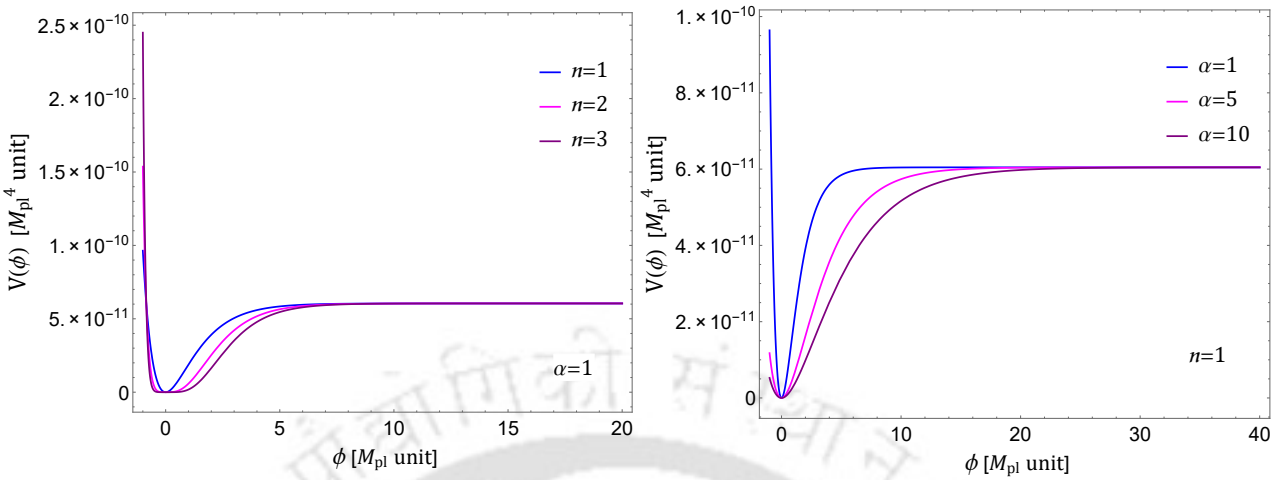


FIGURE 2.7: *Figure represents the $\alpha$-attractor E-type potential model for varying parameters $\alpha$ and $n$.*

In an expanding cosmological background, as the amplitude of the inflaton($\phi_0(t)$) falls with time(see Eq.(2.62)) and naturally assumes $\phi/M_{\rm pl} << 1$ for a significant duration of the reheating phase. Hence, we can safely neglect the higher-order terms in the expansion of the potential. By varying the exponent "$n$" we can achieve different power law forms of the potential, namely, quadratic model(for $n = 1$), quartic model (for $n = 2$), and so on. The model is favored by the latest *Planck*, ACT, DESI, and BICEP/Keck combined (P+ACT+LB+BK18) observational data sets (see the references [43–48]), where $n_s = 0.9743 \pm 0.0034$ at 68% C.L. and 95% C.L. upper limit on tensor-to-scalar ratio $r_{0.05}$ is obtained as $r_{0.05} < 0.038$(see Fig.(2.13)). We will be using these observations throughout. We shall discuss these important observable quantities like $n_s$, $r$, in detail in Section (2.8) on cosmological perturbation theory later. This $\alpha$-attractor E model belongs to the class of large-field inflationary models because the super-Planckian field excursion($\Delta\phi > M_{\rm pl}$) results in a plateau region in the potential (2.75), which gives the slow-roll inflationary phase with sufficient e-folds. In Fig.(2.4), the field excursion or the difference in field amplitude($\Delta\phi$) displaced from the potential minimum to the flat region is greater than the Planck scale $\Delta\phi > M_{\rm pl}$. For $\alpha = 1$, $n = 1$, this potential (2.75) is very similar to the Starobinsky potential model, which is also a large-field inflation model. In Fig.(2.7), we show the structure of the potential during the inflationary and the post-inflationary era for varying parameters ($\alpha$, $n$).

In the context of $\alpha$-attractor E-type potential model, we can derive an expression of the field value for general $n$ at which inflation ends($\epsilon_{\rm V} = 1$).

$$\phi_{\rm end} = \sqrt{\frac{3\alpha}{2}} M_{\rm pl} \ln\left(\frac{2n}{\sqrt{3\alpha}} + 1\right), \tag{2.77}$$

where "end" stands for the value at the end of inflation or at the beginning of reheating, and this has been used as an initial condition in our full numerical post-inflationary solution of

the inflaton in Fig.(2.6). Using this field amplitude in (2.75), we have the potential and the total inflaton energy density at the inflation end as

$$V_{\rm end} = \Lambda^4 \left(\frac{2n}{2n+\sqrt{3\alpha}}\right)^{2n}, \quad \rho_{\rm end} = \frac{3\,\Lambda^4}{2}\left(\frac{2n}{2n+\sqrt{3\alpha}}\right)^{2n}. \tag{2.78}$$

Subject to this $\alpha$-attractor E model, the inflationary slow-roll parameters(see Eq.(2.55)) can be written as

$$\begin{aligned}
\epsilon_{\rm V}(\phi) &= \frac{M_{\rm pl}^2}{2}\left(\frac{V'}{V}\right)^2 = \frac{4n^2}{3\alpha}\frac{1}{\left(e^{\sqrt{\frac{2}{3\alpha}}\cdot\frac{\phi}{M_{\rm pl}}}-1\right)^2}, \\
\eta_{\rm V}(\phi) &= M_{\rm pl}^2\left(\frac{V''}{V}\right) = \frac{4n}{3\alpha}\frac{\left(2n-e^{\sqrt{\frac{2}{3\alpha}}\cdot\frac{\phi}{M_{\rm pl}}}\right)}{\left(e^{\sqrt{\frac{2}{3\alpha}}\cdot\frac{\phi}{M_{\rm pl}}}-1\right)^2}.
\end{aligned} \tag{2.79}$$

We shall next study the two important aspects of the reheating phase. The qualitative discussion is already given in the previous Chapter 1. In this Chapter, the next two sections will be devoted to the quantitative discussion and the development of the perturbative and non-perturbative frameworks of reheating.

## 2.6 Perturbative framework of reheating dynamics

This framework is based on the simultaneous solution of the coupled Boltzmann equations, where the inflaton field interacts with all kinds of SM and BSM particles, and also its interaction with gravity, without having any non-gravitational coupling. At the end of the slow-roll inflationary era, the inflaton field starts oscillating around the potential minima. During oscillation, the field amplitude also falls due to expansion(see Fig.(2.6)), which causes the inflaton energy density($\rho_\phi$) to gradually decrease, and the consequent growth of the energy density of other field components over time. One of the most important features of reheating dynamics is to produce relativistic degrees of freedom from the decaying inflaton, which eventually give rise to a hot, thermalized radiation bath at the end of the reheating phase. To describe the general framework of perturbative reheating, here, we concentrate on the inflaton($\rho_\phi$)-radiation system($\rho_{\rm r}$). In the presence of a direct decay channel between the inflaton and radiation, the inflaton oscillation amplitude decays due to both background expansion and direct decay. The effect of this inflaton decay can be taken into account by introducing an additional decay term with the Hubble damping term in the dynamical Eq.(2.42) as

$$\ddot{\phi} + (3H + \Gamma_\phi)\dot{\phi} + V'(\phi) = 0\,, \tag{2.80}$$

where $\Gamma_\phi$ is the perturbative decay rate of the inflaton. Multiplying both sides of (2.80) with $\dot{\phi}$, we get the evolution equation of the inflaton energy density

$$\begin{aligned}
&\frac{d}{dt}\left(\frac{1}{2}\dot{\phi}^2 + V(\phi)\right) + (3H + \Gamma_\phi)\,\dot{\phi}^2 = 0 \\
&\Rightarrow \dot{\rho_\phi} + 3H\,(\rho_\phi + P_\phi) = -\Gamma_\phi\,(\rho_\phi + P_\phi) \\
&\Rightarrow \dot{\rho_\phi} + 3H\,(1 + w_\phi)\rho_\phi = -\Gamma_\phi(1 + w_\phi)\,\rho_\phi\,.
\end{aligned} \tag{2.81}$$

Inflaton energy density will be transferred to the radiation sector through the decay term $\Gamma_\phi$. The evolution equation of radiation energy density can be derived from the Boltzmann transport equation. Let's consider $f_{\rm r}(t,\vec{p})$ is the phase space distribution function of the relativistic radiation particle with the physical momentum vector $\vec{p}$. With this distribution function, in the presence of interactions, the Boltzmann transport equation is written as[49]

$$\frac{\partial f_{\rm r}(t,\vec{p})}{\partial t} - H|\vec{p}|\frac{\partial f_{\rm r}(t,\vec{p})}{\partial|\vec{p}|} = \mathcal{C}[f_{\rm r}]\,. \tag{2.82}$$

where $\mathcal{C}[f_{\rm r}]$ is the collision function, accounting for different interactions. In the case of radiation, it carries the information of the production of radiation through the decay of the inflaton. To account for the total energy density of produced radiation, we take the momentum space integration of $f_{\rm r}$

$$\rho_{\rm r} = \int \frac{d^3|\vec{p}|}{(2\pi)^3}\,E_p\,f_{\rm r}(t,\vec{p})\,, \tag{2.83}$$

where $E_p$ is the energy per momentum mode, for massless radiation, $E_p = p$.
We take the momentum integration by multiplying $E_p$ on both sides of the Boltzmann equation (2.82), leading to the radiation energy density evolution equation[19, 50]

$$\Rightarrow \dot{\rho}_{\rm r} + 4H\rho_{\rm r} = \Gamma_\phi(1 + w_\phi)\,\rho_\phi\,. \tag{2.84}$$

For a given decay process from inflaton to radiation, the right-hand side of (2.84) gives the energy transfer per spacetime volume from the background to the produced radiation [50]. Now the Hubble parameter $H$ is determined by the total energy density of the inflaton-radiation system

$$H^2 = \frac{(\rho_\phi + \rho_{\rm r})}{3M_{\rm pl}^2}\,. \tag{2.85}$$

Therefore, the perturbative reheating dynamics can be studied by solving the following set of coupled Boltzmann equations

$$\begin{aligned}
&\dot{\rho_\phi} + 3H\,(1 + w_\phi)\rho_\phi = -\Gamma_\phi(1 + w_\phi)\,\rho_\phi\,, \\
&\dot{\rho}_{\rm r} + 4H\rho_{\rm r} = \Gamma_\phi(1 + w_\phi)\,\rho_\phi\,, \\
&H^2 = \frac{(\rho_\phi + \rho_{\rm r})}{3M_{\rm pl}^2}\,.
\end{aligned} \tag{2.86}$$

At the end of inflation, the inflaton energy density is largely dominating over the radiation energy, $\rho_\phi >> \rho_{\rm r}$ and $\rho_{\rm r}(a_{\rm end}) = 0$. In the perturbative regime, as the energy transfer from the background inflaton to the radiation sector happens slowly, $H >> \Gamma_\phi$ condition remains valid till the end of reheating. Hence, the inflaton energy density decays mostly due to the background expansion. In general, the inflaton decay rate $\Gamma_\phi$ is a time-varying function. Depending upon the reheating EoS, different kinds of interactions with the decay products and also the spin-statistics of the decay products, it modifies the reheating dynamics of the universe in many ways, which has been thoroughly studied in many literature [34, 51–58]. However, to describe the basic dynamics, here we shall consider $\Gamma_\phi$ a constant. With these considerations, the set of coupled equations (2.86) leads to the following solutions:

$$\begin{aligned}
\rho_\phi &\simeq \rho_{\rm end}\left(\frac{a}{a_{\rm end}}\right)^{-3(1+w_\phi)}\,,\\
H &\simeq H_{\rm end}\left(\frac{a}{a_{\rm end}}\right)^{-\frac{3}{2}(1+w_\phi)}\,,\\
\rho_{\rm r} &\simeq \frac{2(1+w_\phi)\Gamma_\phi\,\rho_{\rm end}}{(5-3w_\phi)H_{\rm end}}\left(\left(\frac{a}{a_{\rm end}}\right)^{-\frac{3}{2}(1+w_\phi)}-\left(\frac{a}{a_{\rm end}}\right)^{-4}\right)\\
&\Rightarrow \rho_{\rm r} \approx \frac{2(1+w_\phi)\Gamma_\phi\,\rho_{\rm end}}{(5-3w_\phi)H_{\rm end}}\left(\frac{a}{a_{\rm end}}\right)^{-\frac{3}{2}(1+w_\phi)} \quad \text{for } 0\leq w_\phi\leq 1\,.
\end{aligned} \tag{2.87}$$

Therefore, the radiation energy density depends on the decay width $\Gamma_\phi$ as well as the inflaton EoS $w_\phi$. Using the Stefan-Boltzmann law, the temperature of the thermal bath associated with the radiation energy density is given by

$$\rho_{\rm r} = \frac{\pi^2}{30}g_{\rm re}(T_{\rm rad})\,T_{\rm rad}^4\,, \tag{2.88}$$

where $g_{\rm re}(T_{\rm rad})$ is the effective number of relativistic degrees of freedom in the thermal bath, depending upon the temperature of the bath $T_{\rm rad}$. Throughout this thesis, we take $g_{\rm re} = 106.75$ at the time of reheating for the reheating temperature $T_{\rm re} \gtrsim 1$ GeV. Using equations (2.87) and (2.88), the evolution of the bath temperature is computed as

$$T_{\rm rad}(a) \simeq \left(\frac{60(1+w_\phi)\Gamma_\phi\,\rho_{\rm end}}{(5-3w_\phi)\pi^2 g_{\rm re}H_{\rm end}}\right)^{1/4}\left(\frac{a}{a_{\rm end}}\right)^{-\frac{3}{8}(1+w_\phi)}\,. \tag{2.89}$$

In Fig.(2.8), we present the evolution of the inflaton and radiation energy densities and the temperature of the radiation bath during reheating by numerically solving the set of coupled Boltzmann equations (2.86). We see that there is a sharp increment in radiation energy density as well as the bath temperature at the beginning of reheating due to the draining of inflaton energy through $\Gamma_\phi$, and they quickly reach their maximum values. After that, they start decaying due to expansion following the Eq.(2.87). Assuming instantaneous thermalization, the reheating temperature($T_{\rm re}$) of the universe is defined at the point say,

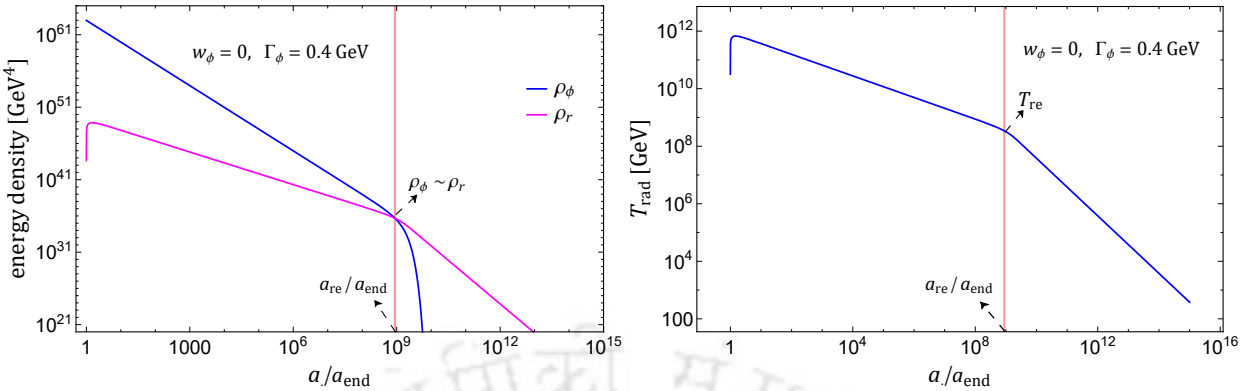


FIGURE 2.8: ***Left Panel:*** *Figure represents the evolution of the inflaton, $\rho_\phi$(blue) and radiation, $\rho_r$(magenta) energy densities with the normalized scale factor $(a/a_{end})$ during reheating.* ***Right Panel:*** *It represents the evolution of thermal bath temperature, $T_{rad}$, with the normalized scale factor during reheating. In both plots, the vertical red lines indicate the end of reheating where $\rho_\phi \sim \rho_r$ condition is satisfied. In this figure, for the parameters, $w_\phi = 0$, $\Gamma_\phi = 0.4$ GeV, we get $T_{re} \sim 10^8$ GeV.*

$a_{re}$ where the condition $\rho_\phi(a_{re}) = \rho_r(a_{re})$ is satisfied, giving the onset of hot, thermal radiation-dominated universe. From (2.87), $a_{re}$ is calculated as

$$\left(\frac{a_{re}}{a_{end}}\right) \approx \left(\frac{(5-3w_\phi)H_{end}}{2(1+w_\phi)\Gamma_\phi}\right)^{\frac{2}{3(1+w_\phi)}} . \tag{2.90}$$

Therefore, in the instantaneous scenario, the reheating temperature will be computed as

$$T_{re} = \left(\frac{30}{\pi^2 g_{re}}\right)^{\frac{1}{4}} \rho_r(a_{re})^{\frac{1}{4}} . \tag{2.91}$$

The Eq.(2.91) is the standard relation to determine the reheating temperature for any specific reheating dynamics. In the absence of direct observational evidence of the reheating phase, the reheating temperature is highly unconstrained by observation. As the reheating phase must end before the BBN phase, therefore, the formation of light elements during the BBN phase requires a lowest possible reheating temperature $T_{BBN}$, and the inflation energy scale decides the maximum limit of reheating temperature $T_{max}$. The conservative estimates of the minimum and maximum values of $T_{re}$, as generally referred to in the literature[7, 59–64], are

$$T_{BBN} \simeq 4\,\text{MeV} \lesssim T_{re} \lesssim T_{max} \simeq 10^{15}\text{GeV} . \tag{2.92}$$

Having presented a brief overview of the perturbative reheating dynamics, we now proceed to study the fundamentals of the non-perturbative aspect of reheating dynamics, which is one of the prime focuses of this thesis.

## 2.7 Non-perturbative framework of reheating dynamics

In Chapter 1, we have already given an introduction to the importance of the non-perturbative framework of reheating dynamics, highlighting the strong limitation of the perturbative framework, based on the system of Boltzmann equations, for the complete understanding of this early universe phase. In this section, we present a quantitative description of the non-perturbative reheating dynamics, discussing about different mathematical tools and techniques to deal with the non-perturbative particle production during the reheating phase. Employing these tools and techniques, we explore the scenarios of Cosmological Gravitational Particle Production(CGPP) and the explosive production of particles through the parametric resonance instability during the preheating phase.

### 2.7.1 Non-perturbative production of scalar fluctuations: General Formalism

In this thesis, we have mainly dealt with the production of spin-0 scalar particles during reheating. To discuss the general non-perturbative formalism of scalar particle production, from the action (2.41), we write the following Lagrangian for the inflaton ($\phi$) and a massive scalar daughter field ($\chi$) non-minimally coupled to gravity in the Jordan frame, and also directly coupled to the inflaton with some interaction

$$\mathcal{L}_{[\phi,\chi]} = -\sqrt{-g}\left(\frac{M_{\rm pl}^2}{2}R + \frac{1}{2}\partial_\mu\phi\partial^\mu\phi + V(\phi) + \frac{1}{2}\partial_\mu\chi\partial^\mu\chi + \frac{1}{2}(m_\chi^2 + F(\phi) + \xi R)\chi^2\right), \tag{2.93}$$

where the background FLRW metric is expressed as $ds^2 = -dt^2 + a^2(t)d\vec{x}^2 = a^2(\eta)\big(-d\eta^2 + d\vec{x}^2\big)$ with $a$ being the scale factor, $\eta$ being the conformal time, defined as $d\eta = \int \frac{dt}{a}$, and $\sqrt{-g} = a^4(\eta)$. Interestingly, in conformal coordinate, the FLRW metric becomes conformally flat with $45^\circ$ light cone. This is the main benefit of working with conformal time. $V(\phi)$ is the inflaton potential. In this thesis, we shall only work with the $\alpha$-attractor E-type potential model (2.75). $m_\chi$ is the bare mass of the produced daughter particles, $\xi$ is the dimensionless non-minimal coupling of $\chi$ with gravity, and $F(\phi)$ is a generic coupling function of the classical background inflaton($\phi$), and the specific form of this function will be discussed later. In the matter Lagrangian, the Ricci scalar $R$ and the coupling function $F(\phi)$ generate a time-dependent effective mass for the $\chi$ field as

$$m_{\rm eff}^2(\eta) = \big(m_\chi^2 + F(\phi(\eta)) + \xi R(\eta)\big)\,. \tag{2.94}$$

From the Eq.(2.18), we can express $R$ as a function of conformal time $\eta$, $R(\eta) = 6\,(a''/a^3)$. The post-inflationary oscillation of the inflaton field(see Fig.(2.6)) and the Ricci scalar induce the oscillatory feature in the effective mass of the daughter field, which gives rise to various non-perturbative effects like parametric resonance, tachyonic instability in the dynamics of the daughter field $\chi$. We shall meticulously investigate these interesting phenomena in the latter part of this thesis.

Expressing the scalar field $\chi$ in terms of Fourier modes,

$$\hat{\chi}(\eta,\vec{x}) = \int \frac{d^3\vec{k}}{(2\pi)^3}\, e^{i\vec{k}.\vec{x}} \left[\chi_{\vec{k}}(\eta)\ \hat{a}_k + \chi^*_{\vec{k}}(\eta)a^\dagger_{-k})\right] , \tag{2.95}$$

and using the Lagrangian (2.93), we obtain the following equation for the mode function $\chi_{\vec{k}}$,

$$\chi''_{\vec{k}} + 2\mathcal{H}\chi'_{\vec{k}} + \left[k^2 + a^2(\eta)\left(m^2_\chi + F(\phi) + \xi R\right)\right]\chi_{\vec{k}} = 0\,, \tag{2.96}$$

where $\mathcal{H} = a'/a$, and all the derivatives are defined with respect to conformal time $\eta$. In Eq. (2.96), we notice the presence of the damping term $2\mathcal{H}\chi'_{\vec{k}}$ which is non-zero for an expanding cosmological background. For convenience, it is conventional to rescale the field properly to absorb the damping term $2\mathcal{H}\chi'_{\vec{k}}$, by defining the rescaled field

$$X_{\vec{k}} = a\chi_{\vec{k}}\,, \tag{2.97}$$

and obtain the following mode equation,

$$X''_{\vec{k}} + \left[k^2 + a^2\big(m^2_\chi + F(\phi)\big) + \frac{a^2R}{6}(6\xi - 1)\right]X_{\vec{k}} = 0\,. \tag{2.98}$$

The bracketed term in the equation above can be identified as a time-dependent frequency $\omega_k$ where

$$\omega^2_k(\eta) = k^2 + a^2\big(m^2_\chi + F(\phi)\big) + \frac{a^2R}{6}(6\xi - 1)\,. \tag{2.99}$$

This $\omega^2_k$ can be negative, giving rise to phenomena like *tachyonic instability dynamics* in many situations in the early universe. In this thesis, we have a significant deal with this distinctive non-perturbative feature in the context of early universe particle production. Likewise, Eq.(2.95), we can decompose the rescaled field operator $\hat{X}(\eta,\ \vec{x})$ in terms of the rescaled Fourier modes $X_{\vec{k}}$ as

$$\hat{X}(\eta,\vec{x}) = \int \frac{d^3\vec{k}}{(2\pi)^3}\, e^{i\vec{k}.\vec{x}} \left[X_{\vec{k}}(\eta)\ \hat{a}_k + X^*_{\vec{k}}(\eta)\hat{a}^\dagger_{-k})\right] . \tag{2.100}$$

The rescaled operator must satisfy the standard quantization condition

$$\left[\hat{X}(\eta,\ \vec{x}),\ \Pi_X(\eta,\vec{y})\right] = \left[\hat{X}(\eta,\ \vec{x}),\ \hat{X}'(\eta,\vec{y})\right] = i\delta^3(\vec{x}-\vec{y})\,. \tag{2.101}$$

Subject to the standard commutation relation between the creation and annihilation operator, $\left[\hat{a}_{\vec{p}},\ \hat{a}^\dagger_{\vec{k}}\right] = (2\pi)^3\delta^3(\vec{p}-\vec{k})$, plugging (2.100) into the field($\hat{X}$)-conjugate momentum($\hat{\Pi}_X$) commutation relation (2.101) gives the following condition:

$$\left(X_k\, X^{*\prime}_k - X^*_k\, X'_k\right) = i \tag{2.102}$$

This is known as the Wronskian condition, giving the normalization factor, $\frac{1}{\sqrt{2\omega_k}}$, for the scalar field quantization. The time dependence in $\omega_k(\eta)$ renders impossible to decompose the scalar field $\chi(\eta, x)$ in Eq. (2.95)into a classical positive/negative frequency basis, with

$$X(\eta) = \frac{e^{-i\omega_k \eta}}{\sqrt{2\omega_k}}\,. \tag{2.103}$$

In other words, the presence of a time-dependent background breaks the time translation symmetry, and the Killing vector field $i\,(\partial/\partial\eta)$ is no longer associated with a positive frequency eigenfunction due to the mixing of positive- and negative-frequency modes in the time-dependent background. However, taking into account the evolution of the frequencies with time, one can reexpress (2.100) as

$$\begin{aligned}\hat{X}(\eta, \vec{x}) = \int \frac{d^3\vec{k}}{(2\pi)^3} \frac{e^{i\vec{k}.\vec{x}}}{\sqrt{2\omega_k(\eta)}} \Big[\big(\alpha_{\vec{k}} e^{-i\Omega_k(\eta)} + \beta_{\vec{k}} e^{i\Omega_k(\eta)}\big)\, \hat{a}_{\vec{k}} \\ +(\alpha^*_{\vec{k}} e^{i\Omega_k(\eta)} + \beta^*_{\vec{k}} e^{-i\Omega_k(\eta)})\hat{a}^\dagger_{-\vec{k}}\Big]\,,\end{aligned} \tag{2.104}$$

with

$$\Omega_k(\eta) = \int^\eta \omega_k(\eta')d\eta'\,, \tag{2.105}$$

and where $\alpha_{\vec{k}}$, $\beta_{\vec{k}}$ are the time-dependent Bogoliubov coefficients satisfying the normalization condition $|\alpha_{\vec{k}}|^2 - |\beta_{\vec{k}}|^2 = 1$, extracted from the Wronskian condition (2.102). We can interpret this evolution in the mode $X_{\vec{k}}(\eta)$

$$X_{\vec{k}}(\eta) = \frac{1}{\sqrt{2\omega_k}}\left[\alpha_{\vec{k}} e^{-i\int^\eta \omega_k(\eta')d\eta'} + \beta_{\vec{k}} e^{i\int^\eta \omega_k(\eta')d\eta'}\right], \tag{2.106}$$

in terms of an evolution in the creation/annihilation operator space. Indeed, rewriting Eq. (2.104) as

$$\begin{aligned}\hat{X}(\eta, \vec{x}) = \int \frac{d^3\vec{k}}{(2\pi)^3} e^{i\vec{k}.\vec{x}} \times \\ \frac{e^{-i\Omega_k}}{\sqrt{2\omega_k}}\left[\alpha_{\vec{k}}\hat{a}_{\vec{k}} + \beta^*_{\vec{k}}\hat{a}^\dagger_{-\vec{k}}\right] + \frac{e^{i\Omega_k}}{\sqrt{2\omega_k}}\left[\beta_{\vec{k}}\hat{a}_{\vec{k}} + \alpha_{\vec{k}}\hat{a}^\dagger_{-\vec{k}}\right]\,,\end{aligned} \tag{2.107}$$

we can define a new set of operators $\tilde{a}_{\vec{k}}$ and $\tilde{a}^\dagger_{-\vec{k}}$ by

$$\tilde{a}_{\vec{k}} = \alpha_{\vec{k}}\hat{a}_{\vec{k}} + \beta^*_{\vec{k}}\hat{a}^\dagger_{-\vec{k}}\,, \quad \tilde{a}^\dagger_{-\vec{k}} = \alpha^*_{\vec{k}}\hat{a}^\dagger_{-\vec{k}} + \beta_{\vec{k}}\hat{a}_{\vec{k}}\,. \tag{2.108}$$

Within this new set of operators, we deduce from the number operator defined by

$$\hat{N} = \int \frac{d^3k}{(2\pi)^3}\tilde{a}^\dagger_{-\vec{k}}\tilde{a}_{\vec{k}}\,, \tag{2.109}$$

that gives

$$_{\rm BD}\langle 0|\hat{N}|0\rangle_{\rm BD} = a^3 n_\chi = \int \frac{d^3k}{(2\pi)^3} {}_{\rm BD}\langle 0|\tilde{a}^\dagger_{-\vec{k}}\tilde{a}_{\vec{k}}|0\rangle_{\rm BD} = \int \frac{d^3k}{(2\pi)^3}|\beta_k|^2\,, \tag{2.110}$$

where we defined the initial vacuum $|0\rangle_{\rm BD}$, called the Bunch-Davies(BD) vacuum [65] with respect to the set of ladder operators $\hat{a}_{\vec{k}}$ at time $\eta \to -\infty$ by $\hat{a}_{\vec{k}}|0\rangle_{\rm BD} = 0$, or $\beta_{\vec{k}}|_{\eta\to-\infty} \to 0$. This Bunch-Davies vacuum state is normalized as ${}_{\rm BD}\langle 0|0\rangle_{\rm BD} = 1$. In the Heisenberg picture, as operator evolution is studied rather than state evolution, a vacuum state corresponding to one set of ladder operators($\hat{a}_{\vec{k}}$, $\hat{a}^\dagger_{\vec{k}}$) will no longer be a vacuum corresponding to some other set of operators say ($\tilde{a}_{\vec{k}}$, $\tilde{a}^\dagger_{-\vec{k}}$), connected to each other through Bogoliubov transformation (2.108). This very fact makes the concept of vacuum ambiguous in a time-dependent background. However, in studies of inflationary perturbations, the evolution of field fluctuations, it is customarily assumed that the modes of perturbations and fluctuations are prepared in the initial Bunch-Davies vacuum state. As $\eta \to -\infty$, the time-dependent scale factor $a(\eta)$ and Ricci scalar $R(\eta)$ in $\omega_k^2(\eta)$(Eq.(2.99)) tend to vanish, making $\omega_k \approx k$. Therefore, at the initial Bunch-Davies vacuum state $|0\rangle_{\rm BD}$, the field mode in Eq.(2.106) takes the following form

$$X_{\vec{k}}(\eta \to -\infty) = \frac{1}{\sqrt{2k}} e^{-i\,k\,\eta}\,. \tag{2.111}$$

In the limit $\eta \to -\infty$, the BD vacuum state (2.111) represents a no-particle, positive-frequency outgoing state. As $\beta_{\vec{k}}|_{\eta\to-\infty} \to 0$, hence, no negative-frequency mode is associated with the BD vacuum solution of the field. Further, the evolution of Bogoliubov coefficients($\alpha_k\,, \beta_k$) can be studied by using the WKB expansion of $X_k$ (2.106) in the field dynamical equation (2.98). This leads to the following equation

$$\left(\frac{\omega_k'}{2\sqrt{2\omega_k}}\beta_k e^{i\int\omega_k\,d\eta} - \sqrt{\frac{\omega_k}{2}}\alpha_k' e^{-i\int\omega_k\,d\eta}\right) + \left(\sqrt{\frac{\omega_k}{2}}\beta_k' e^{i\int\omega_k\,d\eta} - \frac{\omega_k'}{2\sqrt{2\omega_k}}\alpha_k e^{-i\int\omega_k\,d\eta}\right) = 0\,. \tag{2.112}$$

In the first derivative $X_k'$, we have suppressed the terms $\alpha_k'$, $\beta_k'$, and have also used the adiabatic condition, $\left(\frac{\omega_k'}{\omega_k^{3/2}}\right) < 1$. These slowly varying functions will, anyway, contribute to the second derivative of $X_k$ in (2.98), giving the equation (2.112). There is a functional degree of freedom to impose an arbitrary condition between $\alpha_k$ and $\beta_k$. We take it as [66–68]

$$\alpha_k' = \frac{\omega_k'}{2\omega_k} e^{2i\int\omega_k\,d\eta}\,\beta_k\,,\quad \beta_k' = \frac{\omega_k'}{2\omega_k} e^{-2i\int\omega_k\,d\eta}\,\alpha_k\,. \tag{2.113}$$

Indeed, this choice satisfies the dynamical equation (2.98). The eq.(2.113) gives us the time-evolution of $\alpha_k$, $\beta_k$, with the initial conditions, $\alpha_k(\eta \to -\infty) \to 1$, $\beta_k(\eta \to -\infty) \to 0$. Notice that, in the integral (2.110), we have dropped the vector sign of the integration variable $k$. The isotropy of space enables us to write this. Note also that the occupation number, $|\beta_k|^2$, is equivalent to a distribution function $f_\chi(|\vec{k}|, t)$ in the Boltzmann approach

as given in Eq.(2.82). The number density of particles $n_k$ with momentum $k$ can also be obtained with the solution (2.106) noting that [50, 66, 69]

$$n_k = |\beta_k|^2 = \frac{1}{2\omega_k}|\omega_k X_k - iX_k'|^2 = \frac{1}{2\,\omega_k}\left(|X_k'|^2 + \omega_k^2\,|X_k|^2\right) - \frac{1}{2}\,. \tag{2.114}$$

The final expression of $n_k$ is obtained by using the Wronskian condition (2.102).

The whole subject of cosmological particle production is then summarized into computing the value of $\beta_k$, or in other words, the number density spectrum, in varying circumstances. For the purpose of Baryogenesis, explaining the origin of matter-antimatter asymmetry, the number density is an observable quantity of interest. Rather, if we are interested in cosmic relics like dark matter, dark radiation, then the energy density of the produced particles is the quantity of interest to compute the present-day relic abundance. Subject to the Lagrangian (2.93), using Eq.(2.44), we calculate the stress-energy tensor of the $\chi$ field as [68, 69]

$$\begin{aligned} T^{\chi}_{\mu\nu} = {} & (1-2\xi)\partial_\mu\chi\partial_\nu\chi + \left(2\xi - \frac{1}{2}\right) g_{\mu\nu}(\partial_\alpha\chi\partial^\alpha\chi) + 2\xi\left(g_{\mu\nu}\chi\Box\chi - \chi\nabla_\mu\partial_\nu\chi\right) + \xi G_{\mu\nu}\chi^2 \\ & - \frac{1}{2}g_{\mu\nu}\left(m_\chi^2 + F(\phi)\right)\chi^2. \end{aligned} \tag{2.115}$$

where "$\Box$" is the D'Alembertian operator expressed as $\Box \equiv \nabla_\mu\nabla^\mu$ in the curved spacetime, with $\nabla_\mu$ is the covariant derivative. Expressing the above stress-energy tensor (2.115) in terms of the rescaled field operator($\hat{X}(\eta,\vec{x})$), and using the mode expansion (2.100), we can compute the energy density of the field as

$$\begin{aligned} \rho_\chi(\eta) &= {}_{\rm BD}\langle 0|\, T_0^{\chi\,0}\,|0\rangle_{\rm BD} \\ &= a^{-4}(\eta)\int \frac{d^3k}{(2\pi)^3}\left[\frac{1}{2}|X_k'|^2 + \frac{1}{2}\omega_k^2|X_k|^2 + \frac{1}{2}(1-6\xi)\left(\mathcal{H}^2 - \frac{1}{6}a^2R\right)|X_k|^2\right] \\ &\quad - a^{-4}(\eta)\int \frac{d^3k}{(2\pi)^3}(1-6\xi)\mathcal{H}\left(X_kX_k'^* + X_k^*X_k'\right)\,, \end{aligned} \tag{2.116}$$

where $\mathcal{H} = (a'/a)$ is the Hubble parameter, defined in conformal coordinate, and $a' = (da/d\eta)$.

Evidently, in (3+1) dimensional spacetime, there exists a certain non-minimal coupling strength, $\xi = 1/6$ [‡], at which several terms in the above energy density expression (2.116) will vanish. This is known as *conformal limit*, meaning the scalar field is conformally coupled to the gravity sector. A conformally coupled massless spectator scalar field without any non-gravitational coupling doesn't sense the background dynamics due to the conformality of the system. As a result of that, the spectator field continues to remain in the vacuum state until the conformal invariance is broken either by adding mass or non-gravitational

[‡]The conformal coupling for a general spacetime dimension, "D" is given by $\xi(D) = \frac{(D-2)}{4(D-1)}$[70]. For $D = 4$, $\xi = 1/6$. Interestingly, in two dimension, minimal and conformal coupling occur at the same point, $\xi = 0$.

coupling to the system. A conformally coupled scalar field is actually decoupled from the gravity sector. In this conformal limit, many interesting dynamical features of a scalar field system will be discussed in due course.
The energy density integral (2.116) has a UV divergence in the large $k$ limit of the integration domain. To identify this divergent behavior, we consider the field mode (2.111) in the limit $\eta \to -\infty$. Using the vacuum solution (2.111) in (2.116) with vanishing $\mathcal{H}$, $R$ in the $\eta \to -\infty$ limit, we find that the first two non-vanishing terms grow like $k^3$, leading to a quartic divergence of the energy density, $\rho_{\chi_k} \propto k^4$ as $k \to \infty$. This is similar to the well-known divergence of a free field's energy density in Minkowski spacetime. To regularize this divergence in flat-space QFT, the standard method is to introduce a counterterm that renormalizes the divergent vacuum energy term. However, in a curved spacetime where $\omega_k$ is a time-dependent function, the regularization process becomes more subtle as the divergent part of the integral varies with time. One standard method is the Adiabatic regularization prescription to remove the UV divergence in the study of QFT in curved spacetime[71–74]. However, in the present context, to regularize the UV divergence in FLRW spacetime, adopting the technique of renormalization via normal ordering, as illustrated in[69, 75], we compute the UV convergent renormalized energy density. Finally, integrating Eq. (2.114) and (2.116) over all momentum modes, we get the total number and renormalized energy density as [50, 66, 69, 71, 73, 75]

$$
\begin{aligned}
n_\chi &= \frac{1}{a^3}\int \frac{d^3k}{(2\pi)^3} n_k \,, \\
\rho_\chi &= \frac{1}{(2\pi)^3 a^4}\int d^3k \omega_k n_k \,.
\end{aligned}
\tag{2.117}
$$

The general formalism that we have constructed in this section is the main foundation of the non-perturbative study of particle production. In order to get the particle number density spectrum, first we need to solve Eq. (2.98) with Bunch-Davies initial state, and then, by implementing the solution in (2.114), we obtain the number density spectrum of produced particles. Utilizing the spectrum (2.114) in (2.117), we compute the total number and energy density of produced daughter particles in the non-perturbative framework. Based on this general formalism, we now discuss two important aspects of cosmological particle production where the non-perturbative effects are prominent. We shall first discuss the basic features of the Cosmological Gravitational Particle Production(CGPP), where we are solely interested in the gravitational interaction between the inflaton and other SM or BSM sectors with no direct coupling, which is indeed a fundamental portal in nature for the production of particles in the early universe. We next discuss the non-linear early reheating or preheating phase, where the direct coupling, with a sufficiently strong coupling strength, between the background inflaton and daughter particle is necessary for the explosive production through the non-perturbative instability effect.

### 2.7.2 CGPP: Quantum mechanical particle production in a time-dependent background

Over the course of nearly a century, various studies have explored this intriguing phenomenon of cosmological gravitational particle production. The calculability and practical testability of quantum field theory in curved spacetime are provided by the predictions of CGPP. The main principle of CGPP is the quantum mechanical particle production in the expanding background of the early universe, solely facilitated by the gravitational interactions. The changing geometry of the background excites the quantum fluctuations on top of the classical expanding background, resulting in particle production from the quantum vacuum of the spectator field. This CGPP is a semiclassical process in the sense that the background or the external gravitational field is classical, whereas the spectator field is quantized, and the particle production happens by the quantum effect.

**Historical backdrop :**

The way back to 1939, the creation of particle pairs in the expanding universe was first discussed in Schrödinger's seminal work on *The proper Vibrations of the Expanding Universe*[76]. In this work, Schrödinger was the first who envisioned the mixing of positive- and negative-frequency mode solutions of the wave equation in the presence of an expanding background(for instance, see (2.106)). This mixing of positive- and negative-frequency modes was described as "mutual adulteration", which was regarded as an "alarming phenomenon". Interestingly, he identified this adulteration phenomenon as the production(or annihilation) of matter by the expansion of the universe. Although the quantum field-theoretic treatment was not done in this work [76], this idea was marked as a phenomenon of outstanding importance. Contextually, it is relevant to mention the most familiar example of particle production in a strong external field, well-known as *Schwinger Effect*, in which a sufficiently strong electric field leads to the generation of electron-positron pairs from the vacuum[77]. Although this effect was first predicted by Heisenberg and Euler[78] based upon the work[79], the core concept was completely understood in 1951 with a complete description using Quantum Electrodynamics(QED). The basic idea is, in the quantum vacuum, virtual particle–antiparticle pairs are constantly created and annihilated within times allowed by the uncertainty principle. However, if a strong, uniform electric field is present, it can accelerate particles to energies greater than their mass over a distance smaller than or equal to the Compton wavelength of the particle, and then virtual particles can be pulled out of the vacuum and propagate as real particles. The Schwinger mechanism is conceptually related to gravitational particle creation in an expanding universe. In both cases, the vacuum becomes unstable because of the background electromagnetic or gravitational fields. In curved spacetime, the time-dependence of the metric plays the same role as the constant electric field does in flat spacetime in *Schwinger Effect*. Further progress in research on the particle production in a background gravitational field resumed with the thesis of Leonard Parker in 1965 [80]. It is Parker who first presented the complete field-theoretic treatment of this phenomenon. In the conclusion of a 1968 paper [81], Parker

wrote "...for the early stages of a Friedmann expansion, it [particle creation] may well be of great cosmological significance, especially since it seems inescapable if one accepts quantum field theory and general relativity." Later on, he continued to develop this framework in a series of works, first alone [82–84], and then the works in collaboration [71, 85–87]. The Birrell and Davies textbook [70] also beautifully described this phenomenon. In this textbook, the authors have studied the cosmological particle creation for different cosmological spacetimes with varying nature of the scale factor $a(\eta)$. Shortly after the Parker's work in 1968, Zel'dovich in 1970 [88], considered particle production in a homogeneous, anisotropic background metric, called, Kasner metric, a homogeneous, anisotropic metric of the form $ds^2 = (dt)^2 - \sum_{i=1}^{3} t^{2p_i}(dx^i)^2$. It is the vacuum solution of the Einstein equation if the Kasner exponents $p_i$ satisfy $\sum_{i=1}^{3} p_i = \sum_{i=1}^{3} p_i^2 = 1$. Zel'dovich was an admirer of the concept of cosmological particle creation, and he used the Kasner model to explore whether particle creation could isotropize an initially anisotropic universe. And extending this idea, he explained how physical processes could turn an initial anisotropic/inhomogeneous universe into the observed homogeneous/isotropic universe. Zel'dovich carried on this line of research in a series of papers in collaboration with Alexei Starobinsky [89, 90]. Other researchers, including A.A. Starobinsky, A.A. Grib, V.M. Frolov, S.G. Mamayev, and V.M. Mostepanenko, focused on studying particle creation processes in homogeneous and isotropic cosmological backgrounds [91–93]. In the 1980s, with the development of non-standard inflationary cosmology, the CGPP was greatly nurtured in connecting cosmology and elementary particle physics. Inflation and CGPP are deeply interconnected phenomena arising from the dynamics of quantum fields in an evolving spacetime. During inflation, the rapid exponential expansion results in the adiabatic to non-adiabatic transition of the field modes, thereby causing the spontaneous particle creation through purely gravitational effects by breaking quantum vacuum states of the fields. In particular, the amplification of quantum vacuum fluctuations during inflation forms the primordial perturbations for the observed cosmic microwave background anisotropies and large-scale structure, while the same mechanism can produce a stochastic background of relic gravitational waves. Thus, gravitational particle production serves as a natural bridge between the microphysics of quantum field theory and the macroscopic evolution of the universe, linking inflationary dynamics with post-inflationary reheating and subsequent cosmic history.

**Importance of CGPP :**

The schematic representation in Fig.(2.9) nicely shows the fundamental building blocks(Inflation, QFT, General Relativity, and the properties of the spectator particle) upon which this CGPP mechanism is established, and the potential outputs or observables it can generate. Its wide range of output includes the generation of primordial temperature fluctuation, primordial gravitational waves, a possible arena for baryogenesis, a probe of BSM physics, the origin of dark matter and particles in a hidden sector, and CMB isocurvature fluctuations. Apart from this, it also provides the origin of primordial plasma itself through gravitational reheating. This idea was first proposed by Ford[94] and Turner and Widrow[95], who attempted to explain the origin of light scalar (axion) dark matter via CGPP. Subsequent attempts in a se-

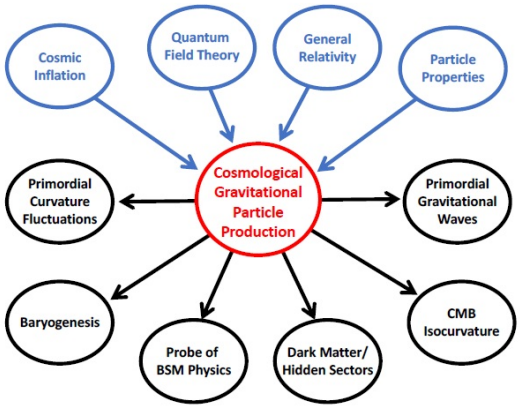


Figure 2.9: *Diagram represents the inputs and potential outputs of the CGPP mechanism. The CGPP framework combines inputs from cosmic inflation, quantum field theory, general relativity, and particle properties to produce observable or potentially observable predictions. This diagram is taken from [69].*

ries of works[68, 69, 75, 96–98] emphasized the novel role of CGPP in producing superheavy dark matter particles having mass($m_\chi$) comparable to the Hubble scale $m_\chi \approx H_{\rm end}$. In this thesis, we have explored an unavoidable production channel of gravitational waves, sourced by the gravitationally produced massless or very low-mass($m_\chi << H_{\rm end}$) particles. Analyzing the produced GW spectrum, we decode the finer details of various non-perturbative signatures of CGPP. This wide range of output proclaims the utmost importance of CGPP in providing a testable link between early-universe dynamics and present-day cosmological observations.

**Theoretical framework :**

We start with the inflaton-spectator scalar field Lagrangian by taking into account only the gravitational interaction terms. From the Lagrangian (2.93), dropping the interaction function $F(\phi)$ with the inflaton background, we write the Lagrangian for the gravitational production as follows:

$$\mathcal{L}_{[\phi,\chi]} = -\sqrt{-g}\left(\frac{M_{\rm pl}^2}{2}R + \frac{1}{2}\partial_\mu\phi\partial^\mu\phi + V(\phi) + \frac{1}{2}\partial_\mu\chi\partial^\mu\chi + \frac{1}{2}(m_\chi^2 + \xi R)\chi^2\right) . \quad (2.118)$$

If we take $\xi = 0$, the system will be purely gravitational, minimally coupled to gravity. This thesis extensively deals with both minimal($\xi = 0$) and non-minimal($\xi \neq 0$) aspects. From the equation of motion(EoM) of the rescaled field mode($X_k$) in Eq.(2.98), we compute the dynamical equation of the field mode in the gravitational production scenario as follows:

$$X_{\vec{k}}'' + \left[k^2 + a^2 m_\chi^2 + \frac{a^2 R}{6}(6\xi - 1)\right] X_{\vec{k}} = 0\,. \quad (2.119)$$

For a massless, minimally coupled system, the above dynamical equation takes the well-known form of the *Mukhanov-Sasaki* equation. From Eq.(2.99), neglecting the non-gravitational interaction term $F(\phi)$, we identify the following time-dependent frequency in the gravitational scenario.

$$\omega_k^2(\eta) = k^2 + a^2 m_\chi^2 + \frac{a^2 R}{6}(6\xi - 1)\,. \tag{2.120}$$

Our main focus is on the study of CGPP in cosmologically relevant spacetimes, which describe the early inflation, post-inflationary reheating, and a subsequent hot Big Bang radiation-dominated era. To study the CGPP mechanism in these evolutionary phases of the early universe, it is always convenient to work in the conformal time($\eta$) coordinate. To solve the dynamical equation (2.119), we compute the evolution of the scale factor in conformal time. Following Eq.(2.64), we integrate $\mathcal{H}(\eta) = \frac{a'}{a} = a_{\rm end} H_{\rm end} \left(\frac{a(\eta)}{a_{\rm end}}\right)^{-\frac{(1+3w_\phi)}{2}}$, to obtain the evolution of the scale factor for any general $w_\phi$ as a function of conformal time as

$$a(\eta) = a_{\rm end} \left(\frac{1+3w_\phi}{2|\eta_{\rm end}|}\right)^{\frac{2}{1+3w_\phi}} \left(\eta - \eta_{\rm end} + \frac{2|\eta_{\rm end}|}{1+3w_\phi}\right)^{\frac{2}{1+3w_\phi}}\,, \tag{2.121}$$

with $a_{\rm end} = -\frac{1}{H_{\rm end}\eta_{\rm end}}$, this also gives the evolution of scale factor during inflation ($w_\phi = -1$),

$$a(\eta) = -\frac{1}{H_{\rm end}\,\eta} \quad \text{for} \quad \eta_I < \eta \leq \eta_{\rm end}. \tag{2.122}$$

where $\eta_I$ is the conformal time at the beginning of inflation, $\eta_I \to -\infty$. Considering pure de Sitter inflation, we take the inflationary Hubble scale and the Hubble scale at the end of inflation same. It is trivial to check that during the transition from inflation to reheating, the scale factor and its first derivative change continuously at the junction point, that is, at the end of inflation, $\eta = \eta_{\rm end}$. Using the expression (2.121), we compute the evolution of the non-minimal coupling($\xi$) associated function in (2.120) during reheating as

$$\frac{1}{6}a^2(\eta)R(\eta) = \frac{2(1-3w_\phi)}{(1+3w_\phi)^2} \frac{1}{\left(\eta - 3\frac{(1+w_\phi)}{(1+3w_\phi)}\eta_{\rm end}\right)^2}. \tag{2.123}$$

For a massless, minimally coupled system, this term $\frac{1}{6}a^2(\eta)R(\eta)$ acts as a source term for the gravitational production of the massless scalar system.

**Asymptotic adiabatic spacetime :** Inflationary spacetime has an appealing property to behave almost adiabatically in the asymptotic past and future. In these asymptotic limits, spacetime evolves very slowly, thereby causing the fluctuations on top of this background to be adiabatic in the asymptotic past and future. This asymptotic flatness is an interesting property of the cosmological spacetime. In particular, one defines a dimensionless parameter $|\omega_k'/\omega_k^2|$ to study the departure from the adiabatic limit. It can be shown explicitly as

$\eta \to \pm\infty$, the ratio approaches $|\omega_k'/\omega_k^2| \to 0$ sufficiently fast, satisfying the adiabatic limit. In the process of transition of the universe from early de Sitter to some post-inflationary phase, this adiabaticity condition gets violated ($|\omega_k'/\omega_k^2| >> 1$) at some intermediate point, resulting in the mixing of positive- and negative-frequency modes, which signals particle production. The violation of the adiabaticity condition depends upon how fast the background expansion is occurring, irrespective of the size of the universe. In the asymptotic future limit, although the universe size is large, the spacetime behaves adiabatically due to the slow expansion rate.

In inflationary spacetime, we define the mode function $X_k(\eta)$ in terms of the adiabatic vacuum solutions during inflation and post-inflationary reheating as follows:

$$X_k(\eta) = \begin{cases} X_k^{(\mathrm{inf})}(\eta) & -\infty < \eta \leq \eta_{\mathrm{end}} \\ \\ \alpha_k X_k^{(\mathrm{reh})} + \beta_k X_k^{(\mathrm{reh})*} & \eta \geq \eta_{\mathrm{end}}\,, \end{cases} \tag{2.124}$$

where $X_k^{(\mathrm{inf})}$ and $X_k^{(\mathrm{reh})}$ are the adiabatic vacuum solutions during inflation and reheating, respectively. In the asymptotic past and future limits, they behave as

$$\begin{aligned} X_k^{(\mathrm{inf})} &\sim \frac{1}{\sqrt{2\omega_k^{(\mathrm{inf})}}} e^{-i\omega_k^{(\mathrm{inf})}\eta} \quad \text{as} \quad \eta \to -\infty\,, \\ X_k^{(\mathrm{reh})} &\sim \frac{1}{\sqrt{2\omega_k^{(\mathrm{reh})}}} e^{-i\omega_k^{(\mathrm{reh})}\eta} \quad \text{as} \quad \eta \to \infty\,. \end{aligned} \tag{2.125}$$

These behaviors in (2.125) justify the asymptotic flatness of the inflationary spacetime in the remote past and distant future. The smooth transition of the universe from early de Sitter to the reheating phase demands that the field solution $X_k$ and its first derivative $X_k'$ must be continuous at the junction $\eta = \eta_{\mathrm{end}}$. Using Eq.(2.124), we compute the Bogoliubov coefficients $\alpha_k, \beta_k$ as follows: [69, 99]

$$\begin{aligned} \alpha_k &= i\left(X_k^{(\mathrm{inf})'}(\eta_{\mathrm{end}}) X_k^{(\mathrm{reh})*}(\eta_{\mathrm{end}}) - X_k^{(\mathrm{inf})}(\eta_{\mathrm{end}}) X_k^{(\mathrm{reh})*'}(\eta_{\mathrm{end}})\right)\,, \\ \beta_k &= -i\left(X_k^{(\mathrm{inf})'}(\eta_{\mathrm{end}}) X_k^{(\mathrm{reh})}(\eta_{\mathrm{end}}) - X_k^{(\mathrm{reh})'}(\eta_{\mathrm{end}}) X_k^{(\mathrm{inf})}(\eta_{\mathrm{end}})\right)\,. \end{aligned} \tag{2.126}$$

where ($'$) denotes the derivative with respect to conformal time, and both the vacuum solutions in the above Eq.(2.126) satisfy the Wronskian condition $\left(X_k^{(\mathrm{inf(reh)})} X_k^{(\mathrm{inf(reh)})*'} - X_k^{(\mathrm{inf(reh)})'} X_k^{(\mathrm{inf(reh)})*}\right) = i$ at any time $\eta$.

### 2.7.3 Non-gravitational particle production during preheating: Parametric Resonance Instability

In the treatment of CGPP in the last subsection, we have concentrated on the particle production solely by the gravitational interaction, i.e. the particle production happens only

due to the background expansion. In the present subsection, we are interested in the particle production with non-gravitational coupling between the inflaton and daughter particle fields. Just after the end of inflation, the inflaton field amplitude remains very high($\phi \sim M_{\rm pl}$ ), and consequently, the energy stored in this field is also very high. In this stage, instead of behaving like an individual inflaton particle(quanta), the entire field behaves like a *coherently oscillating inflaton field*. This behavior can also be thought of as a condensate formed by the superposition of all zero-momentum inflaton particles and coherently oscillating in the expanding background. Therefore, any other daughter fields directly/indirectly coupled with this coherently oscillating inflaton will experience a periodic driving force, and if the coupling strength is appropriate, the field amplitude will be resonantly enhanced, thereby causing an explosive particle production. As the inflaton amplitude falls rapidly due to expansion(see Eq.(2.62)), the span of this era is generically very short, proportional to inverse decay width, and happens within a few e-folds. In this short span, explosive particle production takes place through the mechanism known as *parametric resonance instability*. To investigate the parametric resonance phenomenon during preheating, we exploit the dynamical Eq.(2.96) in the presence of the generic interaction $F(\phi)$. Unlike the previous CGPP scenario, while studying the resonant particle production during preheating, it is convenient to work in cosmic time($t$) coordinate. Therefore, switching from $\eta$ to $t$, we write the field dynamical equation (2.96) for a minimally coupled system in terms of the cosmic coordinate as follows:

$$\ddot{\chi}_{\vec{k}} + 3H\dot{\chi}_{\vec{k}} + \left(\frac{k^2}{a^2} + (m_\chi^2 + F(\phi))\right)\chi_{\vec{k}} = 0. \tag{2.127}$$

Here, all the derivatives are defined in terms of the cosmic coordinate. In the following dynamical Eq.(2.127) there is a damping term, $3H\dot{\chi}_{\vec{k}}$, which is non-zero in an expanding background. After rescaling the field $\chi_{\vec{k}}$ and defining $X_{\vec{k}}(t) = a^{\frac{3}{2}}(t)\chi_{\vec{k}}(t)$, and we obtain the following EoM for the rescaled field $X_k$ in cosmic coordinate

$$\ddot{X}_{\vec{k}} + \left(\frac{k^2}{a^2} + \left(m_\chi^2 + F(\phi)\right) - \frac{9}{4}H^2 - \frac{3}{2}\dot{H}\right)X_{\vec{k}} = 0\,. \tag{2.128}$$

**Introducing interaction :**

In this thesis, we shall consider two types of non-gravitational interactions between inflaton and spectator scalar field: i) Three-leg interaction and ii) Four-leg interaction with the massless daughter field, say $\chi$,

$$\mathcal{L}_{int} = \frac{1}{2}\sigma\phi\chi^2 \quad ; \quad \mathcal{L}_{int} = \frac{1}{2}g^2\phi^2\chi^2\,, \tag{2.129}$$

where $(\sigma, g)$ are the coupling constant. In the present study, the generic coupling function of inflaton, $F(\phi)$, will have the forms $F(\phi) = \sigma\phi, g^2\phi^2$ corresponding to three-leg and four-leg type interactions, respectively. In the usual framework of perturbative field theory, such interactions lead to the decay of inflaton $\phi \to \chi\chi, \phi\phi \to \chi\chi$. We consider coupling parameter

regime where the $\chi$-particle production will be non-perturbative [24, 42, 66, 100]. However, such non-perturbative production stops as time advances. We now discuss different features of the resonant dynamics of the field in the Minkowski and the expanding background.

**Characteristics of narrow and broad resonance in Minkowski space :**

In a static background, $a(t) = 1$, neglecting the red shifting of momentum mode, for a massless field($m_\chi = 0$), the EoM for the field mode (2.128) takes the form

$$\begin{aligned} &\ddot{X}_{\vec{k}} + \Big(k^2 + F(\phi)\Big) X_{\vec{k}} = 0 \\ &\Rightarrow \frac{d^2 X_{\vec{k}}}{dz_n^2} + \frac{4\pi^2}{\left(m_\phi^{\text{end}(n)}\right)^2}\left(k^2 + F(\phi)\right) X_{\vec{k}} = 0\,. \end{aligned} \tag{2.130}$$

As stated earlier, the dimensionless time variable, $z_n = \frac{m_\phi^{\text{end}\,(n)} t}{2\pi}$, and the oscillating inflaton field is expressed as $\phi(z_n) = \phi_0 \mathcal{P}(z_n)$ with amplitude $\phi_0(t)$, for a static background, $\phi_0 = \phi_{\text{end}}$. This is the well-known generalized Hill equation [101]. The solution of such an equation is strongly dependent upon two parameters $(k, q)$. Where the emergent $q$-parameter, identified with the term associated with the purely oscillatory part of the equation, is called the resonance strength parameter, and in a static background, those are,

$$q_g = \frac{g\phi_{\text{end}}}{m_\phi^{\text{end}\,(n)}} \quad \text{for} \quad \phi^2\chi^2 \quad ; \quad q_\sigma = \sqrt{\frac{\sigma\phi_{\text{end}}}{\left(m_\phi^{\text{end}\,(n)}\right)^2}} \quad \text{for} \quad \phi\chi^2\,. \tag{2.131}$$

In terms of $q$ parameter, the EoM (2.130) can be expressed as

$$\begin{aligned} &\frac{d^2 X_{\vec{k}}}{dz_n^2} + 4\pi^2\left(\frac{k^2}{\left(m_\phi^{\text{end}\,(n)}\right)^2} + q_g^2\,\mathcal{P}^2(z_n)\right) X_{\vec{k}} = 0 \quad \text{for} \quad F(\phi) = g^2\phi^2 \\ &\frac{d^2 X_{\vec{k}}}{dz_n^2} + 4\pi^2\left(\frac{k^2}{\left(m_\phi^{\text{end}\,(n)}\right)^2} + q_\sigma^2\,\mathcal{P}(z_n)\right) X_{\vec{k}} = 0 \quad \text{for} \quad F(\phi) = \sigma\phi. \end{aligned} \tag{2.132}$$

Employing *Floquet theorem*[24, 101, 102], solutions of such equations show exponential instability $X_k \propto exp(\tilde{\mu}_k z_n)$ over time for a specific range of parameter values $(k, g)$ forming a band(see Fig.(2.12)) for which $Re\big(\tilde{\mu}_k\big) > 0$, where $\tilde{\mu}_k$ is the rescaled Floquet exponent, $\tilde{\mu}_k = 2\pi\mu_k/m_\phi^{\text{end}\,(n)}$ with $\mu_k$, the Floquet exponent.

However, to explain the phenomena of narrow and broad resonance in a static background, we now consider the quartic interaction, $F(\phi) = g^2\phi^2$, only. For $n = 1$ or $w_\phi = 0$, the EoM (2.132) for $F(\phi) = g^2\phi^2$ can be cast in the following interesting form:

$$\frac{d^2 X_{\vec{k}}}{dz_1^2} + 4\pi^2\left(A_k + \frac{q_g^2}{2}\cos(4\pi z_1)\right) X_{\vec{k}} = 0\,, \tag{2.133}$$

where $A_k^g = \left(\frac{k^2}{(m_\phi^{\text{end}\,(1)})^2} + \frac{q_g^2}{2}\right)$. It represents the dynamical equation of an oscillator with a periodically changing frequency. It can also be compared with the famous *Mathieu equation*[66, 102, 103]. The visible difference between the narrow and broad resonance phenomena in a static background is obvious in Fig.(2.10) in the evolution of $\ln(n_k)$. We numerically solve the dynamical equation (2.132) for $F(\phi) = g^2\phi^2$ with the Bunch-Davies initial condition. Using this solution in the number density spectrum (2.114), we obtain the behaviors presented in Fig.(2.10) for the narrow and broad resonance cases in different coupling regimes. In a static Minkowski background, the condition of *narrow resonance* is $g\phi_{\text{end}} < m_\phi^{\text{end}\,(n)}$, implying $q_g < 1$. In this coupling range, in the narrow resonance regime, the field mode evolves as $X_k \propto e^{\tilde{\mu}_k z_n}$, and the number of $\chi$ particles grows as $n_k \propto e^{2\tilde{\mu}_k z_n}$ from Eq.(2.114). In the top right panel of Fig.(2.10), we see that $\ln(n_k)$ grows as a straight line with a constant slope in the narrow resonance regime. The slope of this line gives us information about the growth index, called *Floquet exponent*. As opposed to the narrow resonance case, when the coupling strength satisfies $g\phi_{\text{end}} > m_\phi^{\text{end}\,(n)}$ with $q > 1$, the resonant production happens in the *broad resonance* regime for a broad range of $k$ values. Unlike the straight line growth of $\ln(n_k)$ in a narrow resonance, the number density grows in a step-like manner in a broad resonance case. Interestingly, we see that between two successive sharp jumps of the amplitude of $\ln(n_k)$ in the domain of broad resonance, there is a constant flat line, which is essentially connected to the time-period of the background inflaton oscillation. From (2.132), we get the typical frequency of the $\chi$ field, $\omega_k^2 \propto (k^2 + g^2\phi^2)$. In the broad resonance regime, as $q_g > 1$, the frequency of oscillation of $\chi$ field is much larger than the inflaton frequency $\omega \propto m_\phi^{\text{end}\,(n)}$ in the static background. Within one period of inflaton oscillation, the field $\chi$ makes $\mathcal{O}(q_g)$ oscillations. Therefore, in the broad resonance regime, the amplitude of $\chi_k$ is minimal at the points where its frequency is maximal, $|\chi_k| \propto \frac{1}{\sqrt{2\omega_k(t)}}$, i.e. at $\phi(t) = \phi_{\text{end}}$, and it grows sufficiently fast, as the inflaton amplitude approaches its minima, $\phi(t) = 0$. As previously explained in the context of CGPP, particle production is intimately tied to the violation of the adiabatic condition, $|\dot{\omega}_k/\omega_k^2| >> 1$. In the present broad resonance case, the adiabaticity condition gets violated as the inflaton field tends to cross its zero minima, violating the above condition. Hence, between two successive zero crossings, we get a constant particle number density, as obvious in the bottom right panel of Fig.(2.10) for the broad resonance case. Therefore, the particle number density is considered to be an adiabatic invariant quantity. The maximum momentum mode for which we get the broad resonance phenomena for a particular coupling strength, can be quantified from the adiabaticity violation condition, $\frac{d\omega_k}{dt} \gtrsim \omega_k^2$. This implies that

$$0 \lesssim k^2 \lesssim \left(g^2\phi\,\omega\phi_0\right)^{2/3} - g^2\phi^2. \tag{2.134}$$

where we approximate $\dot{\phi} \approx \omega\phi_0$ in the small $\phi$ regime.
The maximum momentum will be obtained at

$$\phi \equiv \phi_* \simeq \frac{1}{2}\sqrt{\frac{\omega\phi_0}{g}}\,. \tag{2.135}$$

At this field value, the maximum momentum of the produced particles during the preheating stage will be $k_{\rm max} \approx \sqrt{\frac{g\omega\phi_0}{2}}$. In the oscillatory domain of the background inflaton, during the interval $|\phi| \approx 2\phi_*$, the particle's momentum will be smaller than $k_{\rm max}$, but it will be of the same order of $\sqrt{g\omega\phi_0}$. This makes an important estimation of the coupling-dependent typical momentum range of the produced particles in the broad resonance regime[66, 104, 105]

$$0 \leq k \leq \frac{\sqrt{g\omega\phi_0}}{2}\,. \tag{2.136}$$

In Fig.(2.10), we have chosen the particular momentum from the above relation (2.136). For example, with $g = 2 \times 10^{-4}$, the maximum mode being excited in the broad resonance regime is $k \approx 2.4 \times 10^{-5} M_{\rm pl}$.

**Dynamics of Stochastic resonance in an expanding background:**

In the previous discussion, we briefly described the fundamental properties of the narrow and broad resonance phenomena in the static Minkowski background. We have seen that there exists a specific limit of coupling strength, below which the resonance phenomenon happens in the narrow band and above which it happens in the broad resonance regime. Furthermore, we have computed the typical momentum range of the particles in the broad resonance regime.

In reality, though, the background is dynamic, and hence parameters, particularly the $k$ mode, instead of staying in a specific stability/instability band, it transits from one band to another with the expansion. Thus, in the case of an expanding background, the distinction between stability and instability regions disappears, which is a familiar characteristic of *Stochastic resonance* in a dynamical background. Because of the redshifting of each $k$ mode as well as small coupling strength $g$ or $\sigma$, if we choose any mode from a narrow resonance regime in parameter space, we will not be able to see the resonance phenomenon, as it turns out to be almost instantaneous. Therefore, to observe the exponentially growing solution in time, we need to choose a parameter set from a broad resonance regime with sufficiently high coupling strength $g$. In Fig.(2.11), we have shown the behavior of the field $X_k$ and logarithmic number density $\ln(n_k)$ in an expanding background. Unlike the static background broad resonance profile with an uninterrupted step-like growth of $\ln(n_k)$, in the expanding background, the particle number density saturates at some later time due to the gradual loss of the strength of the resonance parameter $q_{g(\sigma)}$. This late-time saturation of the number density is an important feature of *Stochastic resonance*. Another noticeable difference between Minkowskian broad resonance and stochastic resonance is related to the oscillation phase of the daughter field $X_k$. In an expanding background, the oscillation frequency $\omega_k$ of $X_k$, being time-dependent, causes the phase alteration of $X_k$ between two successive zero crossings of the inflaton field. Therefore, unlike the Minkowski resonance, instead of showing a continuous step-like growth, the logarithmic number density function shows a fluctuating growth over a large time domain in an expanding background; this feature is obvious in the right panel of Fig.(2.11). This interesting phenomenon is nicely

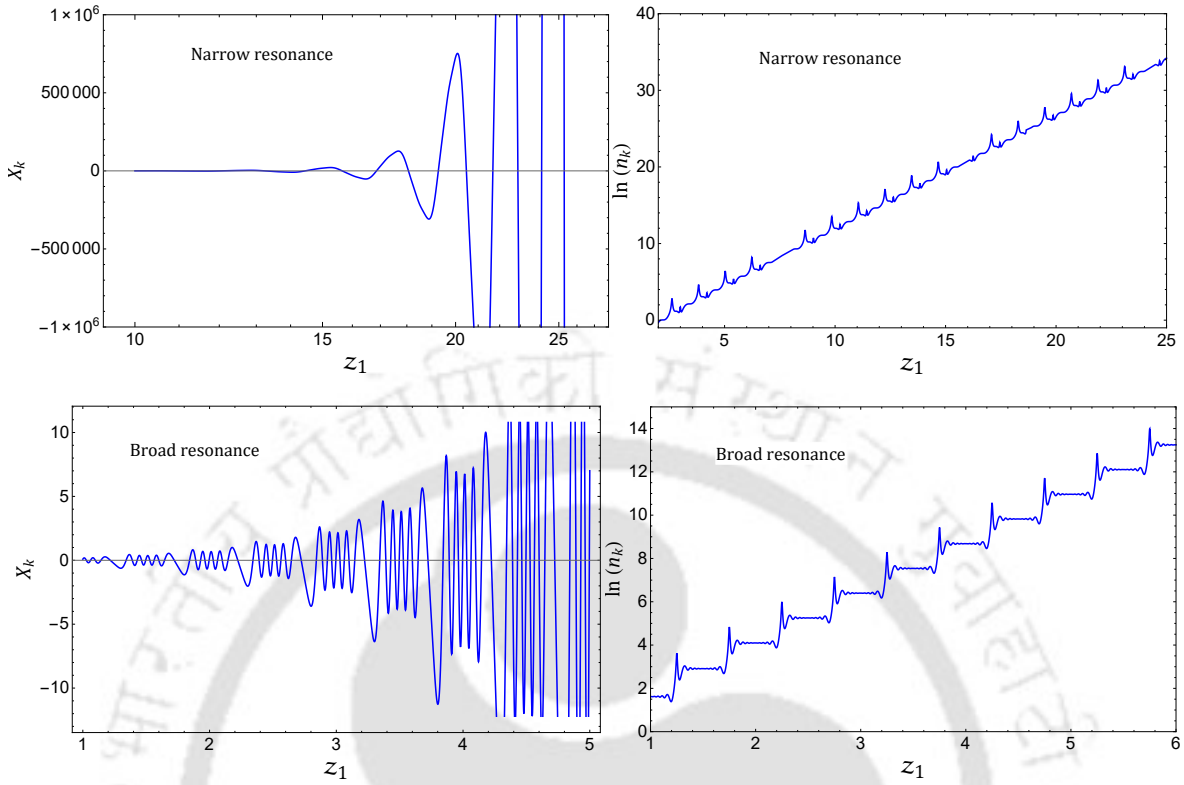


FIGURE 2.10: ***Upper panel:*** *Left plot shows the time evolution of the field mode, and the right plot shows the evolution of the logarithmic occupation number of produced particles $ln(n_k)$ in the narrow resonance regime in the Minkowski space. For narrow resonance, we have chosen the coupling $g = 9 \times 10^{-6}$, or the resonance strength parameter, $q_g \approx 0.7$.* ***Lower panel:*** *Left and right plots show the time evolution of the field mode, and the logarithmic occupation number $ln(n_k)$, respectively, in the broad resonance regime in the Minkowski space. For broad resonance, we have chosen the coupling $g = 2 \times 10^{-4}$, or the resonance strength parameter, $q_g \approx 15.4$, and $k = 6 \times 10^{-6} M_{\rm pl}$. In both panels, the amplitude of $X_k$ is expressed as a dimensionless number. In this figure, we have set $(\alpha, n) = 1$, and the generic interaction $F(\phi) = g^2\phi^2$.*

explained in [66]. In Chapter(4), we shall re-explore all these interesting features of resonant particle production in an expanding background in the language of quantum squeezing.

### Dynamical resonance condition: stability-instability chart

To get an idea of the narrow and broad resonance bands in the momentum space, we construct the coupling vs momentum parameter space during the early reheating phase in a static background ($a(t) = 1$), neglecting the red shifting of momentum mode because of background expansion. Depending upon a specific background, we are to construct this parameter space. Consideration of a static Minkowskian background shows a clear

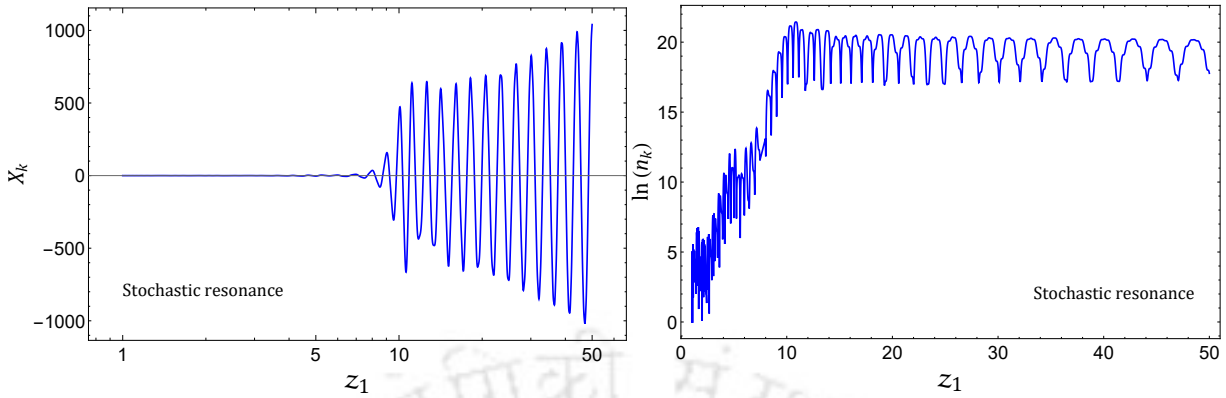


Figure 2.11: *Figure represents the time evolution of the field mode, and the evolution of the logarithmic occupation number $ln(n_k)$ in the expanding background stochastic resonance. We have chosen the coupling $g = 5 \times 10^{-4}$, or the resonance strength parameter, $q_g \approx 38.46$. In this figure also, we set $(\alpha, n) = 1$ with $F(\phi) = g^2\phi^2$.*

distinction between stability and instability regions in the parameter space (see Fig.(2.12)). Any parameter set chosen from the instability region($\mathrm{Re}(\tilde{\mu}_k) > 0$) will lead to an unstable solution interpreted as resonant particle production, and vice versa. Employing the usual Floquet analysis, as described in [24] for the periodically oscillating flat background, we have constructed these $q_{g(\sigma)}$ vs $\tilde{k}$ parameter spaces as shown in Fig.(2.12) for three different models corresponding to background $n = 1, 2, 3$ for two different interactions, where the rescaled momentum mode is defined as $\tilde{k} \equiv (k/m_\phi^{\mathrm{end}\,(n)})$ for any general $n$. The structural difference in parameter space for two different interactions is very evident from the given figure. The *tachyonic instability*$(\omega_k^2 < 0)$[106–109], due to switching sign of $\mathcal{P}(z)$ for trilinear coupling in Eq.(2.132) together with the parametric resonance, cause a very efficient and strong resonance, and because of that, in the lower panel of Fig.(2.12), we notice a very broad instability region in the parameter space for the three given model in comparison with quartic or four-leg interaction.

In the discussion so far, we have talked about the distinctive properties of flat-space resonance and resonance in the non-static background. But the precise condition of resonance for any general $n$ is not specified yet. In the literature, resonance conditions are usually specified by [66, 104, 110], considering $q > 1$, which leads to broad resonance. Otherwise, $q < 1$ gives production in a very narrow resonance regime. Strictly speaking, such a condition defined in flat space is not exactly appropriate, particularly when the driving force namely the inflaton dilutes very fast, $\phi_0 \propto \phi_{\mathrm{end}}(a/a_{\mathrm{end}})^{-3/n+1}$ depending on $n$ values. In the background of such a fast-falling driving force, the resonance parameter $q$ also falls very rapidly as

$$q_g(z_n) = \frac{g\phi_{\mathrm{end}}}{m_\phi^{\mathrm{end}\,(n)}}\left(\frac{z_n}{z_n^{\mathrm{end}}}\right)^{-\frac{1}{n}} \quad ; \quad q_\sigma(z_n) = \sqrt{\frac{\sigma\phi_{\mathrm{end}}}{\left(m_\phi^{\mathrm{end}\,(n)}\right)^2}}\left(\frac{z_n}{z_n^{\mathrm{end}}}\right)^{-\frac{1}{2n}}. \tag{2.137}$$

For those cases, the naive Minkowski resonance condition indeed overestimates the lower limit of the inflaton coupling parameters above which broad-resonance could occur. For the present case with a rapidly decaying $q$-parameter, therefore, we propose a dynamical condition of resonance as follows:

As already stated that the resonant particle production is intimately tied to the violation of the adiabaticity condition, and that is expected to occur while the inflaton crosses zero during its course of oscillation. To achieve significant resonant production within a certain period, one needs to satisfy two important conditions. The first one would be to have the driving force, the oscillating inflaton, executing a few oscillations within the period of interest. The second condition is that within that period the resonance $q$-parameter should remain greater than unity. Combining the preceding two conditions, we state that *for broad resonance to happen while the resonance parameter $q$ time-evolving from its higher initial value to unity, it must execute at least one oscillation.* Bearing this dynamical condition of broad resonance in mind, we derive the lower bound of the inflaton couplings for a general background EoS.

To compute the number of oscillations required for $q$-parameter to change from its large initial value at the end of inflation to unity, we measure the dimensionless time-period of the oscillating inflaton as $z_n^{(\omega)} = m_\phi^{\mathrm{end}\,(n)}/\omega$, where $\omega$ is calculated at $\phi_0 = M_{\rm pl}$. With respect to this, the number of oscillations say $N_{\rm osc}$ becomes,

$$N_{\rm osc} = \frac{z_n - z_n^{\rm end}}{z_n^{(\omega)}} = \begin{cases} \frac{z_n^{\rm end}}{z_n^{(\omega)}} \left( \left( \frac{g\phi_{\rm end}}{m_\phi^{\mathrm{end}\,(n)}} \right)^n - 1 \right) \\ \frac{z_n^{\rm end}}{z_n^{(\omega)}} \left( \left( \frac{\sqrt{\sigma}\phi_{\rm end}}{m_\phi^{\mathrm{end}\,(n)}} \right)^{2n} - 1 \right) \end{cases} . \tag{2.138}$$

This dimensionless time-period $z_n^{(\omega)}$ matches very well with the numerically calculated one. Hence, to achieve efficient resonant production in a broad resonance regime, the minimum criterion that must be fulfilled is $N_{\rm osc} > 1$. Having this criterion, from (2.138) we get the lower bound of the coupling parameter for two interactions as [35, 111]

$$\begin{aligned} g &> \frac{m_\phi^{\mathrm{end}\,(n)}}{\phi_{\rm end}} \left[ 1 + \frac{z_n^{(\omega)}}{z_n^{\rm end}} \right]^{\frac{1}{n}} \\ \sigma &> \frac{\left( m_\phi^{\mathrm{end}\,(n)} \right)^2}{\phi_{\rm end}} \left[ 1 + \frac{z_n^{(\omega)}}{z_n^{\rm end}} \right]^{\frac{1}{n}} . \end{aligned} \tag{2.139}$$

It is very interesting to note that the lower limit of the coupling strength $g$ to achieve efficient resonance in an expanding background also depends upon the time period of background oscillation, besides its dependence on $\phi_{\rm end}$ and $m_\phi^{\mathrm{end}\,(n)}$. Therefore, this limiting value varies from one EoS to another depending upon $\phi_{\rm end}, m_\phi^{\mathrm{end}\,(n)}$ and time-period $z_n^{(\omega)}$.

The above condition sets the minimum possible coupling parameter that one requires at the beginning of the reheating to have efficient broad parametric resonance in an expanding background. However, due to the expanding background, any particular resonant mode $k$

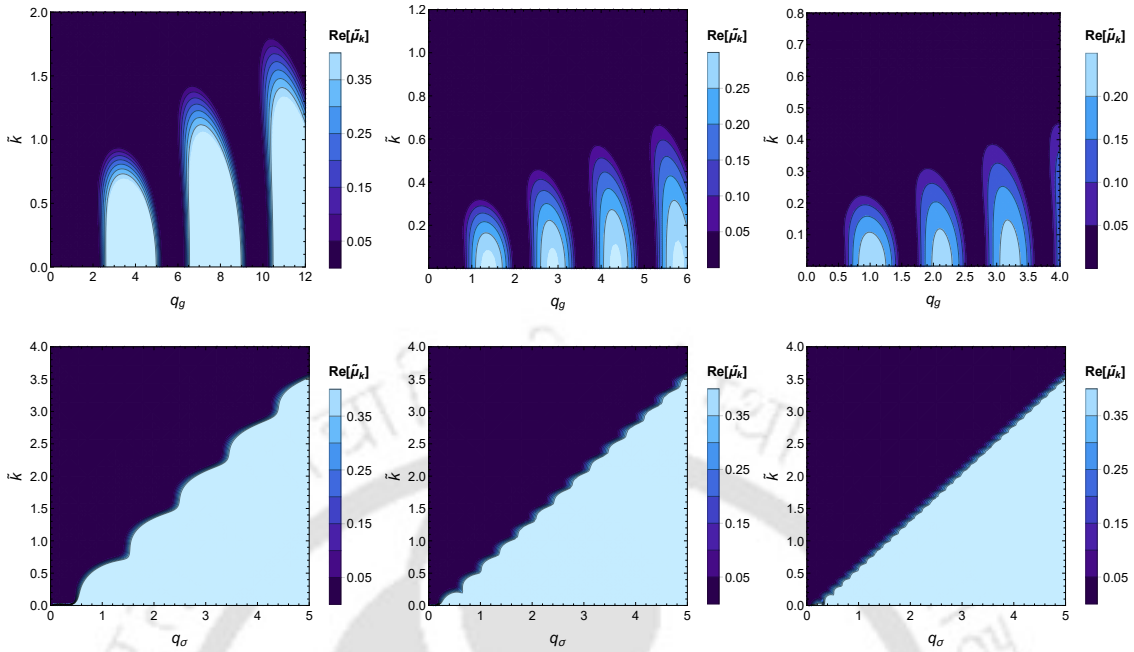


Figure 2.12: ***Upper Panel:*** *Figure represents the flat space parameter space for the model $n = 1$, $n = 2$ and $n = 3$ respectively from the left corresponding to $g^2\phi^2\chi^2$ interaction.* ***Lower Panel :*** *Figure represents the flat space parameter space for the model $n = 1$, $n = 2$ and $n = 3$ respectively from the left corresponding to $\sigma\phi\chi^2$ interaction.*

also becomes non-resonant around its characteristic time scale. For example, in the present context, minimum dimensionless coupling strengths which are necessary to initiate an efficient resonance process are found to be $g = \sigma/m_\phi^{\mathrm{end}\,(n)} = 6 \times 10^{-5}, 4 \times 10^{-5}, 3.77 \times 10^{-5}$ for $n = 1, 2, 3$ respectively. It is important to mention that these lower bounds of coupling parameters are obtained for parametric resonance cases. But for three-leg type interaction, efficient production happens for coupling strength even lower than the given bound due to the presence of the additional tachyonic growth in the system.

Having investigated the non-perturbative aspects of reheating dynamics with a certain degree of rigor, we shall now proceed to study the theory of inflationary cosmological perturbations, which plays a crucial role in connecting the inflationary parameters to the late-time CMB observables. The study of cosmological perturbation theory is also important to understand the dynamics of the real universe, which has tiny perturbations, rather than being perfectly homogeneous and isotropic.

## 2.8 Theory of Inflationary Cosmological Perturbations

Besides generating an isotropic, homogeneous universe at large scales, the superluminal expansion during inflation also plays an instrumental role in stretching out the tiny, sub-

horizon fluctuations to a large cosmological scale, which are believed to seed the large-scale structure of the universe that we observe today. In the last section, we have already talked about the dynamics of a spectator scalar fluctuation($\chi$), generated during inflation, and evolved through post-inflationary phases. The existence of spectator fluctuations leads us to consider the inflaton fluctuations($\delta\phi(\vec{x},\, t)$) on top of the classical, homogeneous inflaton($\phi(t)$) background. However, inflaton fluctuations are somewhat special in comparison with the other spectator fluctuations. During inflation, as the inflaton is the dominant energy component of the universe, its fluctuations naturally generate perturbations in the stress-energy tensor $T^{\phi}_{\mu\nu}$, $\delta\phi \Rightarrow \delta T^{\phi}_{\mu\nu}$. Again, the perturbation in the stress tensor perturbs the spacetime metric through Einstein's equations, $\delta T^{\phi}_{\mu\nu} \Rightarrow \delta G_{\mu\nu} \Rightarrow \delta g_{\mu\nu}$. On the other hand, the dynamics of the inflaton fluctuation is influenced by the perturbed metric through the Klein-Gordon equation of $\delta\phi$, $\delta g_{\mu\nu} \Rightarrow \delta\left(-\partial_\mu\partial^\mu\phi + \frac{\partial V}{\partial\phi}\right) = 0 \Rightarrow \delta\phi$. This logic chain makes us infer that the perturbations in the inflaton field and metric are strongly intertwined with each other, $\delta\phi \Longleftrightarrow \delta g_{\mu\nu}$, and hence, they have to be studied together. If there is a slight disturbance in the background field, it will spread over the whole spacetime by perturbing the metric. The perturbed stress-energy tensor, anyway, generates perturbations in the background energy density, and these primordial density perturbations are responsible for the CMB temperature fluctuations:

$$\delta\phi(\vec{x},\, t) \Rightarrow \delta\rho_\phi(\vec{x},\, t) \Rightarrow \Delta T(\vec{x})\,. \tag{2.140}$$

As long as these fluctuations are tiny, $\delta\phi(\vec{x},\, t) << \phi(t)$, the standard linear perturbation theory suffices to study the evolution of the perturbed quantities.

### 2.8.1 The metric perturbations

The tiny inflaton fluctuations cause small metric perturbations $\delta g_{\mu\nu}$ around the unperturbed background $\bar{g}_{\mu\nu}$, $\delta g_{\mu\nu} << \bar{g}_{\mu\nu}$. We write the most general perturbed FLRW metric in conformal coordinateas[21]

$$ds^2 = a^2(\eta)\left[-(1+2\Phi)d\eta^2 + 2B_i dx^i dx^0 + (\delta_{ij} + h_{ij})\, dx^i dx^j\right]\,. \tag{2.141}$$

where $\Phi$, $B_i$ and $h_{ij}$ are scalar, vector and tensor metric perturbations, respectively, and these are functions of space and time. Here, the Latin indices $i$, $j$ stand for the spatial components, taking $(i,\, j) = 1, 2, 3$, and the Latin indices are on spatial vectors and tensors are raised and lowered by the flat metric $\delta_{ij}$, for example, $h^i_i = \delta^{ij}h_{ij}$.

**Scalar-Vector-Tensor(SVT) decomposition of metric perturbations:**

It is a standard practice to perform a scalar-vector-tensor(SVT) decomposition of the metric perturbations. For the vector perturbations $B_i$, we can express any 3-vector as a linear combination of the gradient of a scalar and a divergenceless vector

$$B_i = \underbrace{\partial_i B}_{\text{scalar}} + \underbrace{\hat{B}_i}_{\text{vector}}\,, \tag{2.142}$$

with $\partial^i \hat{B}_i = 0$. Similarly, any rank two symmetric tensor can be expressed as

$$h_{ij} = \underbrace{2\Psi\delta_{ij} + 2D_{ij}E}_{\text{scalar}} + \underbrace{2\frac{1}{2}\left(\partial_i \hat{E}_j + \partial_j \hat{E}_i\right)}_{\text{vector}} + \underbrace{\hat{h}_{ij}}_{\text{tensor}}, \tag{2.143}$$

where the operator $D_{ij} = \left(\partial_i\partial_j - \frac{1}{3}\delta_{ij}\nabla^2\right)$. Likewise the divergenceless vector $\hat{B}_i$, the hatted quantities satisfy, i.e. $\partial^i \hat{E}_i = 0$, and $\partial^i \hat{h}_{ij} = 0$. Additionally, the tensor components are traceless, $\hat{h}^i_i = 0$. In a $D$-dimensional spacetime, a symmetric tensor has $\frac{D(D+1)}{2}$ degrees of freedom. For $D = 4$, $g_{\mu\nu}$ has 10 degrees of freedom. These 10 degrees of freedom can be decomposed into SVT degrees of freedom as follows:

- 4 scalars: $\Phi$, $\Psi$, $B$, $E$
- 4 vectors: $\hat{B}_i$, $\hat{E}_i$
- 2 tensors: $\hat{h}_{ij}$

This SVT decomposition is a powerful technique because Einstein equations for scalars, vectors and tensors don't mix at the linear order, and we, therefore, can study their evolution separately. In this thesis, we shall focus on the scalar and tensor perturbations, which are the two most important predictions of inflation. Vector perturbations are not produced by inflation; even if they were, they would decay quickly with the expansion of the universe[112]. Finally, we re-express the perturbed metric (2.141) in terms of scalar and tensor degrees of freedom as follows:

$$ds^2 = a^2(\eta)\left[-(1+2\Phi)d\eta^2 + 2\partial_i B dx^i dx^0 + \left((1+2\Psi)\delta_{ij} + 2D_{ij}E + +\hat{h}_{ij}\right)dx^i dx^j\right]. \tag{2.144}$$

Using the property $g^{\mu\alpha}g_{\alpha\nu} = \delta^\mu_\nu$ we find the inverse metric

$$g^{\mu\nu} = a^{-2}(\eta)\begin{pmatrix} (-1+2\Phi) & \partial^i B \\ \partial^i B & (1-2\Psi)\delta^{ij} - 2D^{ij}E \end{pmatrix}. \tag{2.145}$$

**Perturbed Ricci tensor and Ricci scalar:**

In the perturbed FLRW universe with the metric (2.144), we compute the different components of the perturbed Ricci tensor($\delta R_{\mu\nu}$) by varying the expression (2.3)

$$\delta R_{\mu\nu} = \partial_\alpha \delta\Gamma^\alpha_{\mu\nu} - \partial_\nu \delta\Gamma^\alpha_{\mu\alpha} + \delta\Gamma^\alpha_{\alpha\beta}\Gamma^\beta_{\mu\nu} + \Gamma^\alpha_{\alpha\beta}\delta\Gamma^\beta_{\mu\nu} - \delta\Gamma^\beta_{\mu\alpha}\Gamma^\alpha_{\nu\beta} - \Gamma^\beta_{\mu\alpha}\delta\Gamma^\alpha_{\nu\beta}. \tag{2.146}$$

With the following unperturbed background components of $R_{\mu\nu}$

$$R_{00} = -3\frac{a''}{a} + 3\left(\frac{a'}{a}\right)^2,\ R_{0i} = 0,\ R_{ij} = \left(\frac{a''}{a} + \left(\frac{a'}{a}\right)^2\right)\delta_{ij}, \tag{2.147}$$

we find the perturbed components up to the linear order as follows[31]:

$$\delta R_{00} = \frac{a'}{a}\partial_i\partial^i B + \partial_i\partial^i B' + \partial_i\partial^i\Phi - 3\Psi'' + 3\frac{a'}{a}\Phi',$$
$$\delta R_{0i} = \frac{a''}{a}\partial_i B + \left(\frac{a'}{a}\right)^2\partial_i B - 2\partial_i\Psi' + 2\frac{a'}{a}\partial_i\Phi + \partial_k D_i^k E',$$
$$\delta R_{ij} = \left(-\frac{a'}{a}\Phi' + 5\frac{a'}{a}\Psi' - 2\frac{a''}{a}\Phi - 2\left(\frac{a'}{a}\right)^2\Phi + 2\frac{a''}{a}\Psi - +2\left(\frac{a'}{a}\right)^2\Psi + \Psi'' - \partial_k\partial^k\Psi - \frac{a'}{a}\partial_k\partial^k B\right)\delta_{ij}$$
$$- \partial_i\partial_j B' + 2\frac{a'}{a}D_{ij}E' + 2\frac{a''}{a}D_{ij}E + 2\left(\frac{a'}{a}\right)^2 D_{ij}E + D_{ij}E'' - \partial_i\partial_j\Psi - \partial_i\partial_j\Phi - 2\frac{a'}{a}\partial_i\partial_j B$$
$$+ \partial_k\partial_i D_j^k E + \partial_k\partial_j D_i^k E - \partial_k\partial^k D_{ij}E\,. \tag{2.148}$$

With the perturbed components of $\delta R_{\mu\nu}$, we compute the first order perturbed Ricci scalar($\delta R$) as[31]

$$a^2\delta R = \delta g^{\mu\alpha}R_{\alpha\mu} + g^{\mu\alpha}\delta R_{\alpha\mu}$$
$$= \left(-6\frac{a'}{a}\partial_i\partial^i B - \partial_i\partial^i B' - 2\partial_i\partial^i\Phi + 6\Psi'' - 6\frac{a'}{a}\Phi' + 18\frac{a'}{a}\Psi' - 12\frac{a''}{a}\Phi - 4\partial_i\partial^i\Psi + 2\partial_k\partial^i D_i^k E\right). \tag{2.149}$$

From the above expression of the perturbed Ricci scalar (2.149), we can identify the intrinsic curvature of the constant time hypersurfaces as

$$a^2 R_{(3)} = -4\partial_i\partial^i\Psi + 2\partial_k\partial^i D_i^k E = -4\nabla^2\left(\Psi - \frac{1}{3}\nabla^2 E\right). \tag{2.150}$$

This is the three-dimensional Ricci scalar associated with the spatial part $g_{ij}$ of the perturbed metric (2.144) for scalar perturbations, where we define the curvature perturbation as $\left(\Psi - \frac{1}{3}\nabla^2 E\right)$ [113, 114].

**The Gauge problem and Gauge transformation:**

While defining these metric perturbations, we encounter an important subtlety associated with the choice of coordinates, or *gauge choice*. These perturbations in (2.141) are not uniquely defined; rather, they depend upon the choice of coordinates. This coordinate dependence makes it ambiguous to distinguish clearly between the genuine, real perturbation and the fake perturbation arising from a poor choice of coordinates, even if the background is perfectly homogeneous. This is known as *Gauge problem*. Let's illustrate this particular point in a quantitative approach.

- **Gauge transformations:** We consider the coordinate transformation

$$X^\mu \to \tilde{X}^\mu \equiv X^\mu + \xi^\mu(\eta, \vec{x}), \text{ where } \xi^i \equiv \partial^i L(x^\mu) + \hat{L}^i \text{ with } \partial_i\hat{L}^i = 0\,. \tag{2.151}$$

where $\xi^\mu$ is an infinitesimal shift in the spacetime coordinate. Utilizing the invariance of the spacetime interval under general coordinate transformation, we write

$$ds^2 = g_{\mu\nu}dX^\mu dX^\nu = \tilde{g}_{\alpha\beta}(\tilde{X}^\mu)d\tilde{X}^\alpha d\tilde{X}^\beta\,. \tag{2.152}$$

From (2.152), we write the transformation rules of the metric in the new set of coordinates($\tilde{g}_{\mu\nu}$) in terms of the old coordinates($g_{\mu\nu}$) as

$$g_{\mu\nu}(X) = \frac{\partial\tilde{X}^\alpha}{\partial X^\mu}\frac{\partial\tilde{X}^\beta}{\partial X^\nu}\tilde{g}_{\alpha\beta}(\tilde{X})\,. \tag{2.153}$$

This leads to the following transformation laws of the scalar and tensor perturbation variables

$$\begin{aligned}
&\tilde{\Phi} \to \Phi - \xi^{0\prime} - \mathcal{H}\xi^0,\\
&\tilde{B} \to B + \xi^0 - L',\\
&\tilde{\Psi} \to \Psi - \frac{1}{3}\nabla^2 L - \mathcal{H}\xi^0,\\
&\tilde{E} \to E - L,\\
&\hat{h}_{ij} \to h_{ij}\,.
\end{aligned} \tag{2.154}$$

Interestingly, all the perturbation variables, transforming under a gauge transformation, do not represent any physical observable; the only exception is the tensor perturbations($\hat{h}_{ij}$), which are gauge-independent and propagate as primordial gravitational waves in space.

- **Gauge-invariant perturbations:** To eliminate the ambiguous issue of the Gauge problem, one of the ways is to define Gauge-invariant variables that will remain invariant under general coordinate transformations. These are the *Bardeen variables*[112, 115]

$$\Phi_{\rm GI} \equiv \Phi + \mathcal{H}\,(B - E') + (B - E')'\,,\ \Psi_{\rm GI} \equiv -\Psi - \mathcal{H}\,(B - E') + \frac{1}{3}\nabla^2 E\,. \tag{2.155}$$

These Gauge-invariant *Bardeen variables* are considered to be real spacetime perturbations, which can't be removed by a gauge transformation.

### 2.8.2 Matter perturbations

The energy-momentum tensor of matter in an isotropic, homogeneous universe takes the form of an ideal fluid

$$\bar{T}^\mu_\nu = (\bar{\rho} + \bar{P})\bar{U}^\mu\bar{U}_\nu + \bar{P}\delta^\mu_\nu\,, \tag{2.156}$$

where $\bar{\rho}$, $\bar{P}$ are background unperturbed energy and pressure density and $\bar{U}^\mu$ are relative velocity between fluid and observer, for comoving observer, four-velocity becomes $\bar{U}^\mu =$

$-a^{-1}\delta^{\mu}_{0}$ and $\bar{U}_{\mu} = a^{1}\delta^{0}_{\mu}$, which satisfy $\bar{U}^{\mu}\bar{U}_{\mu} = -1$. Perturbing this stress tensor of the perfect fluid we have $T^{\mu}_{\nu} = \bar{T}^{\mu}_{\nu} + \delta T^{\mu}_{\nu}$, where $\delta T^{\mu}_{\nu}$ is the perturbed part of the stress tensor.

$$\delta T^{\mu}_{\nu} = \underbrace{(\delta\rho + \delta P)}_{\text{perturbed energy and pressure}} \bar{U}^{\mu}\bar{U}_{\nu} + (\bar{\rho} + \bar{P}) \underbrace{\left(\delta U^{\mu}\bar{U}_{\nu} + \bar{U}^{\mu}\delta U_{\nu}\right)}_{\text{perturbed velocity part}} + \delta P\delta^{\mu}_{\nu} + \Pi^{\mu}_{\nu} \tag{2.157}$$

where $\Pi^{\mu}_{\nu}$ is the *anisotropic stress tensor*. The spatial part of this tensor can be chosen to be traceless, $\Pi^{i}_{i}$=0, since the effect can be taken care of by redefining the isotropic pressure, $P$. This anisotropic stress tensor can also be taken to be orthogonal to the velocity vector $U^{\mu}$, $U^{\mu}\Pi_{\mu\nu} = 0$. Using the property $U^{\mu}U_{\mu} = -1$ we calculate $\delta g_{\mu\nu}\bar{U}^{\mu}\bar{U}^{\nu} + 2\bar{U}_{\mu}\delta U^{\mu} = 0$. Subject to this condition, we find $\delta U^{0} = a^{-1}\Phi$. Writing $\delta U^{i} = -\frac{v^{i}}{a}$ we get

$$U^{\mu} = a^{-1}\left[(-1 + \Phi), -v^{i}\right] , \tag{2.158}$$

where $v^{i} = dx^{i}/d\eta$ is the coordinate velocity. Using the condition $U^{\mu}U_{\mu} = -1$ we find up to the linear order of perturbation

$$U_{\mu} = a\left[(1 + \Phi) - (\partial_{i}B + v_{i})\right] . \tag{2.159}$$

Utilizing the equations (2.158) and (2.159) in (2.157) we find up to the linear order of perturbation

$$\begin{aligned}
\delta T^{0}_{0} &= -\delta\rho, \\
\delta T^{i}_{0} &= -\left(\bar{\rho} + \bar{P}\right) v^{i} \equiv -q^{i}, \\
\delta T^{0}_{i} &= \left(\bar{\rho} + \bar{P}\right)\left(\partial_{i}B + v_{i}\right) , \\
\delta T^{i}_{j} &= \delta P\delta^{i}_{j} + \Pi^{i}_{j} ,
\end{aligned} \tag{2.160}$$

where $q^{i}$ is the momentum density. In the multicomponent universe, the total stress-energy tensor is the sum of the stress tensors of all the components; $T_{\mu\nu} = \sum_{\rm I} T^{\rm I}_{\mu\nu}$, where "I" varies over all the fluid components. This implies

$$\delta\rho = \sum_{\rm I}\delta\rho_{\rm I},\ \ \delta P = \sum_{\rm I}\delta P_{\rm I},\ \ q^{i} = \sum_{\rm I} q^{i}_{\rm I},\ \ \Pi^{ij} = \sum_{\rm I}\Pi^{ij}_{\rm I} . \tag{2.161}$$

Likewise Eq.(2.153), the stress-energy tensor transforms under general coordinate transformation as

$$T^{\mu}_{\nu}(X) = \frac{\partial\tilde{X}^{\mu}}{\partial X^{\alpha}}\frac{\partial\tilde{X}^{\beta}}{\partial X^{\nu}}\tilde{T}^{\alpha}_{\beta}(\tilde{X}) . \tag{2.162}$$

This leads to the transformation laws of the different components as follows:

$$\begin{aligned}
\tilde{\delta\rho} &\to \delta\rho - \xi^{0}\bar{\rho}' , \\
\tilde{\delta P} &\to \delta P - \xi^{0}\bar{P}' , \\
\tilde{q}_{i} &\to q_{i} + \left(\bar{\rho} + \bar{P}\right) L'_{i} ,
\end{aligned}$$

$$\tilde{v}_i \to v_i + L_i' \,,$$
$$\tilde{\Pi}_{ij} \to \Pi_{ij} \,. \tag{2.163}$$

Likewise the Gauge-invariant *Bardeen variables* in (2.155), we write one popular Gauge-invariant quantity[21, 30, 31]

$$\Delta \equiv \frac{\delta\rho}{\bar{\rho}} + \frac{\bar{\rho}'}{\bar{\rho}}\,(v + B) \,, \tag{2.164}$$

where $v_i = \partial_i v$. This "$\Delta$" is called the *comoving gauge density contrast*. Combining equations (2.150), (2.154), and (2.163), we construct the gauge-invariant comoving curvature perturbation as[31, 113, 114]

$$\mathcal{R} = \left(\Psi - \frac{1}{3}\nabla^2 E\right) + \mathcal{H}(B + v). \tag{2.165}$$

In the latter part of the discussion, we shall show that this gauge-invariant definition of curvature perturbation is connected to the inflaton fluctuation($\delta\phi$) for a particular gauge choice(see Eq.(2.176)).

**Adiabatic perturbations:**

In the universe, filled with multiple fluid components, the *adiabatic perturbations* correspond to the perturbations due to a common, local shift of all background quantities for all the fluids. The *adiabatic perturbations* have the property that the local state of matter, charaterized by the energy or pressure density, at some spacetime point, $(\eta, \vec{x})$ in the perturbed universe, is the same as in the background universe at some slightly different time $\eta + \delta\eta(\vec{x})$. The adiabatic density perturbations are defined as

$$\delta\rho_{\rm I}(\eta, \vec{x}) \equiv \bar{\rho}_{\rm I}(\eta + \delta\eta(\vec{x})) - \bar{\rho}_{\rm I}(\eta) = \bar{\rho}_{\rm I}'\delta\eta(\vec{x}) \,. \tag{2.166}$$

The adiabatic perturbations define the common local shift of time for all the components. Hence, we have

$$\delta\eta = \frac{\delta\rho_{\rm I}}{\bar{\rho}_{\rm I}'} = \frac{\delta\rho_{\rm J}}{\bar{\rho}_{\rm J}'}, \text{ where I, J are two different fluids.} \tag{2.167}$$

In the absence of any energy transfer between the fluid components at the background level, each component individually follows the energy continuity equation (2.7). From the continuity equation, $\bar{\rho}_{\rm I}' = -3\mathcal{H}\,(1 + w_{\rm I})\,\bar{\rho}_{\rm I}$ for a particular component, we, therefore, write

$$\frac{\delta_{\rm I}}{(1 + w_{\rm I})} = \frac{\delta_{\rm J}}{(1 + w_{\rm J})} \quad \text{for all species I and J.} \tag{2.168}$$

where the fractional density contrast is defined as $\delta_{\rm I} \equiv \frac{\delta\rho_{\rm I}}{\bar{\rho}_{\rm I}}$. In the case of adiabatic perturbations, the total density perturbation can be written as

$$\delta\rho_{\rm tot} = \bar{\rho}_{\rm tot}\delta_{\rm tot} = \sum_{\rm I} \bar{\rho}_{\rm I}\delta_{\rm I} \,. \tag{2.169}$$

This expression shows that for adiabatic fluctuations, the total density perturbation is governed by the dominant background component since all the $\delta_{\rm I}$ are comparable, as obvious in (2.167).

**Isocurvature perturbations:**

Unlike the adiabatic perturbations, isocurvature perturbations only correspond to the perturbations between the different components. From Eq.(2.168), for isocurvature fluctuations, the given ratio will change from one species to another. It defines the isocurvature fluctuations as

$$\mathcal{S}_{\rm IJ} \equiv \frac{\delta_{\rm I}}{(1+w_{\rm I})} - \frac{\delta_{\rm J}}{(1+w_{\rm J})}\,. \tag{2.170}$$

The following definitions, therefore, imply that for a single-field inflationary scenario, the perturbations produced during inflation are of the adiabatic type. However, for multifield inflationary models, isocurvature perturbations are expected to be generated, and they might even be cross-correlated to the adiabatic ones[116–118]. In Chapter(6), we shall thoroughly investigate the generation of isocurvature perturbations by the spectator scalar field during inflation and post-inflationary reheating. The current observational constraint on the isocurvature perturbation amplitude in turn constrains the instability growth of the spectator field. The CMB scale isocurvature bound is indeed an important large-scale observational bound that must be respected while studying the dynamics of multiple fields in the early universe.

**Perturbed Stress energy tensor of the inflaton:**

As already explained that the metric perturbations are induced by the energy-momentum tensor of the dominating fluid in the background. In the case of a single-field inflationary model, the perturbation of the inflaton stress tensor leads to the metric perturbations. Perturbing the energy-momentum tensor of the inflaton (2.44), we write

$$\begin{aligned}\delta T^{\phi}_{\mu\nu} = {}& \partial_\mu\delta\phi\partial_\nu\phi + \partial_\mu\phi\partial_\nu\delta\phi - \delta g_{\mu\nu}\left(\frac{1}{2}g^{\alpha\beta}\partial_\alpha\phi\partial_\beta\phi + V(\phi)\right)\\ & - g_{\mu\nu}\left(\frac{1}{2}\delta g^{\alpha\beta}\partial_\alpha\phi\partial_\beta\phi + g^{\alpha\beta}\partial_\alpha\delta\phi\partial_\beta\phi + \frac{\partial V}{\partial\phi}\delta\phi\right)\,.\end{aligned} \tag{2.171}$$

We write the mixed components as

$$\delta T^{\mu(\phi)}_{\nu} = \delta g^{\mu\alpha}T^{(\phi)}_{\alpha\nu} + g^{\mu\alpha}\delta T^{(\phi)}_{\alpha\nu}\,. \tag{2.172}$$

Equation (2.172) leads to the following perturbed components of the inflaton energy-momentum tensor up to the linear order.

$$\delta T^{0(\phi)}_{0} = \Phi\phi'^{2} - \delta\phi'\phi' - a^2\delta\phi\frac{\partial V}{\partial\phi},$$

$$\delta T_0^{i(\phi)} = \partial^i B\phi'^2 + \partial^i\delta\phi',$$
$$\delta T_i^{0(\phi)} = -\frac{\phi'}{a^2}\partial_i(\delta\phi),$$
$$\delta T_j^{i(\phi)} = \left(-\Phi\phi'^2 + \delta\phi'\phi' - a^2\delta\phi\frac{\partial V}{\partial\phi}\right)\delta^i_j\,. \tag{2.173}$$

### 2.8.3 Scalar curvature perturbations: Connection with inflaton fluctuations

At this point, we can show an interesting connection between the inflaton fluctuation $\delta\phi$ and the gauge-invariant curvature perturbation $\mathcal{R}$. If we choose to work in the spatially flat gauge, the definition (2.165) becomes

$$\mathcal{R} = \left(\Psi - \frac{1}{3}\nabla^2 E\right) + \mathcal{H}(B+v) \xrightarrow{\text{spatially flat gauge}} \mathcal{H}(B+v)\,. \tag{2.174}$$

In spatially flat gauge, we set $\Psi = E = 0$. From the equation (2.160), it is clear that the combination $(B+v)$ appears in the off-diagonal elements $\delta T_i^0$ of the perturbed stress tensor of the fluid. Comparing with the linear perturbation $\delta T_i^{0(\phi)}$ of background inflaton field (2.173), we find

$$(B+v) = -\frac{\delta\phi}{\phi'}\,. \tag{2.175}$$

We write $v_i = \partial_i v$, and $\phi(\eta)$ is the homogeneous background field, only depending upon time. In the inflaton-dominated background, recalling Eq.(2.45), we find the sum of unperturbed pressure and energy density $\left(\bar{\rho}+\bar{P}\right) = \left(\frac{\phi'}{a}\right)^2$. Therefore, in the spatially flat gauge, we can conveniently express the curvature perturbation in terms of the inflaton fluctuation

$$\mathcal{R} = -\frac{\mathcal{H}}{\phi'}\delta\phi\,. \tag{2.176}$$

This is an extremely important relation, connecting the primordial density perturbation with the scalar curvature perturbation. This expression will be utilized to derive the relationship between CMB observables and the inflationary slow-roll parameters. In the next part of the discussion, we shall study the dynamics of the inflaton fluctuation within the framework of a massless scalar field evolution in an expanding background, as described in Section(2.7).

It is justified to write the inflaton field as $\phi(\eta,\vec{x}) = \phi(\eta)+\delta\phi(\eta,\vec{x})$, where the fluctuation $\delta\phi$ on top of the homogeneous background $\phi(\eta)$ behaves like a massless fluctuation which follows the dynamical EoM (2.98) for vanishing $m_\chi, \xi, F(\phi)$. By expanding the inflaton Lagrangian (2.41) to the quadratic order in the perturbation $\delta\phi$, we write

$$S^{(2)} = \frac{1}{2}\int d\eta\, d^3x \left((f')^2 - (\nabla f)^2 + \left(\frac{a''}{a} - a^2\frac{\partial^2 V(\phi)}{\partial\phi^2}\right)f^2\right)\,. \tag{2.177}$$

where the rescaled field is defined as $f(\eta,\vec{x}) = a(\eta)\delta\phi(\eta,\vec{x})$. During slow-roll inflation, we have $\eta_{\rm V} = M_{\rm pl}^2\left(\frac{V''}{V}\right) << 1$.(see Eq.(2.55)). Hence, $\frac{a''}{a} = 2a^2H^2 >> a^2V''$, as the constant de Sitter Hubble scale is very high during inflation. Dropping the $V''$ term we write the action

$$S^{(2)} = \frac{1}{2}\int d\eta\, d^3x \left((f')^2 - (\nabla f)^2 + \frac{a''}{a}f^2\right) . \tag{2.178}$$

From the Euler-Lagrange equation, we find the evolution equation of each Fourier mode of $\delta\phi$

$$f_k'' + \left(k^2 - \frac{a''}{a}\right) f_k = 0\,. \tag{2.179}$$

This is the well-known *Mukhanov-Sasaki* equation, which is also followed by any massless, minimally coupled spectator fluctuation(see Eq.(2.98)). With the Bunch-Davies initial vacuum state of each Fourier mode $f_k = \frac{1}{\sqrt{2k}}e^{-ik\eta}$ as $\eta \to -\infty$ and $k|\eta| >> 1$(all the modes were deep inside the horizon), we find the general solution of Eq.(2.179) during de Sitter inflation using the scale factor (2.122)[21, 113, 119]

$$f_k(\eta) = \frac{e^{-ik\eta}}{\sqrt{2k}}\left[1 - \frac{i}{k\eta}\right] . \tag{2.180}$$

Likewise, the spectator field operator, expressed in terms of the ladder operators in (2.100), we can also promote the rescaled inflaton fluctuation to the operator expansion as

$$\hat{f}(\eta,\vec{x}) = \int \frac{d^3\vec{k}}{(2\pi)^3}\, e^{i\vec{k}.\vec{x}}\left[f_{\vec{k}}(\eta)\;\hat{a}_k + f^*_{\vec{k}}(\eta)\hat{a}^\dagger_{-k}\right] . \tag{2.181}$$

As $f(\eta,\vec{x})$ is not giving any background, its vacuum expectation value(VEV) is vanishing, $\langle 0|\,\hat{f}\,|0\rangle = 0$. Only the non-vanishing contribution comes from the variance of the inflaton fluctuations.

$$\begin{aligned}\langle|\hat{f}^2|\rangle &= \langle 0|\,\hat{f}^\dagger(\eta,0)\hat{f}(\eta,0)\,|0\rangle \\ &= \int \frac{d^3k}{(2\pi)^3}|f_k(\eta)|^2 \\ &= \int d(\ln k)\frac{k^3}{2\pi^2}|f_k(\eta)|^2\end{aligned} \tag{2.182}$$

We define the power spectrum as

$$\mathcal{P}_f(k,\eta) \equiv \frac{k^3}{2\pi^2}|f_k(\eta)|^2\,. \tag{2.183}$$

Using the field rescaling, $f_k = a\,\delta\phi_k$, and the solution (2.180), we can write the $\delta\phi$ power spectrum as

$$\mathcal{P}_{\delta\phi}(k,\eta) = a^{-2}\mathcal{P}_f(k,\eta) = \left(\frac{H}{2\pi}\right)^2\left(1 + \left(\frac{k}{aH}\right)^2\right) \xrightarrow{\text{super-horizon modes } k<<aH} \left(\frac{H}{2\pi}\right)^2 . \tag{2.184}$$

We approximate the above power spectrum at the inflation end as

$$\mathcal{P}_{\delta\phi}(k,\eta) \approx \left(\frac{H}{2\pi}\right)^2 . \tag{2.185}$$

Now, exploiting the relation (2.176), we define the curvature perturbation power spectrum as

$$\mathcal{P}_{\mathcal{R}}(k,\eta) = \left(\frac{\mathcal{H}}{\phi'}\right)^2 \mathcal{P}_{\delta\phi}(k,\eta) . \tag{2.186}$$

Similarly, the conserved curvature perturbation power spectrum turns out to be

$$\mathcal{P}_{\mathcal{R}}(k,\eta) = \frac{\mathcal{P}_{\delta\phi}(k,\eta)}{2\,\epsilon_{\rm H}\,M_{\rm pl}^2} = \frac{H^2}{8\pi^2\,\epsilon_{\rm H}\,M_{\rm pl}^2} , \tag{2.187}$$

where the slow-roll parameter $\epsilon_{\rm H}$ is given in Eq.(2.48). Exploiting the equality $\epsilon_{\rm H} = \epsilon_{\rm V} = \frac{M_{\rm pl}^2}{2}\left(\frac{V'}{V}\right)^2$, and the relation $3M_{\rm pl}^2H^2 \simeq V(\phi)$ during inflation, we can reexpress the curvature power spectrum (2.187) as a function of the inflaton potential as

$$\mathcal{P}_{\mathcal{R}}(k,\eta) = \frac{V^3}{12\pi^2\,M_{\rm pl}^6\,(V')^2} . \tag{2.188}$$

So, the power spectrum in this form depends upon the shape of the inflaton potential.

As different modes exit the horizon at different times, hence, $\mathcal{P}_{\mathcal{R}}$ spectrum is expected to have a slight scale dependence, which is basically related to the slow time-variation of $H$ and $\epsilon_{\rm H}$. Near a reference scale $k_*$, the $k$-dependence of the spectrum assumes a power-law form

$$\mathcal{P}_{\mathcal{R}} = A_s \left(\frac{k}{k_*}\right)^{n_s-1} , \tag{2.189}$$

where the amplitude of the scalar curvature power spectrum or the CMB normalization constant is $A_s = 2.12 \times 10^{-9}$ at the CMB pivot scale $(k_*/a_0) \equiv (k_{\rm CMB}/a_0) = 0.05\,{\rm Mpc}^{-1}$ where $a_0$ is the present-day scale factor, normalized to unity, and $n_s$ is the scalar spectral index. The current observational values of these quantities are discussed in Section (2.5). Comparing two equations (2.188) and (2.189), we get the expression of the spectral amplitude $A_s$ at the horizon crossing point of the pivot scale

$$A_s = \frac{V^3}{12\pi^2\,M_{\rm pl}^6\,(V')^2} . \tag{2.190}$$

To define the deviation from the perfect scale-invariance, we introduce the spectral index $n_s$

$$(n_s - 1) = \frac{d\,\ln\mathcal{P}_{\mathcal{R}}}{d\,\ln k} . \tag{2.191}$$

From the relation (2.187), we write

$$\frac{d\,\ln\mathcal{P}_{\mathcal{R}}}{d\,\ln k} = 2\left(\frac{d\,\ln H}{d\,\ln k}\right) - \left(\frac{d\,\ln\epsilon_{\rm H}}{d\,\ln k}\right) . \tag{2.192}$$

For a particular mode $k$, at the point of horizon crossing, we write

$$\ln k = N + \ln H \,. \tag{2.193}$$

This leads to

$$\left(\frac{d\ln H}{d\ln k}\right) = \frac{\epsilon_{\rm H}}{(\epsilon_{\rm H}-1)} \simeq -\epsilon_{\rm H}\,(1+\epsilon_{\rm H}) \approx -\epsilon_{\rm H} \quad \text{taking only first order term} \;. \tag{2.194}$$

The ratio $\left(\frac{d\ln\epsilon_{\rm H}}{d\ln k}\right)$ can be computed as

$$\begin{aligned}\left(\frac{d\ln\epsilon_{\rm H}}{d\ln k}\right) &= \left(\frac{d\ln\epsilon_{\rm H}}{dN}\right)\left(\frac{dN}{d\ln H}\right)\left(\frac{d\ln H}{d\ln k}\right)\\ &\approx \eta_{\rm H}\left(-\frac{1}{\epsilon_{\rm H}}\right)(-\epsilon_{\rm H}) = \eta_{\rm H}\,.\end{aligned} \tag{2.195}$$

Substituting (2.194) and (2.195) to the relation (2.192), we finally obtain the relation between the spectral index $n_s$ and the inflationary slow-roll parameters

$$n_s = (1 - 2\epsilon_{\rm H} - \eta_{\rm H})\,. \tag{2.196}$$

Using the relation (2.55), we express $n_s$ in terms of the inflationary potential model

$$n_s = (1 - 6\epsilon_{\rm V} + 2\eta_{\rm V})\,. \tag{2.197}$$

This relation (2.197) has a great implication as it directly connects the CMB parameter $n_s$ with the inflationary slow-roll parameters. The observationally predicted range of $n_s$ values(see Fig.(2.13)) indicates the departure from the perfect de Sitter inflationary phase with small but non-vanishing slow-roll parameters.

We shall now proceed to study the dynamics of the gauge-invariant tensor perturbations $\hat{h}_{ij}$, which propagate as primordial gravitational waves through space.

### 2.8.4 Tensor perturbations: Generation of Primordial gravitational waves

As we have already discussed in the last subsection, unlike the scalar perturbations, tensor perturbations remain invariant under the general coordinate transformation or gauge transformation. These tensor perturbation components propagate as Gravitational Waves(GWs) through the vast expanse of space without being distorted due to their feeble interaction with matter. This feeble interaction has made GWs a unique messenger to probe the very early universe(the early inflationary era), even much before the generation of CMB radiation. In the Perturbed FLRW metric (2.144), we now only concentrate on the tensor perturbations. The SVT decomposition has made it possible to study the dynamics of each component separately.

$$ds^2 = a^2(\eta)\left[-d\eta^2 + (\delta_{ij} + h_{ij})\,dx^i dx^j\right] \tag{2.198}$$

As already discussed, for the transverse($\partial^i h_i = 0$), traceless($h^i_i = 0$) property, the tensor perturbations $h_{ij}$ have only two degrees of freedom; these two independent modes correspond to "+" and "×", two polarization states of GWs. The tensor perturbations in the presence of anisotropic stress are governed by the following action up to quadratic order [120–122]

$$S_{\rm GW} = \int dx^4\sqrt{-g}\left[-\frac{M_{\rm pl}^2\, g^{\mu\nu}}{8}\partial_\mu h_{ij}\partial_\nu h^{ij} + \frac{1}{2}\Pi_{ij}h^{ij}\right], \tag{2.199}$$

where '$\Pi_{ij}$' is the anisotropic stress, defined as [121] $\Pi^i_j = T^i_j - \bar{P}\delta^i_j$. Here '$\Pi_{ij}$' also satisfies the transverse ($\partial^i\Pi_{ij} = 0$) and traceless ($\Pi^i_i = 0$)) conditions with the unperturbed background pressure $\bar{P}$. Here $\Pi_{ij}$, coupled with the tensor perturbations $h_{ij}$, is acting like an external source. By varying the action (2.199) with $h_{ij}$, we obtain the equation of motion of $h_{ij}$ in the presence of an anisotropic source as follows:

$$h''_{ij}(\eta,\vec{x}) + 2\mathcal{H}h'_{ij}(\eta,\vec{x}) - \nabla^2 h_{ij}(\eta,\vec{x}) = \frac{2}{M_{\rm pl}^2}a^2\Pi_{ij}(\eta,\vec{x}) \tag{2.200}$$

Likewise, scalar fluctuations, the tensor perturbations $h_{ij}(\eta,\boldsymbol{x})$ and the anisotropic stress tensor $\Pi_{ij}(\eta,\vec{x})$ can be decomposed in terms of the Fourier modes, say, $h^\lambda_{\boldsymbol{k}}(\eta)$ and $\Pi^\lambda_k(\eta)$ as follows [17, 120, 121, 123, 124]:

$$\begin{aligned}
\hat{h}_{ij}(\eta,\boldsymbol{x}) &= \sum_{\lambda=+,\times}\int\frac{d^3\vec{k}}{(2\pi)^3}\left[\hat{a}^\lambda_k e^\lambda_{ij}(\vec{k})h^\lambda_k(\eta)e^{i\vec{k}.\vec{x}} + \hat{a}^{\lambda\dagger}_k e^{\lambda *}_{ij}(\vec{k})h^{\lambda *}_k(\eta)e^{-\vec{k}.\vec{x}}\right],\\
\hat{\Pi}_{ij}(\eta,\vec{x}) &= \sum_{\lambda=+,\times}\int\frac{d^3\vec{k}}{(2\pi)^3}\left[\hat{a}^\lambda_k e^\lambda_{ij}(\vec{k})\Pi^\lambda_k(\eta)e^{i\vec{k}.\vec{x}} + \hat{a}^{\lambda\dagger}_k e^{\lambda *}_{ij}(\vec{k})\Pi^{\lambda *}_k(\eta)e^{-\vec{k}.\vec{x}}\right],
\end{aligned} \tag{2.201}$$

where $e^\lambda_{ij}(\boldsymbol{k})$ is the polarization tensor corresponding to the mode with wave vector $\vec{k}$ and the index $\lambda$ represents two polarization states + or × of the GWs. Polarization tensor obeys the relations $\delta^{ij}e^\lambda_{ij}(\vec{k}) = k^i e^\lambda_{ij}(\vec{k}) = 0$, and we shall use the normalization $e^{ij\,\lambda}(\vec{k})e^{\lambda' *}_{ij}(\vec{k}) = 2\delta^{\lambda\lambda'}$. In the above Fourier decompostion, the operators $(\hat{a}^\lambda_k, \hat{a}^{\lambda\dagger}_k)$ are the annihilation and creation operators corresponding to the tensor modes with the wave vector $\vec{k}$ and they satisfy the usual commutation relation $\left[\hat{a}^\lambda_k, \hat{a}^{\lambda'\dagger}_{k'}\right] = (2\pi)^3\delta^3(\vec{k}-\vec{k}')\delta^{\lambda\lambda'}$ and all other combinations are vanishing. The vacuum state $|0\rangle$ is defined as $\hat{a}^\lambda_k|0\rangle = 0$ for all $\vec{k}$ and $\lambda$. Note that $e^\lambda_{ij}(\vec{k})$ is assumed to be real in the linear polarization basis and implying $h^\lambda_{-\boldsymbol{k}}(\eta) = h^{\lambda *}_{\boldsymbol{k}}(\eta)$, and the mode functions $h^\lambda_{\boldsymbol{k}}(\eta)$ satisfy the following inhomogeneous equation [17, 120, 123–127]:

$$h^{\lambda\prime\prime}_{\vec{k}} + 2\frac{a'}{a}h^{\lambda\prime}_{\vec{k}} + k^2 h^\lambda_{\vec{k}} = \frac{2a^2}{M_{\rm pl}^2}e^{ij}_\lambda(\vec{k})P^{lm}_{ij}(\hat{k})T_{lm}(\vec{k},\eta). \tag{2.202}$$

As the left-hand side of the above equation has the transverse-traceless property, to make the right-hand side also transverse and traceless, we operate the transverse-traceless projector $P^{lm}_{ij}(\vec{k})$ on the energy-momentum tensor $T_{ij}(\vec{k},\eta)$. For this type of source, we chose the

linear polarisation basis, in which both polarisation modes contribute equally to the total energy density of the produced gravitational waves (GWs). Henceforth, we drop the polarization index to simplify the notation and incorporate its information into the tensor power spectrum. Following the definition (2.182) for scalar perturbation, we find the variance of the tensor perturbations $\langle 0|\, \hat{h}^{\lambda}_{ij}(\eta)\, (\hat{h}^{ij\,\lambda}(\eta))^{*}\, |0\rangle$. Computing this expectation value, we define the tensor power spectrum as

$$\mathcal{P}_{\rm T}(k,\eta) = 2\frac{k^3}{2\pi^2}|h_{\vec{k}}(\eta)|^2 \sum_{\lambda=+,\times} \delta^{\lambda\lambda} = 4\frac{k^3}{2\pi^2}|h_{\vec{k}}(\eta)|^2. \tag{2.203}$$

Utilizing the Green's function method, the solution of (2.202) for tensor perturbation can be expressed as[128, 129]

$$h_{\vec{k}}(\eta) = h^{\rm pri}_{\vec{k}} + \frac{2e^{ij}(\vec{k})}{M^2_{\rm pl}} \int d\eta_1 \mathcal{G}_k(\eta,\eta_1)\Pi^{\rm TT}_{ij}(\vec{k},\eta_1). \tag{2.204}$$

Here $h^{\rm pri}_{\vec{k}}$ is the homogeneous contributions of the tensor fluctuations, which is the primary tensor perturbation in the absence of any source, and $\mathcal{G}_k(\eta,\eta_1)$ is the retarded propagator by solving Eq.(2.200) with delta function source. In the above Eq.(2.204) we define $\Pi^{\rm TT}_{ij}(\vec{k},\eta_1) = P^{lm}_{ij}(\vec{k})T_{lm}(\eta,\vec{k})$ with $P^{lm}_{ij}(\vec{k})$ and $T_{lm}(\eta,\vec{k})$ being the Fourier transformation of the transverse-traceless projector and the energy-momentum tensor respectively. This projector is defined as

$$P_{lm,ij} = \left(P_{li}(\hat{k})\, P_{mj}(\hat{k}) - \frac{1}{2}P_{lm}(\hat{k})\, P_{ij}(\hat{k})\right), \tag{2.205}$$

where $P_{ij}(\hat{k}) = \left(\delta_{ij} - \hat{k}_i\hat{k}_j\right)$, $\hat{k}_i = (k_i/|k_i|)$. By substituting Eq. (2.204) into Eq. (2.203, we derive the total tensor power spectrum as

$$\mathcal{P}_{\rm T}(k,\eta) = 4\frac{k^3}{2\pi^2}\left(|h^{\rm pri}_{k}|^2 + \underbrace{\frac{4}{M^4_{\rm pl}}\int_{\eta_i}^{\eta_f} d\eta_1 \mathcal{G}_k(\eta,\eta_1)\int_{\eta_i}^{\eta_f} d\eta_2 \mathcal{G}_k(\eta,\eta_2)\Pi^2(k,\eta_1,\eta_2)}_{\text{secondary/induced tensor power spectrum } \mathcal{P}^{\rm sec}_{\rm T}}\right). \tag{2.206}$$

Here, $\eta_i$ and $\eta_f$ represent the initial and final times when the source was active to produce the tensor fluctuations. The term $\Pi^2$ on the right-hand side is defined as the correlator of the source $\Pi^{\rm TT}_{ij}$, given by [129]:

$$\langle 0|\Pi^{\rm TT}_{ij}(\vec{k},\eta_1)\Pi^{\rm TT*}_{ij}(\vec{k}_1,\eta_2)|0\rangle = (2\pi)^3\delta^3(\vec{k}-\vec{k}_1)\Pi^2(k,\eta_1,\eta_2). \tag{2.207}$$

In Chapter(6), we shall extensively study the generation of induced gravitational waves through the gravitationally produced scalar fluctuations within the framework of CGPP. There, we shall compute the whole bracketed quantity in (2.206) for the gravitationally

produced source field. For the time being, we shall concentrate on the dynamics of the inflationary tensor perturbations in the absence of any source term on the right-hand side of (2.202). We write the equation of motion of the primary tensor fluctuation

$$h_k'' + 2\frac{a'}{a}h_k' + k^2 h_k^{\lambda} = 0\,. \tag{2.208}$$

Respecting isotropy, we drop the vector sign of each $k$ mode for the primary tensor perturbations. We rescale the Fourier mode $h_k$ in terms of the Mukhanov-Sasaki variable $u_k$ as $h_k = \left(\sqrt{2}/M_{\rm pl}\right)\left(u_k/a\right)$. The Mukhanov-Sasaki variable satisfies the equation[15–17, 23, 130, 131]

$$u_k'' + \left(k^2 - \frac{a''}{a}\right)u_k = 0\,. \tag{2.209}$$

Using the Bunch-Davies initial vacuum condition, we find exactly the same solution of (2.209) as given in (2.180) during inflation.

$$u_k(\eta) = \frac{1}{\sqrt{2k}}\left[1 + \frac{iH\,a(\eta)}{k}\right]e^{-ik\eta}\,. \tag{2.210}$$

Using the solution (2.210), we obtain the solution of the original field mode $h_k$.

$$h_k(\eta) = \frac{\sqrt{2}}{M_{\rm pl}}\frac{iH}{\sqrt{2k^3}}\left[1 - \frac{ik}{H\,a(\eta)}\right]e^{ik/(H\,a(\eta))} \tag{2.211}$$

Substituting the solution of $h_k$ (2.211) to the tensor power spectrum (2.203), we obtain the primary $\mathcal{P}_{\rm T}^{\rm pri}(k)$ at the inflation end as

$$\mathcal{P}_{\rm T}^{\rm pri}(k) = \frac{2H^2}{\pi^2 M_{\rm pl}^2}\left(1 + \left(\frac{k}{aH}\right)^2\right) \xrightarrow{\text{super-horizon modes } k<<aH} \left(\frac{2H^2}{\pi^2 M_{\rm pl}^2}\right)\,. \tag{2.212}$$

Thus, the primary tensor power spectrum at the end of inflation turns out to be

$$\mathcal{P}_{\rm T}^{\rm pri}(k) \simeq \frac{2H^2}{\pi^2 M_{\rm pl}^2}\,. \tag{2.213}$$

This is the well-known scale-invariant power spectrum often discussed in the context of de Sitter inflation[113, 131–133]. This scale-invariant power spectrum is a robust prediction of inflation, where the tensor perturbation amplitude is directly related to the inflationary Hubble scale. In analogy to the scalar curvature power spectrum (2.189), the scale-dependence of the tensor power spectrum is defined as

$$\mathcal{P}_{\rm T}(k) \equiv A_t\left(\frac{k}{k_*}\right)^{n_t}\,. \tag{2.214}$$

where $n_t$ is the spectral index of the tensor power spectrum. Comparing Eq.(2.214) with (2.213), we write the tensor spectral index as

$$n_t = \left(\frac{d\ln\mathcal{P}_{\rm T}}{d\ln k}\right) = 2\left(\frac{d\ln H}{d\ln k}\right) = -2\,\epsilon_{\rm H}\,. \tag{2.215}$$

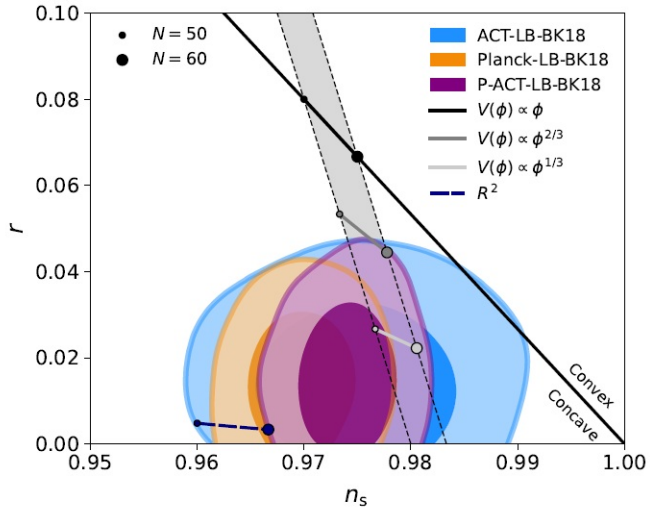


FIGURE 2.13: *The $n_s - r$ parameter space represents the constraints on the scalar and tensor primordial power spectra at the pivot scale $k_* = 0.05\,\mathrm{Mpc}^{-1}$. The constraints on $r$ are driven by the BK18 data[64], while the constraints on $n_s$ are driven by Planck (orange), ACT (blue), or P-ACT (purple). The combined dataset also includes CMB lensing and BAO in all cases. This figure is taken from [43].*

Another quantity, having a great observational significance, is defined as the ratio of the amplitude of the tensor and the scalar curvature power spectrum. This ratio is well-known as *tensor-to-scalar ratio*. Using equations (2.187) and (2.213), we find

$$r \equiv \frac{A_t}{A_s} = 16\,\epsilon_{\mathrm{H}}\,. \tag{2.216}$$

Combining equations (2.213) and (2.216), we establish an interesting relation between the inflationary Hubble scale and the CMB observables

$$H_k = \pi M_{\mathrm{pl}} \sqrt{\frac{r\,A_s}{2}}\,, \tag{2.217}$$

where $H_k$ is the inflationary Hubble scale. Using the current observational upper bound on $r$, as described in Section (2.5), we obtain the highest possible inflationary energy scale.

$$H_k \lesssim (2 \times 10^{-5})\,M_{\mathrm{pl}} = (4.8 \times 10^{13})\,\mathrm{GeV} \;\text{ with }\; r = 0.038 \text{ at } k_* = 0.05\,\mathrm{Mpc}^{-1}. \tag{2.218}$$

### 2.8.5 Connecting $\alpha$-attractor model parameters with the CMB observables

In this subsection, in light of the $\alpha$-attractor E-type potential model, we express various model parameters in terms of the CMB observables $(n_s, r)$. Plugging the expressions of

slow-roll parameters (2.79) in Eq.(2.197) and (2.216), we compute

$$n_s = 1 - \frac{8n}{3\alpha}\frac{\left(n + e^{\sqrt{\frac{2}{3\alpha}}\cdot\frac{\phi_k}{M_{\rm pl}}}\right)}{\left(e^{\sqrt{\frac{2}{3\alpha}}\cdot\frac{\phi_k}{M_{\rm pl}}} - 1\right)^2},$$
$$r = \frac{64n^2}{3\alpha}\frac{1}{\left(e^{\sqrt{\frac{2}{3\alpha}}\cdot\frac{\phi_k}{M_{\rm pl}}} - 1\right)^2}. \tag{2.219}$$

Here, the tensor-to-scalar ratio is computed at the CMB pivot scale $k_*$.

After simplifying Eq.(2.219), we find the inflaton amplitude $\phi_k$ at the horizon crossing of the pivot scale, and $r$ in terms of $n_s$, $\alpha$, $n$ [42].

$$\phi_k = \sqrt{\frac{3\alpha}{2}}\, M_{\rm pl} \ln\left[1 + \frac{4n + \sqrt{16n^2 + 24\alpha n(1-n_s)(1+n)}}{3\alpha(1-n_s)}\right],$$
$$r = \frac{192\,\alpha\, n^2(1-n_s)^2}{\left(4n + \sqrt{16n^2 + 24\alpha\, n(1-n_s)(1+n)}\right)^2}. \tag{2.220}$$

Using Eq.(2.58), the inflationary e-folding number $N_k$ between the horizon exit of the pivot scale $k_*$ at $\phi_k$ and the end of inflation at $\phi_{\rm end}$, is calculated to be

$$N_k = \frac{3\alpha}{4n}\left[\exp\left(\sqrt{\frac{2}{3\alpha}}\left(\frac{\phi_k}{M_{\rm pl}}\right)\right) - \exp\left(\sqrt{\frac{2}{3\alpha}}\left(\frac{\phi_{\rm end}}{M_{\rm pl}}\right)\right) - \sqrt{\frac{2}{3\alpha}}\left(\frac{\phi_k}{M_{\rm pl}} - \frac{\phi_{\rm end}}{M_{\rm pl}}\right)\right]. \tag{2.221}$$

We consider the horizon exit of the pivot scale as the beginning of inflation.

Using equations (2.51) and (2.217), finally, the energy scale of inflation related to the parameter $\Lambda$ in the potential (2.75) can be analytically expressed in terms of CMB parameters as follows [42]:

$$V(\phi_k) = \frac{3\pi^2 A_s M_{\rm pl}^4}{2} r = \Lambda^4\left(1 - e^{-\sqrt{\frac{2}{3\alpha}}\cdot\frac{\phi}{M_{\rm pl}}}\right)^{2n}$$
$$\Rightarrow \Lambda = M_{\rm pl}\left(\frac{3\pi^2 r A_s}{2}\right)^{\frac{1}{4}}\left[\frac{2n(1+2n) + \sqrt{4n^2 + 6\alpha(1+n)(1-n_s)}}{4n(1+n)}\right]^{\frac{n}{2}}. \tag{2.222}$$

All these expressions of the potential model parameters, the inflaton amplitude at the beginning and end of inflation, inflationary e-folding number(see Eqs.(2.77), (2.78), and (2.220)-(2.222)), will be extensively used to study the background dynamics during inflation and the post-inflationary reheating phase throughout this thesis.

In summary, this chapter has presented an overview of the essential theoretical framework that underpins both the standard and extended paradigms of modern cosmology.

Starting from the triumphs and inherent limitations of the standard FLRW cosmology, we motivated the need for an inflationary phase, preceding the hot Big Bang era, whose very dynamics naturally resolve the long-standing horizon, flatness, and monopole problems while simultaneously providing a natural mechanism for the origin of primordial perturbations. We then reviewed the subsequent reheating phase, a crucial bridge between the inflationary and the hot Big Bang epoch, with a significant emphasis on its perturbative and non-perturbative aspects. This intermediate phase not only repopulates the universe with relativistic degrees of freedom but also leaves indelible imprints, from massless and massive(dark matter) particle-production dynamics to stochastic backgrounds of gravitational waves. The treatment of inflationary perturbations further clarifies how tiny quantum vacuum fluctuations of the inflaton evolved into the seed of cosmic structure observed in the CMB temperature anisotropies and the large-scale distribution of matter, and also explains the origin of the nearly scale-invariant tensor perturbations. As an overall impression, these elements illustrate how non-standard extensions of the standard cosmological model enrich our understanding of the early universe and open new observational windows. This foundational framework prepares the ground for an intensive investigation of the non-perturbative signature of reheating through cosmic relics carried out in the subsequent chapters.

CHAPTER 3

# Introduction to Quantum Squeezing and diagnostic of quantum chaos

*" Chaos has become not just theory but also method, not just a canon of beliefs but also a way of doing science."*

—*James Gleick, Chaos: Making a New Science*

## 3.1 Squeezed State Formalism

In cosmology, squeezed states provide a powerful language for describing how small-scale quantum vacuum fluctuations evolve into large-scale classical density perturbations. They capture the memory of how fluctuation modes were stretched, correlated, and amplified by the early inflationary phase of the universe, making squeezing a robust framework linking microscopic quantum behavior with the macroscopic cosmic structure. In this section, we construct the squeezed state formalism, which will be employed later to revisit the phenomenon of explosive particle during the preheating era in the language of quantum squeezing. The interaction between the produced quantum fluctuations and the classical expanding background makes the quantum state of those fluctuations *squeezed*. The investigation of the early universe particle production within the framework of quantum squeezing, indeed, provided us with some insightful ideas regarding the inherent chaotic instability and the eventual thermalization of the system. Thus, treating the interacting system within the squeezing framework opens up a unique possibility to decode various microscopic features of large-scale systems in a cosmological setting. These intriguing aspects will be explored in the next Chapter(4).

It is well known that, upon quantization, the states of a harmonic oscillator are coherent, whereas those of a parametric oscillator (an oscillator with time-dependent frequency) are squeezed. If one measures the uncertainty of two-phase space variables in a squeezed state

corresponding to a particular system, then one will encounter the terms whereupon one grows exponentially, and another one will die out exponentially [134, 135] respecting the Heisenberg Uncertainty Principle. The *squeezing* refers to the unequal distribution of this minimum uncertainty between the two conjugate variables, allowing for enhanced precision in either direction, say, position, with the expense of the reduced precision in the other conjugate direction, i.e. momentum. This fact is nicely depicted in Fig.(3.1). The coherent state is realized in the form of a circle with equal uncertainties of the two variables, whereas for a squeezed state , the circle squeezed along one direction, reducing the uncertainty of one variable, becomes an ellipse.
We introduce the concept of a squeezed state by giving the example of an inverted harmonic oscillator(IHO), which serves as a key toy model for studying squeezed states. The Hamiltonian of IHO, having a potential unbounded from below, is given as

$$\hat{H}_{\rm IHO} = \frac{\hat{p}^2}{2} - \frac{1}{2}k\hat{x}^2 \,. \tag{3.1}$$

where $\hat{x}$, $\hat{p}$ are the position and momentum operators of the quantum system, and $k$ is the frequency of the oscillator. By defining $\hat{x}$ and $\hat{p}$ in terms of raising and lowering operators of the non-inverted oscillator,

$$\hat{x} = \frac{1}{\sqrt{2k}}\left(\hat{a} + \hat{a}^\dagger\right), \quad \hat{p} = -i\sqrt{\frac{k}{2}}\left(\hat{a} - \hat{a}^\dagger\right), \tag{3.2}$$

the inverted oscillator Hamiltonian becomes

$$\hat{H}_{\rm IHO} = -\frac{k}{2}\left(\hat{a}^2 + (\hat{a}^\dagger)^2\right). \tag{3.3}$$

The presence of the $(a^\dagger)^2$ term in the above Hamiltonian (3.3) is responsible for the squeezing of the quantum state for the inverted harmonic oscillator, and we shall make this fact clear while writing the Hamiltonian of the produced fluctuations, interacting with the classical background.

### 3.1.1 Quantum field-theoretic description of squeezed state formalism

As we are interested in applying the squeezed state formalism to the dynamics of quantum fluctuations during early reheating, we need to develop the field-theoretic version of the formalism.

We write the momentum-preserving unitary two-mode squeezing operator $\hat{S}_k(r_k, \varphi_k)$ as[134, 136–138], $\hat{S}_k(r_k, \varphi_k) = e^{\hat{B}_k}$ with

$$\hat{B}_k \equiv \frac{r_k(t)}{2}\left(e^{-2i\varphi_k(t)}\hat{a}_{\vec{k}}(t_0)\hat{a}_{-\vec{k}}(t_0) - e^{2i\varphi_k(t)}\hat{a}^\dagger_{-\vec{k}}(t_0)\hat{a}^\dagger_{\vec{k}}(t_0)\right). \tag{3.4}$$

The anti-hermitian nature $\hat{B}_k^\dagger = -\hat{B}_k$ confirms the unitarity of the squeezing operator in Eq.(3.4). Two parameters $r_k$ and $\varphi_k$ in Eq. (3.4) quantify the amount of squeezing of the

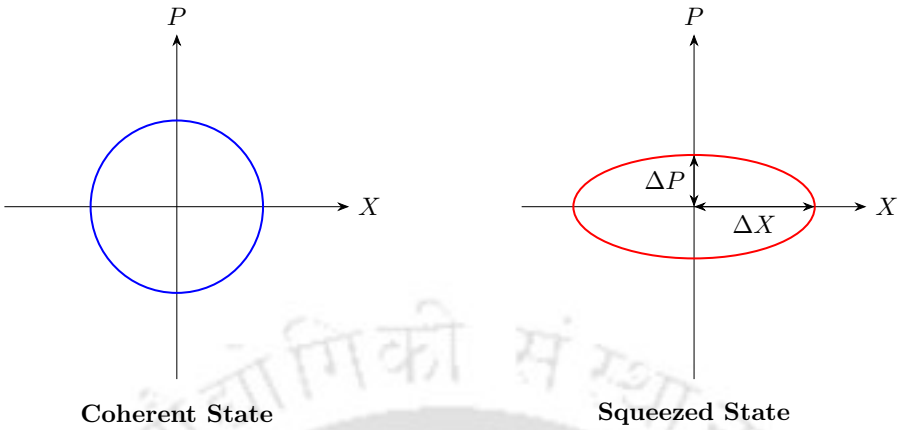


FIGURE 3.1: *Schematic phase-space representation of a coherent state (left) with equal uncertainties along both directions, and a squeezed state (right) exhibiting reduced uncertainty along one direction at the expense of the conjugate variable.*

quantun system in a particular quantum state and its squeezing angle, respectively. To have a complete evolution of a dynamical system, the second operator is the rotation operator, $\hat{R}_k(\theta_k)$, defined as, $\hat{R}_k(\theta_k) = e^{\hat{D}_k}$ with

$$\hat{D}_k \equiv -i\theta_k(t)\Big(\hat{a}^\dagger_{\vec{k}}(t_0)\hat{a}_{\vec{k}}(t_0) + \hat{a}^\dagger_{-\vec{k}}(t_0)\hat{a}_{-\vec{k}}(t_0)\Big), \tag{3.5}$$

where $\hat{D}^\dagger_k = -\hat{D}_k$ as it was in Eq. (3.4). Here rotation operator is characterized by a parameter $\theta_k$, called the rotation angle. In both equations (3.4) and (3.5), the ladder operators are defined at some initial time $t_0$. Combining these two operators $\hat{S}_k(r_k, \varphi_k)$ and $\hat{R}_k(\theta_k)$, one can construct a unitary, momentum-preserving time-evolution operator for every individual scalar mode as,

$$\hat{\mathcal{U}}_k = \hat{S}_k(r_k, \varphi_k)\hat{R}_k(\theta_k). \tag{3.6}$$

Using the operator expansion Baker-Campbell-Hausdorff formula[139] $e^{\hat{O}}\,\hat{A}\,e^{-\hat{O}} = \hat{A} + [\hat{O}, \hat{A}] + [\hat{O}, [\hat{O}, \hat{A}]]/2! + ...$, one can easily check that the application of this unitary evolution operator on the creation and annihilation operators generates their time evolution as

$$\begin{aligned}
\hat{a}_{\vec{k}}(t) &= \hat{\mathcal{U}}^\dagger_k(t, t_0)\hat{a}_{\vec{k}}(t_0)\hat{\mathcal{U}}_k(t, t_0) \Rightarrow \hat{a}_{\vec{k}}(t) = \Big(\cosh r_k e^{-i\theta_k}\hat{a}_{\vec{k}}(t_0) - \sinh r_k e^{i(\theta_k+2\varphi_k)}\hat{a}^\dagger_{-\vec{k}}(t_0)\Big), \\
\hat{a}^\dagger_{\vec{k}}(t) &= \hat{\mathcal{U}}^\dagger_k(t, t_0)\hat{a}^\dagger_{\vec{k}}(t_0)\hat{\mathcal{U}}_k(t, t_0) \Rightarrow \hat{a}^\dagger_{\vec{k}}(t) = \Big(\cosh r_k e^{i\theta_k}\hat{a}^\dagger_{\vec{k}}(t_0) - \sinh r_k e^{-i(\theta_k+2\varphi_k)}\hat{a}_{-\vec{k}}(t_0)\Big).
\end{aligned} \tag{3.7}$$

Following Eq.(2.108), we can express

$$\hat{a}_{\vec{k}}(t) = \alpha_k(t)\hat{a}_{\vec{k}}(t_0) + \beta_k(t)\hat{a}^\dagger_{-\vec{k}}(t_0). \tag{3.8}$$

A comparison between Eq.(3.7) and (3.8) provides one of the forms of two coefficients $\alpha_k(t)$ and $\beta_k(t)$ in terms of $r_k, \varphi_k$ and $\theta_k$ in this two-mode squeezed state formalism. These forms are as follows:

$$\begin{aligned}\alpha_k(t) &= e^{-i\theta_k}\cosh r_k(t),\\ \beta_k(t) &= -e^{(i\theta_k+2i\varphi_k)}\sinh r_k(t).\end{aligned} \tag{3.9}$$

Such choice naturally satisfies the normalization condition, $|\alpha_k(t)|^2 - |\beta_k(t)|^2 = 1$ for a scalar field system. Within this squeezed state framework, we can define an alternative expression of occupation number density $n_k$ which is equivalent to the expression (2.114). It is worth mentioning that the purpose of defining such coefficients, namely Bogoliubov coefficients, is to connect the late-time raising and lowering operators with the operators of initial time. In the Heisenberg picture, as operator evolution is studied rather than state evolution, a vacuum state corresponding to the operators at the initial time will no longer be a vacuum corresponding to the creation and annihilation operators at a late time. Thus, in a dynamical background, the vacuum with respect to the initial operators becomes an excited state with respect to the late-time operators. This argument is already given in Section (2.7). Here we restate the same in the language of the squeezed state formalism. One can construct the late-time number operator($\hat{N}_{\vec{k}}(t)$) using (3.7) and conjugate, $\hat{N}_{\vec{k}}(t) = \hat{a}^\dagger_{\vec{k}}(t)\hat{a}_{\vec{k}}(t)$ and the vacuum expectation value of this late-time number operator in the so-called Bunch-Davis vacuum defined at the initial time($t_0$) can be expressed as

$$\langle \hat{N}_{\vec{k}}(t)\rangle = \left\langle 0_{\vec{k}}\right| \hat{a}^\dagger_{\vec{k}}(t)\hat{a}_{\vec{k}}(t)\left|0_{\vec{k}}\right\rangle = |\beta_k(t)|^2 = \sinh^2 r_k\,. \tag{3.10}$$

The same expression can also be obtained for $-\vec{k}$ mode, $\langle \hat{N}_{-\vec{k}}(t)\rangle = \sinh^2 r_k$. Interesting to note that the evolution of the squeezing parameter $r_k$ influences the time evolution of occupation number density for various modes $\vec{k}$.

### 3.1.2 Two-mode squeezed states for bosonic system

The squeezed state of the produced particles can be determined by the application of the unitary evolution operator (3.6) on a two-mode unsqueezed vacuum state. Borrowing the idea as outlined in [136], we can factorize the full Hilbert space of the system $\boldsymbol{\varepsilon}$ into independent inner products of Hilbert spaces for two opposite momenta modes $\vec{k}$ and $-\vec{k}$, $\boldsymbol{\varepsilon} = \prod_{k\in\mathbb{R}^{3+}} \boldsymbol{\varepsilon}_{\vec{k}} \otimes \boldsymbol{\varepsilon}_{-\vec{k}}$. Using this idea, we can write the two-mode unsqueezed vacuum state as, $\left|0_{\vec{k}}, 0_{-\vec{k}}\right\rangle \equiv \left|0_{\vec{k}}\right\rangle \otimes \left|0_{-\vec{k}}\right\rangle$. Finally the application of two-mode unitary evolution operator (3.6) on the unsqueezed vacuum leads us to the momentum-preserving two-mode squeezed state $|\psi_{\rm sq}\rangle_{\vec{k},-\vec{k}}$[136, 138, 140]*:

$$|\psi_{\rm sq}\rangle_{\vec{k},-\vec{k}} = \hat{S}_k(r_k,\varphi_k)\hat{R}_k(\theta_k)\left|0_{\vec{k}}, 0_{-\vec{k}}\right\rangle = \frac{1}{\cosh r_k}\sum_{n=0}^{\infty} e^{2in\varphi_k}(-1)^n \tanh^n r_k \left|n_{\vec{k}}, n_{-\vec{k}}\right\rangle, \tag{3.11}$$

*Explicitly, the application of Rotation operator on the initial vacuum state keeps it invariant, $\hat{R}_{\vec{k}}(\theta_k)\left|0_{\vec{k}}, 0_{-\vec{k}}\right\rangle = \left|0_{\vec{k}}, 0_{-\vec{k}}\right\rangle$, so vacuum state is rotationally invariant.

where a two-mode excited state is given by

$$\left|n_{\vec{k}}, n_{-\vec{k}}\right\rangle = \sum_{n=0}^{\infty} \frac{1}{n!} \left(\hat{a}^{\dagger}_{\vec{k}}\right)^{n} \left(\hat{a}^{\dagger}_{-\vec{k}}\right)^{n} \left|0_{\vec{k}}, 0_{-\vec{k}}\right\rangle . \tag{3.12}$$

This $|\psi_{\rm sq}\rangle_{\vec{k},-\vec{k}}$ is a two-mode squeezed state, well known in the context of quantum optics as an entangled state[141–143].

These fundamental tools of the squeezed state formalism for a quantum scalar field system will be applied to the study of bosonic preheating in the next chapter.

## 3.2 Diagnostic of quantum chaos: out-of-time-order correlator(OTOC)

OTOC, a nice acronym for out-of-time-order correlator, is one of the diagnostics for detecting the presence of quantum chaos in a system. Unlike a classical system, studying and characterizing the chaos in quantum many-body systems is pretty challenging. For a classical system, if a small perturbation to the initial state of a system causes exponentially diverging phase-space trajectories, then such hypersensitivity to the initial state or initial condition of that system is a clear indication of the presence of chaos. The system's extreme sensitivity to a tiny initial perturbation gives rise to the popular concept of the *Butterfly effect*[144, 145]. In Fig.(3.2), two initially neighbouring trajectories are diverging very fast with time, and this phenomenon resembles, as if a butterfly is flapping its wings. For a classical system, this hypersensitivity can be quantitatively characterized by the Poisson bracket between position ($q$) and momentum ($p$) at unequal times:

$$\{q(t), p(0)\}^2 = \left(\frac{\partial q(t)}{\partial q(0)}\right)^2 \sim \sum_n c_n e^{2\lambda_n t} , \tag{3.13}$$

Where $\lambda_n$, the *Lyapunov exponents* are well-known to give the measure of chaos. In a quantum mechanical system, an analogous quantity can be defined between two operators, replacing the classical Poisson bracket by a Commutation bracket. The quantum mechanical analogue of (3.13) is generically called OTOC $\left[\hat{q}(t), \hat{p}(0)\right]$, which behaves as a Poisson bracket in the semiclassical limit. Likewise, the exponential diverging trajectories in the classical case, the exponential amplification of this commutator is a potential signature of *quantum chaos*. It defines the growing overlap of the time-evolved operator with the operator defined at the initial time. To quantify OTOC, the common practice is the use of a double unequal-time commutator

$$\mathcal{C}(t) \equiv -\langle [\hat{q}(t), \hat{p}(0)]^2 \rangle_{\beta} . \tag{3.14}$$

Where angle brackets $\langle ... \rangle_{\beta}$ stands for thermal average and $\beta$ being the inverse temperature, $\beta = 1/(k_B T)$, where $k_B$ is the Boltzmann constant. Though we are taking commutation between $\hat{q}(t)$ and $\hat{p}(0)$, generically one can consider commutation between any pair of hermitian operators $\hat{W}$, $\hat{V}$,

$$\mathcal{C}(t) \equiv -\langle [\hat{W}(t), \hat{V}(0)]^2 \rangle_{\beta}. \tag{3.15}$$

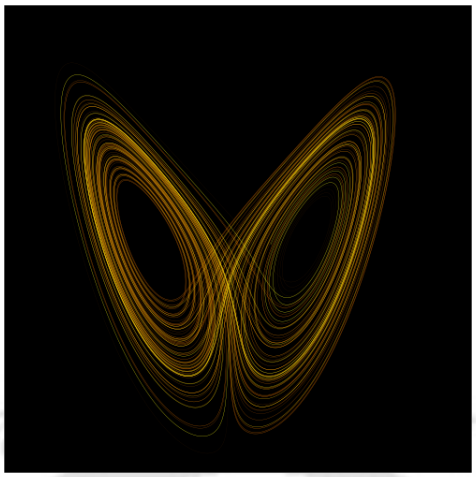

Figure 3.2: *A schematic representation of a chaotic system, having hypersensitivity to the initial conditions. Image courtesy [Wikipedia].*

Therefore, based on the above discussion, a quantum chaotic system is also expected to exhibit exponential growth in OTOC, $\mathcal{C}(t) \sim e^{2\lambda t}$, in a similar fashion to the classical one and we can define the analogous *quantum Lyapunov exponent*($\lambda$) measuring chaos in the quantum system under consideration. In this section, we shall show the OTOC calculation in the two-mode squeezed state formalism. In this formalism, the canonically conjugate phase space operators(field and its conjugate momentum) $(\hat{X}_{\vec{k}}(t), \hat{\Pi}_{X_{\vec{k}}}(t))$ are expressed in terms of time-dependent creation and annihilation operators as

$$\begin{aligned}\hat{X}_{\vec{k}} &= \frac{1}{\sqrt{2\tilde{\omega}_k}}\big[\hat{a}_{\vec{k}}(t) + \hat{a}^{\dagger}_{-\vec{k}}(t)\big] \\ \hat{\Pi}_{X_{\vec{k}}} &= -i\sqrt{\frac{\tilde{\omega}_k}{2}}\big[\hat{a}_{\vec{k}}(t) - \hat{a}^{\dagger}_{-\vec{k}}(t)\big].\end{aligned} \tag{3.16}$$

Where time-independent frequency is denoted by $\tilde{\omega}_k$. The above definition is consistent with the standard quantization condition (2.101). In this definition, we keep the time dependence of the dynamical system in the ladder operators, and in the Heisenberg picture, studying the operator evolution equation, we capture the time evolution of the dynamical system. Using Eq.(3.7), we express the field and conjugate momentum (see Eqs. (4.3)) in terms of three squeezing parameters $(r_k, \varphi_k, \theta_k)$ as

$$\begin{aligned}\hat{X}_{\vec{k}}(t) &= \frac{1}{\sqrt{2\tilde{\omega}_k}}\big(\cosh r_k e^{-i\theta_k} - \sinh r_k e^{-i(\theta_k+2\varphi_k)}\big)\hat{a}_{\vec{k}}(t_0) \\ &\quad + \frac{1}{\sqrt{2\tilde{\omega}_k}}\big(\cosh r_k e^{i\theta_k} - \sinh r_k e^{i(\theta_k+2\varphi_k)}\big)\hat{a}^{\dagger}_{-\vec{k}}(t_0) \\ \hat{\Pi}_{X_{\vec{k}}}(t) &= -i\sqrt{\frac{\tilde{\omega}_k}{2}}\big(\cosh r_k.e^{-i\theta_k} + \sinh r_k.e^{-i(\theta_k+2\varphi_k)}\big)\hat{a}_{\vec{k}}(t_0)\,,\end{aligned}$$

$$+ i\sqrt{\frac{\tilde{\omega}_k}{2}}\big(\text{cosh}r_k e^{i\theta_k} + \sinh r_k e^{i(\theta_k+2\varphi_k)}\big)\hat{a}^{\dagger}_{-\vec{k}}.(t_0). \tag{3.17}$$

Using the above conjugate variables, the commutation relation takes the following simple form,

$$\big[\hat{X}_{\vec{k}}(t), \hat{\Pi}_{X_{\vec{k}'}}(t_0)\big] = i.(2\pi)^3\delta^3(\vec{k}+\vec{k}').f_k(t,t_0), \tag{3.18}$$

where $f_k(t,t_0)$ is defined as[137]

$$f_k(t,t_0) = \frac{1}{2}\Big[\big(\cosh r_k.e^{-i\theta_k} - \sinh r_k.e^{-i(\theta_k+2\varphi_k)}\big)\big(\cosh r_0.e^{i\theta_0} + \sinh r_0.e^{i(\theta_0+2\varphi_0)}\big) + c.c\Big], \tag{3.19}$$

with $(r_0, \theta_0, \varphi_0)$ being the values of the squeezing parameters at initial time $t_0$. The advantage of using such a complex conjugate pair is its being a c-number operator (Eq.(3.18)). Using this property, for every canonically conjugate pair of field variables in momentum space, we can straightforwardly compute the OTOC as

$$\mathcal{C}_{\vec{k}\vec{k}'}(t) = -\langle\big[\hat{X}_{\vec{k}}(t), \hat{\Pi}_{X_{\vec{k}'}}(t_0)\big]^2\rangle_\beta = (2\pi)^6\mathcal{C}_{\vec{k}}(t)(\delta^3(\vec{k}+\vec{k}'))^2\,. \tag{3.20}$$

Clearly, the appearance of the delta function advocates the momentum conservation in the system, which is reminiscent of a homogeneous FLRW background. Ignoring those delta function terms, we concentrate only on the amplitude part

$$\mathcal{C}_{\vec{k}}(t) \sim f_k^2(t,t_0)\,. \tag{3.21}$$

In our subsequent studies, we will mainly focus on this amplitude part for various models. We have already mentioned that not only the commutation between position and momentum operator, but OTOC, in general, can be taken as a double-commutator between any two hermitian operators. Hence, all possible combinations between the field and conjugate momentum can capture the behavior of OTOC. We, therefore, construct a $2\times2$ matrix, $\mathcal{M}_{kk'}$, which is the quantum counterpart of *classical symplectic matrix* having unit determinant consisting of all such combinations of field momenta [137, 146], as

$$\mathcal{M}_{kk'} = -\begin{pmatrix} \big[\hat{X}_{\vec{k}}(t), \hat{X}_{\vec{k}'}(t_0)\big]^2 & \big[\hat{X}_{\vec{k}}(t), \hat{\Pi}_{\vec{k}'}(t_0)\big]^2 \\ \big[\hat{\Pi}_{\vec{k}}(t), \hat{X}_{\vec{k}'}(t_0)\big]^2 & \big[\hat{\Pi}_{\vec{k}}(t), \hat{\Pi}_{\vec{k}'}(t_0)\big]^2 \end{pmatrix} = (2\pi)^6(\delta^3(\vec{k}+\vec{k}'))^2\begin{pmatrix} h_k^2(t,t_0) & f_k^2(t,t_0) \\ g_k^2(t,t_0) & j_k^2(t,t_0) \end{pmatrix}. \tag{3.22}$$

Where assuming the initial squeezing $r_0 \to 0$, all the components of the $c$-number matrix are calculated to be

$$\begin{aligned} f_k(t,t_0) &\approx \cosh r_k\cos(\theta_k-\theta_0) - \sinh r_k\cos(\theta_k-\theta_0+2\varphi_k)\,,\\ g_k(t,t_0) &\approx \cosh r_k\cos(\theta_k-\theta_0) + \sinh r_k\cos(\theta_k-\theta_0+2\varphi_k)\,,\\ h_k(t,t_0) &\approx \cosh r_k\sin(\theta_k-\theta_0) - \sinh r_k\sin(\theta_k-\theta_0+2\varphi_k)\,,\\ j_k(t,t_0) &\approx \cosh r_k\sin(\theta_k-\theta_0) + \sinh r_k\sin(\theta_k-\theta_0+2\varphi_k)\,. \end{aligned} \tag{3.23}$$

From the symplectic matrix, we shall then extract the behavior of OTOC from the dominant eigenvalue of this matrix, and extract the information of "Lyapunov exponent"($\lambda_k$) as discussed before. To this end, let us point out that above expression, we have taken the initial state as an unsqueezed one. But this is not the whole picture, there is also a possibility $r_0 >> 1$. The justification of such consideration is not given here. In the next Chapter(4), the study during the explosive particle production era, where we shall apply all these tools and techniques, will clearly display that such a choice is consistent with the initial condition of the system under study.

CHAPTER 4

# Squeezing, Chaos, Thermalization in a periodically driven Quantum System: Case of Bosonic Preheating

*"The most important thing accomplished by the ultimate discovery of the 3°K radiation background (Penzias and Wilson, 1965) was to force all of us to take seriously the idea that there was an early universe"*

*Steven Weinberg, in The First Three Minutes: A Modern View of the Origin of the universe*

Post-inflationary reheating, an important event in the early universe is responsible for the thermalized universe we see today. Therefore, a theoretical understanding of this phase would be of paramount importance. Inflationary quantum fluctuations are responsible for producing curvature fluctuations, and their subsequent generation of structures is inevitably related to transferring energy from inflaton to matters. Despite having significant efforts [9–12, 14, 24, 66, 100, 103, 104, 110, 147–153], a proper theoretical understanding of this phase is still lacking, particularly due to its complex non-linear evolution, and subsequent thermalization of the produced radiation bath during reheating.

After a quasi-exponential accelerated phase of expansion, known as inflation, as already discussed in Chapter(1) in great detail, the universe is left with a super cold state of vanishing matter, entropy density, and a homogeneous background inflaton field oscillating around its potential minima. Any fundamental field, coupled with such an oscillatory background, will experience a periodic driving force, and its associated particles will be produced by the quantum mechanical particle production mechanism. Such production, therefore, leads to the transfer of energy from the inflaton to standard model fields successfully populating the universe. Typically, such a transferring process involves multiple stages

of evaluation. Depending upon the coupling parameter, the initial stage may be non-perturbative [24, 66, 100, 103, 104, 110, 147–151] followed by perturbative production, or the process could be entirely perturbative [34, 52, 54, 55, 111, 152–154]. However, apart from non-linear nature of production, it is the thermalization of those produced particles in the expanding background which makes the whole process extremely complex and theoretically challenging. Studies of perturbative production and its thermalization have been discussed in the literature [155–158], taking a phenomenological approach with very little foundational progress. Several studies have also been performed for non-perturbative production and their subsequent thermalization by performing lattice simulation [25, 26, 159–162]. However, to the best of our knowledge, a concrete mathematical framework to understand the underlying mechanism of this thermalization process in the context of reheating is far from complete. It is in this realm that we initiate formulating a theoretical framework that we believe to play an instrumental role in understanding such a phase. Apart from its theoretical motivation, it is important to stress that the production and thermalization during reheating may leave an indelible imprint on different cosmological observable related to Cosmic Microwave Background (CMB), baryogenesis, dark matter, and even small-scale structures in the universe.

In this Chapter, we particularly focus on the stage called preheating, when particle production occurs with parametric resonance as a primary mechanism, and hence would naturally last for a very brief initial period of the entire reheating process. The formalism we adopt is based on the recent development [136–138, 163–168] on the application of various intriguing concepts of quantum information theory in the realm of cosmology particularly centered around one of the fundamental questions in theoretical cosmology as to how the quantum correlation of fluctuations generated during inflation is dynamically decohered into post-inflationary classicalized correlation, and what would be the appropriate quantifier of their quantumness [136, 169]. During inflation, the primordial perturbation generically evolves into a squeezed state [134, 140]. Utilizing this squeezed state language and to decode the quantumness of the inflationary correlations, several proposals have been put forth based on quantum information tools in the recent past, namely, observing the Bell violation [163, 170, 171], quantum discord [136, 172–174], quantum stokes parameter [175]. In the quantum field theory framework, on the other hand, the connection between squeezing and chaos has been known for quite some time [176, 177]. The growing interest in quantum information theory further unveiled the idea of OTOC, complexity as an important diagnostic tool to characterize the chaos, first observed in the context of information scrambling by Black holes [178–180]. Utilizing those tools of quantum chaotic growth [137, 138] of the primordial perturbation has also been quantified through diagnostics such as OTOC [181–183], complexity [184–189], and are shown to have signatures in the correlations [190].

This chapter is based on the work [35]. In this chapter, as described above, we shall make use of those different tools and explore the interconnection among resonance, squeezing, and chaos during the preheating phase. We particularly show that the production under the background of a periodic inflaton field during preheating is an ideal quantum chaotic system, where the OTOC of phase space operators exhibits an exponential growth $\sim e^{2\lambda t}$

in time, potentially signalling the chaotic nature of the system under consideration, where $\lambda$, the Lyapunov exponent gives the measure of chaos in the system. A few earlier isolated attempts in this direction can be found in [191, 192], where the chaotic nature of the preheating phase has been indicated without a detailed characterization. We performed a detailed study on this by calculating OTOC as a diagnostic tool for a class of $\alpha-$attractor E-type inflationary potential model and different couplings with daughter fields. We extend our exploration further and shed light on how to quantify the possible thermalization temperature of the system in the parlance of squeezing formalism. From the perspective of a particular observer, the squeezed state is found to be thermal. Utilizing this observation, we arrive at an interesting relation between the squeezing and temperature of the system under consideration. At this juncture, we must remind the reader of a deep connection between chaos and thermalization as conjectured by Maldacena-Shenker-Stanford (MSS)[180] and this states that for any thermal quantum chaotic system, the characteristic Lyapunov exponent ($\lambda$) is constrained by its thermalization temperature $\lambda \leq 2\pi k_B T/\hbar$, where $k_B$ is the Boltzmann constant and $h$ is the Planck constant. Therefore, for any thermal quantum chaotic system, the temperature is set to have a lower bound fixed by the characteristic exponent $\lambda$ of the maximally chaotic system. The temperature defined in the squeezing language is indeed found to satisfy such an upper bound.
The order of construction of this chapter is as follows. In Section 4.1, we construct our model in a two-mode squeezed state language. We derive three dynamical equations for the squeezing parameter ($r_k$), squeezing angle ($\varphi$), and rotation angle ($\theta_k$). The dynamics of these parameters signify the evolution of the quantum state of the produced fluctuation. We also obtain an equivalent expression of occupation number density in terms of the squeezing parameter. In Section 4.2, we calculate OTOC in two-mode squeezed state formalism for four-leg type interaction, and emphasize distinct features of its dynamics for three different background driving sources. In Section 4.3, we repeat the same analysis of Section 4.2 for three-leg type interaction. In Section 4.4, we derive a relation between resonant growth index(*Floquet exponent*) and chaotic growth index(*Lyapunov exponent*) and also study the behavior of the OTOC spectrum. In Section 4.5, we wish to have a semi-classical visualization of the quantum chaotic system by generating Poincaré section. Furthermore, we give an approximate estimate of the thermalized temperature of the system, which is calculated from the squeezed state and the Rayleigh-Jeans spectrum. We also check the consistency of these outcomes with the MSS conjecture. Finally, in Section 4.6, we conclude this chapter by stating the main outcomes of this work.

## 4.1 Produced Fluctuations in Light of the Squeezed State Formalism

In this section, we study the dynamics of the scalar daughter fluctuations produced during the preheating era in light of the squeezed state language(see earlier attempt [193]). To implement the two-mode squeezed state formalism, considering only the non-gravitational

interaction term $F(\phi)$, we express the Lagrangian (2.93) in terms of the rescaled field(see Eq.(2.97)) with two independent modes $(X_{\vec{k}}, X_{-\vec{k}})$,

$$L_X = \frac{1}{2}\int \frac{d^3\vec{k}}{(2\pi)^3}\Big[\dot{X}_{\vec{k}}\dot{X}_{-\vec{k}} - \Big(\frac{k^2}{a^2} - \frac{9}{4}H^2 - \frac{3}{2}\dot{H} + (m_\chi^2 + F(\phi))\Big)X_{\vec{k}}X_{-\vec{k}}\Big], \tag{4.1}$$

and in terms of their canonically conjugate momenta, $\Pi_{X_{-\vec{k}}} = \dot{X}_{\vec{k}}$ and $\Pi_{X_{\vec{k}}} = \dot{X}_{-\vec{k}}$, the Hamiltonian will be

$$H_X = \frac{1}{2}\int \frac{d^3\vec{k}}{(2\pi)^3}\Big[\Pi_{X_{\vec{k}}}\Pi_{X_{-\vec{k}}} + \Big(\frac{k^2}{a^2} - \frac{9}{4}H^2 - \frac{3}{2}\dot{H} + (m_\chi^2 + F(\phi))\Big)X_{\vec{k}}X_{-\vec{k}}\Big]. \tag{4.2}$$

In the squeezed state formalism, the canonically conjugate phase space operators $(\hat{X}_{\vec{k}}(t), \hat{\Pi}_{X_{\vec{k}}}(t))$ are expressed in terms of time-dependent creation and annihilation operators as

$$\begin{aligned}\hat{X}_{\vec{k}} &= \frac{1}{\sqrt{2\tilde{\omega}_k}}\big[\hat{a}_{\vec{k}}(t) + \hat{a}^\dagger_{-\vec{k}}(t)\big]\\ \hat{\Pi}_{X_{\vec{k}}} &= -i\sqrt{\frac{\tilde{\omega}_k}{2}}\big[\hat{a}_{\vec{k}}(t) - \hat{a}^\dagger_{-\vec{k}}(t)\big].\end{aligned} \tag{4.3}$$

Where time-independent frequency is defined as $\tilde{\omega}_k = \sqrt{k^2/a^2 + m_\chi^2}$. The time dependent creation and annihilation operators, $\hat{a}_{\vec{k}}(t)$ and $\hat{a}^\dagger_{-\vec{k}}(t)$ satisfy the standard commutation relation, $\big[\hat{a}_{\vec{p}}, \hat{a}^\dagger_{-\vec{q}}\big] = (2\pi)^3\delta^3(\vec{p}+\vec{q})$. Finally, using Eq.(4.3) in (4.2), we are left with the desired form of the Hamiltonian of this system

$$\hat{H}_X = \frac{1}{2}\int \frac{d^3\vec{k}}{(2\pi)^3}\left[\left(\frac{\omega_k^2(t)}{2\tilde{\omega}_k} + \frac{\tilde{\omega}_k}{2}\right)\left(\hat{a}_{\vec{k}}\hat{a}^\dagger_{\vec{k}} + \hat{a}^\dagger_{-\vec{k}}\hat{a}_{-\vec{k}}\right) + \left(\frac{\omega_k^2(t)}{2\tilde{\omega}_k} - \frac{\tilde{\omega}_k}{2}\right)\left(\hat{a}_{\vec{k}}\hat{a}_{-\vec{k}} + \hat{a}^\dagger_{-\vec{k}}\hat{a}^\dagger_{\vec{k}}\right)\right] \tag{4.4}$$

where, the time-dependent frequency of the system having the generic interaction $F(\phi)$ is $\omega_k^2(t) = \left(\frac{k^2}{a^2} + m_\chi^2 + F(\phi) - \frac{9}{4}H^2 - \frac{3}{2}\dot{H}\right)$.

In the above Hamiltonian, the time-dependent frequency $\omega_k$ encodes the interaction between the daughter field and oscillatory inflaton. The first part of the Hamiltonian (4.4) signifies the collection of free oscillators with equal and opposite momenta, and the second part is their interaction which creates or destroys them leading to well-known two-mode squeezing phenomena between them. Significantly, the classical time-dependent background is responsible for such phenomena. Once we obtained the required Hamiltonian, the Heisenberg operator evolution equation, $\frac{d}{dt}(\hat{a}_{\vec{k}}) = i\big[\hat{H}_X,\ \hat{a}_{\vec{k}}\big]$ is derived as,

$$\frac{d}{dt}(\hat{a}_{\vec{k}}) = i\big[\mathcal{A}\hat{a}_{\vec{k}}(t) + \mathcal{B}\hat{a}^\dagger_{-\vec{k}}(t)\big]\,, \tag{4.5}$$

where the new symbols are

$$\mathcal{A} = \Big(-\frac{\omega_k^2(t)}{2\tilde{\omega}_k} - \frac{\tilde{\omega}_k}{2}\Big) \quad \text{and} \quad \mathcal{B} = \Big(-\frac{\omega_k^2(t)}{2\tilde{\omega}_k} + \frac{\tilde{\omega}_k}{2}\Big). \tag{4.6}$$

Substituting Eq.(3.8) to (4.5), we obtain the time evolution of the Bogoliubov coefficients.

$$\begin{aligned}\frac{d\alpha_k(t)}{dt} &= i\mathcal{A}\alpha_k(t) + i\mathcal{B}\beta_k^*(t)\\ \frac{d\beta_k(t)}{dt} &= i\mathcal{A}\beta_k(t) + i\mathcal{B}\alpha_k^*(t).\end{aligned} \tag{4.7}$$

### 4.1.1 Dynamical equations of $r_k$, $\varphi_k$, $\theta_k$ :

In the previous Chapter(3), we derived the expressions of the Bogoliubov coefficients in terms of $r_k, \theta_k, \varphi_k$ in Eq.(3.9). Plugging the expression (3.9) into Eq.(4.7), we derive the dynamical equations of the squeezing parameters. The utility of the solution of these dynamical equations lies in the study of not only the time evolution of the system but also the squeezed quantum state (3.11). Those equations are as follows:

$$\begin{aligned}\dot{r}_k &= -\mathcal{B}\sin 2\varphi_k\\ \dot{\varphi}_k &= \big(\mathcal{A} - \mathcal{B}\coth 2r_k\cos 2\varphi_k\big)\\ \dot{\theta}_k &= -\big(\mathcal{A} - \mathcal{B}\tanh r_k\cos 2\varphi_k\big).\end{aligned} \tag{4.8}$$

Having analyzed the above three equations, we come to know that none of the dynamical equations of $r_k$, $\varphi_k$, and $\theta_k$ depend upon the rotation angle $\theta_k$. So while studying the dynamics, the system will not exhibit any such sensitive dependence on the rotation angle $\theta_k$.

We have prepared the ground to study the chaotic dynamics of the interacting system during preheating. The next two sections will be devoted to a thorough investigation of the pattern of chaos and the interconnection among the resonance instability, squeezing, and chaos of the bosonic system for quartic and trilinear interactions with the forms of the generic interaction $F(\phi)$ given in (2.129).

## 4.2 Squeezing and OTOC: For quartic interaction ($g^2\phi^2\chi^2$)

In this section, we will concentrate on the study of chaos by explicitly calculating OTOC for $n = 1, 2, 3$ for four-leg or quartic interaction ($g^2\phi^2\chi^2$). The daughter quantum field $\chi$ which experiences periodic driving force due to a coherently oscillating inflaton field, will be observed to undergo resonant amplification. Such resonant amplification will be shown to be chaotic in nature. As discussed before, we compute OTOC on the time-evolving squeezed quantum state and show that such a quantity will exponentially grow with time. The inverse time scale of such exponential growth will be identified as the Lyapunov exponent. We shall discuss the chaotic scenario and its multifarious characteristics with minute details for three different background dynamics. To this end, we would like to point out that in our present analysis, we will confine ourselves strictly to the regime where back-reaction is negligible.

### 4.2.1 Initial condition specification:

To perform a detailed numerical analysis the key dynamical equations are given in (4.8). For the appropriate initial conditions, we first write down the field mode in terms of three squeezing parameters. Replacing Eq. (4.3) in the mode expansion form of rescaled field $\hat{X}(t,\vec{x})$ like (2.100) and also using (3.7), we get the following form

$$\hat{X}(t,\vec{x}) = \int \frac{d^3\vec{k}}{(2\pi)^3}.\Big[X_k(t)\hat{a}_{\vec{k}}(t_0).e^{i\vec{k}.\vec{x}} + X_k^*(t)\hat{a}^\dagger_{\vec{k}}(t_0).e^{-i\vec{k}.\vec{x}}\Big]. \tag{4.9}$$

The general field mode function can further be expressed in terms of squeezing parameters $r_k, \varphi_k, \theta_k$ as

$$X_k(t) = \frac{e^{-i\theta_k}}{\sqrt{2\omega_k}}\big[\cosh r_k - e^{-2i\varphi_k}\sinh r_k\big]. \tag{4.10}$$

The proper specification of the initial condition can be associated with the well-known Bunch-Davies for each mode fluctuation. Now, comparing the BD vacuum condition $\alpha_k(t_0=0)=1,\ \beta_k(t_0=0)=0$ with (3.9) at the initial time $t=t_0=0$, we get the initial conditions for $r_k(t=0)=0$, and $\theta_k(t=0)=2l\pi$, where $l$ is any positive integer including zero. We have the freedom to take any value of $\varphi_k(t=0)$ since all the physical quantities are independent of the squeezing angle $\varphi_k$. Such choices essentially make the initial condition for the initial quantum state to be an unsqueezed one, and that is equivalent to the choice of the Bunch-Davies vacuum. Once initial conditions are properly specified, we are now in a position to proceed with our numerical studies.

### 4.2.2 Computing OTOC for $n = 1$:

We shall now present our numerical results for $r_k, \varphi_k, \theta_k$ solving three coupled differential equations (4.8). We will be interested in those parameters $(k, g)$ that reside in the instability region of the stability-instability chart (see Fig.(2.12)), and hence the resonant solution exists. It is a well-known fact that long-wavelength modes (IR modes) are efficiently amplified during the preheating era. For pictorial representation and comparison, we have chosen three different long-wavelength modes and the inflaton daughter field coupling constant $g = 5\times10^{-4}$. With those parameter choices, we solve for the squeezing parameters shown in Fig.(4.1). During the initial phase of the evolution, the squeezing parameter, $r_k$ grows linearly in time $z_1$ and subsequently saturates. As expected, the slope of the growth increases with decreasing momentum. Long wavelength mode takes a longer time to saturate, which depends on the decreasing amplitude of the background driving force due to Hubble expansion. All these features can indeed be seen in Fig.(4.1). Subject to the variation of $r_k$ as shown in Fig.(4.1) and using Eq. (3.10), we obtain occupation number density, $n_k$ (See Fig.(4.2)), which grows exponentially in time for all three modes under consideration. However, generic dynamical features of squeezing ($r_k$) and number density $\ln(n_k)$ are that they initially grow and reach a peak value, and finally the system relaxes to saturation with small periodic fluctuations. Furthermore, as expected, the long wavelength

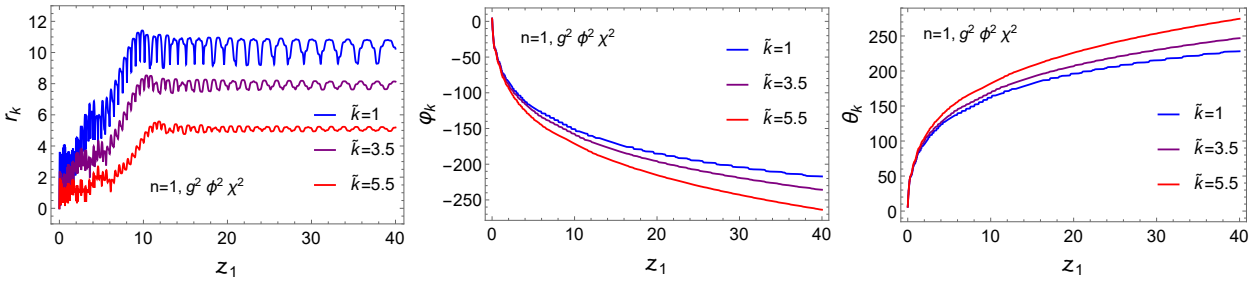


FIGURE 4.1: *Figure represents the time evolution of squeezing parameter($r_k$), squeezing angle($\varphi_k$) and rotation angle($\theta_k$) for three different momentum modes($k$) and the coupling strength is chosen to be $g = 5 \times 10^{-4}$. Here squeezing angle($\varphi_k$) and rotation angle ($\theta_k$) are given in units of radian. Here, we have taken three different modes for which the squeezing parameters grow efficiently, giving a considerable production of particles.*

modes are easily excited than those of the higher momentum mode. These features nicely resemble the thermalization process of any thermodynamic system under perturbation. For every individual mode, the thermalization associated with the saturated region can be said to be achieved at their respective time scale. Long-wavelength modes thermalize faster in time than short-wavelength ones. From Fig.(4.1) we obtain different values of saturation time scale for three different modes having different wavelengths. For $k = m_\phi^{\text{end}(1)}$, we have $z_1 \sim 9.9$, for $k = 3.5 m_\phi^{\text{end}(1)}$, we have $z_1 \sim 10.7$ and for $k = 5.5 m_\phi^{\text{end}(1)}$, we have $z_1 \sim 12$.

For the present system, the reason behind such variation of saturation time scale is hidden in the dynamics of the background periodic driving force due to the coherently oscillating inflaton field. The dimensionless resonance parameter which controls the dynamics is $q_g^2 = (g/m_\phi^{\text{end}(1)})^2 \phi_0^2(t)$. Where, $\phi_0(t)$ is decaying as $\sim a^{-3/2}$ (see Eq.(2.62)). The condition of stochastic resonance in expanding background must satisfy [66], $q_g^4 m_\phi^{\text{end}(1)} \gtrsim H$, we have

$$g\phi_0(t) \gtrsim m_\phi^{\text{end}\,(1)} \left(\frac{H_{\text{end}}}{m_\phi^{\text{end}\,(1)}}\right)^{\frac{1}{4}} \left(\frac{z_1}{z_1^{\text{end}}}\right)^{-\frac{1}{4}}. \tag{4.11}$$

Considering CMB observed value of scalar spectral index $n_s = 0.9743 \pm 0.0034$, we have $H_{\text{end}} \sim 10^{-6} M_{\text{pl}}$. Post-inflationary dynamics leads $H/m_\phi^{\text{end}\,(1)} = (H_{\text{end}}/m_\phi^{\text{end}\,(1)})(z_1^{\text{end}}/z_1)$ very small throughout the entire phase with $m_\phi^{\text{end}\,(1)} \sim 10^{-5} M_{\text{pl}}$. On the other hand, the amplitude of $\phi_0$ also decreases, $\phi_0 \propto z_1^{-1}$ with the background expansion. Therefore, we have competition between the aforesaid two effects. As the dependence of the above condition (4.11) on $H$ is weak ($H^{1/4}$), it has been observed that after a certain number of inflaton oscillations, the above resonance condition (4.11) fails to satisfy, and eventually the resonance process ceases. This causes the saturation in all the physical quantities, namely occupation density ($n_k$), squeezing amplitude ($r_k$), etc, as shown in Fig.(4.1) and Fig.(4.2).

So far, we discussed in detail the dynamics of quantum states of the produced particles in terms of their squeezing parameters and phenomena of chaotic resonance in terms of

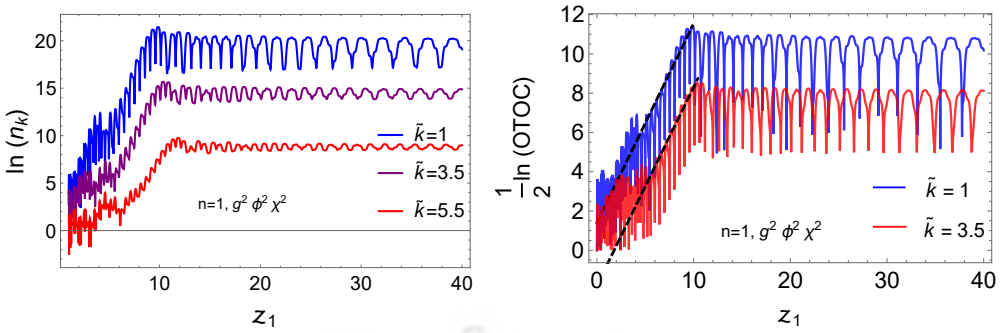


FIGURE 4.2: **Left Panel:***Figure represents the growth of occupation number density $n_k$ for three efficient $k$ modes with $g = 5 \times 10^{-4}$.* **Right Panel:** *Figure represents the time variation of logarithm of OTOC amplitude for two different $k$ modes corresponding to significant production with $g = 5 \times 10^{-4}$. Two black dashed lines for two modes indicate the average straight line-like growth of* ln(OTOC) *and from the slope of those lines we estimate the average growth indices of chaos of the system.*

the field modes. In the following, we will study in detail how such non-trivial behavior of resonance is encoded into OTOC, considered as an interesting diagnostic tool of chaos. We first numerically construct the symplectic matrix in terms of commutators of the field mode and its conjugate momentum. From the dominant eigenvalue of the calculated symplectic matrix (3.22), we identify the OTOC dynamics, which is parametrized by the *Lyapunov exponent*($\lambda_k$).

For a quantum chaotic system the OTOC measured in terms of the function $\mathcal{C}(t)$ is expected to behave as $\mathcal{C}(t) \sim e^{2\lambda t}$ with $\lambda$ being the *quantum Lyapunov exponent*. Therefore, the slope of (1/2)ln(OTOC) in time will give us the information of Lyapunov exponent $\lambda$. In our context we have been using dimensionless time-variable $z_1 = m_\phi^{\text{end}\,(1)} t/2\pi$, and the associated dimensionless Lyapunov exponent will be $\tilde{\lambda} \equiv 2\pi\lambda/m_\phi^{\text{end}\,(1)}$ which implies $\mathcal{C}(z_1) \sim e^{2\tilde{\lambda} z_1}$. In Fig.(4.2), we plotted (1/2)ln(OTOC) vs $z_1$, and linear growth in time can be clearly observed for a finite period of time. Therefore, the initial chaotic nature is manifested through the linear logarithmic growth of OTOC of a quantum field mode which is under the periodic driving force. Our chronological discussions so far seem to suggest that for a quantum chaotic system, squeezing of quantum state parameter $r_k$, logarithmic growth of occupation number density ln($n_k$) and logarithm of the highest OTOC amplitude have some intriguing relation, which we will discuss later. Furthermore, as expected, chaos remains present in the system until the resonance ends or saturation begins, which essentially hints probably the obvious fact that chaos and instability are intimately tied with each other [191]. Now our task is to determine the LE corresponding to different long-wavelength modes. As one observes from Fig.(4.2), growth of $\frac{1}{2}$ ln(OTOC)

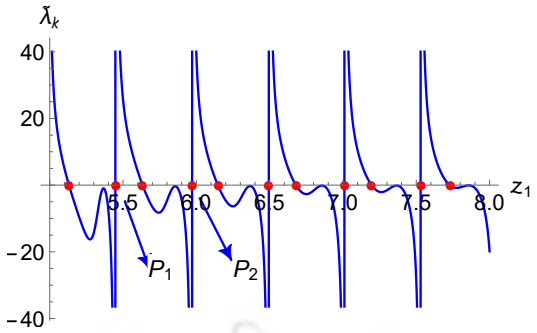


FIGURE 4.3: *Behaviour of Modified Lyapunov exponent(LE)* $\tilde{\lambda}_k$ *for* $k = m_\phi^{\text{end}\,(1)}$

can be fitted by a straight line. We have the expression $\mathcal{C}(z_1) = Ae^{2\tilde{\lambda}z_1}$ such that

$$\ln\,\mathcal{C}(z_1) = \ln A + 2\tilde{\lambda}z_1 \Rightarrow \frac{1}{2}\frac{d}{dz_1}\ln\mathcal{C}(z_1) = \tilde{\lambda}, \tag{4.12}$$

where $A$ is any proportionality constant. For a particular $k$ mode the $\tilde{\lambda}_k = \frac{2\pi\lambda_k}{m_\phi^{\text{end}\,(1)}}$ in above expression (4.12) has many different zeros (red colored points) as in FIG. 4.3. For a particular $k$ mode growth of OTOC depends upon a particular value of the Lyapunov exponent. However, Fig.(4.3) shows a time-varying nature of LE, and we need to determine an effective value of this LE. To do so, we prescribe the following procedure: We numerically compute the oscillation average of the function between two alternative zeros as marked by point $P_1$ at $z_1 = 5.5$ and $P_2$ at $z_1 = 6$ in Fig.(4.3). Repeating this process from the initial time when the growth of a mode starts to the time when it saturates, we define the averaged effective LE ($\tilde{\lambda}_k^{\text{eff}}$) as,

$$\tilde{\lambda}_k^{\text{eff}} = \frac{\sum_{\text{oscillation}}\langle\frac{1}{2}\frac{d}{dz_1}\ln\mathcal{C}(z_1)\rangle|_{\text{oscillations}}}{\text{Number of oscillation}}$$

Using this procedure, we compute effective LE for various $k$ modes, fixing the coupling strength $g$ and also for different coupling parameters $g$ with fixed $k$ mode (see Table 4.1). Finally in Fig.(4.7) we have given pictorial representation of *Lyapunov spectra*, that is $\tilde{\lambda}_k^{\text{eff}}$ vs $\tilde{k} \equiv \left(k/m_\phi^{\text{end}\,(1)}\right)$ and $\tilde{\lambda}_k^{\text{eff}}$ vs $g$. From the figure, it is evident that the variation of LE with $k/m_\phi^{\text{end}\,(n)}$ is not monotonic but rather chaotic. Despite this chaotic behaviour, effectively with increasing $\tilde{k}$ resonance effect decreases as expected. On the other hand, in coupling space, there seems to exist an effective critical coupling around which the system becomes maximally chaotic.

### 4.2.3 For $n = 2$ :

We have explicitly shown all the necessary steps of our study in the previous case for the $n = 1$ model. We present the numerical solution of $r_k, \varphi_k, \theta_k$ using the equations (4.8) in

Table 4.1: *Variation of effective LE*($\tilde{\lambda}_k^{eff}$) *with* $\tilde{k}$ *and coupling strength "g" for* $n = 1(g^2\phi^2\chi^2)$

| | | | | | | | | | | | |
|---|---|---|---|---|---|---|---|---|---|---|---|
| $g = 5 \times 10^{-4}$ | $\tilde{k}$ | 1 | 1.5 | 2 | 2.5 | 3 | 3.5 | 4 | 4.5 | 5 | 6 |
| | $\tilde{\lambda}_k^{\text{eff}}$ | 0.919 | 0.994 | 0.895 | 0.586 | 1.037 | 1.043 | 0.845 | 0.713 | 0.592 | 0.497 |
| $g = 3 \times 10^{-4}$ | $\tilde{k}$ | 1 | 1.5 | 2 | 2.5 | 3 | 3.5 | 4 | 4.5 | 5 | 6 |
| | $\tilde{\lambda}_k^{\text{eff}}$ | 0.475 | 0.712 | 0.704 | 0.930 | 0.575 | 0.690 | 0.601 | 0.411 | 0.406 | 0.201 |
| $\tilde{k} = 1$ | $g \times 10^{-4}$ | 1 | 2 | 3 | 4 | 5 | 6 | 7 | 8 | 9 | 10 |
| | $\tilde{\lambda}_k^{\text{eff}}$ | 0.457 | 0.468 | 0.475 | 0.894 | 0.919 | 1.190 | 1.186 | 1.214 | 1.153 | 1.133 |
| $\tilde{k} = 3$ | $g \times 10^{-4}$ | 1 | 2 | 3 | 4 | 5 | 6 | 7 | 8 | 9 | 10 |
| | $\tilde{\lambda}_k^{\text{eff}}$ | 0.389 | 0.454 | 0.575 | 0.827 | 1.037 | 0.887 | 0.916 | 1.055 | 1.086 | 1.090 |

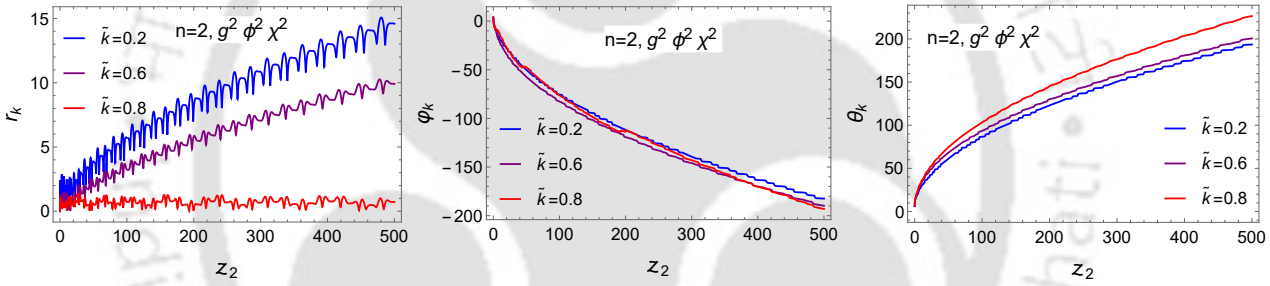


Figure 4.4: *Figure represents the time evolution of squeezing parameter*($r_k$)*, squeezing angle*($\varphi_k$) *and rotation angle*($\theta_k$) *for three efficient k modes, and the coupling strength is chosen to be* $g = 4 \times 10^{-5}$*. Here Squeezing angle*($\varphi_k$) *and rotation angle* ($\theta_k$) *are given in unit of radian.*

the Fig.(4.4). Unlike the model $n = 1$, here the squeezing parameter shows continuous growth over time without any late-time saturation. As the particle number density is tied to the behavior of the squeezing parameter $r_k$, the very nature of $r_k$ will have an impact on $n_k$, and this essentially causes an uninterrupted growth of $n_k$ over time. This feature is special for $n = 2$, when the inflaton field behaves like a relativistic fluid $w_\phi = 1/3$, rendering a vanishing Ricci scalar. Due to this simple fact, the background inflaton field can be made to satisfy $\tilde{\Psi}'' + \bar{\lambda}\tilde{\Psi}^3 = 0$ [104] in conformal coordinate, which is independent of expansion. The solution of this equation is an oscillatory elliptic cosine function with constant amplitude. Such a feature is responsible for the uninterrupted growth of particle number over time for the $n = 2$ model as opposed to other $n$ values. In reality, such an uninterrupted growth process can be terminated by taking into account the backreaction

Table 4.2: *Variation of effective LE($\tilde{\lambda}_k^{eff}$) with $\tilde{k}$ and coupling strength "g" for $n = 2(g^2\phi^2\chi^2)$*

| | | | | | | | | | | | |
|---|---|---|---|---|---|---|---|---|---|---|---|
| $g = 5.5 \times 10^{-5}$ | $\tilde{k}$ | 0.1 | 0.11 | 0.15 | 0.2 | 0.25 | 0.3 | 0.35 | 0.4 | 0.45 | 0.5 |
| | $\tilde{\lambda}_k^{\text{eff}}$ | 0.421 | 0.490 | 0.432 | 0.420 | 0.394 | 0.369 | 0.319 | 0.258 | 0.195 | 0.152 |
| $g = 3.9 \times 10^{-5}$ | $\tilde{k}$ | 0.1 | 0.15 | 0.2 | 0.25 | 0.3 | 0.35 | 0.4 | 0.5 | 0.55 | 0.6 |
| | $\tilde{\lambda}_k^{\text{eff}}$ | 0.319 | 0.381 | 0.534 | 0.600 | 0.626 | 0.493 | 0.549 | 0.609 | 0.932 | 0.258 |
| $\tilde{k} = 0.1$ | $g \times 10^{-5}$ | 1.6 | 1.9 | 2.4 | 3.2 | 3.9 | 4.7 | 5.5 | 6.3 | 7.1 | 7.9 |
| | $\tilde{\lambda}_k^{\text{eff}}$ | 0.358 | 1.228 | 1.007 | 0.507 | 0.319 | 0.324 | 0.421 | 0.355 | 0.258 | 0.374 |
| $\tilde{k} = 0.3$ | $g \times 10^{-5}$ | 1.6 | 1.9 | 2.4 | 3.2 | 3.9 | 4.7 | 5.5 | 6.3 | 7.1 | 7.9 |
| | $\tilde{\lambda}_k^{\text{eff}}$ | 0.841 | 0.974 | 0.295 | 0.416 | 0.626 | 0.316 | 0.369 | 0.349 | 0.290 | 0.286 |

of the produced particle into the background (for details see [104, 162]. In our present study, we are not incorporating those additional effects. For this case, therefore, in a similar manner, we evaluate Eq.(3.23) and, substituting the obtained results in (3.22), we present the behavior of OTOC amplitude in Fig.4.6. We further computed $\tilde{\lambda}_k^{\text{eff}}$ with $\tilde{k}$ and coupling strength $g$. Taking various $k$ modes and coupling strength $g$ given in the Table 4.2, in Fig.(4.7), we show the variation of approximate effective LE with dimensionless momentum mode $\tilde{k} \equiv \left(k/m_\phi^{\text{end}\,(2)}\right)$ and coupling strength $g$. Effective LE takes a prominent peak at some value of $\tilde{k}$ for a given coupling strength, then it gradually decreases with the increase of $\tilde{k}$. This sharp peak indicates the presence of a particular mode, for which the system is maximally chaotic. For the $n = 1$ model, this peak is less sharp compared to the $n = 2$. Variation of effective LE with $g$ follows the more or less same behavior as it does with $\tilde{k}$. For a given $\tilde{k}$, the system peaks at a particular coupling, then it falls with the increase of $g$ with some fluctuations.

### 4.2.4 For $n = 3$ :

This particular value of $n$ induces a stiff fluid of inflaton with an equation of state $w_\phi = 1/2$. In this background, the fluctuations evolve in a somewhat different manner compared to the models $n = 1, 2$. The behavior of squeezing parameters is depicted in Fig.(4.5). Here we observe that the growth time scale of the squeezing parameter $r_k$ is very large and occurs over a very large number of background oscillations as opposed to the previous cases. In Fig.(2.6), it is clearly seen that with the increase of background EoS, the decay rate of inflaton amplitude or in other words, the decay rate of the strength of the driving source gradually falls, causing a slow energy transfer from background to the produced fluctuation. As long as the decay of the inflaton amplitude takes place only

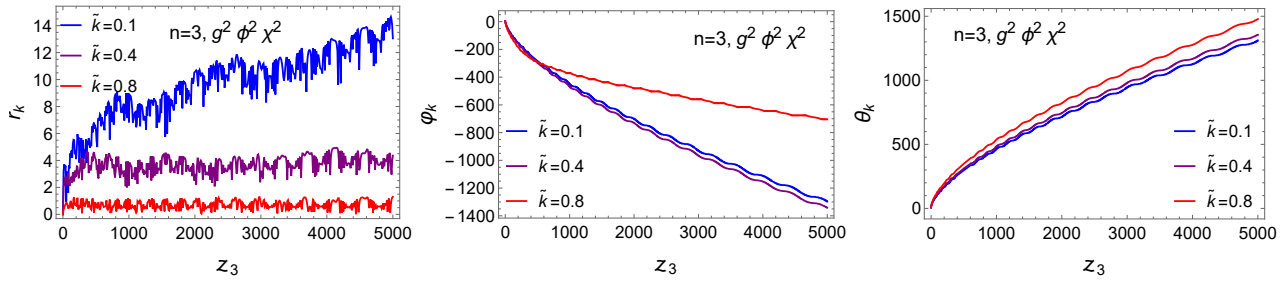


FIGURE 4.5: *Figure represents the time evolution of squeezing parameter ($r_k$), squeezing angle ($\varphi_k$) and rotation angle($\theta_k$) for three k modes corresponding to significant production, and the coupling strength is chosen to be $g = 4 \times 10^{-5}$. Here, the squeezing angle($\varphi_k$) and the rotation angle ($\theta_k$) are given in units of radian.*

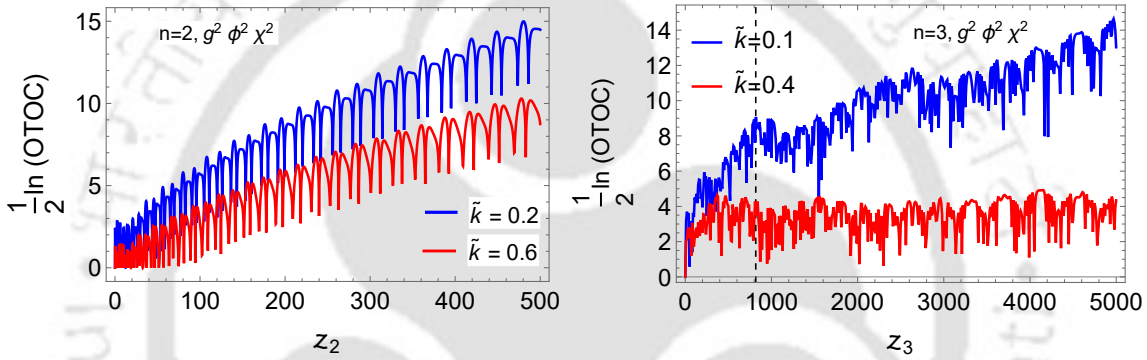


FIGURE 4.6: *Figure represents the time variation of logarithm of OTOC amplitude for $n = 2, 3$ corresponding to two different k modes with coupling strength $g = 4 \times 10^{-5}$ for both cases.*

because of background expansion, this slow energy transfer will essentially cause the $r_k$ amplitude as well as the OTOC amplitude(see Fig.(4.6) to grow very slowly over a long time.

Likewise, $n = 2$ case, the absence of any saturation of OTOC amplitude within a finite time makes the determination of exact $\tilde{\lambda}_k^{\text{eff}}$ for various $\tilde{k}$ and coupling $g$ a bit difficult. In order to have a rough estimate of the growth index of chaos, $\tilde{\lambda}_k^{\text{eff}}$, for different $\tilde{k}$ and $g$, we take the first prominent peak just before a plateau-type region. For example, in Fig.(4.6), we take first peak around $z_3 \sim 820$ for $\tilde{k} = 0.1$( See vertical dashed line in the right figure) and around $z_3 \sim 380$ for $\tilde{k} = 0.4$. Sticking to this idea of local saturation, we have given approximate numerical values of $\tilde{\lambda}_k^{\text{eff}}$ corresponding to a few resonant modes for two different couplings in Table 4.3. We expect that the nature of the variation of $\tilde{\lambda}_k^{\text{eff}}$ with two parameters$(\tilde{k}, g)$ will remain unaffected by the choice of the aforesaid time scale. Stochastic nature, being an inherent property of the system, results in a non-monotonic variation of $\tilde{\lambda}_k^{\text{eff}}$ with $\tilde{k}$ and $g$ as seen in Fig.(4.7).

Table 4.3: *Variation of effective LE*($\tilde{\lambda}_k^{eff}$) *with* $\tilde{k}$ *and coupling strength "g" for* $n = 3(g^2\phi^2\chi^2)$

| | | | | | | |
|---|---|---|---|---|---|---|
| $g = 5.3 \times 10^{-5}$ | $\tilde{k}$ | 0.1 | 0.15 | 0.2 | 0.25 | 0.3 |
| | $\tilde{\lambda}_k^{\text{eff}}$ | $9.639 \times 10^{-3}$ | $12.798 \times 10^{-3}$ | $12.854 \times 10^{-3}$ | $17.701 \times 10^{-3}$ | $8.574 \times 10^{-3}$ |
| $g = 3.5 \times 10^{-5}$ | $\tilde{k}$ | 0.1 | 0.15 | 0.2 | 0.25 | 0.3 |
| | $\tilde{\lambda}_k^{\text{eff}}$ | $9.324 \times 10^{-3}$ | $8.380 \times 10^{-3}$ | $10.059 \times 10^{-3}$ | $7.609 \times 10^{-3}$ | $3.324 \times 10^{-3}$ |
| $\tilde{k} = 0.1$ | $g \times 10^{-5}$ | 1.8 | 3.5 | 5.3 | 7.1 | 8.9 |
| | $\tilde{\lambda}_k^{\text{eff}}$ | $5.530 \times 10^{-3}$ | $9.324 \times 10^{-3}$ | $9.639 \times 10^{-3}$ | $26.524 \times 10^{-3}$ | $9.899 \times 10^{-3}$ |
| $\tilde{k} = 0.3$ | $g \times 10^{-5}$ | 1.8 | 3.5 | 5.3 | 7.1 | 8.9 |
| | $\tilde{\lambda}_k^{\text{eff}}$ | $2.786 \times 10^{-3}$ | $3.324 \times 10^{-3}$ | $8.574 \times 10^{-3}$ | $14.517 \times 10^{-3}$ | $9.127 \times 10^{-2}$ |

## 4.3 Squeezing and OTOC: For trilinear interaction ($\sigma\phi\chi^2$) :

In this section, we shall repeat the same discussion as given in Section (4.2) for three different $n = 1, 2, 3$, taking three-leg interaction $\sigma\phi\chi^2$. Before presenting our numerical results for different models subject to this interaction, we need to give a short discussion on the parametric resonance process for this particular interaction. The structure of the resonance greatly relies on the nature of the interaction. To study the effect of tri-linear interaction on the resonance process, the relevant part in the time-dependent frequency of the massless case $\omega_k^2(t) = \left(\frac{k^2}{a^2} + \sigma\phi - \frac{9}{4}H^2 - \frac{3}{2}\dot{H}\right)$ would be the first two terms. From the evolution of background inflaton in Fig.(2.6), it is evident that when $\phi < 0$ during one half of each oscillation, modes satisfying $k^2 < \sigma|\phi(t)|a^2$ lead to negative $\omega_k^2(t)$. In that case, the well-known *tachyonic instability* sets in, and the modes experience exponential amplification. Therefore, for a linear periodic driving force, the system encounters parametric as well as tachyonic instability, which is a distinctive feature of tri-linear interaction. This process is known as *tachyonic resonance*[106, 107, 109]. Both instability leads to a very efficient production of fluctuation, which causes the preheating phase to end within a few background oscillations. In the later discussion of this section, we will come across this distinctive feature of this particular interaction very closely. Nevertheless, we will follow the same analysis, and the behavior of the three squeezing parameters is depicted in Fig.(4.8) for different values of $n$. Both qualitative and quantitative differences can be observed in the smooth nature of the growth of squeezing and OTOC, along with its amplitude. For $n = 1$, saturation time scale turns out to be for $\tilde{k} = 1$, $z_1 \sim 5.2$, for $\tilde{k} = 2$, $z_1 \sim 6.9$ and for $\tilde{k} = 3$, $z_1 \sim 9.2$. For $n = 2$, due to effective flatness perceived by both background and fluctuations, every mode is expected to have eternal growth in $r_k$. For all the cases, the growth seems to

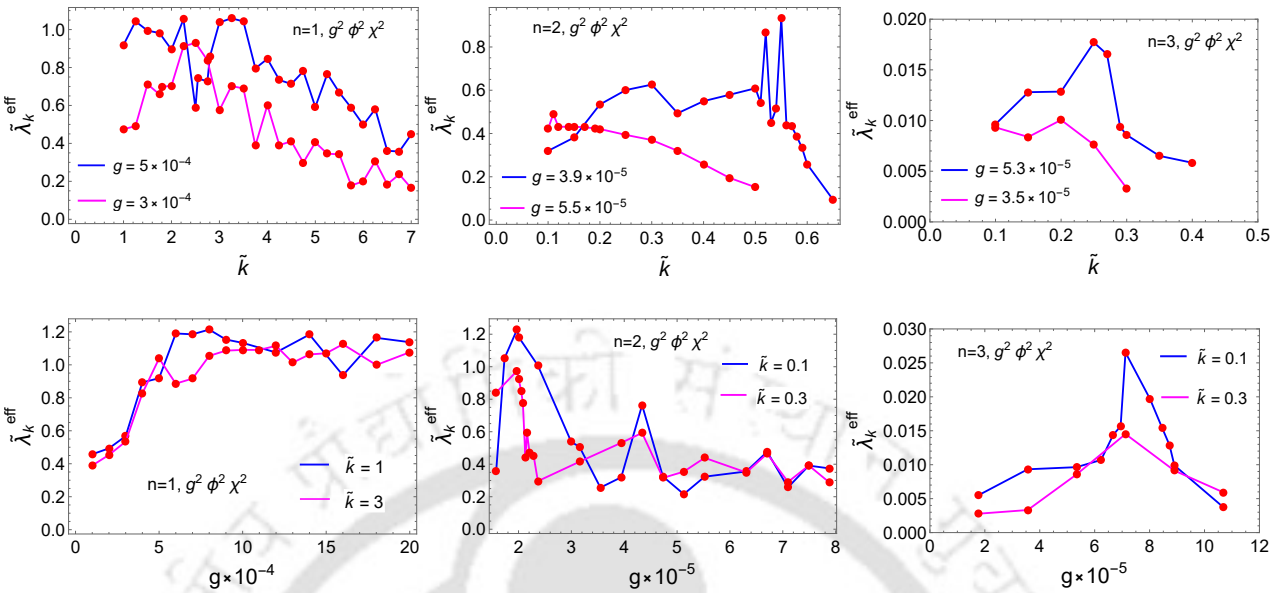


Figure 4.7: *Variation of* $\tilde{\lambda}_k^{\text{eff}}$ *with* $\tilde{k} \equiv (k/m_\phi^{\text{end}\,(n)})$ *and coupling strength* $g$ for three models.

be less stochastic compared to the four-leg interaction. This property will make an impact on the chaotic nature of the system. Using Eq.(3.22), we also plotted the nature of OTOC to capture the chaotic dynamics of the system for three models(See Fig.(4.9). In Fig.(4.9), for $n = 1$ model, we notice that for $\tilde{k} = 1$, OTOC amplitude peaks around $z_1 \sim 5.2$ and $z_1 \sim 9.2$ for $\tilde{k} = 3$ and then it fluctuates without further growth. Finally employing the same methodology that was described in the last Section (4.2), we estimate the effective LE $\tilde{\lambda}_k^{\text{eff}}$ for different values of $k$ with fixed $g$, and for different $g$ with fixed $k$ (see Fig.(4.10)). In the Table 4.4, Table 4.5 and Table 4.6, we have given some numerical values of $\tilde{\lambda}_k^{\text{eff}}$ for different momentum modes $\tilde{k}$ and coupling constant $\tilde{g} \equiv \left(\sigma/m_\phi^{\text{end}\,(n)}\right)$ for three different models.

## 4.4 Relation between Floquet exponent and Lyapunov exponent, and OTOC Spectrum

So far, we have mainly focused on the nature of OTOC and calculated the associated Lyapunov exponents. However, it is understood that such growth is intimately connected to the resonant production of modes. We, therefore, expect to have a direct relationship between the Lyapunov and Floquet exponents, which are the measures of chaos and resonance, respectively, under the influence of a periodic driving force. To establish an approximate analytic relation between those two quantities, we shall resort to the method of

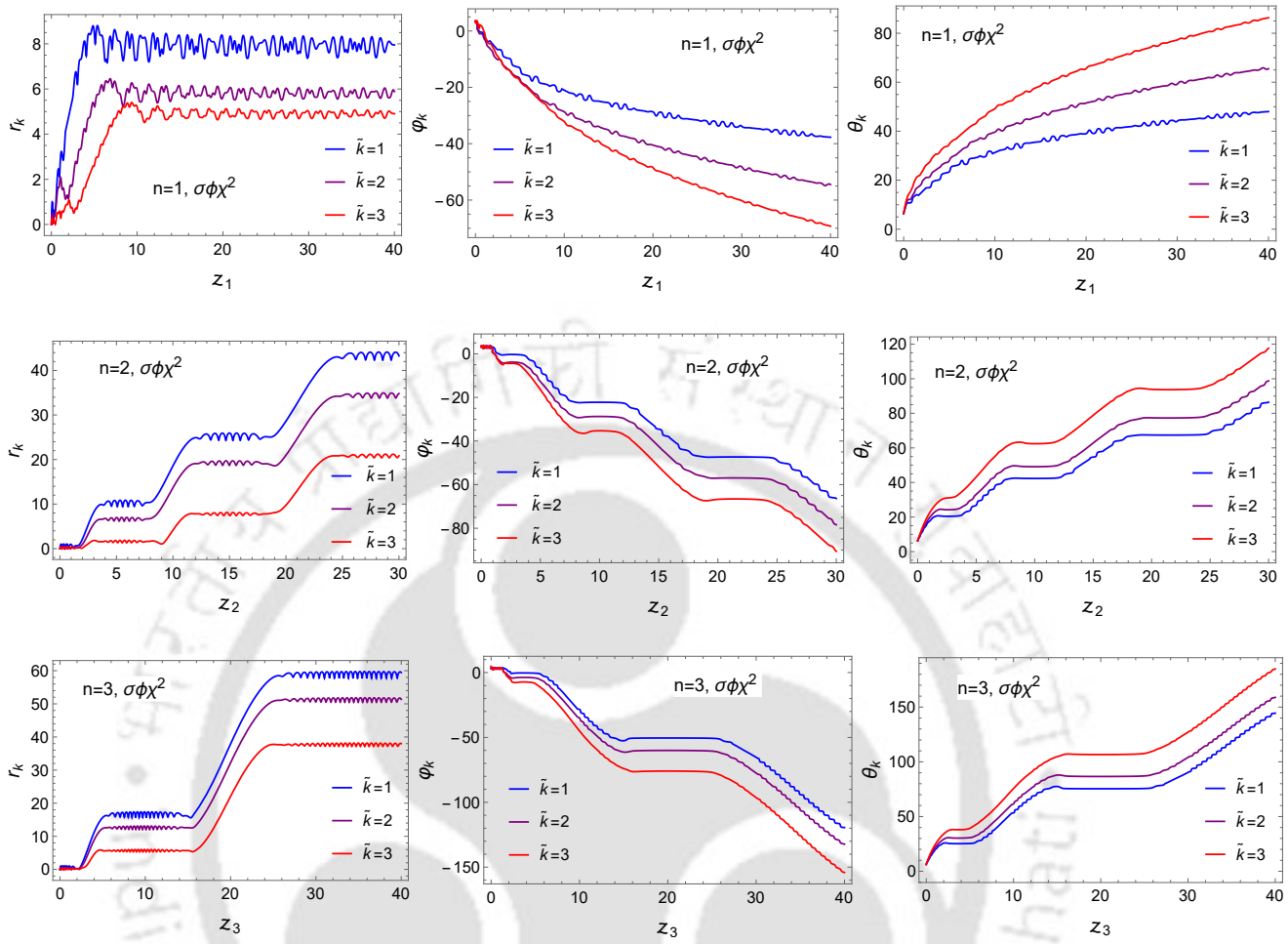


FIGURE 4.8: *Figure represents the time evolution of squeezing parameter($r_k$), squeezing angle($\varphi_k$) and rotation angle($\theta_k$) for $\tilde{k} = 1, 2, 3$ modes with dimensionless coupling strength $\tilde{g} = 8 \times 10^{-5}$ (first row), $\tilde{g} = 9.8 \times 10^{-5}$ (second row), and $\tilde{g} = 1.1 \times 10^{-4}$ (third row). This parameter choice leads to parametric resonance in the system.*

successive scattering on parabolic potential discussed in detail [66, 103]. Here we quote the main results. If we investigate the resonance process more closely, we notice that whenever the background inflaton crosses zero at the minimum, the particle number density shows a sharp growth. Otherwise, particle number density behaves as an adiabatic invariant quantity between two successive zero crossings. Such behavior allows one to obtain an approximate analytical expression of the field mode in terms of Floquet exponent around each zero crossing time, say the $j$-th crossing time is defined to be $t_j$. If one consider $\phi^2\chi^2$ interaction, near $t_j$, massless field mode Eq.(2.128) for $n = 1$ assumes following form in the parabolic potential around $t = t_j$,

$$\frac{d^2X_k}{dt^2} + \left(\frac{k^2}{a^2} + g^2(\phi_0)_j^2(m_\phi^{\text{end}\,(1)})^2(t - t_j)^2\right)X_k = 0 \tag{4.13}$$

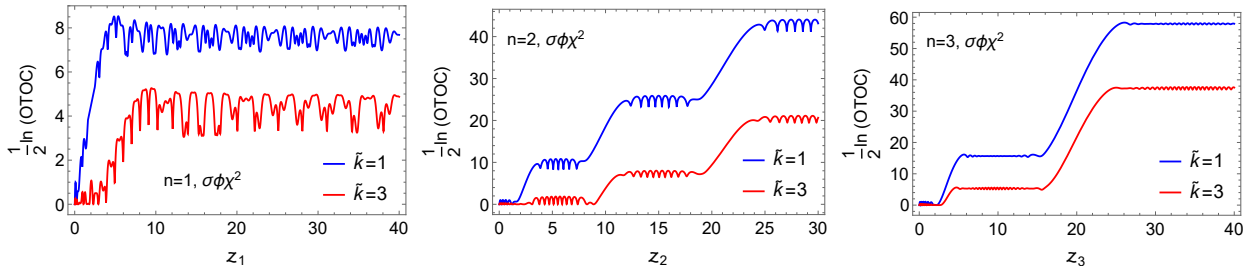


FIGURE 4.9: *Figure represents the time variation of logarithm of OTOC amplitude for two efficient* $\tilde{k} = 1, 3$ *modes with dimensionless coupling strength* $\tilde{g} = 8 \times 10^{-5}$ *(left panel),* $\tilde{g} = 9.8 \times 10^{-5}$ *(middle panel), and* $\tilde{g} = 1.1 \times 10^{-4}$ *(right panel).*

Table 4.4: *Variation of effective LE*($\tilde{\lambda}_k^{\text{eff}}$) *with* $\tilde{k}$ *and dimensionless coupling strength "*$\tilde{g}$*" for* $n = 1(\sigma\phi\chi^2)$

| | | | | | | | | | | | |
|---|---|---|---|---|---|---|---|---|---|---|---|
| $\tilde{g} = 1.6 \times 10^{-4}$ | $\tilde{k}$ | 1 | 1.5 | 2 | 2.5 | 3 | 3.5 | 4 | 4.5 | 5 | 6 |
| | $\tilde{\lambda}_k^{\text{eff}}$ | 2.896 | 1.928 | 1.421 | 1.312 | 1.507 | 1.117 | 0.943 | 0.837 | 0.583 | 0.466 |
| $\tilde{g} = 8 \times 10^{-5}$ | $\tilde{k}$ | 1 | 1.5 | 2 | 2.5 | 3 | 3.5 | 4 | 4.5 | 5 | 6 |
| | $\tilde{\lambda}_k^{\text{eff}}$ | 1.685 | 1.635 | 1.697 | 0.813 | 0.617 | 0.594 | 0.435 | 0.251 | 0.302 | 0.115 |
| $\tilde{k} = 1$ | $\tilde{g} \times 10^{-5}$ | 2.9 | 3.9 | 5.2 | 8 | 9.8 | 11.7 | 16 | 18.2 | 20.8 | 32.5 |
| | $\tilde{\lambda}_k^{\text{eff}}$ | 1.208 | 1.104 | 1.044 | 1.685 | 2.203 | 2.435 | 2.896 | 2.214 | 2.385 | 2.571 |
| $\tilde{k} = 3$ | $\tilde{g} \times 10^{-5}$ | 2.9 | 3.9 | 5.2 | 8 | 9.8 | 11.7 | 16 | 18.2 | 20.8 | 32.5 |
| | $\tilde{\lambda}_k^{\text{eff}}$ | 0.165 | 0.227 | 0.488 | 0.617 | 0.952 | 1.109 | 1.507 | 2.072 | 1.789 | 1.598 |

where $(\phi_{0\ j})$ is the time-dependent amplitude of the inflaton calculated at the instant of the $j$-th crossing $t_j$. For $|t - t_j| > 0$, the adiabaticity condition is satisfied. Using the Bogoliubov method [66, 103],one can compute the rescaled Floquet exponent as

$$\tilde{\mu}_k^j = \ln\left(1 + 2e^{-\pi\kappa_j^2} - 2\sin\theta_j^{\text{tot}} e^{-\frac{\pi}{2}\kappa_j^2}\sqrt{1 + e^{-\pi\kappa_j^2}}\right). \tag{4.14}$$

Where, $\kappa_j^2 = k^2/(a(t_j)^2 g m_\phi^{\text{end}\,(1)}(\phi_0)_j)$, and $\theta_j^{\text{tot}}$ is the total random phase accumulated by the field wave from the initial time to the instant $t_j$. In order to obtain the nature of OTOC spectra as well as the possible relation between Floquet and Lyapunov exponent, we need to evaluate first the commutation relation between field($X_k$) and conjugate momenta($\Pi_k$) as outlined in Chapter(3). We closely follow the reference [66] in deriving the amplitude of

Table 4.5: *Variation of effective LE*($\tilde{\lambda}_k^{\text{eff}}$) *with* $\tilde{k}$ *and dimensionless coupling strength "*$\tilde{g}$*" for* $n = 2(\sigma\phi\chi^2)$

| | | | | | | | |
|---|---|---|---|---|---|---|---|
| $\tilde{g} = 1.9 \times 10^{-4}$ | $\tilde{k}$ | 1 | 1.5 | 2 | 2.5 | 3 | 4 |
| | $\tilde{\lambda}_k^{\text{eff}}$ | 38.066 | 36.861 | 35.799 | 33.094 | 29.545 | 21.114 |
| $\tilde{g} = 9.8 \times 10^{-5}$ | $\tilde{k}$ | 1 | 1.5 | 2 | 2.5 | 3 | 4 |
| | $\tilde{\lambda}_k^{\text{eff}}$ | 27.649 | 25.468 | 24.339 | 20.486 | 12.602 | 6.946 |
| $\tilde{k} = 1$ | $\tilde{g} \times 10^{-5}$ | 3.6 | 6.3 | 9.8 | 14.1 | 19.3 | 25.2 |
| | $\tilde{\lambda}_k^{\text{eff}}$ | 13.385 | 19.452 | 27.649 | 30.519 | 38.066 | 46.235 |
| $\tilde{k} = 3$ | $\tilde{g} \times 10^{-5}$ | 3.6 | 6.3 | 9.8 | 14.1 | 19.3 | 25.2 |
| | $\tilde{\lambda}_k^{\text{eff}}$ | 4.052 | 6.270 | 12.602 | 23.364 | 29.545 | 41.041 |

Table 4.6: *Variation of effective LE*($\tilde{\lambda}_k^{\text{eff}}$) *with* $\tilde{k}$ *and dimensionless coupling strength "*$\tilde{g}$*" for* $n = 3(\sigma\phi\chi^2)$

| | | | | | | | | |
|---|---|---|---|---|---|---|---|---|
| $\tilde{g} = 2.1 \times 10^{-4}$ | $\tilde{k}$ | 1 | 1.5 | 2 | 2.5 | 3 | 3.5 | 4 |
| | $\tilde{\lambda}_k^{\text{eff}}$ | 6.567 | 6.424 | 6.195 | 5.746 | 5.374 | 5.050 | 4.764 |
| $\tilde{g} = 1.1 \times 10^{-4}$ | $\tilde{k}$ | 1 | 1.5 | 2 | 2.5 | 3 | 3.5 | 4 |
| | $\tilde{\lambda}_k^{\text{eff}}$ | 4.360 | 4.419 | 4.280 | 3.926 | 3.134 | 2.184 | 1.996 |
| $\tilde{k} = 1$ | $\tilde{g} \times 10^{-5}$ | 1.8 | 4 | 7.1 | 11.1 | 16 | 28.5 | 44.5 |
| | $\tilde{\lambda}_k^{\text{eff}}$ | 1.460 | 2.407 | 3.347 | 4.360 | 5.542 | 7.585 | 9.518 |
| $\tilde{k} = 3$ | $\tilde{g} \times 10^{-5}$ | 1.8 | 4 | 7.1 | 11.1 | 16 | 28.5 | 44.5 |
| | $\tilde{\lambda}_k^{\text{eff}}$ | 0.057 | 0.732 | 1.737 | 3.134 | 4.433 | 6.848 | 9.123 |

the commutation relations using the asymptotic form of the field mode $X_k$ as in Eq.(2.106). We write the expression of OTOC amplitude as follows:

$$|X_k(t_j)\dot{X}_k^*(t_0) - X_k^*(t_j)\dot{X}_k(t_0)|^2 = \frac{e^{\tilde{\mu}_k^j \cdot j}\omega_k(t_0)(1+\cos\mathcal{V})^2}{2\omega_k(t_j)} \tag{4.15}$$

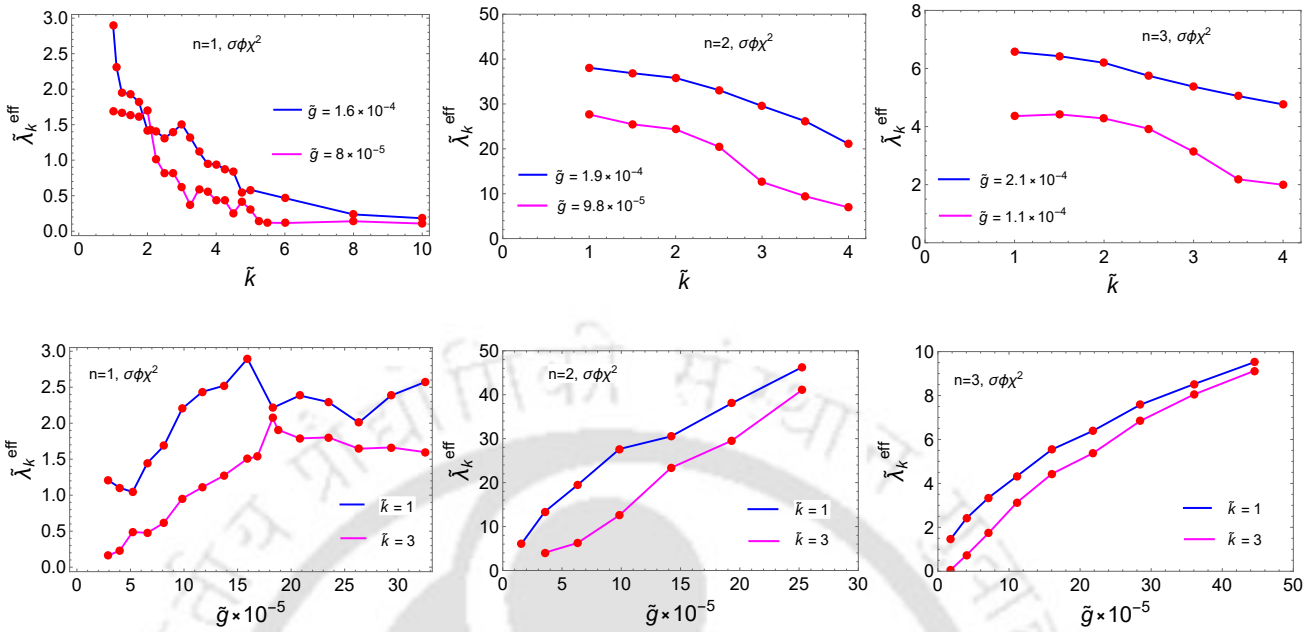


Figure 4.10: *Figure represents the Variation of $\tilde{\lambda}_k^{eff}$ with dimensionless modes $\tilde{k}$ and dimensionless coupling $\tilde{g}$ for three models in three-leg type interaction.*

Where $\mathcal{V}$ is a constant phase, $t_j = \frac{\pi j}{m_\phi^{\text{end }(1)}}$ and $t_0$ is the initial time. Using this amplitude, the expression of OTOC spectra for $\phi^2\chi^2$ type interaction at any later time $t$ becomes

$$\ln(\text{OTOC}) \equiv \ln\Big(1+2e^{-\pi\kappa^2}-2\sin\theta^{\text{tot}}e^{-\frac{\pi}{2}\kappa^2}\sqrt{1+e^{-\pi\kappa^2}}\Big).\frac{m_\phi^{\text{end }(1)}t}{\pi}+\ln\Big(\frac{\omega_k(t_0)}{2\omega_k(t)}\Big)+2\ln(1+\cos\mathcal{V}) \tag{4.16}$$

We have used Eq.(4.14) to reach the final form of the spectra in Eq.(4.16). Now associated with the Lyapunov exponent as outlined in Chapter(3) and using Eq.(2.106) we write, Lyapunov exponent at the instant of $j$-th crossing as,

$$\begin{aligned} e^{2\lambda_k t_j} &= e^{\tilde{\mu}_k^j.j}\Big(\frac{\omega_k(t_0)}{2\omega_k(t_j)}\Big)(1+\cos\mathcal{V})^2 \\ \Rightarrow \tilde{\lambda}_k^j &= \tilde{\mu}_k^j + \frac{1}{j}\ln\Big(\frac{\omega_k(t_0)}{2\omega_k(t_j)}\Big) + \frac{2}{j}\ln(1+\cos\mathcal{V}) \end{aligned} \tag{4.17}$$

Here the out-of-time order commutation of one combination field and conjugate momenta has been defined between $t_0$ and the $j$-th crossing instant $t_j$.
The above expression is true at the point of a particular zero crossing $t_j$. We, therefore, can have an effective relation

$$\tilde{\lambda}_k^{\text{eff}} = \tilde{\mu}_k^{\text{eff}} + \overline{\frac{1}{j}\ln\Big(\frac{\omega_k(t_0)}{2\omega_k(t_j)}\Big)} + 2\,\overline{\frac{1}{j}\ln(1+\cos\mathcal{V})}, \tag{4.18}$$

where the average is taken over time from the initial to the saturation time scale. So practically, we take the average over the number of oscillations executed by the background within the time required for saturation of a particular mode. In the above expression, the phase $\mathcal{V}$ is random around $\pi/2$. So, after taking the average over the entire saturation time scale for a particular mode, the third term will have a vanishing contribution. For the second term, we have numerically found a smaller contribution compared to $\tilde{\mu}_k^{\rm eff}$. Finally, we find $\tilde{\lambda}_k^{\rm eff}$ and $\tilde{\mu}_k^{\rm eff}$ are more or less the same, which is consistent with the numerical result.

From Eq.(4.16), it is clearly seen that the nature of the Floquet exponent governs the spectral nature of OTOC. The growth index of particle number in Eq.(4.14), being a function of random phase in an expanding background, causes somewhat random growth of number density after every zero crossing or every half of a period. This non-monotonic behavior is also reflected in the spectral behavior of OTOC amplitude as shown in Fig.(4.11). The random oscillatory behavior of OTOC amplitude in momentum space is also caused by the randomness of the Floquet exponent in the context of stochastic resonance, as discussed in detail in [66]. Out of three different background driving sources, only for $n = 1$ the system reaches a saturation state * after going through chaotic dynamics within a finite time. While evaluating OTOC spectra numerically for the $n = 1$ model, we have chosen the saturation time corresponding to the maximum mode that will be produced in a broad resonance regime. Unlike the $n = 1$ model, no such saturation is observed for the $n = 2$ model as shown in Fig.(4.6) and Fig.(4.9)(Reason is discussed in Section (4.2). For this case, we computed OTOC spectra by truncating the evolution at any arbitrary instant of time for each momentum mode. With the increase of potential exponent $n$, slow decay of the amplitude of inflaton causes slow growth of OTOC amplitude (See Fig.(4.6) for $n = 3$), and for this, we have considered a local saturation time corresponding to the maximum mode chosen in the spectra in Fig.(4.11), where the coupling parameters are chosen from the broad resonance regime (See the lower bound in Eq.(2.139)). Despite several fluctuations, one common feature observed in the spectra for all the models is that the higher the momentum, the lower the OTOC amplitude, which actually mimics the nature of resonant particle production. The existence of different momentum bands for different values of the resonance strength parameter $(q_g, q_\sigma)$ can be observed to be nicely imprinted in the broad oscillatory feature in the OTOC spectrum, particularly for quadratic coupling. However, for tri-linear coupling due to tachyonic and broad resonance, such an oscillatory nature smoothens out.

## 4.5 Squeezing, Chaos and thermalization

### 4.5.1 Poincaré section: Semi-classical visualization

At the outset of this section, we gain some insight into how the chaotic nature of the system is connected to the squeezing of states. It is known that positive LE signifies

*Late time saturation of different modes can be assumed to be reminiscent of thermalization of a typical thermodynamic system.

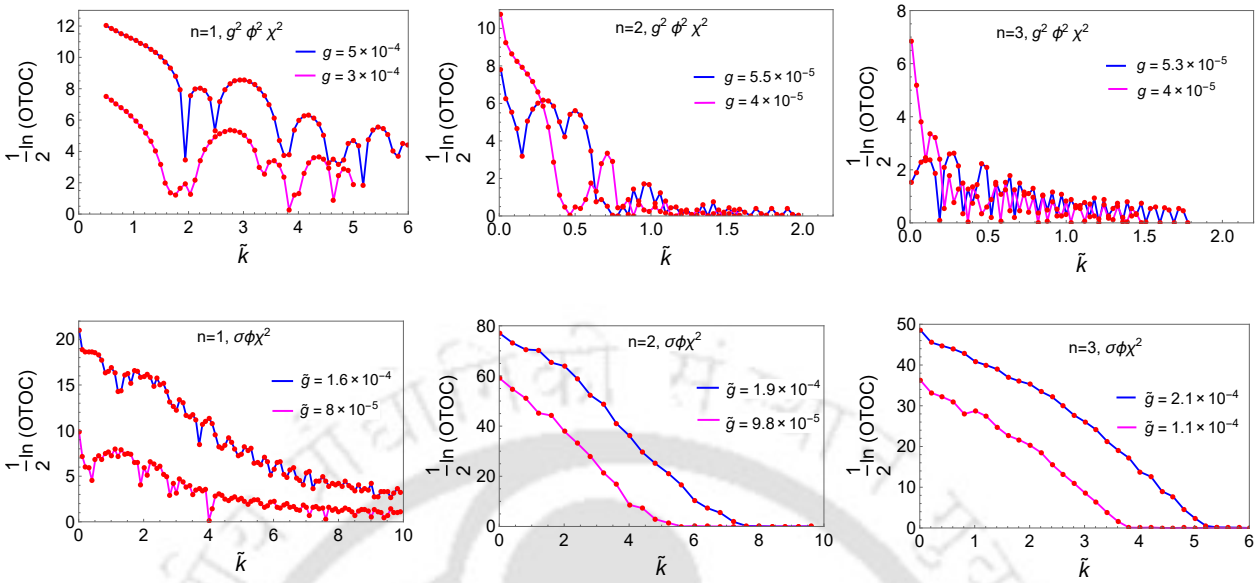


Figure 4.11: *Figure represents the spectral behaviour of* ln(OTOC) *with two different coupling strengths for two interactions.*

the chaotic nature of a system. It actually measures the sensitivity of the system to its initial condition. The well-known method to explore chaotic behavior is to generate and analyze the Poincaré sections, particularly for non-integrable systems. Each field mode of our present system is a periodically driven one-dimensional parametric oscillator, which does not have any conserved quantity. For this system, we identified the semi-classical phase space variables by calculating their expectation values in the squeezed quantum state. We obtain the Poincaré section or a surface of section, by mapping those semi-classical phase space variables projecting onto two dimensions. We generate this Poincaré section by sampling the data points in a 2D plane at a regular interval set by the periodicity of the driving force namely the oscillatory inflaton field. We present Poincaré section for $n = 1$ model for both types of interactions(three-leg and four-leg), besides this, we also give the parametric plot of $X_k$ and $X_k^{'}$, which carries the information of squeezing of the system for both models(See Fig.(4.12). So, for a non-chaotic system, we expect that all the data points will lie in an orbit and will form closed orbits, but here we see that the phase space points are scattered in the plane and are forming a cloud of points, which signifies the presence of chaos in the system. This typical behavior also tells us about the squeezing of the system. Looking at Fig.(4.1), we readily understand that the squeezing parameter of this system corresponding to particular parameter values $(k, g)$ grows over a certain duration and then gets saturated, meaning that after the point of saturation, there is no further squeezing in the system. Furthermore, the growth of OTOC in Fig.(4.2) also exhibits the same behavior. Connecting these two outcomes together, we can state that as long as squeezing is there, the system will remain chaotic, which vindicates the statement that *highly squeezed states*

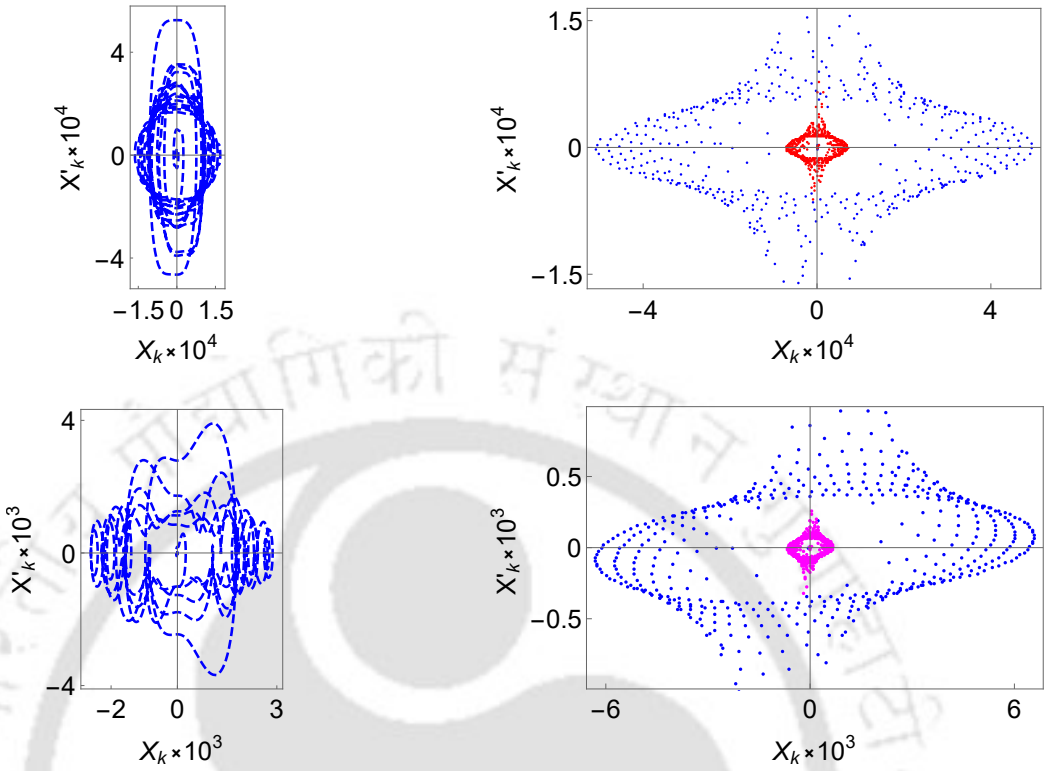


FIGURE 4.12: ***Upper Panel:*** *Figure on the left represents the parametric plot of* $X_k$ *and* $X_k^{'}$ *where* $\tilde{k} = 1$ *and figure on the right represents the Poincaré section for* $n = 1$ *model for* $\phi^2\chi^2$ *interaction. Different colors correspond to different initial conditions. In the Poincaré section, Blue colored points are phase space points for* $\tilde{k} = 1$ *and Red colored points are phase space points for* $\tilde{k} = 3$*. Here dimensionless coupling strength* $g = 5 \times 10^{-4}$*.* ***Lower Panel:*** *Figure on the left represents the parametric plot of* $X_k$ *and* $X_k^{'}$ *where* $\tilde{k} = 1$ *and figure on the right represents the Poincaré section for* $n = 1$ *model for* $\sigma\phi\chi^2$ *interaction. In the Poincaré section, Blue colored points are phase space points for* $\tilde{k} = 1$ *and Magenta colored points are phase space points for* $\tilde{k} = 2$*. Here dimensionless coupling strength* $\tilde{g} = 8 \times 10^{-5}$ *.*

*are prime for quantum chaos.* In the following section, we would like to shed light on the possible thermalization temperature of such a chaotic system.

### 4.5.2 Defining thermalization temperature and Maldacena-Shenker-Stanford (MSS) bound

**MSS bound:** Chaos and thermalization have been the subject of investigation over a long period in non-equilibrium field theory. In this regard an intriguing bound on chaos has been proposed in [180] which we call MSS bound in brief, and the Lyapunov exponent is universally conjectured to be bounded as $\lambda \leq 2\pi(k_B/\hbar)T$, where $T$ is assumed to be the

temperature of the chaotic system when it becomes thermalized after the relaxation from chaotic instability. What it suggests the growth of chaos of a thermal quantum system is bounded by the system temperature $T$. If we reverse this argument, one may arrive at the following universal lower bound on the temperature of a quantum chaotic system $T \geq (\hbar/(2\pi k_B))\lambda$. In other words, if a quantum system thermalizes under the influence of chaotic dynamics, there exists a lower bound on temperature set by the Lyapunov exponent. In our present system, we apply the proposed bound and estimate the minimum possible temperature that the system can achieve. So far, we have discussed the chaotic nature and calculated the value of the associated Lyapunov exponents of a quantum scalar field when coupled with the oscillating inflaton. Further, we have performed our analysis for individual momentum modes and computed the Lyapunov exponent for each mode. Therefore, instead of getting the information about the temperature of the entire system, we will have the information of each mode. Using the bound we may write,

$$T_k \geq \frac{\hbar}{2\pi k_B}\lambda_k. \tag{4.19}$$

Where $\lambda_k$ and $T_k$ are LE and the corresponding minimum possible temperature perceived by the mode. A more rigorous estimation would be to do the analysis in real space by using the lattice simulation technique and identifying the MSS bound. We will defer the lattice studies for our future work. Using the approximate values of effective LE given in Table 4.1 and Table 4.4 for $\phi^2\chi^2$ and $\sigma\phi\chi^2$ interaction respectively, we can identify the lower bound of the temperature of the system by averaging over the resonant momentum band as follows,

$$\bar{T}_{\rm MSS} \geq \frac{\hbar}{2\pi k_B}\frac{\int_{\rm band}\lambda_k k^2 dk}{\int_{\rm band} k^2 dk} \tag{4.20}$$

When the chaotic system reaches thermal equilibrium, the minimum temperature achieved by the system will be given by the following bound in Eq.(4.20). By exploiting this we obtain the lower bound of temperature for different coupling strengths for two different interactions. Using Eq.(4.20), for example, we found $\bar{T}_{\rm MSS} = 2.62 \times 10^{11}(4.76 \times 10^{11})$ GeV for $g = 3 \times 10^{-4}(5 \times 10^{-4})$ in case of $g^2\phi^2\chi^2$ interaction and $\bar{T}_{\rm MSS} = 2.33 \times 10^{11}(4.59 \times 10^{11})$ GeV for $\tilde{g} = 8 \times 10^{-5}(1.6 \times 10^{-4})$ in case of $\sigma\phi\chi^2$ interaction. We find that the lower bound of temperature is indeed approximately the same for different couplings and interactions as represented in Fig.(4.13). However, given the intimate relation between chaos and squeezing, can the squeezing of the daughter particle states also encode the information about the temperature of the system under consideration? In the following we conjecture that squeezed state indeed can encode the temperature of the system under consideration as follows:

**Temperature from Squeezed State:** We have already obtained the squeezed state by the application of the unitary evolution operator $\hat{\mathcal{U}}_k$ on an unsqueezed two-mode vacuum in Eq. (3.11). For that squeezed state, we can define the density matrix for two modes as

$$\hat{\rho}(\vec{k},-\vec{k}) = \frac{1}{\cosh^2 r_k}\sum_{n,n'=0}^{\infty} e^{2i(n-n')\varphi_k}(-1)^{n+n'}\tanh^{n+n'} r_k \left|n_{\vec{k}}, n_{-\vec{k}}\right\rangle\left\langle n'_{\vec{k}}, n'_{-\vec{k}}\right| \tag{4.21}$$

Since one of the two modes is always inaccessible to the observer, we can calculate the reduced density matrix $\hat{\rho}(\vec{k})$ from the full one by tracing out the mode $-\vec{k}$ and get

$$\hat{\rho}(\vec{k}) = \sum_{n=0}^{\infty} \langle n_{-\vec{k}}|\hat{\rho}(\vec{k},-\vec{k})|n_{-\vec{k}}\rangle = \frac{1}{\cosh^2 r_k} \sum_{n=0}^{\infty} \tanh^{2n} r_k |n_{\vec{k}}\rangle\langle n_{\vec{k}}| \tag{4.22}$$

We assume the produced particles are instantaneously thermalized. The above expression of a quantum state can be identified as a thermal squeezed state with inverse temperature defined as [136]

$$\beta_k = -\ln \tanh^2 r_k. \tag{4.23}$$

We can therefore identify this as a system temperature under consideration. As the squeezing parameter $r_k$ is a function of time, $\bar{\beta}_k$ will also vary with time. The very nature of $r_k$ shows a prominent peak near the saturation time scale as seen for $n = 1$ model observed in Fig.(4.1) and Fig.(4.8). The temperature of the system tied with $r_k$ will be maximum at an instant, and for different $k$, this temperature peak position will be different. Collecting only those maximum values, and following the definition of effective MSS bound stated in Eq.(4.20), we define the average system temperature defined for the thermal squeezed state (SS) over the resonance band as

$$\bar{\beta}_{\rm SS} = \frac{1}{\bar{T}_{\rm SS}} = -\frac{2\int_{\rm band} \ln(\tanh r_k) k^2 dk}{\int_{\rm band} k^2 dk}. \tag{4.24}$$

We assumed Boltzmann constant $k_B = 1$ in natural unit. Our motive is to check the consistency of the variation of this average temperature for different coupling with the MSS bound and we anticipate that this temperature variation will abide by the MSS bound for any coupling strength. In the absence of any kind of self-interaction or back-reaction, as late time saturation of $r_k$ is obvious in $n = 1$ model for both the interaction, we concentrate only on $n = 1$ case in order to define an effective temperature of the system. Using the relation (4.24) for two different interactions, we determine an approximate effective temperature that the system can achieve after saturation for different inflaton coupling. For example $\bar{T}_{\rm SS} = 6.75 \times 10^{14}$ GeV for $g = 2 \times 10^{-4}$ in case of $\phi^2\chi^2$ interaction and $\bar{T}_{\rm SS} = 4 \times 10^{13}$ GeV for $\tilde{g} = 3 \times 10^{-5}$ in case of $\phi\chi^2$ interaction, which are greater than the MSS bound we calculated before. We indeed found the MSS bound to be satisfied for different inflaton coupling and parameters as depicted in Fig.(4.13). It has already been shown how non-trivial interaction with a classical background makes the quantum states of the daughter field squeezed. Here, we attempt to estimate the temperature of that thermal squeezed state. As our Present interest is strictly confined to the early preheating phase, so, the temperature defined above should not be thought of as the reheating temperature, which is defined at the end of reheating. Rather, it should be understood as an approximate estimate of system temperature extracted through the squeezing parameter $r_k$ at the end of the chaotic instability phase during preheating. Rayleigh-Jeans Temperature: We would like to stress another consideration in the context of thermalization of a system having a very large occupation number. In this limit, when the system is in thermal equilibrium,

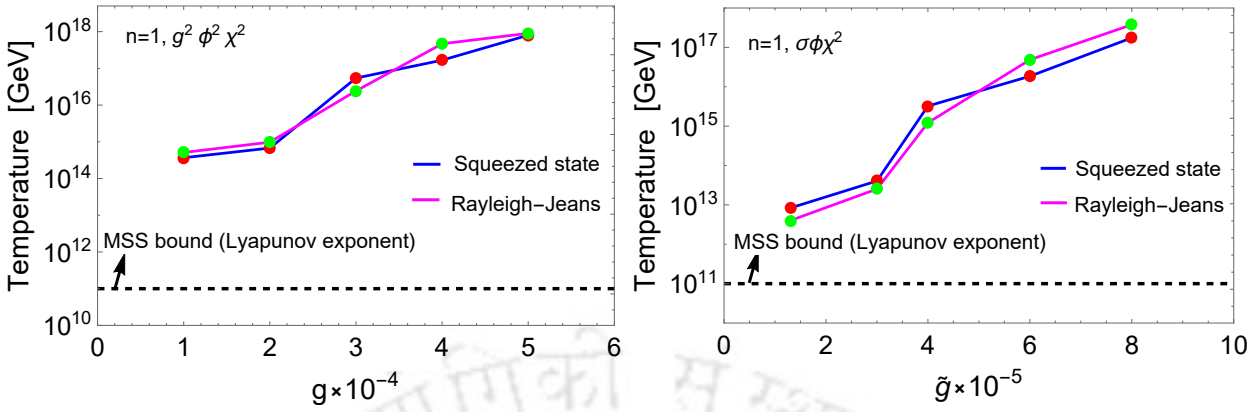


Figure 4.13: **Left Panel:** *Figure represents the variation of effective temperature with coupling strength for four-leg type interaction.* **Right Panel:***Figure represents the variation of effective temperature with coupling strength for three-leg type interaction. It is seen that effective temperatures for different couplings consistently follow the lower bound of temperature for both interactions. Here red dots indicate the temperature obtained through the relation (4.24) and green dots indicate the temperature obtained through the Rayleigh-Jeans formula given in (4.25) for both the interactions.*

the Rayleigh-Jeans spectrum can be defined as $n_k E_k \simeq T_k$, for occupation number $n_k$ and associated energy $E_k$ corresponding to a mode $k$ [159, 162]. In this equation, $T$ is again the temperature of the system under consideration. In our present context energy per mode can be calculated to be $E_k = \langle 1_k | \hat{H}_k | 1_k \rangle = \left( \frac{\Omega_k^2}{2\omega_k} + \frac{\omega_k}{2} \right)$ using the Hamiltonian $H_X$ of the produced massless fluctuation in Eq.(4.4). As the occupation number is usually very high during the preheating phase, to have a better understanding of the thermalization across all the resonant modes for a particular coupling, we can use the combination $n_k E_k$. Following the Eq.(4.24) here also we can define an average temperature using the Rayleigh-Jeans(RJ) formula as

$$\bar{T}_{\rm RJ} = \frac{\int_{\rm band} n_k E_k k^2 dk}{\int_{\rm band} k^2 dk}. \tag{4.25}$$

Most interestingly, we find that the equilibrium temperature predicted by the thermal squeezed state in Eq.(4.24) matches with the thermalized temperature of the system predicted by the Rayleigh-Jeans formula given in Eq.(4.25) pretty well, as shown in Fig.(4.13) by red and green dots accordingly. This indeed establishes a beautiful connection between the non-equilibrium squeezed quantum system with the non-equilibrium preheating phase in the early universe.

Considering an idealised scenario, although we ignore the backscattering effect of the daughter field onto the classical background, in reality, this effect is unavoidable. In fact, this important effect causes system temperatures to drop by many orders compared to the ideal scenario as pointed out in [25, 26] for $n = 2$ model. In these literature, authors have presented the process of thermalization of the system after inflation employing wave kinetic

theory. During the early stage of preheating, energy density of the daughter field grows exponentially in the parametric resonance regime, and the associated occupation number density of the field gets concentrated in the IR regime. The larger the coupling strength, the faster the parametric resonance terminates because of the increasing possibility of back-reaction owing to the gradual increase of energy density in the daughter field sector. The presence of an active background energy source(inflaton energy) causes turbulence to arise in the system in the post-inflationary state. As soon as the resonance ceases, the system shows a greater tendency to transfer its energy from IR to UV regime, and this post-resonance phase is accompanied by the *stationary turbulence* and *free turbulence* stage depending upon the energy stored in the background inflaton field. Eventually, the system thermalizes through the long stage of thermalization classified as *free turbulence*, where the occupation number density of the daughter field approaches the thermal distribution function in a self-similar way with a constant energy density stored in that field. Finally, for the $n = 2$ model with inflaton self-coupling as well as daughter particle self-coupling terms, the thermalization temperature was found to be unacceptably low, that is, $T \sim 100$ eV when the inflaton self-coupling is of the order of $10^{-13}$. Therefore, to achieve a reasonably high reheating temperature in a realistic model, some couplings in the sector of the daughter field (self-coupling, or coupling to the inflaton) have to exceed significantly the scale of the inflaton self-coupling. In the present discussion, one point that also finds relevance is the incomplete decay of the inflaton at the end of preheating. Although the universe transits to a radiation-dominated state with a characteristic EoS 1/3, the rest of the energy in the inflaton sector must be transferred to the daughter sector to achieve a true thermalized state. One possible way that has been elucidated in [162] is the perturbative decay of the inflaton into radiation. Introducing the three-leg type coupling $\sigma\phi\chi^2$, we can complete the decay process to achieve the correct initial condition for the Big Bang. The main purpose of the following discussion is to give some hints at the realistic picture of early preheating and subsequent thermalization phase in the presence of all sorts of backreaction and backscattering effects.

However, in this chapter, we have investigated the thermal behavior of the daughter field system having chaotic instability in the squeezed state language in an idealized preheating scenario, and interestingly, we came up with the findings that the thermal behavior of the scalar daughter field system follows the Bosonic distribution. Since our present analysis is far from complete, and hence the estimation of different temperatures may not strictly be taken as the actual system temperature. At this juncture, therefore, it would be worth pointing out the standard expectation, and we would like to close this section by indicating a naive estimation of the maximum possible temperature the system may attain right after the end of inflation, and that can be calculated by utilizing the following relation $H^2_{\rm end} = 1/(3M^2_{\rm pl})\rho = \pi^2 g_{\rm re}/(90M^2_{\rm pl})T^4$ with $g_{\rm re} = 106.75$ being the effective number of degrees of freedom. In the expression, we considered Stefan-Boltzmann law temperature of radiation energy density $\rho = (g_{\rm re}\pi^2/30)T^4$. Assuming $H_{\rm end} \sim 4 \times 10^{-6} M_{\rm pl}$, one gets $T \sim 2.6 \times 10^{15}$ GeV which anyway falls within the estimation displayed in Fig.(4.13). The over- and underestimation of the temperature concerning the perturbative temperature mentioned above can be avoided by the full lattice simulation, which we consider for our

future study. In addition to that, the extension of the present work to a realistic preheating, thermalization scenario has been intended to be studied separately in future.

## 4.6 Summary

Understanding the non-perturbative dynamics of particle production is of utmost importance, particularly in the quantum field theory framework. In the realm of cosmology, the early universe reheating phase is an interesting laboratory to understand such phenomena. During the reheating phase, inflaton plays the role of periodic driving force which may lead to resonant particle production if the appropriate conditions are satisfied. Extensive exploration has been performed to understand such non-perturbative phenomena with the motivation to successfully reheat our universe. In this chapter, we re-explored such non-perturbative production in the preheating stage and analyzed its underlying physics in relation to quantum squeezing, chaos, and their intriguing connection with thermalization. To the best of our knowledge along that direction, very little attention has been paid (see early references [155–158]) mainly because of a lack of understanding of the possible connection between the reheating and its subsequent evolution to standard cosmology. However, preheating can be assumed as an ideal phase of non-equilibrium processes which demand very special attention from the point of view of theoretical understanding of early universe cosmology. The mechanism of thermalization is of great theoretical importance on its own which is not very well understood. Particularly during reheating, it is believed to have played a significant role in some well-studied cosmological phenomena such as producing matter-anti-matter asymmetry (baryogenesis), and dark matter abundance that we observe today. In the context of perturbative reheating and Lattice studies, the issue of thermalization has been discussed [26, 159, 160, 162]. However, a theoretical understanding of this is still far from complete. In this work, we try to initiate a theoretical exploration of the phenomena of squeezing, chaos, and their deep connection with thermalization during preheating, and we advocate that we have some promising results that are worth exploring with greater detail in the future. For our present study, we have considered two well-studied inflaton interactions with the daughter field, namely $\phi\chi^2$ and $\phi^2\chi^2$. After the inflation, the inflaton field oscillates near the minimum of its potential $\phi^n$ and acts as a quasi-periodic driving force leading to chaotic growth of quantum fluctuation, which is observed to be imprinted in the OTOC of phase space variables. We have computed the associated effective Lyapunov exponent ($\tilde{\lambda}_k^{\text{eff}}$) characterizing the chaos in the system. During this chaotic growth, the quantum state of the produced particles evolved into a squeezed state. We have further explored the underlying connection between the chaotic growth and the squeezing of the quantum states and showed the connection between the Lyapunov exponent and the squeezing parameters. Thermalization is believed to be deeply connected to the chaotic behavior of a system, which is beautifully conjectured [180] by proposing an inequality relating Lyapunov exponent and system temperature under consideration $\lambda \gtrsim T$. By using this, we calculated the approximate lower bound of temperature $\bar{T}_{\text{MSS}}$. We further conjectured a relation between the system temperature

and quantum squeezing averaged over phase space and calculated the temperature $\bar{T}_{\rm SS}$ (see Eq.(4.24)) which indeed satisfies the MSS bound $\bar{T}_{\rm SS} > \bar{T}_{\rm MSS}$. Finally, to validate our aforesaid conjecture, we resort to Rayleigh-Jeans definition of the temperature of a system being in thermal equilibrium. In the classical limit, when the occupation number is very large, a thermalized system satisfies the well-known Rayleigh-Jeans formula $nE \sim T$ with $(n, E)$ being the occupation number and particle energy accordingly. Surprisingly, the temperature $\bar{T}_{\rm RJ}$ derived from the Rayleigh-Jeans formula turned out to be $\bar{T}_{\rm RJ} \approx \bar{T}_{\rm SS}$, which is quite consistent with our definition. To this end, we find that among three different background models, $n = 1, 2, 3$, only $n = 1$ appears to have a close resemblance to the thermalization process of a typical thermodynamic system under perturbation. The process of thermalization itself is a complex phenomenon. In particular, how a quantum system initially prepared in far-from-equilibrium states can evolve into a thermal equilibrium state is still not a completely understood subject. Eigenstate Thermalization Hypothesis(ETH) [194–197] is a well-known proposal towards this direction. In this context, it would be interesting to investigate this ETH in the reheating era, which we have left for our future studies.

CHAPTER 5

# Gravitational production of minimally coupled scalar fluctuation: Generalization of the Bogoliubov vs Boltzmann framework

*" The career of a young theoretical physicist consists of treating the harmonic oscillator in ever-increasing levels of abstraction."*

—*Sidney Coleman*

Having investigated the phenomena of *parametric resonance instability* during the preheating era in the language of quantum squeezing, and establishing a beautiful connection between the non-equilibrium squeezed quantum system with the non-equilibrium preheating phase in the last chapter, we, in this chapter, pay attention to the non-perturbative aspect of gravitational particle(matter and radiation) production during inflation and post-inflationary reheating. This chapter is based on the work [36].

To produce the thermal bath populated by the relativistic degrees of freedom in the post-inflationary reheating, several different production mechanisms have been proposed and studied quite extensively over the years. Gravitational production is one of them, and it has recently re-attracted attention with the development of a novel framework of perturbative gravitational portals during reheating [57, 198, 199] and through several studies on the gravitational production of perturbations of different spins [200–202]. Indeed, the main interest of such a mechanism is that it does not require any new coupling parameter except gravity. It can then be considered as a minimal production, and *should* be added to any extension of the Standard Model. Here, we restrict ourselves to gravitational-type couplings, and we will thus neglect the effects due to the preheating phase [203], or fragmentation

[204–206]. Particularly, the gravitational background dynamics can be sufficient to reheat the universe [54, 58, 154, 207]. The intriguing possibility of quantum mechanical particle production by the dynamical space-time was first put forward by Parker (1969) [82, 83], and then thoroughly studied by many authors, among them is L.H. Ford who applied it in the framework of inflation. In [208, 209] he studied the particle creation due to the abrupt change of space-time metric during its transition from an inflationary era to a subsequent matter or radiation-dominated phase. Subsequently, extensive studies on this gravitational particle production have been performed and possibilities of reheating have also been analyzed* [67, 68, 210–217].

While analyzing gravitational production, two commonly used approaches, namely *Bogoliubov* and *Boltzmann*, are employed to do a quantitative study of particle production, especially in the process of reheating†. ‡ However, the Boltzmann approach is widely used, particularly concerning the production of dark matter *after* the period of inflation, and is based on solving the system of dynamical equations for different energy density components of the system under consideration. The crucial point is that the Boltzmann collision terms are calculated employing the *perturbative* QFT technique, considering a specific inflaton decay/annihilation channel through the exchange of a graviton [34, 57, 154, 220, 221]. Therefore, such an approach typically deals with sub-horizon modes, or short-wavelength modes, which means modes whose lower frequency corresponds (roughly) to the fundamental frequency of the inflaton at the end of inflation. By simple energy conservation principle, the Boltzmann technique does not include the production of super-horizon modes, also called *long-wavelength* modes, like, for instance, quantum fluctuations of stable for particles produced during inflation, which re-enter the horizon during reheating, like spectator dark matter [222–226]. Further, it does not take into account the exact dynamics of the background inflaton and treat interaction perturbatively. This approach can be considered as the one giving the minimal amount of matter (or radiation) produced, being ignorant of the inflationary process, even of its existence.

On the other hand, the Bogoliubov approach is non-perturbative. The same system is solved explicitly in a given dynamical background, keeping all the relevant interactions. Quantum particle production is studied through the evolution of quantum fields in a classical background. The capability of capturing the minute details of background dynamics makes this non-perturbative treatment more complete compared to the perturbative one, *short-wavelength* components as well as *long-wavelength* ones being naturally included in the

*Note that already in 1939 [76], Schrodinger proposed to look at the particle-antiparticle transition in the Universe by solving his equation in a de Sitter space-time, as already discussed while studying the historical backdrop of CGPP mechanism in Chapter(2).

†In [218], authors have compared two approaches for the computation of gravitational particle production from inflation. However, their work considers only an inflaton with an EoS $w_\phi = 0$ and addresses solely the computation of the long-wavelength part of the spectrum (IR). The authors consider the Bogoliubov as well as the Starobinsky stochastic approaches, including a possible non-minimal coupling to gravity of the produced scalar field.

‡In [219], authors have studied the Bogoliubov transformation of parity-violating gravitational waves and spectral behavior across different equations of states. In their work, they have considered the transition from de Sitter inflation to the matter and radiation-dominated phase.

calculation. Indeed, this approach naturally captures both super and sub-horizon modes, and that is found to be important, as we will discuss in detail in this chapter. In a recent very interesting work [227], the authors have shown an equivalence between the *Bogoliubov* and *Boltzmann* approaches. However, they limited themselves to the case when the background dynamics is governed by the matter-like equation of state (EoS) $w_\phi \simeq 0$. In this chapter, we extend the analysis further and show that, in general, the two approaches yield quantitatively very different results for the spectrum particularly for higher values of $w_\phi$. We then explore the dynamics of reheating through this non-perturbative approach which has not been discussed in the literature in this general setup. In this chapter, we focus exclusively on the pure gravitational interaction, and the generalization to non-minimal coupling will be considered in Chapter(6).

Pure gravitational reheating, on the other hand, has already been studied in the Boltzmann framework with significant details [56–58, 199, 201, 228–231]. The unique feature of the mechanism lies in the fact that once we fixed a particular model of inflation, the only parameter that regulates the reheating dynamics is the inflaton EoS, $w_\phi$. The constraints are then very strong. With the variation of $w_\phi$ from $0.65 \to 0.99$ for $\alpha-$attractor model of inflation, the reheating temperature ($T_{\rm re}$) lies within BBN energy scale (i.e., 4 MeV) to $10^6$ GeV [57, 154]. Within the same framework, the gravitationally produced scalar DM was further restricted to be very light (between 0.1 eV and $\sim 1$ keV [57, 154, 221]), and thus excluded by Lyman-$\alpha$ constraints.

In this chapter, we propose to reanalyze the gravitational reheating scenario, considering the perturbative (Boltzmann) and non-perturbative (Bogoliubov) approach, taking into account for the first time, the precise background dynamics. In particular, we investigate the qualitative and quantitative differences arising between the two approaches in terms of the distribution function and its predictions. We show that for super-horizon modes, the non-perturbative Bogoliubov approach yields distinct spectral behavior of the daughter field for which the Boltzmann analysis is not applicable. Moreover, our results indicate that the Bogoliubov method predicts slightly higher reheating temperature for a given equation of state than the Boltzmann one. Nonetheless, through this analysis, we want to advocate that to have a correct prediction, if the inflaton coupling parameters are within the perturbative regime, the Bogoliubov approach can capture the finer aspects of the physics of reheating, which has not been much explored in the literature.

This chapter is organised as follows: In Section 5.1, we present an extensive non-perturbative analytic approach for the sub and super-horizon spectrum of the scalar fluctuation for general reheating EoS. Furthermore, we study the mass-breaking effect of the IR spectrum by including the finite mass, $m_\chi$, of the daughter scalar field. In Section 5.2, we first compute the Boltzmann distribution function of the fluctuation and then compare it qualitatively and quantitatively with the sub-horizon spectrum of the Bogoliubov approach. In section 5.3, using the sub- and super-horizon spectra of the produced fluctuation, we study the pure gravitational reheating dynamics in a non-perturbative approach. Finally, Section 5.4 summarizes this work by briefly stating the important findings of this study.

## 5.1 Fluctuation spectrum for general reheating EoS ($w_\phi$): Analytical approach

The total energy density of produced scalar field fluctuations $\chi$ is computed by integrating the product of $|\beta_k|^2$ by the energy per momentum mode over all scales. Therefore, the nature of the $|\beta_k|^2$ spectrum should be thoroughly studied before proceeding toward the determination of the total energy of gravitationally produced fluctuations. This section will be devoted to the analytic determination of the spectrum in two different regimes. Indeed, the nature of the spectrum differs for sub-horizon modes ($k \gg a_{\rm end}H_{\rm end} \equiv k_{\rm end}$) and super-horizon modes ($k \ll k_{\rm end}$). For sub-horizon modes, for the minimal system($\xi = 0$), the frequency term $\omega_k^2(\eta)$ in Eq.(2.120) is always positive. Indeed, if at the end of inflation, $k > aH$, it will always be the case until present time if $w_\phi > -\frac{1}{3}$, because $H$ decreases as $H \propto a^{-\frac{3(1+w_\phi)}{2}}$. Therefore, those modes will not experience any tachyonic instability. However, as we will discuss later, naively the oscillatory behavior of the Hubble scale during reheating can still have a noticeable effect on those sub-horizon modes. The density spectrum should depend on $w_\phi$, which sets the re-entry time of the mode $k$. But, as we will see in our analysis, it will not be the case for $w_\phi > \frac{1}{9}$. On the other hand, modes satisfying $k^2 < \left(\frac{a''}{a} - a^2 m_\chi^2\right)|_{a_{\rm end}} = a_{\rm end}^2(2H_{\rm end}^2 - m_\chi^2)$ causes frequency $\omega_k^2(\eta)$ to become negative at a given time during inflation and this results tachyonic growth of those mode functions. Upon their horizon exit during inflation, the amplitude of those modes freezes until their re-entry during the post-inflationary evolution. Thus, these super-horizon modes are not in the corresponding Bunch-Davies vacuum in post-inflationary evolution(see Fig.(5.1)). The dependence on $w_\phi$ should then be important to determine the time (scale factor) at re-entry. To accurately track their evolution, one has to follow them from early times, when they were deep inside the horizon [50], until their exit. Besides this, these super-horizon modes, having very long wavelengths, are not affected by the background oscillation of the inflaton during reheating.

In order to compute the full spectrum $|\beta_k|^2$, we compute it separately, first for the super-horizon and then for the sub-horizon modes, as they experience different dynamics in two different regimes. We will then compare the total spectrum with the one obtained using a Boltzmann approach, where we compute the spectrum from Feynman amplitudes through the exchange of a graviton [57, 199].

### 5.1.1 Super-horizon modes spectrum ($k < a_{\rm end}H_{\rm end}$):

The long-wavelength spectrum gets enhanced through tachyonic instability after horizon crossing during inflation. Depending upon different post- inflationary EoS, this large-scale spectrum follows different power-law behavior during reheating. To take into account the spectrum's growth after the horizon crossing, we need to start studying its dynamics from the inflationary era itself. Violation of the adiabaticity condition due to abrupt transition in the mode equation from the de Sitter phase to the oscillatory regime causes particle production observed upon modes re-entry associated with long-wavelength modes. To

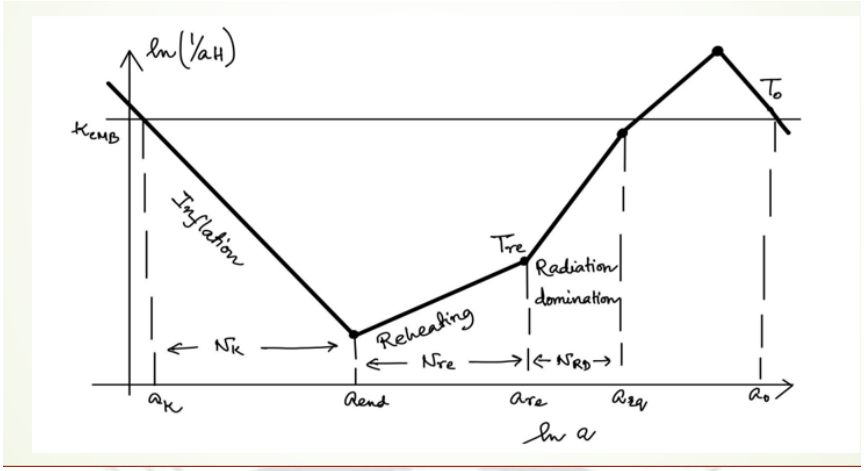


FIGURE 5.1: *The figure represents the evolution of the comoving Hubble horizon through the modified expansion history. The intermediate reheating era modifies the evolution of the fluctuation spectra.*

compute the long-wavelength or IR spectrum, we shall follow the theoretical framework developed in Chapter(2)(see subsection(2.7.2)). We compute the adiabatic vacuum solutions during inflation and the post-inflationary era, from the dynamical equation (2.119) for $\xi = 0$, taking the general form of the scale factor (2.121). Plugging these vacuum solutions into Eq.(2.126), we find the super-horizon modes spectrum.

#### 5.1.1.1 Solution during the inflationary phase ($\eta < \eta_{\rm end}$)

During the de Sitter phase ($\eta \leq \eta_{\rm end}$), the mode equation of a masslesss $\chi$-field for long-wavelength approximation, Eq. (2.119) with $a(\eta)$ given by Eq. (2.122), becomes

$$X_k'' + \left[k^2 - \frac{2}{\eta^2}\right] X_k = 0\,, \tag{5.1}$$

which has for solution the Bunch-Davies mode function [21, 119]

$$\boxed{X_k^{(\rm inf)}(\eta) = \frac{e^{-ik\eta}}{\sqrt{2k}}\left[1 - \frac{i}{k\eta}\right] \simeq -\frac{i}{\sqrt{2}k^{\frac{3}{2}}\eta} e^{-ik\eta}}\,, \tag{5.2}$$

and

$$X_k^{(\rm inf)\prime}(\eta) = \frac{dX_k^{(\rm inf)}(\eta)}{d\eta} \simeq i\frac{e^{-ik\eta}}{\sqrt{2}k^{\frac{3}{2}}\eta^2}\,, \tag{5.3}$$

where we approximate $\frac{k}{a} \ll H_{\rm end} = -\frac{1}{a}\frac{1}{\eta}$, or equivalently $|k\eta| \ll 1$. The divergent term proportional to $\frac{1}{k\eta}$ is clearly the signature of the dominant (tachyonic) negative term $-\frac{a''}{a}$ in Eq. (2.120) with $\xi = 0$. In case of pure de Sitter inflation, one can also understand that,

at $\eta_{\rm end}$, the longer is the wavelength (the smaller is $k$), the sooner the mode enters the divergent regime. We expect then a power spectrum $\propto |X_k^{(\rm inf)}(\eta)|^2$ tilted toward the IR part of the spectrum.

#### 5.1.1.2 Solution during the reheating phase ($\eta > \eta_{\rm end}$)

The same $k$-mode of massless minimally coupled scalar when passing through the reheating phase, dominated by an equation of state $w_\phi$ (for $\eta \geq \eta_{\rm e}$), after implementing Eq. (2.121) in Eq. (2.119), satisfies

$$X_k'' + \left[k^2 - \frac{2(1-3w_\phi)}{(1+3w_\phi)^2}\frac{1}{\left(\eta - 3\mu\eta_{\rm e}\right)^2}\right] X_k = 0\,, \tag{5.4}$$

with

$$\mu = \frac{(1+w_\phi)}{(1+3w_\phi)}\,, \tag{5.5}$$

and whose solution is

$$X_k(\eta) = C_1 2^{2\bar{\nu}}\Gamma(\bar{\nu}+1)\sqrt{2ik\bar{\eta}}I_{\bar{\nu}}(ik\bar{\eta}) + C_2\sqrt{\frac{2ik\bar{\eta}}{\pi}}K_{\bar{\nu}}(ik\bar{\eta})\,, \tag{5.6}$$

where $\bar{\eta} = \eta - 3\mu\eta_{\rm end}$, and $I_{\bar{\nu}}$, $K_{\bar{\nu}}$ are modified Bessel functions of order $\bar{\nu}$ with

$$\bar{\nu} = \frac{3}{2}\frac{(1-w_\phi)}{(1+3w_\phi)} \tag{5.7}$$

with $C_1$ and $C_2$ integration constants. We show in Table (5.1) the values of $\bar{\nu}$ for a set of $w_\phi$. Note that the generic solution obtained in Eq. (5.6) could also have been applied to find

Table 5.1: *Variation of the long-wavelength spectral indices "$\bar{\nu}$" with different EoS "$w_\phi$"*

| $n$ | $w_\phi$ | $\bar{\nu}$ |
|---|---|---|
| 1 | 0 | 3/2 |
| 2 | 1/3 | 1/2 |
| 3 | 1/2 | 3/10 |
| 4 | 3/5 | 3/14 |
| 5 | 2/3 | 1/6 |
| 6 | 5/7 | 3/22 |
| 7 | 3/4 | 3/26 |
| 9 | 4/5 | 3/34 |
| 19 | 9/10 | 3/74 |
| 199 | 99/100 | 3/794 |

the solution $X_k^{(\rm inf)}$ in the de Sitter phase. Indeed, setting $w_\phi = -1$ in (5.6), $\mu = 0 \to \bar{\eta} = \eta$ and $\bar{\nu} = -3/2$, limits of $\bar{\nu}$ for $w_\phi \to -1$. We would have obtained

$$X_k^{(\rm ing)}(\eta) = \sqrt{\frac{\pi}{2k}}\sqrt{2ik|\eta|}I_{-3/2}(ik|\eta|)\,, \tag{5.8}$$

which gives $X_k^{(\rm inf)}(\eta) \sim -1/k^{3/2}\eta$ in the long-wavelength approximation, as obtained in Eq. (5.2). We can also obtain the same expression (5.2) from the general solution in terms of the Hankel function, $X_k^{(\rm inf)}(\eta) = -i\sqrt{\frac{\pi\eta}{2}}H^{(1)}_{3/2}(k|\eta|)$. Therefore, these two forms of $X_k^{(\rm inf)}(\eta)$ in terms of $I_{-3/2}(ik|\eta|)$ and $H^{(1)}_{3/2}(k|\eta|)$ are equivalent to our solution (5.2). Note also that the equation (5.4) is the same for $w_\phi = 0$ and $w_\phi = -1$, replacing $\eta$ by $\bar{\eta}$. However, the solution for $w_\phi = 0$ is non-divergent as $\frac{1}{k\bar{\eta}} \propto \frac{1}{\sqrt{a}} \to 0$ for increasing values of $a$. Even if these remarks may seem too technical, we believe they are important in the context, because several solutions, functions and methods are given in the literature, without underlining their equivalence.

In order to compute the integration constants $C_1$ and $C_2$ for any value of $w_\phi$, we chose the *adiabatic vacuum* for each mode. If spacetime changes very slowly, or equivalently, particle momentum is so large that it hardly feels the background dynamics, the mode function can be safely assumed to behave (and stay) as a positive frequency mode in Minkowski space in its asymptotic limit. This corresponds to the limit $k\eta \gg 1$, and the mode solution (5.6) becomes

$$X_k(\eta) \sim \left[C_1\frac{2^{2\bar{\nu}}\Gamma(\bar{\nu}+1)}{\sqrt{\pi}}e^{ik\bar{\eta}} + C_2 e^{-ik\bar{\eta}}\right]. \tag{5.9}$$

On the other hand, in the adiabatic vacuum limit, the mode function becomes

$$X_k(\eta) \xrightarrow{\eta\to\infty} \frac{e^{-ik\eta}}{\sqrt{2k}}, \tag{5.10}$$

where we used $\eta \to \infty \Rightarrow \bar{\eta} \to \infty$. Comparing (5.9) with (5.10) we then deduce

$$C_1 = 0, \quad C_2 = \frac{1}{\sqrt{2k}}e^{-3ik\mu\eta_{\rm end}} = \frac{1}{\sqrt{2k}}e^{3i\mu\frac{k}{k_{\rm end}}}, \tag{5.11}$$

where $k_{\rm end} = -\frac{1}{\eta_{\rm end}} = a_{\rm end}H_{\rm end}$ is the scale that left the horizon at the end of inflation. Therefore, the adiabatic vacuum solution of massless particles for general EoS $w_\phi$ becomes

$$\boxed{X_k^{(\rm reh)}(\eta) = \sqrt{\frac{\bar{\eta}}{\pi}}e^{i\left(3\mu\frac{k}{k_{\rm end}}+\frac{\pi}{4}\right)} \times K_{\bar{\nu}}(ik\bar{\eta})}\,. \tag{5.12}$$

Note that we recover the plane wave solution of the Minkowski space (Universe with an infinite pressure, or $w_\phi \to \infty$), corresponding to $\bar{\nu} = -\frac{1}{2}$ and $\mu = \frac{1}{3}$, using $K_{-\frac{1}{2}}(x) = \sqrt{\frac{\pi}{2x}}e^{-x}$, as well as for $w_\phi = \frac{1}{3}$ ($\bar{\nu} = \frac{1}{2}$) which are the two conformal situations.

We are interested in the generation of long-wavelength modes satisfying $\frac{k}{k_{\rm end}} \ll 1$. In the limit

$$k \ll a\ H = \frac{a'}{a} \sim \frac{1}{\eta} \Rightarrow \quad k\eta \ll 1\,, \tag{5.13}$$

and using

$$K_{\bar\nu}(x) \ \xrightarrow{x\to 0}\ \frac{1}{2}\Gamma(|\bar\nu|)\left(\frac{2}{x}\right)^{|\bar\nu|}\,, \tag{5.14}$$

we obtain for $\bar\nu > 0$

$$\begin{aligned} X_k^{(\rm reh)}(\eta) &\sim k^{-\bar\nu}\bar\eta^{(\frac{1}{2}-\bar\nu)}\frac{\mathcal{C}}{\sqrt{\pi}}e^{i\left(3\mu\frac{k}{k_{\rm end}}+\frac{\pi}{4}-\frac{\pi\bar\nu}{2}\right)} \\ X_k^{(\rm reh)'}(\eta) &\sim k^{-\bar\nu}\bar\eta^{-(\frac{1}{2}+\bar\nu)}\frac{\mathcal{B}}{\sqrt{\pi}}e^{i\left(3\mu\frac{k}{k_{\rm end}}+\frac{\pi}{4}-\frac{\pi\bar\nu}{2}\right)}\,, \end{aligned} \tag{5.15}$$

with

$$\begin{aligned} \mathcal{B} &= 2^{(\bar\nu-1)}\bar\nu\Gamma(\bar\nu) + 2^{(\bar\nu-2)}\Gamma(\bar\nu) - 2^{\bar\nu}\Gamma(\bar\nu+1) \\ \mathcal{C} &= 2^{(\bar\nu-1)}\Gamma(\bar\nu)\,. \end{aligned}$$

Implementing Eqs. (5.2) and (5.15) into (2.126), we can (at last) compute the long-wavelength spectrum of massless particles during the transition from the de Sitter phase to the Universe with a generic EoS $w_\phi$

$$\boxed{|\beta_k|^2_{\rm IR} = \frac{\mathcal{D}}{2\pi}\left(\frac{k_{\rm end}}{k}\right)^{(2\bar\nu+3)}}\,, \tag{5.16}$$

or

$$\boxed{a^3\left.\frac{dn_\chi}{d\ln k}\right|_{\rm IR} = 2\mathcal{D}\frac{k_{\rm end}^3}{(2\pi)^3}\left(\frac{k_{\rm end}}{k}\right)^{2\bar\nu}} \tag{5.17}$$

with

$$\mathcal{D} = \left(\mathcal{B}(3\mu-1)^{-\frac{1}{2}-\bar\nu} - \mathcal{C}(3\mu-1)^{\frac{1}{2}-\bar\nu}\right)^2 \tag{5.18}$$

and $\bar\nu$ and $\mu$ given by Eqs.(5.5) and (5.7) respectively. The solution $\beta_k$ has been computed by evaluating Eq. (2.126) at the junction point $\eta = \eta_{\rm end} = -\frac{1}{a_{\rm end}H_{\rm end}} = -\frac{1}{k_{\rm end}}$, or $|k\eta_{\rm end}| = \frac{k}{k_{\rm end}}$. In this IR spectrum for massless fluctuations, the spectral index $(-2\bar\nu-3)$, goes from -6 to -3 for $0 \leq w_\phi \lesssim 1$. We show in Fig. (5.2) the spectrum obtained by solving numerically the set of equations, in comparison with our analytical expression (5.16), for three values of $w_\phi$ (0, $\frac{1}{2}$ and $\frac{2}{3}$). In Fig.(5.2), to numerically track the evolution of the IR modes $k \lesssim k_{\rm end}$ from the beginning of early inflation to the horizon reentry during reheating, we solve the dynamical equation (2.119) along with (2.114) taking the Bunch-Davies vacuum state as an initial state of the field at the beginning of inflation. The non-adiabatic evolution of these large scales after horizon exit during inflation is numerically captured by solving this set of equations,

setting the initial time when the largest scale (or the smallest mode) under study was deep inside the horizon during inflation, and the final time is set when this largest scale is well inside the horizon during reheating. We observe a good agreement in the low-frequency regime, with a slope in the spectrum $|\beta_k|^2 \propto k^{-6}$ for $w_\phi = 0$, $\propto k^{-\frac{18}{5}}$ for $w_\phi = \frac{1}{2}$ and $\propto k^{-\frac{10}{3}}$ for $w_\phi = \frac{2}{3}$. Note that the density spectrum becomes flat $\left(\frac{dn_\chi}{d\ln k} \sim |\beta_k|^2 k^3 \sim \text{constant}\right)$ for kination ($w_\phi \to 1, n \to \infty, \bar{\nu} \to 0$).

#### 5.1.1.3 Effects of a finite mass term $m_\chi$

Remark that the spectrum is also flat in the case of finite mass, for $k \ll m_\chi$, when the equation of motion becomes almost independent of $k$. This behavior was already highlighted in recent works [50, 69, 227, 232] for EoS $w_\phi = 0$, and we extend it here for higher EoS. To obtain the scale at which the spectrum of long wavelength becomes flat due to the mass term of the mode, we can look at Eq. (2.119) in the massive minimally coupled case. We then have the dependence of the frequency $\omega_k^2(\eta)$ as a function of the mass of the mode in Eq. (2.120). For convenience in the following discussion, let us rewrite

$$\omega_k^2(\eta) = \left(k^2 + a^2 m_\chi^2 + \left(\frac{3w_\phi - 1}{2}\right) a^2 H^2\right). \tag{5.19}$$

We first determine for which scale factor $a_m$ the mass term $a^2 m_\chi^2$ becomes comparable to the expansion term $\propto a^2 H^2$ and find the value of the Hubble scale at this scale factor $H_m \equiv H(a_m)$,

$$\frac{a_m}{a_{\rm end}} = \left(\sqrt{\frac{2}{|3w_\phi - 1|}} \frac{m_\chi}{H_{\rm end}}\right)^{-\frac{2}{3(1+w_\phi)}}, \tag{5.20}$$

or

$$H_m = \sqrt{\frac{2}{|3w_\phi - 1|}} m_\chi \,. \tag{5.21}$$

Then, it is easy to determine for which scales $k \lesssim k_m$, at horizon reentry after inflation, the mass term dominates over the expansion term, leading to a flat spectrum. We have $k_m \equiv a_m H_m$ and we find the following expression as a function of $w_\phi$ and $m_\chi$

$$\frac{k_m}{k_{\rm end}} = \left(\sqrt{\frac{2}{|3w_\phi - 1|}} \frac{m_\chi}{H_{\rm end}}\right)^{\frac{1+3w_\phi}{3(1+w_\phi)}} \tag{5.22}$$

which matches perfectly the turning point on the different spectra obtained numerically in Figure 5.2. Note that for $w_\phi = 1/3$, as the expansion term $\propto a^2 H^2$ vanishes in Eq. (5.19), the instant $a_m/a_{\rm end}$ becomes

$$\frac{a_m}{a_{\rm end}} = \sqrt{\frac{H_{\rm end}}{m_\chi}}, \tag{5.23}$$

which gives

$$\frac{k_m}{k_{\rm end}} = \sqrt{\frac{m_\chi}{H_{\rm end}}}\,, \tag{5.24}$$

which is also what we observe in Fig. (5.2). So, any $k \lesssim k_m$ suffers from the finite mass-breaking effect of the IR spectrum.

To get further insight, it is interesting to remark that for $w_\phi = 1/3$, there exists an exact solution for the mode equation of the massive field, which we propose to compute. In terms of the Hankel function, the inflationary solution of the massive field is given by

$$X_k^{(\rm inf)}(\eta) = \frac{\sqrt{-\pi\eta}}{2} e^{i(\pi/4+\pi\bar{\nu}_1/2)} H^{(1)}_{\bar{\nu}_1}(k|\eta|)\,, \tag{5.25}$$

where the (mass-dependent) index is now

$$\bar{\nu}_1 = \sqrt{\frac{9}{4} - \frac{m_\chi^2}{H_{\rm end}^2}}\,. \tag{5.26}$$

The adiabatic out-vacuum solution of (2.119) for $\xi = 0$ during reheating for finite mass, $(\frac{m_\chi}{H_{\rm end}}) < 3/2$ and $w_\phi = 1/3$ is

$$X_k^{(\rm reh)}(\eta) = \frac{e^{-\frac{\pi k^2}{8m_\chi a_{\rm end}^2 H_{\rm end}}}}{(2m_\chi a_{\rm end} k_{\rm end})^{1/4}} D_{\bar{\nu}_2}\left(e^{i\frac{\pi}{4}}\sqrt{\frac{2m_\chi}{H_{\rm end}}}(\eta k_{\rm end}+2)\right) \times e^{i\delta}\,, \tag{5.27}$$

where $D_{\bar{\nu}_2}$ is Parabolic Cylinder function with $\bar{\nu}_2 = -\frac{1}{2}\big(1 + \frac{ik^2}{m_\chi a_{\rm end}^2 H_{\rm end}}\big)$, and the phase

$$\delta = \frac{\pi}{8} - \frac{k^2}{4m_\chi a_{\rm end}^2 H_{\rm end}}\ln(2) - \frac{3k^2}{4m_\chi a_{\rm end}^2 H_{\rm end}}\ln\left(\frac{m_\chi}{H_{\rm end}}\right). \tag{5.28}$$

Using (5.25) and (5.27) in (2.126) we obtain the spectral nature in the long-wavelength regime as

$$\boxed{|\beta_k|^2_{{\rm IR},m_\chi\neq 0} \sim \frac{e^{-\frac{\pi H_{\rm end}}{4m_\chi}\left(\frac{k}{k_{\rm end}}\right)^2}}{\sqrt{m_\chi/H_{\rm end}}}\left(\frac{k_{\rm end}}{k}\right)^{2\bar{\nu}_1}}\,. \tag{5.29}$$

In the regime $(k/k_{\rm end}) \ll \sqrt{(m_\chi/H_{\rm end})}$ and $(m_\chi/H_{\rm end}) \ll 3/2$, the spectral nature turns out to be $|\beta_k|^2 \propto \big(k_{\rm end}/k\big)^3$, which justifies the behavior of the spectra for finite mass in the top right panel of Fig.(5.2). This result also agrees with the condition (5.24).

As the general mode solution doesn't exist for any higher Eos $w_\phi > 1/3$, we resort to the approximated method as outlined in [227] to determine at least the behavior of the number density spectrum for the finite mass case. We write the WKB approximated post-inflationary solution as

$$X_k^{(\rm reh)}(\eta) \simeq \frac{e^{-i\Omega_k(\eta)}}{\sqrt{2\omega_k(\eta)}} \tag{5.30}$$

Using the equations (5.25) and (5.30) in (2.126) we find

$$\beta_k \simeq \sqrt{\frac{\pi}{32\bar{\omega}_k(\eta_{\rm end})}}\Bigg[\left(\frac{k}{k_{\rm end}}\right)\left(H^{(1)}_{\bar{\nu}_1+1}(k/k_{\rm end}) - H^{(1)}_{\bar{\nu}_1-1}(k/k_{\rm end})\right) + \left(\frac{\left(\frac{d\bar{\omega}_k(\eta_{\rm end})}{d(\eta k_{\rm end})}\right)}{\bar{\omega}_k(\eta_{\rm end})} - 1 + 2i\bar{\omega}_k(\eta_{\rm end})\right) H^{(1)}_{\bar{\nu}_1}(k/k_{\rm end})\Bigg] \times e^{i\delta} \tag{5.31}$$

Here the phase $\delta = i\left(\frac{3\pi}{4} + \frac{\pi\bar{\nu}_1}{2} - \Omega_k(\eta)\right)$. At the end of inflation ($\eta = \eta_{\rm end}$), the dimensionless terms are given by

$$\bar{\omega}_k(\eta_{\rm end}) = \sqrt{(k/k_{\rm end})^2 + (m_\chi/H_{\rm end})^2 + (3w_\phi - 1)/2}\,,$$
$$\frac{\left(\frac{d\bar{\omega}_k(\eta_{\rm end})}{d(\eta k_{\rm end})}\right)}{\bar{\omega}_k(\eta_{\rm end})} = \left(\frac{H_{\rm end}}{m_\chi}\right)^{5/2}\left(1 + \left(\frac{H_{\rm end}}{m_\chi}\right)^2 \frac{(3w_\phi - 1)}{2}\right)^{-9/4} \tag{5.32}$$

Likewise $w_\phi = 1/3$, in the long-wavelength limit $k/k_{\rm end} \ll 1$, Eq. (5.31) gives the spectral nature $|\beta_k|^2 \propto (k_{\rm end}/k)^3$ for the masses $(m_\chi/H_{\rm end}) \ll 3/2$, which is indeed independent of EoS. For the mass $(m_\chi/H_{\rm end}) > 3/2$, the mass-dependent index $\bar{\nu}_1$ becomes imaginary, this in turn generates an exponential mass-suppressed amplitude of the IR spectrum from the phase part $e^{i\delta}$ in the Eq.(5.31).

Before closing this section, we notice that for light scalar modes with finite mass term $(m_\chi/H_{\rm end}) \ll 3/2$, in the long-wavelength limit $k/k_{\rm end} \ll 1$, the analytic calculations provide flat spectra, whatever the EoS and the specific shape of the inflaton potential. However, it has been shown that the numerical spectra in this limit can be slightly red-tilted depending on the specific inflationary model and evolution of the Hubble scale during inflation [232]. Our analytic approximation assumes an initially constant Hubble rate during the de Sitter phase, which produces a flat long-wavelength spectrum. This is a reasonable assumption for a wide range of inflationary models, corresponding to an inflaton that begins in a very flat potential region, which is valid for $\alpha$-attractor models that we consider as benchmarks in this work. We recover in our numerical results flat spectra in the long-wavelength limit, as can be seen in Figure (5.2) for such inflationary potentials. To this end, we would like to mention that to avoid the infrared logarithmic divergence while studying the gravitational production of massive scalars, we should take the exponent of $|\beta_k|^2$ slightly below 3 (slight deviation from the exact flatness of the spectra). The important physical applications of this thing are nicely explained in [218], which is necessary for the result to be consistent with the Starobinsky stochastic approach to particle production. This important fact has been taken into account while studying the thermal and non-thermal DM phenomenology during the universe's transition from inflation to the radiation-dominated phase, as shown in [233].

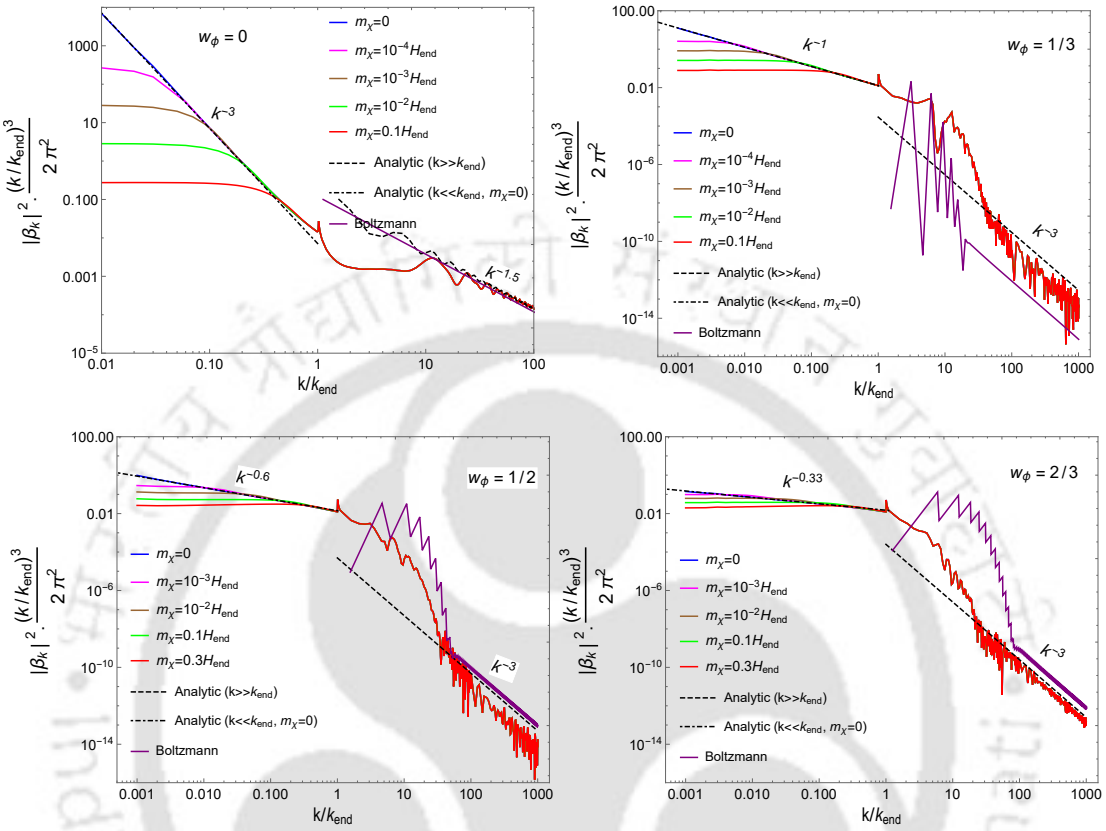


FIGURE 5.2: *Spectral density* $\frac{dn_\chi}{d\log k}$ *in long- and short-wavelength regimes, each panel for a different EoS.* ***Top-Left:*** $w_\phi = 0$. ***Top-Right:*** $w_\phi = 1/3$. ***Bottom-Left:*** $w_\phi = 1/2$. ***Bottom-Right:*** $w_\phi = 2/3$. *The long-wavelength approximations* $k \ll k_{\rm end}$ *from Eq.(5.16) are represented in dash-dotted black for the massless case* $m_\chi = 0$. *The short-wavelength approximations* $k \gg k_{\rm end}$ *from Eqs. (5.58) and (5.60) are represented in dashed black. Numerical results are represented in colored solid lines for different values of* $m_\chi$. *The short-wavelength spectral density obtained through the Boltzmann treatment in Eqs. (5.72) and (5.75) are depicted in solid purple. For all the EoS, the shape of the short-wavelength* $(k \gg k_e)$ *perturbative spectral density obtained through a Boltzmann approach is in accord with the non-perturbative Bogoliubov spectra, although a difference in amplitude is observed. As well, the long-wavelength approximation Eq.(5.16) is consistent with the numerical result for the massless case, while the short-wavelength approximation Eqs. (5.58) and (5.60) are fully consistent with the numerical result deep in the UV. Interestingly, the interference term in (5.58) nicely explains the high-frequency oscillation in the spectrum for* $w_\phi = 0$.

### 5.1.2 Sub-horizon modes spectrum ($k > a_{\rm end}H_{\rm end}$) :

#### 5.1.2.1 Generalities

For modes staying inside the horizon during the whole inflationary phase(never experiencing an adiabatic to non-adiabatic transition), particle production essentially takes place almost immediately after the end of inflation within a very few e-folding numbers, and the coherently oscillating inflaton background becomes the source of the production. Typically, the produced particle number density $|\beta_k|^2$ is bound to be very small, because the divergent term $\propto \frac{1}{k\eta}$ is not present in the solution $X_k^{(\rm inf)}$ in Eq. (5.2), $\omega_k^2$ being always positive. However, the equation of state varying from $-1$ to $w_\phi$, one still has the gravitational production of a certain amount of modes.

In this case, the solution stays adiabatic during all the production process, and one does not need to compute the exact solutions $X_k^{(\rm inf)}(\eta)$ and $X_k^{(\rm reh)}(\eta)$ to find the late-time converging quantity $\beta_k$. Instead, one can compute it directly from the evolution equation of the time-dependent coefficient. Indeed, implementing Eq. (2.106) into

$$X_k'' + \omega_k^2 X_k = 0\,, \tag{5.33}$$

gives in the adiabatic approximation (neglecting second-order derivatives, and considering $\alpha_k \gg \beta_k$) [66–68, 211, 212, 234],

$$\beta_k'(\eta) = \frac{\omega_k'}{2\omega_k} e^{-2i\Omega_k(\eta)}\,, \tag{5.34}$$

or

$$\beta_k(\eta) \simeq \int_{\eta_{\rm end}}^{\eta} d\eta^{'}\, \frac{\omega_k'}{2\omega_k} e^{-2i\Omega_k(\eta^{'})}\,, \tag{5.35}$$

where

$$\Omega_k(\eta^{'}) = \int_{\eta_{\rm end}}^{\eta^{'}} \omega_k(\eta) d\eta = \int_{t_{\rm end}}^{t^{'}} \frac{\omega_k(t)}{a(t)} dt \tag{5.36}$$

and $t_{\rm end}$ stands for the time at the end of inflation. This approach of computing the Bogoliubov coefficient has the advantage of finding the time-independent $\beta_k$ as the limit $\beta_k(\eta \to \infty)$, without the need to find the explicit solution $X_k^{(\rm reh)}(\eta)$.

For the minimal system, using the time-dependent frequency expressed in Eq. (2.120), and working in cosmic time coordinate, we can express

$$a' = a^2 H \;\Rightarrow\; \frac{a''}{a} = 2a'H + aH' = a^2(2H^2 + \dot{H})\,, \tag{5.37}$$

which implies that Eq.(2.120) can be written

$$\omega_k^2(t) = k^2 + a^2(m_\chi^2 - 2H^2 - \dot{H})\,, \tag{5.38}$$

or

$$\frac{\dot{\omega}_k(t)}{\omega_k(t)} = \frac{a^2}{\omega_k^2}\left[H m_\chi^2 - 2H^3 - 3H\dot{H} - \frac{1}{2}\ddot{H}\right]\,. \tag{5.39}$$

Using the development (2.70) for $H$, and with the help of Eq. (2.67), we get at the leading order in $\phi_0(t)/M_{\rm pl}$, the behavior of $\dot{H}(t)$ and $\ddot{H}(t)$ for general $n$

$$\dot{H}(t) \simeq 3\bar{H}^2\left[\left(\mathcal{P}^{2n}-1\right)-\frac{\sqrt{6}\mathcal{P}\sqrt{1-\mathcal{P}^{2n}}}{(n+1)}\left(\frac{\phi_0(t)}{M_{\rm pl}}\right)\right], \tag{5.40}$$

and

$$\begin{aligned}\ddot{H}(t) \simeq \quad & \frac{9\bar{H}^3}{(n+1)}\left[\left(4-(4+2n)\mathcal{P}^{2n}\right)+\left(\frac{\phi_0(t)}{M_{\rm pl}}\right)\sqrt{6}\mathcal{P}\sqrt{1-\mathcal{P}^{2n}}\left(\frac{n+4}{n+1}-\mathcal{P}^{2n}\right)\right] \\ & -6\sqrt{6}n\bar{H}^3\left(\frac{M_{\rm pl}}{\phi_0(t)}\right)\mathcal{P}^{2n-1}\sqrt{1-\mathcal{P}^{2n}}\,.\end{aligned} \tag{5.41}$$

From Eq. (2.70), the leading terms of $H^3$ can be written as

$$H^3(t) \simeq \bar{H}^3\left(1+\frac{3\sqrt{6}\mathcal{P}\sqrt{1-\mathcal{P}^{2n}}}{2(n+1)}\left(\frac{\phi_0(t)}{M_{\rm pl}}\right)\right). \tag{5.42}$$

Finally, using the expressions of $H(t)$ and $\dot{H}(t)$ in Eqs. (2.70) and (5.40) and keeping only the terms up to the first order of $(\phi_0(t)/M_{\rm pl})$ we can write

$$H(t)\dot{H}(t) \simeq 3\bar{H}^3\left[\left(\mathcal{P}^{2n}-1\right)+\frac{\sqrt{6}\mathcal{P}\sqrt{1-\mathcal{P}^{2n}}(\mathcal{P}^{2n}-3)}{2(n+1)}\left(\frac{\phi_0(t)}{M_{\rm pl}}\right)\right]. \tag{5.43}$$

Implementing these developments in Eq. (5.39), we then obtain for $k \gg aH$,

$$\begin{aligned}\frac{\dot{\omega}_k}{\omega_k} \simeq \quad & \frac{1}{\left(\frac{k^2}{a^2}+m_\chi^2\right)}\left[Hm_\chi^2+\left(\frac{7n-11}{n+1}+\frac{9}{n+1}\mathcal{P}^{2n}\right)\bar{H}^3+\frac{3\sqrt{6}\bar{H}^3\mathcal{P}\sqrt{1-\mathcal{P}^{2n}}}{2(n+1)^2}(4n-5)\left(\frac{\phi_0(t)}{M_{\rm pl}}\right)\right. \\ & \left.+3\sqrt{6}n\bar{H}^3\left(\frac{M_{\rm pl}}{\phi_0(t)}\right)\mathcal{P}^{2n-1}\sqrt{1-\mathcal{P}^{2n}}\right].\end{aligned} \tag{5.44}$$

Writing $\bar{H}=H_{\rm end}\left(\frac{t_{\rm end}}{t}\right)$ and $\phi(t)=\phi_{\rm end}\left(\frac{t_{\rm end}}{t}\right)^{\frac{1}{n}}$, we can substitute (5.44) back to Eq.(5.35), with $d\eta'\frac{\omega_k'}{\omega_k}=dt'\frac{\dot{\omega}_k}{\omega_k}$. $\beta_k$ then becomes

$$\begin{aligned}\beta_k \simeq \frac{1}{2}\sum_{\nu,l\neq 0}\int_{t_{\rm end}}^{t}dt'\left(\frac{t_{\rm end}}{t'}\right)^3\left[\mathcal{N}_0 e^{i(\nu+l)\omega t'}\left(\frac{t'}{t_{\rm end}}\right)^{\frac{1}{n}}+\mathcal{N}_1 e^{i\nu\omega t'}+\mathcal{N}_2+\mathcal{N}_3 e^{i(\nu+l)\omega t'}\left(\frac{t_{\rm end}}{t'}\right)^{\frac{1}{n}}\right. \\ \left.+\mathcal{N}_4\left(\frac{t'}{t_{\rm end}}\right)^2+\mathcal{N}_5 e^{i(\nu+l)\omega t'}\left(\frac{t'}{t_{\rm end}}\right)^{\frac{2n-1}{n}}\right]\times\frac{e^{-2i\Omega_k(t')}}{\left(\frac{k^2}{a^2}+m_\chi^2\right)},\end{aligned} \tag{5.45}$$

where we have introduced

$$\mathcal{N}_0=3\sqrt{6}nH_{\rm end}^3\left(\mathcal{P}^{2n-1}\right)_\nu\left(\sqrt{1-\mathcal{P}^{2n}}\right)_l\left(\frac{M_{\rm pl}}{\phi_{\rm end}}\right)\;;\quad \mathcal{N}_1=\frac{9}{n+1}H_{\rm end}^3\,\mathcal{P}_\nu^{2n}\,;$$

$$\mathcal{N}_2 = \frac{7n-11}{n+1}H_{\rm end}^3 \; ; \quad \mathcal{N}_3 = \frac{3\sqrt{6}H_{\rm end}^3\mathcal{P}_\nu\left(\sqrt{1-\mathcal{P}^{2n}}\right)_l}{2(n+1)^2}(4n-5)\left(\frac{\phi_{\rm end}}{M_{\rm pl}}\right) \; ;$$
$$\mathcal{N}_4 = m_\chi^2 H_{\rm end} \; ; \quad \mathcal{N}_5 = \mathcal{N}_4\frac{\sqrt{6}\mathcal{P}_\nu\left(\sqrt{1-\mathcal{P}^{2n}}\right)_l}{2(n+1)}\left(\frac{\phi_{\rm end}}{M_{\rm pl}}\right) . \tag{5.46}$$

Although it is justified to keep only up to the first order terms of $\left(\frac{\phi_0(t)}{M_{\rm pl}}\right)$ for the sake of comparison between the nature of the spectra in the UV regime for two approaches (Boltzmann and Bogoliubov), to achieve an amplitude-wise uniformity between the analytical and the numerically obtained spectrum, it becomes imperative to consider the higher order terms of $\left(\frac{\phi_0(t)}{M_{\rm pl}}\right)$. Although these higher-order terms, decaying rapidly with time, hardly contribute at any late time, from the perspective of initial time $t_{\rm e}$, they have a non- negligible contribution to the total amplitude. This amplitude will also be important for a correct estimate of reheating temperature using this spectrum later. Hence, it is important to keep them while computing the integral (5.35). A complete form of the $\beta_k$ spectrum in the UV regime, including the higher order terms, is given in the Addenda A. Here we shall proceed with the integral (5.45) with the first-order term to compute the nature of the UV spectrum.

In Eq. (5.46), we have introduced separate Fourier series having Fourier components $\mathcal{P}_\nu, \left(\sqrt{1-\mathcal{P}^{2n}}\right)_\nu$ and $\left(\mathcal{P}^{2n-1}\right)_\nu$. In Eq. (5.45), there are terms involving the product of oscillatory phase part and non-oscillatory decaying part, as well as non-oscillatory decaying part only. Due to their specific nature, each part requires separate analytical treatment. To evaluate the integral associated with a term involving the product of oscillatory part and non-oscillatory part (like the first term $\mathcal{N}_0$), we shall use stationary phase approximation [69, 235, 236] and find out the stationary point of the total phase part, $\varphi_\pm(t) \equiv (\nu+l)\omega t - 2\Omega_k(t)$ ($\nu, l$ may be both positive and negative). Defining the time instant of the stationary phase to be $t_k$ at which $\dot{\varphi}_\pm(t_k) = 0$, it is trivial to check that $\varphi_-$ does not have any solution to satisfy the condition $\dot{\varphi}_-(t_k) = 0$, $\Omega_k(t)$ being always positive. Therefore, from now on, we shall only work with $\varphi_+(t)$ to determine the stationary phase solution. The mass term $m_\phi$ appearing in the fundamental frequency $\omega$ of the background inflaton, Eq. (2.69), is a function of time for $n \neq 1$. Considering this time-dependent mass term, we get the following constraint relation of the stationary point

$$\dot{\varphi}_+(t_k) = 0 \Rightarrow (\nu+l)\left(\omega|_{t=t_k} + \dot{\omega}|_{t=t_k}t_k\right) = \frac{2(\omega_k|_{t=t_k})}{a_k}$$
$$\Rightarrow \left(\frac{(\nu+l)\gamma m_\phi^{\rm end}}{2n}\right)^2\left(\frac{a_k}{a_{\rm end}}\right)^{\frac{8-4n}{n+1}} \simeq \left(\frac{k^2}{a_{\rm end}^2} + \left(\frac{a_k}{a_{\rm end}}\right)^2 m_\chi^2\right) \tag{5.47}$$

where

$$\gamma = \sqrt{\frac{\pi n}{(2n-1)}}\frac{\Gamma\left(\frac{1}{2}+\frac{1}{2n}\right)}{\Gamma\left(\frac{1}{2n}\right)} , \tag{5.48}$$

$a_k \equiv a(t=t_k)$, and we supposed $a_{\rm end} \ll a_k$ in the right–hand side of the equation. The time instant $t_k$ should be within the range $t_{\rm end} < t_k < t$; otherwise, the integrand is highly

oscillating and that gives a vanishing contribution. For reheating, the produced particles can be assumed to be massless or $\frac{m_\chi}{m_\phi^{\rm end}} \ll 1$ such that $\mathcal{N}_3, \mathcal{N}_4 \approx 0$. However, for dark matter, those terms may have a significant contribution. Nonetheless, in the following discussions, we consider this approximation, and in such a case, one gets the exact solution for the above stationary phase equation as

$$\frac{a_k}{a_{\rm end}} \propto k^{\frac{n+1}{4-2n}} = k^{\frac{1}{1-3w_\phi}} \tag{5.49}$$

In the high-frequency limit, for $w_\phi < 1/3$, it is indeed clear that $a_{\rm end} < a_k < a(t)$, and we can clearly have a stationary point within the integration range. On the other hand, for $w_\phi > 1/3$, one obtains $a_k < a_{\rm end} < a(t)$ which remains always outside the range of integration, and does not have any stationary point. Therefore, in the following, we compute the number spectrum for two different regimes of the equation of states separately.

#### 5.1.2.2 Spectrum for EoS $0 \leq w_\phi < 1/3$

In the large $k$ limit, considering the dominant term from (5.45), we, therefore, write the spectrum for this EoS range as

$$\beta_k \simeq \frac{1}{2}\sum_{\nu,l\neq 0}\int_{t_{\rm e}}^{t} dt' \left[\mathcal{N}_0 e^{i(\nu+l)\omega t'}\left(\frac{a(t')}{a_{\rm end}}\right)^{-3(1+2w_\phi)} + \mathcal{N}_2\left(\frac{a(t')}{a_{\rm end}}\right)^{-\frac{9(1+w_\phi)}{2}}\right] \times \frac{e^{-2i\Omega_k(t')}}{\left(k^2/a^2\right)} \tag{5.50}$$

One clearly sees that the first term in the above integral has stationary points for $0 \leq w_\phi < 1/3$, whereas the second term does not have such points. Therefore, for the first integral, one can readily use the stationary phase approximation whereas the leading contribution for large $k$ from the second term can be obtained by utilizing the simple integration by parts method.

Employing the stationary phase approximation method, we write the approximate form of the integral (5.50) associated with $\mathcal{N}_0$ term as

$$\beta_k^{(0)} \simeq \sum_{\nu,l>0} \frac{\mathcal{N}_0 a_{\rm end}^2}{2k^2}\left(\frac{a_k}{a_{\rm end}}\right)^{-(1+6w_\phi)} \sqrt{\frac{2\pi}{|\ddot{\varphi}_+(t_k)|}} e^{\pm i\frac{\pi}{4}+i\varphi_+(t_k)} \tag{5.51}$$

Where double derivative of total phase part $\ddot{\varphi}_+(t_k)$ is calculated to be

$$\ddot{\varphi}_+(t_k) = 2(1-3w_\phi)H_{\rm end}\bar{\beta}\left(\frac{\bar{\beta}a_{\rm end}}{k}\right)^{\frac{3(1+3w_\phi)}{2(1-3w_\phi)}}, \tag{5.52}$$

with $\bar{\beta} = \left(\frac{(\nu+l)(1-w_\phi)\gamma m_\phi^{\rm end}}{2(1+w_\phi)}\right)$. Implementing (5.52) in (5.51), we obtain

$$\beta_k^{(0)} \simeq \sum_{\nu,l>0} \frac{\mathcal{N}_0 \bar{\beta}^{p_1}}{2H_{\rm end}^{p_2}}\sqrt{\frac{\pi}{|(1-3w_\phi)|}}\left(\frac{a_{\rm end}H_{\rm end}}{k}\right)^{\frac{9(1-w_\phi)}{4(1-3w_\phi)}} e^{\pm i\frac{\pi}{4}+i\varphi_+(t_k)}$$

$$= \bar{\mathcal{N}}_0 k^{\frac{9(w_\phi-1)}{4(1-3w_\phi)}} e^{\pm i\frac{\pi}{4}+i\varphi_+(t_k)}\,, \tag{5.53}$$

where $\bar{\mathcal{N}}_0 = \sum_{\nu,l>0} \frac{\mathcal{N}_0 \bar{\beta}^{p_1}}{2H_{\rm end}^{p_2}} \sqrt{\frac{\pi}{|(1-3w_\phi)|}} \Big(a_{\rm end}H_{\rm end}\Big)^{\frac{9(1-w_\phi)}{4(1-3w_\phi)}}$, $p_1 = \frac{21w_\phi-1}{4(1-3w_\phi)}$ and $p_2 = \frac{11-15w_\phi}{4(1-3w_\phi)}$.

In the integral (5.45), the oscillatory terms associated with the coefficients $\mathcal{N}_1$ and $\mathcal{N}_3$ also have stationary points. Following exactly the same approach as is followed to reach the expression (5.53) by evaluating the integral (5.50) for $\mathcal{N}_0$, we find the spectra $\propto k^{\frac{15(w_\phi-1)}{4(1-3w_\phi)}}$ and $\propto k^{\frac{21(w_\phi-1)}{4(1-3w_\phi)}}$ for the coefficients $\mathcal{N}_1$ and $\mathcal{N}_3$ respectively. Evidently, the presence of a faster time-decaying term in the amplitude of the coefficient $\mathcal{N}_3$ in Eq.(5.45) essentially causes a sub-dominant spectral index in the associated number density spectrum as compared to $\mathcal{N}_1$ for any $0 \leq w_\phi < 1/3$. Additionally, both the indices for $\mathcal{N}_1$ and $\mathcal{N}_3$ are found to be subdominant as compared to the index $k^{\frac{9(w_\phi-1)}{4(1-3w_\phi)}}$ associated with the coefficient $\mathcal{N}_0$ for any $w_\phi < 1/3$ in the large frequency limit. Hence, the oscillatory terms with the coefficients $\mathcal{N}_1$ and $\mathcal{N}_3$ have been neglected in the integral (5.50).

As mentioned earlier, the second part of the integral (5.50) $\propto \mathcal{N}_2$, which does not contain an oscillatory part, can be solved by an integration by parts. For that, one needs to consider the generic form of integral

$$\begin{aligned} I(x) &= \int_a^b g(t) e^{ix\psi(t)} dt \\ &= \frac{1}{ix}\int_a^b \frac{g(t)}{\dot{\psi}(t)} d(e^{ix\psi(t)}) \\ &= \frac{1}{ix}\frac{g(t)}{\dot{\psi}(t)} e^{ix\psi(t)}\Big|_a^b - \frac{1}{ix}\int_a^b \frac{d}{dt}\left(\frac{g(t)}{\dot{\psi}(t)}\right) e^{ix\psi(t)} dt\,. \end{aligned} \tag{5.54}$$

Because $\psi(t)$ has no stationary point in the given range $[a,b]$, i.e $\dot{\psi}(t) \neq 0$, a simple integration by parts gives a leading asymptotic behavior (Riemann–Lebesgue lemma) [235, 236]

$$I(x) \sim \frac{1}{ix}\frac{g(t)}{\dot{\psi}(t)} e^{ix\psi(t)}\Big|_a^b \qquad \text{as} \quad x \to \infty\,. \tag{5.55}$$

Comparing the integral (5.50) with (5.55) we have for $k \gg a_{\rm end}H_{\rm end}$,

$$x \equiv k/a_{\rm end}H_{\rm end},\ \ \psi(t) \approx -\frac{2H_e t}{(a/a_{\rm end})},\ \ \dot{\psi}(t) \approx \frac{2H_{\rm end}}{(a/a_{\rm end})} \times \underbrace{\left(-\frac{(1+3w_\phi)}{3(1+w_\phi)}\right)}_{f(w_\phi)},$$

$$g(t) = \frac{\mathcal{N}_2}{(k^2/a^2(t))}\left(\frac{a(t)}{a_{\rm end}}\right)^{-\frac{9(1+w_\phi)}{2}}. \tag{5.56}$$

Finally, the second part $\propto \mathcal{N}_2$ of the integral (5.50) becomes

$$\beta_k^{(2)} \simeq \frac{ia_{\rm end}^3}{4k^3 f(w_\phi)} \mathcal{N}_2 e^{-\frac{2ikt_{\rm end}}{a_{\rm end}}} = \bar{\mathcal{N}}_2 k^{-3} e^{i\left(\frac{\pi}{2}-\frac{2kt_{\rm end}}{a_{\rm end}}\right)} \tag{5.57}$$

where $\bar{\mathcal{N}}_2 = \frac{a_{\rm end}^3}{4f(w_\phi)}\mathcal{N}_2$. In the presence of fast decaying terms in the amplitude of Eq. (5.57), the dominant contribution comes from the initial time. Note also that, contrary to the oscillatory term $\propto \mathcal{N}_0$, the spectrum for $|\beta_k^{(2)}|$ does not depend on the EoS, leading to $|\beta_k|^2 \propto k^{-6}$.

Combining Eq. (5.53) and (5.57), we can then obtain the number density spectrum as $n_k = |\beta_k|^2 = |\beta_k^{(0)} + \beta_k^{(2)}|^2$. Upon close inspection, one can notice that for the EoS in the range $0 \leq w_\phi < 1/9$, $|\beta_k^{(0)}|^2$ having a stationary phase contribution dominates over $|\beta_k^{(2)}|^2$ having a non-oscillatory contribution in the high-frequency limit. On the other hand for $1/9 < w_\phi < 1/3$, it is $|\beta_k^{(2)}|^2$ which dominates, $|\beta_k^{(0)}|^2$ having a steeper spectrum. We emphasize that although in our analytical computation we encounter a critical value $w_\phi = 1/9$, our analysis is performed in the inflaton potential $V(\phi) \propto \phi^{2n}$ with $n$ a positive integer, and EoS is defined as $w_\phi = (n-1)/(n+1)$. Hence, the value $w_\phi = 1/9$ is not achieved in the class of models of inflation and reheating considered in this work. Still, this is not a limitation of the theoretical framework constructed in this work. We expect such analytical results to hold in any potential allowing for inflaton oscillations near the minimum, as long as we can expand the oscillating background in terms of its Fourier modes. As a conclusion, the spectral nature of the number density spectrum in the range $0 \leq w_\phi < 1/3$ can be written as follows

$$|\beta_k|^2_{\rm UV, w_\phi<\frac{1}{3}} = \begin{cases} \left(\bar{\mathcal{N}}_0\right)^2 k^{\frac{9(w_\phi-1)}{2-6w_\phi}} + \underbrace{\bar{\mathcal{N}}_0\bar{\mathcal{N}}_2 k^{\frac{45w_\phi-21}{4(1-3w_\phi)}}\cos\psi}_{\text{interference term}} & w_\phi \leq 1/9 \\ \left(\bar{\mathcal{N}}_2\right)^2 k^{-6} + \underbrace{\bar{\mathcal{N}}_0\bar{\mathcal{N}}_2 k^{\frac{45w_\phi-21}{4(1-3w_\phi)}}\cos\psi}_{\text{interference term}} & w_\phi > 1/9 \end{cases} \tag{5.58}$$

where the *quantum interference term (product of an oscillatory and a non-oscillatory function) appears as a fast varying oscillatory term in the number spectrum with momentum-dependent phase factor*, $\psi = \left(\frac{\pi}{4} + \varphi_+(t_k) - 2kt_{\rm end}/a_{\rm end}\right)$. Though the $k$ index of the second term in Eq. (5.58) is sub-leading compared to the first one in both cases, it is this term that results in oscillation in the spectrum, as can indeed be observed in the Top left panel of Fig. (5.2). For $w_\phi = 0$, we indeed recover the leading order spectral behavior $|\beta_k|^2 \propto k^{-\frac{9}{2}}$ discussed in [227, 237], up to the oscillatory term. With the increase of EoS, this oscillation effect in the number density spectrum starts getting washed away because of the gradual decay of the amplitude of the interference term in the large $k$ limit, which is evident from the interference term in Eq. (5.58).

#### 5.1.2.3 Spectrum for EoS $w_\phi \geq 1/3$

In this section, we further generalize the spectrum for EoS $w_\phi \geq 1/3$. The situation becomes drastically different in this case. Indeed, we have shown that Eq. (5.47) has no stationary point within the integration range for $w_\phi \geq 1/3$. As there is no stationary phase in this

range $w_\phi \geq 1/3$, unlike the spectrum (5.50), we need to take into account the contribution of all the terms in Eq. (5.45). Therefore, to estimate the approximate spectral behavior in this EoS range, we should follow the integration by parts method described in the previous subsection.

Comparing the integral (5.45) with (5.55), for $k \gg a_e H_e$, in a similar manner we obtain the functions as given in Eq.(5.56).

We finally end up having the following asymptotic form of the integral (5.45) in large $k$ and massless ($m_\chi \approx 0$) limit for $w_\phi \geq 1/3$.

$$\beta_k \simeq \frac{1}{4if(w_\phi)(k/a_{\rm end})^3} \sum_{\nu,l\neq 0} \left[ \mathcal{N}_0 \left(\frac{a(t)}{a_{\rm end}}\right)^{-6w_\phi} + \left(\mathcal{N}_1 + \mathcal{N}_2\right) \left(\frac{a(t)}{a_{\rm end}}\right)^{-\frac{3(1+3w_\phi)}{2}} + \mathcal{N}_3 \left(\frac{a(t)}{a_{\rm end}}\right)^{-3(1+w_\phi)} \right] \times e^{-\frac{2i(k/a_{\rm end})t}{(a/a_{\rm end})}} \Big|_{t_{\rm end}}^{t} . \tag{5.59}$$

As all the terms in the amplitude part decay fast with time, the dominant contribution will come from the initial time. The final form of the spectrum then becomes

$$\boxed{|\beta_k|^2_{{\rm UV},w_\phi \geq \frac{1}{3}} \simeq \frac{1}{16 f^2(w_\phi)} \left(\frac{a_{\rm end}}{k}\right)^6 \times \sum\sum \left[\mathcal{N}_0 + \mathcal{N}_1 + \mathcal{N}_2 + \mathcal{N}_3\right]^2} \tag{5.60}$$

where $f(w_\phi)$ is given by Eq. (5.56). This equation represents an approximate spectral behavior in the UV regime for $w_\phi \geq 1/3$, taking the background inflaton oscillation effect into account. From Eqs. (5.58) and (5.60), we remark that the spectral index is independent of $w_\phi$ for $w_\phi \geq 1/9$ and in the entire range, the spectral index varies from $-9/2$ to $-6$ for $0 \leq w_\phi \leq 1$. So, unlike the IR divergence in large-scale spectrum (5.16), there is no UV divergence in the number density spectrum. The spectra given in Eqs. (5.16), (5.58), and (5.60) are three important analytic results of this paper. In Figure (5.2), we find a nice agreement between the numerically obtained small-scale spectra and the approximated analytical spectra given by Eqs. (5.58) and (5.60) for different EoS. As already stated earlier, the small-scale modes never experience non-adiabatic evolution, resulting in a low spectral amplitude, $|\beta_k|^2 \ll 1$ for $k \gg k_{\rm end}$. Therefore, to numerically study the spectral behavior in this regime, we rely upon computing the integral (5.35) along with the background dynamical equations (2.43) and (2.46), which are utilized in studying the behavior of the time-dependent frequency term (5.39). In the numerical analysis, we set the potential model parameter $\alpha = 1$. However, the spectral behavior, anyway, is independent of the choice of this parameter. Because of background expansion, the gravitational source term $\frac{a''}{a}$ in Eq.(5.37) rapidly loses its efficiency for further production, thereby causing the stabilization of the amplitude of the integral (5.35) within a few post-inflationary e-folding number. Now, it becomes interesting to compare our result with another approach, the Boltzmann one.

## 5.2 Number density spectrum: Boltzmann versus Bogoliubov

We start this discussion by exploring the perturbative production of massive scalar from the oscillating inflaton condensate which is treated as a classical field. We assume this condensate is homogeneous, decays perturbatively, and it follows the phase space distribution

$$f_\phi(k',t) = (2\pi)^3 n_\phi(t)\delta^{(3)}(\vec{k}')\,, \tag{5.61}$$

where $n_\phi(t)$ is the instantaneous inflaton number density. In the perturbative approach, the phase space distribution of the produced massive scalar field, $f_\chi$, is obtained by solving the Boltzmann transport equation

$$\frac{\partial f_\chi}{\partial t} - H|\vec{p}|\frac{\partial f_\chi}{\partial|\vec{p}|} = C\left[f_\chi\left(|\vec{p}|,t\right)\right], \tag{5.62}$$

where $\mathcal{C}\left[f_\chi\right]$ is the collision term given by

$$\begin{aligned} C\left[f_\chi(|\vec{p}|,t)\right] =& \frac{1}{2p^0}\sum_{\nu=1}^{\infty}\int \frac{d^3\vec{k}'_\nu}{(2\pi)^3 n_\phi}\frac{d^3\vec{p'}}{(2\pi)^3 p^{0\prime}}(2\pi)^4\delta^{(4)}\left(k'_\nu - p - p'\right)|\overline{\mathcal{M}_\nu}|^2_{\phi\to\chi\chi} \\ & \times\left[f_\phi(k')\left(1+f_\chi(p)\right)\left(1+f_\chi(p')\right)\right], \end{aligned} \tag{5.63}$$

with $k'_\nu = (E_\nu, 0)$, the four-momentum of the inflaton condensate and $E_\nu = \nu\omega$ denotes the energy of the inflaton condensate corresponding to the $\nu$-th mode of oscillation and $\omega$ is defined in Eq. (2.69). Vanishing three momenta implies that the inflaton decays to massive particles at its rest frame and $\overline{\mathcal{M}_\nu}$ is the transition amplitude in one oscillation for each oscillating field mode of $\phi$ from coherent condensate state $|\phi\rangle$ to two final particles state $|\chi\chi\rangle$. In the above expression of the collision term, the inverse decay term has been neglected, satisfying the energy-momentum conservation.
From energy-momentum conservation, we have

$$p = p' = \frac{\nu\omega}{2}\sqrt{1-\frac{4m_\chi^2}{(\nu\omega)^2}} \tag{5.64}$$

and considering very low-mass particles, $m_\chi \ll m_\phi$ or massless case, $m_\chi \approx 0$, we can write $p = p' \approx \nu\omega/2$.

Now implementing (5.61) and (5.63) in (5.62), we get

$$\begin{aligned} &\frac{\partial f_\chi}{\partial t} - H|\vec{p}|\frac{\partial f_\chi}{\partial|\vec{p}|} = \sum_{\nu=1}^{\infty}\frac{\pi|\overline{\mathcal{M}_\nu}|^2}{2(p^0)^2}\delta\left(\frac{\nu\omega}{2}-p^0\right)\left(1+2f_\chi(p)\right) \\ &\Rightarrow \frac{d}{dt}f_\chi(|\vec{p}|,t) = \sum_{\nu=1}^{\infty}\frac{2\pi|\overline{\mathcal{M}_\nu}|^2}{\nu^2\omega^2}\delta\left(|\vec{p}|-\frac{\nu\omega}{2}\right) \end{aligned}$$

$$\Rightarrow f_\chi(|\vec{p}|,t) = \sum_{\nu=1}^{\infty} \frac{2\pi}{\nu^2} \int_{t_{\rm end}}^{t} \frac{|\overline{\mathcal{M}_\nu(t')}|^2}{\omega^2(t')} \delta\left(|\vec{p}(t')| - \frac{\nu\omega(t')}{2}\right) dt'$$

$$\Rightarrow f_\chi(|\vec{p}|,t) = \sum_{\nu=1}^{\infty} \frac{2\pi}{\nu^2} \int_{t_{\rm end}}^{t} \frac{|\overline{\mathcal{M}_\nu(t')}|^2}{\omega^2(t')} \delta\left(\frac{|\vec{p}(t)|a(t)}{a(t')} - \frac{\nu\omega(t')}{2}\right) dt' \,. \tag{5.65}$$

In the above expression, for massless particles we have $p^0 = |\vec{p}| = \big(\nu\omega(t)\big)/2$. As here we are talking about gravitational spectra, the condition $f_\chi(p) \ll 1$ is essentially valid. In the second line of Eq. (5.65) we have assumed $\big(1 + 2f_\chi(p)\big) \approx 1$ and in the final line, the product $|\vec{p}(t)|a(t)$ is the comoving momentum.

To evaluate the delta function in the integral (5.65), we introduce a time $\hat{t}$ between the two limits $t_{\rm e}$ and $t$ which satisfies the relation

$$\frac{a(t)}{a(\hat{t})} = \frac{\nu\omega(\hat{t})}{2|\vec{p}(t)|} \,. \tag{5.66}$$

Here we are considering gravitons ($h_{\mu\nu}$) mediated production of a minimally coupled scalar field ($\chi$) from the inflaton background (see [57] for a detailed analysis), and do not consider any other interaction between inflaton and scalar field. For the minimal case, the gravitational interaction gives the following form of the interaction Lagrangian.

$$\mathcal{L}_{\rm int} = -\frac{h^{\mu\nu}}{M_{\rm pl}} \left(T^{\phi}_{\mu\nu} + T^{\chi}_{\mu\nu}\right) \tag{5.67}$$

where $T^{\phi}_{\mu\nu}$, and $T^{\chi}_{\mu\nu}$ are the energy-momentum tensors of the inflaton and scalar field, respectively. Based on the above interaction Lagrangian, we calculate the expression of the transition amplitude $\mathcal{M}_\nu$ as follows: [46, 50, 57]

$$\begin{aligned} \mathcal{M}_\nu &= -\frac{1}{M_{\rm pl}^2} V(\phi_0) \mathcal{P}_\nu^{2n} \left(1 + \frac{2m_\chi^2}{(\nu\omega)^2}\right) \\ &= -\frac{1}{M_{\rm pl}^2} \rho_\phi \mathcal{P}_\nu^{2n} \left(1 + \frac{2m_\chi^2}{(\nu\omega)^2}\right) . \end{aligned} \tag{5.68}$$

Now, if we take into account the symmetry factor associated with two identical final states, then the average transition probability amplitude for massless(or, very low mass) final state particles becomes

$$\sum_{\nu=1}^{\infty} |\overline{\mathcal{M}_\nu}|^2 = \frac{1}{2} \times \sum_{\nu=1}^{\infty} \frac{\rho_\phi^2}{M_{\rm pl}^4} |\mathcal{P}_\nu^{2n}|^2 \,, \tag{5.69}$$

Using Eqs.(5.66) and (5.69) in (5.65) we can then evaluate the phase space distribution function for general EoS in the low mass limit ($m_\chi \approx 0$)

$$f_\chi(p,t) = \sum_{\nu=1}^{\infty} \frac{2\pi|\mathcal{P}_\nu^{2n}|^2}{\nu^3} \frac{\rho_\phi^2(\hat{t})}{M_{\rm pl}^4\omega^2(\hat{t})} \frac{\theta(t-\hat{t})\theta(\hat{t}-t_{\rm end})}{\big|-\omega(\hat{t})H(\hat{t}) - \dot{\omega}(\hat{t})\big|} = \sum_{\nu=1}^{\infty} \frac{2\pi|\mathcal{P}_\nu^{2n}|^2}{\nu^3} \frac{\rho_\phi^2(\hat{t})}{M_{\rm pl}^4\omega^3(\hat{t})H(\hat{t})} \frac{\theta(t-\hat{t})\theta(\hat{t}-t_{\rm end})}{|3w_\phi - 1|}$$

$$= \sum_{\nu=1}^{\infty} \frac{2\pi|\mathcal{P}_{\nu}^{2n}|^2}{\nu^3|3w_\phi-1|}\frac{\rho_\phi^2(t)}{M_{\rm pl}^4\omega^3(t)H(t)}\left(\frac{2p(t)}{\nu\omega(t)}\right)^{\frac{9(w_\phi-1)}{2(1-3w_\phi)}}\theta(t-\hat{t})\theta(\hat{t}-t_{\rm end})$$

$$= \frac{\pi}{4M_{\rm pl}^4|3w_\phi-1|}\frac{\rho_{\rm end}^2}{H_{\rm end}(m_\phi^{\rm end}\gamma)^3}\left(\frac{m_\phi^{\rm end}\gamma}{p(t)(a/a_{\rm end})}\right)^{\frac{9(1-w_\phi)}{2(1-3w_\phi)}}\sum_{\nu=1}^{\infty}|\mathcal{P}_{\nu}^{2n}|^2\left(\frac{\nu}{2}\right)^{\frac{3(1+3w_\phi}{2(1-3w_\phi)}}$$
$$\times\,\theta(t-\hat{t})\theta(\hat{t}-t_{\rm end})$$

$$f_\chi(k,a) = \frac{9\pi}{4}(\gamma)^{\frac{3(1+3w_\phi)}{2(1-3w_\phi)}}\left(\frac{H_{\rm end}}{m_\phi^{\rm end}}\right)^3\left(\frac{a_{\rm end}m_\phi^{\rm end}}{k}\right)^{\frac{9(1-w_\phi)}{2(1-3w_\phi)}}\frac{1}{|(3w_\phi-1)|}\times\sum_{\nu=1}^{\infty}|\mathcal{P}_{\nu}^{2n}|^2\left(\frac{\nu}{2}\right)^{\frac{3(1+3w_\phi)}{2(1-3w_\phi)}}$$
$$\times\,\theta\left(\left(\frac{2k}{\nu a_{\rm end}m_\phi^{\rm end}\gamma}\right)^{\frac{1}{1-3w_\phi}}-1\right)\theta\left(\left(\frac{a}{a_{\rm end}}\right)\left(\frac{2k}{\nu a_{\rm end}m_\phi^{\rm end}\gamma}\right)^{\frac{1}{3w_\phi-1}}-1\right). \qquad (5.70)$$

and $\gamma$ is defined in Eq. (5.48). Using the relations

$$\rho_\phi(\hat{t}) = \rho_\phi(t)\left(\frac{a(\hat{t})}{a(t)}\right)^{-3(1+w_\phi)}\;;H(\hat{t}) = H(t)\left(\frac{a(\hat{t})}{a(t)}\right)^{-\frac{3(1+w_\phi)}{2}}$$
$$\omega(\hat{t}) = \omega(t)\left(\frac{a(\hat{t})}{a(t)}\right)^{-3w_\phi}\;;\quad \rho_{\rm end}^2 = 9M_{\rm pl}^4H_{\rm end}^4 \qquad (5.71)$$

together with $(a(\hat{t})/a(t)) = \left(2p(t)/\nu\omega(t)\right)^{\frac{1}{1-3w_\phi}}$ which is deduced from Eq. (5.66), we finally obtain the distribution function as follows

$$f_\chi^{w_\phi\neq1/3}(k,a) = \frac{9\pi}{4|3w_\phi-1|}\left(\frac{\gamma}{m_\phi^{\rm end}}H_{\rm end}\right)^{\frac{3(1+3w_\phi)}{2(1-3w_\phi)}}\left(\frac{k_{\rm end}}{k}\right)^{\frac{9(1-w_\phi)}{2(1-3w_\phi)}}\sum_{\nu=1}^{\infty}|\mathcal{P}_{\nu}^{2n}|^2\left(\frac{\nu}{2}\right)^{\frac{3(1+3w_\phi)}{2(1-3w_\phi)}}$$
$$\times\,\theta\left(\left(\frac{2k}{\nu a_{\rm end}m_\phi^{\rm end}\gamma}\right)^{\frac{1}{1-3w_\phi}}-1\right)\theta\left(\left(\frac{a}{a_{\rm end}}\right)\left(\frac{2k}{\nu a_{\rm end}m_\phi^{\rm end}\gamma}\right)^{\frac{1}{3w_\phi-1}}-1\right) \qquad (5.72)$$

In the above equation (5.72), $(p(t)a(t) = k)$ is the comoving momentum of the produced particles. To the leading order, this is our main result obtained from the Boltzmann equation, which describes the spectral behavior of the produced particles for the sub-horizon modes if $w_\phi \neq 1/3$. From the distribution function (5.72), we indeed recover the well known spectral nature $f_\chi \propto k^{-9/2}$ for $w_\phi = 0$. If we further compare this with the resulting distribution function Eqs. (5.58) and (5.60) obtained by the Bogoliubov approach, one clearly sees that both match for a matter like reheating equation of state and also the higher equation of state (see Fig.(5.2)). It has already been shown in the Bogoliubov method that the spectral index for UV modes varies from $-9/2$ to $-6$ for $0 \leq w_\phi \leq 1$, therefore, in the computation of energy density, no UV divergence occurs. But, the spectrum (5.72) having

spectral index $\big(9(w_\phi-1)/2(1-3w_\phi)\big)$ appears to be UV divergent both in energy density and particle number density for EoS $w_\phi > 1/3$, which is seemingly in sharp contradiction with the spectrum obtained in the non-perturbative method earlier. Surprisingly, the computation of the full sum containing the Fourier components and two Heaviside functions in the Eq. (5.72) finally generates a convergent spectral nature which agrees well with the Bogoliubov spectrum in the UV regime, as we can see in Fig. (5.2) for $w_\phi = 0,\ 1/2,\ 2/3$. In this regard, a few important points are mentioned by analyzing the massless distribution function in Eq. (5.72).

- For $0 < w_\phi < 1/3$: In this EoS range, $(1-3w_\phi) > 0$ and this makes the index in the first Heaviside function (theta function) of (5.72) always positive. This makes us inclined towards a high-frequency regime, $k/a_{\rm end}m_\phi^{\rm end} > 1$, satisfying the condition $(k/a_{\rm end}m_\phi^{\rm end}) \geq \nu\gamma/2$ to have a non-vanishing value from the first Heaviside function. On the other hand, in the second Heaviside function, the index alters its sign and gets negative in this EoS range. Therefore, in the high-frequency regime, we need to go to a larger time scale, $a(t)/a_{\rm end} \gg 1$, to satisfy the second Heaviside function. From (5.66), such instants say $\hat{t}$ are calculated as $(a(\hat{t})/a_{\rm end}) = \big(2k/\nu a_{\rm end}m_\phi^{\rm end}\gamma\big)^{1/(1-3w_\phi)}$ and these instants are nothing but the stationary points as interpreted in the Bogoliubov approach and they indeed satisfy this second Heaviside function in high-frequency regime. For the stationary points, we get another condition $(k/a_{\rm end}m_\phi^{\rm end}) \leq (\nu\gamma/2)(a(t)/a_{\rm end})^{(1-3w_\phi)}$.
- For $w_\phi > 1/3$: In this EoS range, spectrum index $\big(9(w_\phi-1)/2(1-3w_\phi)\big)$ starts diverging in UV regime. However, to satisfy two Heaviside functions simultaneously, we get more constrained. Now the index of the first theta function gets negative, which eventually gives the condition $\nu\gamma/2 \geq (k/a_{\rm end}m_\phi^{\rm end})$ to satisfy the first theta function. To satisfy the second Heaviside function, we need to choose the time instants satisfying the condition, $(a(t)/a_{\rm end}) \geq \big(\nu a_{\rm end}m_\phi^{\rm end}\gamma/2k\big)^{\frac{1}{(3w_\phi-1)}}$. The condition $\nu\gamma/2 \geq (k/a_{\rm end}m_\phi^{\rm end})$ actually discretizes the computation of the sum in Eq.(5.72) and, for an arbitrary high-frequency mode, we cannot take the sum from any order of Fourier components. If we go on increasing the ratio $\big(k/a_{\rm end}m_\phi^{\rm end}\big)$, we must take higher and higher order of Fourier components $\mathcal{P}_\nu^{2n}$. Again with the increase of order $\nu$, $\mathcal{P}_\nu^{2n}$ drops rapidly, and after the first few terms of the series, it becomes vanishingly small which in turn restricts the maximum range of high-frequency mode up to which one can reach. Beyond that momentum range, the Fourier sum in (5.72) will have a vanishing contribution. Although there is a diverging spectral index in this EoS range, $k^{\frac{9(w_\phi-1)}{2(1-3w_\phi)}}$, the associated Heaviside functions interestingly maintain the convergence in this EoS range, as predicted by the non-perturbative analysis in the previous section.

For the specific case of $w_\phi = 1/3$, we have that

$$f_\chi(|\vec{p}|,t) = \sum_{\nu=1}^{\infty}\frac{2\pi}{\nu^2}\int_{t_{\rm end}}^{t}\frac{|\overline{\mathcal{M}_\nu(t')}|^2}{\omega^2(t')}\frac{a(t')}{a(t)}\delta\Big(|\vec{p}(t)| - \frac{\nu\omega(t)}{2}\Big)dt' \tag{5.73}$$

where now the Dirac delta is independent of the variable of integration $t'$ due to the same redshift of momenta and inflaton frequency, $\omega(t') = \omega(t)\,(a(t)/a(t'))$. Thus, it can be brought out of the integral and we are left with the integral from $t_{\rm e} \to t$ of the quantity

$$\int_{t_{\rm end}}^{t} \frac{a(t')}{a(t)} \frac{|\overline{\mathcal{M}_\nu(t')}|^2}{\omega^2(t')} dt' = |\mathcal{P}_\nu^{2n}|^2 \int_{t_{\rm end}}^{t} \frac{a(t')}{a(t)} \frac{\rho_\phi^2(t')}{2M_{\rm pl}^4 \omega^2(t')} dt' \,. \tag{5.74}$$

Considering the background evolution of the inflaton energy density for $w_\phi = 1/3$ we then obtain the following Boltzmann distribution function

$$\boxed{f_\chi^{w_\phi=1/3}(k,a) = 3\pi \left(\frac{H_{\rm end}}{m_\phi^{\rm end}\gamma}\right)^2 \left[1 - \left(\frac{a_{\rm end}}{a}\right)^3\right] \sum_{\nu=1}^{+\infty} \frac{|\mathcal{P}_\nu^{2n}|^2}{\nu^2} \delta\left(\frac{k}{k_{\rm end}} - \frac{\nu\gamma m_\phi^{\rm end}}{2H_{\rm end}}\right)} \,. \tag{5.75}$$

It corresponds to a series of peaks located at different momenta $(1/2)\nu m_\phi^{\rm end}\gamma$ as previously described in [206] for the distribution function of inflaton quanta produced by inflaton self-interactions in a quartic potential, for which $w_\phi = 1/3$. The appearance of these discrete delta peaks in the momentum space causes the initial rapid fluctuations in the Boltzmann spectrum for $w_\phi = 1/3$ in Fig.(5.2). One should note, however, that in the context of self-interactions, the occupation number was found to rapidly grow after inflation, scaling as $\propto a(t)/a_{\rm end}$ for each peak, signalling the breakdown of the perturbative Boltzmann picture rapidly after inflation. In the case of the gravitational production of quanta, we obtain here that the spectrum is fully determined by what happens at the end of inflation, and the occupation number for each mode is not growing as a function of time, allowing us to consider the Boltzmann computation even at late times for $w_\phi = 1/3$.
To compare the nature of the phase-space distribution function or number density spectrum obtained in two different approaches, we present their behavior in Figure (5.2) for four different EoS $w_\phi = 0,\ 1/3,\ 1/2,\ 2/3$, where we considered a maximum Fourier scale $\nu_{\rm max} = 2000$ for the Boltzmann numerical computation. We observe that the Bogoliubov approach and the Boltzmann approach agree quite well on the shape of the spectrum, as well as with our analytical approximation for all four EoS, and this accordance is true for any higher EoS $w_\phi \geq 1/3$.

## 5.3 Reheating dynamics through minimal gravitational production

In this section, we shall investigate the reheating process through pure gravitational production, considering the full number density spectrum $|\beta_k|^2$ associated with long and short-wavelength modes. In this estimation, we make use of the analytic expressions of the spectrum computed in section 5.1. To determine the reheating temperature through the gravitational excitation of scalar modes, we assume the thermalization of the produced modes once they become subhorizon (particle states). This approximation of fast equilibration

may not be valid depending on the additional interactions to consider among the relativistic particles produced after inflation. Several studies have been focusing on the problem of reaching chemical and kinetic equilibrium for a simple relativistic sector produced during preheating via classical simulations [26, 160, 238, 239] or through perturbative quantum processes during reheating [157, 240–242]. Here, we consider the possibility of producing the light Standard Model (SM) quanta from the inflaton through minimal gravitational interaction, especially in the form of relativistic Higgs bosons. In this case, the large number of degrees of freedom in the SM and the sizable gauge interactions within this sector are expected to efficiently bring the produced relativistic particles into a hot thermal bath. We do not investigate further the complexity of non-instantaneous thermalization during and after reheating, which requires dedicated numerical analysis. Still, we assume we can associate a temperature with the produced relativistic particles at the end of the reheating era.

Our present analysis clearly shows the requirement of a high post-inflationary EoS (or, some stiff matter-dominated phase) to achieve successful reheating through pure gravitational production. It also shows the sensitive dependence of reheating temperature on the inflationary energy scale through the variation of the parameter $\alpha$ in the potential (2.75).

We have obtained the power-law-type behavior of particle number density spectrum in both IR and UV regimes for different EoS and the detailed investigation reveals that the minimum reheating temperature that is BBN (*Big Bang nucleosynthesis*) bound, $T_{\rm re} \sim 1$ MeV, is achieved around $w_\phi = 0.6$ for $\alpha = 1$. If we keep on increasing the parameter value $\alpha$, we keep on getting lower and lower reheating temperatures at higher EoS. The more the value of EoS $w_\phi$ that is closer to the kination regime ($w_\phi \to 1$), the higher the reheating temperature. Indeed, in the gravitational reheating scenario, in the absence of any such specific decay channel for the inlfaton, background inflaton energy density scales as $\rho_\phi \propto a^{-3(1+w_\phi)}$ whereas produced massless fluctuation being radiation scales as $\rho_R \propto a^{-4}$. In order to successfully reheat the universe, $\rho_\phi$ and $\rho_R$ must reach their equality and this essentially requires EoS $w_\phi > 1/3$ in the pure gravitational scenario. Therefore, simple energy scaling confirms the requirement of a higher EoS for gravitational reheating to happen. Now, combining UV and IR modes and using the spectrum given in Eq.(5.16) and (5.85), the total comoving energy density of produced particles can be computed as follows

$$\rho_R a^4 = \int_{k_{\rm re}}^{k_{\rm end}} \frac{k^3}{2\pi^2}|\beta_k|^2_{\rm IR} dk + \int_{k_{\rm end}}^{k_{\rm Planck}} \frac{k^3}{2\pi^2}|\beta_k|^2_{\rm UV} dk$$

$$\Rightarrow \rho_R a^4 = \frac{\mathcal{D} k_{\rm end}^4}{4\pi^3(1-2\bar{\nu})}\left(1-\left(\frac{k_{\rm re}}{k_{\rm end}}\right)^{(1-2\bar{\nu})}\right) + \frac{a_{\rm end}^6 \sum\left[\mathcal{N}_0+\mathcal{N}_1+\mathcal{N}_2+\mathcal{N}_3+\mathcal{N}_8+\mathcal{N}_9\right]^2}{64\pi^2 (f(w_\phi))^2 k_{\rm end}^2} \times \left(1-\left(\frac{k_{\rm end}}{k_{\rm Planck}}\right)^2\right)$$

$$\Rightarrow \rho_R^{\rm com}(\alpha,\ w_\phi) \approx \frac{\mathcal{D}(w_\phi) H_{\rm end}^4(\alpha,\ w_\phi)}{4\pi^3(1-2\bar{\nu}(w_\phi))} + \frac{\sum\left[\mathcal{N}_0+\mathcal{N}_1+\mathcal{N}_2+\mathcal{N}_3+\mathcal{N}_8+\mathcal{N}_9\right]^2}{64\pi^2 (f(w_\phi))^2 H_{\rm end}^2(\alpha,\ w_\phi)}$$

$$\Rightarrow \rho_R^{\rm com}(\alpha,\ w_\phi) \approx \frac{\mathcal{D}(w_\phi)(3w_\phi+1)H_{\rm end}^4(\alpha,\ w_\phi)}{8\pi^3(3w_\phi-1)} + \frac{9(1+w_\phi)^2\sum\left[\mathcal{N}_0+\mathcal{N}_1+\mathcal{N}_2+\mathcal{N}_3+\mathcal{N}_8+\mathcal{N}_9\right]^2}{64\pi^2(1+3w_\phi)^2H_{\rm end}^2(\alpha,\ w_\phi)} \tag{5.76}$$

In the expression above, the first part is associated with the large-scale (IR) contribution and the second part is associated with the small-scale (UV) contribution, where the coefficients $\mathcal{N}_i$ are functions of the model parameter $\alpha$ and the EoS $w_\phi$ as defined earlier and in the Addenda A. Another EoS dependent function $\mathcal{D}$ is defined in (5.18). Here $k_{\rm re} = a_{\rm re}H_{\rm re}$ is the scale that entered the horizon at the end of reheating, and $a_{\rm re}, H_{\rm re}$ are the scale factor and Hubble scale at the end of reheating. Furthermore, in the comoving energy density expression, we take the IR cut-off at the scale $k_{\rm re}$ and we take the UV cut-off at the Planck energy scale, $k_{\rm Planck}$. It is important to note that while defining any physical quantity like energy density or temperature associated with fluctuations, we shall consider solely the contribution of the causal modes, which are well inside the horizon at the time of computing the quantity of interest. The highest accessible scale in the finite time scale of reheating is $k_{\rm re}$, and the modes in the range $k_{\rm re} \leq k \leq k_{\rm end}$ are well inside the horizon at the end of reheating, hence contributing to the total energy density of produced particles [46]. Therefore, $k_{\rm re}$ is considered to be the IR limit in the computation of $\rho_R^{\rm com}$ at the time of reheating in Eq.(5.76). The very nature of the UV spectrum shows no small-scale divergence at all in the computation of the energy density for the entire range of EoS $0 \leq w_\phi \leq 1$, whereas the very nature of the IR spectrum (see (5.16)) suggests a large-scale divergence in the total energy density for $w_\phi < 1/3$, and a logarithmic divergence for $w_\phi = 1/3$. However, in the entire range $w_\phi > 1/3$, there is no IR divergence in the energy density spectrum. Therefore, in the gravitational reheating scenario with $w_\phi \geq 3/5$, we are free from both IR and UV divergence of the comoving energy spectra. As $k_{\rm Planck} \gg k_{\rm end}$ and $k_{\rm RH} \ll k_{\rm end}$, in both the cases for $w_\phi > 1/3$, the significant contribution in energy comes around the scale, which leaves the Hubble horizon at the inflation end, which is $k = k_{\rm end}$.

As we are dealing with pure gravitational production here, the evolution of background inflaton energy density will mostly be affected by background expansion rather than the backreaction of produced fluctuations, as mentioned before. Therefore, background energy density evolves as

$$\rho_\phi(a) \simeq (3M_{\rm pl}^2H_{\rm end}^2)\left(\frac{a}{a_{\rm end}}\right)^{-3(1+w_\phi)} \tag{5.77}$$

Different spectral behavior causes different reheating e-folding number $N_{\rm re} \equiv \ln\left(\frac{a_{\rm re}}{a_{\rm end}}\right)$ for different EoS. In order to obtain $N_{\rm re}$ for different $w_\phi$, the condition $\rho_\phi(a) = \rho_R(a)$ has to be met at some point, say, at $a_{\rm re}$ during the reheating phase. We have,

$$\left(\frac{a_{\rm re}}{a_{\rm end}}\right) = \left(\frac{3M_{\rm pl}^2H_{\rm end}^2}{\rho_R^{\rm com}}\right)^{\frac{1}{(3w_\phi-1)}} \tag{5.78}$$

Finally, combining both IR and UV scale contributions, we end up having the expression

of reheating temperature achieved in the pure gravitational reheating scenario as

$$T_{\rm re} = \left(\frac{30}{g_{\rm re}\pi^2}\right)^{\frac{1}{4}} \left(3M_{\rm pl}^2 H_{\rm end}^2\right)^{\frac{1}{1-3w_\phi}} \left(\rho_R^{\rm com}\right)^{-\frac{3(1+w_\phi)}{4(1-3w_\phi)}} \tag{5.79}$$

where $g_{\rm re}$ is the total relativistic degrees of freedom at the time of reheating, which is given by $g_{\rm re} = 106.75$ in the SM for $T_{\rm re} \gtrsim 1$ GeV. Eq. (5.79) along with (5.76) are two important results of this work, giving us a particular reheating temperature corresponding to a specific reheating EoS within the Bogoliubov approach. Our detailed numerical results of reheating dynamics based on this non-perturbative formalism compared with the Boltzmann approach are given in Table 5.2 for different values of $w_\phi$. We note that both approaches agree quite well numerically. The slight discrepancy in the temperature prediction is caused by the addition of the IR contribution to the total energy density as well as the slightly higher spectral amplitude obtained in the non-perturbative Bogoliubov treatment, compared to the Boltzmann one, around the scale $k \sim k_{\rm end}$, for any $w_\phi > 1/3$. Now, to understand the individual contributions of the IR and UV components of radiation energy density $\rho_{\rm R}^{\rm com}$ from Eq.(5.76), we also calculated the reheating temperatures for these two components separately for varying EoS as shown in Fig.(5.3). Evidently, in this non-perturbative minimal reheating scenario, the small-scale(UV) contribution in the energy density is slightly larger than the large-scale(IR) contribution, causing the difference in the reheating temperatures as computed through UV and IR modes separately in Fig.(5.3).

Table 5.2: *Variation of reheating temperature with various EoS for $\alpha = 1$. Here, we have given both Boltzmann and Bogoliubov predictions for comparison.*

| Bogoliubov | | Boltzmann | |
|---|---|---|---|
| $w_\phi$ | $T_{\rm re}$ (GeV) | $w_\phi$ | $T_{\rm re}$ (GeV) |
| 3/5 | $1.12 \times 10^{-3}$ | 3/5 | $9.40 \times 10^{-4}$ |
| 2/3 | 2.17 | 2/3 | 0.97 |
| 5/7 | 58.26 | 5/7 | 11.76 |
| 3/4 | $3.54 \times 10^{2}$ | 3/4 | $2.42 \times 10^{2}$ |
| 4/5 | $5.84 \times 10^{3}$ | 4/5 | $2.54 \times 10^{3}$ |

## 5.4 Summary

In this chapter, we have computed the long and short-wavelength spectra of a massless scalar fluctuation during inflation and post-inflationary reheating employing the non-perturbative

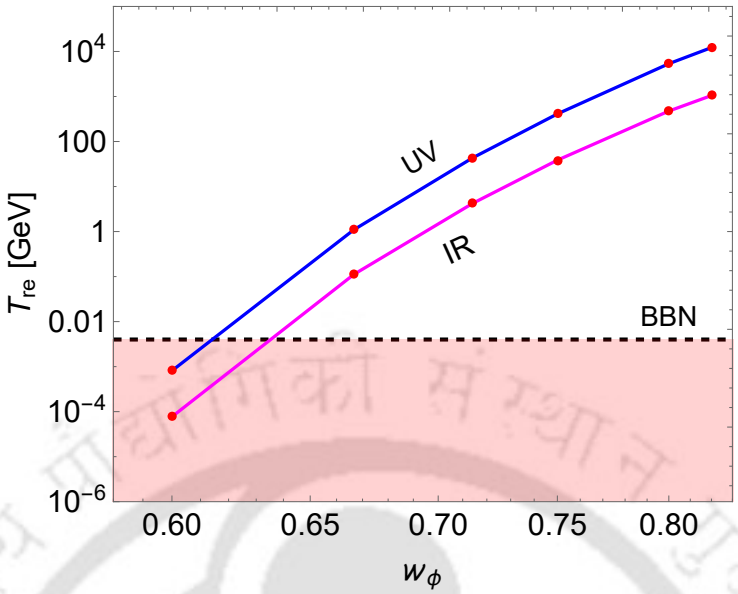


Figure 5.3: *The figure represents the individual contribution of IR and UV components of* $\rho_{\rm R}^{\rm com}$ *in Eq.(5.76) to the reheating temperature for varying EoS. The BBN temperature here is taken to be* 4 *MeV.*

Bogoliubov treatment in the pure gravitational reheating scenario. In the long-wavelength regime, we found that in the case of a transition from de Sitter inflation to general reheating EoS $w_\phi$, the spectral index varies from -6 to -3 for $0 \leq w_\phi \leq 1$. The lower the reheating EoS $w_\phi$, the heavier the red tilt of the spectrum in the IR regime. This IR behavior of the spectra is obtained within a purely non-perturbative treatment as the perturbative (or Boltzmann) approach fails to track the super-horizon evolution of the fluctuation.

We have also studied the mass-breaking effect or the departure of the large-scale spectra from the massless limit. We have analytically computed the relationship between field mass ($m_\chi$) and the IR scale ($k_m$) below which all the modes suffer from the finite mass effect for any general reheating EoS. For any $m_\chi/H_{\rm end} \gtrsim 3/2$, the large-scale spectrum is found to experience an exponential mass-suppression effect. Interestingly, we find that for the masses $m_\chi/H_{\rm end} \ll 3/2$, the $k^3\left|\beta_k\right|^2$ spectral shape always remains flat irrespective of the post-inflationary EoS. Our numerical result also supports this analytical finding.
However, for the short-wavelength modes, we find that the post-inflationary inflaton oscillation plays a very important role in computing the sub-horizon spectrum in the non-perturbative treatment. Our study reveals that the product of an oscillatory term and a non-oscillatory term in the expression of $|\beta_k|^2_{\rm UV}$ results in the appearance of an interference term which nicely explains the origin of the momentum-space oscillations in the high-frequency regime of the spectrum as we can see in Fig. (5.2). For $w_\phi = 0$, we recover the known UV spectral index to be -9/2 with small oscillations over it. Interestingly, we find the EoS $w_\phi = 1/9$, at which the dominant spectral index turns out to be -6, and

for any $1/9 \leq w_\phi \lesssim 1$, the spectral index remains -6 independent of the choice of $w_\phi$. Therefore, in the entire range $0 \leq w_\phi \lesssim 1$, the UV spectral index varies from $-9/2$ to -6. Unlike the long-wavelength regime, there is no UV divergence in the short-wavelength regime of the number density spectrum. We have also found an agreement in the spectral behavior between two approaches, using the Bogoliubov formalism or solving the associated Boltzmann equation, in the UV regime for any EoS $0 \leq w_\phi \lesssim 1$.

In the present study, we have also looked at how to achieve a successful reheating scenario from the non-perturbative approach. Such a gravitational reheating scenario is drawing much attention because of its simpler mechanism where a dynamical background itself suffices the conditions for successful reheating without the requirement of any complicated non-minimal coupling between produced fluctuation and inflaton or with gravity. In our work, we have studied this reheating scenario employing a non-perturbative Bogoliubov approach. We presented our result in Section 5.3, summarizing the variation of the reheating temperature with $w_\phi$ in Table 5.2. Our analysis shows that maintaining a reheating temperature above the BBN energy scale requires $w_\phi \gtrsim 0.6$. Evidently, to achieve radiation domination through purely gravitational production, the Universe has to transit to a higher post-inflationary EoS. It is interesting to note that there is a one-to-one correspondence between reheating temperature and reheating EoS, so a particular EoS can uniquely specify a particular $T_{\rm re}$ as given in Table 5.2. However, such a gravitational reheating scenario generally faces the challenge of overproducing primary gravitational waves (PGWs) [58, 111, 228, 243]. As well, the generation of light scalar perturbations from inflation and reheating may suffer from the problem of a too large isocurvature power spectrum $\mathcal{P}_S(k)$ for these modes. These isocurvature perturbations are tightly constrained by *Planck* data at CMB horizon crossing scale, $k_*/a_0 = 0.05$ Mpc$^{-1}$, with $a_0$ be the present-day scale factor. In this work, we are focusing on the gravitational production of a scalar fluctuation minimally coupled to gravity, $\xi = 0$. In several recent studies [69, 223, 224, 244–246], it has been clearly pointed out that for $w_\phi = 0$, a massless scalar fluctuation must have a lower limit of non-minimal coupling strength, $\xi \gtrsim 0.027$ to prevent the overproduction of isocurvature fluctuation at the CMB scale respecting the current isocurvature bound $\mathcal{P}_S(k_*) < 8.3 \times 10^{-11}$ [7, 8]. This rules out the possibility of a minimally coupled scalar field for $w_\phi = 0$ due to the heavily red-tilted large-scale spectrum, $|\beta_k|^2_{\rm IR} \propto k^{-6}$. On the contrary, for $w_\phi > 1/3$, the appearance of strong post-inflationary *tachyonic instability* beyond a certain coupling strength ($\xi > 1/6$) for the large scales imposes upper bounds on $\xi$ respecting the isocurvature constraint at the CMB scale. These possibilities are explored in the recent studies [46, 246] quite extensively. It has also been found that, as one approaches $w_\phi = 1/3$, the value of $\xi$ remains unconstrained subject to this large-scale isocurvature bound.

This chapter demonstrates the gravitational particle production phenomenon of a minimally coupled system, based on the semi-classical gravity treatment, where the dynamical background is classical, and the produced fluctuations are quantum. This treatment of particle production within a classical gravitational background is an effective description, and at sufficiently high energies, when the inflaton field value is not far from the Planck scale, the quantum gravity effects are expected to become relevant. As pointed out in [247], the

effective field theory operators can significantly enhance the particle production immediately after inflation. Additionally, in the higher EoS regime (for $n > 1$), self-interactions of the inflaton can generate loop-induced corrections such as the *Coleman–Weinberg potential*, which may modify the effective potential, particularly at small field values. In this chapter, we have focused on the leading-order (tree-level) dynamics and have not included these radiative corrections explicitly to the background inflaton potential, which is expected to further alter the early-universe reheating and dark matter studies. However, the detailed investigation of these effects lies beyond the scope of this thesis and is left for our future endeavour.

# Addenda

## A Higher order sub-horizon spectrum

### A.1 UV($k > a_{\rm end}H_{\rm end}$) modes spectrum including higher-order terms of $\left(\frac{\phi_0(t)}{M_{\rm pl}}\right)$ :

In the expressions of $H(t)$, $H^3(t)$, $\dot{H}(t)$ and $\ddot{H}(t)$, we truncate the expansions at the order three $\left(\frac{\phi_0(t)}{M_{\rm pl}}\right)^3$ through an amplitude comparison with the other higher-order terms($\mathcal{O}(4)$, $\mathcal{O}(5)$ etc.).
The expression of the Hubble scale up to $O(4)$ higher-order terms is given as,

$$H(t) \simeq \bar{H}\left(1+\frac{\mathcal{P}\sqrt{6(1-\mathcal{P}^{2n})}}{2(n+1)}\left(\frac{\phi_0(t)}{M_{\rm pl}}\right)-\frac{3\mathcal{P}^2}{2(n+1)^2}\left(\frac{\phi_0(t)}{M_{\rm pl}}\right)^2+\frac{3\sqrt{6}\mathcal{P}^3\sqrt{(1-\mathcal{P}^{2n})}}{4(n+1)^3}\left(\frac{\phi_0(t)}{M_{\rm pl}}\right)^3\right) \tag{5.80}$$

Subject to this Hubble scale (5.80), the expressions of $H^3$, $\dot{H}$, $H\dot{H}$ and $\ddot{H}$ with the higher-order terms can be written as follows

$$\begin{aligned}
H^3(t) &\simeq \bar{H}^3\Bigg(1+\frac{3\mathcal{P}\sqrt{6(1-\mathcal{P}^{2n})}}{2(n+1)}\left(\frac{\phi_0(t)}{M_{\rm pl}}\right)-\frac{9\mathcal{P}^2\mathcal{P}^{2n}}{2(n+1)^2}\left(\frac{\phi_0(t)}{M_{\rm pl}}\right)^2\\
&\quad-\frac{3\sqrt{6}\mathcal{P}^3\sqrt{(1-\mathcal{P}^{2n})}}{4(n+1)^3}\left(2+\mathcal{P}^{2n}\right)\left(\frac{\phi_0(t)}{M_{\rm pl}}\right)^3\Bigg)\\
\dot{H}(t) &\simeq 3\bar{H}^2\Bigg(\left(\mathcal{P}^{2n}-1\right)-\frac{\sqrt{6}\mathcal{P}\sqrt{1-\mathcal{P}^{2n}}}{(n+1)}\left(\frac{\phi_0(t)}{M_{\rm pl}}\right)+\frac{9\mathcal{P}^2}{2(n+1)^2}\left(2\mathcal{P}^{2n}-3\right)\left(\frac{\phi_0(t)}{M_{\rm pl}}\right)^2\Bigg)\\
H(t)\dot{H}(t) &\simeq 3\bar{H}^3\Bigg(\left(\mathcal{P}^{2n}-1\right)+\frac{\sqrt{6}\mathcal{P}\sqrt{1-\mathcal{P}^{2n}}}{2(n+1)}\left(\mathcal{P}^{2n}-3\right)\left(\frac{\phi_0(t)}{M_{\rm pl}}\right)+\frac{3\mathcal{P}^2}{2(n+1)^2}\left(3\mathcal{P}^{2n}-4\right)\left(\frac{\phi_0(t)}{M_{\rm pl}}\right)^2\\
&\quad+\frac{3\sqrt{6}\mathcal{P}^3\sqrt{1-\mathcal{P}^{2n}}}{4(n+1)^3}\left(3\mathcal{P}^{2n}-2\right)\left(\frac{\Phi(t)}{M_{\rm pl}}\right)^3\Bigg)\\
\ddot{H}(t) &\simeq \frac{9\bar{H}^3}{(n+1)}\Bigg(\left(4-(4+2n)\mathcal{P}^{2n}\right)+\sqrt{6}\mathcal{P}\sqrt{1-\mathcal{P}^{2n}}\left(\frac{n+4}{n+1}-\mathcal{P}^{2n}\right)\left(\frac{\phi_0(t)}{M_{\rm pl}}\right)\\
&\quad+\frac{3\mathcal{P}^2}{(n+1)}\left(\frac{3n+4}{n+1}-3\mathcal{P}^{2n}\right)\left(\frac{\phi_0(t)}{M_{\rm pl}}\right)^2+\frac{3\sqrt{6}\mathcal{P}^3\sqrt{1-\mathcal{P}^{2n}}}{(n+1)^2}\left(\frac{\phi_0(t)}{M_{\rm pl}}\right)^3\Bigg)\\
&\quad-6\sqrt{6}n\bar{H}^3\left(\frac{M_{\rm pl}}{\phi_0(t)}\right)\mathcal{P}^{2n-1}\sqrt{1-\mathcal{P}^{2n}}
\end{aligned} \tag{5.81}$$

Substituting the Equations (5.80) and (5.81) to (5.39) we obtain

$$\frac{\dot{\omega}_k}{\omega_k} \simeq \frac{1}{\left(\frac{k^2}{a^2}+m_\chi^2\right)}\Bigg[Hm_\chi^2+\left(\frac{7n-11}{n+1}+\frac{9}{n+1}\mathcal{P}^{2n}\right)\bar{H}^3+\frac{3\sqrt{6}\bar{H}^3\mathcal{P}\sqrt{1-\mathcal{P}^{2n}}}{2(n+1)^2}(4n-5)\left(\frac{\phi_0(t)}{M_{\rm pl}}\right)$$
$$\underbrace{+\frac{9\bar{H}^3\mathcal{P}^2}{2(n+1)^2}\left(\frac{3n}{n+1}+2\mathcal{P}^{2n}\right)\left(\frac{\phi_0(t)}{M_{\rm pl}}\right)^2+\frac{3\sqrt{6}\bar{H}^3\mathcal{P}^3\sqrt{1-\mathcal{P}^{2n}}}{4(n+1)^3}\left(4-25\mathcal{P}^{2n}\right)\left(\frac{\phi_0(t)}{M_{\rm pl}}\right)^3}_{\text{Additional higher-order terms}}$$
$$+3\sqrt{6}n\bar{H}^3\left(\frac{M_{\rm pl}}{\phi_0(t)}\right)\mathcal{P}^{2n-1}\sqrt{1-\mathcal{P}^{2n}}\Bigg] \tag{5.82}$$

Similarly, we can define the integral (5.45) with the modified expression (5.82) as

$$\beta_k \simeq \frac{1}{2}\sum_{\nu,l\neq 0}\int_{t_{\rm end}}^{t}dt'\left(\frac{t_{\rm end}}{t'}\right)^3\Bigg[\mathcal{N}_0e^{i(\nu+l)\omega t'}\left(\frac{t'}{t_{\rm end}}\right)^{\frac{1}{n}}+\mathcal{N}_1e^{i\nu\omega t'}+\mathcal{N}_2+\mathcal{N}_3e^{i(\nu+l)\omega t'}\left(\frac{t_{\rm end}}{t}\right)^{\frac{1}{n}}$$
$$+\mathcal{N}_4\left(\frac{t'}{t_{\rm end}}\right)^2+\mathcal{N}_5e^{i(\nu+l)\omega t'}\left(\frac{t'}{t_{\rm end}}\right)^{\frac{2n-1}{n}}$$
$$\underbrace{+\mathcal{N}_6e^{i\nu\omega t'}\left(\frac{t'}{t_{\rm end}}\right)^{\frac{2(n-1)}{n}}+\mathcal{N}_7e^{i(\nu+l)\omega t'}\left(\frac{t'}{t_{\rm end}}\right)^{\frac{2n-3}{n}}+\mathcal{N}_8e^{i\nu\omega t'}\left(\frac{t_{\rm end}}{t}\right)^{\frac{2}{n}}+\mathcal{N}_9e^{i(\nu+l)\omega t'}\left(\frac{t_{\rm end}}{t}\right)^{\frac{3}{n}}}_{\text{Additional coefficients}}\Bigg]$$
$$\times\frac{e^{-2i\Omega_k(t')}}{\left(\frac{k^2}{a^2}+m_\chi^2\right)}, \tag{5.83}$$

where newly defined indices are

$$\mathcal{N}_6=-\mathcal{N}_4\frac{3\mathcal{P}_\nu^2}{2(n+1)^2}\left(\frac{\phi_{\rm end}}{M_P}\right)^2;\ \mathcal{N}_7=\mathcal{N}_4\frac{3\sqrt{6}\mathcal{P}_\nu^3\left(\sqrt{1-\mathcal{P}^{2n}}\right)_l}{4(n+1)^3}\left(\frac{\phi_{\rm end}}{M_{\rm pl}}\right)^3;$$
$$\mathcal{N}_8=\frac{9H_{\rm end}^3}{2(n+1)^2}\left(\frac{3n\mathcal{P}_\nu^2}{n+1}+2\mathcal{P}_\nu^{2(n+1)}\right)\left(\frac{\phi_{\rm end}}{M_{\rm pl}}\right)^2;$$
$$\mathcal{N}_9=\frac{3\sqrt{6}H_{\rm end}^3}{4(n+1)^3}\left(4\mathcal{P}_\nu^3\left(\sqrt{1-\mathcal{P}^{2n}}\right)_l-25\mathcal{P}_\nu^{3+2n}\left(\sqrt{1-\mathcal{P}^{2n}}\right)_l\right)\left(\frac{\phi_{\rm end}}{M_{\rm pl}}\right)^3. \tag{5.84}$$

Here, we introduce a few other separate Fourier series having Fourier components $\mathcal{P}_\nu^2, \mathcal{P}_\nu^3, \mathcal{P}_\nu^{2(n+1)}$ and $\mathcal{P}_\nu^{3+2n}$.

In the range $0 \leq w_\phi < 1/3$, as we have argued in (5.50), the integrals associated with the coefficients $\mathcal{N}_1$, $\mathcal{N}_3$ will not contribute to the stationary points considerably because of the subdominant spectral indices. Likewise, for massless or very low-mass case($m_\chi \approx 0$), additional higher-order terms with the coefficients $\mathcal{N}_8$ and $\mathcal{N}_9$ have even smaller contributions compared to $\mathcal{N}_1, \mathcal{N}_3$. Therefore, in the range $0 \leq w_\phi < 1/3$, the spectral behavior in Eq.(5.58) will remain unchanged by adding higher-order terms.

In the range $w_\phi > 1/3$, these additional higher-order terms have a significant contribution to the total amplitude of the spectrum. Evaluating the integral (5.83) for $w_\phi > 1/3$ and proceeding along the same way as described in Section 5.1 (see Eqs.(5.54)-(5.60)) we finally obtain the modified UV spectrum as follows

$$\boxed{|\beta_k|^2_{\rm UV} \simeq \frac{1}{16(f(w_\phi))^2}\left(\frac{a_{\rm e}}{k}\right)^6 \times \sum\sum\left[\mathcal{N}_0+\mathcal{N}_1+\mathcal{N}_2+\mathcal{N}_3+\mathcal{N}_8+\mathcal{N}_9\right]^2} \tag{5.85}$$

Although the terms associated with $\mathcal{N}_3, \mathcal{N}_8, \mathcal{N}_9$ are faster decaying, while evaluating the integral (5.83), they have a non-negligible contribution to the total amplitude from the perspective of initial time.

CHAPTER 6

# Gravitational production of nonminimally coupled scalar fluctuation: Gravitational wave and Reheating phenomenology

*" When gravitational waves reach the earth, the waves stretch and squeeze space. This is a tiny stretch and squeeze. Far too small to detect with ordinary human senses."*

— *Kip Thorne*

Primordial Gravitational wave (GW) is one of the unique observable predictions of the inflationary paradigm [9–12, 14, 17–19, 21–23, 123, 124, 248, 249]. Given the advent of a large number of existing [250–261] and upcoming [262–268] GWs detection experiments, inflationary framework proves to be an interesting playground to look for new physics at very high energy scales [269, 270]. Exponential expansion leading to tachyonic growth of the super-horizon modes, and their subsequent evolution are known to be imprinted in the distribution of various cosmological relics such as Cosmic Microwave Background (CMB), Dark Matter (DM), GWs in the form of various correlations of scalar, vector and tensor fluctuations. Over the years enormous efforts have been put into estimating those correlations through the CMB anisotropy ([7] and references therein), dark and baryonic matter distribution [271, 272], and placed tight constraints on the possible physics of inflation. Out of those different relics, GW is said to be unique due to its extremely weak (Planck-suppressed) but universal coupling. Whereas weak coupling renders it an ideal probe of the very early universe, universal coupling, on the other hand, enables it to probe into the nature of all fundamental interactions in both the visible and dark sectors.

Utilizing inflation as a mechanism and the subsequent reheating phase, in the first part of this chapter, we intend to probe the non-minimal gravitational coupling $\xi R\chi^2$ with a real scalar field $\chi$ through its imprints on the primordial GW spectrum. Such coupling is assumed to be inevitable in the low-energy effective theory for the scalar field when coupled with gravity. Nonminimal couplings are generated by quantum corrections even if they are not present in the classical action [273]. The coupling is actually required if the scalar field theory is to be renormalizable in a classical gravitational background [274, 275]. Non-minimal gravitational coupling has been extensively explored in the context of inflation [276–288], reheating [289–299], DM [68, 69, 300–309], and dark energy [310–313]. In the present chapter, however, we focus on the dynamics of super-Hubble modes during inflation and reheating, the associated induced GW spectrum, and the reheating phenomenology, solely assisted by the large-scale fluctuations. These particular aspects of the present study have been less explored in the literature. The Chapter(6) is based on two works [246] and [46].

This chapter is divided into two parts. In the first part based on [246], we have studied that depending on the strength of the non-minimal coupling, a certain range of super-Hubble modes of the scalar field realises tachyonic growth and may lead to potentially detectable secondary gravitational waves (SGW). Our analysis further reveals that the post-inflationary reheating phase plays an instrumental role. In the perturbative framework, the reheating phase is described by the equation of state $w_\phi$ of inflaton and reheating temperature $T_{\rm re}$. The instability that we pointed out for the super-Hubble modes turned out to be significant during the reheating phase, particularly for two distinct regions in the $(w_\phi, \xi)$ parameter space. Whereas for the equation of state $w_\phi < 1/3$, instability arises for $\xi < 1/6$, for $w_\phi > 1/3$, on the other hand, $\xi$ should be greater than the conformal limit $1/6$. Such instability helps to enhance the overall growth of the amplitude of the scalar field modes after they enter into the reheating phase and depends upon the reheating parameters, namely $w_\phi$ and reheating temperature $T_{\rm re}$. Further, the cosmological background driven by matter fields with a stiff equation of state is known to amplify GW amplitude when propagating through such a background [133]. In the first part of this chapter, we explore that a combination of the above two non-trivial effects indeed leads to strong GW production for the stiff equation of state. For the $w_\phi < 1/3$, on the other hand, the growth is weaker, but GW acquires a non-trivial spectral behavior near the CMB scales that can have an appreciable impact on the tensor-to-scalar ratio. Taking into account CMB constraints on the inflationary tensor power spectrum, and BBN constraints on an effective number of degrees of freedom we demonstrate that SGW induced by non-minimal coupling put a tighter constraint on non-minimal coupling parameters $\xi$ as compared to the values generically assumed in the earlier studies [58, 230, 314] and also constraint recently reported considering primary gravitational waves [315]. Respecting all the existing observational constraints, we finally estimate the range of non-minimal coupling against different reheating models that can be probed by the various upcoming GW experiments such as BBO, DECIGO, LISA, and ET.

In the second part of this chapter, based on [46], we have mainly focused on the possibility of the universe's reheating in the presence of nonminimally coupled gravitationally produced

scalar fluctuation. For the minimally coupled theory, after their horizon exit during inflation, the super-horizon modes of massless fields remain constant until their reentry during the standard Big Bang evolution. Therefore, such a scenario generally predicts low reheating temperature [36, 57, 154]. However, it has been observed that for a non-minimally coupled scalar field namely $\xi\chi^2 R$, the super-horizon modes can grow due to *tachyonic instability* [246, 293–302]. In this work, we shall demonstrate that such modes reentering the horizon after the conclusion of inflation can successfully reheat the universe without any further coupling parameter in the inflaton sector and predict a high reheating temperature. Since the reheating is solely aided by the infrared modes and produced by non-minimal gravitational interaction, we shall call it "Non-minimal Infrared Gravitational Reheating". Reheating governed by purely gravitational interaction has recently been discussed in the literature [154, 230, 293, 316]. In all these studies, the focus has been on sub-Hubble modes during the reheating phase. The dynamics of these modes are well described by the standard Boltzmann equation, which assumes inflaton decay into massless radiation. This decay process is mediated by gravitons through minimal gravitational interactions of the form $(1/M_{\rm pl})h_{\mu\nu}T^{\mu\nu}_{\chi}$. Such scenarios have gained significant interest due to their universal nature and model-independent predictions, particularly in determining the reheating temperature and dark matter mass. The predictions of gravitational reheating scenarios depend entirely on inflationary parameters, particularly the inflaton equation of state (EoS) $w_\phi$. For instance, if the inflaton potential follows a standard power-law form near its minimum, $V(\phi) \sim \phi^{2n}$, the effective inflaton EoS, given by $w_\phi = (n-1)/(n+1)$, governs the entire reheating dynamics. However, this compelling scenario is ruled out for any value of $0 \leq w_\phi \leq 1$ due to constraints from Big Bang nucleosynthesis (BBN)*. Specifically, it is inconsistent with the observed effective number of relativistic degrees of freedom, $\Delta N_{\rm eff} \sim 0.284$ [7, 8] latest observation, and the lower bound on the reheating temperature, $T_{\rm re}^{\rm min} \sim T_{\rm BBN} \simeq 4$ MeV. [59, 61, 317]. Subsequently, the model with non-minimal coupling where the radiation field is gravitationally coupled is studied [58, 230] to evade such a problem. It is indeed demonstrated that for a sufficiently large value of $\xi$ the universe can be reheated with $w_\phi > 1/3$ in consistent with Big Bang nucleosynthesis(BBN) observation. One should remember that in all the aforesaid studies, the standard Boltzmann framework has been adopted, which deals with only the sub-Hubble modes of the fluctuation.

In this study, we shall compare two different production mechanisms stated above. We analyze the contribution of both super- and sub-Hubble modes, which are produced during and after inflation in the process of reheating. Our analysis reveals that since reheating is a gradual process, a large number of super-horizon modes will enter the horizon during this process, resulting in a non-negligible contribution compared to the modes causally produced via Boltzmann dynamics from the inflaton decay. Indeed, in some regions of parameter space, we show that the energy density associated with the inflationary super-horizon modes of radiation field non-minimally coupled with gravity $\xi\chi^2 R$ can supersede the contribution from their causal counterpart produced solely from the inflaton decay.

*Recently proposed gravitational neutrino reheating [56, 231] scenarios alleviate such constraints, making the framework viable for any inflaton EoS $w_\phi > 1/3$.

The latest precision observation by ACT, DESI [43, 44], combined with *Planck*, however, seemingly make a large number of well-motivated inflationary models disfavored. However, inference on any inflationary model based on observation must include its post-inflationary dynamics. It is important to note that the predictions of any inflationary model, and their relation to the CMB anisotropies, are intimately tied to the post-inflationary reheating phase. This intriguing connection was first explored by Kamionkowski et al. in [318]. Consequently, CMB observations, together with the underlying reheating mechanism, play a crucial role in constraining any given inflationary model. In this light, any new reheating scenario—such as the one we present in this work—should be examined through the lens of CMB observations to obtain the correct constraints on inflationary models. In this paper, we propose a new gravitational reheating mechanism, discuss its indirect impact, and revisit the possible constraint on the parameter space of the $\alpha-$attractor model in light of the latest ACT, DESI observations.

The order of construction of Part I of this chapter is as follows: In Section 6.1, we elaborately discuss the super-horizon instability dynamics(*tachyonic instability*) of the scalar field in the presence of the non-minimal coupling with gravity $\xi\chi^2 R$ and we also compute the associated long-wavelength field solutions during reheating corresponding to three different ranges of non-minimal coupling strength, $0 \leq \xi < 3/16, \xi = 3/16, \xi > 3/16$ in the entire range of post-inflationary EoS $0 \leq w_\phi \leq 1$. Further, we thoroughly investigate the behavior of the scalar power spectrum and explicitly point out the salient features of this spectrum for varying parameters ($w_\phi$, $\xi$). We close this section by giving a short discussion on the model-independent definition of the reheating parameters ($N_{\rm re}$, $T_{\rm re}$). In Section 6.2, we discuss the dynamics of the tensor fluctuations with (secondary gravitational waves, SGW) and without (primary gravitational waves, PGW) the anisotropy sourced by the gravitationally produced scalar field. In this section, our prime focus is on the effect of the parametric instability being caused by the non-minimal coupling of the scalar field on the gravitational wave spectrum(PGW+SGW) for both $w_\phi < 1/3$ and $w_\phi > 1/3$. Here we compute the primary as well as the secondary gravitational wave spectrum and show the nature of the full spectrum for varying parameters ($w_\phi$, $T_{\rm re}$, $\xi$, $r_{0.05}$). Furthermore, we constrain the coupling strength $\xi$ in light of the present-day tensor-to-scalar ratio at the CMB scale $r_{0.05} \leq 0.036$, the $\Delta N_{\rm eff} \leq 0.284$, and the present-day isocurvature bound as reported by the recent *Planck* 2018 observation. We also constrain the negative $\xi$ values based on the observational bounds in the present scenario. We also provide a feasible parameter space of the parameter set ($T_{\rm re}$, $\xi$) that future GW detectors like LISA, DECIGO, BBO, ET, etc can detect. Section 6.3 summarizes the main findings of part I by shedding light on some possible directions of this work that are left for future endeavors. In Addenda 6.4, we have studied the behavior of the suppression factor $\left(1 - \frac{a^2\xi\langle\chi^2\rangle}{M_{\rm pl}^2}\right)^{-2}$ that we encounter in the dynamics of the secondary gravitational waves for different reheating parameters($w_\phi$, $T_{\rm re}$, $H_{\rm end}$, $\xi$). In Addenda 6.5, we illustrate the computation of the secondary GW spectrum for $w_\phi < 1/3$ and $w_\phi > 1/3$.

Part II of this chapter is constructed as follows: In Section 6.6, we study the non-perturbative dynamics of the *infrared gravitational reheating*. In Section 6.7, we do a

comparative study between the non-minimal coupling-induced perturbative gravitational reheating and the non-perturbative infrared reheating. In Section 6.8.2, we show that based on observational bounds on the tensor-to-scalar ratio and the isocurvature perturbation amplitude, there exists an upper limit on the coupling strength ($\xi_{\rm max}$). In Section 6.9, considering the induced gravitational wave, we further obtain a lower limit on the coupling strength($\xi_{\rm min}$) based on the $\Delta N_{\rm eff}$ bound for the primary gravitational wave(PGW). Finally, we identify the region of $\xi$ vs $\alpha$ and $\xi$ vs $T_{\rm re}$ parameter spaces, which are fully consistent with all the observational bounds and latest ACT results. Finally, Section 6.10 summarizes the main outcomes of this study. In Addenda 6.11, we compute the expression of the isocurvature perturbation amplitude for massless fluctuations. In Appendix 6.12, we do a comparative analysis between the Jordan and Einstein frame $T_{\rm re}$ vs $\xi$ predictions for different reheating EoS.

# Part I

# Probing a nonminimal coupling through super-horizon instability and secondary gravitational waves

## 6.1 IR Spectrum of Nonminimally Coupled Gravitationally Produced Massless Particles

We shall begin with the computation of the adiabatic vacuum solutions during inflation and the post-inflationary phase for the nonminimally coupled massless scalar fluctuation. Using the scale factor (2.121) in the dynamical Eq.(2.119), we write the equation of motion during de Sitter inflation ($\eta \leq \eta_{\rm end}$) as,

$$X_k'' + \underbrace{\left[k^2 - \frac{2(1-6\xi)}{\eta^2}\right]}_{\omega_k^2} X_k = 0. \tag{6.1}$$

From the above equation, it can be noted that long wavelength modes after their horizon crossing become tachyonic ($\omega_k^2 < 0$) for $0 \leq \xi < 1/6$. As $\xi$ exceeds the conformal limit $\xi = 1/6$, this instability ceases to exist.

The general solution of this equation is

$$X_k = C_1\sqrt{|\eta|}J_{\nu_1}(k|\eta|) + C_2\sqrt{|\eta|}Y_{\nu_1}(k|\eta|). \tag{6.2}$$

With the order of the Bessel functions $\nu_1 = \sqrt{9-48\xi}/2$ and $C_1, C_2$ are integration constants. To evaluate $\alpha_k$ and $\beta_k$, we need to define first the vacuum solution $X_k^{(\rm inf)}$ during inflation. To compute the de Sitter vacuum solution, we use the Bunch-Davies vacuum condition at the beginning of inflation. In this limit $k|\eta| >> 1$, the mode solution (6.2) becomes,

$$X_k(\eta) \sim \frac{1}{\sqrt{2\pi k}}\left[(C_1 - iC_2)e^{-i(k\eta+\pi/4+\pi\nu_1/2)} + (C_1+iC_2)e^{i(k\eta+\pi/4+\pi\nu_1/2)}\right]. \tag{6.3}$$

In the asymptotic in-vacuum limit, the positive-frequency outgoing mode function behaves as

$$X_k(\eta) \xrightarrow{\eta\to-\infty} \frac{e^{-ik\eta}}{\sqrt{2k}}. \tag{6.4}$$

Comparing (6.3) with (6.4) we have

$$C_1 = \frac{\sqrt{\pi}}{2}e^{i(\pi/4+\pi\nu_1/2)}, \quad C_2 = \frac{i\sqrt{\pi}}{2}e^{i(\pi/4+\pi\nu_1/2)}. \tag{6.5}$$

Therefore, the adiabatic vacuum solution during de Sitter inflation is

$$X_k^{(\rm inf)} = \frac{\sqrt{-\pi\eta}}{2}e^{i(\pi/4+\pi\nu_1/2)}H_{\nu_1}^{(1)}(-k\eta). \tag{6.6}$$

Similarly the dynamical equation for general post-inflationary($\eta > \eta_{\rm end}$) EoS "$w_\phi$" is

$$X_k'' + \underbrace{\left[k^2 - \frac{2(1-3w_\phi)(1-6\xi)}{(1+3w_\phi)^2\left(\eta + \frac{3(1+w_\phi)}{a_{\rm end}H_{\rm end}(1+3w_\phi)}\right)^2}\right]}_{\omega_k^2} X_k = 0, \tag{6.7}$$

From the above equation, it can be again noted that the modes which were stable during inflation for $\xi > 1/6$ become tachyonic ($\omega_k^2 < 0$) during reheating for $w_\phi > 1/3$ [302]. We will see that this will play a significant role in our subsequent studies. The general solution of this equation is

$$X_k(\eta) = C_3 4^{\nu_2}\Gamma(\nu_2+1)\sqrt{2ik\bar{\eta}}I_{\nu_2}(ik\bar{\eta}) + C_4\sqrt{\frac{2ik\bar{\eta}}{\pi}}K_{\nu_2}(ik\bar{\eta}). \tag{6.8}$$

Where we use the symbol $\bar{\eta} = (\eta + 3\mu/a_{\rm end}H_{\rm end})$. $I_{\nu_2}$ and $K_{\nu_2}$ are modified Bessel functions of order $\nu_2$ with

$$\mu = \frac{(1+w_\phi)}{(1+3w_\phi)}, \quad \nu_2 = \frac{\sqrt{3(1+w_\phi)\Big(3(1-w_\phi)^2 + 16\xi(3w_\phi-1)\Big)}}{2\sqrt{1+3w_\phi}\sqrt{1+4w_\phi+3w_\phi^2}}. \tag{6.9}$$

and $C_3, C_4$ are the integration constants.

We now seek the solution of (6.7) compatible with the requirements of an adiabatic vacuum. If spacetime changes very slowly or equivalently particle momentum is so large that it hardly feels the background dynamics, the mode function can be safely assumed to behave as a positive frequency mode in Minkowski space in its asymptotic limit. For this we assume the ($k\eta >> 1$) limit, and the mode solution (6.8) transforms into,

$$X_k(\eta) \sim \left[C_3\frac{2^{2\nu_2}\Gamma(\nu_2+1)}{\sqrt{\pi}}e^{ik\bar{\eta}} + C_4 e^{-ik\bar{\eta}}\right]. \tag{6.10}$$

In the adiabatic out-vacuum limit that is for $\eta >> 1$ or equivalently $a(\eta) \to \infty$ mode function behaves as a positive frequency state

$$X_k(\eta) \xrightarrow{\eta\to\infty} \frac{e^{-ik\eta}}{\sqrt{2k}}, \tag{6.11}$$

Comparing (6.10) with (6.11) we have

$$C_3 = 0, \quad C_4 = \frac{1}{\sqrt{2k}}\exp\left[\frac{3ik\mu}{a_{\rm end}H_{\rm end}}\right]. \tag{6.12}$$

Therefore, the adiabatic vacuum solution of massless particles for general reheating EoS "$w_\phi$" becomes

$$X_k^{(\rm reh)}(\eta) = \sqrt{\frac{\bar{\eta}}{\pi}}\exp\left[\frac{3ik\mu}{a_{\rm end}H_{\rm end}} + \frac{i\pi}{4}\right]K_{\nu_2}(ik\bar{\eta}). \tag{6.13}$$

It is important to note that depending upon the value of the non-minimal coupling constant $\xi$, the order of the inflationary vacuum solution $\nu_1$ becomes positive for $0 \le \xi < 3/16$, zero for $\xi = 3/16$, and imaginary for $\xi > 3/16$. In addition to this, the index of post-inflationary vacuum solution $\nu_2$ also becomes imaginary in the range $\xi > 3/16$ for EoS $0 \le w_\phi < 1/3$

and it becomes real positive for $1/3 \leq w_\phi \leq 1$. This varying nature of the indices $\nu_1, \nu_2$ depending upon different ranges of non-minimal coupling strength and post-inflationary EoS greatly influences the nature of the post-inflationary field solution. Now we shall compute the field solution during reheating for general EoS in three specified ranges of the non-minimal coupling strength $\xi$.

### 6.1.1 Field solution at large scale for $0 \leq w_\phi < 1/3$

#### 6.1.1.1 For $0 \leq \xi < 3/16$ :

As mentioned earlier in Chapter(2), the general field solution in a particular phase can be expressed as a linear combination of the respective vacuum solution with the help of Bogoliubov coefficients $\alpha_k$ and $\beta_k$ (See Eq.(2.124) and (2.126)). So, our main task is to compute $\alpha_k$ and $\beta_k$ using the relations in (2.126). In this specified range of $\xi$, we get both $\nu_1$ and $\nu_2$ to be positive definite. Substituting these vacuum solutions (6.6) and (6.13) into (2.126), in long-wavelength limit $k/k_{\rm end} << 1$, we compute the Bogoliubov coefficients as

$$\alpha_k \approx \frac{\Gamma(\nu_1)\Gamma(\nu_2)2^{\nu_1}}{8\pi}\left(\frac{2}{3\mu-1}\right)^{\nu_2}\left(\frac{3\mu(1-2\nu_1)+2(\nu_1-\nu_2)}{\sqrt{(3\mu-1)}}\right)\left(\frac{1}{\bar{k}}\right)^{\nu_1+\nu_2} e^{i\left(\frac{\pi\nu_1}{2}+\frac{\pi\nu_2}{2}+\frac{\pi}{2}-3\mu\bar{k}\right)},$$
$$\beta_k \approx \alpha_k e^{i\left(-\pi\nu_2-\frac{\pi}{2}+6\mu\bar{k}\right)} \tag{6.14}$$

For a simplified expression, we define a new symbol $\bar{k} = k/k_{\rm end}$. We define the energy density of the produced particles at a time during reheating when the associated longest wavelength is well inside the horizon. In this sense, we always have $k\eta > 1$ for any mode that contributes to the energy density. Using the long-wavelength approximated form of the coefficients $\alpha_k$ and $\beta_k$(See Eq.(6.14)) in (2.124), we obtain the general long-wavelength solution of the scalar field for general EoS in the specified $\xi$ range for $k\eta >> 1$ as

$$X_k^{\rm long}(\eta) \approx \frac{\Gamma(\nu_1)\Gamma(\nu_2)2^{\nu_1}}{4\pi\sqrt{k_{\rm end}}}\left(\frac{2}{3\mu-1}\right)^{\nu_2}\left(\frac{3\mu(1-2\nu_1)+2(\nu_1-\nu_2)}{\sqrt{2(3\mu-1)}}\right)\frac{\cos(k\eta)}{\bar{k}^{(\nu_1+\nu_2+1/2)}} \tag{6.15}$$

where $k_{\rm end} = a_{\rm end}H_{\rm end}$ is the scale that leaves the horizon at the end of inflation.

#### 6.1.1.2 For $\xi = 3/16$ :

For this particular value of the coupling strength $\xi$, $\nu_1$ vanishes. Following the same procedure, in the long-wavelength limit, $\alpha_k$ and $\beta_k$ can now be evaluated as

$$\alpha_k \approx -\frac{\Gamma(\nu_2)}{2}\left(\frac{2}{3\mu-1}\right)^{\nu_2}\left(\frac{3\mu-2\nu_2}{4\sqrt{(3\mu-1)}}+\frac{i\sqrt{3\mu-1}}{\pi}\right)\frac{\exp\left(i(\pi\nu_2/2-\pi/2-3\mu\bar{k})\right)}{\bar{k}^{\nu_2}} \tag{6.16a}$$

$$\beta_k \approx \frac{\Gamma(\nu_2)}{2}\left(\frac{2}{3\mu-1}\right)^{\nu_2}\left(\frac{3\mu-2\nu_2}{4\sqrt{(3\mu-1)}}+\frac{i\sqrt{3\mu-1}}{\pi}\right)\frac{\exp\left(i(-\pi\nu_2/2+3\mu\bar{k})\right)}{\bar{k}^{\nu_2}} \tag{6.16b}$$

Associated general field solution for $\xi = 3/16$ in $k\eta >> 1$ limit becomes

$$X_k^{\rm long}(\eta) \approx \frac{\Gamma(\nu_2)}{\sqrt{2k_{\rm end}}}\left(\frac{2}{3\mu-1}\right)^{\nu_2}\left(\frac{3\mu-2\nu_2}{4\sqrt{(3\mu-1)}}+\frac{i\sqrt{3\mu-1}}{\pi}\right)\frac{i\sin(k\eta)}{\bar{k}^{\nu_2+1/2}} \tag{6.17}$$

#### 6.1.1.3 For $\xi > 3/16$ :

In this range of $\xi$ values, $\nu_1$ and $\nu_2$ become imaginary. Long-wavelength approximated Bogoliubov coefficients are

$$\alpha_k \approx \left(K_{\nu_2}\left(i\bar{k}(3\mu-1)\right)H_{\nu_1}^{(1)}(\bar{k})\left(\frac{3\mu}{\sqrt{3\mu-1}}\right)+\bar{k}\sqrt{3\mu-1}\left(H_{\nu_1-1}^{(1)}(\bar{k})-H_{\nu_1+1}^{(1)}(\bar{k})\right)\right) \times \exp(i(\pi/2)-3\mu\bar{k})\frac{\exp(-\pi\tilde{\nu}_1/2)}{4} \tag{6.18a}$$

$$\beta_k \approx \left(K_{\nu_2}\left(i\bar{k}(3\mu-1)\right)H_{\nu_1}^{(1)}(\bar{k})\left(\frac{3\mu}{\sqrt{3\mu-1}}\right)+\bar{k}\sqrt{3\mu-1}\left(H_{\nu_1-1}^{(1)}(\bar{k})-H_{\nu_1+1}^{(1)}(\bar{k})\right)\right) \times \exp(3\mu\bar{k})\frac{\exp(-\pi\tilde{\nu}_1/2)}{4} \tag{6.18b}$$

General field solution for $\xi > 3/16$ becomes

$$X_k^{\rm long}(\eta) \approx \frac{\exp(-\pi\tilde{\nu}_1/2)}{4\sqrt{2k_{\rm end}}}\left(K_{\nu_2}\left(i\bar{k}(3\mu-1)\right)H_{\nu_1}^{(1)}(\bar{k})\left(\frac{3\mu}{\sqrt{3\mu-1}}\right)+\bar{k}\sqrt{3\mu-1} \times\left(H_{\nu_1-1}^{(1)}(\bar{k})-H_{\nu_1+1}^{(1)}(\bar{k})\right)\right)\frac{\cos(k\eta)}{\bar{k}^{1/2}} \tag{6.19}$$

where $\tilde{\nu}_1 = (\sqrt{48\xi-9})/2$.

### 6.1.2 Field solution at large scale for $1/3 \leq w_\phi \leq 1$

#### 6.1.2.1 For $0 \leq \xi < 3/16$ :

Likewise in the previous case, the indices $\nu_1, \nu_2$ are also real positive in this EoS range. In the limit $k/k_{\rm end} << 1$, using equations (6.6),(6.13), and (2.126), we obtain Bogoliubov coefficients as

$$\alpha_k \approx -\frac{\Gamma(\nu_1)\Gamma(\nu_2)2^{\nu_1}}{8\pi}\left(\frac{2}{3\mu-1}\right)^{\nu_2}\left(\frac{3\mu(1-2\nu_1)+2(\nu_1-\nu_2)}{\sqrt{(3\mu-1)}}\right)\frac{\exp\left(i(\pi\nu_1/2+\pi\nu_2/2-\pi/2-3\mu\bar{k})\right)}{\bar{k}^{(\nu_1+\nu_2)}} \tag{6.20a}$$

$$\beta_k \approx \frac{\Gamma(\nu_1)\Gamma(\nu_2)2^{\nu_1}}{8\pi}\left(\frac{2}{3\mu-1}\right)^{\nu_2}\left(\frac{3\mu(1-2\nu_1)+2(\nu_1-\nu_2)}{\sqrt{(3\mu-1)}}\right)\frac{\exp\left(i(\pi\nu_1/2-\pi\nu_2/2+3\mu\bar{k})\right)}{\bar{k}^{(\nu_1+\nu_2)}} \tag{6.20b}$$

Subject to the following coefficients, the general field solution in $k\eta >> 1$ limit becomes

$$X_k^{\rm long}(\eta) \approx \frac{\Gamma(\nu_1)\Gamma(\nu_2)2^{\nu_1}}{4\pi\sqrt{k_{\rm end}}}\left(\frac{2}{3\mu-1}\right)^{\nu_2}\left(\frac{3\mu(1-2\nu_1)+2(\nu_1-\nu_2)}{\sqrt{2(3\mu-1)}}\right)\frac{i\sin(k\eta)}{\bar{k}^{(\nu_1+\nu_2+1/2)}} \tag{6.21}$$

#### 6.1.2.2 For $\xi = 3/16$ :

For this particular value of $\xi$, the expression of Bogoliubov coefficients as well as general field solution will remain the same for this EoS range $1/3 \leq w_\phi \leq 1$ also. Here also we obtain $\alpha_k$ and $\beta_k$ as

$$\alpha_k \approx -\frac{\Gamma(\nu_2)}{2}\left(\frac{2}{3\mu-1}\right)^{\nu_2}\left(\frac{3\mu-2\nu_2}{4\sqrt{(3\mu-1)}}+\frac{i\sqrt{3\mu-1}}{\pi}\right)\frac{\exp\left(i(\pi\nu_2/2-\pi/2-3\mu\bar{k})\right)}{\bar{k}^{\nu_2}} \tag{6.22a}$$

$$\beta_k \approx \frac{\Gamma(\nu_2)}{2}\left(\frac{2}{3\mu-1}\right)^{\nu_2}\left(\frac{3\mu-2\nu_2}{4\sqrt{(3\mu-1)}}+\frac{i\sqrt{3\mu-1}}{\pi}\right)\frac{\exp\left(i(-\pi\nu_2/2+3\mu\bar{k})\right)}{\bar{k}^{\nu_2}} \tag{6.22b}$$

Associated general field solution for $\xi = 3/16$ in $k\eta >> 1$ limit will be

$$X_k^{\rm long}(\eta) \approx \frac{\Gamma(\nu_2)}{\sqrt{2k_{\rm end}}}\left(\frac{2}{3\mu-1}\right)^{\nu_2}\left(\frac{3\mu-2\nu_2}{4\sqrt{(3\mu-1)}}+\frac{i\sqrt{3\mu-1}}{\pi}\right)\frac{i\sin(k\eta)}{\bar{k}^{\nu_2+1/2}} \tag{6.23}$$

#### 6.1.2.3 For $\xi > 3/16$ :

A significant difference in terms of spectral behavior will appear between two given EoS ranges in this particular case $\xi > 3/16$. In this case, we get one index $\nu_1$ to be imaginary as expected but another index $\nu_2$ to be real positive which differs from the previous case for $0 \leq w_\phi < 1/3$. This causes a noticeable change in the spectral behavior as we see soon. Long-wavelength approximated coefficients are evaluated to be

$$\begin{aligned}\alpha_k \approx & \frac{\Gamma(\nu_2)\exp(-\pi\tilde{\nu}_1/2)}{8}\left(\frac{3\mu-2\nu_2}{\sqrt{(3\mu-1)}}H^{(1)}_{\nu_1}(\bar{k})+\bar{k}\sqrt{3\mu-1}\Big(H^{(1)}_{\nu_1-1}(\bar{k})-H^{(1)}_{\nu_1+1}(\bar{k})\Big)\right)\\ & \times\frac{\exp\left(i(\pi\nu_2/2+\pi/2-3\mu\bar{k})\right)}{\bar{k}^{\nu_2}}\left(\frac{2}{3\mu-1}\right)^{\nu_2}\end{aligned} \tag{6.24a}$$

$$\begin{aligned}\beta_k \approx & \frac{\Gamma(\nu_2)\exp(-\pi\tilde{\nu}_1/2)}{8}\left(\frac{3\mu-2\nu_2}{\sqrt{(3\mu-1)}}H^{(1)}_{\nu_1}(\bar{k})+\bar{k}\sqrt{3\mu-1}\Big(H^{(1)}_{\nu_1-1}(\bar{k})-H^{(1)}_{\nu_1+1}(\bar{k})\Big)\right)\\ & \times\frac{\exp\left(i(3\mu\bar{k}-\pi\nu_2/2)\right)}{\bar{k}^{\nu_2}}\left(\frac{2}{3\mu-1}\right)^{\nu_2}\end{aligned} \tag{6.24b}$$

Therefore, the associated general field solution takes the following form.

$$X_k^{\rm long}(\eta) \approx \frac{\Gamma(\nu_2)\exp(-\pi\tilde{\nu}_1/2)}{4\sqrt{2k_{\rm end}}}\left(\frac{3\mu-2\nu_2}{\sqrt{(3\mu-1)}}H^{(1)}_{\nu_1}(\bar{k})+\bar{k}\sqrt{3\mu-1}\Big(H^{(1)}_{\nu_1-1}(\bar{k})-H^{(1)}_{\nu_1+1}(\bar{k})\Big)\right)$$
$$\times\frac{\cos(k\eta)}{\bar{k}^{\nu_2+1/2}}\left(\frac{2}{3\mu-1}\right)^{\nu_2} \tag{6.25}$$

From our analysis so far it is revealed that the long-wavelength scalar field modes gets amplified through tachyonic instability during and after inflation depending upon the value of $(\xi, w_\phi)$. To this end let us reiterate again that for $0 \leq \xi < 1/6$ long wavelength modes after their horizon crossing during inflation, get amplified due to the tachyonic instability effect (see Eq.(6.1)). As $\xi$ exceeds the conformal limit $\xi = 1/6$, the inflationary instability diminishes, whereas new tachyonic instability develops during reheating, particularly for stiff equation of state $w_\phi > 1/3$ (see Eq.(6.7). To identify this instability effect, in particular, one defines a dimensionless parameter $|\omega_k'/\omega_k^2|$ to study the departure from the adiabatic limit(see the discussion in subsection(2.7.2) of Chapter(2)). It can be shown explicitly as $\eta \to \pm\infty$, the ratio approaches $|\omega_k'/\omega_k^2| \to 0$ sufficiently fast. In the process of transition of the universe from early de Sitter to the post-inflationary reheating phase, this adiabaticity condition gets violated ($|\omega_k'/\omega_k^2| >> 1$) at some intermediate point (See Fig.6.1), and causes particle production associated with long-wavelength modes. However, small scales $k > a_{\rm end}H_{\rm end}$ residing inside the horizon generally remain adiabatic without any parametric growth. Enhancement of the scalar field modes due to those instabilities can indeed be observed in Fig.6.2. In this figure, we have plotted the time evolution of different field modes assuming $\xi = 3$ for three different equations of state $w_\phi = (0, 1/3, 1/2)$. It can indeed be seen that for $\xi > 1/6, w_\phi > 1/3$, the amplitude of the original field modes $\chi_k$ increases appreciably. The excitation of these large-scale modes due to the instability effect during and after inflation for different parameter regions of $\xi$ and $w_\phi$ motivates us to investigate the induced GWs. In the subsequent study of the generation of secondary GWs sourced by the anisotropy, we pay attention to the long-wavelength modes of the source, that lie in the range $k_* < k < k_{\rm end}$ where $(k_*/a_0) = 0.05{\rm Mpc}^{-1}$ is the present-day CMB pivot scale.

### 6.1.3 Behavior of scalar field energy density spectrum "$\rho_{\chi_k}(\eta)$"

While defining the anisotropic stress tensor to calculate the induced GW spectrum later, we require the nature of the power spectrum of the source field($\chi$). However, we shall soon see in the subsequent section that the gravitational wave energy density spectrum follows the spectral behavior of the field energy density spectrum($\rho_{\chi_k}$) in the long-wavelength regime $k << k_{\rm re}$. According to the standard definition given in [21], we define the field power spectrum of the produced fluctuations corresponding to the original field mode $\chi_k$ as $\mathcal{P}_\chi(k,\eta) = \frac{k^3}{2\pi^2a^2}|X_k|^2$. Excluding the non-minimal coupling term, the standard expression of energy density in terms of rescaled field mode($X_k$) and its derivative($X_k'$) is $\rho_\chi = \frac{1}{4\pi^2a^4}\int d(\ln k)k^3(|X_k'|^2 + k^2|X_k|^2)$[68, 69]. Hence associated energy density spectrum can be expressed as $\rho_{\chi_k}(\eta) = \frac{k^3}{4\pi^2a^4}(|X_k'|^2 + k^2|X_k|^2) = (k^2/a^2)\,\mathcal{P}_\chi(k,\eta)$. Now we shall

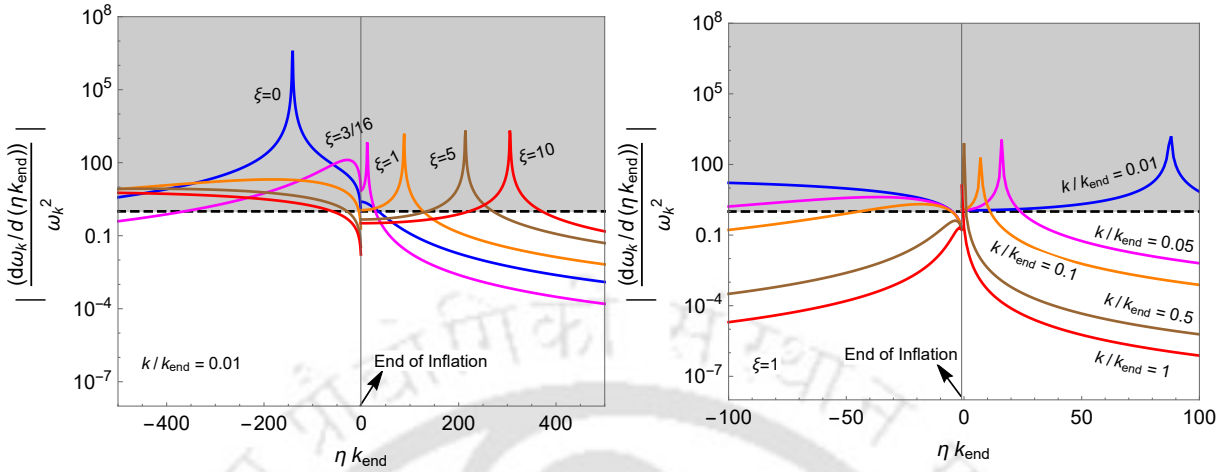


FIGURE 6.1: *Figure represents the measure of adiabaticity violation in terms of parameter* $|(d\omega_k/d(\eta k_{\rm end})/\omega_k^2|$ *with* $\eta k_{\rm end}$ *for different coupling strengths* $\xi$ *(left panel) and different scales* $k/k_{\rm end}$ *(right panel) for a specific EoS* $w_\phi = 1/2$*. In both panels, the black dashed line indicates adiabaticity parameter,* $|(d\omega_k/d(\eta k_{\rm end})/\omega_k^2| = 1$*. Any value of* $|(d\omega_k/d(\eta k_{\rm end})/\omega_k^2| > 1$ *depicted by the gray shaded region indicates the violation of adiabaticity. In the left panel of this figure, for the given scale* $k/k_{\rm end} = 0.01$*, with the increase of* $\xi$ *values, the peak of the adiabaticity parameter gradually shifts from the inflationary to the post-inflationary phase. This indicates that the super-horizon modes can still grow during reheating for higher coupling* $\xi$*. For* $\xi = 0$*, the instability effect is only present in the inflationary phase. In the right panel, it shows that for a given non-minimal coupling* $\xi$ *with the increase of* $k/k_{\rm end}$ *(small scale), the modes tend to remain adiabatic through the evolution.*

discuss the spectral features of $\rho_{\chi_k}$in the entire post-inflationary EoS range $0 \leq w_\phi \leq 1$ for three different $\xi$ ranges.

#### 6.1.3.1 For $0 \leq w_\phi < 1/3$ :

$$\rho_{\chi_k}(\eta > \eta_{\rm end}) = \frac{k^2}{a^2}\mathcal{P}_\chi(k, \eta > \eta_{\rm end}) \propto \begin{cases} (\cos^2(k\eta)/a(\eta)^4)(k/k_{\rm end})^{2(2-\nu_1-\nu_2)} & \text{for} \quad 0 \leq \xi < 3/16 \\ (\sin^2(k\eta)/a(\eta)^4)(k/k_{\rm end})^{2(2-\nu_2)} & \text{for} \quad \xi = 3/16 \\ (1/a(\eta)^4)(k/k_{\rm end})^4 & \text{for} \quad \xi > 3/16 \end{cases} \tag{6.26}$$

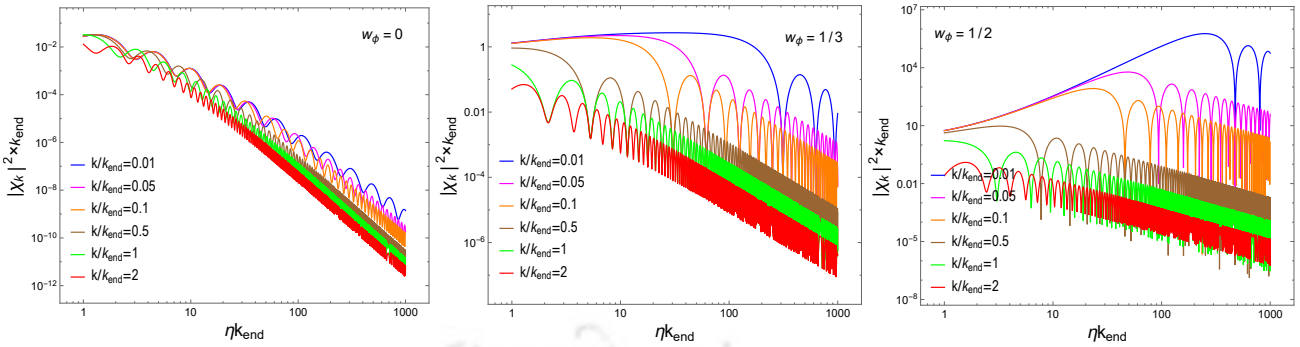


FIGURE 6.2: *Figure represents the time-evolution of dimensionless field amplitude square* $(|\chi_k|^2 \times k_{\rm end})$ *associated with some large scale*$(k < k_{\rm end})$ *and small scale*$(k > k_{\rm end})$ *modes for three different EoS. In all three plots, we choose the non-minimal coupling strength to be* $\xi = 3$*. It is clearly seen that for* $\xi > 1/6$*, the post-inflationary instability effect associated with long-wavelength modes is effective for* $w_\phi > 1/3$ *as discussed earlier.*

#### 6.1.3.2 For $1/3 \leq w_\phi \leq 1$ :

$$\rho_{\chi_k}(\eta > \eta_{\rm end}) \propto \begin{cases} (\sin^2(k\eta)/a(\eta)^4)(k/k_{\rm end})^{2(2-\nu_1-\nu_2)} & \text{for} \quad 0 \leq \xi < 3/16 \\ (\sin^2(k\eta)/a(\eta)^4)(k/k_{\rm end})^{2(2-\nu_2)} & \text{for} \quad \xi = 3/16 \\ (\cos^2(k\eta)/a(\eta)^4)(k/k_{\rm end})^{2(2-\nu_2)} & \text{for} \quad \xi > 3/16 \end{cases} \tag{6.27}$$

Depending upon EoS in three ranges $0 \leq w_\phi < 1/3$, $w_\phi = 1/3$, and $1/3 \leq w_\phi \leq 1$, the scalar field energy density spectrum $\rho_{\chi_k}(\eta)$ has interesting spectral behavior with the variation of coupling strength $\xi$. We first illustrate those important features of the $\rho_{\chi_k}(\eta)$ spectrum at a fixed time(and this is true for any time) for varying EoS $w_\phi$ in different ranges of $\xi$ values. We shall next discuss the behavior of the spectrum at varying instants of time for a fixed coupling strength.

#### 6.1.3.3 Spectral behavior of "$\rho_{\chi_k}(\eta)$" at a fixed time :

We first study the nature of the energy density spectrum for varying coupling strength at a fixed time during reheating.

- For $0 \leq w_\phi < 1/3$ : Examining the spectrum as given in (6.26) for $0 \leq w_\phi < 1/3$, we find that for $0 \leq \xi < 1/6$, the spectrum is always red-tilted or IR divergent $\rho_{\chi_k}(\eta) \propto k^{2(2-\nu_1-\nu_2)}$ with $(2-\nu_1-\nu_2) < 0$. However, the amount of red tilt depends upon the choice of EoS $w_\phi$ through the following relations,

$$\nu_1 = \frac{\sqrt{9-48\xi}}{2} \quad ; \quad \nu_2 = \frac{\sqrt{3(1+w_\phi)\Big(3(1-w_\phi)^2 + 16\xi(3w_\phi - 1)\Big)}}{2\sqrt{1+3w_\phi}\sqrt{1+4w_\phi+3w_\phi^2}}. \tag{6.28}$$

With the above mentioned parameter ranges $\nu_2$ should lie within $\sqrt{9-48\xi}/2 > \nu_2 > 1/2$. For example, as $w_\phi$ approaches zero the spectrum becomes maximally red-tilted $\rho_{\chi_k}(\eta) \propto k^{2(2-2\nu_1)}$ for given $\xi < 1/6$ up to the sinusoidal function of $k$. Such red tilt can indeed be observed in the blue curve in the left panel of Fig.(6.3). Furthermore, there exists a critical coupling strength $\xi_{\rm cri}$ lying in this range $0 < \xi_{\rm cri} < 1/6$, at which energy spectrum becomes scale-invariant giving $(4-2(\nu_1+\nu_2)) = 0$ (see the magenta line in the left panel of Fig.(6.3). Therefore, for $0 < \xi_{\rm cri} < 1/6$, energy spectrum remains IR divergent in the range $0 \leq \xi < \xi_{\rm cri}$ and it turns blue-tilted $(4-2(\nu_1+\nu_2)) > 0$ for $\xi > \xi_{\rm cri}$. Due to this red-tilted behavior of the energy density spectrum, the gravitational wave amplitude would be very large at the CMB scale. The *Planck* constraint on tensor to scalar ratio $r_{0.05} < 0.036$ will, therefore be shown to set a lower limit on the value of $\xi$. Once $\xi$ exceeds conformal limit $\xi > 1/6$, the spectrum remains blue-tilted till one reaches the $\xi = 3/16$. As $\xi$ exceeds $3/16$, both the indices $\nu_1, \nu_2$ being imaginary results in the energy density spectrum to be insensitive to the non-minimal coupling strength with $\rho_{\chi_k}(\eta) \propto k^4$. In the left panel of Fig.6.3 we can indeed see the blue titled spectrum for $\xi = (3/16,\ 1,\ 4)$ in brown, green and red respectively. In summary, in the entire range of $\xi > \xi_{\rm cri}$, the spectrum being blue-tilted draws the maximum contribution to the amplitude of the scalar power spectrum amplitude for those modes which left the horizon at the inflation end, that is $k_{\rm end}$.

- For $w_\phi = 1/3$ : For this particular value of the equation of state, $\nu_2 = 1/2$, irrespective of the choice of $\xi$, and in the range $0 \leq \xi < 1/6$, $\nu_1$ lies within $[3/2, 1/2)$. Consequently, we obtain a scale-invariant energy density spectrum(see the blue line in the middle panel of Fig.(6.3) for $\xi = 0$, and a blue-tilted spectrum in the range $0 < \xi < 1/6$. As $\xi$ exceeds the conformal limit, the index $\nu_1$ gradually decreases with the increase of $\xi$ up to $\xi = 3/16$, and in this range, $\nu_1$ lies within $(0.5, 0]$. According to the spectral index given in Eq.(6.27), the spectrum in the range $1/6 < \xi \leq 3/16$ becomes blue-tilted as shown in magenta and brown colors for $\xi = (0.18, 3/16)$ respectively in the middle panel of Fig. 6.3. For $\xi > 3/16$, $\nu_1$ becomes imaginary as is obvious from (6.28). With the further increase of $\xi$, the independence of $\nu_2$ makes the slope of the spectrum completely insensitive to the coupling strength in the entire range $\xi > 3/16$ although our numerical analysis shows very slow growth of the amplitude with increasing $\xi$ (see the green and red lines in the middle panel of Fig.6.3 for $\xi = (1,\ 4)$ respectively). From the spectral index given in Eq.(6.27), in the range $\xi \geq 3/16$, the power spectrum behaves as $\rho_{\chi_k}(\eta) \propto k^3$.

- For $1/3 < w_\phi \leq 1$ :

  Contrary to the previous case, the energy density spectrum for $1/3 < w_\phi \leq 1$, is blue-tilted in the range $0 \leq \xi < 3/16$ as obvious in the right panel of Fig.(6.3) for $\xi = 0$ (blue line, also see the magenta and brown lines in the right panel of Fig.(6.3). However, for $\xi > 3/16$, the energy spectrum has some noticeable features. For this case $\nu_2$ should lie within the range $(1/2, \sqrt{3\xi/2})$. Given an EoS $w_\phi > 1/3$, there exists a

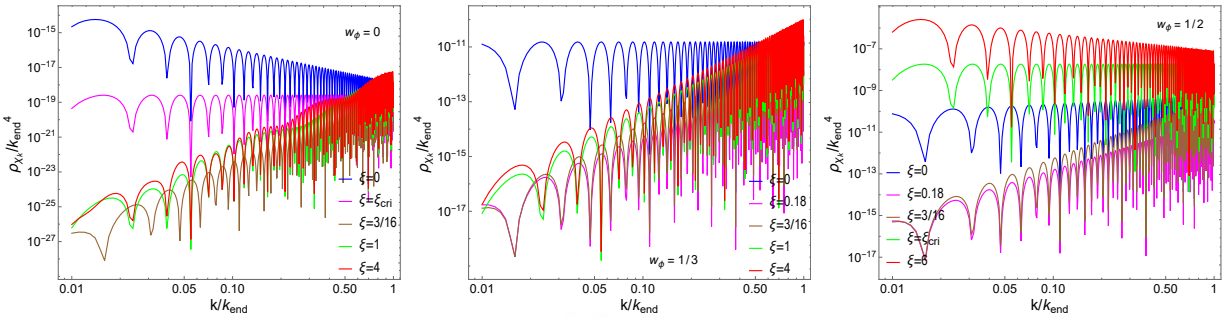


FIGURE 6.3: *Figure represents the variation of dimensionless scalar field energy density spectrum* $\rho_{\chi_k}(\eta)/k_{\rm end}^4$ *with non-minimal coupling strength* $\xi$ *for three reheating EoS,* $w_\phi = 0,\ 1/3,\ 1/2$. *For* $w_\phi = 0$, *the critical coupling* $\xi_{\rm cri} = 5/48$, *and for* $w_\phi = 1/2$, *critical coupling* $\xi_{\rm cri} \approx 4.073$.

particular coupling strength say, $\xi_{\rm cri} = \frac{(9w_\phi+7)(15w_\phi+1)}{48(3w_\phi-1)}$, at which the spectrum becomes perfectly scale-invariant giving $(2-\nu_2) = 0$ (see Eq.(6.27)). For $3/16 < \xi < \xi_{\rm cri}$, spectrum $\rho_{\chi_k}$ remains blue-tilted, $(2-\nu_2) > 0$ and turns into red-tilted or IR divergent, $(2-\nu_2) < 0$ for $\xi > \xi_{\rm cri}$. In the right panel of Fig.6.3, we notice the scale-invariant and red-tilted spectrum for $\xi = (\xi_{\rm cri},\ 6)$ in green and red lines respectively.

All these important characteristics of the energy density spectrum are shown in Fig.6.3 for three EoS $w_\phi = 0, w_\phi = 1/3,$ and $w_\phi = 1/2$ for different $\xi$ values at some point of time during reheating. Variations of spectral tilt with the variation of $\xi$ are believed to leave a discernible imprint on the induced GWs spectrum, which we intend to investigate in the subsequent section.

#### 6.1.3.4 Spectral behavior of "$\rho_{\chi_k}(\eta)$" for varying time :

Here we show for a certain coupling strength how the spectral shape will change over time during the reheating phase. We notice that as we go deep into the reheating phase $\eta >> \eta_{\rm end}$, the amplitude of the spectrum gets diminished for a given $k$-mode as obvious in Fig.6.4, and this is because of the decaying nature of every mode after horizon reentry during reheating. For the chosen value of coupling strength $\xi = 3$, the blue-tilted nature of the energy density spectra for $w_\phi = 0,\ 1/3,\ 1/2$ are also consistent with the expressions given in Eqs. (6.26) and (6.27).

### 6.1.4 Model-independent description of Reheating Parameters $(N_{\rm re},\ T_{\rm re})$ :

In this subsection, we introduce pivotal inflationary parameters namely the inflationary energy scale ($H_{\rm end}$), the duration of the inflationary period denoted by e-folding number $N_*$, and define a crucial reheating parameter, namely the *Reheating Temperature* ($T_{\rm re}$). From

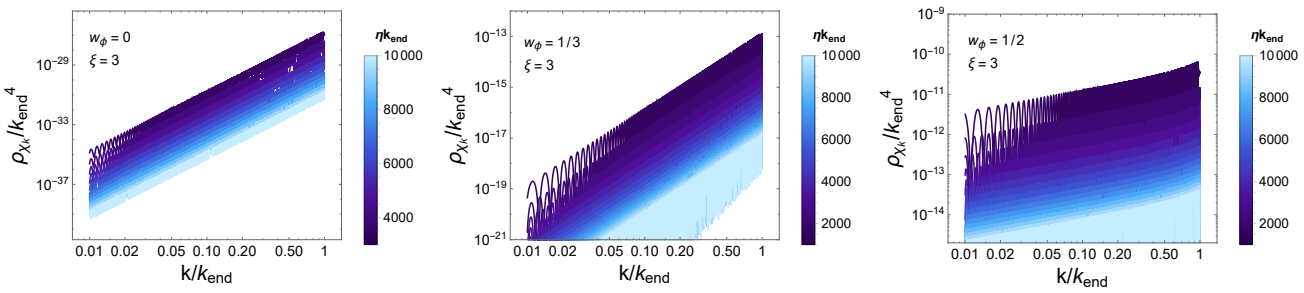


FIGURE 6.4: *Figure represents the behavior of dimensionless scalar field energy density spectrum $\rho_{\chi_k}(\eta)/k_{\rm end}^4$ for three EoS and a specific coupling strength $\xi = 3$ with the variation of dimensionless time-variable $\eta k_{\rm end}$ indicated by the color bar where the color gradient is indicating this time-evolution in the post-inflationary phase.*

the CMB pivot scale, we have $(k_*/a_0) = 0.05{\rm Mpc}^{-1}$ where $a_0$ is the present-day scale factor, and $k_{\rm end}$ denotes the wave number that crosses the Hubble radius at the end of inflation, and connecting these two scales, we express $k_{\rm end} = k_* {\rm e}^{N_k}$.

Assuming the reheating dynamics are characterized by an average inflaton equation of state $w_\phi$, the evolution of the inflaton energy density during this period is described by the simple expression $\rho_\phi = \rho_{\rm end}(a_{\rm end}/a)^{3(1+w_\phi)}$, where $\rho_{\rm end} = 3H_{\rm end}^2 M_{\rm pl}^2$ is the total inflaton energy density at the end of inflation.

The reheating temperature is conventionally defined at the end of the reheating period, where the radiation energy density equals the inflaton energy density, i.e., $\rho_{\rm R}(\eta_{\rm re}) = \rho_\phi(\eta_{\rm re})$, with $\eta_{\rm re}$ being the conformal time defined at the end of the reheating period. Employing this condition, the *Reheating Temperature* ($T_{\rm re}$) can be expressed as [133, 318]

$$T_{\rm re} = \left(\frac{90 H_{\rm end}^2 M_{\rm pl}^2}{\pi^2 g_{\rm re}}\right)^{1/4} \exp\left[-\frac{3N_{\rm re}}{4}(1+w_\phi)\right]. \tag{6.29}$$

Alternatively, the duration of the reheating period can be expressed as [318]

$$N_{\rm re} = \frac{1}{3(1+w_\phi)} \ln\left(\frac{90 H_{\rm end}^2 M_{\rm pl}^2}{\pi^2 g_{\rm re} T_{\rm re}^4}\right). \tag{6.30}$$

Here, $g_{\rm re} = 106.75$ represents the number of relativistic degrees of freedom at the beginning of the radiation epoch.

Assuming negligible entropy production after reheating, leading to the conservation of comoving entropy density ($a^3(\eta \geq \eta_{\rm re})s = {\rm const}$), we can establish a connection between the lowest possible mode re-entering the horizon at the end of reheating and the reheating temperature as

$$(k_{\rm re}/a_0) = \left(\frac{43}{11 g_{\rm re}}\right)^{1/3} \left(\frac{\pi^2 g_{\rm re}}{90}\right)^{1/2} \left(\frac{T_{\rm re} T_0}{M_{\rm pl}}\right) \simeq 1.82 \times 10^5 \left(\frac{T_{\rm re}}{10^{-2}\ {\rm GeV}}\right) {\rm Mpc}^{-1}. \tag{6.31}$$

By utilizing Eq. (6.30), we can define the largest mode that left the horizon at the end of inflation as

$$(k_{\rm end}/a_0) = \left(\frac{43}{11 g_{\rm re}}\right)^{1/3} \left(\frac{\pi^2 g_{\rm re}}{90}\right)^{\alpha_1} \frac{H_{\rm end}^{1-2\alpha_1} T_{\rm re}^{4\alpha_1-1} T_0}{M_{\rm pl}^{2\alpha_1}}, \tag{6.32}$$

where $\alpha_1 = 1/3(1+w_\phi)$ and $T_0 = 2.725$ K is the present-day CMB temperature.

## 6.2 Production of Gravitational Waves

In this section, our primary interest is to investigate the effect of the produced scalar fluctuations in the presence of non-minimal coupling as a possible source of anisotropy on gravitational waves. The perturbed FLRW metric, considering only the tensor perturbations, can be written as

$$ds^2 = a^2(\eta)\left[-d\eta^2 + (\delta_{ij} + h_{ij}) dx^i dx^j\right], \tag{6.33}$$

where "$\eta$" is the conformal time and $h_{ij}$ is the traceless tensor, i.e. $\partial^i h_{ij} = h^i_i = 0$. The tensor perturbations in the presence of anisotropic stress are governed by the following action up to quadratic order [**?** ]

$$S_{GW} = \int dx^4 \sqrt{-g}\left[-\frac{g^{\mu\nu}}{64\pi G}\partial_\mu h_{ij}\partial_\nu h_{ij} + \frac{1}{2}\Pi_{ij} h_{ij}\right], \tag{6.34}$$

where '$\Pi_{ij}$' is the anisotropic stress, defined as $\Pi^i_j = T^i_j - P\delta^i_j$. Here $\Pi_{ij}$' also satisfies the transverse ($\partial^i \Pi_{ij} = 0$) and traceless ($\Pi^i_i = 0$)) conditions. Here $\Pi_{ij}$ is coupled with the tensor perturbations $h_{ij}$ acting like an external source. From the expression of the stress-energy tensor of a massless scalar field having non-minimal gravity coupling(see Eq.(2.115)), we write the expression of anisotropic stress tensor as

$$\Pi_{ij} \sim (1-2\xi)\partial_i\chi\partial_j\chi - 2\xi\chi\partial_i\partial_j\chi + \xi\chi^2 G_{ij} \tag{6.35}$$

By varying $h_{ij}$ in action (6.34), we obtain the equation of motions of $h_{ij}$ [319]

$$h''_{ij}(\eta,\vec{x}) + 2\mathcal{H}h'_{ij}(\eta,\vec{x}) - \nabla^2 h_{ij}(\eta,\vec{x}) = 16\pi G a^2 \left(1 - \frac{a^2\xi\langle\chi^2\rangle}{M_{pl}^2}\right)^{-1}\Big((1-2\xi)\partial_i\chi\partial_j\chi - 2\xi\chi\partial_i\partial_j\chi\Big), \tag{6.36}$$

where the vacuum expectation value of fluctuations square can be expressed in terms of Fourier modes as

$$\langle\chi^2\rangle = \frac{1}{a^2}\int_{k_{\rm re}}^{k_{\rm end}} \frac{k^3}{2\pi^2}|X_k|^2\, d(\ln(k)). \tag{6.37}$$

For our specific choices of $\xi$, $a^2\xi\langle\chi^2\rangle < M_{\rm pl}^2$ should always be satisfied. Therefore, $\left(1-a^2\xi\langle\chi^2\rangle/M_{\rm pl}^2\right)\approx 1$ is well justified(See the details in the Addenda 6.4).
Utilizing Eqs. (2.100) and (6.35), we can write the Fourier expression of the source term as

$$\Pi_{ij}^{\rm TT}(\vec{k},\eta) = \frac{(2\xi-1)P_{ij}^{lm}(\hat{k})}{(2\pi)^3a^2(\eta)}\int d^3q q_l(k-q)_m\left(\hat{a}_{\vec{q}}X_{\vec{q}}(\eta)+\hat{a}^\dagger_{-\vec{q}}X^*_{\vec{q}}(\eta)\right)\left(\hat{a}_{\vec{k}-\vec{q}}X_{\vec{k}-\vec{q}}(\eta)+\hat{a}^\dagger_{-(\vec{k}-\vec{q})}X^*_{\vec{k}-\vec{q}}(\eta)\right)$$
$$+\frac{2\xi P_{ij}^{lm}(\hat{k})}{(2\pi)^3a^2(\eta)}\int d^3q q_l q_m\left(\hat{a}_{\vec{q}}X_{\vec{q}}(\eta)+\hat{a}^\dagger_{-\vec{q}}X^*_{\vec{q}}(\eta)\right)\left(\hat{a}_{\vec{k}-\vec{q}}X_{\vec{k}-\vec{q}}(\eta)+\hat{a}^\dagger_{-(\vec{k}-\vec{q})}X^*_{\vec{k}-\vec{q}}(\eta)\right). \tag{6.38}$$

The creation ($\hat{a}_{\vec{q}}$) and annihilation $\hat{a}^\dagger_{-\vec{q}}$ operators which contribute to the expectation value of Eq.(6.38) are

$$\langle 0|\hat{a}_{\vec{q}}\hat{a}_{\vec{k}-\vec{q}}\hat{a}^\dagger_{\vec{q}_1}\hat{a}^\dagger_{\vec{k}_1-\vec{q}_1}|0\rangle = (2\pi)^6\left[\delta^{(3)}(\vec{k}-\vec{q}-\vec{q}_1)+\delta^{(3)}(\vec{q}-\vec{q}_1)\right]\delta^{(3)}(\vec{k}-\vec{k}_1), \tag{6.39a}$$
$$\langle 0|\hat{a}_{\vec{q}}\hat{a}^\dagger_{-(\vec{k}-\vec{q})}\hat{a}_{\vec{q}_1}\hat{a}^\dagger_{-(\vec{k}_1-\vec{q}_1)}|0\rangle = (2\pi)^6\delta^{(3)}(\vec{k})\delta^{(3)}(\vec{k}_1-\vec{k}), \tag{6.39b}$$

where we used the following commutation relation $[\hat{a}_{\vec{k}},\hat{a}^\dagger_{\vec{k}_1}] = (2\pi)^3\delta^{(3)}(\vec{k}-\vec{k}_1)$. Since the second term Eq.(6.39b) does not contribute to $\Pi^2(k,\eta,\eta_1)$ due to the finite momenta i.e. $k=k_1\neq 0$. The only term Eq.(6.39a) contributes to the final expression of the correlator as

$$\Pi^2(k,\eta_1,\eta_2) = \frac{1}{4\pi^2a^2(\eta_1)a^2(\eta_2)}\int dqq^6\int d\gamma(1-\gamma^2)^2\langle X_{\vec{q}}(\eta_1)X_{\vec{k}-\vec{q}}(\eta_1)X^*_{\vec{q}}(\eta_2)X^*_{\vec{k}-\vec{q}}(\eta_2)\rangle \tag{6.40}$$

where $\gamma=\hat{k}\cdot\hat{q}=\cos(\theta)$, where $\theta$ is the angle between $\vec{k}$ and $\vec{q}$.

Now utilizing Eq.(6.40) in Eq.(2.206) we have found the tensor power spectrum to be

$$\mathcal{P}_{\rm T}^{\rm sec}(k,\eta) = \frac{k^3}{2\pi^2}\frac{4}{\pi^2M_{\rm pl}^4}\times\int_0^\infty dqq^6\int_{-1}^1 d\gamma(1-\gamma^2)^2$$
$$\times\int_{\eta_{\rm end}}^\eta d\eta_1\frac{\mathcal{G}_k^{\rm re}(\eta,\eta_1)}{a^2(\eta_1)}\int_{\eta_{\rm end}}^\eta d\eta_2\frac{\mathcal{G}_k^{\rm re}(\eta,\eta_2)}{a^2(\eta_2)}\langle X_{\vec{q}}(\eta_1)X_{\vec{k}-\vec{q}}(\eta_1)X^*_{\vec{q}}(\eta_2)X^*_{\vec{k}-\vec{q}}(\eta_2)\rangle \tag{6.41}$$

Here $\mathcal{P}_{\rm T}^{\rm sec}(k,\eta)$ defines the secondary tensor power spectrum during reheating at conformal time $\eta$ induced due to massless scalar field $\chi$.

### 6.2.1 Evolution of Primordial Tensor Power spectrum during Reheating:

This subsection provides a concise overview of the primary tensor power spectrum and its evolution resulting from quantum fluctuations during inflation. Within the context of a

simple slow-roll inflationary background, the primary tensor power spectrum resulting from quantum production can be approximated as [131–133]:

$$\mathcal{P}_{\rm T}^{\rm pri}(k,\eta_{\rm end}) \approx \frac{2}{\pi^2}\left(\frac{H_{\rm end}}{M_{\rm pl}}\right)^2\left(1+\frac{k^2}{k_{\rm end}^2}\right) \tag{6.42}$$

Here, $k_{\rm end}$ represents the highest momentum leaving the horizon at the end of inflation.

Following inflation, the reheating phase converts inflaton energy into radiation, leading to a radiation-dominated universe characterized by the equation of state ($w_\phi$) and reheating temperature ($T_{\rm re}$). The Hubble parameter evolves as $H^2 = H_{\rm end}^2(a/a_{\rm end})^{-3(1+w_\phi)}$, influencing the scale factor's evolution $a(\eta) \approx a_{\rm end}(\eta/\eta_{\rm end})^{2/(1+3w_\phi)}$. This results in the evolution of tensor fluctuations $h_{\vec{k}}$ during reheating without any source term:

$$h_{\vec{k}}''(x) + \frac{4}{1+3w_\phi}\frac{1}{x}h_{\vec{k}}'(x) + h_{\vec{k}}(x) = 0. \tag{6.43}$$

Here, we introduce the dimensionless variable $x = k\eta$. The well-known solution to this equation is given by:

$$h_{\vec{k}}(x) = \mathcal{C}_1 x^{l(w_\phi)} J_{l(w_\phi)}(x) + \mathcal{C}_2 x^{l(w_\phi)} J_{-l(w_\phi)}(x), \tag{6.44}$$

where $J_l(x)$ is the Bessel function of order $l(w_\phi) = 3(w_\phi - 1)/2(1+3w_\phi)$ and the two integration constants $\mathcal{C}_1$ and $\mathcal{C}_2$ contain critical information regarding the origin of tensor fluctuations during inflation. Determining these constants involves satisfying continuity conditions for both tensor fluctuations and their first derivatives at $\eta = \eta_{\rm end}$. Focusing on modes beyond the Hubble radius at the end of inflation, we can calculate $\mathcal{C}_1$ and $\mathcal{C}_2$ in the super-horizon limit ($x_{\rm e} = k\eta_{\rm end} \ll 1$). The expressions are as follows:

$$\mathcal{C}_1 = \frac{\pi}{2\sin(l\pi)}\left(\frac{k}{k_{\rm end}}\right)^{2(1-l)}\left(\frac{1}{\Gamma(2-l)} + \frac{1}{\Gamma(1-l)}\right) h_{\vec{k}}(k,\eta_{\rm end}), \tag{6.45}$$

$$\mathcal{C}_2 = \frac{\pi}{2\sin(l\pi)}\left(\frac{1}{\Gamma(l)} - \frac{1}{\Gamma(1+l)}\left(\frac{k}{k_{\rm end}}\right)^2\right) h_{\vec{k}}(k,\eta_{\rm end}) \tag{6.46}$$

where $h_{\vec{k}}(k,\eta_{\rm end})$ is the amplitude of tensor fluctuation at the inflation end [131, 133]. In the general scenario, the parameter $w_\phi$ lies within $0 \le w_\phi \le 1$, causing $l(w_\phi)$ to take negative values consistently. Given our interest in scales beyond the horizon at the end of inflation (i.e., $k < k_{\rm end}$, implying $k/k_{\rm end} < 1$), we assert that $\mathcal{C}_2$ greatly dominates over $\mathcal{C}_1$.

Finally, utilizing Eqs.(6.44) and (6.46) in Eq.(2.206), we obtain the primary GW spectrum at the end of reheating as [131]:

$$\mathcal{P}_{\rm T}^{\rm pri}(k,\eta_{\rm re}) = \frac{\pi^2}{4\sin^2(l\pi)\Gamma^2(l)}\left(1 - \frac{1}{l}\left(\frac{k}{k_{\rm end}}\right)^2\right)^2 \mathcal{P}_{\rm T}^{\rm pri}(k,\eta_{\rm end}). \tag{6.47}$$

### 6.2.2 Productions of Secondary Tensor Power spectrum during Reheating:

As previously discussed in Section 6.1, due to non-minimal coupling results in the growth of the scalar fluctuation due to instability. For a high value of $\xi > 1$, it is evident from the right panel of Fig.(6.2) that for any EoS $0 \leq w_\phi \leq 1$, the effect of this instability is much stronger for large scales($k < k_{\rm end}$), leading to growth of amplitude as depicted in Fig.(6.2). Such growth is prominent exclusively in reheating scenarios where $w_\phi > 1/3$ in larger $\xi$ regimes. On the contrary, for $w_\phi < 1/3$, the growth of the large-scale modes becomes significant in the lower $\xi$ regimes, particularly below the conformal limit $0 \leq \xi < 1/6$, which causes an enhanced energy density spectrum $\rho_{\chi_k}$ as shown in the left panel of Fig.(6.3).

The secondary tensor power spectrum $\mathcal{P}_{\rm T}^{\rm sec}(k,\eta)$ corresponding to this period is detailed in Eq. (6.41), where $\mathcal{G}_k^{\rm re}(\eta,\eta_1)$ represents the Green's function associated with Eq. (2.200), satisfying the following differential equation [133]

$$\mathcal{G}_k''(\eta,\eta_1) + 2\mathcal{H}\mathcal{G}_k'(\eta,\eta_1) + k^2\mathcal{G}_k(\eta,\eta_1) = \delta(\eta-\eta_1). \tag{6.48}$$

The Green's function during the reheating epoch is expressed as [133]

$$\mathcal{G}_k^{\rm re}(\eta,\eta_1) = \Theta(\eta-\eta_1)\frac{\pi\eta^l\eta_1^{1-l}}{2\sin(l\pi)}\left[J_l(k\eta)J_{-l}(k\eta_1) - J_{-l}(k\eta)J_l(k\eta_1).\right] \tag{6.49}$$

Utilizing Eq. (6.25) and (6.49) in Eq. (6.41), we have obtained the general expressio of the secondary tensor power spectrum due to the massless scalar field $\chi$ at the end of the reheating era $\eta = \eta_{\rm re}$ as follows,

$$\mathcal{P}_{\rm T}^{\rm sec}(k,\eta_{\rm re}) = \frac{2\mathcal{A}^2H_{\rm end}^4}{\pi^4M_{\rm pl}^4}\left(\frac{k}{k_{\rm end}}\right)^{4+2\delta-4\nu_2}\left(\int_{x_{\rm e}}^{x_{\rm re}} dx_1 x_1^{-\delta}\mathcal{G}_k^{\rm re}(x_{\rm re},x_1)\mathcal{I}(x_1)\right)^2\mathcal{F}(k), \tag{6.50}$$

where $\delta(w_\phi) = 4/(1+3w_\phi)$. This equation introduces one dimensionless variable: $x \equiv k\eta$ or $x_1 = k\eta_1$. The time integral limits range from $x_{\rm e} = k\eta_{\rm end}$ to $x_{\rm re} = k\eta_{\rm re}$. The momentum integral part $\mathcal{F}(k)$ is detailed in the Addenda 6.5.

Upon evaluating all the integrals, the resulting secondary tensor power spectrum at the end of reheating for $w_\phi > 1/3$ and $\xi > 3/16$ turns out to be

$$\mathcal{P}_{\rm T}^{\rm sec}(k,\eta_{\rm re}) = \frac{2\mathcal{A}_3^2H_{\rm end}^4}{\pi^4M_{\rm pl}^4}\left(\frac{k}{k_{\rm end}}\right)^{4+2\delta-4\nu_2}\mathcal{I}_t^2(x_{\rm re},x_{\rm e})\mathcal{F}(k). \tag{6.51}$$

Here, $\mathcal{A}_3$ is defined as

$$\mathcal{A}_3 \approx \left(\frac{\Gamma(\nu_2)\exp(-\pi\tilde{\nu}_1/2)}{4}\left(\frac{2}{3\mu-1}\right)^{\nu_2}\sqrt{3\mu-1}\left|\frac{(\pi+i\cosh(\pi\tilde{\nu}_1)\Gamma(1-i\tilde{\nu}_1)\Gamma(i\tilde{\nu}_1))}{\pi\Gamma(i\tilde{\nu}_1)}\right|\right)^2, \tag{6.52}$$

whereas the time integral part $\mathcal{I}_t$ is defined as (see the details in Addenda 6.5)

$$\mathcal{I}_t(x_{\rm re}, x_{\rm e}) = \int_{x_{\rm e}}^{x_{\rm re}} dx_1 x_1^{-\delta} \mathcal{I}(x_1) \mathcal{G}_k^{\rm re}(x_{\rm re}, x_1), \tag{6.53}$$

and

$$\mathcal{F}(k) \simeq \frac{16}{15} \left\{ \frac{1}{6-2\nu_2} \left( 1 - \left( \frac{k_{\rm min}}{k} \right)^{6-2\nu_2} \right) + \frac{1}{5-4\nu_2} \left( \left( \frac{k_{\rm end}}{k} \right)^{5-4\nu_2} - 1 \right) \right\}. \tag{6.54}$$

Proceeding in the same way, utilizing the Eq.(6.26) we obtain the secondary tensor power spectrum for $w_\phi < 1/3$ and $\xi < 3/16$ as

$$\mathcal{P}_{\rm T}^{\rm sec}(k, \eta_{\rm re}) = \frac{2\mathcal{A}_1^2 H_{\rm end}^4}{\pi^4 M_{\rm pl}^4} \left( \frac{k}{k_{\rm end}} \right)^{4+2\delta-4(\nu_1+\nu_2)} \mathcal{I}_t^2(x_{\rm re}, x_{\rm e}) \mathcal{E}(k). \tag{6.55}$$

where $\mathcal{A}_1$ is defined as

$$\mathcal{A}_1 \approx \left( \frac{\Gamma(\nu_1)\Gamma(\nu_2) 2^{\nu_1}}{8\pi} \left( \frac{2}{3\mu-1} \right)^{\nu_2} \left( \frac{3\mu(1-2\nu_1) + 2(\nu_1-\nu_2)}{\sqrt{(3\mu-1)}} \right) \right)^2. \tag{6.56}$$

Here, the expression of the time integral $\mathcal{I}_t(x_{\rm re}, x_{\rm e})$ will remain unchanged and momentum-integral will be modified as

$$\mathcal{E}(k) \simeq \frac{16}{15} \left\{ \frac{1}{6-2(\nu_1+\nu_2)} \left( 1 - \left( \frac{k_{\rm min}}{k} \right)^{6-2(\nu_1+\nu_2)} \right) + \frac{1}{5-4(\nu_1+\nu_2)} \left( \left( \frac{k_{\rm end}}{k} \right)^{5-4(\nu_1+\nu_2)} - 1 \right) \right\}. \tag{6.57}$$

Now we shall define the dimensionless energy density of the gravitational waves $\Omega_{\rm gw}(k)h^2$ for *today* in the following subsection.

### 6.2.3 GW spectrum for today :

During the reheating and radiation-dominated epochs, perturbation modes progressively re-enter the Hubble radius, producing a stochastic gravitational wave (GW) signal. When produced in the early universe, this GW signal is assumed to possess statistical homogeneity, isotropy, and Gaussianity, inheriting properties from the FLRW universe, whether during inflation or the thermal era.

Due to the weak interaction of gravity with matter, GWs are decoupled from the rest of the universe at the Planck scale. Neglecting interactions with ordinary matter and self-interactions, we assume that sub-Hubble GWs propagate freely in space after their production or re-entry into the Hubble radius. The GW energy density decays with the expansion of the universe, mimicking the behavior of radiation, i.e., $\rho_{\rm gw} \propto a^{-4}$. Meanwhile, the physical wave number of GWs evolves as $k/a$. Deep inside the radiation-dominated

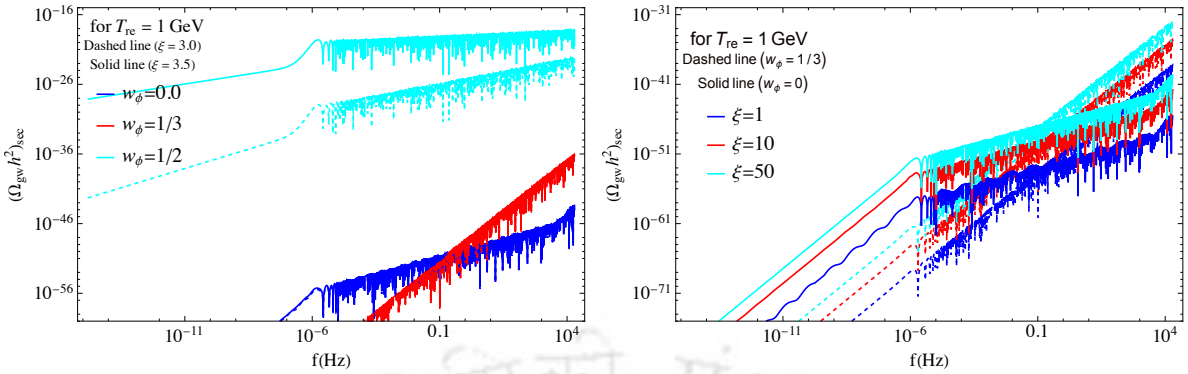


FIGURE 6.5: *In this figure, we have shown the present-day dimensionless gravitational waves energy density* $(\Omega_{\rm gw}h^2)_{\rm sec}$ *(induced by the scalar field only) as a function of frequency* $f$ *(Hz). The left panel illustrates the dependency of the EoS* $w_\phi = 0, 1/3,$ *&* $1/2$ *for two specific values of the coupling constant* $\xi = 3.5$ *(indicated by solid lines) and* $\xi = 3.0$ *(indicated by dashed lines). In the right panel, we have shown how the spectral energy density evolves for the coupling constants* $\xi = 1, 10,$ *&* $50$*, with fixed EoS values* $w_\phi = 0$ *(indicated by solid lines) and* $w_\phi = 1/3$ *(indicated by dashed lines). In both panels, we have considered the reheating temperature of our universe to be* $T_{\rm re} = 1$ *GeV.*

universe, given the spectrum, the normalized GW energy density parameter at any time $\eta$ is defined as

$$\Omega_{\rm gw}(k,\eta) = \frac{\rho_{\rm gw}(k,\eta)}{\rho_c(\eta)} = \frac{k^2\mathcal{P}_{\rm T}^{\rm rad}(k,\eta)}{12a^2(\eta)H^2(\eta)}. \tag{6.58}$$

Here, the critical energy density $\rho_c(\eta) = 3H^2(\eta)M_{\rm pl}^2$, and $M_{\rm pl} \simeq 2.43 \times 10^{18}$ GeV represents the reduced *Planck* mass. The tensor power spectrum $\mathcal{P}_{\rm T}^{\rm rad}(k,\eta)$ during radiation-dominated era can further be expressed in terms of the spectrum at the end of reheating as [133].

$$\mathcal{P}_{\rm T}^{\rm rad}(k,\eta) = \left(1 + \frac{k^2}{k_{\rm re}^2}\right)\frac{\mathcal{P}_{\rm T}(k,\eta_{\rm re})}{2k^2\eta^2}. \tag{6.59}$$

As is well-established, the energy density of gravitational waves (GWs) exhibits a behavior akin to radiation, scaling as $\rho_{\rm gw} \propto a^{-4}$. Our focus lies on modes that are well within the Hubble radius at a later time, particularly in proximity to the radiation-matter equality epoch during radiation domination. We express the dimensionless energy density parameter $\Omega_{\rm gw}(k)$ today in terms of $\Omega_{\rm gw}(k,\eta)$ as follows, as described in [131, 133]:

$$\Omega_{\rm gw}(k)h^2 = \left(\frac{g_{r,\rm eq}}{g_{r,0}}\right)\left(\frac{g_{s,0}}{g_{s,\rm eq}}\right)^{4/3}\Omega_R h^2\Omega_{\rm gw}(k,\eta) \approx \left(\frac{g_{r,0}}{g_{r,\rm eq}}\right)^{1/3}\Omega_R h^2\Omega_{\rm gw}(k,\eta). \tag{6.60}$$

Here, $\Omega_R h^2 = 4.3 \times 10^{-5}$, representing the dimensionless energy density of radiation at the present epoch. $g_{r,\rm eq}$ and $g_{r,0}$ represent the number of relativistic degrees of freedom at radiation-matter equality and in the present era, respectively, whereas $g_{s,\rm eq}$ and $g_{s,0}$ signify

the number of such degrees of freedom contributing to entropy at these respective epochs. In our calculation we adopt the value $g_{r,0} \simeq g_{s,0} = 3.35$.

***Primary GWs spectrum today(PGWs):*** After the reheating epoch, the subsequent era is predominantly characterized by radiation. Now utilizing Eqs (6.47) and (6.58) in Eq.(6.60) we have found that the PGWs *today* can be estimated as [133]

$$\Omega_{\rm gw}^{\rm pri}(k)h^2 \simeq 1.12\cdot 10^{-17}\left(\frac{\Omega_R h^2}{4.3\times 10^{-5}}\right)\left(\frac{H_{\rm end}}{10^{-5}M_{\rm pl}}\right)^2 \times \begin{cases} \mathcal{D}_1 & \text{for } \; k < k_{\rm re} \\ \mathcal{D}_2(k/k_{\rm re})^{n_w} & \text{for } \; k_{\rm re} < k < k_{\rm end} \end{cases}. \tag{6.61}$$

Here, we introduce the parameter $n_w = 2(3w_\phi - 1)/(1+3w_\phi)$, and define $\mathcal{D}_1 = \pi^2 2^{2l}/4\sin^2(l\pi)\Gamma^2(l)$ $\times\, \Gamma^2(1-l) \simeq \mathcal{O}(1)$ and $\mathcal{D}_2 \simeq \left(\pi^2/2\sin^2(l\pi)\Gamma^2(l)\right)\cos^2\left(-k/k_{\rm re} + (1-2l)\pi/4\right) \simeq \mathcal{O}(1)$.

***Secondary GWs spectrum today(SGWs):*** Similarly, using Eqs. (6.51), (6.55), and (6.58) in Eq.(6.60) we have found that the secondary GWs spectrum for the modes $k_* \leq k \leq k_{\rm end}$ can be estimated as

$$\Omega_{\rm gw}^{\rm sec}(k)h^2 \simeq 2.22\times 10^{-26}\left(\frac{\Omega_R h^2}{4.3\times 10^{-5}}\right)\left(\frac{H_{\rm end}}{10^{-5}M_{\rm pl}}\right)^4\left(1+\frac{k^2}{k_{\rm re}^2}\right)\mathcal{I}_t^2(k,\eta_{\rm re}) \times \begin{cases} \mathcal{A}_1^2\left(\frac{k}{k_{\rm end}}\right)^{4+2\delta-4(\nu_1+\nu_2)}\mathcal{E}(k) & \text{for } \; w_\phi < 1/3,\; \xi < 3/16 \\ \mathcal{A}_3^2\left(\frac{k}{k_{\rm end}}\right)^{4+2\delta-4\nu_2}\mathcal{F}(k) & \text{for } \; w_\phi > 1/3,\; \xi > 3/16 \end{cases} \tag{6.62}$$

In this context, $\mathcal{I}_t(k,\eta_{\rm re})$ represents the time integral as defined in Eq. (6.53), while $\mathcal{A}_3$ and $\mathcal{A}_1$ denote the constant coefficients consisting of the EoS parameter and coupling strength $(w_\phi,\ \xi)$, as outlined in Eq.(6.52), and (6.56).

- For $w_\phi > 1/3,\ \xi > 3/16$ : This the region of parameter space, for which the scalar field growth is prominent for the range of scales which has wider detection prospects of a large pool of ongoing and future GW experiments. We consider two distinct regimes to analyze the spectral behavior of secondary gravitational waves: $k \ll k_{\rm re}$ and $k_{\rm re} \ll k < k_{\rm end}$. In the super-horizon limit, the SGW spectrum follows the relation $\Omega_{\rm gw}^{\rm sec}(k \ll k_{\rm re})h^2 \propto f^{4(2-\nu_2)}$. In contrast, in the sub-horizon limit, the spectrum exhibits a behavior of $\Omega_{\rm gw}^{\rm sec}(k \gg k_{\rm re})h^2 \propto f^{6+\delta-4\nu_2}$ (for further details, refer to the Addenda 6.5).

  For an EoS with $w_\phi > 1/3$ and a coupling parameter $\xi > 1/6$, a post-inflationary parametric instability raises the overall production of the scalar field during the reheating era. On the contrary, for $w_\phi \leq 1/3$, no such post-inflationary instability

occurs. In Fig.(6.5), we showed how such growths are imprinted in SGWs depending upon $w_\phi$ and the coupling parameter $\xi$. In the left panel, we examine three EoS values: $w_\phi = 0$, $1/3$, and $1/2$, with a fixed reheating temperature of $T_{\rm re} = 1$ GeV. The secondary GW spectrum generically acquires a common factor $\Omega_{\rm gw}^{\rm sec}(k)h^2 \propto (k_{\rm end}/k_{\rm re})^{\frac{6w_\phi-2}{1+3w_\phi}}$ (see the detailed calculation in Addenda 6.5). The factor immediately suggests that for $w_\phi < 1/3$ ($w_\phi > 1/3$), the amplitude of the spectrum is suppressed (enhanced) as $k_{\rm end}/k_{\rm re} >> 1$. This suppression or enhancement can indeed be seen from the left panel of Fig.(6.5). Detailed calculation further indicates that when $w_\phi \leq 1/3$, the secondary GW production is always overshadowed by the primary production for all scales as far as larger coupling values, $\xi > 3/16$, are concerned. However, for $w_\phi = 1/2$ (i.e., $w_\phi > 1/3$) in the larger coupling regime, the production of SGWs due to the scalar field is enhanced in super-horizon modes, potentially surpassing the primary gravitational wave production.

In the top left panel of Fig.(6.6), we explore the dependency of the coupling parameter $\xi$ for two different EoS values: $w_\phi = 0$ and $1/3$. As neither of these EoS values induces instability in the system, no growth in the scalar field occurs during the reheating era (see Fig.(6.2)). Consequently, the secondary production of gravitational waves is negligible, and the strength of the gravitational wave spectrum remains considerably lower than that of the primary gravitational waves, even when a very high coupling constant $\xi$ is considered.

To this end, we would like to discuss the generic characteristics of the total GW spectrum (PGWs + SGWs) in terms of the reheating parameters, non-minimal coupling, and the inflationary energy scale. In the top left panel, we show the dependency of the reheating temperature on the GW spectrum, with a fixed equation of state $w_\phi = 3/5$ and a coupling constant $\xi = 2.90$. Evidently, in the intermediate frequency range, the secondary production of GWs can surpass the primary gravitational waves (PGWs). The decreasing temperature turns out to increase the overall amplitude of the spectrum through the factor $\Omega_{\rm gw}(k)h^2 \propto {T_{\rm re}}^{\frac{8(1-3w_\phi)}{3(1+w_\phi)}} \propto {T_{\rm re}}^{-4/3}$ for $k < k_{\rm re}$, $w_\phi = 3/5$, and $\Omega_{\rm gw}(k)h^2 \propto {T_{\rm re}}^{\frac{4(1-3w_\phi)}{3(1+w_\phi)}} \propto {T_{\rm re}}^{-2/3}$ for $k > k_{\rm re}$, $w_\phi = 3/5$. Beyond a certain reheating temperature, however, the large-scale spectrum can exceed the present bound on the tensor-to-scalar ratio $r_{0.05} \leq 0.036$ from the recent *Planck*-2018 results [8], which we discuss in the subsequent section. The spectrum can intersect with future GW sensitivity curves for specific parameter sets, such as LISA, DECIGO, and BBO.

This enhancement of the SGWs with decreasing reheating temperature is effective only for $w_\phi > 1/3$ reheating scenarios due to post-inflationary instability to the scalar field mode. Further lowering the reheating temperature implies an increase in the duration of the reheating period. A longer reheating period implies that the scalar field experiences instability for a longer period, resulting in greater growth.

Similarly, in the top right panel of Fig.(6.6), we show the evolution of the final GW

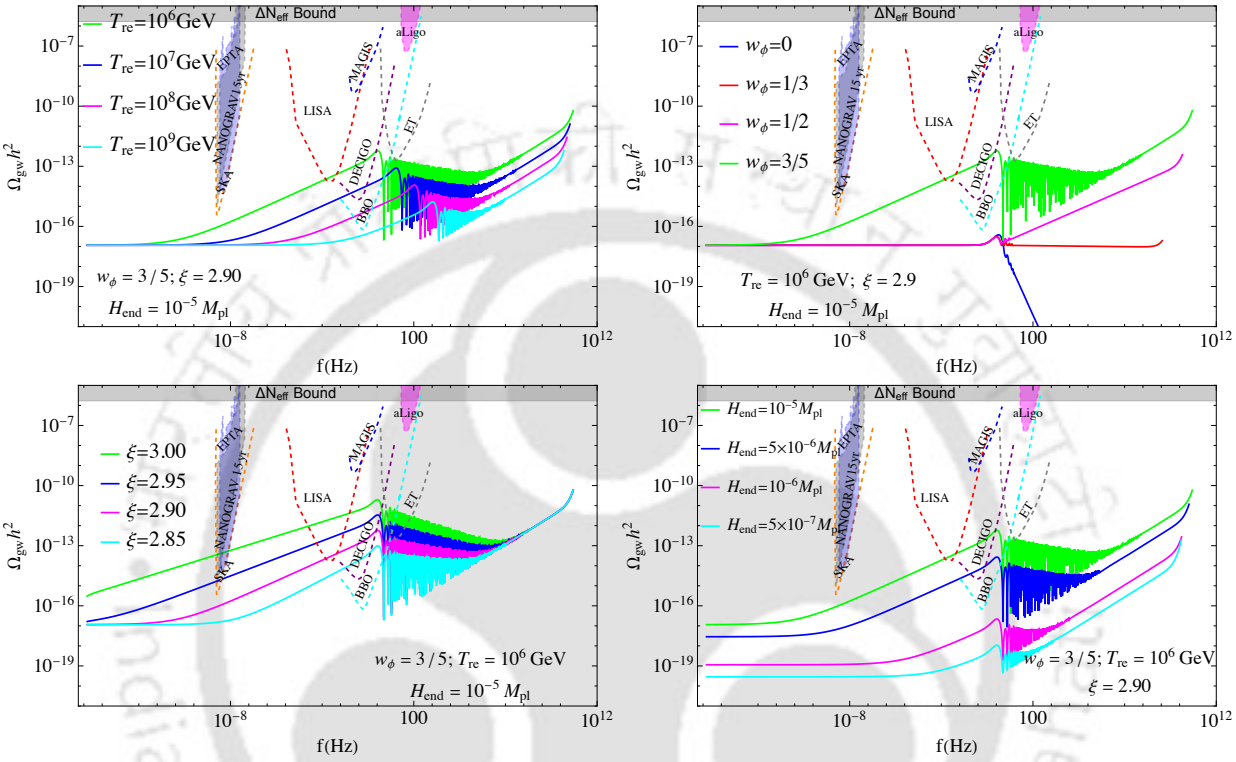


FIGURE 6.6: *The figure presents the combined GW spectrum today for different theory parameters. In the top-left panel, we illustrate the dependence of the GW spectrum on the reheating temperature $T_{\rm re}$ for a fixed EoS $w_\phi = 3/5$ with a coupling parameter $\xi = 3.0$. The top-right panel shows the GW spectra for four different EoS values: $w_\phi = 0, 1/3, 1/2,$ and $3/5$, assuming a fixed reheating temperature of $T_{\rm re} = 10^6$ GeV and a coupling constant $\xi = 2.90$. The bottom-left panel demonstrates the influence of the coupling constant $\xi$ on the GW spectrum, where we assume a fixed reheating scenario with $T_{\rm re} = 10^6$ GeV and $w_\phi = 3/5$. In all three of these plots, we have adopted the maximal allowed value of the tensor-to-scalar ratio, $r_{0.05} \simeq 0.036$, as constrained by the Planck observations. Finally, in the bottom-right panel, we explore the impact of varying the tensor-to-scalar ratio on the GW spectrum for a fixed reheating scenario with $T_{\rm re} = 10^6$ GeV, $w_\phi = 3/5$, and $\xi = 2.90$.*

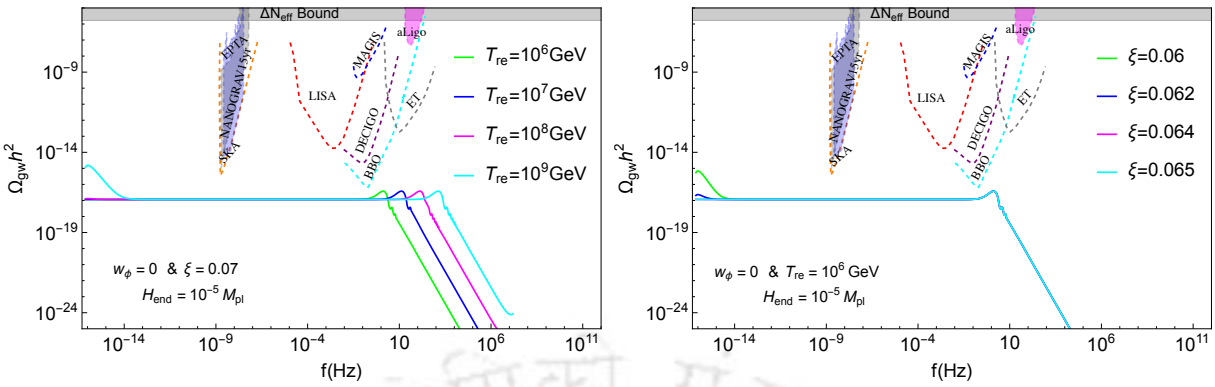


FIGURE 6.7: *The figure presents the combined GW spectrum today for different theory parameters. In the left panel of this figure, we show the variation of the GW spectrum for different reheating temperatures with a fixed coupling strength* $\xi = 0.07$ *and reheating EoS* $w_\phi = 0$*. In the right panel, we show the dependence of the spectrum on the coupling strength* $\xi$ *for a fixed reheating temperature* $T_{\rm re} = 10^6$ *GeV and EoS* $w_\phi = 0$*. In these two plots, we have taken the maximal value of the Hubble scale* $H_{\rm end} = 10^{-5} M_{\rm pl}$*.*

spectrum for different EoS values, indicated by four different colors. We assume $\xi = 2.90$ and $T_{\rm re} = 10^6$ GeV. For $w_\phi = 0, 1/3, 1/2$ the PGW dominates the entire spectrum. Although for $w_\phi > 1/3$ and $\xi > 1$, there is instability (as seen in Fig.6.2), this growth is insufficient to produce GWs of strength which can surpass the PGWs generated during inflation. SGW turns out to dominate only when $w_\phi \geq 3/5$. For example assuming $w_\phi = 3/5$ the spectrum transforms from scale-invariant to blue tilted in the small frequency(large scale) range $f^{8-4\nu_2} = f^{0.41}$, and from blue tilted to red-tiled $f^{6+\delta-4\nu_2} = f^{-0.16}$ for the modes $k > k_{\rm re}$(small scale) as indeed observed in green curve. Therefore, for a fixed reheating temperature and coupling constant ($\xi > 1$), there exists a threshold EoS value above which the scalar field growth is sufficient to produce enough SGWs to overtake the PGWs.

In the bottom left panel of Fig. 6.6, we examine the effect of the coupling constant $\xi$, with a fixed equation of state $w_\phi = 3/5$ and reheating temperature $T_{\rm re} = 10^6$ GeV. The results show that increasing the coupling parameter enhances the scalar field's growth, thereby enhancing the GW spectrum. The spectral behavior is the same as the previous one with blue tilt in the small frequency(large scale) range $f^{8-4\nu_2}$, and red-tilt $f^{6+\delta-4\nu_2}$ for the modes $k > k_{\rm re}$(small scale) as indeed observed in the green curve. For fixed reheating scenarios, a critical value of the coupling constant $\xi_{\rm max}$ exists above which the tensor fluctuations can be overproduced violating bound on tensor-to-scalar ratio $r_{0.05} \leq 0.036$ set by the *Planck*.

In the bottom right panel of Fig. 6.6, we demonstrate how the gravitational wave (GW) spectrum energy density varies with the inflationary energy scale $H_{\rm end}$ for a fixed reheating temperature of $T_{\rm re} = 10^6$ GeV and a fixed EoS $w_\phi = 3/5$, with the coupling parameter $\xi = 2.90$. Since the GW spectral energy density follows $\Omega_{\rm gw} h^2 \propto H_{\rm end}^4$, a

decrease in $H_{\rm end}$ naturally leads to a reduction of the total GWs strength.

For a fixed reheating temperature, lowering the inflationary energy scale by reducing $H_{\rm end}$ leads to a shorter reheating period (see Eq.(6.30)). The duration of this period is intimately tied to the growth of the scalar field. When the inflationary energy scale $H_{\rm end}$ is reduced, it not only limits the growth of the scalar field during reheating but also affects its initial production during inflation since the scalar field's amplitude depends on the inflationary energy scale. As a result, the overall amplitude of the gravitational wave (GW) spectrum decreases as $H_{\rm end}$ is lowered.

Considering these factors, we find that with $H_{\rm end} = 10^{-5} M_{\rm pl}$, $w_\phi = 3/5$, $T_{\rm re} = 10^6$ GeV, and $\xi = 2.9$, the tensor fluctuations are strong enough to be detected by future sensitivity curves like LISA, DECIGO, and BBO. However, with a lower value like $H_{\rm end} = 5 \times 10^{-6} M_{\rm pl}$, the amplitude is suppressed, allowing detection by DECIGO and BBO but not by LISA. For $H_{\rm end} \leq 10^{-6} M_{\rm pl}$, the signal is too weak to be detected by upcoming experiments. Therefore, the inflationary energy scale significantly impacts the production of secondary GWs via the scalar field dynamics.

In all figures, at very high-frequency ranges near $f_{\rm end} = (k_{\rm end}/2\pi)$, the spectrum follows the $\Omega_{\rm gw} h^2(f) \propto f^{n_w}$ [131, 133] behavior, which is due to PGWs contributions at these frequencies. At very high frequencies, PGWs dominate over SGWs. As seen in Fig.(6.4), when the modes become sub-horizon, the scalar field growth subsides because of adiabatic evolution, leading to insufficient to produce significant anisotropy.

- For $0 \leq w_\phi < 1/3$, $\xi < 3/16$: In this region of parameter space the infrared scalar field growth turned out to be relevant around the CMB scales. *Planck* is the only experiment that can place constraints. Likewise, the previous case for $w_\phi > 1/3$, we consider here also two distinct regimes of the SGW spectrum, $k \ll k_{\rm re}$ and $k_{\rm re} \ll k < k_{\rm end}$. For the super-horizon modes, the SGW spectrum follows the relation $\Omega^{\rm sec}_{\rm gw}(k \ll k_{\rm re}) h^2 \propto f^{4(2-\nu_1-\nu_2)}$. In contrast, for sub-horizon modes, the spectrum exhibits a behavior of $\Omega^{\rm sec}_{\rm gw}(k \gg k_{\rm re}) h^2 \propto f^{6+\delta-4(\nu_1+\nu_2)}$ (for detailed calculation see Appendix 6.5). Unlike $w_\phi > 1/3$, for this case the GW spectrum exhibits a sharp enhancement $\big((2-\nu_1-\nu_2) < 0\big)$ in the long- wavelength modes $k << k_{\rm re}$ particularly for $\xi < 1/6$. We have presented the dependence of GW spectrum (PGW+SGW) on reheating temperature $T_{\rm re}$, and the coupling strength $\xi$ for EoS $w_\phi = 0$ in the above Fig. 6.7. As stated earlier, for lower EoS for the modes around the CMB pivot scale $k_*$, the GW spectrum receives a significant correction due to tachyonic instability. This makes the spectrum IR divergent with enhanced amplitude, and its value freezes at the end of inflation. Therefore, as the duration of reheating decreases or reheating temperature increases, the GW amplitude enhances as $\Omega_{\rm gw}(k) h^2 \propto (k_{\rm end}/k_{\rm re})^{4-2\delta} \propto T_{\rm re}^{\frac{8(1-3w_\phi)}{3(1+w_\phi)}} \propto T_{\rm re}^{8/3}$ due to less dilution. For example if $w_\phi = 0$, $\Omega_{\rm gw}(k) h^2 \propto T_{\rm re}^{8/3}$ for $w_\phi = 0$ (see left panel of Fig. 6.7). The right panel depicts the GW spectral behavior for different non-minimal coupling strength $\xi$ with $w_\phi = 0$, $T_{\rm re} = 10^6$ GeV.

In the regime $k << k_{\rm re}$, it grows as $\Omega_{\rm gw}(k)h^2 \propto (k/k_{\rm end})^{8-4(\nu_1+\nu_2)}$. The spectral index $\big(4(\nu_1+\nu_2)-8\big)$ gradually increases with the decrease of $\xi$. This is a distinctive feature of the gravitational wave spectrum for $w_\phi < 1/3$, which essentially puts a lower bound on $\xi$ set by CMB observation.

**Constraining the coupling strength $\xi$ from the tensor-to-scalar ratio bound:**

- Constraining positive $\xi$ values for $w_\phi > 1/3$ : We have discovered that for $w_\phi > 1/3$ reheating scenarios, the scalar field undergoes a tachyonic instability beyond a threshold of the coupling constant $\xi$, particularly for the super-horizon modes, and generates large tensor fluctuations even at CMB scales. The current observational bound on the tensor-to-scalar ratio at CMB scales $r_{0.05} \leq 0.036$, [8] can impose a stringent constraint on the coupling parameter $\xi$ through the following equation (assuming all contributions originate from secondary sources),

$$r_{0.05} \simeq \frac{2\mathcal{A}_3^2 H_{\rm end}^4}{\pi^4 M_{\rm pl}^4 A_s}\left\{\frac{1}{2l(\delta-2)}+\frac{1}{4l(1-l)-2l\delta}\right\}^2 \frac{8(1+2\nu_2)}{15(3-\nu_2)(4\nu_2-5)} \times \left(\frac{90H_{\rm end}^2 M_{\rm pl}^2}{\pi^2 g_{\rm re} T_{\rm re}^4}\right)^{\frac{2(3w_\phi-1)}{3(1+w_\phi)}} \left(\frac{k_*}{k_{\rm end}}\right)^{4(2-\nu_2)} \leq 0.036 \tag{6.63}$$

From Eq.(6.63), it is evident that the reheating temperature $T_{\rm re}$ and the average equation of state $w_\phi$, has a very sensitive dependence on the maximum coupling strength $\xi_{\rm max}$ to prevent the overproduction of tensor fluctuations at the CMB scale. In Fig.6.6, coupling parameter has been chosen in a narrow range $2.85 \leq \xi < 3$ preventing the overproduction of large-scale(CMB scale) tensor fluctuations. For $w_\phi = 3/5$ and $T_{\rm re} = 10^6$ GeV, we have found the highest possible value of coupling strength $\xi_{\rm max} \approx 2.9867$(See Table 6.1). The SGW strength will be significant to overcome the PGW one for any $\xi$ close to this $\xi_{\rm max}$, $\xi \lesssim \xi_{\rm max}$. In the bottom left panel of Fig.6.6, for any $\xi \geq 3$, total GW strength exceeds the maximum limit $\Omega_{\rm gw}h^2 \gtrsim 1.42 \times 10^{-16}$ at the CMB scale, hence it is disfavored by the current observation. All the solid curves in the left panel of Figure (6.8) depict maximum allowed values of $\xi_{\rm max}$ as a function of $w_\phi$ for different values of $T_{\rm re}$. And $\xi_{\rm max}$ represents the value of the coupling constant for a specific set of parameters exceeding which would violate the current bound on $r_{0.05}$ [8]. For instance, when $w_\phi = 0.5$ and $T_{\rm re} = 10^{-2}$ GeV, the maximum value of the coupling constant is $\xi_{\rm max} \simeq 3.73$. On the other hand, if the reheating temperature is $T_{\rm re} = 10^6$ GeV with the same EoS, the bound turns out to be $\xi_{\rm max} \simeq 3.99$. The plot shows that $\xi_{\rm max}$ decreases with a reduction in the reheating temperature due to the prolonged duration of the reheating era implying longer period of super-horizon growth. We have listed the maximum allowed values of $\xi$ for different reheating temperatures and equation of state in Table 6.1. It varies within $\sim (2, 4)$. Maximum limit on $\xi$ is not sensitive to $r$ value. For example, future experiments such as LiteBIRD ([320–323]) will be able to detect $r < 0.002$ at 95% C.L (accounting

for both statistical and systematic uncertainties)[321]. Subject to this new bound we obtain $\xi_{\rm max} = (4.045,\ 3.089,\ 2.785,\ 2.640,\ 2.465,\ 2.277)$ corresponding to EoS $w_\phi = (1/2,\ 3/5,\ 2/3,\ 5/7,\ 4/5,\ 99/100)$ respectively for the reheating temperature $T_{\rm re} = 10^6$GeV, which is not significantly different from that of the *Planck* bound. We have already discussed the bound on $\xi$ for $r_{0.05} = 10^{-4}$( see Table 6.1) which anyway falls within the LiteBIRD limit. Henceforth, we shall stick to the current *Planck* bound $r_{0.05} \lesssim 0.036$ while constraining the coupling for other EoS.

- Constraining negative $\xi$ values for $w_\phi \geq 1/3$: In this EoS range, the dynamical equations (6.1) and (6.7) clearly show the presence of a strong inflationary IR instability but the absence of post-inflationary instability for any negative $\xi$ value. Subject to CMB bound, and considering the reheating parameters $(T_{\rm re},\ H_{\rm end}) = (10^6{\rm GeV},\ 10^{-5}M_{\rm pl})$, we find $\xi_{\rm min} = (-0.15333,\ -0.14079,\ -0.13346,\ -0.12866,\ -0.12085,\ -0.10659)$ for the reheating EoS $w_\phi = (1/2,\ 3/5,\ 2/3,\ 5/7,\ 4/5,\ 99/100)$ respectively. Therefore, any $|\xi| > |\xi_{\rm min}|$ is strictly prohibited for any $w_\phi > 1/3$ based on the present study. We also further check that for a given EoS, the lower bound does not vary much with the reheating temperature. For instance, for $w_\phi = 3/5$, we get $\xi_{\rm min} = (-0.11,\ -0.12483,\ -0.14079,\ -0.158)$ for $T_{\rm re} = (10^{-2},\ 10^2,\ 10^6,\ 10^{10})$GeV respectively.

- Constraining positive $\xi$ values for $w_\phi < 1/3$ : In a similar fashion, for $w_\phi < 1/3$, we calculate the tensor-to-scalar ratio at the CMB scale $r_{0.05}$ as

$$r_{0.05} \simeq \frac{2\mathcal{A}_1^2 H_{\rm end}^4}{\pi^4 M_{\rm pl}^4 A_s}\left\{\frac{1}{2l(\delta-2)} + \frac{1}{4l(1-l)-2l\delta}\right\}^2 \frac{8(1+2(\nu_1+\nu_2))}{15(3-(\nu_1+\nu_2))(4(\nu_1+\nu_2)-5)} \times \left(\frac{90H_{\rm end}^2 M_{\rm pl}^2}{\pi^2 g_{\rm re} T_{\rm re}^4}\right)^{\frac{2(3w_\phi-1)}{3(1+w_\phi)}} \left(\frac{k_*}{k_{\rm end}}\right)^{4(2-\nu_1-\nu_2)} \leq 0.036 \tag{6.64}$$

The negative value of the index $(2-\nu_1-\nu_2)$ in the lower the value of $\xi < 1/6$ gives significant GW strength for $w_\phi < 1/3$. This fact sets the lower limit of $\xi_{\rm min}$ that satisfies the observational bound on $r_{0.05}$. For instance, for $w_\phi = 0$, we obtain $\xi_{\rm min} \simeq (0.02036,\ 0.04179,\ 0.05935,\ 0.07394)$, and for $w_\phi = 0.1$, we obtain $\xi_{\rm min} \simeq (5.4\times10^{-4},\ 0.01569,\ 0.02916,\ 0.04119)$ for $T_{\rm re} = (10^{-2},\ 10^2,\ 10^6,\ 10^{10})$ GeV respectively and for $w_\phi = 0.2$, we obtain $\xi_{\rm min} \simeq (3.35\times10^{-3},\ 0.01104)$ for $T_{\rm re} = (\ 10^6,\ 10^{10})$ GeV respectively. For $w_\phi = 0.2$, no lower limit exists for the temperatures $T_{\rm re} = (10^{-2},\ 10^2)$ GeV. In the right panel of Fig.6.7, we have considered a narrow range of $0.06 < \xi \leq 0.065$ for $w_\phi = 0$ and $T_{\rm re} = 10^6$ GeV, and shown how the GW spectrum changes near the CMB scale within the *Planck* limit. The larger value of $\xi$ is unconstrained due to less GW production at the CMB scale ($k << k_{\rm end}$). Interestingly, we also find that as one gradually approaches $w_\phi = 1/3$, the coupling remains unconstrained, for secondary GW is

| | $T_{\rm re}$ (GeV) | $w_\phi = 0$ | $w_\phi = 1/2$ | $w_\phi = 3/5$ | $w_\phi = 4/5$ | $w_\phi = 99/100$ |
|---|---|---|---|---|---|---|
| $r_{0.05} = 0.036$ | $10^{-2}$ | 0.02036 | 3.7312 | 2.7649 | 2.1056 | 1.8818 |
| | $10^{2}$ | 0.04179 | 3.8599 | 2.9034 | 2.2611 | 2.0529 |
| | $10^{6}$ | 0.05935 | 3.9955 | 2.9867 | 2.4342 | 2.2482 |
| $r_{0.05} = 10^{-4}$ | $10^{-2}$ | 0.01668 | 3.7950 | 2.8136 | 2.1443 | 1.9168 |
| | $10^{2}$ | 0.03903 | 3.9289 | 2.9569 | 2.3059 | 2.095 |
| | $10^{6}$ | 0.05728 | 4.0691 | 3.1111 | 2.4859 | 2.299 |

Table 6.1: *In the above table, we have listed the minimum possible values $\xi_{\rm min}$ for $w_\phi = 0$ and maximum possible values $\xi_{\rm max}$ for higher reheating EoS $w_\phi = 1/2,\ 3/5,\ 4/5,\ 0.99$ for different reheating temperatures $T_{\rm re}$. The lower bound $\xi_{\rm min}$ for $w_\phi = 0$ is derived from Eq. (6.64) and the upper bound $\xi_{\rm max}$ for higher EoS $w_\phi > 1/3$ is derived from Eq. (6.63) to avoid the overproduction of tensor perturbations at the CMB scale. Based on recent observations from Planck, We consider the upper bound on the tensor-to-scalar ratio to be $r_{0.05} = 0.036$. We also show the slight variation of both $\xi_{\rm min}$ and $\xi_{\rm max}$ with tensor-to-scalar ratio by considering another value at the CMB scale $r_{0.05} = 10^{-4}$.*

subdominant compared to the primary one. As an example, for $w_\phi = 0.33$ and $\xi = 0$, we find $r_{0.05} = (2.88 \times 10^{-11},\ 3.46 \times 10^{-11},\ 4.17 \times 10^{-11},\ 5 \times 10^{-11})$ for $T_{\rm re} = (10^{-2},\ 10^{2},\ 10^{6},\ 10^{10})$ GeV respectively.

- Constraining negative $\xi$ values for $w_\phi < 1/3$ : In this range, according to the dynamical equations (6.1) and (6.7), both inflationary and post-inflationary instability causes large GW production. For instance, for $w_\phi = 0$ and $T_{\rm re} = 10^6$ GeV, we find $r_{0.05} \approx (10^{26},\ 10^{24},\ 3.73 \times 10^{23},\ 7 \times 10^{23})$ for the coupling strength $\xi = (-0.01, -0.1, -1, -10)$ respectively. Therefore, the entire negative $\xi$ regime is found to be completely incompatible with CMB at least for $w_\phi = 0$.

**Constraining $\xi$ from the isocurvature bound:** A similar bound on the non-minimal coupling can also be obtained from the isocurvature constraint. The current constraints on the isocurvature power spectrum by *Planck* are defined to be $\beta_{\rm iso} \equiv \mathcal{P}_{\mathcal{S}}(k_*)/\left(\mathcal{P}_{\mathcal{R}}(k_*) + \mathcal{P}_{\mathcal{S}}(k_*)\right) \lesssim 0.038$ at the 95% C.L for the *Planck* pivot scale $k_*$. The large-scale instability of the scalar field inevitably generates strong isocurvature perturbation at the CMB scale. In the recent literature [244] and [245], authors have investigated such perturbation from the non-minimally coupled scalar field and background inflaton field. The pivot scale amplitude of curvature power spectrum $\mathcal{P}_{\mathcal{R}}(k_*) = 2.1 \times 10^{-9}$ gives the upper bound of the

amplitude of isocurvature power spectrum at CMB scale $\mathcal{P}_{\mathcal{S}}(k_*) \lesssim 8.3 \times 10^{-11}$[8]. The second-order isocurvature power spectrum is evaluated by using the following expression as [69, 75, 244, 245, 324–326]

$$\mathcal{P}_{\mathcal{S}}(k) = \frac{1}{\rho_\chi^2}\frac{k^3}{2\pi^2}\int d^3\vec{x}\langle\delta\rho_\chi(\vec{x})\delta\rho_\chi(0)\rangle e^{-i\vec{k}.\vec{x}} = \frac{k^3}{(2\pi)^5\rho_\chi^2 a^8}\int d^3\vec{p}\; P_X\left(p, |\vec{p}-\vec{k}|\right) \tag{6.65}$$

where $\rho_\chi$ and $\delta\rho_\chi$ are energy-density, and

$$P_X(p,q) = |X_p'|^2|X_q'|^2 + a^4 m_\chi^4 |X_p|^2|X_q|^2 \tag{6.66}$$

- Isocurvature constraint for $w_\phi > 1/3$: With the help of the equations (6.25), (6.122), and (6.123) we compute the isocurvature amplitude at the CMB scale, and we obtained the maximum bound on $\xi$ for $w_\phi > 1/3$. The maximum values tunes out to be $\xi_{\rm max} = (3.750,\ 2.981,\ 2.545,\ 2.477)$ for EoS $w_\phi = (1/2,\ 3/5,\ 4/5,\ 99/100)$ respectively for the reheating temperature $T_{\rm re} = 10^6$GeV and $H_{\rm end} = 10^{-5}M_{\rm pl}$. For a given EoS, this maximum limit of $\xi$ does not vary much for a wide range of reheating temperatures. For example, for $w_\phi = 1/2$, we get $\xi_{\rm max} = (3.761,\ 3.755,\ 3.750,\ 3.744)$ for $T_{\rm re} = (10^{-2}, 10^2, 10^6, 10^{10})$ GeV respectively. Interestingly, these $\xi_{\rm max}$ values are close to the values we obtained from the tensor-to-scalar ratio discussed earlier (See Table 6.1).

- Isocurvature constraint for $w_\phi < 1/3$: In [245], for $w_\phi = 0$, authors have found a lower limit of $\xi \gtrsim 0.027$ for the massless non-minimally coupled scalar fluctuations from the current isocurvature bound $\mathcal{P}_S(k_*) < 8.3 \times 10^{-11}$. Interestingly, for $w_\phi = 0$, this lower boundary of $\xi$ from the isocurvature constraint is close to the prediction of CMB scale tensor-to-scalar ratio bound $r_{0.05} \leq 0.036$ as discussed above.

**Constraining the coupling strength $\xi$ and reheating dynamics through $\Delta N_{\rm eff}$:** The total radiation energy density around the time of decoupling influences the cosmic microwave background (CMB). At that epoch, neutrinos comprised a significant fraction of the radiative energy, but additional radiation (such as dark radiation or primordial gravitational waves) may also impact the CMB spectrum. In this context, treating the $\chi$ field as dark radiation significantly affects the CMB spectra through the extra radiation component. The effective number of neutrino species, $N_{\rm eff}$, which represents the energy density stored in relativistic components (radiation), is defined as

$$\rho_{\rm ra} = \rho_\gamma + \rho_\nu + \rho_{\rm x} = \left[1 + \frac{7}{8}\left(\frac{4}{11}\right)^{4/3} N_{\rm eff}\right]\rho_\gamma \tag{6.67}$$

where $\rho_\gamma$, $\rho_\nu$, and $\rho_{\rm x}$ are the energy densities of photons, neutrinos, and extra radiation components (massless scalar field ($\rho_\chi$) or primordial gravitational waves ($\rho_{\rm gw}$)), respectively. From Eq. (6.67), the excess radiation component can be defined as:

$$\rho_\chi = \frac{7}{8}\left(\frac{4}{11}\right)^{4/3}\rho_\gamma \Delta N_{\rm eff} \tag{6.68}$$

where $\Delta N_{\rm eff} = N_{\rm eff} - N_\nu$ represents the extra relativistic degrees of freedom. Here, $\rho_x$ includes both dark radiation $\rho_\chi$ and primordial gravitational waves $\rho_{\rm gw}$, with $N_{\rm eff}$ being the observed total relativistic degrees of freedom and $N_\nu = 3.044$ representing the standard model neutrino degrees of freedom [54, 111, 327–329].

To determine the contribution of the dark radiation, specifically the massless scalar field $\chi$, we can express Eq. (6.68) as:

$$\rho_\chi = \frac{1}{2\pi^2 a^4}\int_{k_{\rm re}}^{k_{\rm end}} \frac{dk}{k} k^4 |\beta_k|^2 = \frac{7}{8}\left(\frac{4}{11}\right)^{4/3} \rho_\gamma \Delta N_\chi \tag{6.69}$$

where $\Delta N_\chi$ is the extra relativistic degree of freedom due to the dark radiation field $\chi$. This computation of $\rho_\chi$ in different $\xi$ ranges is detailed in the Eqs.(6.106)-(6.112). For the sake of convenience, we introduce a new dimensionless variable $\Omega_\chi(\eta_{\rm re}) = \rho_\chi(\eta_{\rm re})/\rho_{\rm c}(\eta_{\rm re})$, where $\rho_{\rm c}(\eta_{\rm re}) = 3H_{\rm re}^2 M_{\rm pl}^2$ is the background energy density at the end of reheating. As both the background energy density ($\rho_c$) and the massless scalar field (considered as dark radiation $\rho_\chi$) goes as $a^{-4}$ due the background expansion, the fractional energy density $\Omega_\chi(\eta > \eta_{\rm re} < \eta_{\rm eq})$ remain conserved during radiation dominated era. The present-day fractional energy density of the $\chi$ field can be expressed as

$$\Omega_\chi h^2 \simeq \left(\frac{g_{r,0}}{g_{r,\rm eq}}\right)^{1/3} \Omega_{\rm R} h^2\, \Omega_\chi(\eta_{\rm re}) \tag{6.70}$$

where $\Omega_{\rm R} h^2 \simeq 4.3 \times 10^{-5}$ [8] denotes the dimensionless energy density of radiation at the current epoch. Here, $g_{r,\rm eq}$ and $g_{r,0}$ represent the number of relativistic degrees of freedom at the epochs of radiation-matter equality and the present day, respectively. By expressing Eq. (6.69) in terms of this dimensionless variable, we obtain

$$\Omega_\chi h^2 = \frac{7}{8}\left(\frac{4}{11}\right)^{4/3} \Omega_\gamma h^2 \Delta N_\chi \simeq 1.6 \times 10^{-6} \left(\frac{\Delta N_\chi}{0.284}\right) \tag{6.71}$$

where $\Omega_\gamma h^2 = 2.47 \times 10^{-5}$ is the present-day photon energy density [8]. The latest Planck data with Baryon Acoustic Oscillation (BAO) predicts $\Delta N_{\rm eff} \leq 0.284$ (within $2\sigma$ range) [8]. Using this bound as an upper limit, we can further constrain the coupling parameter $\xi$ through Eq.(6.71).

We find that coupling strength $\xi$ is further constrained through $\Delta N_{\rm eff}$ for $w_\phi > 1/3$. In Fig.(6.8), we have plotted the upper limit of the coupling parameter $\xi_{\rm max}$ as a function of the average equation of state $w_\phi > 1/3$ for five different reheating temperatures. Lowering the reheating temperature for a fixed EoS tightens the constraint on $\xi$. For example, if the EoS is $w_\phi = 0.5$ and the reheating temperature of our universe is $T_{\rm re} = 10^{-2}$ GeV, then to satisfy the current $\Delta N_{\rm eff}$ bound, the maximum allowed value of the coupling parameter is $\xi_{\rm max} \simeq 4.02$. Note this is greater than the bound we obtained from the tensor-to-ratio ($\xi_{\rm max} \simeq 3.73$) discussed before. On the other hand, if the reheating temperature is $T_{\rm re} = 10^6$

GeV with the same EoS, the bound is $\xi_{\rm max} \simeq 4.99$, which is again higher than the bound from the tensor to ratio ($\xi_{\rm max} \simeq 3.99$) discussed before.

It is to be noted that combining constraints from the tensor-to-scalar ratio and from $\Delta N_{\rm eff}$ yields significant insights. In the lower reheating temperature case as one reduces the equation state the tensor to scalar ratio tends (solid lines) to provide stronger constraints on $\xi_{\rm max}$ than the $\Delta N_{\rm eff}$, and $\Delta N_{\rm eff}$ leads to the maximum possible value of equation state $w_\phi$ (set by dashed lines). For instance, with $w_\phi = 0.6$ and a reheating temperature of $T_{\rm re} = 10^{-2}$ GeV, the $\Delta N_{\rm eff}$ constraint predicts a maximum allowable value of the coupling constant $\xi_{\rm max} \simeq 0.205$. In contrast, under the same reheating parameters, the tensor-to-scalar ratio constraint allows a higher upper bound for the coupling constant, $\xi_{\rm max} \simeq 2.765$. Therefore, we get an allowed region of $\xi$ bounded by solid and dashed lines which satisfy both the constraints. This is indeed the case for red, blue, and magenta curves as depicted in the left panel of Fig.6.8 for $T_{\rm re} = (10^{-2}, 10^2, 10^6)$ GeV accordingly. However, with the higher temperature, the constraint from *Planck* on tensor to scalar ratio becomes increasingly important and tends to prove the entire bound on $\xi$. This indeed can be observed for cyan and brown curves with $T_{\rm re} = (10^{14}, 10^{10})$ GeV, respectively.

Unlike $w_\phi > 1/3$, for $w_\phi < 1/3$, we don't get any new constrain on $\xi$ through $\Delta N_{\rm eff}$ bound. As discussed earlier, for $w_\phi < 1/3$, as enhancement effect is important in the range $\xi < 1/6$, we find the lower limit of coupling $\xi_{\rm min} < \xi_{\rm cri} < 1/6$ satisfying the tensor-to-scalar ratio bound $r_{0.05} \leq 0.036$. The energy spectrum remains blue-tilted in the entire range $\xi > \xi_{\rm cri}$. For example, for $\xi = 0$, exploiting the Equations (6.69)-(6.71) we obtain for $w_\phi = (0,\ 0.1,\ 0.2)$, $\Delta N_{\rm eff} = (2.88 \times 10^{-13},\ 7 \times 10^{-13},\ 1.77 \times 10^{-12})$ for a wide range of reheating temperatures $T_{\rm re} = (10^{-2} - 10^{10})$ GeV(Detail computations of $\rho_\chi$ for $w_\phi < 1/3$ are given in the part II of this chapter.(see Eqs.(6.106)-(6.112))). These values are far below the maximum limit $\Delta N_{\rm eff} \leq 0.284$ for the lowest possible value of $\xi = 0$, meaning no lower limit can be imposed on $\xi$ through $\Delta N_{\rm eff}$ for $w_\phi < 1/3$. If we choose $\xi > \xi_{\rm cri}$, although the energy spectrum is blue-tilted, the secondary GW energy strength is too weak to overtake the primary strength around $k_{\rm end}$(see Fig.6.5). Therefore, in this regime, the PGW contribution always dominates the total GW energy density $\Omega_{\rm gw}h^2$.

Similarly, primordial gravitational waves (PGWs) with frequencies $\geq 10^{-15}$ Hz may contribute significantly to the radiation density of the Universe during the decoupling of the cosmic microwave background (CMB). It can also be treated as an extra relativistic degree of freedom symbolized as $\Delta N_{\rm gw}$. Hence, we can similarly express it as [133, 330]

$$\Omega_{\rm gw}h^2 = \frac{7}{8}\left(\frac{4}{11}\right)^{4/3}\Omega_\gamma h^2 \Delta N_{\rm gw} \simeq 1.6 \times 10^{-6}\left(\frac{\Delta N_{\rm gw}}{0.284}\right) \tag{6.72}$$

where $\Omega_{\rm gw}h^2$ is the present-day dimensionless energy density of the gravitational waves produced in the early universe and it is defined as

$$\Omega_{\rm gw}h^2 = \int_{k_{\rm min}}^{k_{\rm end}} \frac{dk}{k}\Omega_{\rm gw}(k)h_0^2 \tag{6.73}$$

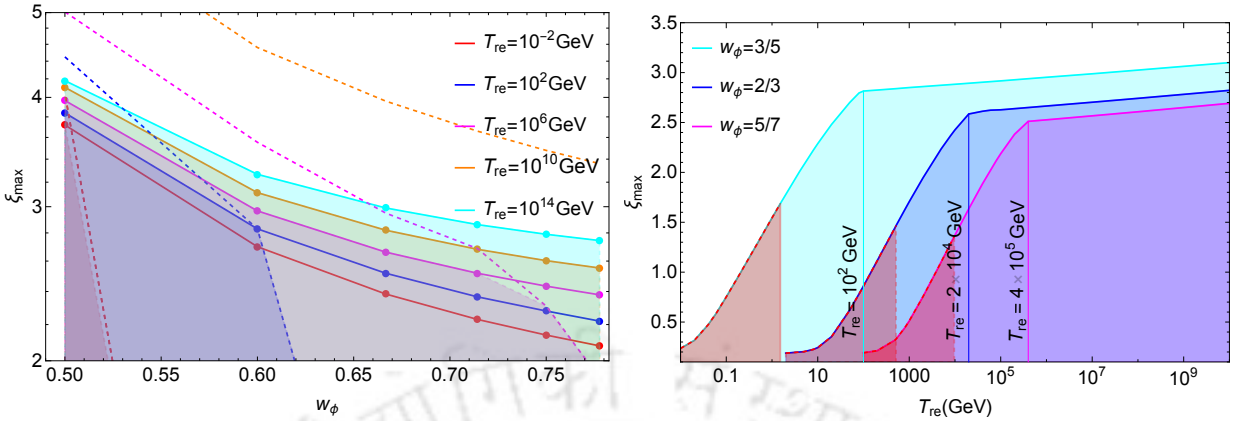


FIGURE 6.8: *In the left panel, we present the maximum allowed values of the coupling constant, $\xi_{\rm max}$, as a function of $w_\phi$. The colored dashed lines represent $\xi_{\rm max}$ values calculated from the $\Delta N_{\rm eff}$ bound (see Eq. (6.71)). In contrast, the solid colored lines indicate the limit derived from the tensor-to-scalar ratio (see Eq. (6.63)). Different colors represent different $T_{\rm re}$ values. By combining both limits, we identify a common region allowed under both bounds, represented by the shaded areas corresponding to each color. In the right panel, we plot $\xi_{\rm max}$ as a function of $T_{\rm re}$ for three discrete values of the equation of state: $w_\phi = 3/5$ (cyan), $w_\phi = 2/3$ (blue), and $w_\phi = 5/7$ (magenta). Combining both constraints, this plot shows the common allowed region, free from the $\Delta N_{\rm eff}$ and the tensor-to-scalar ratio bounds. The three vertical lines labeled by specific $T_{\rm re}$ values divided the shaded regions into two. Above this temperature, the tensor-to-scalar ratio imposes a stricter constraint on the coupling parameter $\xi$ compared to the $\Delta N_{\rm eff}$ bound. Three red-shaded regions indicate that these reheating temperatures are not allowed for the specified set of $w_\phi$ values as it violates $\Delta N_{\rm eff}$ bound at high frequency near $k_{\rm end}$ primarily sourced by PGWs.*

here $\Omega_{\rm gw}(k)h^2$ is the total contributions from both primary and secondary gravitational waves. To this end, we should point out that the GW is a secondary contribution

Assuming the present-day photon density parameter is $\Omega_\gamma h^2 \simeq 2.47\times10^{-5}$, a combination of the latest Planck-2018 and Baryon Acoustic Oscillation (BAO) data predicts $\Delta N_{\rm eff} \simeq 0.284$ (within a $2\sigma$ range) [8]. Consequently, this prediction sets an upper limit on primordial gravitational waves, such that $\Omega_{\rm gw}h^2 < 1.6 \times 10^{-6}$ [331]. Using this result, we derive the following inequality [133, 331, 332]

$$\Omega_{\rm gw}h^2 \leq 1.6 \times 10^{-6} \left(\frac{\Delta N_{\rm gw}}{0.284}\right) \tag{6.74}$$

The constraint presented in Eq. (6.74) imposes a constraints on the reheating temperature;

$$T_{\rm min} \geq \left(\frac{90 H_{\rm end}^2 M_{\rm pl}^2}{\pi^2 g_{\rm re}}\right)^{1/4} \beta^{\frac{3(1+w_\phi)}{4(3w_\phi-1)}} \left(\frac{0.284}{\Delta N_{\rm gw}}\right)^{\frac{3(1+w_\phi)}{4(3w_\phi-1)}} \tag{6.75}$$

Here $T_{\rm min}$ is the lowest possible reheating temperature to ensure the overproduction of the extra relativistic degree of freedom due to the PGWs. In the above we defined

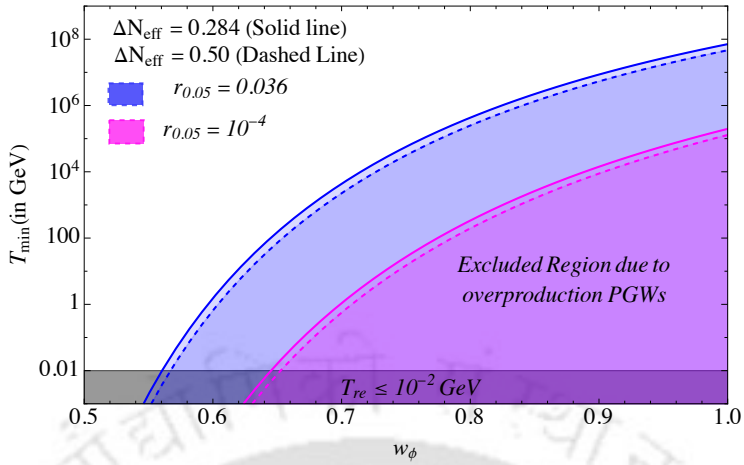


FIGURE 6.9: *The figure above shows the minimum allowed reheating temperature $T_{min}$ (in GeV) as a function of $w_\phi$. The blue lines correspond to $r_{0.05} = 0.36$, while the magenta lines represent $r_{0.05} = 10^{-4}$. The solid lines indicate $\Delta N_{\rm eff} = 0.284$, and the dashed lines indicate $\Delta N_{\rm eff} = 0.50$. The shaded regions in color mark areas that were excluded due to the overproduction of primary gravitational waves at the high-frequency end $f = f_{\rm end} = (k_{\rm end}/2\pi)$. The gray region at the bottom is excluded due to the minimum reheating temperature required by Big Bang nucleosynthesis (BBN), which is about $T_{\rm re} \simeq 10^{-2}$ GeV.*

$\beta = 1.43 \times 10^{-11}\mathcal{D}_2(H_{\rm end}/10^{-5}M_{\rm pl})^2/(n_w)$. It is crucial to emphasize that this lower bound on the reheating temperature applies exclusively to the equation of state $w_\phi > 1/3$.

Using Eq. (6.75), we have generated a parameter space plot of $T_{\rm min}$ as a function of the average equation of state ($w_\phi$) in Fig. (6.9), showing the minimum permissible reheating temperature as a function of $w_\phi$. In this figure, the blue lines correspond to $r_{0.05} = 0.036$, and the magenta lines to $r_{0.05} = 10^{-4}$. Solid lines represent $\Delta N_{\rm eff} = 0.284$, while dashed lines correspond to $\Delta N_{\rm eff} = 0.50$. The shaded regions indicate areas excluded due to the overproduction of gravitational waves at high frequencies. The gray shaded region at the bottom excludes reheating temperatures lower than the BBN bound, i.e., $T_{\rm re}^{\rm BBN} \simeq 10^{-2}$ GeV. While considering a stiff equation of state ($w_\phi > 1/3$), this bound must be taken into account. In all our plots, we have ensured that this bound is respected to avoid the overproduction of gravitational waves from primary quantum fluctuations during inflation.

**Constraining Reheating Dynamics and Coupling Parameters $\xi$ via Future Gravitational Wave Experiments:** As depicted in Fig. (6.6), for an appropriate set of reheating parameters and coupling constant $\xi$, the production of secondary gravitational waves (SGWs) by the scalar field is significant enough to pass through the sensitivity curves of several forthcoming gravitational wave (GW) detectors, including LISA, DECIGO, BBO, ET, and others. This observation suggests that future GW detectors could probe non-minimal coupling and associated dynamics in the early universe, potentially placing stringent constraints on the coupling parameter $\xi$ and the reheating dynamics. In this

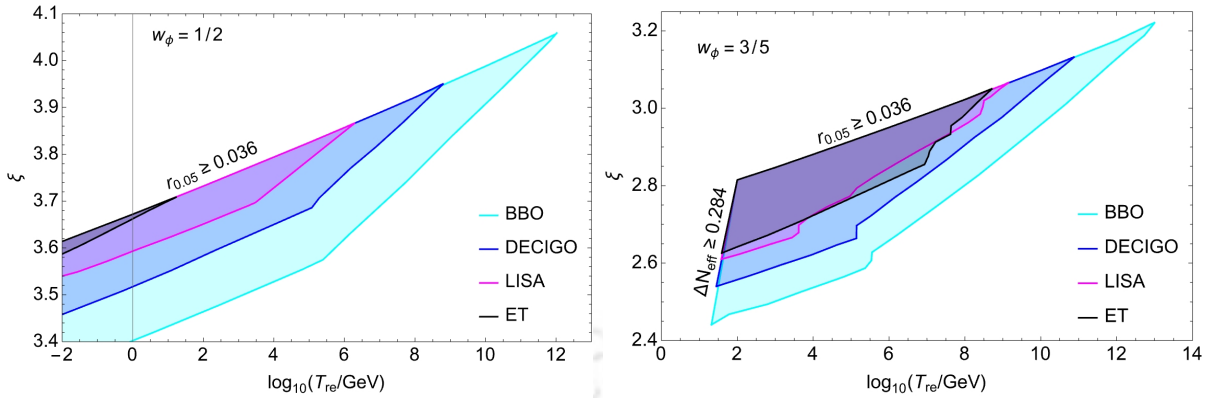


FIGURE 6.10: *In the figure above, we present the estimated parameter space of the coupling constant $\xi$ versus the reheating temperature $T_{\rm re}$ for two different equations of state (EoS): $w_\phi = 1/2$, and $w_\phi = 3/5$. These estimates can be tested by future gravitational wave (GW) detectors, including LISA (magenta), DECIGO (blue), BBO (cyan), and ET (gray). Within this parameter space, the signal generated by the scalar field $\chi$ can be detected by these GW experiments. In both plots, the upper bound comes from the tensor to scalar ratio at the CMB scale where in the right panel at a lower temperature the $\Delta N_{\rm eff}$ puts a stronger constraint on the coupling parameter $\xi$.*

section, we point out the parameter space in which these detectors are expected to explore these dynamics.

Focusing on future GW experiments such as LISA, DECIGO, BBO, and ET, we utilize the proposed sensitivity curves to estimate the parameter ranges for $\xi$ and the reheating temperature $T_{\rm re}$ for two different equations of state, $w_\phi = 1/2$ and $w_\phi = 3/5$, as shown in Fig. (6.10). The shaded regions indicate the parameter space where the signal produced by the scalar field is expected to be detectable by these experiments, provided $\xi$ falls within the specified range for a given reheating temperature and equation of state. Notably, the upper bound on $\xi$ remains the same for all experiments, despite differing sensitivity thresholds. This is because the upper limit on $\xi$ is determined by the tensor-to-scalar ratio constraint by *Planck* and the $\Delta N_{\rm eff}$ bound (as illustrated in Fig. (6.8)). Consequently, for values of $\xi$ exceeding a certain threshold, the signal, although potentially detectable, is excluded due to the overproduction of tensor fluctuations and additional relativistic degrees of freedom.

In the right panel of Fig. (6.10), we observe that when the reheating temperature is relatively low, and the scalar field is considered as dark radiation, $\Delta N_{\rm eff}$ imposes stricter constraints on $\xi$, as discussed earlier. Conversely, in the case of $w_\phi = 0.5$ (see in the left panel of Fig.(6.10)), the tensor-to-scalar ratio constraint is more restrictive than the $\Delta N_{\rm eff}$ constraint. For all the plots the lower boundary is fixed by the lowest values of the gravitational wave strength (sensitivity line) that a particular experiment could measure.

To this end, we would like to point out that in the present study, we solely focus on the long-wavelength modes($k < k_{\rm end}$) of the scalar fluctuations that suffer from tachyonic instability. The longer the wavelength, the stronger the instability and the larger the source

field amplitude. Our study revealed that the presence of such instability causes large GW and isocurvature production, and gives tight constraints on $\xi$ which one should keep in mind in future studies. At this point let us mention the recent works [245, 294, 298], where authors have explored the effect of $\xi$ on the dynamics of the scalar fluctuations, particularly for sub-horizon modes ($k \gtrsim k_{\rm end}$). In order to obtain parametric resonance, the authors assumed a value of $\xi$ that is much larger than the bound we obtained. In our entire study, we have established that for higher EoS, the large-scale modes get enhanced even at a relatively lower $\xi$ value compared to the small-scale parametric resonance studied in [245, 294, 298]. It has also been found that beyond a certain $\xi$, the appearance of long-wavelength instability results in the development of a larger two-point correlation function $\langle\chi^2\rangle$(see the Addenda 6.4) which eventually generates a back-reaction effect on the inflaton background. However, to address all these subtle issues, we may resort to the lattice study, which is beyond the scope of the present work, and we leave it for our future endeavor.

## 6.3 Summary

In this section, we summarize the key findings of this study.

- Production of scalar fluctuations and infrared instability:

  In this study, we investigate the production of a massless scalar field in the presence of a $\xi R\chi^2$ coupling during both inflation and reheating. We found that for $\xi < 1/6$ and $w_\phi < 1/3$, the infrared(IR) instability helps scalar field fluctuation to grow both during and after inflation. Such growth turns out to be maximal for $\xi = 0$. It potentially violates the *Planck* bound on $r$ through its secondary GW production, thereby setting a tight constraint on the minimum value of $\xi$. On the contrary, for $\xi > 1/6$, and $w_\phi > 1/3$ the infrared modes of the scalar field grow due to post-inflationary instability, and such instability grows with increasing $\xi$. Therefore, in this case, the associated induced gravitational waves put a tight constraint on the maximum value of $\xi$. Thus, in both cases, the infrared instability plays a pivotal role in constraining the non-minimal coupling strength.

- Constraining $\xi$ through $\Delta N_{\rm eff}$, $r_{0.05}$, and isocurvature bound:

  To obtain the constraint on $\xi$, we mainly consider the observational bounds on the effective number of degrees of freedom $\Delta N_{\rm eff}$ at the time of BBN and *Planck*'s upper limit on tensor to scalar ratio $r_{0.05}$ at the pivot scale $(k_*/a_0) = 0.05\ {\rm Mpc}^{-1}$. The scalar field generated due to infrared instability can be treated as a possible candidate for dark radiation which contributes to $\Delta N_{\rm eff}$. On the other hand, associated secondary GW can affect both $\Delta N_{\rm eff}$ and in estimating the energy scale of inflation through $r$. Except for a few reheating parameters($w_\phi > 1/3$, $N_{\rm re}, T_{\rm re}$), we have obtained bounds on maximum possible values of the coupling strength $\xi_{\rm max}$ as illustrated in Fig.(6.8). In the higher reheating temperature regime, we find stronger constraints

from the tensor-to-scalar ratio bound that shrinks the maximum allowed region of $\xi$ for given reheating parameters. Combining the latest *Planck*-2018 data of both $r_{0.05} < 0.036$ and $\Delta N_{\rm eff} \simeq 0.284$ for $w_\phi \geq 1/2$, we find that there exists an upper limit on $\xi < \xi_{\rm max}(\simeq 4)$, and hence arbitrarily large values of $\xi$ are hardly acceptable. Likewise, for $w_\phi = 0$, we find that there exists a lower limit on $\xi > \xi_{\rm min}(\simeq 0.02)$, and hence vanishing non-minimal coupling or in other words, the minimal scenario may not be tenable. We have also briefly discussed the constraints on $\xi$ based on current isocurvature bound at the CMB pivot scale, $\mathcal{P}_{\mathcal{S}}(k_*) \lesssim 8.3 \times 10^{-11}$. Interestingly, we have found an almost similar prediction of both minimum(for $w_\phi = 0$) and maximum bounds(for $w_\phi > 1/3$) on $\xi$ as obtained through the tensor-to-scalar ratio and the isocurvature bound.

- Constraining negative $\xi$ values:

  we have also estimated the possible constraint on negative $\xi$ values. Our study reveals that for $w_\phi = 0$, the presence of strong inflationary and post-inflationary IR instability of the source field results in a heavily red-tilted energy-density spectrum, and this also results high value of $r_{0.05}$ which may violate the CMB bound. Hence, negative $\xi$ values are found to be completely forbidden for $w_\phi = 0$. On the contrary, for $w_\phi > 1/3$, we find lower limits of negative $\xi$ for different reheating parameters($w_\phi$, $T_{\rm re}$, $H_{\rm end}$), and for a given $w_\phi$, the typical values of negative $\xi$ don't vary much for a wide range of reheating temperatures as discussed in Section 6.2. This is opposite to the case of putting upper limits on positive $\xi$ for any $w_\phi > 1/3$.

- Detection prospect:

  Furthermore, we have found a distinctive gravitational wave spectrum for different parameters, which could be detectable by future GW detectors, allowing for more robust constraints on the coupling parameters and reheating dynamics in the near future GW experiments Towards the end, given the constraints from all the observations from *Planck*, we derived the region of parameter space in $(T_{\rm re}, \xi)$ plane which can be probed by future experiments such as BBO, DECIGO, LISA, and ET, particularly for a stiff inflaton equation of state.

# Addenda

## 6.4 Analyzing the behavior of the suppression factor $\left(1 - a^2\xi\langle\chi^2\rangle/M_{\rm pl}^2\right)^{-2}$

This factor might play a very crucial role in estimating the strength of the secondary GW spectrum for larger values of the two-point correlation function $\langle\chi^2\rangle$. Therefore, the typical values of this suppression factor in the different ranges of $\xi$ must be analyzed very carefully. With the help of the equations (6.15),(6.25) and (6.37) we can compute the typical values of the two-point correlation function $\langle\chi^2\rangle$ with varying theory parameters.

The behavior of $\left(1 - a^2\xi\langle\chi^2\rangle/M_{\rm pl}^2\right)^2$ is depicted in Fig.(6.11) for different reheating EoS in two regimes $w_\phi < 1/3$ and $w_\phi > 1/3$. In the higher EoS $w_\phi > 1/3$, and $\xi > 3/16$ regime, we observed that it can become larger than unity, as evident in Fig.(6.11). For instance, for $T_{\rm re} = 10^6$ GeV and $H_{\rm end} = 10^{-5}M_{\rm pl}$, we get $\xi = (14.94,\ 10.75,\ 9.27,\ 7.77)$ for $w_\phi = (1/2, 3/5, 2/3, 4/5)$ respectively, and beyond these typical values, the suppression factor starts diverging($a^2\xi\langle\chi^2\rangle >> M_{\rm pl}^2$) with further increase of the coupling strength as shown in Fig.(6.11)(middle row, right panel). The last two bottom plots of Fig.(6.11) represent the variation of the said quantity in terms of $T_{\rm re}$ and $H_{\rm end}$ for different EoS with a fixed $\xi$. We see that for $\xi = 6, H_{\rm end} = 10^{-5}M_{\rm pl}$, the factor grows rapidly with the decrease of $T_{\rm re}$(bottom row, left panel), and for $\xi = 10, T_{\rm re} = 10^6$ GeV, the suppression term grows with $H_{\rm end}$ for higher reheating EoS $w_\phi = 2/3, 4/5$(bottom row, right panel). However, our analysis has already shown well below the above values of $\xi$, we have found either large GW or isocurvature modes which already violate the *Planck* bound.

## 6.5 Computing the Secondary Tensor power spectrum

As we are mainly interested in the higher post-inflationary EoS regime, $w_\phi > 1/3$, so, we shall first share a detailed calculation of the tensor power spectrum during reheating for a generalized power law type matter power spectrum in stiff EoS regime $w_\phi > 1/3$. The computation of the tensor power spectrum for $w_\phi < 1/3$ will follow the same procedure.

### 6.5.1 For $w_\phi > 1/3$ :

For $w_\phi > 1/3$ and $\xi > 3/16$, combining Eqs. (6.25) and (6.27) we can write the matter power spectrum in terms of the rescaled field $X_k$ for long-wavelength modes as follows.

$$\mathcal{P}_X(k,\eta) = \frac{k^3}{2\pi^2}\left|X_k^{\rm long}(k,\eta)\right|^2 = \frac{\mathcal{A}_3}{\pi^2}\,k_{\rm end}^2\,\mathcal{I}(k,\eta)\left(\frac{k}{k_{\rm end}}\right)^{2(1-\nu_2)} \tag{6.76}$$

In the above equation, $\mathcal{A}_3$ is a constant part depending on the initial parameters as given in (6.106) and $\mathcal{I} = \cos^2(k\eta)$ is the time-dependent part of the matter power spectrum.

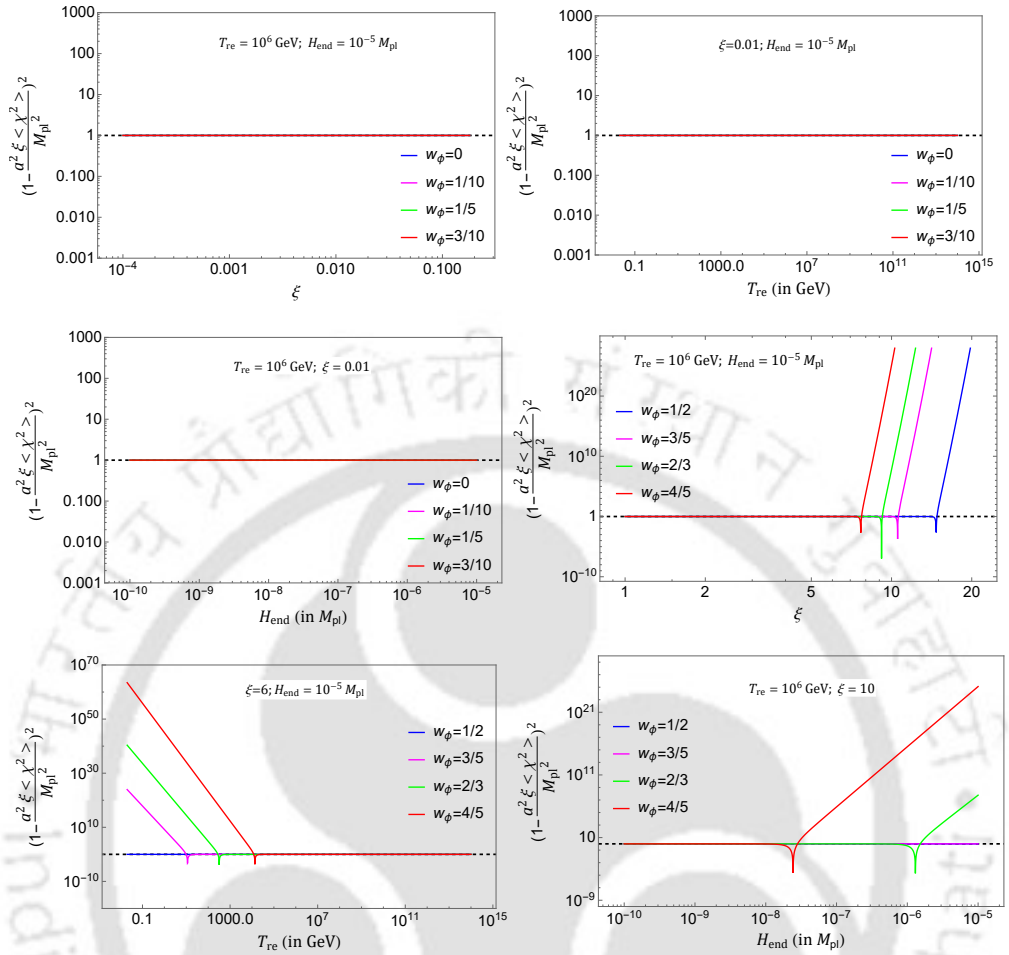


FIGURE 6.11: *The figure presents the behavior of the suppression factor with the variation of three parameters* $\xi, T_{re}, H_{end}$ *for different reheating EoS in the regimes* $w_\phi < 1/3$ *and* $w_\phi > 1/3$. *In all the plots, the black dotted line depicts* $\left(1-\frac{a^2\xi\langle\chi^2\rangle}{M_{pl}^2}\right)^2 = 1$

Now we can write the tensor power spectrum in terms of the matter power spectrum as

$$\mathcal{P}_T^{sec}(k,\eta_{re}) = \frac{8}{M_{pl}^4}\left(\int_{x_e}^{x_{re}} dx_1 \frac{\mathcal{G}_k^{re}(x_{re},x_1)}{a^2(x_1)}\right)^2 \times \int_{k_{min}}^{k_{end}} \frac{dq}{k}\int_{-1}^{1} d\gamma(1-\gamma^2)^2 \frac{(q/k)^3\mathcal{P}_X(q,\eta_1)\mathcal{P}_X(|\vec{k}-\vec{q}|\eta_1)}{|1-q/k|^3} \tag{6.77}$$

Now using Eq.(6.76) in the above Eq.(6.77) we get the following form.

$$\begin{aligned}\mathcal{P}_T^{sec}(k,\eta_{re}) =& \frac{8\mathcal{A}_3^2 k_{end}^4}{\pi^4 M_{pl}^4}\left(\int_{x_e}^{x_{re}} dx_1 \frac{\mathcal{G}_k^{re}(x_{re},x_1)}{a^2(x_1)}\mathcal{I}(x_1)\right)^2 \\ &\times \int_{k_{min}}^{k_{end}} \frac{dq}{k}\int_{-1}^{1} d\gamma(1-\gamma^2)^2 \frac{(q/k)^3(q/k_{end})^{2(1-\nu_2)}(|\vec{k}-\vec{q}|/k_{end})^{2(1-\nu_2)}}{|1-q/k|^3}\end{aligned} \tag{6.78}$$

During the reheating era, the scale factor can be approximately written as $a^2(\eta) \approx a^2_{\rm end}(x/x_{\rm e})^{\delta}$, we recall that $\delta(w_\phi) = 4/(1+3w_\phi)$. We obtain the following expression by substituting this approximate form of the scale factor to the above Eq.(6.78).

$$\begin{aligned}\mathcal{P}_{\rm T}^{\rm sec}(k,\eta_{\rm re}) &= \frac{8\mathcal{A}_3^2 H_{\rm end}^4}{\pi^4 M_{\rm pl}^4}\left(\frac{k}{k_{\rm end}}\right)^{4+2\delta-4\nu_2}\left(\int_{x_{\rm e}}^{x_{\rm re}} dx_1 x_1^{-\delta}\mathcal{G}_k^{\rm re}(x_{\rm re},x_1)\mathcal{I}(x_1)\right)^2 \\ &\times \int_{k_{\rm min}}^{k_{\rm end}}\frac{dq}{k}\int_{-1}^{1} d\gamma(1-\gamma^2)^2(q/k)^{5-2\nu_2}(|1-q/k|)^{-(1+2\nu_2)} \\ &= \frac{8\mathcal{A}_3^2 H_{\rm end}^4}{\pi^4 M_{\rm pl}^4}\left(\frac{k}{k_{\rm end}}\right)^{4+2\delta-4\nu_2}\left(\underbrace{\int_{x_{\rm e}}^{x_{\rm re}} dx_1 x_1^{-\delta}\mathcal{G}_k^{\rm re}(x_{\rm re},x_1)\mathcal{I}(x_1)}_{\text{Time Integral}}\right)^2 \mathcal{F}(k) \qquad (6.79)\end{aligned}$$

where we define $\mathcal{F}(k)$ as

$$\mathcal{F}(k) = \int_{u_{\rm min}}^{u_{\rm max}} du \int_{-1}^{1} d\gamma(1-\gamma^2)^2 u^{5-2\nu_2}(1+u^2-2u\gamma)^{-(\nu_2+1/2)} \qquad (6.80)$$

#### 6.5.1.1 Computation of $\mathcal{F}(k)$ :

Here we define another variable $u = q/k$. In order to perform the momentum integral, we have to break it into two separate limits, i.e. $u_{\rm min} \leq u < 1$ and $1 < u \leq u_{\rm max}$, where $u_{\rm min} = k_{\rm min}/k$ and $u_{\rm max} = k_f/k$ where $k_{\rm min}$ represents the largest observable scale as of today( CMB scale, $k_*$) and $k_{\rm end}$ represent the largest mode that leaves the horizon at the end of inflation.

Now in the following range $u_{\rm min} \leq u < 1$ the above integral (6.80) boils down to

$$\mathcal{F}_1 \simeq \int_{u_{\rm min}}^{1} du u^{5-2\nu_2}\int_{-1}^{1} d\gamma(1-\gamma^2)^2 = \frac{16}{15(6-2\nu_2)}\left\{1-\left(\frac{k_{\rm min}}{k}\right)^{6-2\nu_2}\right\} \qquad (6.81)$$

where we have used $(1+u^2-2\gamma u) \simeq 1$. On the other hand for $1 < u \leq u_{\rm max}$ range the above integral Eq.(6.80) boils down to the following one.

$$\begin{aligned}\mathcal{F}_2 &\simeq \int_{1}^{u_{\rm max}} du \int_{-1}^{1} d\gamma(1-\gamma^2)^2 u^{5-2\nu_2}u^{-(2\nu_2+1)} = \frac{16}{15(5-4\nu_2)}\left\{\left(\frac{k_{\rm end}}{k}\right)^{5-4\nu_2} - 1\right\} \\ &= \frac{16}{15(5-4\nu_2)}\left(\frac{k_{\rm end}}{k}\right)^{5-4\nu_2}\left\{1-\left(\frac{k}{k_{\rm end}}\right)^{5-4\nu_2}\right\} \qquad (6.82)\end{aligned}$$

where we have used $(1+u^2-2\gamma u) \simeq u^2$.

Now combining Eq.(6.81) and Eq.(6.82) we get

$$\mathcal{F}(k) = (\mathcal{F}_1 + \mathcal{F}_2) \simeq \frac{16}{15}\left\{\frac{1}{6-2\nu_2}\left(1-\left(\frac{k_{\rm min}}{k}\right)^{6-2\nu_2}\right) + \frac{1}{5-4\nu_2}\left(\left(\frac{k_{\rm end}}{k}\right)^{5-4\nu_2} - 1\right)\right\} \tag{6.83}$$

#### 6.5.1.2 Simplification of the Time Integral :

During reheating, the Green's function of Eq.(2.200) is

$$\mathcal{G}_k^{\rm re}(x, x_1) = \frac{\pi x^l x_1^{1-l}}{2\sin(l\pi)}(J_l(x)J_{-l}(x_1) - J_{-l}(x)J_l(x_1)) \tag{6.84}$$

We recall again $l(w_\phi) = 3(w_\phi - 1)/2(1+3w_\phi)$. Now using Eq.(6.84) we are going to perform the time integral part of Eq.(6.79)

$$\begin{aligned}
\mathcal{I}_t(x_{\rm re}, x_{\rm e}) &= \int_{x_{\rm e}}^{x_{\rm re}} dx_1 x_1^{-\delta}\mathcal{I}(x_1)\mathcal{G}_k^{\rm re}(x_{\rm re}, x_1) = \frac{\pi}{2\sin(l\pi)}\frac{x_{\rm re}^l x_1^{2-2l-\delta}}{2^{1+l}} \\
&\times \left(-x_1^{2l}J_{-l}(x_{\rm re})\Gamma\left[1-\frac{\delta}{2}\right]\text{HypergeometricPFQRegularized}\left[\left\{1-\frac{\delta}{2}\right\}, \left\{1+l, 2-\frac{\delta}{2}\right\}, -\frac{x_1^2}{4}\right]\right)\Bigg|_{x_{\rm e}}^{x_{\rm re}} \\
&+ 4^l J_l(x_{\rm re})\Gamma\left[1-l-\frac{\delta}{2}\right]\frac{\pi}{2\sin(l\pi)}\frac{x_{\rm re}^l x_1^{2-2l-\delta}}{2^{1+l}} \\
&\times \text{HypergeometricPFQRegularized}\left[\left\{1-l-\frac{\delta}{2}\right\}, \left\{1-l, 2-l-\frac{\delta}{2}\right\}, -\frac{x_1^2}{4}\right]\Bigg|_{x_{\rm e}}^{x_{\rm re}}
\end{aligned} \tag{6.85}$$

$$\mathcal{I}_t(x_{\rm re}, x_{\rm e}) = (\mathcal{I}_t(x_{\rm re}, x_{\rm re}) - \mathcal{I}_t(x_{\rm re}, x_{\rm e})) \simeq \mathcal{I}_t(x_{\rm re}, x_{\rm re}) \tag{6.86}$$

For the sub-horizon limit i.e.

$$\begin{aligned}
\mathcal{I}_t(x_{\rm re}, x_{\rm e}) &\simeq -\frac{\pi}{2\sin(l\pi)}\frac{2^{1-l-\delta}\pi}{\Gamma(l+\delta/2)\Gamma(\delta/2)}x_{\rm re}^l\left[\csc(\pi\delta/2)J_{-l}(x_{\rm re}) - \csc\left[\pi(2l+\delta)/2\right]J_l(x_{\rm re})\right] \\
&\simeq -\frac{2^{1-l-\delta}\pi\Gamma(1-l)\Gamma(l)}{2\Gamma(l+\delta/2)\Gamma(\delta/2)}x_{\rm re}^l\sqrt{\frac{2}{\pi x_{\rm re}}}
\end{aligned} \tag{6.87}$$

Plugging the above Eq.(6.87) into the Eq.(6.79)we have the following expression.

$$\lim_{k>>k_{\rm re}}\mathcal{P}_{\rm T}^{\rm sec}(k, \eta_{\rm re}) \simeq \frac{2\mathcal{A}_3^2 H_{\rm end}^4}{\pi^4 M_{\rm pl}^4}\frac{2^{1-2l-2\delta}\pi\Gamma^2(1-l)\Gamma^2(l)}{\Gamma^2(l+\frac{\delta}{2})\Gamma^2\left(\frac{\delta}{2}\right)}\frac{8(1+2\nu_2)}{15(3-\nu_2)(4\nu_2-5)}\left(\frac{k_{\rm re}}{k_{\rm end}}\right)^{\delta}\left(\frac{k}{k_{\rm end}}\right)^{4+\delta-4\nu_2} \tag{6.88}$$

Similarly for the super-horizon limit i.e. $x_{\rm re} << 1$ limit, the above integral boils down to the simplified form below.

$$\lim_{k<<k_{\rm re}}\mathcal{I}_t(x_{\rm re}, x_{\rm e}) \simeq x_{\rm re}^{2-\delta}\left\{\frac{1}{2l(\delta-2)} + \frac{1}{4l(1-l)-2l\delta}\right\} \tag{6.89}$$

Now utilizing this expression in Eq.(6.79) we obtain the tensor power spectrum at the super-horizon scale behaving as

$$\lim_{k<<k_{\rm re}} \mathcal{P}_{\rm T}^{\rm sec}(k,\eta_{\rm re}) \simeq \frac{2\mathcal{A}_3^2 H_{\rm end}^4}{\pi^4 M_{\rm pl}^4}\left\{\frac{1}{2l(\delta-2)}+\frac{1}{4l(1-l)-2l\delta}\right\}^2 \mathcal{F}(k)\left(\frac{k_{\rm end}}{k_{\rm re}}\right)^{4-2\delta}\left(\frac{k}{k_{\rm end}}\right)^{4(2-\nu_2)}$$
$$\simeq \frac{2\mathcal{A}_3^2 H_{\rm end}^4}{\pi^4 M_{\rm pl}^4}\left\{\frac{1}{2l(\delta-2)}+\frac{1}{4l(1-l)-2l\delta}\right\}^2 \frac{8(1+2\nu_2)}{15(3-\nu_2)(4\nu_2-5)}\left(\frac{k_{\rm end}}{k_{\rm re}}\right)^{4-2\delta}\left(\frac{k}{k_{\rm end}}\right)^{4(2-\nu_2)} \tag{6.90}$$

**GWs spectral behavior for extreme limit $k << k_{\rm re}$ and $k >> k_{\rm re}$:** During the radiation-dominated era, the spectral energy density can be written as

$$\Omega_{\rm gw}(k,\eta) = \frac{\rho_{\rm gw}(k,\eta)}{\rho_c(\eta)} = \frac{1}{12}\frac{k^2\mathcal{P}_{\rm T}^{\rm rad}(k,\eta)}{a^2(\eta)H^2(\eta)} \tag{6.91}$$

where $\mathcal{P}_{\rm T}^{\rm rad}(k,\eta)$ is the tensor power spectrum during radiation dominated era and it can be written in terms of $\mathcal{P}_{\rm T}(k,\eta_{\rm re})$ as

$$\mathcal{P}_{\rm T}^{\rm rad}(k,\eta) = \left(1+\frac{k^2}{k_{\rm re}^2}\right)\frac{\mathcal{P}_{\rm T}(k,\eta_{\rm re})}{2k^2\eta^2} \tag{6.92}$$

Now utilizing Eq.(6.92) and (6.90) in Eq.(6.91) we obtain the GW spectrum behaving in super-horizon limit as

$$\lim_{k<<k_{\rm re}} \Omega_{\rm gw}(k,\eta) \simeq \frac{2\mathcal{A}_3^2 H_{\rm end}^4}{24\pi^4 M_{\rm pl}^4}\left\{\frac{1}{2l(\delta-2)}+\frac{1}{4l(1-l)-2l\delta}\right\}^2 \frac{8(1+2\nu_2)}{15(3-\nu_2)(4\nu_2-5)}\left(\frac{k_{\rm end}}{k_{\rm re}}\right)^{4-2\delta}$$
$$\times\left(\frac{k}{k_{\rm end}}\right)^{2(4-2\nu_2)} \tag{6.93}$$

Similarly, for sub-horizon modes, using Eq.(6.88) and (6.92) in Eq.(6.91), the GW spectral energy density can be written as

$$\lim_{k>>k_{\rm re}} \Omega_{\rm gw}(k,\eta) \simeq \frac{2\mathcal{A}_3^2 H_{\rm end}^4}{24\pi^4 M_{\rm pl}^4}\frac{2^{1-2l-2\delta}\pi\Gamma^2(1-l)\Gamma^2(l)}{\Gamma^2(l+\frac{\delta}{2})\Gamma^2\left(\frac{\delta}{2}\right)}\frac{8(1+2\nu_2)}{15(3-\nu_2)(4\nu_2-5)}\left(\frac{k_{\rm end}}{k_{\rm re}}\right)^{2-\delta}\left(\frac{k}{k_{\rm end}}\right)^{6+\delta-4\nu_2} \tag{6.94}$$

### 6.5.2 For $w_\phi < 1/3$ :

It is already discussed in Section 6.1, for $w_\phi < 1/3$, the system experiences greater enhancement in the long-wavelength regime in the range $\xi < 1/6$. Combining Eqs. (6.15) and (6.26) we obtain the expression of the field power spectrum as

$$\mathcal{P}_X(k,\eta) = \frac{k^3}{2\pi^2}\left|X_k^{\rm long}(k,\eta)\right|^2 = \frac{\mathcal{A}_1}{\pi^2}\,k_{\rm end}^2\,\mathcal{I}(k,\eta)\left(\frac{k}{k_{\rm end}}\right)^{2(1-\nu_1-\nu_2)} \tag{6.95}$$

In the above equation, $\mathcal{A}_1$ is a constant part depending on the initial parameters as given in (6.100) and $\mathcal{I} = \cos^2(k\eta)$ is the time-dependent part of the matter power spectrum as it was for $w_\phi > 1/3$. Subject to this field power spectrum, following the same steps as followed in the previous case, we obtain the secondary tensor power spectrum as

$$\mathcal{P}_{\rm T}^{\rm sec}(k,\eta_{\rm re}) = \frac{8\mathcal{A}_1^2 k_{\rm end}^4}{\pi^4 M_{\rm pl}^4}\left(\int_{x_e}^{x_{\rm re}} dx_1 \frac{\mathcal{G}_k^{\rm re}(x_{\rm re},x_1)}{a^2(x_1)}\mathcal{I}(x_1)\right)^2 \times \int_{k_{\rm min}}^{k_{\rm end}} \frac{dq}{k}\int_{-1}^{1} d\gamma(1-\gamma^2)^2 \frac{(q/k)^3 (q/k_{\rm end})^{2(1-\nu_1-\nu_2)}(|\vec{k}-\vec{q}|/k_{\rm end})^{2(1-\nu_1-\nu_2)}}{|1-q/k|^3} \tag{6.96}$$

Comparing Eqs. (6.78) and (6.96), apart from the time-independent amplitude part($\mathcal{A}_1$ and $\mathcal{A}_3$), we notice the only difference in the index of $(q/k_{\rm end})$ and $\left(|\vec{k}-\vec{q}|/k_{\rm end}\right)$ ratios. This fact confirms that the substitution of $(\nu_1+\nu_2)$ in place of $\nu_2$ will essentially reproduce all the results up to Eq.(6.94) for $w_\phi < 1/3$ in a similar fashion. Simplification of the following time-integral in (6.96) gives the same expression as in (6.85). Following the same procedure, the above momentum integral is simplified as

$$\mathcal{E}(k) \simeq \frac{16}{15}\left\{\frac{1}{6-2(\nu_1+\nu_2)}\left(1-\left(\frac{k_{\rm min}}{k}\right)^{6-2(\nu_1+\nu_2)}\right)+\frac{1}{5-4(\nu_1+\nu_2)}\left(\left(\frac{k_{\rm end}}{k}\right)^{5-4(\nu_1+\nu_2)}-1\right)\right\} \tag{6.97}$$

Having followed the same methodology as outlined in the previous case for $w_\phi > 1/3$, we finally reach the GW spectrums in both super-horizon and sub-horizon limits as follows:

**GW spectrum in super-horizon($k << k_{\rm re}$) limit:** Likewise (6.93), we compute the GW energy density spectrum for super-horizon modes, $k << k_{\rm re}$ as

$$\lim_{k<<k_{\rm re}} \Omega_{\rm gw}(k,\eta) \simeq \frac{2\mathcal{A}_1^2 H_{\rm end}^4}{24\pi^4 M_{\rm pl}^4}\left\{\frac{1}{2l(\delta-2)}+\frac{1}{4l(1-l)-2l\delta}\right\}^2 \times \frac{8(1+2(\nu_1+\nu_2))}{15(3-(\nu_1+\nu_2))(4(\nu_1+\nu_2)-5)}\left(\frac{k_{\rm end}}{k_{\rm re}}\right)^{4-2\delta}\left(\frac{k}{k_{\rm end}}\right)^{2(4-2(\nu_1+\nu_2))} \tag{6.98}$$

**GW spectrum in sub-horizon($k >> k_{\rm re}$) limit:** Likewise (6.94), we compute the GW energy density spectrum for sub-horizon modes, $k >> k_{\rm re}$ as

$$\lim_{k>>k_{\rm re}} \Omega_{\rm gw}(k,\eta) \simeq \frac{2\mathcal{A}_1^2 H_{\rm end}^4}{24\pi^4 M_{\rm pl}^4}\frac{2^{1-2l-2\delta}\pi\Gamma^2(1-l)\Gamma^2(l)}{\Gamma^2(l+\frac{\delta}{2})\Gamma^2\left(\frac{\delta}{2}\right)} \times \frac{8(1+2(\nu_1+\nu_2))}{15(3-(\nu_1+\nu_2))(4(\nu_1+\nu_2)-5)}\left(\frac{k_{\rm end}}{k_{\rm re}}\right)^{2-\delta}\left(\frac{k}{k_{\rm end}}\right)^{6+\delta-4(\nu_1+\nu_2)} \tag{6.99}$$

# Part II

# Nonminimal infrared gravitational reheating in light of ACT observation

## 6.6 Infrared Gravitational Reheating: Defining Reheating parameters ($N_{\rm re}$, $T_{\rm re}$)

The super-horizon growth beyond a certain threshold of $\xi$ essentially directs us to investigate the possibility of successful reheating without invoking any further new physics in the inflaton sector. The non-minimal coupling between gravity and radiation provides us with an extra gravitational parameter $\xi$, which can be tuned to obtain radiation energy density that can surpass the contribution from the sub-Hubble modes, and lead to successful reheating. Therefore, controlling $\xi$ can give rise to a large reheating temperature as compared to the pure gravitational reheating scenario [54, 111, 154]. In the present section, exploiting all the energy density spectra derived in Section 6.1 for $w_\phi > 1/3$ (see Eq.(6.27)), we shall thoroughly investigate the reheating dynamics by these infrared scalar fluctuations, and also derive the important expressions of reheating parameters $(N_{\rm re}, T_{\rm re})$ in different ranges of coupling parameter $\xi$.

For a minimally coupled inflaton without any additional interaction, inflaton energy density scales as $\rho_\phi \propto a^{-3(1+w_\phi)}$ whereas produced massless fluctuations, being radiation, scale as $\rho_\chi \propto a^{-4}$. To successfully reheat the universe, $\rho_\phi$ and $\rho_\chi$ must be equal at a point where reheating is assumed to end, and standard radiation domination starts. Note from the Fig.6.1 that adiabaticity violation occurs for a brief period of time, and hence, like conventional perturbative reheating, production of infrared radiation is not a gradual process. This essentially suggests that such infrared radiation can dominate over the background inflaton only for $w_\phi > 1/3$. Therefore, in the subsequent part of the discussion on energy density, we shall only focus on the spectrum for $w_\phi > 1/3$.

### 6.6.1 Reheating parameters $N_{\rm re}, T_{\rm re}$ for $0 \leq \xi < 3/16$

In this parameter range of interest, we have the number spectrum, behaving as $|\beta_k|^2 \propto (k/k_{\rm end})^{-2(\nu_1+\nu_2)}$. Utilizing the spectrum, the total comoving energy density is computed to be

$$\rho_\chi^{\rm com} = \rho_\chi \left(\frac{a}{a_{\rm end}}\right)^4 = \frac{1}{2\pi^2}\int_{k_{\rm re}}^{k_{\rm end}} k^4 |\beta_k|^2 d(\ln(k)) \approx \frac{\mathcal{A}_1 H_{\rm end}^4}{4\pi^2\left(2-(\nu_1+\nu_2)\right)} \tag{6.100}$$

$$\text{Where,} \quad \mathcal{A}_1 = \left(\frac{\Gamma(\nu_1)\Gamma(\nu_2)2^{\nu_1}}{8\pi}\left(\frac{2}{3\mu-1}\right)^{\nu_2}\left(\frac{3\mu(1-2\nu_1)+2(\nu_1-\nu_2)}{\sqrt{(3\mu-1)}}\right)\right)^2 \tag{6.101}$$

For $w_\phi > 1/3$, in this specified range of $\xi$, we always have $(4-2(\nu_1+\nu_2)) > 0$. Therefore, the maximum contribution to energy is coming from largest mode $k_{\rm end}$ corresponding to the end of inflation. This property of the blue-tilted spectrum is used to reach the final expression of $\rho_\chi^{\rm com}$ in Eq.(6.100). *The highest accessible scale in the finite time scale of reheating is $k_{\rm re}$ and the modes in the range $k_{\rm re} \leq k \leq k_{\rm end}$ are well inside the horizon at the end of reheating, and hence contribute to the total energy density of produced particles. This is why $k_{\rm re}$ is considered to be the IR limit in the computation of the above integration.*

Reheating will be concluded when background energy density will be equal to total radiation energy density $\rho_\chi$, the reheating parameters, namely the reheating e-folding number $N_{\rm re} = \ln(a_{\rm re}/a_{\rm end})$, is calculated as

$$\rho_{\rm end}\left(\frac{a_{\rm re}}{a_{\rm end}}\right)^{-3(1+w_\phi)} = \rho_\chi^{\rm com}\left(\frac{a_{\rm re}}{a_{\rm end}}\right)^{-4} \implies N_{\rm re} = \frac{1}{(1-3w_\phi)}\ln\left(\frac{\rho_\chi^{\rm com}}{\rho_{\rm end}}\right), \tag{6.102}$$

and the reheating temperature $T_{\rm re}$ is calculated as

$$\rho_\chi^{\rm com} e^{-4N_{\rm re}} = \frac{\pi^2 g_{\rm re}}{30}T_{\rm re}^4 \implies T_{\rm re} = \left(\frac{30}{g_{\rm re}\pi^2}\right)^{\frac{1}{4}}(\rho_{\rm end})^{\frac{1}{1-3w_\phi}}(\rho_\chi^{\rm com})^{-\frac{3(1+w_\phi)}{4(1-3w_\phi)}}. \tag{6.103}$$

Where the background energy density at inflation end is $\rho_{\rm end} = 3M_{\rm pl}^2H_{\rm end}^2$, $g_{\rm re} = 106.75$ is the total number of relativistic degrees of freedom at the time of reheating in the standard model(SM) for $T_{\rm re} \gtrsim 1$ GeV. Important to note that as long as the energy spectrum remains blue-tilted, the expressions of both $N_{\rm re}$ and $T_{\rm re}$ in Eq.(6.102) and (6.103) hold true. For any value of coupling strength lying in the range $0 \leq \xi < 3/16$, we can utilize above two equations for a given comoving energy density $\rho_\chi^{\rm com}$ to identify the respective reheating parameters. For example, for $w_\phi = 3/5$, we get the reheating temperatures $T_{\rm re} = (6.16\times10^{-4},\ 7.95\times10^{-6})$ GeV for the coupling $\xi = (0, 0.1)$ respectively. Similarly, for $w_\phi = 9/11$, we get $T_{\rm re} = (3.83\times10^3,\ 2.43\times10^2)$ GeV for the coupling $\xi = (0, 0.1)$ respectively. In this particular range of coupling strength, increasing $\xi$ lowers the temperature as can be recovered from Fig.(6.12). As one gradually approaches the conformal limit $\xi = 1/6$, large-scale production diminishes substantially, which causes this particular behavior.

### 6.6.2 Reheating parameters $N_{\rm re}, T_{\rm re}$ for $\xi = 3/16$

This is a special case for which the number spectrum behaves as $|\beta_k|^2 \propto (k/k_{\rm end})^{-2\nu_2}$. Likewise the previous case, total comoving energy density for $\xi = 3/16$ is evaluated to be

$$\rho_\chi^{\rm com} \approx \frac{\mathcal{A}_2 H_{\rm end}^4}{4\pi^2(2-\nu_2)}, \quad \text{where,} \quad \mathcal{A}_2 = \left(\frac{\Gamma(\nu_2)}{2}\left(\frac{2}{3\mu-1}\right)^{\nu_2}\left|\frac{3\mu-2\nu_2}{4\sqrt{(3\mu-1)}} + \frac{i\sqrt{3\mu-1}}{\pi}\right|\right)^2. \tag{6.104}$$

As discussed in the previous case, the energy spectrum being blue-tilted for $\xi = 3/16$, here we have the similar expressions of reheating parameters $N_{\rm re}, T_{\rm re}$ with $\rho_\chi^{\rm com}$ in Eq.(6.104).

$$\begin{aligned} N_{\rm re} &= \frac{1}{(1-3w_\phi)}\ln\left(\frac{\rho_\chi^{\rm com}}{\rho_{\rm end}}\right) \\ T_{\rm re} &= \left(\frac{30}{g_{\rm re}\pi^2}\right)^{\frac{1}{4}}(\rho_{\rm end})^{\frac{1}{1-3w_\phi}}(\rho_\chi^{\rm com})^{-\frac{3(1+w_\phi)}{4(1-3w_\phi)}} \end{aligned} \tag{6.105}$$

For $\xi = 3/16$, we get $T_{\rm re} = (3.8\times10^{-5},\ 8.96\times10^2)$GeV for $w_\phi = (3/5,\ 9/11)$ respectively.

### 6.6.3 Reheating parameters $N_{\rm re}, T_{\rm re}$ for $\xi > 3/16$

For this case, there exists a critical coupling strength $\xi_{\rm cri}(w_\phi) = \frac{(9w_\phi+7)(15w_\phi+1)}{48(3w_\phi-1)}$, which demarcates two regions with a junction at $\xi = \xi_{\rm cri}$. For $w_\phi > 1/3$, the energy-density spectra, $k^4|\beta_k|^2$ becomes perfectly scale-invariant at this critical value. For any $\xi < \xi_{\rm cri}$, the energy spectra remain blue-tilted and turn into red-tilted (or IR divergent) in the regime $\xi > \xi_{\rm cri}$ (see Fig.(6.3)). In this range, we shall compute the reheating parameters in three different regimes.

#### 6.6.3.1 For $3/16 < \xi < \xi_{\rm cri}$ :

For $3/16 < \xi < \xi_{\rm cri}$, the energy spectrum behaves as $k^4|\beta_k|^2 \propto (k/k_{\rm end})^{4-2\nu_2}$, and the comoving energy density is calculated to be

$$\rho_\chi^{\rm com} \approx \frac{\mathcal{A}_3 H_{\rm end}^4}{4\pi^2\,(2-\nu_2)} \tag{6.106}$$

where

$$\mathcal{A}_3 \approx \left(\frac{\Gamma(\nu_2)\exp(-\pi\tilde{\nu}_1/2)}{4(3\mu-1)^{-1/2}}\left(\frac{2}{3\mu-1}\right)^{\nu_2}\left|\frac{(\pi+i\cosh(\pi\tilde{\nu}_1)\Gamma(1-i\tilde{\nu}_1)\Gamma(i\tilde{\nu}_1))}{\pi\Gamma(i\tilde{\nu}_1)}\right|\right)^2. \tag{6.107}$$

The corresponding reheating parameters become,

$$\begin{aligned} N_{\rm re} &= \frac{1}{(1-3w_\phi)}\ln\left(\frac{\rho_\chi^{\rm com}}{\rho_{\rm end}}\right), \\ T_{\rm re} &= \left(\frac{30}{g_{\rm re}\pi^2}\right)^{\frac{1}{4}}\left(\rho_{\rm end}\right)^{\frac{1}{1-3w_\phi}}\left(\rho_\chi^{\rm com}\right)^{-\frac{3(1+w_\phi)}{4(1-3w_\phi)}}. \end{aligned} \tag{6.108}$$

For example, for $w_\phi = 3/5$, we find $T_{\rm re} = (9.94\times10^{-3},\ 5.48\times10^{-2})$ GeV, and for $w_\phi = 9/11$, we find $T_{\rm re} = (9.13\times10^{4},\ 5.66\times10^{5})$ GeV for $\xi = (2, 2.5)$ respectively. Likewise, growing instability with growing $\xi$ causes the increase in temperature in this range of coupling strength also.

#### 6.6.3.2 For $\xi = \xi_{\rm cri}$ :

At this junction point, total energy density is computed as

$$\rho_\chi^{\rm com} = \frac{\mathcal{A}_3 H_{\rm end}^4}{2\pi^2}\ln\left(\frac{k_{\rm end}}{k_{\rm re}}\right) \simeq \frac{\mathcal{A}_3 H_{\rm end}^4(1+3w_\phi)}{4\pi^2}N_{\rm re}. \tag{6.109}$$

Subject to this total energy density, we get the following equation of $N_{\rm re}$,

$$\left(\exp\left(N_{\rm re}(1-3w_\phi)\right) - \frac{\mathcal{A}_3 H_{\rm end}^4(1+3w_\phi)}{4\pi^2\rho_{\rm end}}N_{\rm re}\right) = 0. \tag{6.110}$$

We numerically solve the above equation to find the root $N_{\rm re}$ for a given $w_\phi$. Using Eq.(6.109) and the solution of the Eq.(6.110), reheating temperature is calculated to be

$$T_{\rm re} = \left(\frac{30}{g_{\rm re}\pi^2}\right)^{\frac{1}{4}} \left(\rho_\chi^{\rm com}\right)^{\frac{1}{4}} \exp(-N_{\rm re}). \tag{6.111}$$

We calculate this critical coupling $\xi_{\rm cri} \simeq (3.23,\ 2.73)$ for $w_\phi = (3/5,\ 9/11)$ respectively. At this critical point, we find the temperatures $T_{\rm re} = (13.83,\ 3.14\times10^6)$ GeV for the two given EoS.

#### 6.6.3.3 For $\xi > \xi_{\rm cri}$ :

After crossing the critical coupling or the junction $\xi_{\rm cri}$, the energy spectrum turns out to be red-tilted. The larger the $\xi$, the heavier the red-tilting of the energy spectrum. Therefore, large scales are now dominantly contributing to the total energy density of the system. Total energy density is now computed as

$$\rho_\chi^{\rm com} = \frac{\mathcal{A}_3 H_{\rm end}^4}{4\pi^2(\nu_2-2)}\left(\frac{k_{\rm end}}{k_{\rm re}}\right)^{2\nu_2-4} \simeq \frac{\mathcal{A}_3 H_{\rm end}^4}{4\pi^2(\nu_2-2)}\exp\Big((1+3w_\phi)(\nu_2-2)N_{\rm re}\Big) \tag{6.112}$$

For this energy density, the reheating e-folding number is calculated to be

$$N_{\rm re} = \frac{\ln\left((4\pi^2(\nu_2-2)\rho_{\rm end})/\mathcal{A}_3 H_{\rm end}^4\right)}{\nu_2(1+3w_\phi)-3(1+w_\phi)} \tag{6.113}$$

The reheating temperature associated with the energy density (6.112) and e-folding number (6.113) now becomes

$$T_{\rm re} = \left(\frac{30}{g_{\rm re}\pi^2}\right)^{\frac{1}{4}} \left(\frac{\mathcal{A}_3 H_{\rm end}^4}{4\pi^2(\nu_2-2)}\right)^{\frac{1}{4}} \left(\frac{4\pi^2\rho_{\rm end}(\nu_2-2)}{\mathcal{A}_3 H_{\rm end}^4}\right)^{\frac{(1+3w_\phi)(\nu_2-2)-4}{4\left(\nu_2(1+3w_\phi)-3(1+w_\phi)\right)}} \tag{6.114}$$

In this red-tilted regime of the energy spectrum(IR divergent energy spectrum), we get a high reheating temperature. With the increase of the coupling $\xi$, the reheating temperature rises rapidly and reaches the maximum limit($T_{\rm re} \sim 10^{15}$GeV) for a coupling strength $\xi \lesssim 50$ as obvious in Fig.(6.12). For example, for $w_\phi = 3/5$, we find $T_{\rm re} = (3.24\times10^3,\ 4.5\times10^6)$ GeV, and for $w_\phi = 9/11$, we get $T_{\rm re} = (3.36\times10^9,\ 4.5\times10^{10})$ for $\xi = (3.5, 4)$ respectively. Thus, using all these expressions of $T_{\rm re}$, we study the variation of reheating temperature with respect to the non-minimal coupling strength in this *infrared gravitational reheating scenario*.

To this end, we would like to point out a subtle aspect regarding the consideration of the time-averaged EoS $w_\phi = (n-1)/(n+1)$, specifically the omission of post-inflationary inflaton oscillations when computing the fluctuation spectra. In this work, we propose a special kind of reheating scenario, solely facilitated by the large-scale fluctuations, $k << k_{\rm end}$. These long-wavelength modes are subject to strong post-inflationary super-horizon instability

beyond a certain coupling strength. Upon horizon reentry at some later time during reheating, they contribute to the total radiation energy density. These scales, having very long wavelengths, cannot sense the small-scale background oscillations after horizon reentry, as the oscillatory feature gradually becomes insignificant at the late stage of reheating. Furthermore, with the increase of the potential exponent $n$, the oscillation time-period of the background also increases, $T \propto \omega^{-1} \propto m_\phi^{-1}$(see Eq.(2.69)). So, the background oscillation feature becomes less prominent for higher EoS. Our study reveals that even for a small nonminimal coupling, much smaller than that required for the small-scale resonance instability($\xi > 50$) as shown in [245], the substantial growth of these large scales due to super-horizon *tachyonic instability* can successfully reheat the universe. In the subsequent discussion, we shall constrain this reheating dynamics by the CMB scale GW and isocurvature bounds within a very narrow range of $\xi$ values. The large CMB scale will also remain unaffected by the background oscillation. Therefore, for these very long-wavelength classical modes, the consideration of the time-averaged EoS is justified.

## 6.7 Comparing perturbative and infrared reheating

In the previous section, we have calculated the reheating parameters $T_{\rm re}$ and $N_{\rm re}$ taking into account the contribution from the infrared modes which are produced during inflation. However, the usual approach to reheating is to simultaneously solve the Boltzmann equations for decaying inflaton and radiation. Such an approach naturally deals with the excitation of sub-Hubble modes [36] and their subsequent thermalization at the end of reheating. In this section, we shall discuss the growth of sub-horizon modes using the standard perturbative technique, i.e., the Boltzmann approach, and compare its contribution with that of the super-horizon components discussed in the previous section. In order to do this, we need to track the evolution of the inflaton ($\rho_\phi$) and the radiation ($\rho_\chi$) energy densities during reheating, we solve the following set of coupled Boltzmann equations

$$\dot{\rho_\phi} + 3H(1+w_\phi)\rho_\phi = -Q, \quad ; \quad \dot{\rho_\chi} + 4H\rho_\chi = Q, \quad ; \quad H^2 = \frac{\rho_\phi + \rho_\chi}{3\,M_{\rm pl}^2}\,, \tag{6.115}$$

where $Q$ is the production rate, the amount of energy transferred per unit time, and the unit volume. Since the inflaton primarily governs the total energy density during the reheating period, the expansion rate associated with the term $3H\,(1+w_\phi)\,\rho_\phi$ significantly surpasses the reaction rate $Q$. As a result, the inflaton part of Eq.(6.115) can be solved analytically by disregarding the right-hand side, leading to the solution,

$$\rho_\phi(a) \simeq \rho_{\rm end}\left(\frac{a}{a_{\rm end}}\right)^{-3(1+w_\phi)},$$

with the corresponding Hubble rate

$$\bar{H}(a) \simeq H_{\rm end}\left(\frac{a}{a_{\rm end}}\right)^{-\frac{3}{2}(1+w_\phi)}.$$

In the present context, we consider a non-minimally coupled scalar field ($\chi$) as radiation discussed earlier. The total production rate must be the sum of the minimal and the non-minimal gravitational interactions. To this end, *it is important to note that for a non-minimally coupled theory, frame ambiguity exists in the computation of the perturbative production rate, and this is what we analyze now in the following discussion.*

By utilizing the conformal transformation, the production rate of massless non-minimally coupled scalar field $\chi$ has already been computed [58, 333] in the Einstein frame and studied their implication in the reheating dynamics. However, note that in the super-horizon analysis as discussed in the previous section, one usually solves for the $\chi$ field in the Jordan frame. Hence, in order to compare with the results we obtained for the infrared modes, we shall compute the scalar field production rate in the Jordan frame. For completeness, we also analyze the difference in predictions for both frames. Any dissimilarity in the outcomes will indicate the fundamental difference in these frame transformations. The total production rate expressions in two frames (see the detailed derivation in the Appendix 7.2) are given by,

$$Q \simeq \frac{\rho_\phi^2\, m_\phi}{8\,\pi\, M_{\rm pl}^4}\,\mathcal{S}_{\rm n}^{\xi}\,, \tag{6.116}$$

where given the inflaton potential Eq.(2.75), $\mathcal{S}_{\rm n}^{\xi}$ are time independent constant, and the expressions are,

$$\mathcal{S}_{\rm n}^{\xi} = \begin{cases} \left((1-6\xi)^2 \sum_{\nu=1}^{\infty} \gamma\,\nu\,|\mathcal{P}_\nu^{2n}|^2\right) & \text{Jordon frame} \\ \underbrace{\left(\sum_{\nu=1}^{\infty} \gamma\,\nu\,|\mathcal{P}_\nu^{2n}|^2\right)}_{\text{for minimal case}} + \underbrace{\left(\xi^2 \sum_{\nu=1}^{\infty} \gamma\,\nu \left|2\,\mathcal{P}_\nu^{2n} + \frac{2n\,(2n-1)\,\gamma^2\,\nu^2}{2}|\mathcal{P}_\nu|^2\right|^2\right)}_{\text{additional term for non-minimal case}} & \text{Einstein frame} \end{cases} \tag{6.117}$$

It is interesting to note the important difference in decay rates of the inflaton, or in other words, the production rate of the conformally coupled $\chi$ field in both frames. The noticeable difference can be observed at $\xi = 1/6$. The Jordan frame production rate vanishes at this special point, as expected due to the conformal property of the massless scalar field. On the other hand, in Einstein's frame, such a property ceases to exist, which is also reflected in the above formula, yielding non-vanishing production.

Utilizing Eq.(6.7) along with the interaction rate Eqs.(6.116) and (6.117) in Eq.(6.115), one can obtain the radiation energy density as follows

$$\rho_\chi(a) \simeq \mathcal{S}_{\rm n}^{\xi} \frac{9\,H_{\rm end}^3\, m_\phi^{\rm end}}{4\,\pi\,(1+15\,w_\phi)} \left(\frac{a_{\rm end}}{a}\right)^4 \left[1 - \left(\frac{a}{a_{\rm end}}\right)^{-\frac{1+15w_\phi}{2}}\right], \tag{6.118}$$

where $m_\phi^{\rm end}$ is the inflaton mass at the end of inflation. In the presence of the non-minimal coupling, therefore, the reheating temperature $T_{\rm re}$ and reheating e-folding number $N_{\rm re}$ can

be expressed for any arbitrary value of the $\xi$ as,

$$T_{\rm re} \simeq 0.5 M_{\rm pl} \left(\frac{3\,\mathcal{S}_{\rm n}^{\xi}}{4\pi(1+15w_\phi)}\frac{m_\phi^{\rm end}}{M_{\rm pl}}\right)^{\frac{3(1+w_\phi)}{4(3w_\phi-1)}} \left(\frac{H_{\rm end}}{M_{\rm pl}}\right)^{\frac{9w_\phi+1}{4(3w_\phi-1)}} \tag{6.119}$$

$$N_{\rm re} = \frac{1}{(3\,w_\phi-1)} \ln\left[\left(\frac{4\,\pi\,(1+15\,w_\phi)}{3\,\mathcal{S}_{\rm n}^{\xi}}\right)\left(\frac{M_{\rm pl}}{H_{\rm end}}\right)\left(\frac{M_{\rm pl}}{m_\phi^{\rm end}}\right)\right] \tag{6.120}$$

For the varying non-minimal coupling associated function $\mathcal{S}_{\rm n}^{\xi}$ in two frames, we obtain different predictions of reheating parameters, specifically around the conformality, $\xi \sim 1/6$. As pointed out earlier, since $\mathcal{S}_{\rm n}^{\xi} \propto (1-6\xi)$ in the Jordan frame, the radiation temperature clearly vanishes, as there is no radiation production as opposed to the Einstein frame temperature. This can also be observed from our full numerical computation depicted in Fig.(6.17) in Addenda 6.12. In Fig.(6.17), it is seen that in the higher non-minimal coupling regime, $\xi > 1$, pertinent to the present analysis, frame ambiguity is gone. Therefore, in the subsequent discussion, we shall stick to the Jordan frame while comparing the perturbative and non-perturbative reheating parameter predictions.

### 6.7.1 Comparing perturbative and non-perturbative approaches in infrared gravitational production

Non-minimal coupling produces large infrared fluctuations via tachyonic instability. After the end of inflation, on the other hand, the perturbative effect (effect of small scales) on reheating cannot be ignored. To compare the contribution of these two production processes, we further realized that it is appropriate to consider the Jordan frame. Hence, in this frame, assuming both the contributions as independent in Fig.(6.12), we have shown how non-perturbative infrared predictions of reheating temperature surpass that of the perturbative prediction beyond a certain coupling strength. These takeover happen around $\xi \approx (4,\ 2.9,\ 2.4,\ 2.2)$ for $w_\phi = (1/2,\ 3/5,\ 5/7,\ 9/11)$, respectively(see also Table 6.2 showing the reheating temperature predictions for three EoS). Therefore, the usual perturbative approach as discussed in [58, 333] can be observed to greatly underestimate the value of reheating temperature as depicted in dotted lines as compared to the infrared contribution depicted in solid lines in Fig.(6.12). For example, it requires as large as $\xi \simeq 10^5$ to reach the maximum reheating temperature $T_{\rm max} \simeq 10^{15}$ GeV in the perturbative approach as indicated by the point where all the dashed-colored lines meet in Fig.(6.12). On the contrary, a value as small as $\xi \lesssim 50$ turned out to be sufficient to obtain maximum reheating temperature from the super-horizon modes, as can be seen from the converging solid color lines.

To this end, let us briefly state the peculiar feature (dominance of perturbative prediction over the non-perturbative) observed in Fig.(6.12), particularly in the coupling range $1/6 < \xi < \xi_{\rm cri}$. As stated earlier, infrared instability is expected to be suppressed around the conformal value $\xi \gtrsim 1/6$, and becomes stronger only for larger values of $\xi \gtrsim \xi_{\rm cri}$, beyond

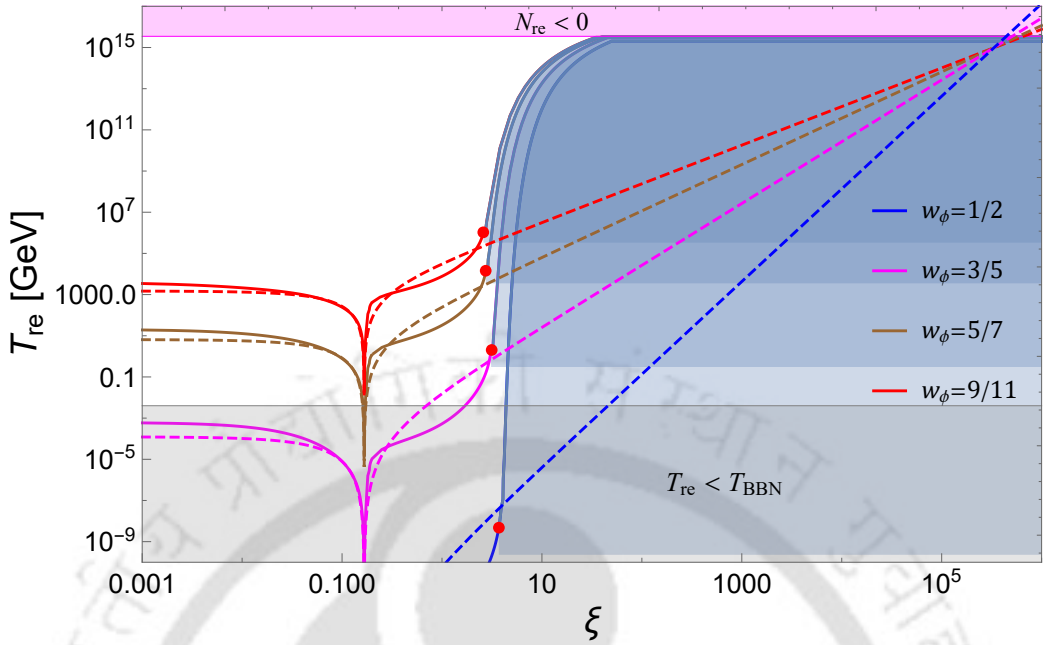


FIGURE 6.12: *Figure represents a comparison of $T_{re}$ vs $\xi$ variation for different EoS between perturbative(Jordan frame) and non-perturbative analysis. Solid lines correspond to the non-perturbative or Bogoliubov predictions, and dashed lines correspond to the perturbative Boltzmann predictions in the Jordan frame. Red dots on each color line indicate the maximum value of the coupling strength, $\xi_{max}$, corresponding to each EoS consistent with large-scale observational bounds ( gravitational wave and isocurvature), and the overlapping shaded region is ruled out by the latest CMB scale tensor-to-scalar ratio and isocurvature bounds for all four EoS. For a given EoS, any $\xi$, exceeding the red dot is disallowed by observation, and its associated $T_{re}$ lies inside the shaded region. There are four demarcating lines inside the shaded region. From the top, the first one corresponds to $w_\phi = 9/11$, the second one to $w_\phi = 5/7$, the third one to $w_\phi = 3/5$, and the fourth one to $w_\phi = 1/2$.*

which the energy spectrum becomes red-tilted. The moment the spectrum becomes red tilted, one naturally expects the total energy budget to be dominated by the super-horizon mode. This is when all the solid curves corresponding to the contribution from the infrared modes start to show an upward trend with increasing $\xi > \xi_{cri}$ becoming stiff, surpassing the contribution from that of the perturbative sub-horizon contribution.

Our analysis so far, therefore, indicates that by increasing the $\xi$ value, we can increase the radiation temperature as high as $10^{15}$ GeV, and the infrared modes solely contribute to that high reheating temperature. Note that the origin of such a high temperature is due to the infrared divergent energy spectrum, particularly for $w_\phi > 1/3$. However, in the subsequent sections, we shall see that from the observational perspective, this IR divergent energy spectrum, particularly at the large (CMB) scales, often becomes problematic and is tightly constrained by observational bounds, like the tensor-to-scalar ratio and the

Table 6.2: *Variation of reheating temperature with EoS and non-minimal coupling strength for $\alpha = 1$. Here we have given the perturbative and non-perturbative predictions for comparison. The Jordan(Einstein) frame predictions are given without and with braces in the perturbative analysis.*

| EoS ($w_\phi$) | Non-perturbative | | Perturbative | |
|---|---|---|---|---|
| | $\xi$ | $T_{\rm re}$ (GeV) | $\xi$ | $T_{\rm re}$ (GeV) |
| 3/5 | 0 | $6.16 \times 10^{-4}$ | 0 | $6 \times 10^{-4}\,(6 \times 10^{-4})$ |
| | 3/16 | $3.8 \times 10^{-5}$ | 3/16 | $9.38 \times 10^{-6}\,(2.0 \times 10^{-3})$ |
| | 1 | $5.3 \times 10^{-4}$ | 1 | $7.5 \times 10^{-2}\,(1.3 \times 10^{-1})$ |
| | $\xi_{\rm max} = 2.95$ | 3.3 | $\xi_{\rm max} = 2.95$ | 2.8 (2.7) |
| | $\xi_{\rm cri}(3/5)$ | 13.84 | $\xi_{\rm cri}(3/5)$ | 3.73 (3.0) |
| 5/7 | 0 | 20.35 | 0 | 6.5 (6.5) |
| | 3/16 | 3.14 | 3/16 | $2.87 \times 10^{-1}$ (17) |
| | 1 | 32.4 | 1 | $2.43 \times 10^{2}\,(4.0 \times 10^{2})$ |
| | $\xi_{\rm max} = 2.63$ | $5.63 \times 10^{3}$ | $\xi_{\rm max} = 2.63$ | $2.78 \times 10^{3}\,(2.6 \times 10^{3})$ |
| | $\xi_{\rm cri}(5/7)$ | $4.93 \times 10^{4}$ | $\xi_{\rm cri}(5/7)$ | $3.43 \times 10^{3}\,(3.0 \times 10^{3})$ |
| 9/11 | 0 | $3.83 \times 10^{3}$ | 0 | $2.0 \times 10^{3}$ $(2.0 \times 10^{3})$ |
| | 3/16 | $8.96 \times 10^{2}$ | 3/16 | $1.48 \times 10^{2}$ $(3.0 \times 10^{3})$ |
| | 1 | $7.68 \times 10^{3}$ | 1 | $4.09 \times 10^{4}\,(4.0 \times 10^{4})$ |
| | $\xi_{\rm max} = 2.51$ | $6 \times 10^{5}$ | $\xi_{\rm max} = 2.51$ | $2.84 \times 10^{5}\,(10^{5})$ |
| | $\xi_{\rm cri}(9/11)$ | $3.14 \times 10^{6}$ | $\xi_{\rm cri}(9/11)$ | $3.37 \times 10^{5}\,(2.0 \times 10^{5})$ |

isocurvature constraint. We now derive the constraints on $\xi$ in light of the latest *Planck*, ACT, DESI, and BICEP/Keck combined (P+ACT+LB+BK18) bound on tensor-to-scalar ratio and isocurvature at the CMB scale provided in [43, 44]. The constraints on $\xi$ will, anyway, further constrain the present infrared reheating dynamics. This is the subject of our subsequent discussion.

## 6.8 Constraints from Gravitational Wave and Isocurvature Perturbation

Gravitational waves (GWs) probe very deep in the early universe due to their extremely weak coupling with matter fields. Therefore, any early universe model that can generate GW can, in principle, be constrained through direct or indirect observation.

### 6.8.1 Constraining the infrared reheating dynamics through tensor-to-scalar ratio $r_{0.05}$:

For stiff EoS $w_\phi > 1/3$, a stronger IR instability (tachyonic instability) of the scalar fluctuations generates larger tensor fluctuations even at the Cosmic Microwave Background(CMB) scale beyond a certain threshold of $\xi$. In this discussion, we shall closely follow the GW analysis from the first part of this chapter(see Section(6.2)) to write down the expression of the secondary tensor power spectrum being sourced by these scalar fluctuations. Following the expression of the tensor power spectrum (6.63), and assuming that maximum contributions originate from secondary sources (i.e., the scalar fields), we obtain the tensor-to-scalar ratio at the CMB pivot scale as

$$r_{0.05} \simeq \frac{2\mathcal{A}_3^2 H_{\rm end}^4}{\pi^4 M_{\rm pl}^4 A_s}\left\{\frac{1}{2l(\delta-2)}+\frac{1}{4l(1-l)-2l\delta}\right\}^2 \frac{8(1+2\nu_2)}{15(3-\nu_2)(4\nu_2-5)} \times e^{\left(N_{\rm re}(6w_\phi-2)\right)}\left(\frac{k_*}{k_{\rm end}}\right)^{4(2-\nu_2)} \leq 0.038 \tag{6.121}$$

where the above parameters are expressed in terms of $w_\phi$ and $\xi$ as $l = 3(w_\phi - 1)/2(1 + 3w_\phi)$, $\delta = 4/(1+3w_\phi)$. The ratio $(k_{\rm end}/k_{\rm re})$ is written as $(k_{\rm end}/k_{\rm re}) = \exp\left(N_{\rm re}(1+3w_\phi)/2\right)$. Here "$k_*$" is the pivot scale or CMB scale, $(k_*/a_0) = 0.05{\rm Mpc}^{-1}$ and $a_0$ is the present scale factor. According to the combined(P+ACT+LB+BK18) data set, there is no significant improvement in the tensor-to-scalar ratio bound, $r_{0.05} < 0.038$ at the 95% C.L [43]. This slight modification of the maximum $r_{0.05}$ bound will not relax the upper limit on $\xi$ much. In the background of the present reheating scenario, from the above inequality (6.121), for a given reheating EoS $w_\phi > 1/3$, we obtain a maximum value of coupling strength $\xi_{\rm max}$ to prevent the overproduction of tensor fluctuations at the CMB scale. Any coupling strength $\xi > \xi_{\rm max}$, represented by the red dots in the Fig.(6.12), is discarded by the current tensor-to-scalar ratio bound at the CMB scale, which is depicted by the blue shaded region. This upper boundary of $\xi$ in turn sets the maximum allowed reheating temperature for a given EoS in the present reheating scenario.

### 6.8.2 Constraints from isocurvature power spectrum $\mathcal{P}_{\mathcal{S}}(k_*)$ :

As we have observed, massless scalar long-wavelength modes experience substantial post-inflationary growth, being driven by the super-horizon instability induced by the non-minimal gravity coupling as previously illustrated. This large-scale instability inevitably generates significant isocurvature fluctuations at the CMB scale. The current constraint on the isocurvature power spectrum by *Planck* 2018 is defined to be $\beta_{\rm iso} \equiv \mathcal{P}_{\mathcal{S}}(k_*)/\left(\mathcal{P}_{\mathcal{R}}(k_*) + \mathcal{P}_{\mathcal{S}}(k_*)\right) \lesssim 0.038$ at the 95% C.L for the pivot scale or CMB scale $k_*$[7]. The pivot scale amplitude of curvature power spectrum $\mathcal{P}_{\mathcal{R}}(k_*) = 2.1 \times 10^{-9}$ gives the upper bound of the amplitude of isocurvature power spectrum at CMB scale $\mathcal{P}_{\mathcal{S}}(k_*) \lesssim 8.3 \times 10^{-11}$[7, 8]. This large-scale upper bound of the isocurvature power spectrum constrains the reheating dynamics further. The second-order isocurvature power spectrum is evaluated by using the following expression

as [69, 75, 244, 245, 324–326]

$$\mathcal{P}_{\mathcal{S}}(k) = \frac{1}{\rho_\chi^2}\frac{k^3}{2\pi^2}\int d^3\vec{x}\langle\delta\rho_\chi(\vec{x})\delta\rho_\chi(0)\rangle e^{-i\vec{k}.\vec{x}} = \frac{k^3}{(2\pi)^5\rho_\chi^2 a^8}\int d^3\vec{p}\, P_X\left(p, |\vec{p}-\vec{k}|\right) \tag{6.122}$$

where $\rho_\chi$ and $\delta\rho_\chi$ are energy-density and its fluctuation of the field having finite mass $m_\chi$, and the functional integrand for non-zero mass is given by

$$P_X(p,q) = |X_p'|^2|X_q'|^2 + a^4 m_\chi^4|X_p|^2|X_q|^2 + a^2 m_\chi^2\left[(X_p X_p'^*)(X_q X_q'^*) + h.c\right]. \tag{6.123}$$

As here we are dealing with purely massless fields, only the non-vanishing contribution will come from the first term of the expression of $P_X(p,q)$ above, and similarly, $\rho_\chi$ is the energy-density of the massless scalar. To evaluate this integral, we shall exploit the late-time post-inflationary solutions of the rescaled field mode $X_k$ in different ranges of $\xi$ values as found in [246]. Further, let us point out that although we have a strong large-scale fluctuation, it should not influence the total curvature power spectrum. We find that a fluctuation without its associated homogeneous background will not contribute to the total curvature perturbation amplitude; hence, these large-scale fluctuations solely contribute to the isocurvature mode. Since this is not obvious, we provide a detailed calculation on this issue in Appendix 7.2.

For $w_\phi > 1/3$ and $\xi > 3/16$, evaluating the integral (6.122), we find the expression of the large-scale isocurvature power spectrum for massless fluctuation as follows:

$$\mathcal{P}_{\mathcal{S}}(k) = \frac{\mathcal{A}_3^2 k_{\rm end}^8 \mathcal{I}_2}{(2\pi)^4(3-2\nu_2)\rho_\chi^2 a^8}\left(\frac{k}{k_{\rm end}}\right)^{(8-4\nu_2)}. \tag{6.124}$$

The detailed computation of the above Eq.(6.124) with the functional form of $\mathcal{I}_2$ is found in Addeda 6.11. Substituting the expressions (6.106) and (6.112) into (6.124) we compute the expressions of the isocurvature power spectrum in the large scale($k << k_{\rm end}$) as follows:

$$\mathcal{P}_{\mathcal{S}}(k) = \left(\frac{k}{k_{\rm end}}\right)^{(8-4\nu_2)}\left(\frac{2-\nu_2}{\sqrt{3-2\nu_2}}\right)^2 \mathcal{I}_2 \times \begin{cases} 1 & \text{for } 3/16 < \xi < \xi_{\rm cri} \\ e^{(1+3w_\phi)(4-2\nu_2)N_{\rm re}} & \text{for } \xi > \xi_{\rm cri} \end{cases}. \tag{6.125}$$

Interestingly, we have obtained the same spectral index $(8-4\nu_2)$ as it is found in tensor power spectrum for $k << k_{\rm re}$ in Eq. (6.63). This confirms a behavioral similarity between isocurvature and tensor power spectrum in the long-wavelength regime ($k << k_{\rm re}$) for a given $w_\phi$ and coupling strength $\xi$. The CMB constraint on isocurvature spectrum $\mathcal{P}_{\mathcal{S}}(k_*) < 8.3\times10^{-11}$ immediately gives an another upper bound on $\xi_{\rm max}$. Our numerical computation shows that both the upper bounds from tensor to scalar ratio, derived from Eq.(6.121), and isocurvature constraints, derived from Eq.(6.125), are approximately the same clearly depicted in Fig.(6.13). The reason behind this can be explained through the relation between isocurvature and tensor power spectrum at the CMB scale. Using the inequality $r_{0.05} = \mathcal{P}_{\rm T}(k_*)/\mathcal{P}_{\mathcal{R}}(k_*) \lesssim 0.038$, we can express $\mathcal{P}_{\mathcal{R}}(k_*) = \mathcal{P}_{\rm T}(k_*)/\left(r_{0.05} \lesssim 0.038\right)$. Substituting this

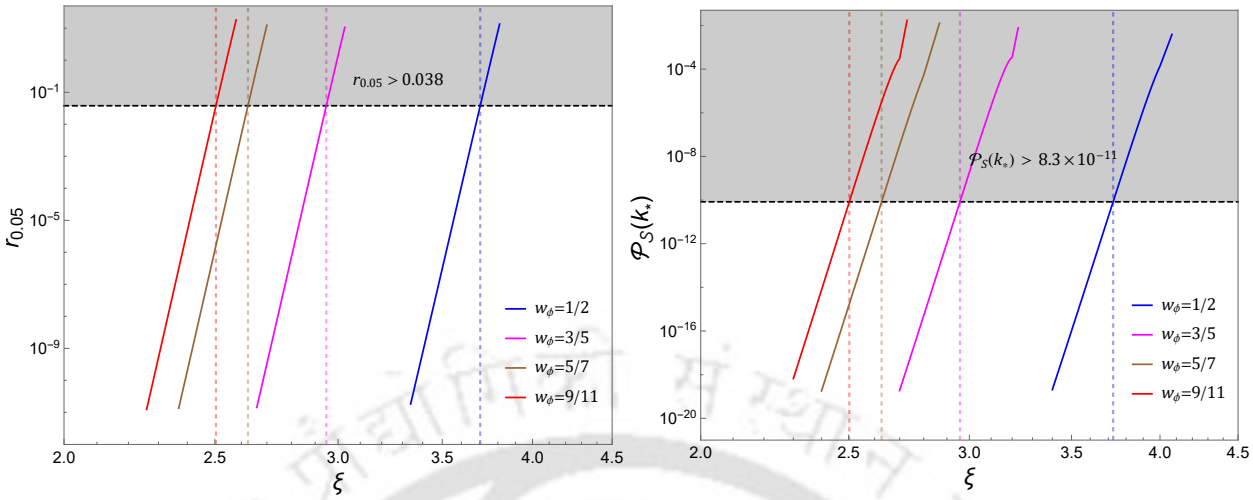


FIGURE 6.13: ***Left Panel***: *Figure represents constraints on $\xi$ for different post-inflationary EoS. The horizontal black dashed line indicates the maximum bound on $r$ at the CMB scale, $r_{0.05} = 0.038$, and the vertical colored dashed lines show the maximum allowed value of the coupling $\xi_{\rm max}$ for different EoS subject to this bound. For a given EoS, $r_{0.05}$ for any $\xi > \xi_{\rm max}$(shaded region) is hence disallowed by the current bound.* ***Right panel***: *Figure represents the constraints on $\xi$ from isocurvature power spectrum for different post-inflationary EoS. The horizontal black dashed line indicates the current bound on CMB scale isocurvature amplitude $\mathcal{P}_{\mathcal{S}}(k_*) = 8.3 \times 10^{-11}$, and the vertical colored dashed lines show the maximum allowed value of $\xi$ for different EoS. For a given EoS, $\mathcal{P}_{\mathcal{S}}(k_*)$ for any $\xi > \xi_{\rm max}$(shaded region) is hence disallowed by the current isocurvature bound.*

scalar power spectrum amplitude into $\beta_{\rm iso}$, the relation $\beta_{\rm iso} = \mathcal{P}_{\mathcal{S}}(k_*)/\left(\mathcal{P}_{\mathcal{R}}(k_*) + \mathcal{P}_{\mathcal{S}}(k_*)\right) \sim 0.038$ can be translated into the approximate relation $\mathcal{P}_{\mathcal{S}}(k_*) \approx 1.04\mathcal{P}_{\rm T}(k_*)$. This relation suggests that these two bounds predict more or less the same maximum bound $\xi_{\rm max}$ for any particular reheating EoS.

Based on these two large-scale observational bounds, we get a very narrow allowed regime in the reheating parameter space, where the non-perturbative prediction surpasses the perturbative prediction, as obvious in Fig.(6.12). The red dots in Fig.(6.12) indicate the $\xi_{\rm max}$ values for four different EoS respecting the relevant observational bounds as already discussed in this Section. For example, we get the narrow ranges, $2.9 \lesssim \xi \lesssim 2.95$, $2.4 \lesssim \xi \lesssim 2.63$, and $2.2 \lesssim \xi \lesssim 2.51$ for $w_\phi = 3/5,\ 5/7,\ 9/11$ respectively, where the non-perturbative prediction slightly overtakes the perturbative one. It is in this coupling range, the infrared fluctuations are dominated, and hence one should expect the production of gravitational waves, which can be relevant for the existing and upcoming gravitational waves experiments.

## 6.9 GW signature of infrared gravitational reheating

In light of the current CMB scale tensor-to-scalar ratio and isocurvature bound as discussed above, we get a very narrow range of allowed coupling strength for any EoS $w_\phi > 1/3$. And each $w_\phi$ has a maximum limit of $\xi$ consistent with the current bounds of $\mathcal{P}_{\mathcal{S}}(k_*)$ and $r_{0.05} \lesssim 0.038$ as discussed. In this section, we study the spectral nature of the total gravitational wave spectrum, combining the primary and secondary parts in all frequency scales.

**Behavior of primary gravitational wave (PGW) spectrum today :** The PGW spectrum is the one that originates from quantum fluctuation during inflation. The present-day PGW spectrum are read as [131, 133, 246, 334]:

$$\Omega_{\rm gw}^{\rm pri}(k)h^2 \simeq \Omega_R h^2 \left(\frac{H_{\rm end}^2}{12\pi^2 M_{\rm pl}^2}\right) \times \begin{cases} 1 & \text{for} \quad k < k_{\rm re} \\ \frac{(1+3w_\phi)^{(2-n_w)}}{\pi}\Gamma^2\left(\frac{5+3w_\phi}{2+6w_\phi}\right)\left(\frac{k}{k_{\rm re}}\right)^{n_w} & \text{for} \quad k_{\rm re} < k < k_{\rm end} \end{cases} . \tag{6.126}$$

where the spectral index "$n_w$" is defined as $n_w = 2(3w_\phi - 1)/(1+3w_\phi)$, and $\Omega_{\rm R}h^2 \simeq 4.3\times10^{-5}$ denotes the dimensionless energy density of radiation at the current epoch[8].

**Behavior of scalar induced secondary gravitational wave(SGW) spectrum today :**

Likewise, the primary spectra, we can also define the scalar field-induced secondary spectra for today in the regime $\xi > 3/16$ as illustrated in (6.127)

$$\begin{aligned} \Omega_{\rm gw}^{\rm sec}(k)h^2 =& \frac{(1+k^2/k_{\rm re}^2)\,\mathcal{P}_{\rm T}^{\rm sec}(k,\eta_{\rm re})}{24} \simeq \Omega_R h^2 \frac{\mathcal{A}_3^2 H_{\rm end}^4}{12\pi^4 M_{\rm pl}^4} \frac{8(1+2\nu_2)}{15(3-\nu_2)(4\nu_2-5)} \left(\frac{k_{\rm end}}{k_{\rm re}}\right)^{4-2\delta} \\ & \times \begin{cases} \left(\frac{1}{2l(\delta-2)} + \frac{1}{4l(1-l)-2l\delta}\right)^2 \left(\frac{k}{k_{\rm end}}\right)^{8-4\nu_2} & \text{for} \quad k < k_{\rm re} \\ \frac{2^{1-2l-2\delta}\pi\Gamma^2(1-l)\Gamma^2(l)}{\Gamma^2(l+\frac{\delta}{2})\Gamma^2\left(\frac{\delta}{2}\right)} \left(\frac{k_{\rm end}}{k_{\rm re}}\right)^{\delta-2} \left(\frac{k}{k_{\rm end}}\right)^{6+\delta-4\nu_2} & \text{for} \quad k_{\rm re} < k < k_{\rm end} \end{cases} \end{aligned} \tag{6.127}$$

where the indices $l,\ \delta$ are functions of $w_\phi$ as defined earlier.

Combining these two spectra, we define the total gravitational wave spectrum for today, $\Omega_{\rm gw}h^2 = (\Omega_{\rm gw}^{\rm pri}(k)h^2 + \Omega_{\rm gw}^{\rm sec}(k)h^2)$, whose spectral nature is depicted in Fig.(6.14) in the present reheating background, and they are consistent with the current observational bounds at CMB scales discussed in the sections above. In addition, we also take into account $\Delta N_{\rm eff}$ bound on GW energy density $\Omega_{\rm gw}h^2 \lesssim 1.7\times10^{-6}$ [331] where generically high-frequency modes contribute. In Fig.(6.14), in all the plots, one common feature we notice is that at low and intermediate frequency ranges, the secondary strength significantly surpasses the primary one beyond a certain coupling for a given $w_\phi$. In this coupling regime, the total

GW spectrum assumes a broken power law form with three different spectral indices as

$$\Omega_{\rm gw}(k)h^2 \propto \begin{cases} k^{8-4\nu_2} & \text{for } k < k_{\rm re} \\ k^{6+\delta-4\nu_2} & \text{for } k_{\rm re} < k < k_{\rm SB} \\ k^{n_w} & \text{for } k_{\rm SB} < k < k_{\rm end} \end{cases} \tag{6.128}$$

Where $k_{\rm SB}$ corresponds to spectral breaking scale at which $\Omega^{\rm sec}_{\rm gw}(k)h^2 = \Omega^{\rm pri}_{\rm gw}(k)h^2$ is satisfied, and above this, the primary GW spectrum dominates. Equating the Eq. (6.127) with (6.126) and simplifying we get this characteristic frequency as

$$\left(\frac{k_{\rm SB}}{k_{\rm end}}\right) = \left(\mathcal{C}\ \exp\left(\frac{N_{\rm re}}{2}(1+3w_\phi)(\delta+n_w-2)\right)\right)^{\frac{1}{(6+\delta-4\nu_2-n_w)}} \tag{6.129}$$

where

$$\mathcal{C} = \left(\frac{M_{\rm pl}}{\mathcal{A}_3\, H_{\rm end}}\right)^2 \frac{15(3-\nu_2)(4\nu_2-5)}{8(1+2\nu_2)}(1+3w_\phi)^{(2-n_w)}\Gamma^2\left(\frac{5+3w_\phi}{2+6w_\phi}\right)\left(\frac{\Gamma^2(l+\frac{\delta}{2})\Gamma^2\left(\frac{\delta}{2}\right)}{2^{1-2l-2\delta}\Gamma^2(1-l)\Gamma^2(l)}\right)$$

For example, $w_\phi = 3/5$ and the coupling strength $\xi = 2.9$, the primary GW spectrum becomes dominant for $\mathrm{f_{SB}} = k_{\rm SB}/2\pi \sim 1.84\times10^{-3}$ Hz, for $w_\phi = 2/3$ and $\xi = 2.6$, this occurs around $\mathrm{f_{SB}} \sim 7.17\times10^{-2}$ Hz, for $w_\phi = 5/7$ and $\xi = 2.5$, this occurs around $\mathrm{f_{SB}} \sim 3.43$ Hz, and for $w_\phi = 9/11$ and $\xi = 2.4$, we get $\mathrm{f_{SB}} \sim 1.52\times10^{3}$ Hz. All the features can be observed in the figure (6.14). Further, in all the plots, the blue-tilted nature in the low-frequency regime($k < k_{\rm re}$), and the mixed nature(red-tilted for $k_{\rm re} < k < k_{\rm SB}$ and blue-tilted for $k_{\rm SB} < k < k_{\rm end}$) in the intermediate frequency regime($k_{\rm re} < k < k_{\rm end}$) nicely follow the spectral nature as given in Eq.(6.128) for all EoS. It is important to note that in the range $k_{\rm SB} < k < k_{\rm end}$, the PGW spectral index $n_w$ will remain valid up to the maximum frequency $k_{\rm end}$. However, if one assumes modes $k > k_{\rm end}$, that remain sub-horizon during inflation, the spectral density can be assumed to be convergent. For example, in Chapter(5), we have shown that for a massless minimally coupled scalar field spectral behavior of the number density assumes convergent form $|\beta_k|^2 \propto k^{-6}$, irrespective of the EoS. Furthermore, the behavior of GW is similar to that of a massless minimally coupled scalar field; hence, the PGW spectrum will also remain convergent beyond $k > k_{\rm end}$. Thus it does not violate the $\Delta N_{\rm eff}$ bound at any higher frequency. Interestingly, we also observe that the enhanced GW spectra in the intermediate frequency range pass through various sensitivity curves like LISA, BBO, DECIGO, and some parts of ET also. This detection prospect indeed opens up a possibility to probe such a reheating scenario through future GW observatories.

### 6.9.1 Constraining "$\xi$" vs "$\alpha$" parameter space based on observational bounds :

Finally, we constrain the theory parameter space $(\xi, \alpha)$ appropriately taking into account reheating dynamics and the latest ACT, DESI data as depicted in Fig.(6.15). The figure

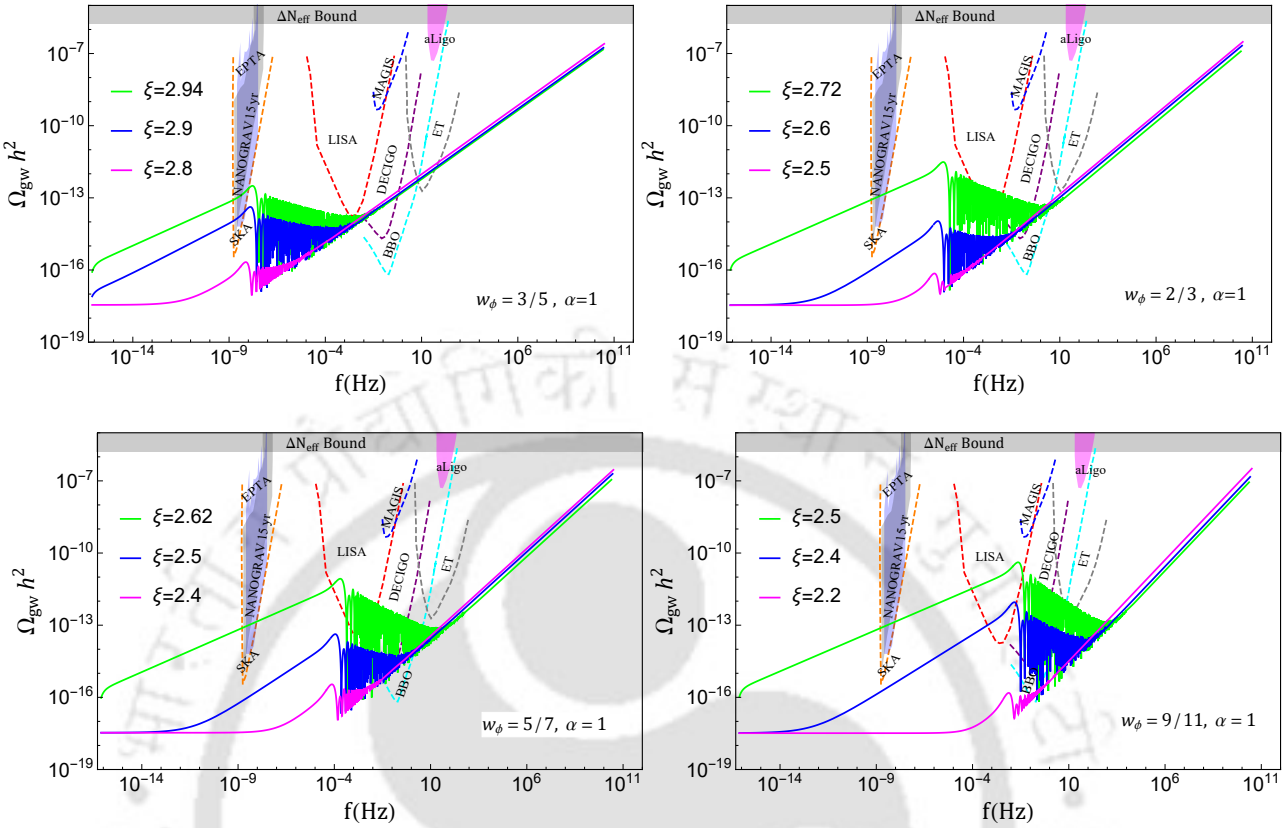


FIGURE 6.14: *Figure represents the total gravitational wave spectra (PGW+SGW) for today with the variation of non-minimal coupling strength for different reheating EoS in the non-minimal coupling-induced infrared reheating background. For each EoS, a particular coupling $\xi$ exists at which primary strength starts to overcome the secondary one at all frequency regimes, and the total GW spectrum closely follows the primary behavior, as obvious in this figure. For instance, for $w_\phi = 2/3$, $\xi \lesssim 2.5$, PGW strength starts to surpass the secondary strength in the entire frequency scale. In this plot, we have taken the lowest frequency, $f_* = (k_*/2\pi) \sim 7.75 \times 10^{-17}$ Hz, and the highest frequency, $f_{\rm end} = (k_{\rm end}/2\pi) \sim 10^{11}$ Hz for all the EoS.*

indicates that for a given EoS, there exists a maximum limit of $\alpha$ associated with each value of $\xi$ within the allowed range of coupling strength, $\xi \leq \xi_{\rm max}$. For smaller $\xi$ values primary GW (see Eq.(2.220), (6.126)) dominates over the secondary one, and hence the upper limit on $\alpha$ is nearly constant for any EoS. Such behavior can be clearly observed in the left panel of Fig.(6.15). For example, we obtain $\alpha_{\rm max} \simeq 17$ for the coupling strength in the range $1.92 \lesssim \xi \lesssim 2.6$ for $w_\phi = 2/3$. Upon increasing the coupling beyond $\xi \gtrsim 2.6$, secondary GW production is expected to become significant, causing the rapid growth of $r_{0.05}$, and also the enhancement of the large-scale field amplitude quickly violates the isocurvature bound, setting a maximum value of $\xi \sim 2.7251$, and the parameter $\alpha$ sharply drops to unity at the

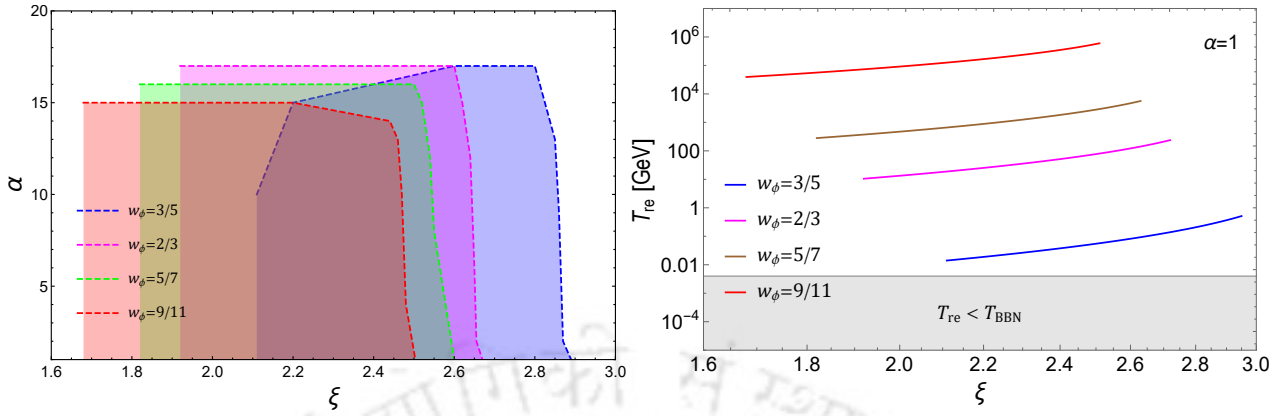


FIGURE 6.15: ***Left panel:*** *Figure represents the allowed $\xi$ vs $\alpha$ parameter space in this infrared gravitational reheating dynamics for different reheating EoS. In this figure, the color-shaded regions provide an admissible parameter set $(\xi, \alpha)$ for different EoS based on the bounds, $r_{0.05} \lesssim 0.038$, $\mathcal{P}_{\mathcal{S}}(k_*) \lesssim 8.3 \times 10^{-11}$, $\Omega_{\rm gw}h^2 \lesssim 9.54 \times 10^{-7}$, and $T_{\rm re} \gtrsim 4$ MeV.* ***Right panel:*** *Figure represents the variation of the infrared gravitational reheating temperature with the non-minimal coupling strength within its allowed range($\xi_{\rm min} \leq \xi \leq \xi_{\rm max}$) for different reheating EoS.*

maximum value $\xi_{\rm max}$. *In the proximity of $\xi = \xi_{\rm max}$, a sudden and rapid rise of $r_{0.05}$ is a prominent signature of the production of secondary gravitational waves (see dashed color lines in Fig.(6.16)). Any $\xi < 1.92$ is discarded because of the overproduction of primary gravitational wave, violating the $\Delta N_{\rm eff}$ bound.* For $w_\phi = 2/3$, we therefore get a very narrow allowed range of coupling parameter, $1.92 \lesssim \xi \lesssim 2.7251$.

Likewise for the other two EoS $w_\phi = (5/7,\ 9/11)$, the allowed range of $\xi$ and the upper limit of $\alpha$ is $(1.82 \lesssim \xi \lesssim 2.6256,\ 16)$ and $(1.68 \lesssim \xi \lesssim 2.5041,\ 15)$ respectively. Unlike the above three EoS, for $w_\phi = 3/5$, the constancy of the upper limit of $\alpha$ for smaller $\xi$ is absent owing to the satisfaction of the lowest reheating temperature bound $T_{\rm BBN}$. For a smaller $\xi$, maximum $\alpha$ is obtained taking the lowest temperature bound into account, which lowers the maximum possible $\alpha$ for coupling in the range $2.11 \lesssim \xi \lesssim 2.6$ as shown in the blue line in the left panel of Fig.(6.15). At $\xi = 2.6$, $\alpha$ becomes maximum $\alpha_{\rm max} = 17$, and further increase of $\xi$ gradually lowers $\alpha$ as discussed before. For this EoS, we obtain the allowed $\xi$ range and upper limit of $\alpha$ as $(2.11 \lesssim \xi \lesssim 2.9483,\ 17)$.

In Fig.(6.16) we summarize the final constraints on the model parameters taking all the relevant constraints into account, namely the bound on tensor-to-scalar ratio ($r_{0.05} \lesssim 0.038$), isocurvature ($\mathcal{P}_{\mathcal{S}}(k_*) \lesssim 8.3 \times 10^{-11}$), BBN constraint on $\Delta N_{\rm eff} < 0.17$ ($\Omega_{\rm gw}h^2 \lesssim 9.54 \times 10^{-7}$), and the lowest possible reheating temperature $T_{\rm re} = T_{\rm BBN} \sim 4$ MeV), in light of combined P+ACT+LB+BK18 observational data sets (see the references [43, 44]). In Fig.(6.16), using Eq.(2.220), we have presented the $\alpha$-attractor E-model prediction of $n_s, r_{0.05}$ parameters for varying $\alpha$(solid color lines) on top of the observational contour provided by the latest *Planck*, ACT, DESI, and BICEP/Keck combined (P+ACT+LB+BK18) observational data

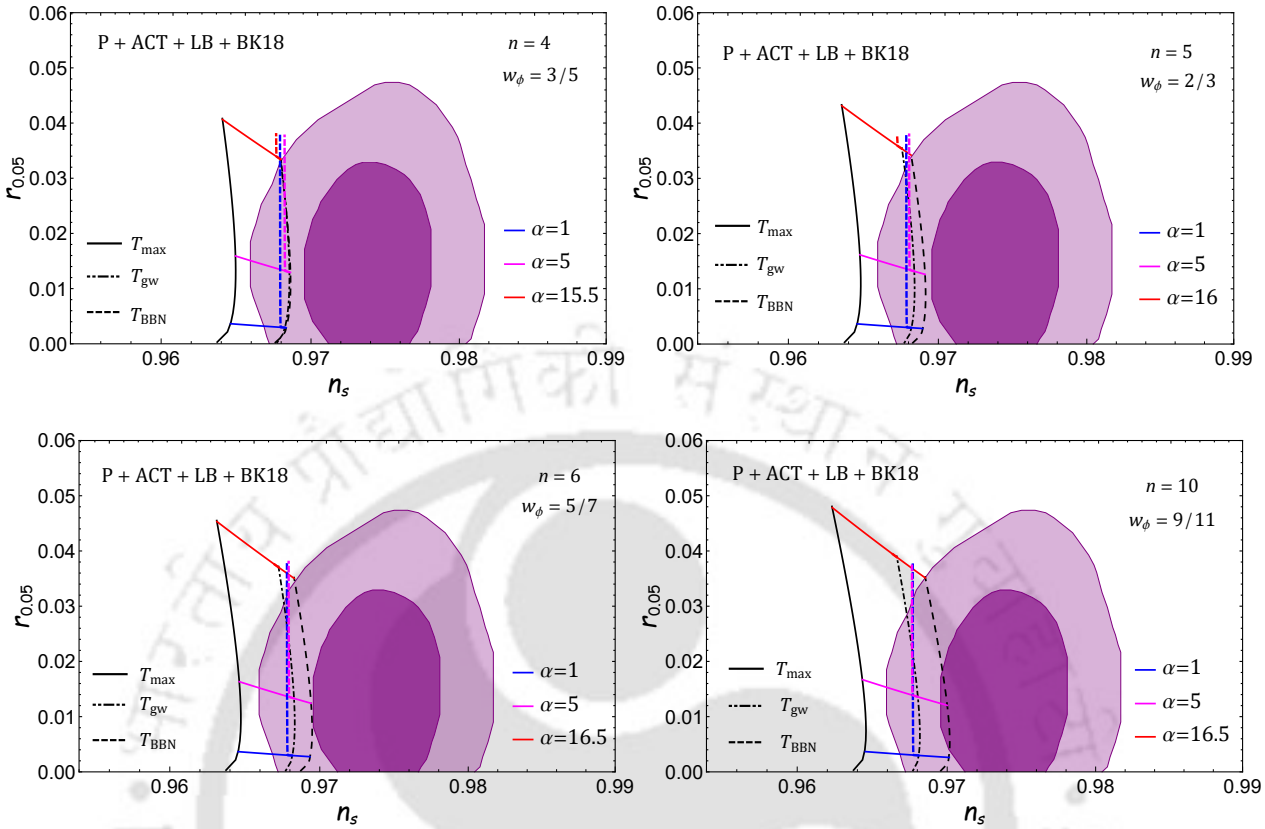


FIGURE 6.16: *Figure represents the $n_s, r_{0.05}$ parameters predicted by the $\alpha$-attractor E-model (solid blue, magenta, red lines), and the infrared gravitational reheating dynamics(dashed blue, magenta, red lines) within its allowed coupling regime($\xi_{\rm min} \leq \xi \leq \xi_{\rm max}$) in the $n_s - r_{0.05}$ contour based on the latest Planck, ACT, DESI, and BICEP/Keck combined (**P+ACT+LB+BK18**)(Purple) data sets for four different reheating EoS. Here $T_{\rm max} \sim 10^{15}$ GeV (solid black line), $T_{\rm BBN} = 4$ MeV (dashed black line), and $T_{\rm gw}$(black dot-dashed line) is the minimum reheating temperature satisfying the $\Delta N_{\rm eff}$ bound of PGW.*

sets [43, 44]. These predictions span reheating temperatures from the maximum reheating temperature, $T_{\rm max} \sim 10^{15}$ GeV (solid black lines) to the BBN temperature, $T_{\rm BBN} = 4$ MeV (dashed black lines). When $w_\phi \geq 3/5$, the minimum reheating temperature, $T_{\rm gw}$, derived from satisfying the BBN constraint of the maximum PGW amplitude at the scale $k = k_{\rm end}$, is stronger than the BBN temperature[246]. This is illustrated in Fig. (6.16) with a black dot-dashed line. Within the full parameter range, the model clearly falls within the $2\sigma$ region of the observational contour and outside of $1\sigma$ region. In this Fig.(6.16), with every solid color line for $\alpha$-attractor E-model, we associate a dashed color line representing the predictions of $n_s, r_{0.05}$ parameters of the infrared reheating dynamics. It is seen that for $w_\phi \geq 3/5$, each dashed color line meets the solid line where it cuts the $T_{\rm gw}$ black dot-dashed line. This feature is caused by setting the lower limit($\xi_{\rm min}$) of coupling strength

respecting the $\Delta N_{\rm eff}$ bound of PGW as discussed earlier. With further increase of $\xi$, the infrared reheating prediction of $r_{0.05}$ parameters noticeably departs from the $\alpha$-attractor model prediction, showing a steep rise towards the maximum $r_{0.05} \simeq 0.038$ at $\xi \simeq \xi_{\rm max}$ owing to the substantial growth of secondary tensor fluctuations as already stated. For $w_\phi = 5/7$, $9/11$ and $\alpha = 16.5$, as the maximum contribution to $r_{0.05}$ comes from PGW production (Eq.(2.220)), we find overlapping red dashed lines on the solid lines, as obvious in the bottom panel of Fig.(6.16). The tight constraint, represented by dashed color lines (blue, magenta, red), can be observed lying within the $2\sigma$ region of the $n_s - r_{0.05}$ reported by the ACT collaboration.

**Final infrared reheating temperature($T_{\rm re}$) vs $\xi$ parameter space :** Subject to all relevant latest observational bounds, we have shown the variation of reheating temperature within the allowed range of coupling strength ($\xi_{\rm min} \leq \xi \leq \xi_{\rm max}$) for different $w_\phi$ in the right panel of Fig.(6.15). In the present *infrared gravitational reheating* scenario, we find the lowest possible EoS $w_\phi \simeq 3/5$, which is consistent with the bounds ($T_{\rm BBN}$, $\Delta N_{\rm eff}$, $r_{0.05}$, $\mathcal{P}_{\mathcal{S}}(k_*)$). In the right panel of Fig.(6.15), $\Omega_{\rm gw}h^2 \lesssim 9.54 \times 10^{-7}$ imposes the lower limit $\xi_{\rm min}$ for all four EoS. Whereas, for all the EoS, $\xi_{\rm max}$ is set by the tensor-to-scalar ratio bound as mentioned earlier. This indeed is a striking improvement of the reheating parameter space compared to the non-perturbative minimal gravitational reheating scenario [36]. In the minimal scenario, although we achieved $T_{\rm BBN}$, we failed to satisfy the PGW $\Delta N_{\rm eff}$ constraint for $w_\phi \simeq 3/5$. Whereas in the non-minimal scenario, we respect all these relevant observational bounds in the entire range $w_\phi \gtrsim 3/5$ and achieve successful reheating and a notable induced GW signal.

## 6.10 Summary

Inflation is intimately tied to the physics of reheating. While constraining inflation via observation, one must take into account the physics of reheating. Over the years, different reheating mechanisms have been proposed. In this work, we have proposed a new reheating scenario driven by non-minimally coupled ($\xi\chi^2 R$) scalar field. Taking $\alpha-$attractor as a potential candidate for an inflation model, and embedding our proposed reheating scenario, we finally place constraints on the model parameters in light of the latest ACT, DESI results.

a) Production of scalar fluctuations through infrared instability and reheating: Non-minimal coupling induces super-horizon instability in the scalar field both during and after inflation. Such instability produces large infrared fluctuations, and upon entering the post-inflationary phase, those modes successfully reheat the universe. For $w_\phi < 1/3$, we find reheating cannot be achieved due to the fact that the inflaton field dilutes more slowly than the infrared fluctuation. On the contrary, for $w_\phi > 1/3$, we find that infrared fluctuation can successfully reheat the universe due to faster dilution of the inflaton field. We have compared our non-perturbative infrared results with that of the perturbative one. In the perturbative reheating, one needs to calculate the width of the inflaton decaying into

radiation. In the present context, since radiation is non-minimally coupled, decay widths are computed both in Jordan and Einstein frames. Important to note that perturbative reheating describes the dynamics of sub-Hubble modes and always ignores the modes that are outside the horizon. Therefore, while studying the post-inflationary reheating phase, one must take into account the super-Hubble modes separately, which are usually ignored in the literature. And in the present context, we indeed found that it is the infrared modes that actually dominate over the perturbative sub-Hubble modes above a critical coupling strength.

This essentially results in a noticeable difference in the $T_{\rm re}$ vs $\xi$ parameter space as shown in Fig.(6.12) as compared to the perturbative results. In Fig.(6.17), we have also shown a comparison between the Jordan and Einstein frame reheating parameter space. Interestingly, near the conformal limit, we find a discrepancy in the predictions of these two frames, which justifies the non-equivalence between these two frames in the non-minimal coupling induced reheating scenario.

In this context, we would like to mention one important point. In our present model, the parametric resonance can be sourced by two factors: i) Oscillation of the curvature scalar $R$ along with sufficiently high non-minimal coupling strength $\xi > 50$, that can lead to strong non-perturbative resonance particularly for the modes $k \sim k_{\rm end}$, as discussed in [245], and ii) For equation of state $w_\phi > 1/3$, there exists self resonance phenomena[335] that can give rise to radiation domination early. This self-resonance can have an impact depending upon its strength, which needs detailed investigation. We can compare the efficiency of the self-resonance dynamics with the present reheating scenario, which is left for our future endeavour.

b) Impact of ACT, DESI on the $\alpha-$attractor along with infrared reheating :
Besides being a dominant radiation component to reheat the universe, this massless scalar also generates significant anisotropies to source notable induced gravitational waves. We find that for $w_\phi > 1/3$, the growing $\xi$ of the field causes larger tensor and isocurvature fluctuations at the CMB scale. Therefore, the latest (P+ACT+LB+BK18) bound $r_{0.05} \lesssim 0.038$, and the *Planck* 2018 bound $\mathcal{P}_{\mathcal{S}}(k_*) \lesssim 8.3 \times 10^{-11}$ put tight constraint on maximum $\xi$. Furthermore, for a given EoS, low $\xi$ causes low reheating temperature, and hence enhances the duration of reheating, producing stronger high-frequency gravitational waves. Hence, the BBN bound $\Omega_{\rm gw}h^2 \lesssim 9.54 \times 10^{-7}$ imposes further constraint on minimum value of $\xi$. Thus, different observations tighten the associated reheating dynamics. We find the lowest possible EoS, $w_\phi = 3/5$, which successfully reheats the universe satisfying all relevant bounds ($T_{\rm BBN}$, $r_{0.05}$, $\mathcal{P}_{\mathcal{S}}(k_*)$, $\Delta N_{\rm eff}$) in the coupling range $2.11 \lesssim \xi \lesssim 2.9483$. After considering all the latest bounds, for a given EoS, $w_\phi \geq 3/5$, we find that the small-scales (UV) analyzed by perturbative treatment give higher reheating temperature than the IR modes in a larger portion within the allowed regime($\xi_{\rm min} \leq \xi \leq \xi_{\rm max}$) of the reheating parameter space.

c) Detectability of the GW signal: Furthermore, we have found a distinctive gravitational wave spectrum for different reheating parameters($w_\phi$, $\alpha$, $T_{\rm re}$, $\xi$) which is strong enough to be detected by various GW observatories(see Fig.(6.14)), allowing for more robust constraints on the coupling parameters and the reheating dynamics in the near future GW

experiments.

# Addenda

## 6.11 Computation of Isocurvature power spectrum :

For stiff EoS $w_\phi > 1/3$, the large-scale fluctuation strength becomes significant in the range $\xi > 3/16$. Therefore, in the present reheating scenario, we shall confine ourselves to this particular regime while computing the isocurvature power spectrum amplitude.
For $w_\phi > 1/3$ and $\xi > 3/16$, with the knowledge of $\alpha_k, \beta_k$ in this regime, we obtain the following long-wavelength post-inflationary field solutions at a very late time $k\eta >> 1$(see Eq.(6.25)).

$$X_k^{\rm long}(\eta) \approx \frac{\Gamma(\nu_2)\exp(-\pi\tilde{\nu}_1/2)}{4\sqrt{2k_{\rm end}}}\left(\frac{3\mu-2\nu_2}{\sqrt{(3\mu-1)}}H^{(1)}_{\nu_1}(\bar{k}) + \bar{k}\sqrt{3\mu-1}\Big(H^{(1)}_{\nu_1-1}(\bar{k}) - H^{(1)}_{\nu_1+1}(\bar{k})\Big)\right) \times \frac{\cos(k\eta)}{\bar{k}^{\nu_2+1/2}}\left(\frac{2}{3\mu-1}\right)^{\nu_2} \tag{6.130}$$

The time-derivative of this solution can be approximated as

$$(X_k^{\rm long})'(\eta) \approx \frac{\Gamma(\nu_2)\exp(-\pi\tilde{\nu}_1/2)\sqrt{k_{\rm end}}}{2\sqrt{2}}\sqrt{3\mu-1}\left(\frac{2}{3\mu-1}\right)^{\nu_2}\frac{(\pi + i\cosh(\pi\tilde{\nu}_1)\Gamma(1-i\tilde{\nu}_1)\Gamma(i\tilde{\nu}_1))}{\pi\Gamma(i\tilde{\nu}_1)} \times \left(\frac{\bar{k}}{2}\right)^{i\tilde{\nu}_1}(\bar{k})^{(1/2-\nu_2)}\cos(k\eta)$$

$$\Rightarrow \left|(X_k^{\rm long})'(\eta)\right|^2 \approx 2\mathcal{A}_3 k_{\rm end}\left(\frac{k}{k_{\rm end}}\right)^{1-2\nu_2}\cos^2(k\eta) \tag{6.131}$$

Therefore, in the massless limit $m_\chi \approx 0$, the integrand $P_X(p, |\vec{p}-\vec{k}|)$ in Eq.(6.123) can be written as

$$P_X(p, |\vec{p}-\vec{k}) = 4\mathcal{A}_3^2 k_{\rm end}^2\left(\frac{p}{k_{\rm end}}\right)^{1-2\nu_2}\left(\frac{|\vec{p}-\vec{k}|}{k_{\rm end}}\right)^{1-2\nu_2}\cos^2(p\eta)\,\cos^2(|\vec{p}-\vec{k}|\eta) \tag{6.132}$$

The expression of this integrand (6.132) is true for any $\xi > 3/16$ for EoS $w_\phi > 1/3$. In the entire range $\xi > 3/16$, total energy-density of the system $\rho_\chi$ will be different below$(3/16 < \xi < \xi_{\rm cri})$ and above$(\xi > \xi_{\rm cri})$ the critical coupling $\xi_{\rm cri}$ (See Equations (6.106) and (6.112)). This creates a difference in the amplitude of the isocurvature power spectrum (6.122). We first express the integral (6.122) in terms of the general energy-density function $\rho_\chi$ to compute the integration. Plugging the expression (6.132) into the integral (6.122) we have

$$\mathcal{P}_{\mathcal{S}}(k) = \frac{4\mathcal{A}_3^2 k_{\rm end}^5}{(2\pi)^4\rho_\chi^2 a^8}\left(\frac{k}{k_{\rm end}}\right)^{5-4\nu_2}\cos^2(p\eta)\,\cos^2(|\vec{p}-\vec{k}|\eta)\int_{k_{\rm min}}^{k_{\rm max}}p^2dp\int_{-1}^{1}d\gamma\left(\frac{p}{k}\right)^{(1-2\nu_2)}$$

$$\times \left(\frac{|\vec{p}-\vec{k}|}{k}\right)^{(1-2\nu_2)}$$
$$\approx \frac{\mathcal{A}_3^2 k_{\rm end}^8}{(2\pi)^4 \rho_\chi^2 a^8}\left(\frac{k}{k_{\rm end}}\right)^{8-4\nu_2}\int_{u_{\rm min}}^{u_{\rm max}} u^{(3-2\nu_2)}du \underbrace{\int_{-1}^{1} d\gamma\ \left(1+u^2-2u\gamma\right)^{(1/2-\nu_2)}}_{\text{angular integral}} \quad (6.133)$$

where "$\gamma$" is the angle between two momentum vectors $\vec{p}$ and $\vec{k}$, $\cos(\gamma)=\hat{p}.\hat{k}$. The dimensionless quantity $u$ is defined to be $u=(p/k)$ where $u_{\rm min}=(k_{\rm min}/k)$ and $u_{\rm max}=(k_{\rm max}/k)$, where $k_{\rm min}$ is considered to be the present-day horizon scale(smaller than CMB scale), and $k_{\rm max}$ is considered to be $k_{\rm end}$. We have to first perform the angular integral before going to the momentum part.

*Angular integral :*

The angular integral is calculated to be

$$\mathcal{I}_1=\int_{-1}^{1} d\gamma\ \left(1+u^2-2u\gamma\right)^{(1/2-\nu_2)}=\frac{1}{u(3-2\nu_2)}\left[(1+u)^{(3-2\nu_2)}-(1-u)^{(3-2\nu_2)}\right] \quad (6.134)$$

Substituting the angular integral (6.134) back to (6.133) we have

$$\mathcal{P}_{\mathcal{S}}(k)=\frac{\mathcal{A}_3^2 k_{\rm end}^8}{(2\pi)^4(3-2\nu_2)\rho_\chi^2 a^8}\left(\frac{k}{k_{\rm end}}\right)^{8-4\nu_2}\underbrace{\int_{u_{\rm min}}^{u_{\rm max}} du\ \frac{\left[(1+u)^{(3-2\nu_2)}-(1-u)^{(3-2\nu_2)}\right]}{u^{2(\nu_2-1)}}}_{\text{momentum integral}} \quad (6.135)$$

*Simplification of momentum integral :*

Evaluating the following momentum integral we get

$$\begin{aligned}\mathcal{I}_2&=\int_{u_{\rm min}}^{u_{\rm max}} du\ \frac{\left[(1+u)^{(3-2\nu_2)}-(1-u)^{(3-2\nu_2)}\right]}{u^{2(\nu_2-1)}}\\&=\frac{u^{3-2\nu_2}}{(3-2\nu_2)}\left[{}_2F_1\Big((2\nu_2-3),(3-2\nu_2);(4-2\nu_2);-u\Big)-{}_2F_1\Big((2\nu_2-3),(3-2\nu_2);(4-2\nu_2);u\Big)\right]_{u_{\rm min}}^{u_{\rm max}}\\&=I_2(u_{\rm max})-I_2(u_{\rm min}) \quad (6.136)\end{aligned}$$

where ${}_2F_1(a,b;c;z)$ is a Gaussian or ordinary Hypergeometric function with four arguments. In the long-wavelength regime($k << k_{\rm end}$), we simplify the following expression $I_2$ for two limits separately.

*For upper limit $u_{\rm max}$ :*

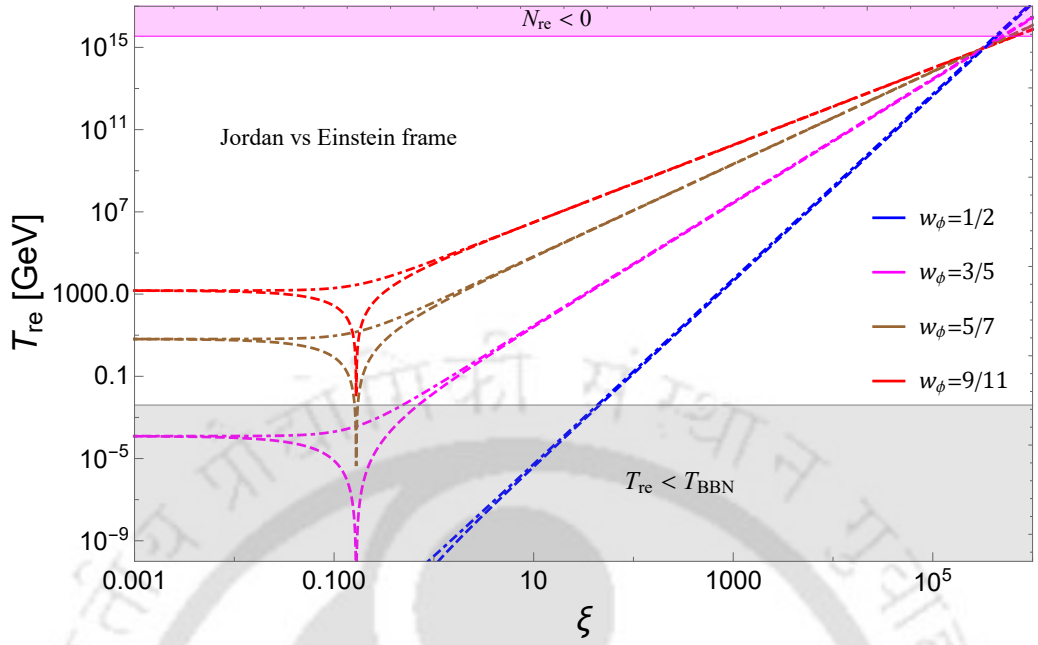


FIGURE 6.17: *Figure represents a comparison of $T_{re}$ vs $\xi$ variation for different EoS between the perturbative studies in the Jordan and Einstein frames. Dashed lines correspond to the perturbative predictions in the Jordan frame, and the dot-dashed lines correspond to the Einstein frame predictions. Except near the conformal limit, $\xi \sim 1/6$, it shows almost the same temperature predictions made by the studies in two different frames.*

For large $u$ limit, the expression (6.136) can be approximated as

$$I_2(u_{\rm max}) \approx \left( \frac{(-1)^{(2\nu_2-3)}\big(-1+(-1)^{(3-2\nu_2)}\big)\Gamma(4\nu_2-6)\Gamma(4-2\nu_2)}{(3-2\nu_2)\Gamma(2\nu_2-3)} + \frac{u_{\rm max}^{(6-4\nu_2)}}{(6-4\nu_2)}\big(1+(-1)^{(4-2\nu_2)}\big) \right) \tag{6.137}$$

*For lower limit $u_{\rm min}$ :*

For small $u$ limit, expression (6.136) can be approximated as

$$I_2(u_{\rm min}) \approx \frac{(3-2\nu_2)}{(2-\nu_2)} u_{\rm min}^{(4-2\nu_2)} \tag{6.138}$$

Using Equations (6.137) and (6.138) in (6.135), we write the final form of the isocurvature power spectrum amplitude in terms of total energy-density $\rho_\chi$ as follows:

$$\mathcal{P}_{\mathcal{S}}(k) = \frac{\mathcal{A}_3^2 k_{\rm end}^8}{(2\pi)^4(3-2\nu_2)\rho_\chi^2 a^8}\Big(I_2(u_{\rm max}) - I_2(u_{\rm min})\Big)\left(\frac{k}{k_{\rm end}}\right)^{(8-4\nu_2)} \tag{6.139}$$

## 6.12 Comparing the perturbative approach in Jordan and Einstein frame

Based on the production rates given in Eq.(6.117), we have compared the contribution in Jordan and Einstein frames in Fig.(6.17). It clearly shows that in the Einstein frame, the conformal behavior of a massless scalar field is lost and giving rise to a non-vanishing production in the time-dependent background at $\xi = 1/6$. Whereas such production is indeed vanishing in the Jordan frame, as expected. This indicates a notable departure of the Einstein frame prediction from the Jordan frame and establishes the non-equivalence of these two frames in the context of perturbative reheating predictions. It is interesting to explore such non-equivalence further in the quantum regime.

CHAPTER 7

# Conclusions and outlook

*"We're always, by the way, in fundamental physics, always trying to investigate those things in which we don't understand the conclusions. After we've checked them enough, we're okay."*

*Richard P. Feynman*

## 7.1 Conclusions

Post-inflationary reheating is an integral part of the early universe dynamics, which is of utmost importance in studying the cosmic history of the universe. It bridges the enormous gap in energy and time scales between the end of inflation and the beginning of the Big Bang nucleosynthesis phase. This theoretically proposed important intermediate phase is poorly understood to date due to the absence of any direct observational evidence. Besides generating proper initial conditions for the hot, thermal universe, the modified expansion and thermal history of the universe during reheating also abundantly produce different cosmological relics like gravitational waves, dark matter, dark radiation, etc. Although this phase is highly unconstrained from the observational perspective, it leaves distinct signatures on these cosmic relics and also subtle imprints on CMB anisotropies, by which this important phase of the early universe can be indirectly constrained. In this thesis, we have investigated various non-perturbative aspects of reheating dynamics and their imprint on cosmic relics to a great extent. The chapterwise summary of this thesis is as follows:

Chapter(1) begins with an introductory note to the historical development of the scientific ideas and different theoretical frameworks upon which the foundation of modern cosmology is built. After introducing the historical backdrop, we present the transition of modern cosmology from a primary theoretical playground to a precision observational

science with the accidental discovery of CMB in 1965, and the advancement of precise measurements of CMB anisotropies.
In Chapter(2), we first present a concise overview of the Standard Big Bang cosmology. After describing the major successes and important drawbacks of this model, we introduce the inflationary Non-standard cosmology. We demonstrate the importance of the early accelerated inflationary era in solving various cosmological puzzles and also providing plausible explanations for the generation of CMB anisotropies and the large-scale structure formation of the universe. We have then reviewed the subsequent reheating phase, a crucial bridge between the inflationary and the hot Big Bang epoch. The treatment of inflationary perturbations further clarifies how tiny quantum vacuum fluctuations of the inflaton evolved into the seed of cosmic structure observed in the CMB temperature anisotropies and the large-scale distribution of matter, and also explains the origin of the nearly scale-invariant tensor perturbations. Taken together, these elements illustrate how non-standard extensions of the standard cosmological model enrich our understanding of the early universe and open new observational windows.
In cosmology, squeezed states provide a powerful language for describing how small-scale quantum vacuum fluctuations evolve into large-scale classical density perturbations. They capture the memory of how fluctuation modes were stretched, correlated, and amplified by the early inflationary phase of the universe, making squeezing a robust framework linking microscopic quantum behavior with the macroscopic cosmic structure. In Chapter(3), we first construct the squeezed state formalism, which is employed later to revisit the phenomenon of explosive particle production during the preheating era in the language of quantum squeezing. The interaction between the produced quantum fluctuations and the classical expanding background makes the quantum state of those fluctuations *squeezed*. The investigation of the early universe particle production within the framework of quantum squeezing, indeed, provided us with some insightful ideas regarding the inherent chaotic instability and the eventual thermalization of the system. We next briefly discussed the basic definition and the quantum field theoretic description of *out-of-time-order correlator*(OTOC), a diagnostic of quantum chaos. Thus, treating the interacting system within the squeezing framework opens up a unique possibility to decode various microscopic features of large-scale systems in a cosmological setting.

In Chapter(4), we have done a detailed theoretical exploration of the phenomena of particle production, resonance, squeezing, and chaos of the non-perturbative system that emerge in the early reheating phase, known as *preheating*. The early reheating or *preheating* era, being a highly out-of-equilibrium phase, creates a congenial environment for the exploration of the aforementioned connections of these fundamental properties. Here, we have tried to establish a connection between squeezing, chaos, and the inherent instability of a bosonic system in a cosmological background. The post-inflationary oscillation of the classical inflaton background periodically drives the bosonic fluctuations coupled to it, and this periodic drive makes the fluctuation system intrinsically chaotic owing to the inherent *parametric resonance instability*. Non-trivial interactions of the quantum fluctuations with the classical inflaton background also make the system squeezed. To diagnose the presence of *quantum chaos* in the system, we computed one of the important

diagnostics of quantum chaos, OTOC or *out-of-time-order correlator* of the phase space variables for this bosonic system. We have studied the dynamics of the squeezing parameter characterizing the amount of squeezing present in the bosonic system for tri-linear and quartic interactions. For a quantum chaotic system, OTOC is known to exhibit exponential growth over time. In the present cosmological scenario, we have found that the growth of OTOC, the growth of the squeezing parameter, and the parametric resonance instability in the system are intrinsically connected to each other. The more the squeezing, the more the chaos in the system. Due to the presence of an expanding background, the periodic driving source gradually loses its strength, resulting in the eventual relaxation of the fluctuation system from the chaotic instability to a thermalized state. Thermalization is believed to be deeply connected to the chaotic behavior of a system, which is beautifully conjectured [180] by proposing an inequality relating Lyapunov exponent(a measure of chaos) and system temperature under consideration(well-known MSS bound). By using this bound, we calculated the approximate lower bound of the temperature of the thermalized system at the end of preheating. We further conjectured a relation between the system temperature and quantum squeezing averaged over phase space, which interestingly satisfies the MSS bound and the well-known Rayleigh-Jeans formula for the temperature. Finally, we came up with the findings that the thermalized temperature of the system at the end of chaotic instability nicely follows the bosonic distribution function in this early reheating era. This indeed establishes a beautiful connection between the non-equilibrium squeezed quantum system with the non-equilibrium preheating phase in the early universe.

In Chapter(5), we have extensively studied the long-wavelength(IR) and short-wavelength(UV) spectrum of *minimally coupled* massless or low mass scalar fluctuation, considering minute post-inflationary background oscillation effect for general reheating equation of state(EoS). We find that the large-scale spectrum is hardly sensitive to the oscillation effect of the background, whereas this oscillation effect becomes extremely important while computing the spectrum of the UV modes. We also find an IR divergent number density spectrum for any reheating EoS lying between 0 to 1. On the other hand, we always get UV-convergent number and energy-density spectra. Interestingly, the UV number density spectral index is found to be -6 irrespective of the reheating EoS for any EoS $\geq 1/3$. This is one of the important findings of this study. Our study also provides a viable explanation of the small-scale oscillation in the momentum space of no. density spectrum through the appearance of an *interference term* in the spectrum. Furthermore, we study the mass-breaking effect of the IR spectrum by including the finite mass, $m_\chi$, of the daughter scalar field. We show that for $m_\chi/H_{\rm end} > 3/2$, the IR spectrum of scalar fluctuations experiences exponential mass suppression, while for smaller masses, $m_\chi/H_{\rm end} < 3/2$, the spectrum remains flat in the IR regime regardless of the post-inflationary EoS. For any general EoS, we also compute a specific IR scale, $k_m$, of fluctuations below which the IR spectrum will suffer from this finite mass effect. We also do a comparative study of the small-scale UV spectra obtained through perturbative or *Boltzmann* and non-perturbative or *Bogoliubov* treatment. In some literature [227, 237], people analytically studied the UV spectra for a single EoS $w_\phi = 0$. In this work, we have provided an analytical approach to study the behavior of UV spectra in a general reheating background. Interestingly, for any general reheating EoS, we

find a behavioral similarity in the UV spectra obtained through two different approaches, as mentioned before. Therefore, in this minimal scenario, the production of small-scale fluctuations through *graviton exchange* process [34, 54, 57, 154, 220] in perturbative treatment is found to be equivalent to the production of UV fluctuations in non-perturbative treatment by taking higher order inflaton oscillation effect into account for any general EoS. This is another intriguing outcome of this study. Furthermore, this study offers a proper non-perturbative approach to study the gravitational reheating dynamics, considering all the scales(UV and IR) of a fluctuation in a general reheating background.

In Chapter(6), we have extended the idea of the minimally coupled scalar field dynamics of the previous chapter by including the nonminimal coupling between the scalar field and gravity. The nonminimal gravity coupling gives rise to various interesting dynamical features in the scalar field system. The appearance of post-inflationary *tachyonic instability* for higher reheating EoS and coupling strength signals a striking departure from the dynamics of a minimally coupled system in long-wavelength regime. There exists a large number of recent literature [58, 230, 314, 315], where authors took arbitrarily large nonminimal coupling strength while studying the dynamics of the scalar fluctuation. Our study reveals that the nonminimal coupling-induced post-inflationary IR instability, a distinctive non-perturbative feature, causes a significant enhancement of the fluctuations in the higher coupling regime, which, unlike the aforementioned literature, essentially forbids us from taking sufficiently large coupling strength respecting various large-scale observations.

In Part I of this chapter, we have explored an unavoidable production channel of induced gravitational waves without considering any non-gravitational interactions of the source field. we have considered massless or very low mass non-minimally coupled scalar fluctuations, which acted as a potential source of secondary gravitational waves(SGWs). We have found that the presence of strong IR instability in the system causes a substantial growth in the scalar field amplitude, leading to pronounced production of SGWs in the low and intermediate-frequency ranges that are strong enough to be detected by *Planck* and future gravitational wave detectors like LISA, BBO, DECIGO and ET. Such growth in super-horizon modes of the scalar field and associated GW production may have a significant effect on the strength of the tensor fluctuation at the CMB scales and the number of relativistic degrees of freedom at the time of CMB decoupling. The present-day CMB scale tensor-to-scalar ratio bound, CMB scale isocurvature bound, and the bound on the total number of relativistic degrees of freedom finally imposed tight constraints on the upper and lower boundary of the non-minimal coupling strength. Constraining nonminimal coupling between gravity and a spectator scalar fluctuation based on present large-scale observation is one of the notable outcomes of this study.

In Part II of this chapter, we have proposed a novel reheating scenario facilitated by nonminimal coupling induced large-scale infrared fluctuations generated during inflation. In this work, we have investigated the possibility of reheating and the existence of a distinct gravitational wave signal through significant anisotropies, generated by the large-scale fluctuations of the nonminimally coupled field simultaneously. Besides being a possible source of anisotropy, we have also considered the massless or very low mass fluctuation to be a dominant radiation component in the post-inflationary phase, which gives successful

reheating. We call this special kind of reheating scenario *infrared gravitational reheating* . We have also done a comparative study with the prediction of reheating parameters made by perturbative or Boltzmann analysis in the presence of nonminimal curvature coupling in both Jordan and Einstein frames. *Interestingly, we found a non-equivalence of these two frames in the context of perturbative reheating predictions.* Perturbative or Boltzmann approach, solely confined to the sub-horizon modes, can't capture the dynamics of super-horizon modes. Therefore, due to the absence of non-minimal coupling-induced IR instability, the Boltzmann method is found to predict relatively lower reheating temperature for a given coupling as compared to the non-perturbative treatment. We have also found that in non-perturbative treatment, the significant IR instability causes the reheating temperature to reach the maximum limit at a much smaller coupling strength as compared to the perturbative treatment. Finally, embedding this infrared reheating scenario into the well-known $\alpha-$attractor inflationary model, we examine possible constraints on the model parameters in light of the latest Atacama Cosmology Telescope (ACT), Dark Energy Spectroscopic Instrument (DESI) results. In light of the latest large-scale observational bounds as addressed in part I of this chapter, we also constrain the present reheating dynamics. Subject to those bounds, we find a very narrow allowed range of non-minimal coupling strength and reheating temperature parameter space for different reheating EoS. And these non-perturbative constraints, anyway, rule out a large region of temperature vs coupling parameter space predicted by Boltzmann analysis. Likewise, in the previous work, interestingly, we also find here within the admissible range of coupling strength, the induced GW strength surpasses the PGW strength at low and intermediate frequency ranges, and the induced strength is strong enough to pass through various GW sensitivity curves like LISA, BBO, DECIGO, and some parts of ET also. This detection prospect indeed opens up a possibility of probing such a reheating scenario through future GW observatories.

## 7.2 Future Outlook

In my doctoral work, I have explored an important aspect of the reheating era and have rigorously studied various mechanisms of non-thermal particle production in this early era, and their subtle imprint on the cosmological relics. These ideas can be further extended in a few more interesting directions.

### Thermalization of hot plasma during reheating

The mechanism of thermalization of the non-thermally produced particles during reheating is of great theoretical importance on its own, as this is important for setting the initial condition for the hot Big Bang phase. In particular, it is believed to have played a significant role in some well-studied cosmological phenomena, such as producing matter-antimatter asymmetry (baryogenesis), and dark matter abundance that we observe today. In Chapter(4), we investigated an intriguing interconnection in an idealized preheating scenario where the produced fluctuations don't interact with the background. However, in

reality, the backscattering effect is inescapable. Incorporating this important effect in the system, we can extend the dynamics of the coupled inflaton, daughter field system up to the end of the reheating phase by performing a rigorous LATTICE analysis and also intend to thoroughly study the dynamics of the squeezed quantum state of the daughter fluctuation in a more realistic scenario. This would be a novel approach to unravel the microphysics of the post-inflationary thermalization of the hot plasma within the framework of quantum squeezing.

**Massive test scalar or Dark matter sourcing Gravitational waves:**

The production of sub- and super-Hubble mass particles is a well-known fact in the context of cosmological gravitational particle production. We can also study the effect of a massive test scalar as a possible source of anisotropy on the spectrum of secondary gravitational waves. These massive gravitationally produced scalars can be treated as possible candidates for dark matter(DM), producing gravitational waves. We have already explored that the nontrivial dynamics of the universe during the finite reheating phase have a great impact on the massless and massive particle spectra. This opens up another interesting side to probe DM masses satisfying the present relic abundance through the induced GW signal. It is expected to probe a particular range of gravitationally produced DM masses through future GW observatories.

**Impact of large-scale fluctuations on the Dark Matter phenomenology**

Exploration of the thermal(WIMP), non-thermal(FIMP) production of Dark Matter(DM) by taking the large-scale fluctuations of the DM field into account is indeed an interesting aspect of DM phenomenology, having a potential connection to early universe physics. Most of the literature has studied the DM production mechanism confined to the causal scales or sub-Hubble modes. Our study reveals that in the presence of non-minimal gravity-fluctuation coupling(mainly scalar fluctuations), a significant large-scale instability is present in the system. Hence, the large-scale dynamics of the DM field are expected to leave a visible imprint on the entire DM freeze-in and freeze-out parameter space.

**Impact of early universe particle production on large-scale structure formation**

Infrared fluctuations, generated during inflation and propagating through the reheating phase, may provide nontrivial corrections to the primordial initial conditions relevant for structure formation. Nonlinear dynamics and gravity coupling can enhance long-wavelength modes during reheating, potentially leaving subtle imprints on the growth of large-scale structures or higher-order correlations. Exploring these effects in a consistent dynamical framework remains an important direction for future work.

# Appendices

# Calculation of oscillatory Hubble scale for general reheating EoS

In a general reheating background, for a power-law-type inflationary potential, we compute the expression of the Hubble scale with the fast-varying oscillatory part. Plugging Eq.(2.66) into the expression of Hubble scale (2.46) with a generic inflaton potential $V(\phi)$, we write

$$H^2 = \frac{1}{3M_{\rm pl}^2}\Big[\frac{1}{2}\Big(\dot{\phi}_0(t)\mathcal{P}(t) + \phi_0(t)\dot{\mathcal{P}}(t)\Big)^2 + V(\phi_0)\mathcal{P}^{2n}\Big]\,. \tag{1}$$

At the earlier stage of reheating, the expansion rate is larger than the perturbative decay rate, i.e. $H >> \Gamma_\phi$. Neglecting the term $\Gamma_\phi(1+w_\phi)\rho_\phi$ in the continuity equation, we approximately write

$$\dot{\rho}_\phi + 3H(1+w_\phi)\rho_\phi \simeq 0 \Rightarrow \dot{\phi}_0(t) \simeq -\frac{6Hn}{n+1}\frac{V(\phi_0)}{V'(\phi_0)} \Rightarrow \dot{\phi}_0(t) \simeq -\frac{3H\phi_0}{n+1}\,. \tag{2}$$

To reach the final expression in the Eq.(2) we have used the form of energy density $\rho_\phi = V(\phi_0)$ with the oscillation average $\langle\mathcal{P}^{2n}\rangle = \frac{1}{n+1}$ and the ratio $\frac{V(\phi_0)}{V'(\phi_0)} = \frac{\phi_0}{2n}$ can be easily calculated from the potential Eq.(2.76). Substituting Eq.(2) to (1), we write

$$\begin{aligned}
H^2 &= \frac{1}{3M_{\rm pl}^2}\Big[\frac{1}{2}\Big(\phi_0(t)\dot{\mathcal{P}}(t) - \frac{3H\phi_0\mathcal{P}(t)}{n+1}\Big)^2 + V(\phi_0)\mathcal{P}^{2n}\Big] \\
\Rightarrow H^2 &= \frac{1}{3M_{\rm pl}^2}\Big[\frac{1}{2}\phi_0^2(t)\Big(\dot{\mathcal{P}}(t) - \frac{3H\mathcal{P}(t)}{n+1}\Big)^2 + V(\phi_0)\mathcal{P}^{2n}\Big] \\
\Rightarrow H &= \frac{\sqrt{1 + \frac{4M_{\rm pl}^2(n+1)^2}{3\mathcal{P}^2\dot{\mathcal{P}}^2\phi_0^4}\Big(1 - \frac{3\mathcal{P}^2\phi_0^2}{2M_{\rm pl}^2(n+1)^2}\Big)\Big(\frac{1}{2}\phi_0^2\dot{\mathcal{P}}^2 + V(\phi_0)\mathcal{P}^{2n}\Big)} - 1}{M_{\rm pl}^2\Big(\frac{2(n+1)}{\mathcal{P}\dot{\mathcal{P}}\phi_0^2} - \frac{3\mathcal{P}}{\dot{\mathcal{P}}(n+1)M_{\rm pl}^2}\Big)}\,.
\end{aligned} \tag{3}$$

Now we will simplify Eq. (3) with the help of Eq. (2.76), (2.67) and (2.68). Taking the entire function in the numerator under the square root of (3), we write

$$\text{Numerator} = \left(1 + \frac{4M_{\rm pl}^2(n+1)^2}{3\mathcal{P}^2\dot{\mathcal{P}}^2\phi_0^4}\Big(1 - \frac{3\mathcal{P}^2\phi_0^2}{2M_{\rm pl}^2(n+1)^2}\Big)\Big(\frac{1}{2}\phi_0^2\dot{\mathcal{P}}^2 + V(\phi_0)\mathcal{P}^{2n}\Big)\right)$$

$$
\begin{aligned}
&= 1 + \Big(2\frac{M_{\rm pl}^2(n+1)^2}{3\mathcal{P}^2\phi_0^2} - 1\Big)\Big(1 + \frac{V(\phi_0)\mathcal{P}^{2n}}{\frac{1}{2}\phi_0^2\dot{\mathcal{P}}^2}\Big) \\
&= \frac{2M_{\rm pl}^2(n+1)^2}{3\mathcal{P}^2\phi_0^2} + \frac{2M_{\rm pl}^2(n+1)^2}{3\mathcal{P}^2\phi_0^2}\Big(\frac{\mathcal{P}^{2n}}{1-\mathcal{P}^{2n}}\Big) - \Big(\frac{\mathcal{P}^{\bar{n}}}{1-\mathcal{P}^{2n}}\Big) \\
&= \frac{2M_{\rm pl}^2(n+1)^2}{3\mathcal{P}^2\phi_0^2}\Big(\frac{1}{1-\mathcal{P}^{2n}}\Big) - \Big(\frac{\mathcal{P}^{2n}}{1-\mathcal{P}^{2n}}\Big) \\
&\simeq \frac{2M_{\rm pl}^2(n+1)^2}{3\mathcal{P}^2\phi_0^2}\Big(\frac{1}{1-\mathcal{P}^{2n}}\Big)\,. \qquad (4)
\end{aligned}
$$

In the above equation, we have two terms, the first one of which will grow with time, as $\phi_0^2(t)$ decays, whereas the second one is only a periodic function having no such monotonic growth or decay over time. Hence, in the final line, we have dropped that oscillatory term. We now write the whole expression of the numerator

$$
\text{Numerator} \simeq \frac{2M_{\rm pl}(n+1)}{\sqrt{6}\mathcal{P}\phi_0\sqrt{(1-\mathcal{P}^{2n})}} - 1\,. \qquad (5)
$$

Now, from the denominator of Eq.(3)

$$
\text{Denominator} = \frac{2M_{\rm pl}^2(n+1)}{\mathcal{P}\dot{\mathcal{P}}\phi_0^2}\Big(1 - \frac{3\mathcal{P}^2\phi_0^2}{2(n+1)^2M_{\rm pl}^2}\Big)\,. \qquad (6)
$$

Using Eqs.(5) and (6), we reach an approximate expression of $H$ as

$$
H \simeq \frac{\Big(2M_{\rm pl}\dot{\mathcal{P}}\phi_0(n+1) - \sqrt{6}\mathcal{P}\dot{\mathcal{P}}\phi_0^2\sqrt{(1-\mathcal{P}^{2n})}\Big)}{2\sqrt{6}M_{\rm pl}^2(n+1)\sqrt{(1-\mathcal{P}^{2n})}}\,. \qquad (7)
$$

As $\phi_0(t)$ is gradually decaying, we have dropped the terms containing higher powers of $\phi_0(t)$ to reach Eq.(7). Finally, using Eq.(2.67), the expression (7) can be written in the following simplified form

$$
\boxed{H(t) \simeq \bar{H}(t)\left(1 + \underbrace{\frac{\sqrt{6}\mathcal{P}(t)\sqrt{1-\mathcal{P}(t)^{2n}}}{2(n+1)}\left(\frac{\phi_0(t)}{M_{\rm pl}}\right)}_{H_{\rm fast}}\right)}\,. \qquad (8)
$$

# Calculation of the perturbative production rate

In the computation of perturbative production rates for both minimal and non-minimal cases, we follow the metric signature $(+,-,-,-,)$ for computational simplicity. The final results will certainly remain independent of the metric signature.

## For minimal case

The energy-momentum tensor for the minimally coupled scalar inflaton field is given by,

$$T^{\phi}_{\mu\nu} = \partial_\mu\phi\partial_\nu\phi - \frac{1}{2}\eta_{\mu\nu}(\partial^\alpha\phi\partial_\alpha\phi - V(\phi)). \tag{9}$$

For the minimally coupled scalar fluctuation, the energy-momentum tensor is given by

$$T^{\chi}_{\mu\nu} = \partial_\mu\chi\partial_\nu\chi - \frac{1}{2}\eta_{\mu\nu}(\partial^\alpha\chi\partial_\alpha\chi - m_\chi^2\,\chi^2). \tag{10}$$

Note that minimal coupling with gravity always leads to a three-point vertex at the tree level(see the left panel of Fig.(1)). For the minimal case, the gravitational interaction takes the following form.

$$\mathcal{L}_{\rm int} = -\frac{h^{\mu\nu}}{M_{\rm pl}}\left(T^{\phi}_{\mu\nu} + T^{\chi}_{\mu\nu}\right) \tag{11}$$

where $T^{\phi}_{\mu\nu}$, and $T^{\chi}_{\mu\nu}$ are given by Eqs.(9) and (10). Further treating the inflaton as a classical background, the transition probability turns out to be proportional to the energy-momentum tensor as

$$\mathcal{M}^{\phi}_{\mu\nu} = -i\frac{T^{\phi}_{\mu\nu}}{M_{\rm pl}} = -\frac{i}{M_{\rm pl}}\left\{\partial_\mu\phi\,\partial_\nu\phi - \frac{1}{2}\eta_{\mu\nu}\left(\partial^\alpha\phi\,\partial_\alpha\phi - V(\phi)\right)\right\} \tag{12}$$

for $\phi\,\phi\,h_{\mu\nu}$ vertices (see left panel of Fig. 1). For $\chi^2\,h_{\mu\nu}$ vertices, however, it is,

$$\mathcal{M}^{\chi}_{\rho\sigma} = -\frac{2\,i}{M_{\rm pl}}\left(p_{1\rho}p_{2\sigma} + p_{1\sigma}p_{2\rho} - \eta_{\rho\sigma}(p_1\cdot p_2 + m_\chi^2)\right), \tag{13}$$

where "$p_1$" and "$p_2$" are the final state $\chi$ particle's four-momenta. The final scattering amplitude is expressed as,

$$\mathcal{M}^{\phi\chi} = \mathcal{M}^{\phi}_{\mu\nu}\,\Pi^{\mu\nu\rho\sigma}\,\mathcal{M}^{\chi}_{\rho\sigma}, \tag{14}$$

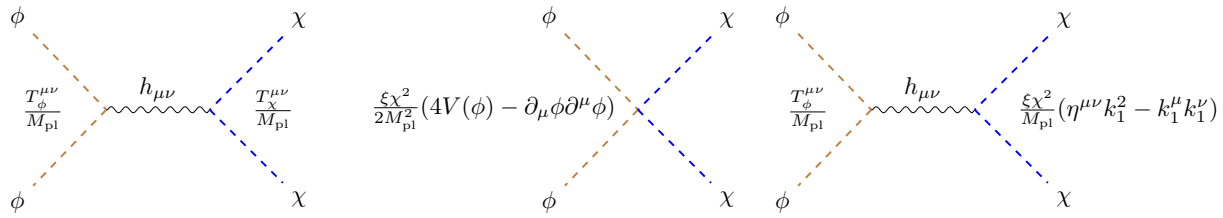


Figure 1: Feynman diagrams illustrating the perturbative gravitational production of the scalar field ($\chi$) in the minimal scenario (left), the Einstein frame (middle), and the Jordan frame (right) in the non-minimal coupling scenarios.

where $\Pi^{\mu\nu\rho\sigma}$ is the graviton propagator for the canonical field $h_{\mu\nu}$ with momentum $\sqrt{s}$,

$$\Pi^{\mu\nu\rho\sigma} = \frac{1}{2\,s}\left(\eta^{\mu\rho}\eta^{\nu\sigma} + \eta^{\mu\sigma}\eta^{\nu\rho} - \eta^{\mu\nu}\eta^{\rho\sigma}\right). \tag{15}$$

where "$s$" is the Mandelstam variable defined in terms of the background condensate energy. Utilizing the above expression of the propagator we obtained,

$$M^{\phi}_{\mu\nu}\,\Pi^{\mu\nu\rho\sigma} = \frac{1}{M_{\rm pl}\,s}\left[\partial^\rho\phi\partial^\sigma\phi - \eta^{\rho\sigma}V(\phi)\right], \tag{16}$$

$$\mathcal{M}^{\phi\chi} = \frac{2}{M^2_{\rm pl}s}\left(\partial^\rho\phi\partial^\sigma\phi - \eta^{\rho\sigma}V(\phi)\right)\left(p_{1\rho}p_{2\sigma} + p_{1\sigma}p_{2\rho} - \eta_{\rho\sigma}(p_1\cdot p_2 + m_\chi^2)\right). \tag{17}$$

Expanding and simplifying the above equation, we have

$$\mathcal{M}^{\phi\chi} = \frac{2\,i}{M^2_{\rm pl}\,s}\left[(\partial^\rho\phi\,p_{1\rho})(\partial^\sigma\phi\,p_{2\sigma}) + (\partial^\rho\phi\,p_{2\rho})(\partial^\sigma\phi\,p_{1\sigma}) - 2p_1\cdot p_2 V(\phi) + 4V(\phi)(p_1\cdot p_2 + m_\chi^2)\right]. \tag{18}$$

For a homogeneous field $\phi(t)$, $\partial_\mu\phi = \dot\phi$ and spatial derivatives vanish. Substituting this,

$$\mathcal{M}^{\phi\chi} = \frac{2\,i}{M^2_{\rm pl}\,s}\left[2\,\dot\phi^2\,p_1^0\,p_2^0 - \dot\phi^2(p_1\cdot p_2 + m_\chi^2) + 2p_1\cdot p_2\,V(\phi) + 4\,m_\chi^2\,V(\phi)\right]. \tag{19}$$

For the inflaton condensate, we can use the transition amplitude $\mathcal{M}_\nu$ for each oscillating field mode of $\phi$, defined the main text. In this case, the four-momentum of the $\nu$-th oscillation mode is given by $p_\nu = \sqrt{s} = (E_\nu, 0)$ where $E_\nu = \nu\,\omega$ represents the energy of the $\nu$-th oscillation mode. The four-momenta $p_1 = (E_\nu/2, \vec{p})$ and $p_2 = (E_\nu/2, -\vec{p})$, $s = (p_1 + p_2)^2 = E_\nu^2$ and $p_1\cdot p_2 = E_\nu^2/2 - m_\chi^2$. Finally from Eq.(19), we obtain

$$|\mathcal{M}^{\phi\chi}_\nu|^2 = \frac{1}{M^4_{\rm pl}}V(\phi)^2\left(1 + \frac{2m_\chi^2}{E_\nu^2}\right)^2. \tag{20}$$

Using $V(\phi) = V(\phi_0)\,\mathcal{P}^{2n}(t) = \rho_\phi\sum_\nu \mathcal{P}^{2n}_\nu\,e^{-i\nu\omega t}$ and $\rho_\phi \simeq V(\phi_0)$,

$$|\mathcal{M}^{\phi\chi}_\nu|^2 = \frac{\rho_\phi^2}{M^4_{\rm pl}}\left(1 + \frac{2\,m_\chi^2}{\nu^2\,\omega^2}\right)^2|\mathcal{P}^{2n}_\nu|^2. \tag{21}$$

To calculate the decay width, we have used the following relation [336],

$$\Gamma_\phi = \frac{1}{8\pi(1+w_\phi)\rho_\phi}\sum_\nu E_\nu\,|\mathcal{M}_\nu^{\phi\chi}|^2\left(1-\frac{4\,m_\chi^2}{E_\nu^2}\right)^{1/2} \tag{22}$$

and the final expression for the decay width will be

$$\Gamma_\phi = \frac{\rho_\phi}{8\,\pi(1+w_\phi)M_{\rm pl}^4}\sum_\nu \nu\,\omega\,|\mathcal{P}_\nu^{2n}|^2\left(1-\frac{4m_\chi^2}{\nu^2\omega^2}\right)^{\frac{1}{2}}\left(1+\frac{2m_\chi^2}{\nu^2\omega^2}\right). \tag{23}$$

For massless radiation $m_\chi = 0$ and $\omega = \gamma\, m_\phi(t)$, so the production rate

$$\boxed{Q(t) = (1+w_\phi)\,\Gamma_\phi\,\rho_\phi = \frac{\rho_\phi^2\, m_\phi}{8\pi M_{\rm pl}^4}\sum_\nu \gamma\,\nu\,|\mathcal{P}_\nu^{2n}|^2} \tag{24}$$

# For non-minimal case

## Einstein frame analysis :

In the presence of non-minimal coupling between the massless scalar and gravity, we write down the total action of the inflaton-scalar field system in the Jordan frame as follows:

$$S = \int\sqrt{-g}\,d^4x\left(-\frac{M_{\rm pl}^2}{2}\Omega^2 R + \frac{1}{2}\partial_\mu\phi\partial^\mu\phi - V(\phi) + \frac{1}{2}\partial_\mu\chi\partial^\mu\chi\right), \tag{25}$$

with the conformal factor $\Omega^2$ is given by

$$\Omega^2 \equiv \left(1+\frac{\xi\chi^2}{M_{\rm pl}^2}\right). \tag{26}$$

To deal with a non-minimally coupled system, It is convenient to switch to the Einstein frame by the following metric redefinition:

$$g_{\mu\nu}^{\rm E} = \Omega^2 g_{\mu\nu} \tag{27}$$

Under this transformation the Jordan frame Ricci scalar is transformed as [337]

$$R = \Omega^2\left(R^{\rm E} + 6\nabla_\mu\nabla^\mu{\rm ln}\Omega - 6g^{{\rm E}\mu\nu}\partial_\mu{\rm ln}\Omega\;\partial_\nu{\rm ln}\Omega\right). \tag{28}$$

Second term in the above equation being the total divergence term will not contribute to the Einstein frame action. Therefore, eliminating the term we find the Einstein frame action as follows:

$$S_{\rm E} = \int\sqrt{-g^{\rm E}}d^4x\left(-\frac{M_{\rm pl}^2}{2}R^{\rm E} + \frac{1}{2\Omega^2}\partial_\mu\phi\partial^\mu\phi + \frac{1}{2\Omega^2}\partial_\mu\chi\partial^\mu\chi + \frac{6M_{\rm pl}^2}{2}g^{{\rm E}\mu\nu}\partial_\mu{\rm ln}\Omega\;\partial_\nu{\rm ln}\Omega - \frac{V(\phi)}{\Omega^4}\right) \tag{29}$$

As we are interested in the small-field limit $\frac{\xi\,\chi^2}{M_{\rm pl}^2} << 1$, the conformal factor(26) is approximated as

$$\Omega \approx \left(1 + \frac{\xi\chi^2}{2M_{\rm pl}^2}\right). \tag{30}$$

Let us now simplify the Einstein frame inflaton-scalar field Lagrangian (29) as follows:

$$\begin{aligned}
\mathcal{L}_{\rm E} &= \left(\frac{1}{2\Omega^2}\partial_\mu\phi\partial^\mu\phi + \frac{1}{2\Omega^2}\partial_\mu\chi\partial^\mu\chi + 3M_{\rm pl}^2\, g^{{\rm E}\mu\nu}\partial_\mu{\rm ln}\Omega\;\partial_\nu{\rm ln}\Omega - \frac{V(\phi)}{\Omega^4}\right) \\
&= \frac{1}{2\Omega^2}\partial_\mu\phi\partial^\mu\phi + \frac{1}{2\Omega^2}\partial_\mu\chi\partial^\mu\chi + \frac{3M_{\rm pl}^2\, g^{{\rm E}\mu\nu}}{\Omega^2}\left(\frac{\partial\Omega}{\partial\chi}\right)^2\partial_\mu\chi\partial_\nu\chi - \frac{V(\phi)}{\Omega^4} \\
&\approx \left(1 - \frac{\xi\chi^2}{M_{\rm pl}^2}\right)\frac{\partial_\mu\phi\partial^\mu\phi}{2} + \left(\frac{3\,\xi^2\chi^2}{M_{\rm pl}^2} + \frac{1}{2}\right)\left(1 - \frac{\xi\,\chi^2}{M_{\rm pl}^2}\right)\partial_\mu\chi\partial^\mu\chi - V(\phi)\left(1 - \frac{2\,\xi\chi^2}{M_{\rm pl}^2}\right) \\
&\approx \Bigg(\underbrace{\frac{1}{2}\partial_\mu\phi\partial^\mu\phi - V(\phi) + \frac{1}{2}\partial_\mu\chi\partial^\mu\chi}_{\text{free Lagrangian}} + \underbrace{\frac{\chi^2}{2}\partial_\mu\chi\partial^\mu\chi\left(\frac{6\xi^2}{M_{\rm pl}^2} - \frac{\xi}{M_{\rm pl}^2}\right)}_{\text{non-canonical kinetic terms}}\Bigg) + \underbrace{\frac{\xi\,\chi^2}{M_{\rm pl}^2}\left(2\,V(\phi) - \frac{1}{2}\partial_\mu\phi\,\partial^\mu\phi\right)}_{\text{effective interaction Lagrangian } \mathcal{L}_{\rm E}^{\rm eff}} \\
&+ {\rm h.o}
\end{aligned} \tag{31}$$

In the present study, as we are considering a massless scalar field without any self-interaction, the free Lagrangian part of $\chi$ field doesn't contain any potential part. Evidently, in the Einstein frame Lagrangian (31) we encounter the non-canonical kinetic terms of the massless scalar field $\chi$, which vanishes at $\xi = 1/6$. The following effective interaction Lagrangian $\mathcal{L}_{\rm E}^{\rm eff}$ gives the production of massless scalars from the background inflaton condensate, $|\phi\rangle \to |\chi\chi\rangle$, which is non-vanishing at the conformal limit. Working in the weak field limit, with an expansion in powers of the gravitational coupling $G$ and taking the terms up to the linear order of perturbation, we write the Einstein frame metric as follows [338]:

$$\begin{aligned}
g_{\mu\nu}^{\rm E} &= \eta_{\mu\nu} + 2\frac{h_{\mu\nu}}{M_{\rm pl}} \\
g^{{\rm E}\,\mu\nu} &= \eta^{\mu\nu} - 2\frac{h^{\mu\nu}}{M_{\rm pl}} \\
\sqrt{-g^{\rm E}} &= 1 + \frac{\eta^{\mu\nu}h_{\mu\nu}}{M_{\rm pl}}
\end{aligned} \tag{32}$$

where $\eta_{\mu\nu}$ is the flat-space metric, and $h_{\mu\nu}$ is the perturbation (graviton field) on top of the flat metric. Using the expansions of (32) in the action (29) and from the free Lagrangian and non-canonical kinetic terms involving parts of the Einstein frame Lagrangian $\mathcal{L}_{\rm E}$, we obtain the following leading-order gravitational interactions.

$$\mathcal{L}_{\rm E}^{\rm int} \supset -\frac{h_{\mu\nu}}{M_{\rm pl}}\left(T^{\phi\,\mu\nu} + T^{\chi\,\mu\nu}\left(1 + \frac{6\xi^2\,\chi^2}{M_{\rm pl}^2} - \frac{\xi\chi^2}{M_{\rm pl}^2}\right)\right) \tag{33}$$

where $T^{\phi}_{\mu\nu}$, and $T^{\chi}_{\mu\nu}$ are given by Eqs.(9) and (10). Setting $\xi = 0$ in (33), we can get back the minimal interaction (11) as expected. From the effective interaction Lagrangian $\mathcal{L}^{\rm eff}_{\rm E}$ we obtain the following gravitational interaction Lagrangian.

$$\mathcal{L}^{\rm int}_{\rm E} \supset \left(\frac{\xi\,\chi^2}{M^2_{\rm pl}}\right)\left(2V(\phi) - \frac{1}{2}\partial_\mu\phi\partial^\mu\phi\right) + \left(\frac{\xi\,\chi^2}{M^2_{\rm pl}}\right)\left(\frac{h_{\mu\nu}}{M_{\rm pl}}\right)\left(\partial^\mu\phi\partial^\nu\phi + \eta^{\mu\nu}\left(2V(\phi) - \frac{\partial_\alpha\phi\partial^\alpha\phi}{2}\right)\right) \tag{34}$$

Finally, combining (33) and (34), we write the total Einstein frame interaction Lagrangian as follows:

$$\mathcal{L}^{\rm int}_{\rm E} = -h_{\mu\nu}\Bigg(\underbrace{\frac{T^{\phi\,\mu\nu}}{M_{\rm pl}} + \frac{T^{\chi\,\mu\nu}}{M_{\rm pl}}}_{\text{minimal interaction}} \underbrace{- \frac{\xi\,\chi^2}{M^3_{\rm pl}}\left(\partial^\mu\phi\partial^\nu\phi + \eta^{\mu\nu}\left(2V(\phi) - \frac{\partial_\alpha\phi\partial^\alpha\phi}{2}\right)\right) + \frac{T^{\chi\,\mu\nu}}{M^3_{\rm pl}}\left(6\xi^2\,\chi^2 - \xi\chi^2\right)}_{\text{non-minimal gravitational interaction with } M_{\rm pl}^{-3} \text{ suppression}}\Bigg)$$
$$+ \underbrace{\left(\frac{\xi\,\chi^2}{M^2_{\rm pl}}\right)\left(2V(\phi) - \frac{1}{2}\partial_\mu\phi\partial^\mu\phi\right)}_{\text{non-minimal gravitational interaction with } M_{\rm pl}^{-2} \text{ suppression}} \tag{35}$$

We finally proceed to study the non-minimal production of massless scalar fluctuations from the background inflaton condensate with the leading $1/M^2_{\rm pl}$ suppressed term in the interaction Lagrangian (35). Therefore, the $1/M^2_{\rm pl}$ suppressed interaction leads to the process $|\phi\rangle \to |\chi\chi\rangle$ with a transition amplitude(like an interaction process, $\phi\phi \to \chi\chi$, where $\phi$ is an oscillating condensate)

$$\mathcal{M}^{\phi\chi}_{\xi} = -\frac{i\xi}{M^2_{\rm pl}}\left(2V(\phi) - \frac{1}{2}\partial_\mu\phi\partial^\mu\phi\right)$$
$$\mathcal{M}^{\phi\chi}_{\xi} = -\frac{i\xi}{M^2_{\rm pl}}\sum_{\nu=1}^{\infty}\left(2\rho_\phi\mathcal{P}^{2n}_\nu + \frac{2n(2n-1)\gamma^2\nu^2\rho_\phi|\mathcal{P}_\nu|^2}{2}\right)$$
$$|\mathcal{M}^{\phi\chi}_{\xi}|^2 = \left(\frac{\xi\rho_\phi}{M^2_{\rm pl}}\right)^2\sum_{\nu=1}^{\infty}\left|\left(2\mathcal{P}^{2n}_\nu + \frac{2n(2n-1)\gamma^2\nu^2|\mathcal{P}_\nu|^2}{2}\right)\right|^2 \tag{36}$$

To reach the final line of the Eq.(36) we have utilized the equations (2.64), (2.66) and (2.69) along with the relations [35, 36]

$$\dot\phi(t) \approx -i\nu\phi_0(t)\omega(t)\mathcal{P}(t)\,,\ V(\phi) = \rho_\phi(t)\mathcal{P}^{2n}(t)\,,\ m_\phi(t) = \sqrt{6n(2n-1)}H(a)\left(\frac{M_{\rm pl}}{\phi_0}\right) \tag{37}$$

Using the non-minimal transition amplitude (36) in the equations (22) and (24), we finally obtain the following expression of non-minimal coupling-induced production rate.

$$\boxed{Q(t) = \frac{\xi^2\rho^2_\phi\,m_\phi}{8\pi M^4_{\rm pl}}\sum_{\nu=1}^{\infty}\nu\gamma\left|\left(2\mathcal{P}^{2n}_\nu + \frac{2n(2n-1)\gamma^2\nu^2|\mathcal{P}_\nu|^2}{2}\right)\right|^2} \tag{38}$$

### Jordan frame analysis :

Considering only the inflaton-scalar fluctuation part in the Lagrangian, from (25) we write the Jordan frame action as follows:

$$S = \int \sqrt{-g} d^4x \left( \frac{1}{2}\partial_\mu\phi\partial^\mu\phi - V(\phi) + \frac{1}{2}\partial_\mu\chi\partial^\mu\chi - \frac{1}{2}\xi\chi^2 R \right) \tag{39}$$

Likewise, Einstein frame gravitational field perturbation (see Eq.(32)), we also quantize the gravitational field by taking the linear order metric perturbation in the Jordan frame. Under this metric perturbation, the curvature scalar up to the first order metric perturbation is written as follows [338]:

$$R^{(1)} = \frac{2}{M_{\rm pl}} \left( \eta_{\alpha\beta}\partial_\mu\partial^\mu h^{\alpha\beta} - \partial_\mu\partial_\nu h^{\mu\nu} \right) \tag{40}$$

Substituting (40) to the action (39), we write the Jordan frame action as a function of the perturbed metric field as follows:

$$S = \int d^4x \left( 1 + \frac{\eta^{\mu\nu}h_{\mu\nu}}{M_{\rm pl}} \right) \times \left( \frac{\left( \eta^{\mu\nu} - \frac{2h^{\mu\nu}}{M_{\rm pl}} \right) \left( \partial_\mu\phi\partial_\nu\phi + \partial_\mu\chi\partial_\nu\chi \right)}{2} - V(\phi) + \frac{\xi\chi^2}{M_{\rm pl}} \left( \partial_\mu\partial_\nu h^{\mu\nu} - \eta_{\alpha\beta}\partial_\mu\partial^\mu h^{\alpha\beta} \right) \right) \tag{41}$$

The above action (41) leads to the following gravitational interaction in the Jordan frame:

$$\mathcal{L}_{\rm int} = \underbrace{-\frac{h^{\mu\nu}}{M_{\rm pl}} \left( T^\phi_{\mu\nu} + T^\chi_{\mu\nu} \right)}_{\text{minimal interaction}} + \underbrace{\left( \frac{\xi\,\chi^2}{M_{\rm pl}} \right) \left( \partial_\mu\partial_\nu h^{\mu\nu} - \eta_{\alpha\beta}\partial_\mu\partial^\mu h^{\alpha\beta} \right)}_{\text{non-minimal interaction } \mathcal{L}^\xi_{\rm int}} \tag{42}$$

Likewise the Einstein frame, we can also generate the minimal gravitational interaction setting $\xi = 0$ in (42). To study the non-minimal production of $\chi$ particles from the background inflaton condensate, we consider the second-order scattering matrix term, $S^{(2)}_{fi}$, which gives the gravity-mediated non-minimal production processes. The non-minimal coupling associated relevant second-order matrix element is written as follows:

$$\begin{aligned} S^{\xi\,(2)}_{fi} =& \frac{\xi}{2M^2_{\rm pl}} \int d^4x \int d^4y \, \langle f | \, T \Big[ h^{\mu\nu}(x) T^\phi_{\mu\nu}(x) \chi^2(y) \left( \partial_\mu\partial_\nu h^{\mu\nu}(y) - \eta_{\alpha\beta}\partial_\mu\partial^\mu h^{\alpha\beta}(y) \right) \\ &+ h^{\mu\nu}(y) T^\phi_{\mu\nu}(y) \chi^2(x) \left( \partial_\mu\partial_\nu h^{\mu\nu}(x) - \eta_{\alpha\beta}\partial_\mu\partial^\mu h^{\alpha\beta}(x) \right) \Big] \, | i \rangle \end{aligned} \tag{43}$$

where "$i$" and "$f$" stand for initial inflaton condensate, $|\phi\rangle$, and final $\chi$ particles state, $|\chi\chi\rangle$, respectively. To proceed to compute these matrix elements, we first quantize the graviton field($h_{\mu\nu}$), and the scalar field($\chi$).

$$\hat{\chi}(x) = \int d\Pi_k \left( \hat{a}_{\vec{k}} e^{-ik_\mu x^\mu} + \text{h.c} \right)$$

$$\hat{h}^{\mu\nu}(x) = \sum_{\lambda=++,--} \int d\Pi_k \left(\epsilon^{\lambda\,\mu\nu}(k)\hat{a}^{\lambda}_{\vec{k}} e^{-ik_\mu x^\mu} + \text{h.c}\right) \tag{44}$$

where $d\Pi_k = \frac{d^3k}{(2\pi)^3\sqrt{2k^0}}$ is the phase-space factor. The polarization tensor for the spin-2 graviton field and the creation, annihilation operators of the scalar field satisfy the following relations:

$$\begin{aligned}
&\sum_{\lambda=++,--} \epsilon^{\lambda\,\mu\nu}(k)\left(\epsilon^{\lambda\,\alpha\beta}(k)\right)^* = \frac{1}{2}\left(\eta^{\mu\alpha}\eta^{\nu\beta} + \eta^{\mu\beta}\eta^{\nu\alpha} + \eta^{\mu\nu}\eta^{\alpha\beta}\right) = P^{\mu\nu\alpha\beta} \\
&\left[\hat{a}^{\lambda}_{\vec{p}}, \hat{a}^{\lambda'\,\dagger}_{\vec{k}}\right] = (2\pi)^3\delta^3(\vec{p}-\vec{k})\delta^{\lambda\lambda'}
\end{aligned} \tag{45}$$

Using (44) in (43) we compute the expression of the matrix element associated with the first term $h^{\mu\nu}(x)T^{\phi}_{\mu\nu}(x)\chi^2(y)\left(\partial_\mu\partial_\nu h^{\mu\nu}(y) - \eta_{\alpha\beta}\partial_\mu\partial^\mu h^{\alpha\beta}(y)\right)$ as follows:

$$\begin{aligned}
S^{\xi\,(2)}_{\phi\to\chi\chi} \supset &\frac{\xi}{M^2_{\text{pl}}}\sum_{\lambda\lambda'}\int d^4x\int d^4y\int d\Pi_{k_1}\int d\Pi_{k_2}\int d\Pi_p\int d\Pi_q T^{\phi}_{\mu\nu}(x)\sqrt{p^0_1 p^0_2} \\
&\times\langle 0|\left(\epsilon^{\lambda\,\mu\nu}(k_1)\hat{a}^{\lambda}_{\vec{k}_1}e^{-ik_{1\mu}x^\mu} + \text{h.c}\right)\left(\epsilon^{\lambda'\,\alpha\beta}(k_2)\hat{a}^{\lambda'}_{\vec{k}_2}e^{-ik_{2\alpha}y^\alpha} + \text{h.c}\right) \\
&\times\left(\eta_{\alpha\beta}(k_2)_\mu(k_2)^\mu - (k_2)_\alpha(k_2)_\beta\right)|0\rangle\,\langle 0|\,\hat{a}_{\vec{p}_1}\hat{a}_{\vec{p}_2}\left(\hat{a}_{\vec{p}}e^{-ip_\mu y^\mu} + \text{h.c}\right)\left(\hat{a}_{\vec{q}}e^{-iq_\mu y^\mu} + \text{h.c}\right)|0\rangle
\end{aligned} \tag{46}$$

where $p_1,\ p_2$ are the final state four-momenta. The contraction of the graviton operators finally leads to the following propagator[338, 339].

$$D^{\mu\nu\alpha\beta}(x-y) = \lim_{\epsilon\to 0^+}\int\frac{d^4k_1}{(2\pi)^4}\frac{i}{k_1^2+i\epsilon}e^{-ik_1(x-y)}P^{\mu\nu\alpha\beta} \tag{47}$$

It gives

$$T^{\phi}_{\mu\nu}P^{\mu\nu\alpha\beta} = \left(\partial^\alpha\phi\partial^\beta\phi - \eta^{\alpha\beta}V(\phi)\right) \tag{48}$$

Using (47) and (48) in (46), after some straightforward computations we reach

$$\begin{aligned}
S^{\xi\,(2)}_{\phi\to\chi\chi} \supset &\frac{\xi}{M^2_{\text{pl}}}\int d^4x\int e^{i(p_2+p_2)y}d^4y\times\lim_{\epsilon\to 0^+}\int\frac{d^4k_1}{(2\pi)^4}\frac{ie^{-ik_1(x-y)}}{k_1^2+i\epsilon}\left(\partial^\alpha\phi\partial^\beta\phi - \eta^{\alpha\beta}V(\phi)\right) \\
&\times\left(\eta_{\alpha\beta}(k_1)_\mu(k_1)^\mu - (k_1)_\alpha(k_1)_\beta\right) \\
=&\frac{i\xi}{M^2_{\text{pl}}}\int d^4x e^{-ik_1x}\int d^4y\int\frac{d^4k_1}{(2\pi)^4}\frac{e^{i(k_1+p_1+p_2)y}}{k_1^2} \\
&\times\left(\partial^\alpha\phi\partial_\alpha\phi(k_1)_\beta(k_1)^\beta - \partial^\alpha\phi(k_1)_\alpha\partial^\beta\phi(k_1)_\beta - 3V(\phi)(k_1)_\beta(k_1)^\beta\right)
\end{aligned} \tag{49}$$

For homogeneous inflaton background, i.e., $\phi = \phi(t)$, we write inflaton-scalar field system's kinematics as

$$p_1\,.\,p_2 = \frac{s}{2},\quad p^0_1 = p^0_2 = \frac{\sqrt{s}}{2},\quad s = (p_1+p_2)^2 \tag{50}$$

where "$s$" is the Mandelstam variable defined earlier in the case of minimal production. Using the equations (2.66), (37), and (50) in (49) we write

$$S^{\xi\,(2)}_{\phi\to\chi\chi} \supset -\frac{3i\xi\rho_\phi}{M^2_{\rm pl}}\sum_\nu \mathcal{P}^{2n}_\nu \int d^4x e^{-i(\nu\omega-p^0_1-p^0_2)t+i(p_1+p_2)_j x^j}$$
$$= -\frac{3i\xi\rho_\phi}{M^2_{\rm pl}}(2\pi)^4\sum_\nu \mathcal{P}^{2n}_\nu \delta(\nu\omega-p^0_1-p^0_2)\delta^3(\vec{p}_1+\vec{p}_2) \tag{51}$$

We obtain the same result from the second element of the S-matrix (43) also. Combining these two, we write the final expression of the non-minimal coupling associated second-order S-matrix element as follows:

$$S^{\xi\,(2)}_{\phi\to\chi\chi} = -\frac{6i\xi\rho_\phi}{M^2_{\rm pl}}(2\pi)^4\sum_\nu \mathcal{P}^{2n}_\nu \delta(\nu\omega-p^0_1-p^0_2)\delta^3(\vec{p}_1+\vec{p}_2) \tag{52}$$

Using the minimal interaction in the Jordan frame interaction Lagrangian (42), we can compute the gravity-mediated minimal production of massless $\chi$ particles from the background inflaton condensate. We find the second-order S-matrix element for the minimal process as follows [339] :

$$S^{\xi=0\,(2)}_{\phi\to\chi\chi} = \frac{i\rho_\phi}{M^2_{\rm pl}}(2\pi)^4\sum_\nu \mathcal{P}^{2n}_\nu \delta(\nu\omega-p^0_1-p^0_2)\delta^3(\vec{p}_1+\vec{p}_2) \tag{53}$$

Therefore, we write the full expression of the S-matrix element describing the gravitational production of massless scalar particles from the inflaton condensate in the Jordan frame as follows:

$$S^{(2)}_{\phi\to\chi\chi} = \left(S^{\xi=0\,(2)}_{\phi\to\chi\chi} + S^{\xi\,(2)}_{\phi\to\chi\chi}\right) = \frac{(1-6\xi)i\rho_\phi}{M^2_{\rm pl}}(2\pi)^4\sum_\nu \mathcal{P}^{2n}_\nu \delta(\nu\omega-p^0_1-p^0_2)\delta^3(\vec{p}_1+\vec{p}_2) \tag{54}$$

From (54), we write the total transition amplitude of this gravitational production process as

$$\left|\mathcal{M}^{\phi\chi}\right|^2 = \frac{(1-6\xi)^2\rho^2_\phi}{M^4_{\rm pl}}\sum_{\nu=1}^{\infty}|\mathcal{P}^{2n}_\nu|^2 \tag{55}$$

**Using the Feynman rule**: We can also directly derive this transition amplitude by using the Feynman rule. In the Jordan frame, the Feynman diagram for the production of scalar fluctuations $\chi$ from the background condensate in the presence of non-minimal coupling $\xi$ is shown in Fig.(1) (see the right most plot). So, the expression of partial amplitudes for $\phi\,\phi\,h_{\mu\nu}$ vertices is the same as we defined in Eq.(12). Here, the partial amplitude for $\chi^2\,h_{\mu\nu}$ vertices is different, which is

$$\mathcal{M}^{\chi}_{\rho\sigma} = -\frac{2\,i\,\xi}{M_{\rm pl}}(\eta_{\rho\sigma}\,k_{1\alpha}\,k^\alpha_1 - k_{1\rho}\,k_{1\sigma})\,, \tag{56}$$

where $k_1 = (p_1 + p_2)$ momentum of the propagator. Therefore, the final scattering amplitude is

$$\begin{aligned}\mathcal{M}_{\xi}^{\phi\chi} &= \mathcal{M}^{\phi}_{\mu\nu}\,\Pi^{\mu\nu\rho\sigma}\,\mathcal{M}^{\chi}_{\rho\sigma} \\ &= \frac{2\,i\,\xi}{M_{\rm pl}^2 s}\left(\partial^{\rho}\phi\partial^{\sigma}\phi - \eta^{\rho\sigma}V(\phi)\right)\left(\eta_{\rho\sigma}\,k_{1\alpha}\,k_1^{\alpha} - k_{1\rho}\,k_{1\sigma}\right) \\ &= \frac{2\,i\,\xi}{M_{\rm pl}^2 s}\left[(\dot{\phi}^2\,k_1^2 - \dot{\phi}^2\,k_1^0\,k_1^0) - (V(\phi)\eta_{\rho\sigma}\,\eta^{\rho\sigma}\,k_1^2 + V(\phi)k_1^2)\right] \\ &= -\frac{6\,i\,\xi}{M_{\rm pl}^2}V(\phi) \quad [\text{where}\;\; k_1^2 = s\,, k_1^0 = \sqrt{s},\; \eta_{\rho\sigma}\,\eta^{\rho\sigma} = 4]\end{aligned} \tag{57}$$

The total scattering amplitude is

$$\begin{aligned}\mathcal{M}^{\phi\chi} &= \mathcal{M}^{\phi\chi}_{\xi=0} + \mathcal{M}^{\phi\chi}_{\xi} \\ &= \frac{i\,(1-6\,\xi)}{M_{\rm pl}^2}V(\phi)\end{aligned} \tag{58}$$

which is the same as we find in Eq.(55). Using this total transition amplitude (55) in the equations (22) and (24), we finally obtain the following expression of the Jordan frame total gravitational production rate.

$$\boxed{Q(t) = \frac{(1-6\xi)^2\rho_{\phi}^2\,m_{\phi}}{8\pi M_{\rm pl}^4}\sum_{\nu=1}^{\infty}\gamma\,\nu\,|\mathcal{P}_{\nu}^{2n}|^2} \tag{59}$$

Clearly, unlike the Einstein frame (38), this production rate vanishes at the conformal limit, $\xi = 1/6$.

# Total Curvature power spectrum in terms of inflaton ($\mathcal{P}_{\delta\phi}$) and the scalar field($\mathcal{P}_{\chi}$) power spectrum

We write the conformal coordinate perturbed metric considering only the scalar degrees of freedom as

$$ds^2 = a^2(\eta)\left[-(1+2\Phi)d\eta^2 + 2\partial_i B dx^i dx^0 + ((1+2\Psi)\delta_{ij} + 2D_{ij}E)\,dx^i dx^j\right] \tag{60}$$

where $\Phi,\ \Psi,\ B,\ E$ are four scalar degrees of freedom, the operator $D_{ij} = \left(\partial_i\partial_j - \frac{1}{3}\delta_{ij}\nabla^2\right)$. Using the property $g^{\mu\alpha}g_{\alpha\nu} = \delta^\mu_\nu$ we find the inverse metric

$$g^{\mu\nu} = a^{-2}(\eta)\begin{pmatrix} (-1+2\Phi) & \partial^i B \\ \partial^i B & (1-2\Psi)\delta^{ij} - 2D^{ij}E \end{pmatrix} \tag{61}$$

In the isotropic and homogeneous universe, the stress-energy tensor of a perfect fluid is written as

$$\bar{T}^\mu_\nu = (\bar{\rho} + \bar{P})\bar{U}^\mu\bar{U}_\nu + \bar{P}\delta^\mu_\nu \tag{62}$$

where $\bar{\rho},\ \bar{P}$ are background unperturbed energy and pressure density and $\bar{U}^\mu$ are relative velocity between fluid and observer, for comoving observer, four-velocity becomes $\bar{U}^\mu = -a^{-1}\delta^\mu_0$ and $\bar{U}_\mu = a^1\delta^0_\mu$, which satisfy $\bar{U}^\mu\bar{U}_\mu = -1$. Perturbing this stress tensor of the perfect fluid we have $T^\mu_\nu = \bar{T}^\mu_\nu + \delta T^\mu_\nu$, where $\delta T^\mu_\nu$ is the perturbed part of the stress tensor.

$$\delta T^\mu_\nu = \underbrace{(\delta\rho + \delta P)}_{\text{perturbed energy and pressure}}\bar{U}^\mu\bar{U}_\nu + (\bar{\rho}+\bar{P})\underbrace{\left(\delta U^\mu\bar{U}_\nu + \bar{U}^\mu\delta U_\nu\right)}_{\text{perturbed velocity part}} + \delta P\delta^\mu_\nu \tag{63}$$

Using the property $U^\mu U_\nu = -1$ we calculate $\delta g_{\mu\nu}\bar{U}^\mu\bar{U}^\nu + 2\bar{U}_\mu\delta U^\mu = 0$. Subject to this condition, we find $\delta U^0 = a^{-1}\Phi$. Writing $\delta U^i = -\frac{v^i}{a}$ we get

$$U^\mu = a^{-1}\left[(-1+\Phi), -v^i\right] \tag{64}$$

where $v^i = dx^i/d\eta$ is the coordinate velocity. Using the condition $U^\mu U_\mu = -1$ we find up to the linear order of perturbation

$$U_\mu = a\left[(1+\Phi) - (\partial_i B + v_i)\right] \tag{65}$$

Utilizing the equations (64) and (65) in (63) we find up to the linear order of perturbation

$$\delta T_i^0 = (\bar{\rho} + \bar{P})\,(\partial_i B + v_i) \tag{66}$$

Subject to the scalar metric perturbation (60) we find the gauge invariant expression of curvature perturbation as[21, 31, 114, 120, 340]

$$\mathcal{R} = \left(\Psi - \frac{1}{3}\nabla^2 E\right) + \mathcal{H}(B+v) \xrightarrow{\text{spatially flat gauge}} \mathcal{H}(B+v) \tag{67}$$

So, in spatially flat gauge, we can connect the scalar curvature perturbation to the $(0i)$ component of $\delta T^\mu_\nu$ in (66).
In the present context, in addition to the inflaton fluctuation($\delta\phi$), we have another fluid component, the massless scalar fluctuation($\chi$). Therefore, the left hand side of (66) will contain the contributions of both $\delta\phi$ and $\chi$, $\left(\delta T_i^{0(\phi)} + \delta T_i^{0(\chi)}\right)$.
We have the expression of the stress-energy tensor of the minimally coupled inflaton field as

$$T^{(\phi)}_{\mu\nu} = \partial_\mu\phi\partial_\nu\phi - g_{\mu\nu}\left(\frac{1}{2}\partial_\alpha\phi\partial^\alpha\phi + V(\phi)\right) \tag{68}$$

From (68) considering only the linear perturbation terms we get

$$\begin{aligned}
\delta T^{\mu(\phi)}_\nu &= \delta g^{\mu\alpha} T^{(\phi)}_{\alpha\nu} + g^{\mu\alpha}\delta T^{(\phi)}_{\alpha\nu} \\
\Rightarrow \delta T_i^{0(\phi)} &= \delta g^{0i} T^{(\phi)}_{ii} + g^{00}\delta T^{(\phi)}_{0i} + g^{0i}\delta T^{(\phi)}_{ii} \\
&= \frac{\partial^i B}{a^2}\underbrace{\left(\frac{1}{2}(\phi')^2 - a^2 V(\phi)\right)}_{T^{(\phi)}_{ii}}\delta_{ii} + \frac{(2\Phi-1)}{a^2}\underbrace{\left(\partial_i(\delta\phi)\phi' + \frac{1}{2}\partial_i B(\phi')^2 - \partial_i B a^2 V(\phi)\right)}_{\delta T^{(\phi)}_{0i}} \\
&\quad + \frac{\partial^i B}{a^2}\left(\delta\phi'\phi' - a^2\frac{\partial V}{\partial\phi}\delta\phi\right)\delta_{ii} + \text{h.o} \\
&= -\frac{\phi'}{a^2}\partial_i(\delta\phi)
\end{aligned} \tag{69}$$

We have the expression of the stress-energy tensor of the non-minimally coupled massless scalar fluctuation as [68, 69]

$$\delta T^{(\chi)}_{\mu\nu}(\eta,\vec{x}) = (1-2\xi)\partial_\mu\chi\partial_\nu\chi + \left(2\xi - \frac{1}{2}\right)g_{\mu\nu}(\partial_\alpha\chi\partial^\alpha\chi) + 2\xi\left(g_{\mu\nu}\chi\Box\chi - \chi\nabla_\mu\partial_\nu\chi\right) + \xi G_{\mu\nu}\chi^2 \tag{70}$$

This gives

$$\begin{aligned}
\delta T^{\alpha(\chi)}_\mu &= (1-2\xi)g^{\nu\alpha}\partial_\mu\chi\partial_\nu\chi + \left(2\xi - \frac{1}{2}\right)g^{\nu\alpha}g_{\mu\nu}(\partial_\beta\chi\partial^\beta\chi) + 2\xi g^{\nu\alpha}g_{\mu\nu}\chi\Box\chi - 2\xi\chi g^{\nu\alpha}\nabla_\mu\partial_\nu\chi \\
&\quad + \xi g^{\nu\alpha}G_{\mu\nu}\chi^2
\end{aligned}$$

$$= (1-2\xi)g^{\nu\alpha}\partial_\mu\chi\partial_\nu\chi + \left(2\xi - \frac{1}{2}\right) g^{\nu\alpha}g_{\mu\nu}(\partial_\beta\chi\partial^\beta\chi) + 2\xi g^{\nu\alpha}g_{\mu\nu}\chi\Box\chi$$
$$- 2\xi\chi g^{\nu\alpha}\left(\partial_\mu\partial_\nu\chi - \Gamma^\gamma_{\mu\nu}\partial_\gamma\chi\right) + \xi g^{\nu\alpha}G_{\mu\nu}\chi^2 \tag{71}$$

We now simplify the expression (71) for $\alpha = 0,\ \mu = i$.

$$\begin{aligned} g^{\nu 0}g_{i\nu} &= g^{00}g_{i0} + g^{j0}g_{ij} \\ &= (2\Phi - 1)\partial_i B + \partial^j B\left((1+2\Psi)\delta_{ij} + D_{ij}E\right) \\ &= -\partial_i B + \partial_i B + \text{h.o} \\ &= 0 \end{aligned} \tag{72}$$

As the product (72) vanishes in linear order, we need to evaluate only three terms in (71).

$$\begin{aligned} (1).\quad (1-2\xi)g^{0\nu}\partial_i\chi\partial_\nu\chi &= (1-2\xi)\left(g^{00}\partial_i\chi\partial_0\chi + g^{j0}\partial_i\chi\partial_j\chi\right) \\ &= \frac{(1-2\xi)}{a^2}\left((2\Phi-1)\chi'\partial_i\chi + \partial^j B\partial_i\chi\partial_j\chi\right) \\ &= \frac{(2\xi-1)}{a^2}\chi'\partial_i\chi + \text{h.o} \end{aligned} \tag{73}$$

$$\begin{aligned} (2).\quad -2\xi\chi g^{0\nu}\left(\partial_i\partial_\nu\chi - \Gamma^\gamma_{i\nu}\partial_\gamma\chi\right) &= 2\xi\chi\left(g^{0\nu}\Gamma^\gamma_{i\nu}\partial_\gamma\chi - g^{00}\partial_i\chi' - g^{j0}\partial_i\partial_j\chi\right) \\ &= 2\xi\chi \\ &\times\left(\frac{(2\Phi-1)}{a^2}\mathcal{H}\delta^j_i\partial_j\chi + \frac{\partial_i B}{a^2}\mathcal{H}\chi' + \frac{(1-2\Phi)}{a^2}\partial_i\chi' - \frac{\partial^j B}{a^2}\partial_i\partial_j\chi\right) \\ &= \frac{2\xi\chi}{a^2}\left(\partial_i\chi' - \mathcal{H}\partial_i\chi\right) + \text{h.o} \end{aligned} \tag{74}$$

$$\begin{aligned} (3).\quad \xi g^{0\nu}G_{i\nu}\chi^2 &= \xi\chi^2\left(g^{00}G_{i0} + g^{0j}G_{ij}\right) \\ &= \frac{\xi\chi^2}{a^2}\left((2\Phi-1)\underbrace{G_{i0}}_{=0} + \partial^j B G_{ij}\right) \\ &= -\frac{\xi\chi^2}{a^2}\partial_i B\left(\mathcal{H}' + \mathcal{H}^2\right) \end{aligned} \tag{75}$$

As there is a product of perturbation and fluctuation, the above term in (75) can be dropped. Combining (73) and (74), taking only the linear perturbation terms, we end up having

$$\delta T_i^{0(\chi)} = \frac{2\xi}{a^2}\left(\chi'\partial_i\chi + \chi\partial_i\chi' - \mathcal{H}\chi\partial_i\chi\right) - \frac{\chi'\partial_i\chi}{a^2} \tag{76}$$

Plugging the expressions (69) and (76) into (66) we write

$$(\bar{\rho} + \bar{P})\partial_i\left(B + v\right) = \left(\delta T_i^{0(\phi)} + \delta T_i^{0(\chi)}\right)$$

$$\Rightarrow (\bar{\rho}+\bar{P})\partial_i\left(B+v\right) = -\frac{1}{a^2}\Bigg(\underbrace{\left(\phi'\partial_i\delta\phi+\chi'\partial_i\chi\right)}_{\text{minimal term}}+\underbrace{2\xi\left(\chi'\partial_i\chi+\chi\partial_i\chi'-\mathcal{H}\chi\partial_i\chi\right)}_{\text{non-minimal term}}\Bigg) \tag{77}$$

Integrating Eq.(77) we can compute $(B+v)$ in terms of inflaton fluctuation $\delta\phi$ and the additional scalar fluctuation $\chi$. Using the expression of $(B+v)$ as a function of $\delta\phi$, $\chi$ in the Eq.(67), we can directly connect the curvature perturbation to the fluctuations in spatially flat gauge system.
Integrating (77) we write

$$(\bar{\rho}+\bar{P})(B+v) = -\frac{\phi'\delta\phi}{a^2}-\frac{1}{a^2}\int\chi'\partial_i\chi dx^i-\frac{2\xi}{a^2}\left(\chi\chi'\big|_{-\infty}^{\infty}-\int\chi\partial_i\chi' dx^i+\int\chi\partial_i\chi' dx^i-\frac{\mathcal{H}}{2}\chi^2\big|_{-\infty}^{\infty}\right) \tag{78}$$

Considering all the fluctuations to vanish at spatial infinity, we are left with the following expression.

$$(B+v) = -\frac{\delta\phi}{\phi'}-\frac{1}{(\phi')^2}\int\chi'\partial_i\chi dx^i \tag{79}$$

Substituting the Eq.(79) to (67) we express the scalar curvature perturbation as

$$\mathcal{R} = -\frac{\mathcal{H}\delta\phi}{\phi'}-\frac{\mathcal{H}}{(\phi')^2}\int\chi'\partial_i\chi dx^i \tag{80}$$

We write down the scalar field quantization as

$$\chi(\eta,\vec{x}) = \int\frac{d^3\vec{k}}{(2\pi)^3}\left(\chi_{\vec{k}}(\eta)\hat{a}_{\vec{k}}+\chi^*_{\vec{k}}(\eta)\hat{a}^\dagger_{\vec{k}}\right)e^{i\vec{k}.\vec{x}} \tag{81}$$

Plugging Eq.(81) into (80) we have

$$\begin{aligned}\mathcal{R} &= -\frac{\mathcal{H}\delta\phi}{\phi'}-\frac{\mathcal{H}}{(\phi')^2}\int\frac{d^3\vec{k}d^3\vec{p}dx}{(2\pi)^6}\left(\chi'_{\vec{k}}\hat{a}_{\vec{k}}+\chi'^*_{\vec{k}}\hat{a}^\dagger_{\vec{k}}\right)(ip_i)\left(\chi_{\vec{p}}\hat{a}_{\vec{p}}+\chi^*_{\vec{p}}\hat{a}^\dagger_{\vec{p}}\right).e^{i(\vec{k}+\vec{p}).\vec{x}}\\ &= -\frac{\mathcal{H}\delta\phi}{\phi'}+\frac{\mathcal{H}}{(\phi')^2}\int\frac{d^3\vec{k}}{\pi(2\pi)^3}\left(\chi'_{\vec{k}}\hat{a}_{\vec{k}}+\chi'^*_{\vec{k}}\hat{a}^\dagger_{\vec{k}}\right)(ik^2k_i)\left(\chi_{-\vec{k}}\hat{a}_{-\vec{k}}+\chi^*_{-\vec{k}}\hat{a}^\dagger_{-\vec{k}}\right)\end{aligned} \tag{82}$$

Let's first calculate the VEV of curvature perturbation. From the Eq.(82) we write

$$\begin{aligned}\langle\mathcal{R}_k\rangle &= -\underbrace{\frac{\mathcal{H}\langle\delta\phi_k\rangle}{\phi'}}_{=0}+\frac{\mathcal{H}}{(\phi')^2}\int\frac{d^3\vec{k}}{\pi(2\pi)^3}(ik^2k_i)\langle0|\left(\chi'_{\vec{k}}\hat{a}_{\vec{k}}+\chi'^*_{\vec{k}}\hat{a}^\dagger_{\vec{k}}\right)\left(\chi_{-\vec{k}}\hat{a}_{-\vec{k}}+\chi^*_{-\vec{k}}\hat{a}^\dagger_{-\vec{k}}\right)|0\rangle\\ &= \frac{\mathcal{H}}{(\phi')^2}\int\frac{d^3\vec{k}}{\pi(2\pi)^3}(ik^2k_i)\langle0|\left(\chi'_{\vec{k}}\chi^*_{-\vec{k}}\hat{a}_{\vec{k}}\hat{a}^\dagger_{-\vec{k}}+\chi_{-\vec{k}}\chi'^*_{\vec{k}}\hat{a}^\dagger_{\vec{k}}\hat{a}_{-\vec{k}}\right)|0\rangle\\ &= \frac{i\mathcal{H}}{\pi(\phi')^2}\int\frac{d^3\vec{k}}{(2\pi)^3}(k^2k_i)\chi'_{\vec{k}}\chi^*_{-\vec{k}}(2\pi)^3\delta^3(2\vec{k})\end{aligned}$$

$$= 0 \tag{83}$$

So, in presence of an additional fluctuation we also obtain a vanishing VEV of curvature perturbation.

We shall now compute the variance of the curvature perturbation $\langle|\mathcal{R}_k|^2\rangle$. This variance expression will acquire the following non-zero terms.

$$\begin{aligned}\langle|\mathcal{R}_k|^2\rangle = &\frac{\mathcal{H}^2\langle|\delta\phi_k|^2\rangle}{\phi'^2} + \frac{\mathcal{H}^2}{(\phi')^4}\int \frac{d^3\vec{k}_1 d^3\vec{k}_2}{\pi^2(2\pi)^6}(k_1k_2)^2(k_1)_i(k_2)_j \\ &\times \langle 0|\left(\left(\chi'_{\vec{k}_1}\hat{a}_{\vec{k}_1} + \chi'^*_{\vec{k}_1}\hat{a}^\dagger_{\vec{k}_1}\right)\left(\chi_{-\vec{k}_1}\hat{a}_{-\vec{k}_1} + \chi^*_{-\vec{k}_1}\hat{a}^\dagger_{-\vec{k}_1}\right)\left(\chi'_{\vec{k}_2}\hat{a}_{\vec{k}_2} + \chi'^*_{\vec{k}_2}\hat{a}^\dagger_{\vec{k}_2}\right)^\dagger\right. \\ &\left.\times\left(\chi_{-\vec{k}_2}\hat{a}_{-\vec{k}_2} + \chi^*_{-\vec{k}_2}\hat{a}^\dagger_{-\vec{k}_2}\right)^\dagger\right)|0\rangle\end{aligned} \tag{84}$$

In this expression, any $\delta\phi$ and $\chi$ cross term doesn't survive due to the presence of the terms like the product of three creation and annihilation operators, and the VEV of such terms are always zero.

In the second term of the above Eq.(84), only the following combinations will have non-vanishing VEV. Employing the Wick's theorem we get

$$\begin{aligned}\langle 0|\left(\hat{a}_{\vec{k}_1}\hat{a}_{-\vec{k}_1}\hat{a}^\dagger_{\vec{k}_2}\hat{a}^\dagger_{-\vec{k}_2}\right)|0\rangle &= (2\pi)^6\left(\delta^3(\vec{k}_1-\vec{k}_2)\delta^3(\vec{k}_1-\vec{k}_2) + \delta^3(\vec{k}_1+\vec{k}_2)\delta^3(\vec{k}_1+\vec{k}_2)\right) \\ \langle 0|\left(\hat{a}_{\vec{k}_1}\hat{a}^\dagger_{-\vec{k}_1}\hat{a}_{\vec{k}_2}\hat{a}^\dagger_{-\vec{k}_2}\right)|0\rangle &= (2\pi)^6\delta^3(2\vec{k}_1)\delta^3(2\vec{k}_2)\end{aligned} \tag{85}$$

The second combination of creation and annihilation operators in Eq.(85) will be vanishing for any finite $\vec{k}_1,\ \vec{k}_2 \neq 0$. So, this will also not contribute to the variance (84). We finally write

$$\begin{aligned}\langle|\mathcal{R}_k|^2\rangle &= \frac{\mathcal{H}^2\langle|\delta\phi_k|^2\rangle}{\phi'^2} + \frac{\mathcal{H}^2}{(\phi')^4}\int\frac{d^3\vec{k}_1 d^3\vec{k}_2}{\pi^2}(k_1k_2)^2(k_1)_i(k_2)_j \\ &\times\left(\chi'_{\vec{k}_1}\chi'^*_{\vec{k}_2}\chi_{-\vec{k}_1}\chi^*_{-\vec{k}_2}\left(\delta^3(\vec{k}_1-\vec{k}_2)\delta^3(\vec{k}_1-\vec{k}_2)+\delta^3(\vec{k}_1+\vec{k}_2)\delta^3(\vec{k}_1+\vec{k}_2)\right)\right) \\ &= \frac{\mathcal{H}^2\langle|\delta\phi_k|^2\rangle}{\phi'^2} + \frac{\mathcal{H}^2}{(\phi')^4}\int\frac{d^3\vec{k}_1}{\pi^2}(k_1)^4\delta^3(0)|\chi'_{\vec{k}_1}|^2|\chi_{\vec{k}_1}|^2\left((k_1)_i(k_1)_j-(k_1)_i(k_1)_j\right) \\ &= \frac{\mathcal{H}^2\langle|\delta\phi_k|^2\rangle}{\phi'^2}\end{aligned} \tag{86}$$

From this result, we can infer that in a single-field inflationary scenario, any fluctuation without an associated classical homogeneous background will not contribute to the scalar curvature perturbation. And in a multi-field inflationary scenario, associated fluctuations of multiple fluid components or background components will contribute to the curvature perturbation [341, 342]. Therefore, in the present context, the significant super-horizon post-inflationary instability of the massless scalar($\chi$) will not affect the scalar curvature power spectrum, and hence this has an impact on the isocurvature mode that is discussed in Section 6.8.2.

# Bibliography


[1] A.A. Penzias and R.W. Wilson, *A measurement of excess antenna temperature at 4080 mc/s*, *The Astrophysical Journal* **142** (1965) 419.

[2] R.H. Dicke, P.J.E. Peebles, P.G. Roll and D.T. Wilkinson, *Cosmic black-body radiation*, *The Astrophysical Journal* **142** (1965) 414.

[3] G.F. Smoot, C.L. Bennett, A. Kogut, E.L. Wright, J. Aymon, N.W. Boggess et al., *Structure in the COBE differential microwave radiometer first-year maps*, *Astrophysical Journal Letters* **396** (1992) L1.

[4] G.F. Smoot, *Nobel lecture: Cosmic microwave background radiation anisotropies: Their discovery and utilization*, *Rev. Mod. Phys.* **79** (2007) 1349.

[5] Planck collaboration, *Planck 2015 results. XIII. Cosmological parameters*, *Astron. Astrophys.* **594** (2016) A13 [1502.01589].

[6] Planck collaboration, *Planck 2015 results. XX. Constraints on inflation*, *Astron. Astrophys.* **594** (2016) A20 [1502.02114].

[7] Planck collaboration, *Planck 2018 results. X. Constraints on inflation*, *Astron. Astrophys.* **641** (2020) A10 [1807.06211].

[8] Planck collaboration, *Planck 2018 results. VI. Cosmological parameters*, *Astron. Astrophys.* **641** (2020) A6 [1807.06209].

[9] A.H. Guth, *The Inflationary Universe: A Possible Solution to the Horizon and Flatness Problems*, *Phys. Rev. D* **23** (1981) 347.

[10] L. Senatore, *Lectures on Inflation*, in *Theoretical Advanced Study Institute in Elementary Particle Physics: New Frontiers in Fields and Strings*, pp. 447–543, 2017, DOI [1609.00716].

[11] A.D. Linde, *A New Inflationary Universe Scenario: A Possible Solution of the Horizon, Flatness, Homogeneity, Isotropy and Primordial Monopole Problems*, *Phys. Lett. B* **108** (1982) 389.

[12] A. Albrecht and P.J. Steinhardt, *Cosmology for Grand Unified Theories with Radiatively Induced Symmetry Breaking*, *Phys. Rev. Lett.* **48** (1982) 1220.

[13] A.A. Starobinsky, *A New Type of Isotropic Cosmological Models Without Singularity*, *Phys. Lett. B* **91** (1980) 99.

[14] M. Lemoine, J. Martin and P. Peter, eds., *Inflationary cosmology* (2008), 10.1007/978-3-540-74353-8.

[15] J. Martin, *Inflation and precision cosmology*, 2003.

[16] J. Martin, *Inflationary cosmological perturbations of quantum-mechanical origin*, in *Lecture Notes in Physics*, p. 199–244, Springer-Verlag DOI.

[17] L. Sriramkumar, *An introduction to inflation and cosmological perturbation theory*, 2009.

[18] A. Linde, *Inflationary Cosmology after Planck 2013*, in *100e Ecole d'Ete de Physique: Post-Planck Cosmology*, pp. 231–316, 2015, DOI [1402.0526].

[19] O.F. Piattella, *Lecture Notes in Cosmology*, UNITEXT for Physics, Springer, Cham (2018), 10.1007/978-3-319-95570-4, [1803.00070].

[20] D. Baumann, *Cosmological inflation: Theory and observations*, *Advanced Science Letters* **2** (2009) 105–120.

[21] D. Baumann, *Primordial Cosmology*, *PoS* **TASI2017** (2018) 009 [1807.03098].

[22] D. Baumann and H.V. Peiris, *Cosmological Inflation: Theory and Observations*, *Adv. Sci. Lett.* **2** (2009) 105 [0810.3022].

[23] B.A. Bassett, S. Tsujikawa and D. Wands, *Inflation dynamics and reheating*, *Reviews of Modern Physics* **78** (2006) 537–589.

[24] K.D. Lozanov, *Lectures on Reheating after Inflation*, 1907.04402.

[25] R. Micha and I.I. Tkachev, *Relativistic turbulence: A long way from preheating to equilibrium*, *Physical Review Letters* **90** (2003) .

[26] R. Micha and I.I. Tkachev, *Turbulent thermalization*, *Phys. Rev. D* **70** (2004) 043538 [hep-ph/0403101].

[27] I. Tkachev, S. Khlebnikov, L. Kofman and A. Linde, *Cosmic strings from preheating*, *Physics Letters B* **440** (1998) 262–268.

[28] A. Rajantie and E.J. Copeland, *Phase transitions from preheating in gauge theories*, *Physical Review Letters* **85** (2000) 916–919.

[29] J.-F. Dufaux, D.G. Figueroa and J. García-Bellido, *Gravitational waves from abelian gauge fields and cosmic strings at preheating*, *Physical Review D* **82** (2010) .

[30] D. Baumann, *Inflation*, in *Theoretical Advanced Study Institute in Elementary Particle Physics: Physics of the Large and the Small*, pp. 523–686, 2011, DOI [0907.5424].

[31] A. Riotto, *Inflation and the theory of cosmological perturbations*, 2017.

[32] A.D. Linde, *Chaotic Inflation*, *Phys. Lett. B* **129** (1983) 177.

[33] A.D. Linde, *Particle physics and inflationary cosmology*, vol. 5 (1990), [hep-th/0503203].

[34] M.A.G. Garcia, K. Kaneta, Y. Mambrini and K.A. Olive, *Reheating and Post-inflationary Production of Dark Matter*, *Phys. Rev. D* **101** (2020) 123507 [2004.08404].

[35] A. Chakraborty and D. Maity, *Squeezing, chaos and thermalization in periodically driven quantum systems: the case of bosonic preheating*, *JHEP* **02** (2024) 110 [2309.10116].

[36] A. Chakraborty, S. Clery, M.R. Haque, D. Maity and Y. Mambrini, *Generalizing the Bogoliubov vs Boltzmann approaches in gravitational production*, *Phys. Rev. D* **112** (2025) 043511 [2503.21877].

[37] R. Kallosh, A. Linde and D. Roest, *Superconformal Inflationary $\alpha$-Attractors*, *JHEP* **11** (2013) 198 [1311.0472].

[38] R. Kallosh and A. Linde, *Polynomial $\alpha$-attractors*, *JCAP* **04** (2022) 017 [2202.06492].

[39] M. Galante, R. Kallosh, A. Linde and D. Roest, *Unity of Cosmological Inflation Attractors*, *Phys. Rev. Lett.* **114** (2015) 141302 [1412.3797].

[40] J. Martin, C. Ringeval, R. Trotta and V. Vennin, *The Best Inflationary Models After Planck*, *JCAP* **03** (2014) 039 [1312.3529].

[41] J.L. Cook, E. Dimastrogiovanni, D.A. Easson and L.M. Krauss, *Reheating predictions in single field inflation*, *JCAP* **04** (2015) 047 [1502.04673].

[42] M. Drewes, J.U. Kang and U.R. Mun, *CMB constraints on the inflaton couplings and reheating temperature in $\alpha$-attractor inflation*, *JHEP* **11** (2017) 072 [1708.01197].

[43] ACT collaboration, *The Atacama Cosmology Telescope: DR6 Constraints on Extended Cosmological Models*, 2503.14454.

[44] ACT collaboration, *The Atacama Cosmology Telescope: DR6 Power Spectra, Likelihoods and $\Lambda$CDM Parameters*, 2503.14452.

[45] M. Drees and Y. Xu, *Refined Predictions for Starobinsky Inflation and Post-inflationary Constraints in Light of ACT*, 2504.20757.

[46] A. Chakraborty, D. Maity and R. Mondal, *Nonminimal infrared gravitational reheating in light of ACT observation*, 2506.02141.

[47] R. Mondal, S. Mondal and A. Chakraborty, *Constraining Reheating Temperature, Inflaton-SM Coupling and Dark Matter Mass in Light of ACT DR6 Observations*, 2505.13387.

[48] M.R. Haque, S. Pal and D. Paul, *ACT DR6 Insights on the Inflationary Attractor models and Reheating*, 2505.01517.

[49] E.W. Kolb and M.S. Turner, *The Early Universe*, vol. 69 (1990), 10.1201/9780429492860.

[50] M.A.G. Garcia, M. Pierre and S. Verner, *Scalar dark matter production from preheating and structure formation constraints*, *Phys. Rev. D* **107** (2023) 043530 [2206.08940].

[51] P. Adshead, Y. Cui and J. Shelton, *Chilly dark sectors and asymmetric reheating*, *Journal of High Energy Physics* **2016** (2016) .

[52] M.A.G. Garcia, K. Kaneta, Y. Mambrini and K.A. Olive, *Inflaton Oscillations and Post-Inflationary Reheating*, *JCAP* **04** (2021) 012 [2012.10756].

[53] P. Adshead, P. Ralegankar and J. Shelton, *Reheating in two-sector cosmology*, *Journal of High Energy Physics* **2019** (2019) .

[54] M.R. Haque, D. Maity and R. Mondal, *WIMPs, FIMPs, and Inflaton phenomenology via reheating, CMB and* $\Delta N_{eff}$, *JHEP* **09** (2023) 012 [2301.01641].

[55] M.R. Haque, D. Maity and P. Saha, *Two-phase reheating: CMB constraints on inflation and dark matter phenomenology*, *Phys. Rev. D* **102** (2020) 083534 [2009.02794].

[56] M.R. Haque, D. Maity and R. Mondal, *Gravitational neutrino reheating*, *Phys. Rev. D* **109** (2024) 063543 [2311.07684].

[57] S. Clery, Y. Mambrini, K.A. Olive and S. Verner, *Gravitational portals in the early Universe*, *Phys. Rev. D* **105** (2022) 075005 [2112.15214].

[58] B. Barman, S. Cléry, R.T. Co, Y. Mambrini and K.A. Olive, *Gravity as a portal to reheating, leptogenesis and dark matter*, *JHEP* **12** (2022) 072 [2210.05716].

[59] S. Sarkar, *Big bang nucleosynthesis and physics beyond the standard model*, *Reports on Progress in Physics* **59** (1996) 1493–1609.

[60] S. Hannestad, *What is the lowest possible reheating temperature?*, *Physical Review D* **70** (2004) .

[61] M. Kawasaki, K. Kohri and N. Sugiyama, *MeV scale reheating temperature and thermalization of neutrino background*, *Phys. Rev. D* **62** (2000) 023506 [astro-ph/0002127].

[62] N. Barbieri, T. Brinckmann, S. Gariazzo, M. Lattanzi, S. Pastor and O. Pisanti, *Current constraints on cosmological scenarios with very low reheating temperatures*, 2501.01369.

[63] P. de Salas, M. Lattanzi, G. Mangano, G. Miele, S. Pastor and O. Pisanti, *Bounds on very low reheating scenarios after planck*, *Physical Review D* **92** (2015) .

[64] P. Ade, Z. Ahmed, M. Amiri, D. Barkats, R.B. Thakur, C. Bischoff et al., *Improved constraints on primordial gravitational waves using planck , wmap, and bicep/ keck observations through the 2018 observing season*, *Physical Review Letters* **127** (2021) .

[65] T.S. Bunch and P.C.W. Davies, *Quantum Field Theory in de Sitter Space: Renormalization by Point Splitting*, *Proc. Roy. Soc. Lond. A* **360** (1978) 117.

[66] L. Kofman, A.D. Linde and A.A. Starobinsky, *Towards the theory of reheating after inflation*, *Phys. Rev. D* **56** (1997) 3258 [hep-ph/9704452].

[67] Y. Ema, R. Jinno, K. Mukaida and K. Nakayama, *Gravitational particle production in oscillating backgrounds and its cosmological implications*, *Phys. Rev. D* **94** (2016) 063517 [1604.08898].

[68] Y. Ema, K. Nakayama and Y. Tang, *Production of Purely Gravitational Dark Matter*, *JHEP* **09** (2018) 135 [1804.07471].

[69] E.W. Kolb and A.J. Long, *Cosmological gravitational particle production and its implications for cosmological relics*, 2312.09042.

[70] N.D. Birrell and P.C.W. Davies, *Quantum field theory in curved spacetime*, in *Quantum Fields in Curved Space*, Cambridge Monographs on Mathematical Physics, p. 36–88, Cambridge University Press (1982).

[71] L. Parker and S.A. Fulling, *Adiabatic regularization of the energy-momentum tensor of a quantized field in homogeneous spaces*, *Phys. Rev. D* **9** (1974) 341.

[72] S. Fulling and L. Parker, *Renormalization in the theory of a quantized scalar field interacting with a robertson-walker spacetime*, *Annals of Physics* **87** (1974) 176.

[73] P.R. Anderson and L. Parker, *Adiabatic regularization in closed robertson-walker universes*, *Phys. Rev. D* **36** (1987) 2963.

[74] L. Parker and D. Toms, *Quantum Field Theory in Curved Spacetime: Quantized Fields and Gravity*, Cambridge Monographs on Mathematical Physics, Cambridge University Press (2009).

[75] D.J.H. Chung, E.W. Kolb, A. Riotto and L. Senatore, *Isocurvature constraints on gravitationally produced superheavy dark matter*, *Phys. Rev. D* **72** (2005) 023511 [astro-ph/0411468].

[76] E. Schro¨dinger, *The proper vibrations of the expanding universe*, *Physica* **6** (1939) 899.

[77] J. Martin, *Inflationary perturbations: The Cosmological Schwinger effect*, *Lect. Notes Phys.* **738** (2008) 193 [0704.3540].

[78] W. Heisenberg and H. Euler, *Consequences of dirac theory of the positron*, 2006.

[79] F. Sauter, *Uber das Verhalten eines Elektrons im homogenen elektrischen Feld nach der relativistischen Theorie Diracs*, *Z. Phys.* **69** (1931) 742.

[80] L.E. Parker, *The creation of particles in an expanding universe*, 2025.

[81] L. Parker, *Particle creation in expanding universes*, *Phys. Rev. Lett.* **21** (1968) 562.

[82] L. Parker, *Quantized fields and particle creation in expanding universes. i*, *Phys. Rev.* **183** (1969) 1057.

[83] L. Parker, *Quantized fields and particle creation in expanding universes. ii*, *Phys. Rev. D* **3** (1971) 346.

[84] L. Parker, *Particle creation in isotropic cosmologies*, *Phys. Rev. Lett.* **28** (1972) 705.

[85] L.H. Ford and L. Parker, *Infrared divergences in a class of robertson-walker universes*, *Phys. Rev. D* **16** (1977) 245.

[86] L.H. Ford and L. Parker, *Quantized gravitational wave perturbations in robertson-walker universes*, *Phys. Rev. D* **16** (1977) 1601.

[87] L.H. Ford and L. Parker, *Creation of particles by singularities in asymptotically flat spacetimes*, *Phys. Rev. D* **17** (1978) 1485.

[88] Y.B. Zel'dovich, *Particle Production in Cosmology*, *Soviet Journal of Experimental and Theoretical Physics Letters* **12** (1970) 307.

[89] Y.B. Zel'dovich and A.A. Starobinsky, *Particle Production and Vacuum Polarization in an Anisotropic Gravitational Field*, *Sov. Phys. JETP* **34** (1972) 1159.

[90] Y.B. Zel'dovich and A.A. Starobinsky, *Rate of particle production in gravitational fields*, *JETP Lett.* **26** (1977) 252.

[91] V.M. Frolov, S.G. Mamaev and V.M. Mostepanenko, *On the Difference in Creation of Particles with Spin 0 and 1/2 in Isotropic Cosmologies*, *Phys. Lett. A* **55** (1976) 389.

[92] A.A. Grib, S.G. Mamaev and V.M. Mostepanenko, *Particle Creation from Vacuum in Homogeneous Isotropic Models of the Universe*, *Gen. Rel. Grav.* **7** (1976) 535.

[93] A.A. Grib, S.G. Mamayev and V.M. Mostepanenko, *Vacuum quantum effects in strong fields*, Friedmann Laboratory Publishing, St.Petersburg (1994).

[94] L.H. Ford, *Gravitational Particle Creation and Inflation*, *Phys. Rev. D* **35** (1987) 2955.

[95] M.S. Turner and L.M. Widrow, *Gravitational Production of Scalar Particles in Inflationary Universe Models*, *Phys. Rev. D* **37** (1988) 3428.

[96] D.J.H. Chung, *Classical Inflation Field Induced Creation of Superheavy Dark Matter*, *Phys. Rev. D* **67** (2003) 083514 [hep-ph/9809489].

[97] V.A. Kuzmin and I.I. Tkachev, *Ultrahigh-energy cosmic rays, superheavy long-lived particles, and matter creation after inflation*, *Journal of Experimental and Theoretical Physics Letters* **68** (1998) 271–275.

[98] V. Kuzmin and I. Tkachev, *Matter creation via vacuum fluctuations in the early universe and observed ultrahigh-energy cosmic ray events*, *Phys. Rev. D* **59** (1999) 123006 [hep-ph/9809547].

[99] M.R. de Garcia Maia, *Spectrum and energy density of relic gravitons in flat Robertson-Walker universes*, *Phys. Rev. D* **48** (1993) 647.

[100] M.A. Amin, M.P. Hertzberg, D.I. Kaiser and J. Karouby, *Nonperturbative Dynamics Of Reheating After Inflation: A Review*, *Int. J. Mod. Phys. D* **24** (2014) 1530003 [1410.3808].

[101] W. Magnus and S. Winkler, *Hill's Equation*, Interscience tracts in pure and applied mathematics, Interscience Publishers (1966).

[102] N. McLachlan, *Theory and Application of Mathieu Functions*, Clarendon Press (1947).

[103] L. Kofman, A.D. Linde and A.A. Starobinsky, *Reheating after inflation*, *Phys. Rev. Lett.* **73** (1994) 3195 [hep-th/9405187].

[104] P.B. Greene, L. Kofman, A.D. Linde and A.A. Starobinsky, *Structure of resonance in preheating after inflation*, *Phys. Rev. D* **56** (1997) 6175 [hep-ph/9705347].

[105] D.G. Figueroa and F. Torrenti, *Parametric resonance in the early Universe—a fitting analysis*, *JCAP* **02** (2017) 001 [1609.05197].

[106] J.F. Dufaux, G.N. Felder, L. Kofman, M. Peloso and D. Podolsky, *Preheating with trilinear interactions: Tachyonic resonance*, *JCAP* **07** (2006) 006 [hep-ph/0602144].

[107] G.N. Felder, L. Kofman and A.D. Linde, *Tachyonic instability and dynamics of spontaneous symmetry breaking*, *Phys. Rev. D* **64** (2001) 123517 [hep-th/0106179].

[108] G.N. Felder, J. Garcia-Bellido, P.B. Greene, L. Kofman, A.D. Linde and I. Tkachev, *Dynamics of symmetry breaking and tachyonic preheating*, *Phys. Rev. Lett.* **87** (2001) 011601 [hep-ph/0012142].

[109] A.A. Abolhasani, H. Firouzjahi and M.M. Sheikh-Jabbari, *Tachyonic Resonance Preheating in Expanding Universe*, *Phys. Rev. D* **81** (2010) 043524 [0912.1021].

[110] P.B. Greene and L. Kofman, *On the theory of fermionic preheating*, *Phys. Rev. D* **62** (2000) 123516 [hep-ph/0003018].

[111] A. Chakraborty, M.R. Haque, D. Maity and R. Mondal, *Inflaton phenomenology via reheating in light of primordial gravitational waves and the latest BICEP/Keck data*, *Phys. Rev. D* **108** (2023) 023515 [2304.13637].

[112] J.M. Bardeen, *Gauge-invariant cosmological perturbations*, *Phys. Rev. D* **22** (1980) 1882.

[113] D. Baumann, *Cosmology: Part iii mathematical tripos*, 2015.

[114] D. Baumann, *Cosmology*, Cambridge University Press (7, 2022), 10.1017/9781108937092.

[115] J.M. Bardeen, P.J. Steinhardt and M.S. Turner, *Spontaneous creation of almost scale-free density perturbations in an inflationary universe*, *Phys. Rev. D* **28** (1983) 679.

[116] N. Bartolo, S. Matarrese and A. Riotto, *Oscillations during inflation and cosmological density perturbations*, *Phys. Rev. D* **64** (2001) 083514 [astro-ph/0106022].

[117] N. Bartolo, S. Matarrese and A. Riotto, *Adiabatic and isocurvature perturbations from inflation: Power spectra and consistency relations*, *Phys. Rev. D* **64** (2001) 123504 [astro-ph/0107502].

[118] D. Wands, N. Bartolo, S. Matarrese and A. Riotto, *An Observational test of two-field inflation*, *Phys. Rev. D* **66** (2002) 043520 [astro-ph/0205253].

[119] A. Riotto, *Inflation and the theory of cosmological perturbations*, *ICTP Lect. Notes Ser.* **14** (2003) 317 [hep-ph/0210162].

[120] V.F. Mukhanov, H.A. Feldman and R. Brandenberger, *Theory of cosmological perturbations*, *Physics Reports* **215** (1992) 203.

[121] L.A. Boyle and P.J. Steinhardt, *Probing the early universe with inflationary gravitational waves*, *Physical Review D* **77** (2008) .

[122] J.M. Maldacena, *Non-Gaussian features of primordial fluctuations in single field inflationary models*, *JHEP* **05** (2003) 013 [astro-ph/0210603].

[123] J. Martin, *Inflation and precision cosmology*, *Braz. J. Phys.* **34** (2004) 1307 [astro-ph/0312492].

[124] J. Martin, *Inflationary cosmological perturbations of quantum-mechanical origin*, *Lect. Notes Phys.* **669** (2005) 199 [hep-th/0406011].

[125] L. Sorbo, *Parity violation in the cosmic microwave background from a pseudoscalar inflaton*, *Journal of Cosmology and Astroparticle Physics* **2011** (2011) 003–003.

[126] R. Sharma, K. Subramanian and T. Seshadri, *Gravitational wave generation in a viable scenario of inflationary magnetogenesis*, *Physical Review D* **101** (2020) .

[127] C. Caprini and L. Sorbo, *Adding helicity to inflationary magnetogenesis*, *Journal of Cosmology and Astroparticle Physics* **2014** (2014) 056–056.

[128] J.L. Cook and L. Sorbo, *Particle production during inflation and gravitational waves detectable by ground-based interferometers*, *Phys. Rev. D* **85** (2012) 023534.

[129] D.G. Figueroa and F. Torrentí, *Gravitational wave production from preheating: parameter dependence*, *Journal of Cosmology and Astroparticle Physics* **2017** (2017) 057–057.

[130] R. Brandenberger, H. Feldman and V. Mukhanov, *Classical and quantum theory of perturbations in inflationary universe models*, 1993.

[131] M.R. Haque, D. Maity, T. Paul and L. Sriramkumar, *Decoding the phases of early and late time reheating through imprints on primordial gravitational waves*, *Phys. Rev. D* **104** (2021) 063513 [2105.09242].

[132] M.C. Guzzetti, N. Bartolo, M. Liguori and S. Matarrese, *Gravitational waves from inflation*, *Riv. Nuovo Cim.* **39** (2016) 399 [1605.01615].

[133] S. Maiti, D. Maity and L. Sriramkumar, *Constraining inflationary magnetogenesis and reheating via GWs in light of PTA data*, 2401.01864.

[134] A. Albrecht, P. Ferreira, M. Joyce and T. Prokopec, *Inflation and squeezed quantum states*, *Phys. Rev. D* **50** (1994) 4807 [astro-ph/9303001].

[135] K. Hashimoto, K.-B. Huh, K.-Y. Kim and R. Watanabe, *Exponential growth of out-of-time-order correlator without chaos: inverted harmonic oscillator*, *JHEP* **11** (2020) 068 [2007.04746].

[136] J. Martin and V. Vennin, *Quantum Discord of Cosmic Inflation: Can we Show that CMB Anisotropies are of Quantum-Mechanical Origin?*, *Phys. Rev. D* **93** (2016) 023505 [1510.04038].

[137] S.S. Haque and B. Underwood, *Squeezed out-of-time-order correlator and cosmology*, *Phys. Rev. D* **103** (2021) 023533 [2010.08629].

[138] A. Bhattacharyya, S. Das, S.S. Haque and B. Underwood, *Rise of cosmological complexity: Saturation of growth and chaos*, *Phys. Rev. Res.* **2** (2020) 033273 [2005.10854].

[139] B.C. Hall, *The baker—campbell—hausdorff formula*, in *Lie Groups, Lie Algebras, and Representations: An Elementary Introduction*, (New York, NY), pp. 63–90, Springer New York (2003), DOI.

[140] L.P. Grishchuk and Y.V. Sidorov, *Squeezed quantum states of relic gravitons and primordial density fluctuations*, *Phys. Rev. D* **42** (1990) 3413.

[141] P.M. Radmore and S.M. Barnett, *Methods in theoretical quantum optics*, 1997, https://api.semanticscholar.org/CorpusID:61184177.

[142] C.M. Caves and B.L. Schumaker, *New formalism for two-photon quantum optics. i. quadrature phases and squeezed states*, *Phys. Rev. A* **31** (1985) 3068.

[143] B.L. Schumaker and C.M. Caves, *New formalism for two-photon quantum optics. ii. mathematical foundation and compact notation*, *Phys. Rev. A* **31** (1985) 3093.

[144] E.N. Lorenz, *Deterministic nonperiodic flow*, *Journal of Atmospheric Sciences* **20** (1963) 130 .

[145] B.-W. Shen, R.A. Pielke, X. Zeng, J. Cui, S. Faghih-Naini, W. Paxson et al., *Three kinds of butterfly effects within lorenz models*, *Encyclopedia* **2** (2022) 1250.

[146] H. Gharibyan, M. Hanada, B. Swingle and M. Tezuka, *Quantum Lyapunov Spectrum*, *JHEP* **04** (2019) 082 [1809.01671].

[147] S. Tsujikawa, K.-i. Maeda and T. Torii, *Preheating of the nonminimally coupled inflaton field*, *Phys. Rev. D* **61** (2000) 103501 [hep-ph/9910214].

[148] Y. Shtanov, J.H. Traschen and R.H. Brandenberger, *Universe reheating after inflation*, *Phys. Rev. D* **51** (1995) 5438 [hep-ph/9407247].

[149] D.I. Kaiser, *Post inflation reheating in an expanding universe*, *Phys. Rev. D* **53** (1996) 1776 [astro-ph/9507108].

[150] D.I. Podolsky and A.A. Starobinsky, *Chaotic reheating*, *Grav. Cosmol. Suppl.* **8N1** (2002) 13 [astro-ph/0204327].

[151] G. Palma and V.H. Cardenas, *Resonance enhancement of particle production during reheating*, *Class. Quant. Grav.* **18** (2001) 2233 [gr-qc/0012005].

[152] L. Abbott, E. Farhi and M.B. Wise, *Particle production in the new inflationary cosmology*, *Physics Letters B* **117** (1982) 29.

[153] A.D. Dolgov and A.D. Linde, *Baryon Asymmetry in Inflationary Universe*, *Phys. Lett. B* **116** (1982) 329.

[154] M.R. Haque and D. Maity, *Gravitational reheating*, *Phys. Rev. D* **107** (2023) 043531 [2201.02348].

[155] D.T. Son, *Reheating and thermalization in a simple scalar model*, *Phys. Rev. D* **54** (1996) 3745 [hep-ph/9604340].

[156] J. McDonald, *Reheating temperature and inflaton mass bounds from thermalization after inflation*, *Phys. Rev. D* **61** (2000) 083513 [hep-ph/9909467].

[157] K. Harigaya and K. Mukaida, *Thermalization after/during Reheating*, *JHEP* **05** (2014) 006 [1312.3097].

[158] K. Mukaida and M. Yamada, *Thermalization Process after Inflation and Effective Potential of Scalar Field*, *JCAP* **02** (2016) 003 [1506.07661].

[159] D.I. Podolsky, G.N. Felder, L. Kofman and M. Peloso, *Equation of state and beginning of thermalization after preheating*, *Phys. Rev. D* **73** (2006) 023501 [hep-ph/0507096].

[160] G.N. Felder and L. Kofman, *The Development of equilibrium after preheating*, *Phys. Rev. D* **63** (2001) 103503 [hep-ph/0011160].

[161] M. Desroche, G.N. Felder, J.M. Kratochvil and A.D. Linde, *Preheating in new inflation*, *Phys. Rev. D* **71** (2005) 103516 [hep-th/0501080].

[162] D. Maity and P. Saha, *(P)reheating after minimal Plateau Inflation and constraints from CMB*, *JCAP* **07** (2019) 018 [1811.11173].

[163] J. Martin, *Cosmic Inflation, Quantum Information and the Pioneering Role of John S Bell in Cosmology*, *Universe* **5** (2019) 92 [1904.00083].

[164] S. Choudhury, *The Cosmological OTOC: Formulating new cosmological micro-canonical correlation functions for random chaotic fluctuations in Out-of-Equilibrium Quantum Statistical Field Theory*, *Symmetry* **12** (2020) 1527 [2005.11750].

[165] S. Choudhury, *The Cosmological OTOC: A New Proposal for Quantifying Auto-correlated Random Non-chaotic Primordial Fluctuations*, *Symmetry* **13** (2021) 599 [2106.01305].

[166] K. Adhikari, S. Choudhury, H.N. Pandya and R. Srivastava, *Primordial Gravitational Wave Circuit Complexity*, *Symmetry* **15** (2023) 664 [2108.10334].

[167] S. Banerjee, S. Choudhury, S. Chowdhury, J. Knaute, S. Panda and K. Shirish, *Thermalization in Quenched Open Quantum Cosmology*, 2104.10692.

[168] P. Bhargava, S. Choudhury, S. Chowdhury, A. Mishara, S.P. Selvam, S. Panda et al., *Quantum aspects of chaos and complexity from bouncing cosmology: A study with two-mode single field squeezed state formalism*, *SciPost Phys. Core* **4** (2021) 026 [2009.03893].

[169] J. Martin, A. Micheli and V. Vennin, *Comparing quantumness criteria*, *EPL* **142** (2023) 18001 [2211.10114].

[170] S. Kanno and J. Soda, *Bell Inequality and Its Application to Cosmology*, *Galaxies* **5** (2017) 99.

[171] S. Kanno and J. Soda, *Infinite violation of Bell inequalities in inflation*, *Phys. Rev. D* **96** (2017) 083501 [1705.06199].

[172] S. Kanno, J.P. Shock and J. Soda, *Quantum discord in de Sitter space*, *Phys. Rev. D* **94** (2016) 125014 [1608.02853].

[173] H. Ollivier and W.H. Zurek, *Introducing Quantum Discord*, *Phys. Rev. Lett.* **88** (2001) 017901 [quant-ph/0105072].

[174] L. Henderson and V. Vedral, *Classical, quantum and total correlations*, *Journal of Physics A: Mathematical and General* **34** (2001) 6899.

[175] D. Maity and S. Pal, *Probing non-classicality of primordial gravitational waves and magnetic field through quantum Poincare sphere*, *Phys. Lett. B* **835** (2022) 137503 [2107.12793].

[176] K.N. Alekseev and J. Peř ina, *Light squeezing at the transition to quantum chaos*, *Physical Review E* **57** (1998) 4023.

[177] L. Song, D. Yan, J. Ma and X. Wang, *Spin squeezing as an indicator of quantum chaos in the dicke model*, *Phys. Rev. E* **79** (2009) 046220.

[178] Y. Sekino and L. Susskind, *Fast Scramblers*, *JHEP* **10** (2008) 065 [0808.2096].

[179] P. Hayden and J. Preskill, *Black holes as mirrors: Quantum information in random subsystems*, *JHEP* **09** (2007) 120 [0708.4025].

[180] J. Maldacena, S.H. Shenker and D. Stanford, *A bound on chaos*, *JHEP* **08** (2016) 106 [1503.01409].

[181] K. Hashimoto, K. Murata and R. Yoshii, *Out-of-time-order correlators in quantum mechanics*, *JHEP* **10** (2017) 138 [1703.09435].

[182] E.B. Rozenbaum, S. Ganeshan and V. Galitski, *Lyapunov Exponent and Out-of-Time-Ordered Correlator's Growth Rate in a Chaotic System*, *Phys. Rev. Lett.* **118** (2017) 086801 [1609.01707].

[183] S. Das, B. Ezhuthachan, A. Kundu, S. Porey and B. Roy, *Critical quenches, OTOCs and early-time chaos*, *JHEP* **07** (2022) 046 [2108.12884].

[184] T. Ali, A. Bhattacharyya, S.S. Haque, E.H. Kim, N. Moynihan and J. Murugan, *Chaos and Complexity in Quantum Mechanics*, *Phys. Rev. D* **101** (2020) 026021 [1905.13534].

[185] R.-Q. Yang and K.-Y. Kim, *Time evolution of the complexity in chaotic systems: a concrete example*, *JHEP* **05** (2020) 045 [1906.02052].

[186] V. Balasubramanian, M. Decross, A. Kar and O. Parrikar, *Quantum Complexity of Time Evolution with Chaotic Hamiltonians*, *JHEP* **01** (2020) 134 [1905.05765].

[187] K. Adhikari, S. Choudhury, S. Chowdhury, K. Shirish and A. Swain, *Circuit complexity as a novel probe of quantum entanglement: A study with black hole gas in arbitrary dimensions*, *Phys. Rev. D* **104** (2021) 065002 [2104.13940].

[188] S. Choudhury, A. Mukherjee, N. Pandey and A. Roy, *Causality Constraint on Circuit Complexity from COSMOEFT*, *Fortsch. Phys.* **71** (2023) 2200199 [2111.11468].

[189] K. Adhikari and S. Choudhury, *Cosmological Krylov Complexity*, *Fortsch. Phys.* **70** (2022) 2200126 [2203.14330].

[190] M. Park and P. Saha, *Primordial Cosmic Complexity and effects of Reheating*, 2212.13723.

[191] S.E. Joras and V.H. Cardenas, *Chaos and preheating*, *Phys. Rev. D* **67** (2003) 043501 [gr-qc/0108088].

[192] Y. Jin and S. Tsujikawa, *Chaotic dynamics in preheating after inflation*, *Class. Quant. Grav.* **23** (2006) 353 [hep-ph/0411164].

[193] S. Hirai, *Squeeze parameters in reheating*, *Progress of Theoretical Physics* **103** (2000) 1161.

[194] M. Srednicki, *Chaos and Quantum Thermalization*, cond-mat/9403051.

[195] L. D'Alessio, Y. Kafri, A. Polkovnikov and M. Rigol, *From quantum chaos and eigenstate thermalization to statistical mechanics and thermodynamics*, *Adv. Phys.* **65** (2016) 239 [1509.06411].

[196] L. Foini and J. Kurchan, *Eigenstate thermalization hypothesis and out of time order correlators*, *Phys. Rev. E* **99** (2019) 042139 [1803.10658].

[197] M. Brenes, S. Pappalardi, M.T. Mitchison, J. Goold and A. Silva, *Out-of-time-order correlations and the fine structure of eigenstate thermalization*, *Phys. Rev. E* **104** (2021) 034120 [2103.01161].

[198] N. Bernal, M. Dutra, Y. Mambrini, K. Olive, M. Peloso and M. Pierre, *Spin-2 Portal Dark Matter*, *Phys. Rev. D* **97** (2018) 115020 [1803.01866].

[199] Y. Mambrini and K.A. Olive, *Gravitational Production of Dark Matter during Reheating*, *Phys. Rev. D* **103** (2021) 115009 [2102.06214].

[200] A. Ahmed, B. Grzadkowski and A. Socha, *Gravitational production of vector dark matter*, *JHEP* **08** (2020) 059 [2005.01766].

[201] K. Kaneta, W. Ke, Y. Mambrini, K.A. Olive and S. Verner, *Gravitational production of spin-3/2 particles during reheating*, *Phys. Rev. D* **108** (2023) 115027 [2309.15146].

[202] G. Choi, W. Ke and K.A. Olive, *Minimal production of prompt gravitational waves during reheating*, *Phys. Rev. D* **109** (2024) 083516 [2402.04310].

[203] M.A.G. Garcia, K. Kaneta, Y. Mambrini, K.A. Olive and S. Verner, *Freeze-in from preheating*, *JCAP* **03** (2022) 016 [2109.13280].

[204] M.A.G. Garcia, M. Gross, Y. Mambrini, K.A. Olive, M. Pierre and J.-H. Yoon, *Effects of fragmentation on post-inflationary reheating*, *JCAP* **12** (2023) 028 [2308.16231].

[205] M.A.G. Garcia and M. Pierre, *Gravitational wave signatures of post-fragmentation reheating*, *JCAP* **09** (2024) 054 [2404.16932].

[206] M.A.G. Garcia and M. Pierre, *Reheating after inflaton fragmentation*, *JCAP* **11** (2023) 004 [2306.08038].

[207] B. Barman, N. Bernal and J. Rubio, *Rescuing gravitational-reheating in chaotic inflation*, *JCAP* **05** (2024) 072 [2310.06039].

[208] L.H. Ford, *Gravitational particle creation and inflation*, *Phys. Rev. D* **35** (1987) 2955.

[209] L.H. Ford, *Cosmological particle production: a review*, *Rept. Prog. Phys.* **84** (2021) [2112.02444].

[210] A.D. Dolgov and D.P. Kirilova, *ON PARTICLE CREATION BY A TIME DEPENDENT SCALAR FIELD*, *Sov. J. Nucl. Phys.* **51** (1990) 172.

[211] D.J.H. Chung, E.W. Kolb and A.J. Long, *Gravitational production of super-Hubble-mass particles: an analytic approach*, *JHEP* **01** (2019) 189 [1812.00211].

[212] E.E. Basso and D.J.H. Chung, *Computation of gravitational particle production using adiabatic invariants*, *JHEP* **11** (2021) 146 [2108.01653].

[213] S. Hashiba and J. Yokoyama, *Gravitational reheating through conformally coupled superheavy scalar particles*, *JCAP* **01** (2019) 028 [1809.05410].

[214] S. Hashiba and J. Yokoyama, *Gravitational particle creation for dark matter and reheating*, *Phys. Rev. D* **99** (2019) 043008 [1812.10032].

[215] N. Herring, D. Boyanovsky and A.R. Zentner, *Nonadiabatic cosmological production of ultralight dark matter*, *Phys. Rev. D* **101** (2020) 083516 [1912.10859].

[216] J. Lankinen, O. Kerppo and I. Vilja, *Reheating via gravitational particle production in the kination epoch*, *Phys. Rev. D* **101** (2020) 063529 [1910.07520].

[217] C. Pallis, *Kination-dominated reheating and cold dark matter abundance*, *Nucl. Phys. B* **751** (2006) 129 [hep-ph/0510234].

[218] D. Feiteira and O. Lebedev, *Cosmological gravitational particle production: Starobinsky vs Bogolyubov, uncertainties, and issues*, 2503.14652.

[219] S. Alexander, H. Bernardo, Y.S. Li and C. Niu, *Vacuum Amplification of Chiral Gravitational Waves and the Stochastic Gravitational Wave Background*, 2411.04233.

[220] T. Moroi and W. Yin, *Particle Production from Oscillating Scalar Field and Consistency of Boltzmann Equation*, *JHEP* **03** (2021) 296 [2011.12285].

[221] M.R. Haque and D. Maity, *Gravitational dark matter: Free streaming and phase space distribution*, *Phys. Rev. D* **106** (2022) 023506 [2112.14668].

[222] T. Markkanen, A. Rajantie and T. Tenkanen, *Spectator Dark Matter*, *Phys. Rev. D* **98** (2018) 123532 [1811.02586].

[223] G. Choi, M.A.G. Garcia, W. Ke, Y. Mambrini, K.A. Olive and S. Verner, *Inflaton production of scalar dark matter through fluctuations and scattering*, *Phys. Rev. D* **110** (2024) 083512 [2406.06696].

[224] M.A.G. Garcia, W. Ke, Y. Mambrini, K.A. Olive and S. Verner, *Scalar field fluctuations and the production of dark matter*, *JCAP* **08** (2025) 039 [2502.20471].

[225] K. Enqvist, S. Nurmi, T. Tenkanen and K. Tuominen, *Standard Model with a real singlet scalar and inflation*, *JCAP* **08** (2014) 035 [1407.0659].

[226] T. Tenkanen, *Dark matter from scalar field fluctuations*, *Phys. Rev. Lett.* **123** (2019) 061302 [1905.01214].

[227] K. Kaneta, S.M. Lee and K.-y. Oda, *Boltzmann or Bogoliubov? Approaches compared in gravitational particle production*, *JCAP* **09** (2022) 018 [2206.10929].

[228] B. Barman, S. Jyoti Das, M.R. Haque and Y. Mambrini, *Leptogenesis, primordial gravitational waves, and PBH-induced reheating*, *Phys. Rev. D* **110** (2024) 043528 [2403.05626].

[229] M.A.G. Garcia, K. Kaneta, W. Ke, Y. Mambrini, K.A. Olive and S. Verner, *The role of vectors in reheating*, *JCAP* **06** (2024) 014 [2311.14794].

[230] S. Clery, Y. Mambrini, K.A. Olive, A. Shkerin and S. Verner, *Gravitational portals with nonminimal couplings*, *Phys. Rev. D* **105** (2022) 095042 [2203.02004].

[231] M.R. Haque, D. Maity and R. Mondal, *Thermal and non-thermal dark matters with gravitational neutrino reheating*, 2408.12450.

[232] L. Jenks, E.W. Kolb and K. Thyme, *Gravitational particle production of scalars: analytic and numerical approaches including early reheating*, *JHEP* **05** (2025) 077 [2410.03938].

[233] A. Chakraborty, D. Maity and R. Mondal, *Dark matters are Inert, or FIMPy, or WIMPy or UFOy: An inflationary gravitational particle production*, 2603.04155.

[234] Y. Ema, R. Jinno, K. Mukaida and K. Nakayama, *Gravitational Effects on Inflaton Decay*, *JCAP* **05** (2015) 038 [1502.02475].

[235] M.J. Ablowitz and A.S. Fokas, *Fundamentals and techniques of complex function theory*, in *Complex Variables: Introduction and Applications*, Cambridge Texts in Applied Mathematics, p. 1–2, Cambridge University Press (2003).

[236] M.S. Rozman, *The method of stationary phase*, 2017.

[237] E. Basso, D.J.H. Chung, E.W. Kolb and A.J. Long, *Quantum interference in gravitational particle production*, *JHEP* **12** (2022) 108 [2209.01713].

[238] R. Micha and I.I. Tkachev, *Relativistic turbulence: A Long way from preheating to equilibrium*, *Phys. Rev. Lett.* **90** (2003) 121301 [hep-ph/0210202].

[239] J.-H. Yoon, S. Cléry, M. Gross and Y. Mambrini, *Preheating with deep learning*, *JCAP* **08** (2024) 031 [2405.08901].

[240] S. Davidson and S. Sarkar, *Thermalization after inflation*, *JHEP* **11** (2000) 012 [hep-ph/0009078].

[241] A. Kurkela and G.D. Moore, *Thermalization in Weakly Coupled Nonabelian Plasmas*, *JHEP* **12** (2011) 044 [1107.5050].

[242] K. Mukaida and M. Yamada, *Perturbative reheating and thermalization of pure Yang-Mills plasma*, *JHEP* **05** (2024) 174 [2402.14054].

[243] B. Barman, A. Ghoshal, B. Grzadkowski and A. Socha, *Measuring inflaton couplings via primordial gravitational waves*, *JHEP* **07** (2023) 231 [2305.00027].

[244] M.A.G. Garcia, M. Pierre and S. Verner, *Isocurvature constraints on scalar dark matter production from the inflaton*, *Phys. Rev. D* **107** (2023) 123508 [2303.07359].

[245] M.A.G. Garcia, M. Pierre and S. Verner, *New window into gravitationally produced scalar dark matter*, *Phys. Rev. D* **108** (2023) 115024 [2305.14446].

[246] A. Chakraborty, S. Maiti and D. Maity, *Probing a nonminimal coupling through superhorizon instability and secondary gravitational waves*, *Phys. Rev. D* **111** (2025) 083505 [2408.07767].

[247] O. Lebedev, *Scalar overproduction in standard cosmology and predictivity of non-thermal dark matter*, *JCAP* **02** (2023) 032 [2210.02293].

[248] V. Mukhanov, H. Feldman and R. Brandenberger, *Theory of cosmological perturbations*, *Physics Reports* **215** (1992) 203.

[249] B.A. Bassett, S. Tsujikawa and D. Wands, *Inflation dynamics and reheating*, *Rev. Mod. Phys.* **78** (2006) 537.

[250] LIGO Scientific, Virgo collaboration, *Observation of Gravitational Waves from a Binary Black Hole Merger*, *Phys. Rev. Lett.* **116** (2016) 061102 [1602.03837].

[251] LIGO Scientific, Virgo collaboration, *GW150914: The Advanced LIGO Detectors in the Era of First Discoveries*, *Phys. Rev. Lett.* **116** (2016) 131103 [1602.03838].

[252] LIGO Scientific, VIRGO collaboration, *GW170104: Observation of a 50-Solar-Mass Binary Black Hole Coalescence at Redshift 0.2*, *Phys. Rev. Lett.* **118** (2017) 221101 [1706.01812].

[253] LIGO Scientific, Virgo collaboration, *Upper Limits on the Stochastic Gravitational-Wave Background from Advanced LIGO's First Observing Run*, *Phys. Rev. Lett.* **118** (2017) 121101 [1612.02029].

[254] NANOGrav collaboration, *The NANOGrav 12.5 yr Data Set: Search for an Isotropic Stochastic Gravitational-wave Background*, *Astrophys. J. Lett.* **905** (2020) L34 [2009.04496].

[255] NANOGrav collaboration, *The NANOGrav 15 yr Data Set: Evidence for a Gravitational-wave Background*, *Astrophys. J. Lett.* **951** (2023) L8 [2306.16213].

[256] NANOGrav collaboration, *The NANOGrav 15 yr Data Set: Observations and Timing of 68 Millisecond Pulsars*, *Astrophys. J. Lett.* **951** (2023) L9 [2306.16217].

[257] EPTA, InPTA: collaboration, *The second data release from the European Pulsar Timing Array - III. Search for gravitational wave signals*, *Astron. Astrophys.* **678** (2023) A50 [2306.16214].

[258] EPTA, InPTA collaboration, *The second data release from the European Pulsar Timing Array - IV. Implications for massive black holes, dark matter, and the early Universe*, *Astron. Astrophys.* **685** (2024) A94 [2306.16227].

[259] D.J. Reardon et al., *Search for an Isotropic Gravitational-wave Background with the Parkes Pulsar Timing Array*, *Astrophys. J. Lett.* **951** (2023) L6 [2306.16215].

[260] A. Zic et al., *The Parkes Pulsar Timing Array third data release*, *Publ. Astron. Soc. Austral.* **40** (2023) e049 [2306.16230].

[261] H. Xu et al., *Searching for the Nano-Hertz Stochastic Gravitational Wave Background with the Chinese Pulsar Timing Array Data Release I*, *Res. Astron. Astrophys.* **23** (2023) 075024 [2306.16216].

[262] M. Punturo, M. Abernathy, F. Acernese, B. Allen, N. Andersson, K. Arun et al., *The einstein telescope: a third-generation gravitational wave observatory*, *Classical and Quantum Gravity* **27** (2010) 194002.

[263] B. Sathyaprakash et al., *Scientific Objectives of Einstein Telescope*, *Class. Quant. Grav.* **29** (2012) 124013 [1206.0331].

[264] J. Crowder and N.J. Cornish, *Beyond LISA: Exploring future gravitational wave missions*, *Phys. Rev. D* **72** (2005) 083005 [gr-qc/0506015].

[265] V. Corbin and N.J. Cornish, *Detecting the cosmic gravitational wave background with the big bang observer*, *Class. Quant. Grav.* **23** (2006) 2435 [gr-qc/0512039].

[266] J. Baker et al., *Space Based Gravitational Wave Astronomy Beyond LISA*, *Bull. Am. Astron. Soc.* **51** (2019) 243 [1907.11305].

[267] E. Barausse, E. Berti, T. Hertog, S.A. Hughes, P. Jetzer, P. Pani et al., *Prospects for fundamental physics with lisa*, *General Relativity and Gravitation* **52** (2020) .

[268] G. Janssen et al., *Gravitational wave astronomy with the SKA*, *PoS* **AASKA14** (2015) 037 [1501.00127].

[269] N. Arkani-Hamed and J. Maldacena, *Cosmological Collider Physics*, 1503.08043.

[270] X. Chen and Y. Wang, *Large non-Gaussianities with Intermediate Shapes from Quasi-Single Field Inflation*, *Phys. Rev. D* **81** (2010) 063511 [0909.0496].

[271] DESI collaboration, *DESI 2024 VI: cosmological constraints from the measurements of baryon acoustic oscillations*, *JCAP* **02** (2025) 021 [2404.03002].

[272] eBOSS collaboration, *The 16th Data Release of the Sloan Digital Sky Surveys: First Release from the APOGEE-2 Southern Survey and Full Release of eBOSS Spectra*, *Astrophys. J. Suppl.* **249** (2020) 3 [1912.02905].

[273] A. Linde, *Scalar field fluctuations in the expanding universe and the new inflationary universe scenario*, *Physics Letters B* **116** (1982) 335.

[274] D.Z. Freedman, I.J. Muzinich and E.J. Weinberg, *On the Energy-Momentum Tensor in Gauge Field Theories*, *Annals Phys.* **87** (1974) 95.

[275] D.Z. Freedman and E.J. Weinberg, *The energy-momentum tensor in scalar and gauge field theories*, *Annals of Physics* **87** (1974) 354.

[276] V. Faraoni, *Nonminimal coupling of the scalar field and inflation*, *Physical Review D* **53** (1996) 6813–6821.

[277] S. Tsujikawa, *Power-law inflation with a nonminimally coupled scalar field*, *Phys. Rev. D* **62** (2000) 043512.

[278] E. Komatsu and T. Futamase, *Complete constraints on a nonminimally coupled chaotic inflationary scenario from the cosmic microwave background*, *Physical Review D* **59** (1999) .

[279] F. Lucchin, S. Matarrese and M. Pollock, *Inflation with a non-minimally coupled scalar field*, *Physics Letters B* **167** (1986) 163.

[280] B. Spokoiny, *Inflation and generation of perturbations in broken-symmetric theory of gravity*, *Physics Letters B* **147** (1984) 39.

[281] T. Futamase and K.-i. Maeda, *Chaotic inflationary scenario of the universe with a nonminimally coupled "inflaton" field*, *Phys. Rev. D* **39** (1989) 399.

[282] M. Shokri, J. Sadeghi, M.R. Setare and S. Capozziello, *Nonminimal coupling inflation with constant slow roll*, *International Journal of Modern Physics D* **30** (2021) 2150070.

[283] S. Capozziello and R. de Ritis, *Nöther's symmetries and exact solutions in flat non-minimally coupled cosmological models*, *Classical and Quantum Gravity* **11** (1994) 107.

[284] K. NOZARI and S.D. SADATIAN, *Non-minimal inflation after wmap3*, *Modern Physics Letters A* **23** (2008) 2933–2945.

[285] C. Gomes, J. Rosa and O. Bertolami, *Inflation in non-minimal matter-curvature coupling theories*, *Journal of Cosmology and Astroparticle Physics* **2017** (2017) 021–021.

[286] P. Sarkar, Ashmita and P.K. Das, *Non-minimal inflation with a scalar-curvature mixing term* $\frac{1}{2}\xi r\phi^2$, 2023.

[287] S. Pi, Y.-l. Zhang, Q.-G. Huang and M. Sasaki, *Scalaron from $R^2$-gravity as a heavy field*, *JCAP* **05** (2018) 042 [1712.09896].

[288] X. Wang, Y.-l. Zhang and M. Sasaki, *Enhanced curvature perturbation and primordial black hole formation in two-stage inflation with a break*, *JCAP* **07** (2024) 076 [2404.02492].

[289] B.A. Bassett and S. Liberati, *Geometric reheating after inflation*, *Phys. Rev. D* **58** (1998) 021302 [hep-ph/9709417].

[290] S. Tsujikawa, K.-i. Maeda and T. Torii, *Resonant particle production with nonminimally coupled scalar fields in preheating after inflation*, *Phys. Rev. D* **60** (1999) 063515 [hep-ph/9901306].

[291] S. Tsujikawa, K.-i. Maeda and T. Torii, *Preheating with nonminimally coupled scalar fields in higher curvature inflation models*, *Phys. Rev. D* **60** (1999) 123505 [hep-ph/9906501].

[292] Y. Ema, R. Jinno, K. Mukaida and K. Nakayama, *Violent preheating in inflation with nonminimal coupling*, *Journal of Cosmology and Astroparticle Physics* **2017** (2017) 045–045.

[293] K. Dimopoulos and T. Markkanen, *Non-minimal gravitational reheating during kination*, *Journal of Cosmology and Astroparticle Physics* **2018** (2018) 021–021.

[294] D.G. Figueroa, A. Florio, T. Opferkuch and B.A. Stefanek, *Lattice simulations of non-minimally coupled scalar fields in the Jordan frame*, *SciPost Phys.* **15** (2023) 077 [2112.08388].

[295] T. Opferkuch, P. Schwaller and B.A. Stefanek, *Ricci Reheating*, *JCAP* **07** (2019) 016 [1905.06823].

[296] D. Bettoni, A. Lopez-Eiguren and J. Rubio, *Hubble-induced phase transitions on the lattice with applications to Ricci reheating*, *JCAP* **01** (2022) 002 [2107.09671].

[297] G. Laverda and J. Rubio, *Ricci reheating reloaded*, *JCAP* **03** (2024) 033 [2307.03774].

[298] D.G. Figueroa and N. Loayza, *Geometric reheating of the Universe*, 2406.02689.

[299] G. Laverda and J. Rubio, *The rise and fall of the Standard-Model Higgs: electroweak vacuum stability during kination*, *JHEP* **05** (2024) 339 [2402.06000].

[300] T. Markkanen and S. Nurmi, *Dark matter from gravitational particle production at reheating*, *JCAP* **02** (2017) 008 [1512.07288].

[301] T. Markkanen, *Light scalars on cosmological backgrounds*, *JHEP* **01** (2018) 116 [1711.07502].

[302] M. Fairbairn, K. Kainulainen, T. Markkanen and S. Nurmi, *Despicable Dark Relics: generated by gravity with unconstrained masses*, *JCAP* **04** (2019) 005 [1808.08236].

[303] K. Kainulainen, O. Koskivaara and S. Nurmi, *Tachyonic production of dark relics: a non-perturbative quantum study*, *JHEP* **04** (2023) 043 [2209.10945].

[304] O. Lebedev, T. Solomko and J.-H. Yoon, *Dark matter production via a non-minimal coupling to gravity*, *JCAP* **02** (2023) 035 [2211.11773].

[305] Z. Yu, C. Fu and Z.-K. Guo, *Particle production during inflation with a nonminimally coupled spectator scalar field*, *Physical Review D* **108** (2023) .

[306] J.A.R. Cembranos, L.J. Garay, A. Parra-López and J.M. Sánchez Velázquez, *Vector dark matter production during inflation and reheating*, *JCAP* **02** (2024) 013 [2310.07515].

[307] E.W. Kolb and A.J. Long, *Completely dark photons from gravitational particle production during the inflationary era*, *JHEP* **03** (2021) 283 [2009.03828].

[308] C. Capanelli, L. Jenks, E.W. Kolb and E. McDonough, *Gravitational Production of Completely Dark Photons with Nonminimal Couplings to Gravity*, 2405.19390.

[309] C. Capanelli, L. Jenks, E.W. Kolb and E. McDonough, *Runaway Gravitational Production of Dark Photons*, *Phys. Rev. Lett.* **133** (2024) 061602 [2403.15536].

[310] M.R. Setare and E.C. Vagenas, *Non-minimal coupling of the phantom field and cosmic acceleration*, *Astrophys. Space Sci.* **330** (2010) 145 [0906.4237].

[311] M. Sami, M. Shahalam, M. Skugoreva, A. Toporensky, M. Shahalam, M. Skugoreva et al., *Cosmological dynamics of non-minimally coupled scalar field system and its late time cosmic relevance*, *Phys. Rev. D* **86** (2012) 103532 [1207.6691].

[312] R. Kase and S. Tsujikawa, *Scalar-Field Dark Energy Nonminimally and Kinetically Coupled to Dark Matter*, *Phys. Rev. D* **101** (2020) 063511 [1910.02699].

[313] G. Ye, M. Martinelli, B. Hu and A. Silvestri, *Non-minimally coupled gravity as a physically viable fit to DESI 2024 BAO*, 2407.15832.

[314] A. Ghoshal, D. Paul and S. Pal, *Primordial Gravitational Waves as Probe of Dark Matter in Interferometer Missions: Fisher Forecast and MCMC*, 2405.06741.

[315] S. Maity and M.R. Haque, *Probing the early universe with future GW observatories*, 2407.18246.

[316] T. Nakama and J. Yokoyama, *Reheating through the Higgs amplified by spinodal instabilities and gravitational creation of gravitons*, *PTEP* **2019** (2019) 033E02 [1803.07111].

[317] S. Hannestad, *What is the lowest possible reheating temperature?*, *Phys. Rev. D* **70** (2004) 043506 [astro-ph/0403291].

[318] L. Dai, M. Kamionkowski and J. Wang, *Reheating constraints to inflationary models*, *Phys. Rev. Lett.* **113** (2014) 041302.

[319] C. Fu, P. Wu and H. Yu, *Production of gravitational waves during preheating with nonminimal coupling*, *Phys. Rev. D* **97** (2018) 081303 [1711.10888].

[320] LiteBIRD collaboration, *Tensor-to-scalar ratio forecasts for extended LiteBIRD frequency configurations*, *Astron. Astrophys.* **676** (2023) A42 [2302.05228].

[321] LiteBIRD collaboration, *Probing Cosmic Inflation with the LiteBIRD Cosmic Microwave Background Polarization Survey*, *PTEP* **2023** (2023) 042F01 [2202.02773].

[322] M. Drewes, L. Ming and I. Oldengott, *LiteBIRD and CMB-S4 sensitivities to reheating in plateau models of inflation*, *JCAP* **05** (2024) 081 [2303.13503].

[323] M. Drewes and L. Ming, *Connecting Cosmic Inflation to Particle Physics with LiteBIRD, CMB-S4, EUCLID, and SKA*, *Phys. Rev. Lett.* **133** (2024) 031001 [2208.07609].

[324] D.J.H. Chung and H. Yoo, *Isocurvature Perturbations and Non-Gaussianity of Gravitationally Produced Nonthermal Dark Matter*, *Phys. Rev. D* **87** (2013) 023516 [1110.5931].

[325] S. Ling and A.J. Long, *Superheavy scalar dark matter from gravitational particle production in $\alpha$-attractor models of inflation*, *Phys. Rev. D* **103** (2021) 103532 [2101.11621].

[326] A.R. Liddle and A. Mazumdar, *Perturbation amplitude in isocurvature inflation scenarios*, *Phys. Rev. D* **61** (2000) 123507 [astro-ph/9912349].

[327] J.J. Bennett, G. Buldgen, P.F. De Salas, M. Drewes, S. Gariazzo, S. Pastor et al., *Towards a precision calculation of $N_{\rm eff}$ in the Standard Model II: Neutrino decoupling in the presence of flavour oscillations and finite-temperature QED*, *JCAP* **04** (2021) 073 [2012.02726].

[328] J. Froustey, C. Pitrou and M.C. Volpe, *Neutrino decoupling including flavour oscillations and primordial nucleosynthesis*, *JCAP* **12** (2020) 015 [2008.01074].

[329] K. Akita and M. Yamaguchi, *A precision calculation of relic neutrino decoupling*, *JCAP* **08** (2020) 012 [2005.07047].

[330] C. Caprini and D.G. Figueroa, *Cosmological Backgrounds of Gravitational Waves*, *Class. Quant. Grav.* **35** (2018) 163001 [1801.04268].

[331] T.J. Clarke, E.J. Copeland and A. Moss, *Constraints on primordial gravitational waves from the Cosmic Microwave Background*, *JCAP* **10** (2020) 002 [2004.11396].

[332] T.L. Smith, E. Pierpaoli and M. Kamionkowski, *A new cosmic microwave background constraint to primordial gravitational waves*, *Phys. Rev. Lett.* **97** (2006) 021301 [astro-ph/0603144].

[333] R.T. Co, Y. Mambrini and K.A. Olive, *Inflationary gravitational leptogenesis*, *Phys. Rev. D* **106** (2022) 075006 [2205.01689].

[334] S. Maiti, D. Maity and R. Srikanth, *Probing Reheating Phase via Non-Helical Magnetogenesis and Secondary Gravitational Waves*, 2505.13623.

[335] K.D. Lozanov and M.A. Amin, *Self-resonance after inflation: oscillons, transients and radiation domination*, *Phys. Rev. D* **97** (2018) 023533 [1710.06851].

[336] M.A.G. Garcia, K. Kaneta, Y. Mambrini and K.A. Olive, *Reheating and post-inflationary production of dark matter*, *Phys. Rev. D* **101** (2020) 123507.

[337] Y. Fujii and K. Maeda, *The Scalar-Tensor Theory of Gravitation*, Cambridge University Press (2003).

[338] B.R. Holstein, *Graviton Physics*, *Am. J. Phys.* **74** (2006) 1002 [gr-qc/0607045].

[339] A. Ahmed, B. Grzadkowski and A. Socha, *Higgs boson induced reheating and ultraviolet frozen-in dark matter*, *JHEP* **02** (2023) 196 [2207.11218].

[340] R. Brandenberger, H. Feldman and V. Mukhanov, *Classical and quantum theory of perturbations in inflationary universe models*, 1993.

[341] J. White, M. Minamitsuji and M. Sasaki, *Curvature perturbation in multi-field inflation with non-minimal coupling*, *JCAP* **07** (2012) 039 [1205.0656].

[342] D.H. Lyth and D. Wands, *Generating the curvature perturbation without an inflaton*, *Phys. Lett. B* **524** (2002) 5 [hep-ph/0110002].